Southern California Earthquake Center

2010 Annual Meeting

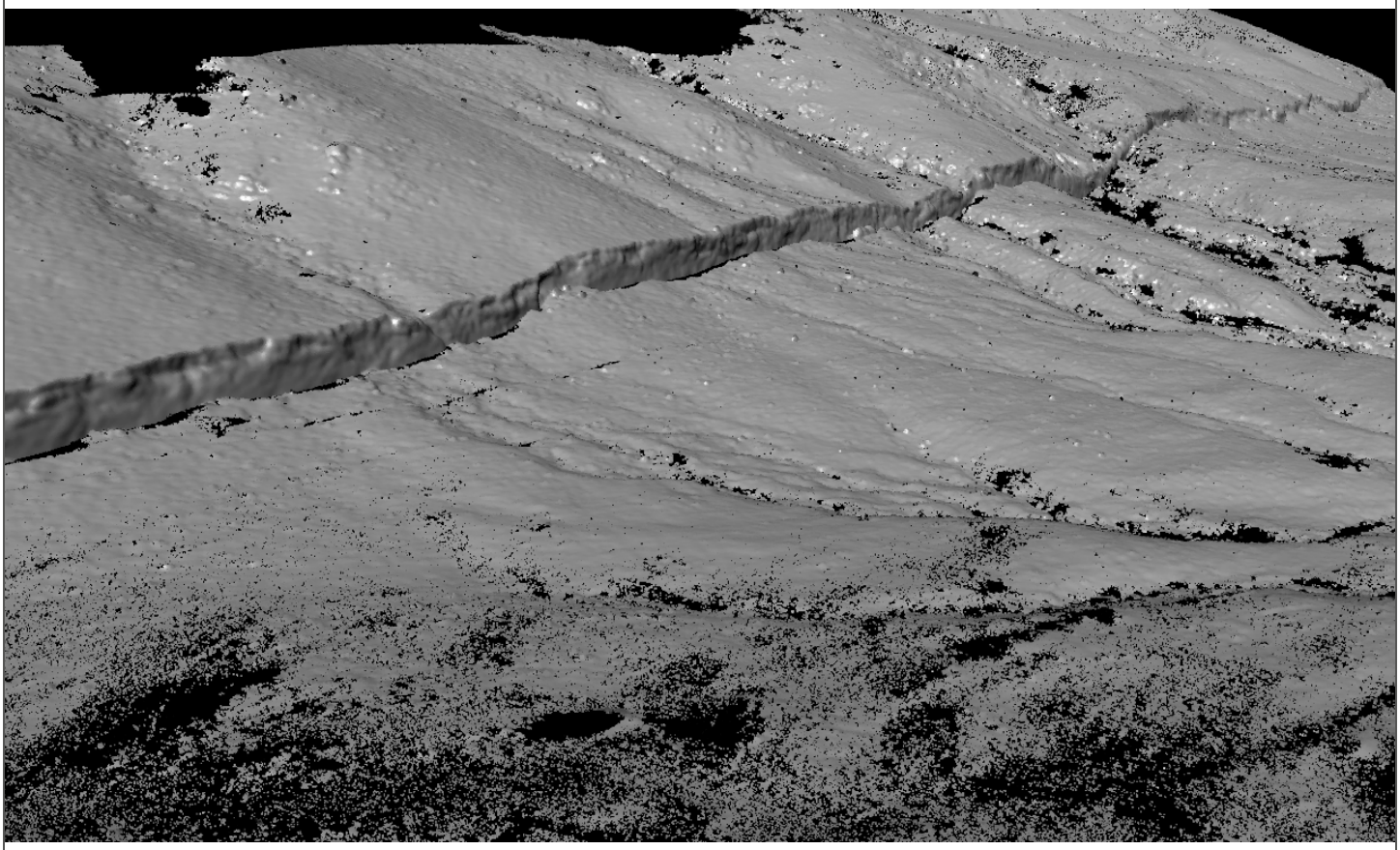

Proceedings and Abstracts, Volume XX

September 11-15, 2010

SCEC

an NSF+USGS center

ANNUAL MEETING

of the

Southern California Earthquake Center

Proceedings and Abstracts, Volume XX

Cover Image: Section of the Borrego fault rupture formed during the 4 April 2010 El Mayor-Cucapah earthquake. (*Peter Gold, Austin Elliott, Michael Oskin, and Alejandro Hinojosa. Image was generated in LidarViewer software developed by Oliver Kreylos at the W.M. Keck Center for Active Visualization in the Earth Sciences (KeckCAVES) at UC Davis.*)

SCEC ORGANIZATION

Center Director, *Tom Jordan*

Deputy Director, *Greg Beroza*

Associate Director for Administration, *John McRaney*

Associate Director for Communication, Education, and Outreach, *Mark Benthien*

Associate Director for Information Technology, *Phil Maechling*

Special Projects and Events Coordinator, *Tran Huynh*

Research Contracts and Grants Coordinator, *Karen Young*

Administrative Coordinator, *Deborah Gormley*

Education Programs Manager, *Robert de Groot*

Digital Products Manager, *John Marquis*

Research Programmers, *Scott Callaghan, Sandarsh Kumar, Maria Liukis, Kevin Milner, Patrick Small*

Systems Administrator, *John Yu*

SCEC PLANNING COMMITTEE

Chair, *Greg Beroza*

Seismology, *Egill Hauksson, Elizabeth Cochran*

Tectonic Geodesy, *Jessica Moraleda, Rowena Lohman*

Earthquake Geology, *Mike Oskin, James Dolan*

Unified Structural Representation, *John Shaw, Kim Olsen*

Fault and Rupture Mechanics, *Judith Chester, Ruth Harris*

Crustal Deformation Modeling, *Liz Hearn, Kaj Johnson*

Lithospheric Architecture and Dynamics, *Paul Davis, Thorsten Becker*

Earthquake Forecasting and Predictability, *Terry Tullis, Jeanne Hardebeck*

Ground Motion Prediction, *Brad Aagaard, Rob Graves*

Seismic Hazard and Risk Analysis, *Paul Somerville, Nicolas Luco*

Southern San Andreas Fault Evaluation, *Tom Rockwell, Kate Scharer*

Working Group on California Earthquake Probabilities, *Ned Field*

Collaboratory for the tudy of Earthquake Predictability, *Tom Jordan, Danijel Schorlemmer*

Extreme Ground Motion, *Tom Hanks*

Community Modeling Environment, *Phil Maechling*

SCEC ADVISORY COUNCIL

Mary Lou Zoback, *Chair, Risk Management Solutions*

Jeffrey Freymueller, *Chair-Designate, U. Alaska*

Gail Atkinson, *U. Western Ontario*

Roger Bilham, *U. of Colorado (new member 2010)*

Donna Eberhart-Phillips, *UC Davis*

John Filson, *U.S. Geological Survey (Emeritus)*

Jim Goltz, *CalEMA*

Steve Mahin, *PEER*

Anne Meltzer, *Lehigh University*

Denis Mileti, *U. Colorado (Emeritus)*

M. Meghan Miller, *UNAVCO*

Farzad Naeim, *John A. Martin & Associates (new member 2010)*

John Vidale, *U. Washington (new member 2010)*

Andrew Whittaker, *U. Buffalo (new member 2010)*

SCEC BOARD OF DIRECTORS

Tom Jordan, *Chair, USC*

Lisa Grant-Ludwig, *Vice-Chair, UCI*

Ralph Archuleta, *UCSB*

Peter Bird, *UCLA*

David Bowman, *CSUF*

Tom Brocher, *USGS Menlo, liaison (non-voting)*

Emily Brodsky, *UCSC*

Jim Brune, *UNR*

Steve Day, *SDSU*

James Dieterich, *UCR*

Yuri Fialko, *UCSD*

Tom Herring, *MIT*

Ken Hudnut, *USGS Pasadena, liaison (non-voting)*

Nadia Lapusta, *CalTech*

Jim Rice, *Harvard*

Paul Segall, *Stanford*

Bruce Shaw, *Columbia*

Jill McCarthy, *USGS Golden, liaison (non-voting)*

Table of Contents

Table of Contents

SCEC Annual Meeting Program

SATURDAY, SEPTEMBER 11, 2010

09:00 – 18:30 Registration Check-In

10:00 – 17:30 Workshop on Transient Anomalous Strain Detection (*pages 5*)

12:00 – 13:30 Lunch (*Tapestry Room, Terrace Restaurant*)

13:30 – 17:30 Extreme Ground Motion Workshop: The Last Hurrah (*pages 6*)

13:30 – 17:30 Source Inversion Validation Workshop – Session I (*pages 7*)

18:00 – 20:00 Dinner (*Poolside*)

18:00 – 20:00 SCEC Intern Program Reception (*Tapestry Room*)

SUNDAY, SEPTEMBER 12, 2010

07:00 – 18:30 Registration Check-In

07:00 – 08:00 Breakfast (*Poolside*)

08:00 – 12:00 Source Inversion Validation Workshop – Session II (*pages 7*)

08:00 – 12:00 SCEC CME Leadership Meeting (*Oasis Room 3*)

08:00 – 17:00 Coulomb 3.2 Short Course (*pages 8*)

09:30 – 12:00 Southern San Andreas Fault Evaluation Workshop (*page 9*)

10:00 – 16:00 Great California ShakeOut Workshop for Science Educators (*page 10*)

12:00 – 13:00 Lunch (*Terrace Restaurant, Poolside*)

13:00 – 15:00 Salton Seismic Imaging Project Meeting (*Horizon Ballroom I*)

13:00 – 17:00 Engineering Workshop on Tall Building Safety (*pages 11-12*)

13:00 – 17:00 UCERF3/GPS Working Group Meeting (*Oasis Room 3*)

13:00 – 17:00 Poster Session Set-Up: Group 1 Posters (*Plaza Ballroom*)

17:00 – 18:00 **Special Talk** (*Horizon Ballroom I*)
Comparison of the 1960 and 2010 Chilean Earthquakes (*Hiroo Kanamori*)

18:00 – 20:00 SCEC Annual Meeting Ice-Breaker / Welcome Reception (*Poolside*)

18:30 SCEC Advisory Council Working Dinner (*Boardroom*)

20:00 – 22:30 Poster Session I: Group 1 Posters (*Plaza Ballroom*)

MONDAY, SEPTEMBER 13, 2010

07:00 – 08:00 Registration Check-In

07:00 – 08:00 Breakfast (*Poolside*)

Annual Meeting Session I (*Horizon Ballroom*)

08:00 Welcome and State of the Center (*Tom Jordan*)

08:30 Report from NSF (*Greg Anderson*)

08:45 Report from USGS (*Dave Applegate*)

09:00 Communication, Education, & Outreach Highlights (*Mark Benthien*)

09:30 SCEC Science Accomplishments (*Greg Beroza*)

10:30 Break

Annual Meeting Session II (*Horizon Ballroom*)

11:00 – 11:30 **Plenary Talk:** The January 12, 2010, Mw 7.0 Earthquake in Haiti: Context and Mechanism (*Eric Calais*)

11:30 – 13:00 **Science Discussion:** How should SCEC participate in national and international partnerships to promote earthquake system science?

(Moderators: *Ralph Archuleta, Joann Stock*)

13:00 – 14:30 Lunch (*Poolside*)

14:30 – 16:00 Poster Session II: Group 1 Posters (*Plaza Ballroom*)

Annual Meeting Session III (*Horizon Ballroom*)

16:00 – 16:30 **Plenary Talk:** Performance of Structures in the 27 February 2010 Great Maule Earthquake (*Jose Restrepo*)

16:30 – 18:00 **Science Discussion:** How can earthquake scientists most effectively work with earthquake engineers to reduce earthquake risk?

(Moderators: *Nico Luco, Paul Somerville*)

18:00 – 19:00 Poster Session Set-Up: Group 2 Posters (*Plaza Ballroom*)

19:00 – 21:00 SCEC Honors Banquet (*Poolside*)

21:00 – 22:30 Poster Session III: Group 2 Posters (*Plaza Ballroom*)

TUESDAY, SEPTEMBER 14, 2010

07:00 – 08:00 Breakfast (*Poolside*)

Annual Meeting Session IV (*Horizon Ballroom*)

08:00 – 08:30 **Plenary Talk:** Distribution and Kinematics of Surface Ruptures Associated with the El Mayor-Cucapah Earthquake Sequence (*John Fletcher*)

08:30 – 10:00 **Science Discussion:** How can we better prepare for, and respond to, future earthquakes?

(Moderators: *Elizabeth Cochran, Mike Oskin*)

10:00 Break

Annual Meeting Session V (*Horizon Ballroom*)

10:30 – 11:00 **Plenary Talk:** Triggering by Seismic Waves and Implications for Earthquake Predictability (*Emily Brodsky*)

11:00 – 12:30 **Science Discussion:** What do we need to do to understand better the physics of earthquake faulting?

(Moderators: *Jeanne Hardebeck, Eric Dunham*)

12:30 – 14:00 Lunch (*Poolside*)

12:30 SCEC Advisory Council Working Lunch, Executive Session (*Boardroom*)

14:00 – 15:30 Poster Session IV: Group 2 Posters (*Plaza Ballroom*)

Annual Meeting Session VI (*Horizon Ballroom*)

15:30 – 16:00 **Plenary Talk:** Behavior of the Deep Roots of Faults (*Greg Hirth*)

16:00 – 17:30 **Science Discussion:** How does the large scale architecture of the plate boundary inform our understanding of earthquake occurrence?

(Moderators: *Kaj Johnson, Liz Hearn*)

17:30 – 18:30 2011 Science Collaboration and Planning (*Greg Beroza*)

19:00 – 21:00 Dinner (*Poolside*)

20:00 SCEC Advisory Council Executive Session (*Boardroom*)

21:00 – 22:30 Poster Session V: Group 2 Posters (*Plaza Ballroom*)

WEDNESDAY, SEPTEMBER 15, 2010

07:00 – 08:00 Remove Posters (*Plaza Ballroom*)

07:00 – 08:00 Breakfast (*Poolside*)

Annual Meeting Session VII (*Horizon Ballroom*)

08:00 – 08:30 **Plenary Talk:** Petrified Earthquakes: Structural Properties of Damaged Rocks within the San Andreas Fault Zone (*Ory Dor*)

08:30 – 10:00 **Science Discussion:** What do we need to do to forecast better the timing, extent, and properties of future earthquake ruptures?

(Moderators: *Ned Field, Terry Tullis*)

10:00 – 10:30 Break

10:30 – 11:00 Report from the SCEC Advisory Council (*Jeff Freymueller*)

11:00 – 11:30 Science Collaboration Wrap-Up (*Greg Beroza*)

11:30 – 12:00 SCEC4 Planning Session (*Tom Jordan*)

12:00 Adjourn

12:00 – 14:00 SCEC Board Lunch Meeting (*Boardroom*)

12:00 – 14:00 SCEC Planning Committee Lunch Meeting (*Palm Canyon Room*)

13:00 – 17:00 Fault Database Coordination and Implementation Meeting (*Oasis 2*)

13:00 – 17:00 El Mayor-Cucapah Science Coordination Meeting (*Horizon Ballroom*)

Workshop Descriptions and Agendas

Workshop on Transient Anomalous Strain Detection

Organizers: Rowena Lohman, Jessica Murray-Moraleda

The Transient Detection Test Exercise is a project in support of one of the SCEC3 priority science objectives, to "develop a geodetic network processing system that will detect anomalous strain transients." Fulfilling this objective will fill a major need of the geodetic community. A means for systematically searching geodetic data for transient signals has obvious applications for network operations, hazard monitoring, and event response, and may lead to identification of events that would otherwise go (or have gone) unnoticed.

As part of the test exercise, datasets are distributed to participants who then apply their detection methodology and report back on any transient signals they find in the test data. We are currently in Phase III of the project. Phases I and II used synthetic GPS datasets. Phase III test data are comprised of synthetic and real GPS observations. Test data, results from completed phases, and further information are available at *http://groups.google.com/group/SCECtransient*.

The objectives of the workshop will be to assess what we have learned to-date, discuss directions on which to focus as the project moves forward, and establish a timeline for these activities. Presentations and discussion in the first half of the workshop will cover advances in methodologies made over the past year by participating groups, improvements to synthetic data, release of the true signals present in Phase III synthetic data, and review of Phase III participants' results. In the second half of the workshop participants will address future directions, with particular focus on 1) application of methods to real data, 2) steps needed for operational deployment of algorithms, and 3) extension of testing to data types other than GPS.

All interested individuals are encouraged to attend, regardless of whether they have participated in the test exercise up to this stage.

SATURDAY, SEPTEMBER 11, 2010 — *Palm Canyon Room*

10:00 – 10:15 Update on the test exercise – developments over the past year and topics to discuss at the workshop (*Jessica Murray-Moraleda*)

10:15 – 12:00 Presentations on different methodologies including results – *15 mins each*

Kang Hyeun | John Langbein | Sharon Kedar | Brad Lipovsky | Matt Weller | Bill Holt | Zhen Liu and Jessica Murray-Moraleda

12:00 – 13:00 Lunch (*Tapestry Room, Terrace Restaurant*)

13:00 – 14:00 Presentations on different methodologies including results – *continued*
Junichi Fukuda and Paul Segall | Jeff McGuire | Maud Comboul | Zhonwen Zhan and Mark Simons

14:00 – 14:20 Test Data

- Synthetic data and FAKENET code – innovations since last year (*Duncan Agnew*)
- Real Data – overview of how it was process (*Tom Herring*)

14:20 – 14:40 Phase II Results (*Rowena Lohman*) and Discussion

14:40 – 15:00 Break

15:00 – 15:30 Discussion and Forward Planning

Extreme Ground Motion (ExGM) Workshop: The Last Hurrah

Organizers: Tom Hanks, Norm Abrahamson

Apart from the hiatus in 2009, ExGM/SCEC workshops have been part of the SCEC Annual Meeting since 2005, when the ExGM research program began. These workshops have been attended by a large number of scientists of many different interests, in part because of the wide-ranging research supported by ExGM. As of this writing in the first week in August, the Final Report of the ExGM research program is being prepared, and a summary of it will be presented at the workshop. Other presentations will focus on results more recent than the last ExGM/SCEC workshop two years ago. These include progress in the dynamic rupture code validation models and applications, dynamic fragility calculations for PBRs, several dozen new exposure ages determined from the abundance of 36Cl, and a new, more rigorous formalism for the Points In Hazard Space graphic that summarizes so much of the ExGM research.

The Cooperative Agreement with the Department of Energy will end on September 30, 2010, and the ExGM research program as we have known it for the last five years will also end. We do, however, expect that various threads of the ExGM fabric will continue for some time to come. One of these is the Ground Motion Simulation effort, long an important matter for SCEC scientists that has been also supported by ExGM and PG&E. Recent developments in this continuing activity will also be summarized at this workshop.

SATURDAY, SEPTEMBER 11, 2010 — *Horizon Ballroom 1*

13:30 – 14:00	Review of ExGM Research Program and Summary of Final Report (*Tom Hanks*)
14:00 – 14:30	Failure Probabilities of PBRs and PBRs in Hazard Space (*Jack Baker*)
14:30 – 15:10	Quaternary Geology/Geomorphology and PSHA at Low Hazard Levels (*John Whitney*)
15:10 – 15:30	Discussion
15:30 – 15:45	Break
	Event Frequencies and Ground-Motion Simulations
15:45 – 16:00	Summary of the Project and Approach (*Norm Abrahamson*)
16:00 – 16:15	Update of the "100 Runs" Task (*Ruth Harris*)
16:15 – 16:45	Points in Hazard Space
16:45 – 17:30	Discussion: Future Plans for Ground-Motion Simulations / Future ExGM Research at SCEC

Source Inversion Validation (SIV) Workshop

Organizers: P. Martin Mai, Morgan Page, Danijel Schorlemmer

Earthquake source inversions image the spatio-temporal rupture evolution on one or more fault planes using seismic and/or geodetic data. Source inversion methods thus represent important research tools in seismology to unravel the complexity of the earthquake rupture process. Researchers are using source-inversion results to study earthquake mechanics, to develop spontaneous dynamic rupture models, to build models for generating rupture realizations for ground-motion simulations, and to perform Coulomb-stress modeling. In all these applications, the underlying finite-source rupture models are treated as "data" (input information), but the uncertainties in these data (i.e. source models obtained from solving an inherently ill-posed inverse problem) are hardly known, and almost always neglected. The Source Inversion Validation (SIV) project is born out of recent efforts to better understand the intra-event variability of earthquake rupture models, as documented in the finite-source rupture model database.

During this workshop will review our recent activities and results regarding Green's function testing and a forward-modeling exercise for a finite-fault kinematic rupture. Additionally, we will examine initial inversion results for a first test problem, discussing also optimal seismic-network geometries for finite-fault studies.

We invite presentations that discuss SIV modeling/testing results, but also general contributions on source-inversion methodologies, analysis of resolution and model errors, and source-model variability in general. New approaches to source inversion and error characterization are also welcome. Presentations that highlight robust features of sources inversions or discriminate between artifacts and true heterogeneities are particularly encouraged.

SATURDAY, SEPTEMBER 11, 2010 — *Horizon Ballroom II*

Session I Review of SIV Activities and Green's Function Results

Session II Results from Forward-Modeling Exercise

SUNDAY, SEPTEMBER 12, 2010 — *Horizon Ballroom II*

Session III Initial Inversion Results and Seismic-Network Geometry

Session IV Break-Out Session and Open Discussion

Coulomb 3.2 Short Course

Organizers: Ross Stein, Shinji Today, Jian Lin, Volkan Sevilgen

SUNDAY, SEPTEMBER 11, 2010 (08:00 – 17:00) — *Palm Canyon Room*

Coulomb is a free, full-day course guaranteed to turn novices into experts. There are 1600 registered Coulomb users worldwide, so you don't have to take the class to use Coulomb, but you will learn faster with us. You'll receive a bound User Guide, and you'll download Coulomb onto your own laptop beforehand for the course. We use the 'push-pull' teaching method, with one maniac in front of the room keying and talking, and the other 3 working behind the participants, giving individual attention and slowing the leader down when needed: No one gets lost!

The program, user guide, and tutorial files are freely available from *http://www.coulombstress.org*. Coulomb runs on Macs, PCs, and Linux boxes. It is a MATLAB application, so you'll need to install MATLAB 7.4 or later. We will have a temporary site license for MATLAB at course. You will be asked to register Coulomb when you first launch.

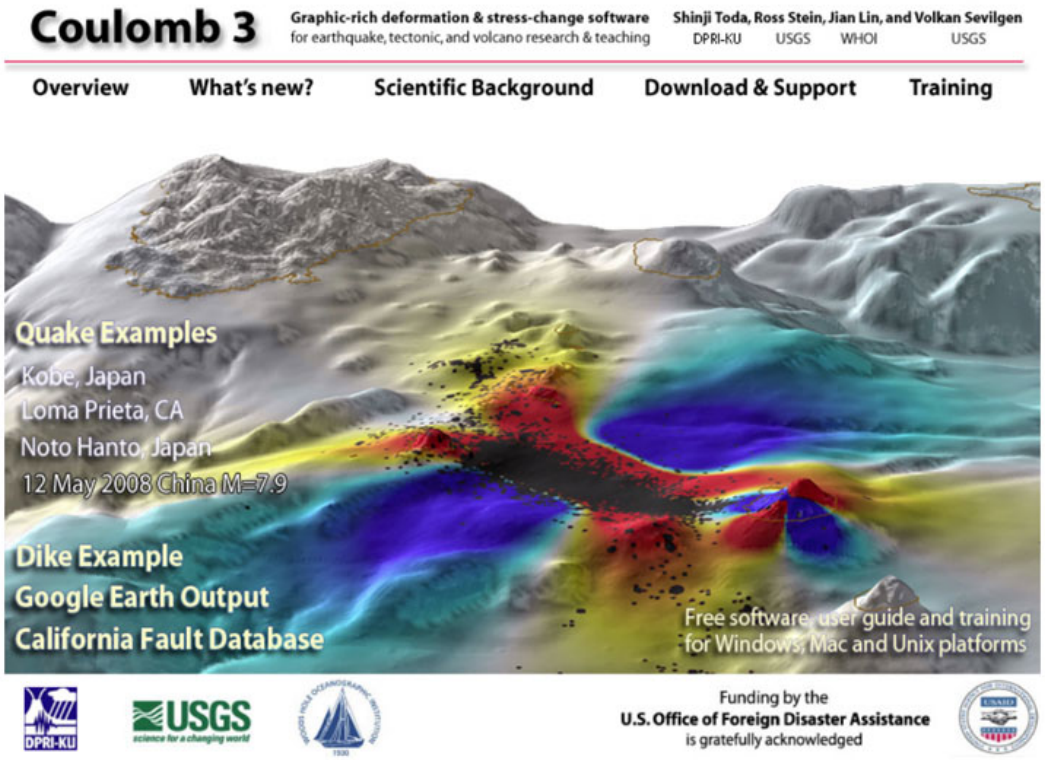

Why Coulomb?

We learn best when we can see and explore alternatives quickly. So Coulomb's principal features are ease of input, rapid interactive modification, and intuitive visualization of the results. Coulomb calculates displacements, strains, and stresses caused by fault slip, magmatic intrusion or dike expansion. Typical uses are how an earthquake promotes or inhibits failure on nearby faults, or how fault slip or dike expansion will compress a nearby magma chamber. Geologic deformation associated with faults and fault-bend folds is also a useful application. Calculations are made in an elastic halfspace with uniform isotropic elastic properties following Okada [1992]. The internal graphics are intended for publication, and can be imported into Google Earth, illustration or animation programs.

Class Plan

In the morning, we'll introduce you to Coulomb analysis and explain our approach to modeling. Then you'll learn how to build and use input files, add active faults, earthquakes, and coastlines, calculate displacements and strains, and create publication-quality PDF and numerical output files. We'll also show you how to taper or tile the fault slip, and how to import the SCEC faults and variable-slip source models from databases. In the afternoon, we'll drink a lot of espresso, and will focus on Coulomb stress analysis for seismic and volcanic investigations, and show you how to display your results in Google Earth. We'll let you resolve stress changes on faults in their rake directions or on optimal planes. You'll learn how to view all these results graphically in 3D or to output numerical tables.

Southern San Andreas Fault Evaluation (SoSAFE) Workshop

Organizers: Kate Scharer, Tom Rockwell

The primary goal of the Southern San Andreas Fault Evaluation project is to understand the timing of and slip due to earthquakes that occurred on the southern San Andreas and San Jacinto faults over the last 2000 years. This workshop will combine both individual presentations and group discussion. The presentations include summaries of major results of SoSAFE research projects. Discussions are designed to address field- and technology-related challenges in paleoseismology and slip rate studies.

SUNDAY, SEPTEMBER 11, 2010 — *Horizon Ballroom I*

09:30	Field and LiDAR measurements of offsets along the Clark fault (*J. Barrett Salisbury*) and the southernmost San Andreas (*Pat Williams*)
09:50	Earthquakes and offsets in the Carrizo Plain (*Sinan Akciz*)
10:10	Discussion of observations, approaches, uncertainties in field and LiDAR measurements of slip
10:30	Break
10:35	Earthquakes and slip rates from Mystic Lake area, San Jacinto fault (*Nate Onderdonk* / *Tom Rockwell* / *Sally McGill*)
10:55	Salton Sea: new CHIRP data and normal fault activity (*Graham Kent* / *Neal Driscoll)*
11:15	San Gorgonio Pass update (*Dick Heermance* / *Doug Yule*)
11:30	Earthquake correlations through the Mojave section (*Kate Scharer*)
11:40	Discussion: Earthquake response on the SAF. Given experience in recent earthquakes, what technologies should be adopted? Should we assign areas or other coordination given likely limitations to internet access?

The Great California ShakeOut Workshop for Science Educators

Organizers: Robert de Groot

Welcome to Palm Springs, a town that sits next to one of the most famous faults in the world - the San Andreas. Participants will learn about earthquakes in California and make connections to topics such as plate tectonics, faults, and earthquake hazards throughout the state. You will learn about the Great California ShakeOut and how you can participate. This workshop will include a plate tectonics activity and participants will learn how earthquake scientists create simulated "big ones" using supercomputers. There will be an opportunity to discuss earthquake preparedness and what one should do before, during, and after an earthquake. Every participant will receive earthquake education resources to take back to their educational environment. If you teach about earthquakes in your school, library, museum, park, home school, or other learning environment you are welcome to join us for this workshop.

Important Note: *While open to the entire SCEC community this workshop is primarily designed for K-12 science educators that work in formal and informal learning environments. Special emphasis will be placed on providing content and activities related to basic earthquake science and preparedness.*

SUNDAY, SEPTEMBER 11, 2010 — *Oasis Room 2*

10:00 – 10:45	Welcome and Introduction to the Great California ShakeOut – *Robert de Groot* (USC) and *Kathleen Springer* (San Bernardino County Museum)
10:45 – 11:30	San Andreas Fault GPS Exercise – *Sarah Robinson* (ASU)
11:30 – 12:15	GPS Research Program Presentation – Teachers from CSUSB/ EarthScope Research Experiences for Teachers (RET) Program and *Sally McGill* (CSUSB)
12:15 – 13:00	Lunch, Networking, and GPS Teachers Set Up Poster
13:00 – 13:45	Paleoseismology – *Kris Weaver-Bowman* (CSUSF)
13:45 – 14:15	Illuminating Earthquake Hazards Using LiDAR – *Sarah Robinson* (ASU)
14:15 – 14:30	Break
14:30 – 15:15	Quake Cather Network – *Elizabeth Cochran* (UCR)
15:15 – 15:45	Great California ShakeOut Resources – *Kathleen Springer (SBCM)*, *Robert de Groot* (USC), and *Yessenia Robles* (CSULB)
15:45 – 16:00	Tying it all together and Adjourn
17:00 – 18:00	**Presentation:** *Hiroo Kanamori* (Caltech) "Comparison of the 1960 and 2010 Chilean Earthquakes"
18:00 – 20:00	**SCEC Annual Meeting Ice-Breaker / Welcome Reception**
20:00 – 22:30	**SCEC Poster Session:** An opportunity to learn more about current research in earthquake science in a lively and interactive setting. Also, join the teachers from the CSUSB/EarthScope RET program as they present their GPS research at this session.

Engineering Workshop on Tall Building Safety

Organizers: Nico Luco, Paul Somerville, and Swami Krishnan

At present there are contrasting viewpoints on the issue of tall building safety in Southern California, with some researchers suggesting that tall buildings may be particularly vulnerable while design professionals tend to think that they may be safer than other categories of buildings. The purpose of this workshop is to stimulate discussion on the topic of tall building safety in Southern California, with a special focus on earthquake ground motions simulated by SCEC, their scientific basis and validity, their appropriate use, and their relevance to the issue of tall building safety. The workshop will begin with presentations on ground motions that have been simulated by SCEC and used in analyses of building response. Next, there will be mini-debates on the following three questions, based in part on past and ongoing SCEC research: Are SCEC ground motion simulations improbably high? Do simulated and recorded time histories produce different building responses? What different perspectives come from deterministic scenarios (such as ShakeOut and other scenarios generated by SCEC) vs. probabilistic risk (as used in CyberShake and building codes)? There will then be a summary of the debates as they relate to different perspectives on tall building safety, and discussion of research topics that could help resolve differences of opinion. It is expected that the workshop will lead to a better mutual understanding of different viewpoints, and to the identification of future work in which SCEC research can contribute further to the evaluation of tall building safety in Southern California.

SUNDAY, SEPTEMBER 11, 2010 — *Horizon Ballroom II*

13:00 – 13:10 Purpose(s) of Workshop (*Paul Somerville*)

13:10 – 13:55 Ground Motion Products Available from SCEC and their Physics Basis (*Rob Graves*)

Simulated Time Histories

- Broadband Platform (1D, others can use)
- CyberShake (3D, in house use)
- TeraShake etc (long period) – *Kim Olsen*

Time Histories Provided to TBI and Other Presenters to Come

- Puente Hills
- Southern San Andreas (ShakeOut)
- Northern San Andreas (1906 and repeats)
- Hayward

Response Spectra

- OpenSHA (others can use)
- CyberShake (in house use)

Debates Related to Tall Building Safety

13:55 – 14:40 Are SCEC Simulations Improbably High?

- Yes: *Lisa Star*, *Farzad Naeim* (presented by *Paul Somerville*)
- No: *Tom Heaton*

14:40 – 14:50 Break

14:50 – 15:35 Do Simulated and Recorded Time Histories Produce Different Building Responses?

- Yes: *Farzin Zareian*
- No: *Nirmal Jayaram / Nilesh Shome*

15:35 – 16:20 What Different Perspectives Come From Deterministic Scenario vs. Probabilistic Risk?

- Deterministic Scenario (but with spatially varying buildings): *Abbie Liel*
- Probabilistic Risk (with simulated ground motions): *Swami Krishnan*

16:20 – 16:30 Summary of Debates and Different Perspectives on Building Safety (*Nico Luco*)

16:30 – 17:00 Discussion of Future Work related to Tall Building Safety (*Swami Krishnan*)

State of SCEC, 2010

Thomas H. Jordan
SCEC Director

Welcome to the 2010 Annual Meeting

This will be SCEC's 20th Annual Meeting—twenty years already!—and our fourth community-wide gathering under the five-year SCEC3 program. The agenda for this big anniversary features some very interesting talks by keynote speakers, discussion sessions on major themes, many outstanding poster presentations, and a variety of IT demonstrations, education & outreach activities, and social gatherings. Seven workshops and several project coordination sessions are scheduled before and after the main meeting.

The week's activities will bring together a substantial collaboration in geoscience: 545 people have pre-registered (Figure 1), and 310 poster abstracts have been submitted—the most ever for a SCEC annual meeting. Among this year's pre-registrants are 160 first-time attendees, so we will welcome many new faces!

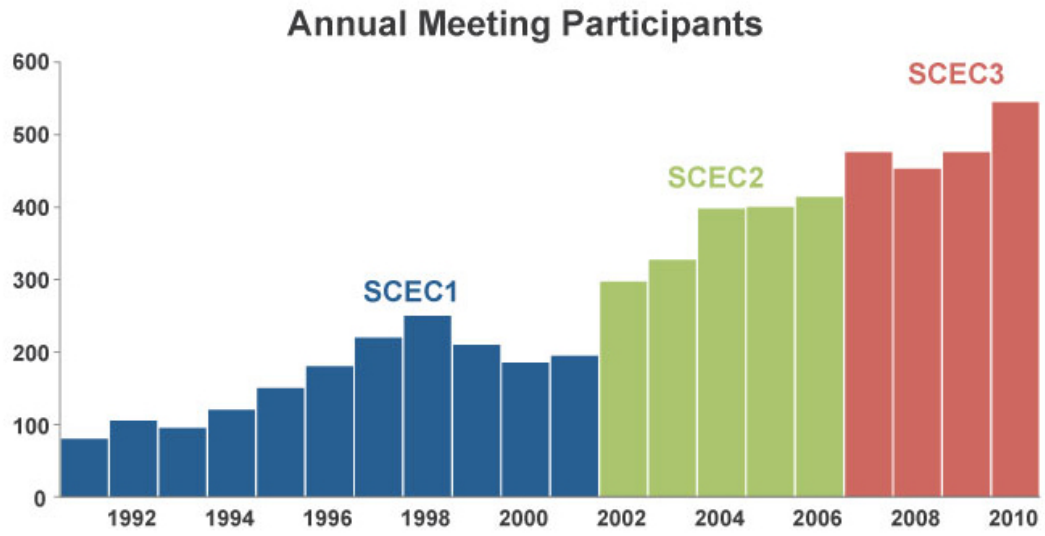

Figure 1. Registrants at SCEC Annual Meetings, 1991-2010. Number for 2010 (545) is pre-registrants.

Goals of the Meeting

Our annual meetings are designed to achieve three goals: to share research results and plans in the sessions, at the meals, and around the pool; to mark our progress toward the priority objectives of the SCEC3 science plan given in Table 1; and to incorporate your ideas for new research into the annual and long-range planning processes. A draft of the 2011 Science Plan, prepared by Deputy Director Greg Beroza and the Planning Committee, is included in this meeting volume.

Greg and the PC have put together an impressive report (also included in the meeting volume) on the research projects supported by SCEC during the past year. This annual report demonstrates substantial progress towards the SCEC3 objectives. Greg will highlight the research results in his

plenary address on Monday morning. The poster presentations at the Annual Meeting will provide a forum for more detailed discussions and interchange of ideas.

Table 1. Priority Science Objectives for SCEC3

1. Improve the unified structural representation and employ it to develop system-level models for earth-quake forecasting and ground motion prediction
2. Develop an extended earthquake rupture forecast to drive physics-based SHA
3. Define slip rate and earthquake history of southern San Andreas fault system for last 2000 years
4. Investigate implications of geodetic/geologic rate discrepancies
5. Develop a system-level deformation and stress-evolution model
6. Map seismicity and source parameters in relation to known faults
7. Develop a geodetic network processing system that will detect anomalous strain transients
8. Test of scientific prediction hypotheses against reference models to understand the physical basis of earthquake predictability
9. Determine the origin and evolution of on- and off-fault damage as a function of depth
10. Test hypotheses for dynamic fault weakening
11. Assess predictability of rupture extent and direction on major faults
12. Describe heterogeneities in the stress, strain, geometry, and material properties of fault zones and understand their origin and interactions by modeling ruptures and rupture sequences
13. Predict broadband ground motions for a comprehensive set of large scenario earthquakes
14. Develop kinematic rupture representations consistent with dynamic rupture models
15. Investigate bounds on the upper limit of ground motion
16. Develop high-frequency simulation methods and investigate the upper frequency limit of deterministic ground motion predictions
17. Validate earthquake simulations and verify simulation methodologies
18. Collaborate with earthquake engineers to develop rupture-to-rafters simulation capability for physics-based risk analysis
19. Prepare for post-earthquake response.

SCEC4 Proposal

A special goal of this year's meeting is to look beyond the annual cycle toward SCEC4, the next five-year phase of the Center (2012-2017). The SCEC4 proposal was submitted in early March to our sponsoring agencies, the National Science Foundation (NSF) and the U.S. Geological Survey (USGS). Both agencies convened a panel for a joint site review, held at USC on June 21-24. We are expecting to receive news about the status of the proposal from our agency representatives in the first session of the meeting on Monday morning.

The SCEC4 scientific program is framed in terms of a very challenging, long-term research goal: *to understand how seismic hazards change across all time scales of interest, from millennia to seconds*. This problem is well suited to SCEC's integrated approach to earthquake system science. Earthquakes emerge from complex, multiscale interactions within active fault systems that are opaque, and are thus difficult to observe. They cascade as chaotic chain reactions through the natural and built environments, and are thus difficult to predict. We propose a 5-year research program that will focus on time-dependent seismic hazard analysis—the geoscience required to "track earthquake cascades" (Figure 2).

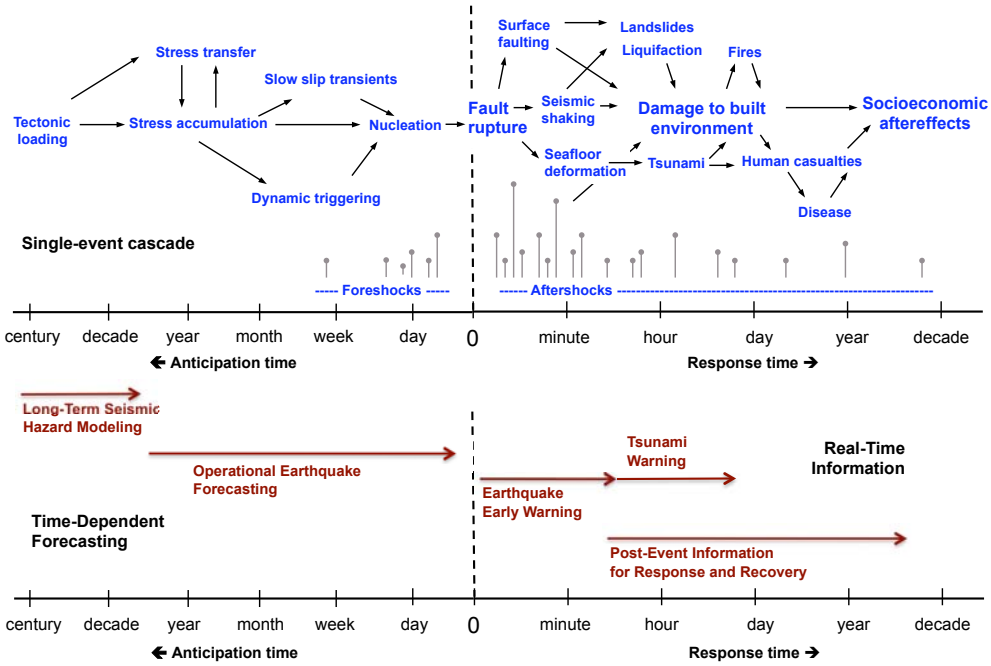

Figure 2. Earthquake processes (in blue) cascade through the natural and built environments, depicted here for a single damaging event on a nonlinear timeline. Advancing the science behind long-term hazard modeling, operational forecasting, earthquake early warning, and delivery of post-event information (in red) will help reduce seismic risk and improve community resilience.

The SCEC4 science plan was developed by the Center's Board of Directors and Planning Committee with broad input from the SCEC community. A committee chaired by Nadia Lapusta assessed the basic research that will be needed to move towards the Center's scientific goals, identifying six fundamental problems in earthquake physics:

a. Stress transfer from plate motion to crustal faults: long-term fault slip rates

b. Stress-mediated fault interactions and earthquake clustering: evaluation of mechanisms

c. Evolution of fault resistance during seismic slip: scale-appropriate laws for rupture modeling

d. Structure and evolution of fault zones and systems: relation to earthquake physics

e. Causes and effects of transient deformations: slow slip events and tectonic tremor

f. Seismic wave generation and scattering: prediction of strong ground motions

These problems are clearly interrelated and require an interdisciplinary, multi-institutional approach. Each was described in the proposal by a short problem statement, a set of SCEC4 objectives, and a listing of priorities and requirements.

We reformulated our working group structure in accordance with the overall SCEC4 research plan, which is organized around a set of four system-level challenges. (1) discover the physics of fault failure; (2) improve earthquake forecasts by understanding fault-system evolution and the physical basis for earthquake predictability; (3) predict ground motions and their effects on the built environment by simulating earthquakes with realistic source characteristics and three-dimensional representations of geologic structures; and (4) improve the technologies that can reduce long-term

earthquake risk, provide short-term earthquake forecasts and earthquake early warning, and enhance emergency response.

We developed a coherent set of interdisciplinary research initiatives that will focus on special fault study areas, the development of a community geodetic model for Southern California (which will combine GPS and InSAR data), and a community stress model. The latter will provide a new platform for the integration of various constraints on earthquake-producing stresses. Improvements will be made to SCEC's unified structural representation and its statewide extensions. The SCEC4 program, which lies squarely within Pascal's Quadrant, has been designed to help:

- transform long-term seismic hazard analysis, the most important geotechnology for characterizing seismic hazards and reducing earthquake risk, into a physics-based science
- develop operational earthquake forecasting into a capability that can provide authoritative information about the time dependence of seismic hazards to aid communities in preparing for potentially destructive earthquakes
- enable earthquake early warning—advanced notification that an earthquake is underway and predictions of when strong shaking will arrive at more distant sites
- improve the delivery of post-event information about strong ground motions and secondary hazards

The Center will create, prototype, and refine these capabilities in partnership with the USGS and other responsible government agencies. SCEC4 contributions will include research within the Collaboratory for the Study of Earthquake Predictability (CSEP), a cyberinfrastructure for the prospective (and retrospective) testing of forecasting models against authoritative data.

The SCEC4 organizational structure will comprise disciplinary working groups, interdisciplinary focus groups, special projects, and technical activity groups. The Southern San Andreas Fault Evaluation (SoSAFE) project, which has been funded by the USGS Multi-Hazards Demonstration Project for the last four years, will be transformed into a standing interdisciplinary focus group to coordinate research on the San Andreas and the San Jacinto master faults. Research in seismic hazard and risk analysis will be bolstered through an Implementation Interface that will include educational as well as research partnerships with practicing engineers, geotechnical consultants, building officials, emergency managers, financial institutions, and insurers. A set of special projects funded separately by the NSF, USGS, and other agencies will leverage core research support.

The theme of the CEO program during SCEC4 will be *creating an earthquake and tsunami resilient California.* SCEC and its partners in the statewide Earthquake Country Alliance will prepare individuals and organizations for making decisions (split-second and long-term) in response to changing seismic hazards and introduce them to the new technologies of operational earthquake forecasting and earthquake early warning. A public education and preparedness thrust area will educate people of all ages—in California, across the country, and internationally—about earthquakes, and motivate them to become prepared. A K-14 earthquake education initiative will seek to improve earth science education and school earthquake safety, and SCEC's experiential learning and career advancement program will provide students and early-career scientists with research opportunities and networking to encourage and sustain careers in science and engineering.

The SCEC leadership is committed to the growth of a diverse scientific community, and the SCEC4 diversity plan provides a strategy and review process to pursue this goal. It recognizes that the most effective long-term strategy is to promote diversity among students and early-career scientists; i.e., to address the "pipeline problem."

The SCEC4 management plan contains specific "smart & green" objectives that will contribute to a sustainable future for the Center. The Center will continue to work towards an effective post-earthquake scientific response, in coordination with the USGS, California Geological Survey, and other organizations.

Organization and Leadership

SCEC is an institution-based center, governed by a Board of Directors, who represent its members. The membership currently stands at 16 core institutions and 57 participating institutions (Table 2). SCEC currently involves more than 800 scientists and other experts in active SCEC projects. A key measure of the size of the SCEC community—registrants at our Annual Meetings—is shown for the entire history of the Center in Figure 1. With the current number topping last year's by 17%, it is clear that participation in SCEC is continuing to grow.

Table 2. SCEC Institutions (March 1, 2010)

Core Institutions (16)	Participation Institutions (57)
California Institute of Technology Columbia University Harvard University Massachusetts Institute of Technology San Diego State University Stanford University U.S. Geological Survey, Golden U.S. Geological Survey, Menlo Park U.S. Geological Survey, Pasadena University of California, Los Angeles University of California, Riverside University of California, San Diego University of California, Santa Barbara University of California, Santa Cruz University of Nevada, Reno University of Southern California (lead) **New SCEC4 Core Institutions:** California Geological Survey CalState Consortium	Appalachian State University; Arizona State University; Berkeley Geochron Center; Boston University; Brown University; Cal-Poly, Pomona; Cal-State, Chico; Cal-State, Long Beach; Cal-State, Fullerton; Cal-State, Northridge; Cal-State, San Bernardino; California Geological Survey; Carnegie Mellon University; Case Western Reserve University; CICESE (Mexico); Cornell University; Disaster Prevention Research Institute, Kyoto University (Japan); ETH (Switzerland); Georgia Tech; Institute of Earth Sciences of Academia Sinica (Taiwan); Earthquake Research Institute, University of Tokyo (Japan); Indiana University; Institute of Geological and Nuclear Sciences (New Zealand); Jet Propulsion Laboratory; Los Alamos National Laboratory; Lawrence Livermore National Laboratory; National Taiwan University (Taiwan); National Central University (Taiwan); Ohio State University; Oregon State University; Pennsylvania State University; Princeton University; Purdue University; SUNY at Stony Brook; Texas A&M University; University of Arizona; UC, Berkeley; UC, Davis; UC, Irvine; University of British Columbia (Canada); University of Cincinnati; University of Colorado; University of Illinois; University of Massachusetts; University of Miami; University of Missouri-Columbia; University of New Hampshire; University of Oklahoma; University of Oregon; University of Texas-El Paso; University of Utah; University of Western Ontario (Canada); University of Wisconsin; University of Wyoming; URS Corporation; Utah State University; Woods Hole Oceanographic Institution

The current core institutions have all committed resources to SCEC4. Two new institutions have requested to join the core, the California Geological Survey (CGS) and California State University Center for Collaborative Earthquake Science (CSUCCES), and a third, UC Davis, is exploring the possibility. CSUCCES, a 6-campus consortium of CalState (the nation's largest university system), will be included as a "distributed" core institution in SCEC4. This 6-campus consortium of CalState—the nation's largest university system—will be included as a "distributed" core institution in SCEC4. The CSUCCES initiative, led by Prof. David Bowman of CalState Fullerton, will benefit an outstanding group of faculty and students who have contributed substantially to the SCEC research program.

Board of Directors. Under the SCEC3 by-laws, each core institution appoints one member to the Board of Directors, and two at-large members are elected by the Board from the participating institutions. The Board is chaired by the Center Director, who also serves as the USC representative; the Vice-Chair is Lisa Grant Ludwig. The complete Board of Directors is listed on page ii of the meeting volume.

Advisory Council. The Center's external Advisory Council (AC), chaired by Dr. Mary Lou Zoback, is charged with developing an overview of SCEC operations and advising the Director and the Board. Since the inception of SCEC in 1991, the AC has played a major role in maintaining the

vitality of the organization and helping its leadership chart new directions. A verbatim copy of the AC's 2009 report follows this report in the meeting volume.

Dr. Zoback has announced her intention to step down as AC chair after completing this year's report. She has been an outstanding leader, and we will use the opportunity at the meeting to thank her for her efforts on behalf of the SCEC community. Other members cycling off the Council will be Patti Guatteri, Kate Miller, John Rudnicki, and Lloyd Cluff. We are fortunate that such excellent scientists have been willing to lend us their advice.

I am very happy to report that Jeff Freymueller has agreed to take over as AC chair. Jeff is very experienced in the ways of SCEC, having served on the SCIGN advisory committee from 1998 to 2002 and the AC since the beginning of SCEC2 in 2002. Please join me in welcoming him to this important leadership role.

We can also look forward to welcoming five new members to the AC: Roger Bilham (U. Colorado), Farzad Naiem (John A. Martin & Associates), Meghan Miller (UNAVCO), John Vidale (U. Washington), and Andrew Whittaker (U. Buffalo). Two additional members, Donna Eberhart-Phillips (U.C. Davis) and Bob Lillie (Oregon State U.), will begin their terms in 2011. All of them will bring exceptional qualities and experience to the AC.

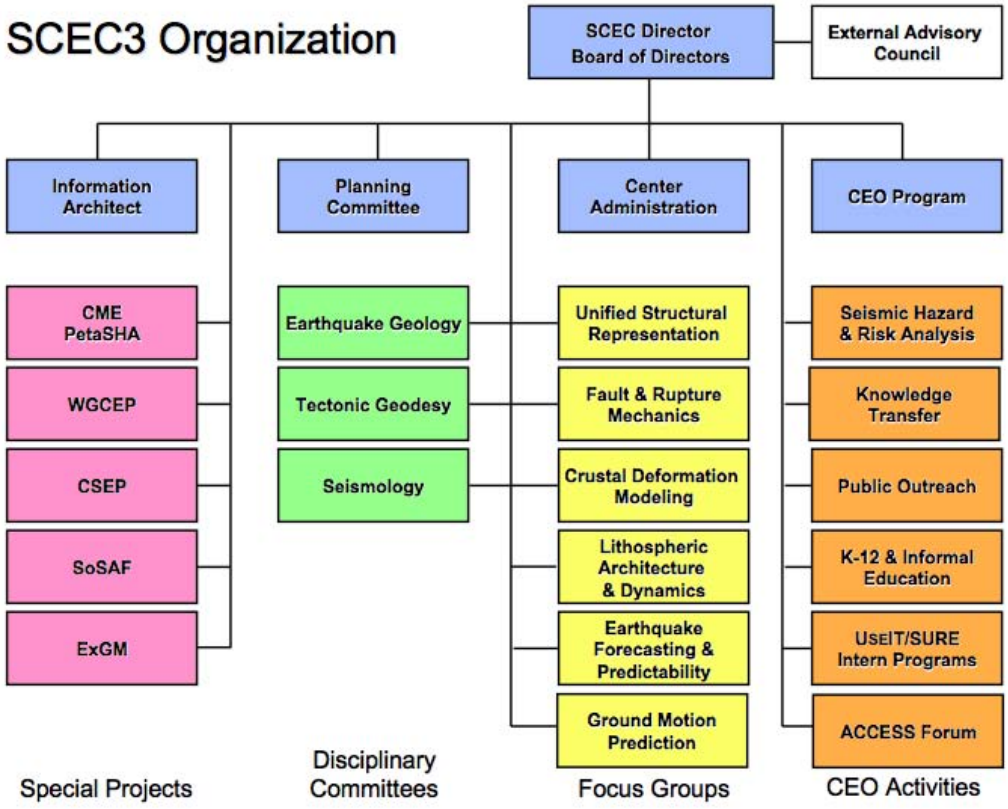

Figure 3. The SCEC3 organization chart, showing the disciplinary committees (green), focus groups (yellow), special projects (pink), CEO activities (orange), management offices (blue), and the external advisory council (white).

Table 3. SCEC3 Working Group Leadership

Disciplinary Committees	
Geology	Mike Oskin*
	James Dolan
Seismology	Egill Hauksson*
	Elizabeth Cochran
Geodesy	Jessica Murray-Moraleda*
	Rowena Lohman
Focus Groups	
Structural Representation	John Shaw*
	Kim Olsen
Fault & Rupture Mechanics	Judi Chester*
	Ruth Harris
Crustal Deformation Modeling	Liz Hearn*
	Kaj Johnson
Lithospheric Architecture & Dynamics	Paul Davis*
	Thorsten Becker
Earthquake Forecasting & Predictability	Terry Tullis*
	Jeanne Hardebeck
Ground Motion Prediction	Brad Aagaard*
	Rob Graves
Seismic Hazard & Risk Analysis	Paul Somerville*
	Nico Luco
Special Project Groups	
Community Modeling Environment	Phil Maechling*
WG on Calif. Earthquake Probabilities	Ned Field*
Collaboratory for Study of Equake Predictability	Tom Jordan
	Danijel Schorlemmer*
Southern San Andreas Fault Project	Tom Rockwell*
	Kate Scharer
Extreme Ground Motion	Tom Hanks*

* *Planning Committee members*

Working Groups. The SCEC organization comprises a number of disciplinary committees, focus groups, and special project teams (Figure 3). These working groups have been the engines of its success. The discussions organized by the working-group leaders at the Annual Meeting have provided critical input to the SCEC planning process.

The Center supports disciplinary science through three standing committees in Seismology, Tectonic Geodesy, and Earthquake Geology (green boxes of Figure 3). They are responsible for disciplinary activities relevant to the SCEC Science Plan, and they make recommendations to the Planning Committee regarding the support of disciplinary research and infrastructure.

SCEC coordinates earthquake system science through five interdisciplinary focus groups (yellow boxes): Unified Structural Representation (USR), Fault & Rupture Mechanics (FARM), Crustal Deformation Modeling (CDM), Lithospheric Architecture & Dynamics (LAD), Earthquake Forecasting & Predictability (EFP), and Ground Motion Prediction (GMP).

A sixth interdisciplinary focus group on Seismic Hazard & Risk Analysis (SHRA) manages the "implementation interface" as part of SCEC Communication, Education & Outreach (CEO) program (orange box). In particular, SHRA coordinates research partnerships with earthquake

engineering organizations in end-to-end simulation and other aspects of risk analysis and mitigation.

SCEC sponsors Technical Activity Groups (TAGs), which self-organize to develop and test critical methodologies for solving specific problems. TAGs have formed to verify the complex computer calculations needed for wave propagation and dynamic rupture problems, to assess the accuracy and resolving power of source inversions, and to develop geodetic transient detectors and earthquake simulators. TAGs share a *modus operandi:* the posing of well-defined "standard problems", solution of these problems by different researchers using alternative algorithms or codes, a common cyberspace for comparing solutions, and meetings to discuss discrepancies and potential improvements.

Planning Committee. The SCEC Planning Committee (PC) is chaired by the SCEC Deputy Director, Greg Beroza, and comprises the leaders of the SCEC science working groups—disciplinary committees, focus groups, and special project groups—who together with their co-leaders guide SCEC's research program (Table 3).

The PC has the responsibility for formulating the Center's science plan, conducting proposal reviews, and recommending projects to the Board for SCEC support. Its members will play key roles in formulating the SCEC4 proposal. Therefore, I urge you to use the opportunity of the Annual Meeting to communicate your thoughts about future research plans to them.

Center Budget and Project Funding

In 2010, SCEC received $3.0M from NSF and $1.1M from the USGS under its five-year cooperative agreements with these two agencies. Supplementing the $4.1M in base funding was $240K from the USGS Multi-Hazards Demonstration Project for SoSAFE and $80K from Pacific Gas & Electric Company for the rupture dynamics project. Other funds available for core projects included $20K from the Keck CSEP grant, $200K from the geodesy royalty funds, $58K from the UCERF3 project, and $80K rolled over from the 2009-2010 Director's. Therefore, SCEC core funding for 2010 totaled $4,778K.

The base budget approved by the Board of Directors for this year allocated $3,514K for science activities managed by the SCEC Planning Committee; $463K (including $25K for intern programs) for communication, education, and outreach activities, managed by the CEO Associate Director, Mark Benthien; $170K for information technology, managed by Associate Director for Information Technology, Phil Maechling; $301K for administration and $200K for meetings, managed by the Associate Director for Administration, John McRaney; and $130K for the Director's reserve account.

Structuring of the SCEC program for 2010 began with the working-group discussions at our last Annual Meeting in September, 2009. An RFP was issued in October, 2009, and 171 proposals (including collaborative proposals) requesting a total of $5,276K were submitted in November, 2009. All proposals were independently reviewed by the Director and Deputy Director. Each proposal was also independently reviewed by the leaders and/or co-leaders of three relevant focus groups or disciplinary committees. (Reviewers were required to recuse themselves when they had a conflict of interest.) The Planning Committee met on January 11-12, 2010, and spent two days discussing every proposal. The objective was to formulate a coherent, budget-balanced science program consistent with SCEC's basic mission, short-term objectives, long-term goals, and institutional composition. Proposals were evaluated according to the following criteria:

1. Scientific merit of the proposed research
2. Competence and performance of the investigators, especially in regard to past SCEC-sponsored research
3. Priority of the proposed project for short-term SCEC objectives as stated in the RFP
4. Promise of the proposed project for contributing to long-term SCEC goals as reflected in the SCEC3 science plan
5. Commitment of the P.I. and institution to the SCEC mission
6. Value of the proposed research relative to its cost
7. Ability to leverage the cost of the proposed research through other funding sources
8. Involvement of students and junior investigators
9. Involvement of women and underrepresented groups
10. Innovative or "risky" ideas that have a reasonable chance of leading to new insights or advances in earthquake physics and/or seismic hazard analysis.
11. The need to achieve a balanced budget while maintaining a reasonable level of scientific continuity given very limited overall center funding.

The recommendations of the PC were reviewed by the SCEC Board of Directors at a meeting on January 31-February 1, 2010. The Board voted unanimously to accept the PC's recommendations. After minor adjustments and a review of the proposed program by the NSF and USGS, I as Center Director approved the final program in March, 2010.

Communication, Education, and Outreach

Through its CEO Program, SCEC offers a wide range of student research experiences, web-based education tools, classroom curricula, museum displays, public information brochures, online newsletters, workshops, and technical publications. Highlights of CEO activities for the past year are reported in the meeting volume by the Associate Director for CEO, Mark Benthien, who will present an oral summary on Monday morning.

Immediately following the 2009 SCEC Annual Meeting, a major review meeting was held of the SCEC CEO program. An extensive evaluation document was prepared in summer 2009 by evaluation consultants, which an external review panel used as the basis of its analysis. The review panel's report was quite thorough and provided several excellent recommendations. Overall, their analysis was that the SCEC CEO program is excellent and should be an example to all similar programs. The review was very important to the SCEC4 proposal process and was supported with funding from the NSF.

SCEC has led the development of the Earthquake Country Alliance (ECA), an umbrella organization that includes earthquake scientists and engineers, preparedness experts, response and recovery officials, news media representatives, community leaders, and education specialists. The ECA has become our primary framework for developing partnerships, products, and services for the general public. SCEC maintains the ECA web portal (*www.earthquakecountry.org*), which provides multimedia information about living in earthquake country, answers to frequently asked questions, and descriptions of other resources and services provided by ECA members.

A major focus of the ECA and the SCEC/CEO programs during the past year has been the expansion of the Great California ShakeOut, which was held in mid-October, 2009, with over 6.9 million participants statewide. ShakeOut is now an annual event and recruitment for the 2010 drill is on track to exceed the participation in 2009. The ShakeOut is also expanding to other regions. New Zealand's Great West Coast ShakeOut was the first test of the concept in another area, held the day after the 2009 SCEC Annual Meeting, The British Columbia ShakeOut on January 26, 2011, will be the next non-California drill, along with a local drill in Oregon (Washington may join in

2012 as part of a Cascadia ShakeOut). In April, 2011, the Great Central US ShakeOut will be held as part of the lead up to the New Madrid Bicentennial. And in 2012, Utah and possibly New Zealand (nationwide) will launch ShakeOut drills. ShakeOut has really changed the way people and organizations are approaching the problems of earthquake preparedness. The SCEC staff, led by Mark Benthien, really put a huge effort into supporting ShakeOut, and the Annual Meeting will be an appropriate time to thank them for contributing to its success.

Owing to increased cooperation across California fostered by ShakeOut, the 1906 San Francisco Earthquake Centennial, and other events aimed at increasing community resiliency to earthquakes, the ECA has been broadened into a statewide organization with a number of regional chapters (see Mark's report for a more complete description). We look forward to working with our partners around the state in future preparedness activities such as the ShakeOut. I would like to encourage California members of the SCEC community to register for the ShakeOut (at *www.shakeout.org*) and to encourage their institutions to join USC and others that are already registered.

SCEC CEO staff continues to work with museums and other informal education venues to develop content and programs for earthquake education and to distribute SCEC resources, such as the extensive set of publications that has grown out of *Putting Down Roots in Earthquake Country*. In 2008, SCEC organized a group of museums and other locations interested in earthquake education into a network of *Earthquake Education and Public Information Centers* (Earthquake EPIcenters), which has since been expanded to over 50 venues distributed throughout California. The EPIcenters are essential partners in the ShakeOut, as many hold public events on drill day, and help promote participation.

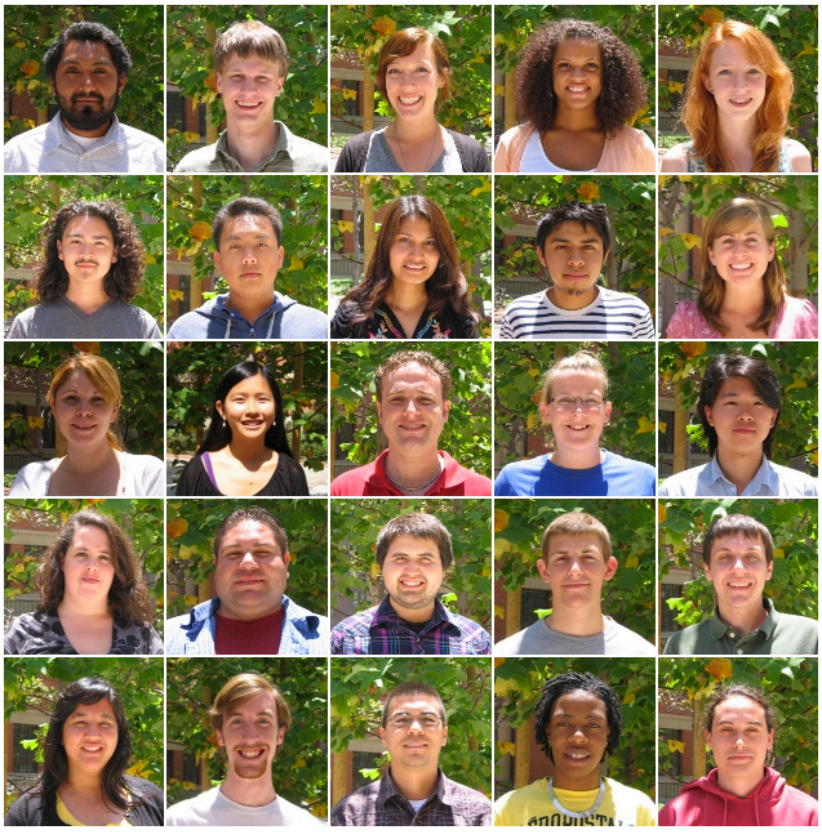

Figure 4. This "Brady Bunch" picture shows the students from around the country who participated in the 2010 UseIT summer program at USC. At the center is Michael Ihrig, an ACCESS-U intern and alumnus of UseIT, who helped to supervise the UseIT activities. Many will be attending the Annual Meeting to present posters, demos, and animations.

SCEC is very active in the earth science education community, participating in organizations such as the National Association of Geoscience Teachers, The Coalition for Earth System Education, and local and national science educator organizations (e.g. NSTA). SCEC Education Programs Manager Bob de Groot leads these efforts. In 2010 SCEC is collaborating with IRIS and EarthScope in developing the content for the San Andreas fault Active Earth Kiosk, building on a workshop SCEC co-organized in 2009. Also in 2010, Arizona State University, the OpenTopography Facility, and SCEC developed three earth science education products to inform students and other audiences about LiDAR and its application to active tectonics research.

Bob de Groot is also skillfully leading SCEC's Office for Experiential Learning and Career Development. His office manages three SCEC intern programs: Summer Undergraduate Research Experiences (SURE, 189 interns since 1994), Undergraduate Studies in Earthquake Information Technology (USEIT, 148 interns since 2002), and Advancement of Cyberinfrastructure Careers through Earthquake System Science (ACCESS, 31 since 2007). The ELCA office promotes diversity in the scientific workforce and the professional development of early-career scientists (Figure 4). As someone very involved in these intern programs, I really enjoy seeing the students grapple with the tough but engaging problems of cutting-edge earthquake science. For example, the "grand challenge" for this year's USEIT program was to *develop a Seismic Crisis Visualization System based on SCEC-VDO that can display information needed for operational earthquake forecasting*. Many of the summer interns will be presenting their work at this meeting, and I hope you'll have the opportunity to check out their posters and demos.

A Word of Thanks

As SCEC Director, I want to express my deep appreciation to all of you for your attendance at the Annual Meeting and your sustained commitment to the collaboration. Greg Beroza and the PC for have developed a brilliant program, so the entire meeting should be a pleasant experience for us all. I'd especially like to thank Tran Huynh, the SCEC Special Projects and Events Coordinator, and her associates for their hard work and exceptional skill in organizing this meeting and arranging its many moving parts. Please do not hesitate to contact me, Greg, Tran, or other members of the SCEC team if you have questions or comments about our meeting activities and future plans. Now please enjoy Palm Springs and its surrounding tectonic environment!

Report of the Advisory Council

Southern California Earthquake Center

2009 SCEC Annual Meeting

Advisory Council Membership

Mary Lou Zoback, Risk Management Solutions-RMS (Chair)*

Gail Atkinson, University of Western Ontario*

Lloyd S. Cluff, Pacific Gas and Electric Company

John Filson, USGS (Emeritus)*

Jeffrey T. Freymueller, University of Alaska*

Jim Goltz, CA Emergency Management Agency*

Mariagiovanna Guatteri, Swiss Re Capital Markets*

Anne Meltzer, Lehigh University

Dennis Miletti, University of Colorado, Boulder (Emeritus)*

Kate C. Miller, University of Texas at El Paso*

Steve Mahin, Pacific Earthquake Engineering Research Center (PEER)

John Rudnicki, Northwestern University*

****Attended 2009 Annual Meeting and contributed to this report***

Introduction

The Advisory Council of the Southern California Earthquake Center (SCEC) met during the 2009 SCEC Annual Meeting, held in Palm Springs, California, 13-16 September 2009. The principal meeting of the Advisory Council was during the afternoon and early evening of 15 September; an earlier session was held prior to the start of the Annual Meeting on 13 September to outline areas of focus. The Council chair summarized the principal Council findings and recommendations in an oral report delivered during the closing session of the Annual Meeting on the morning of 16 September.

Prior to the Annual Meeting on 11 September the SCEC Director circulated to the Advisory Council a confidential report summarizing how SCEC had responded to Advisory Council recommendations from the previous year and raised a number of new and continuing issues warranting Council attention. Those issues included:

- Evaluation of the Communication, Education, and Outreach (CEO) Program
- Input on Collaboratory for the Study of Earthquake Predictability (CSEP)
- Advice on initiatives in earthquake simulation and ground motion prediction
- Input on SCEC4 planning process
- Leadership development /succession planning within SCEC
- Science planning discussions at annual meeting

After a few general remarks below, we provide input on these issues raised by the Director in his 11 September mailing; we also comment on a number of recurring topics (documenting and leveraging SCEC3 earthquake system science accomplishments, visibility and vital role of workshops within SCEC) and make

recommendations on some additional issues raised by the AC at this meeting. Those additional issues include:

- Risk and crisis communication training
- Expanding high risk/high return research opportunities

Some General Impressions

Congratulations are in order on multiple fronts. The unparalleled success of the November 2008 Southern CA ShakeOut drill, actively engaging more than 5.5 million Southern Californians and a myriad of local, state and federal agencies to prepare for a large earthquake, was the culmination of years of planning by SCEC's CEO program, under Mark Benthien's superb leadership. Informed by social science research on effective messaging, the ShakeOut exercise was backed by a detailed and scientifically rigorous scenario developed with input from more than 100 earthquake scientists and experts in diverse fields led by Lucy Jones, USGS. The exercise was an integrative opportunity that involved the entire SCEC community. SCEC's researchers used ShakeOut to design and test post-quake response programs. We view the ShakeOut exercise as a unique scientific leadership outcome that was only possible as a result of the shared vision, the stature, strong participatory spirit, and integrative organization of SCEC as a dedicated science center.

While on the topic of CEO, we also want to strongly commend the outstanding, on-going commitment to involving undergrads in SCEC research through intern programs under the leadership of Bob de Groot. The enthusiasm, breadth and diversity of the outstanding undergrads getting an opportunity to participate directly in earth science research is inspiring. We are pleased that so many of them take advantage of the opportunity to participate in the annual meeting and present posters on their work.

Since members of the Advisory Council are not also members of SCEC, the Annual Meeting provides an important opportunity for Council members to assess the community's annual progress on the Center's goals and programs. The 2009 meeting and associated workshops proved again to be impressive demonstrations of the energy and enthusiasm of the SCEC community. The 121 registrants who were attending their first SCEC Annual Meeting (more than 25% of the 460+ total registrants), including many students and interns, provided heartening evidence of the center's growing participation and its compelling mission. The Advisory Council particularly applauds SCEC's continually strengthening of partnerships with the earthquake engineering community. It is heartening to see their ranks grow at each meeting.

The Advisory Council also lauds the entire SCEC membership for its persistently selfless community spirit which enables considerable progress in developing communal, system-level models and representations that are advancing the goals of both fundamental and applied earthquake system science. In particular, we would like to recognize Deputy Director Greg Beroza's superb leadership of the science collaboration process. Beroza's kickoff keynote on SCEC scientific accomplishment did a superb job of highlighting breakthrough science and the progress made towards SCEC3 goals. We found the new structure of the 2009 meeting particularly conducive to interactive discussion. The uncompeted, 2 hour plenary sessions were kicked off by outstanding and provocative overview talks mostly by early-career scientists and were then followed by 1.5 hours of open discussion around a focused but complex question involving the entire SECE membership and actively moderated by group leaders in the topical areas.

Finally, the Advisory Council would like to particularly acknowledge Tom Jordan's exemplary leadership of SCEC over the past 9 years. Tom arrived in 2000 and brought an infusion of energy and creative ideas to SCEC as it went into its SCEC3 planning process. Under his direction the SCEC3 proposal was funded and a number of new research directions were launched. Tom's vision and ability to cultivate and seize funding opportunities outside of the core support has brought new perspectives, expertise and tools to address earthquake system science. Under Tom's initiative and leadership, SCEC now leads the earthquake science community in active engagement of the high performance computing community, as evidenced once again by the success of their $1.6/24 months PetaSHA3 NSF grant in a highly competitive pool. In addition, the new $2M, 32-month grant from the California Earthquake Authority for work on UCERF3 is particularly rewarding. The UCERF2 analysis succeeded in a uniform statewide assessment of earthquake likelihood consistent with the 150+ years of historical seismicity data, but left a number of significant issues impacting earthquake likelihood unresolved and outstanding. The fact that the CEA was interested and willing to fund

the follow-up research for an improved reassessment is a strong statement of their perceived value of this endeavor.

As Tom is always the first to admit, the outstanding staff support provided by John McRaney, SCEC's Associate Director of Administration and Tran Huynh, Special Project Manager, are vital to the success of SCEC. John and Tran keep SCEC running smoothly and money flowing to researchers in a timely fashion, they make sure workshops are easy to organize and run flawlessly, and we especially thank them for providing all manner of cheerful and indefatigable assistance, while managing all the details involved in carrying out another highly successful Annual Meeting.

Looking Forward

Before moving to our recommendations on specific topics, the Advisory Council noted several issues for the leadership to be mindful of:

- Maintain focus and avoid getting spread too thin (especially going into new funding cycle)
- Continue to take advantage of creative funding opportunities, seek ways of engaging new core sponsors, as well as explore untapped potential funding sources including some kind of industrial associates program or perhaps a utilities/infrastructure owners groups.

When the above points were raised in the oral presentation of the AC report at the Annual Meeting on Sept 16, they led to a vigorous discussion as to whether the AC was providing conflicting advice. The AC does not feel that the suggestion to be mindful of focus contradicts the advice to continue to seek and take advantage of new research and funding opportunities. One reason for suggested focus is a simple matter of resources – USGS funding has been flat, and while NSF funding has been going up slightly, we think a big increase in core funding is unlikely and certainly will not be enough to do all SCEC would like to do. Therefore, some choices will need to be made. We feel it is far better for SCEC to make these choices rather than have them made for them or have to make them suddenly without sufficient thought. The need for focus is also relevant to prevent overloading and eroding what has been an outstanding level of staff support. All of the AC recommendations below for new efforts emphasize collaboration or interaction with other agencies that could provide additional support to the proposed SCEC activities or leverage SCEC activities with modest support levels.

Focus is also important for perception of SCEC3 accomplishments and for the SCEC4 proposal presentation. We feel that SCEC must avoid the impression (and reality) of going in too many (e.g., 19) directions. We suggest that a better impact and marketing strategy for SCEC4 would be to organize around 2 to 4 main themes or grand challenges. We don't think it is prudent or wise for the AC to make recommendations on dropping specific programs. However, we feel an evaluation in terms of the question "is impact on the field and practitioners commensurate with 20 year investment" is a useful context to weigh SCEC3 accomplishments and use for planning for SCEC4. In terms of CEO activities, the answer to that question would be a resounding yes. In other areas, such as ground motion modeling, the discussion on that topic at the Annual Meeting highlighted the fact that more effort is needed to understand and provide the kind of products and outcomes that will facilitate adoption of ground motion simulations by the engineering community. This is not a comment on the scientific quality of that research (which is excellent), but rather a recommendation that SCEC4 should continue and extend its initiatives to improve communications with engineering users, and thereby gain a wider appreciation and application of their scientific products.

CEO Program

Formal Evaluation of the CEO Program

Following up on past AC recommendations, a formal retrospective review of the CEO program over the past 5 years occurred directly following the 2009 Annual Meeting. One important rationale for the review was to help assess the impact of the CEO program and to provide supporting information and data on its efficacy for the SCEC4 proposal. Two members of the AC, Dennis Mileti and Mary Lou Zoback, served on the review panel. The panel's report was submitted to SCEC on December 1, 2009 and was forwarded to the AC by Director Jordan on the same day.

The Advisory Committee will respond to the "Phase 1" retrospective CEO evaluation within the January 2010 timeframe.

In last two years the AC has also recommend a second (Phase II) forward-looking review of the CEO program utilizing an external panel informed by a wide range of disciplines (e.g., marketing and psychology) to explore potential new CEO activities and directions, and refining existing ones.

The Advisory Committee will update last year's recommendation proposing a phase II planning effort following its evaluation of the Phase I review.

ShakeOut and the Earthquake Country Alliance

The 2008 Southern California ShakeOut became the largest earthquake drill in history and it was an unparalleled success: it had 5.5 million participants, broad-based appeal from many constituent categories, and it was very effective at publicizing the M7.8 southern San Andreas scenario and its impact throughout the region. And, even thought it was not funded, we congratulate SCEC CEO for interesting a non-SCEC University of California social scientist in writing a proposal to the National Science Foundation to evaluate the ShakeOut and to inform future best practices.

We also congratulate the SCEC CEO for both growing the Earthquake Country Alliance throughout southern California and effectively utilizing this broad "Alliance" to support the 2008 ShakeOut and also for taking the "Alliance" and future ShakeOuts state-wide. The creation of a single, state-wide annual preparedness event and the creation of a state-wide earthquake "Alliance" of regional preparedness partners are herculean accomplishments that will contribute to earthquake safety in the state for many years to come. These represent the largest steps forward for public earthquake preparedness in California in decades. These achievements are particularly noteworthy considering that they were made without any additional funding beyond core SCEC CEO staff salary funding.

We have two recommendations for these efforts:

1. We support the SCEC CEO Program's decision to continue with its plans to grow the "Alliance" and to conduct state-wide annual ShakeOuts in the future. However, we recommend that SCEC CEO give consideration to seeking funding from agencies such as the California Emergency Management Agency (Cal-EMA) to support these state- wide activities so that they may be enriched where appropriate.
2. We recommend that SCEC CEO continue to work with its partners to identify year- round public education and outreach activities to supplement the now annual ShakeOut events. It is well established scientifically that ongoing, repetitive messaging over the long-haul is more effective at motivating public preparedness action-taking than any annual (or rare anniversary event) public information program. We feel that positioning the annual ShakeOut as the "crown jewel" in an ongoing and year-long public preparedness information campaign that delivers preparedness information to the public, regardless if they seek it out on their own or not, would be the most effective strategy.

Targeted Leveraging of CEO Activities

We heartily applaud the accomplishments of SCEC's CEO Program in leveraging funds for its activities. According to the Phase I report, more than $4.4M of outside funds were leveraged to support the ECA and ShakeOut activities between 2003-2009 (compared to $2.7M in core funding over the same time interval). In fact, AC knows of no other science center in the country that has accomplished as much leveraged success for CEO activities as has SCEC's CEO Program. People in other states and even nations use the SCEC CEO Program as the "gold standard" to which they aspire and seek to replicate. We will not here offer more detailed comments on the accomplishments of this program since an elaborate evaluation of the SCEC CEO program has recently been completed.

We recommend SCEC CEO play off their success and consider two innovative pathways for leveraging additional future funding:

1. ***Engage in program activities social and behavioral scientists that can carry out related research drawing on their own funding resources.*** Some elements of the SCEC CEO Program, e.g., the ShakeOut exercise, have drawn the attention of hazards researchers in the social and behavioral sciences across the nation. We recommend that the SCEC CEO Program capitalize on their strong reputation by either working with and through social scientists on the Advisory Council or on its own to seek out and involve social and behavioral scientist researchers (at the University of Southern California, at other California universities, and at universities in other states). Although there are likely diverse mechanisms available to create such involvement, we foresee two SCEC CEO objectives that might be addressed:

    a. First, increase the number of social scientists that provide input to CEO activities, e.g., on-line questionnaire development from public involvement in the ShakeOuts, analysis and publication of journal articles based on the data collected, assessment of participation in the Earthquake Country Alliance, etc.

    b. Second, grow enthusiasm in these social and behavioral scientists for writing proposals to outside funding agencies with which they might be already familiar to do research whose findings might inform subsequent CEO activities. Although what might actually be researched would depend on the interests of the involved social and behavioral scientists, candidate fundable projects for external funding that we can imagine include: laboratory testing of messages contained in the document "Putting Down Roots in Earthquake Country", exploring which elements of ShakeOut are most and least effective, and more.

2. ***Explore special grants/contracts with federal agencies.*** The ability of SCEC to attract external funds for CEO research are impacted by the fact that SCEC does not, nor should it have, affiliated social and behavioral scientists with Ph.D.s who can complete for research funds from national funding agencies, e.g., the National Science Foundation. However, this does not constrain SCEC CEO from using its existing hard won national reputation for success from seeking funding from federal agencies with program missions, e.g., the Federal Emergency Management Agency (FEMA). Moreover, a catastrophic earthquake in southern California is one of the fifteen high profile catastrophic events singled out by the U.S. Department of Homeland Security, FEMA's parent agency, as deserving of special national preparedness attention. We recommend that that the SCEC CEO Program capitalize on this overlapping "event of interest" with FEMA/DHS, by either working with appropriate members of the External Advisory Council, SCEC scientists, others, or act on its own to explore what SCEC CEO activities match FEMA preparedness program elements for possible FEMA funding for future SCEC CEO activities, or possibly, FEMA core funding.

Risk Communication

Several decades ago the subdiscipline of risk communication (also known as crisis communication) arose from the merger of the disciplines of psychology, sociology and public relations. Today, risk communication is a well developed, scientifically-informed, and diverse enterprise legitimated by specialty area classification in professional research associations. It is an established service routinely provided by consulting firms and it is often used to inform public communication practices in both government agencies, e.g., the U.S. Department of Homeland Security, the U.S. Environmental Protection Agency, and by private sector hazard- related businesses.

SCEC currently does not have a public information officer trained in risk communication to speak on its behalf when scientific information developed by SCEC is made public. Instead, some SCEC scientists speak out publically on their own on matters regarding earthquake occurrence and risk without the benefit of what is known from risk communication research about how to maximizing both the appropriateness and effectiveness of their public statements. We recommend that:

1. SCEC determine how to appropriately access the knowledge and techniques in risk communication, and, then, how to make some appropriate and acceptable level of training in public risk and crisis communication available to SCEC scientists who might speak publicly for SCEC on matters of earthquake occurrence and risk.

Collaboratory for the Study of Earthquake Predictability (CSEP)

The SCEC leadership and staff are to be commended for developing and implementing CSEP for the testing of earthquake prediction techniques and aiding and promoting the development of test centers in several other countries besides the U. S. Crucial to the development of CSEP was funding provided by the Keck Foundation, approximately $425K for each of three years. The rational, quantitative, and transparent approach to the evaluation of earthquake prediction techniques developed by CSEP is sorely needed by the earthquake community, relevant government organizations, private interests, and the public in general. SCEC now faces major challenges to ensure the future of CSEP. The Keck Foundation funding will come to an end in early 2010. CSEP's first challenge is to secure significant new support in order to continue to be active at near its current level. The second challenge requires that SCEC "walk a fine line" between evaluation of earthquake prediction methodologies and endorsement of methodologies and specific earthquake predictions.

CSEP provides a platform for the testing of earthquake prediction techniques in an open and standardized manner. This platform includes evaluation software and access to data needed in proposed earthquake prediction processes. Replica CSEP testing centers have been established in New Zealand, Japan, and Switzerland. These serve as evidence of the acceptance and enthusiasm for the CSEP concept as developed by SCEC. Regions currently falling under testing for prediction techniques include California, Italy, Japan, New Zealand, and the northwest and southwest Pacific. The international dimension of the CSEP concept allows collaboration in development of evaluation procedures and software, and provides a broad, consistent base of experience in earthquake prediction.

Assuming that CSEP has now reached a development plateau, SCEC now faces the problem of sustaining the CSEP effort. An obvious source of funding should be the U. S. Geological Survey (USGS), the agency that has responsibility for evaluating earthquake predictions in the United States and its territories. It is unlikely that USGS funding could reach the level provided by Keck or that the USGS could provide support for foreign CSEP centers. The Federal Emergency Management Agency (FEMA) and other federal and state agencies involved in public safety and continuity of operations may represent additional sources of support.

In approaching other funding sources, SCEC should emphasize the point that CSEP is providing a service to the earthquake research community by evaluating earthquake prediction methods. In particular, since other federal agencies, such as the National Science Foundation (NSF) and National Aeronautics and Space Administration (NASA), support earthquake prediction research, they should feel some obligation to support the open and objective evaluation of prediction methods developed with their support. Private sector utilities and financial interests may also have an interest in the evaluation of prediction techniques. Finally, the concepts developed by CSEP may have application in evaluating long-range earthquake hazard studies such as fault rupture forecasts and earthquake hazard assessments.

As the current private funding environment is rather challenging, one idea to build this support for CSEP could be to create a consortium of private entities stakeholders, e.g. insurance companies. Possibly such a consortium could be explored at a workshop with industry representative's design to engage them in discussion with CSEP scientists to discuss industry informational needs and possible CSEP products that could address those needs. In the consortium model, each member company would pay a small annual fee and participate in an annual one-day meeting to discuss the research directions and results. This may provide additional visibility to CSEP in the private sector and could lay down the foundation for larger financial support. Additional visibility in the private sector could also be achieved by approaching media such as, e.g., Bloomberg News, Insurance Day or other similar trade magazines.

SCEC should be cautious to avoid potential liability exposure in its CSEP work. CSEP should be limited to the evaluation of prediction techniques and not stray into the endorsement of specific techniques or specific predictions. As a private institution, the University of Southern California (USC) may face litigious exposure related to earthquake predictions from which state and federal institutions and agencies are immune.

However, as CSEP is gaining increasing public visibility, the role of CSEP scientists should also include a strict collaboration with policy makers and communication with the media. The task of translating scientific results into risk communication and decision making is very critical and difficult at the same time, and therefore it should be carefully addressed within CSEP planning.

We recommend that:

1. The SCEC CSEP effort should be continued as a valuable platform for the open, rigorous, and consistent evaluation of earthquake prediction methodologies.
2. SCEC CSEP should continue its foreign involvements but limit these to collaboration on implementation of evaluation procedures and to sharing results and evaluation outcomes.
3. Because of likely funding restrictions, SCEC CSEP should evolve from its current developmental phase to one of sustained operations based on the evaluation concepts already established.
4. SCEC should explore public and private sector partnerships to expand the awareness, scope, role as well as and future support for CSEP operations.
    a. Target public sector groups include the USGS, NSF, NASA, FEMA, CALEMA and other agencies with concerns in earthquake prediction, either through their statutory evaluation and public safety responsibilities or through support of earthquake prediction research.
    b. A consortium of private entity stakeholders (e.g. insurance industry and, potentially, capital markets) could be established in order to raise some private funding while building momentum and visibility within the private sector.
        i. An excellent method of raising awareness and interest from the private sector would be for SCEC/CSEP to host a workshop soliciting input from industry representative on which potential products and timeframes would be of most interest.
    c. A process should be established for the exchange of forecast concepts and results between the CEA-funded UCERF3 California earthquake likelihood study and CSEP.
5. SCEC should seek assessment by the legal offices of USC any concerns regarding liability exposure that may result for CSEP activities and determine which, if any, specific steps might mitigate those concerns.
6. Given the critical role that CSEP may have in evaluating predictions and reporting results, SCEC should review the social sciences research literature on the societal aspects of earthquake prediction and adopt and apply relevant aspects of this research.

Initiative in Earthquake Simulation and Ground Motion Prediction

Another special project area within SCEC that is undergoing rapid growth is large-scale earthquake simulation and ground motion prediction. It is the view of the Advisory Council that physics-based simulations and coupled hazard assessments represent a valuable integration of much of the knowledge and new understanding gained from SCEC's earthquake system science approach. These simulations are gaining more acceptance in the engineering design community, particularly as an important alternative to the use of a limited set of 'real' earthquake recordings and as a means to explore ground motions expected at a site for various scenarios and conditions. The simulations are also being used as a means to provide theoretical confirmation and physical insights into the commonly-used empirical ground-motion prediction equations that form the backbone of probabilistic seismic hazard analysis. We agree that this remains a critical direction for SCEC.

Despite these successes and the important role of simulation in encapsulating scientific knowledge of earthquake ground motions and effects, there remains a palpable resistance within the practical engineering community to the use of simulated motions in the place of "real" records, due to qualms amongst the engineering community that the state-of-the-art in ground-motion simulation may not be sufficiently advanced to apply simulated motions to real engineering design problems. SCEC has a valuable role to play in engaging with the engineering community so that they better understand the strengths and limitations of simulated ground motions – and, just as importantly, SCEC scientists need to better understand the engineering perspective, including an appreciation for what is important in earthquake records from a structural analysis perspective.

The Advisory Council recommends:

1. A strong focus on understanding those aspects of ground motion prediction that have significant engineering impact
2. A strong connection between simulation and empirical validation with existing data – what aspects of simulation-based predictions can be validated with ground-motion data, and what aspects are currently untestable? Are there alternative ways to test such aspects?
3. More close collaboration between the Ground Motion Simulation group and the Fault and Rupture Mechanics focus group with an attempt to include or evaluate some of the more elaborate physical modeling being developing. For example, how much complexity of fault geometry is needed to accurately simulate strong ground motions for engineering applications? Does off-fault damage affect strong ground motions, and if so how should it be included?
4. Consider a robust code validation effort, similar to CSEP, and conducted jointly with leaders in the earthquake engineering community, for ground-motion simulation methods. Such an effort could be critical in establishing user acceptance of simulated ground motions as input to engineering designs.
    a. The effort should include comprehensive analysis and documentation of the sensitivity of simulation-based ground motions to the input parameters (and their interaction and uncertainties), with investigation of the extent to which each input parameter can be determined and constrained by data.
    b. b. Considerable thought should be given to the most effective organization and home of such a code validation effort so that it would have the greatest likelihood of success in attracting NSF Engineering funding.
5. Consider also providing suites of ground motions and documentation to engineering groups, in collaboration with them, to allow them to better evaluate the engineering implications of using simulated ground motions in comparison to recorded motions. For example, PEER recently completed an important evaluation project of ground-motion selection and scaling methods, from the perspective of the sensitivity of structural response to the input motions:

    http://peer.berkeley.edu/publications/peer_reports/reports_2009/reports_2009.html

    All of the proposed selection and scaling methods for this exercise (which engineers were free to propose according to their preferred methods) began with "real" earthquake records. An extension to this project that considered the role of simulated motions would be very useful and would build acceptance for such motions within the engineering community.

The engineering community has indicated their need for understanding the sensitivity of simulations to input source conditions (this was a focus of the engineering feedback comments at the SCEC workshop). Acceptance of simulated records for engineering applications will grow with further engagement and collaboration with engineers in the use of simulations. In short, engineers need to understand the simulations and their uncertainties in order to use them. Just as importantly, scientists need to understand how simulations are used in order to generate them effectively.

Leadership Development

The AC is very impressed with SCEC's effort to constantly renew its leadership group and to be cognizant of and proactive about the need for succession planning at the director's level. We make special note of the diversity and youth present both within the SCEC community and within the Planning Committee. Rotation within the leadership group is essential for the health of the center and this is clearly ongoing. It is critical that young scientists learn to fully appreciate the importance of participating in leadership activities to the success of a large collaborative interdisciplinary research community. We again, encourage SCEC senior leadership to continue to remember that leadership skills are learned and that they should remain attentive to mentoring and leadership development of new members of the leadership group.

In thinking about the future, the AC wishes to first gratefully acknowledge USC's long-term generous support of SCEC. USC's support of SCEC in the form of facilities, key scientific hires to its faculty, and outstanding staff has been central to the success of SCEC. We also want to recognize and thank USC for its strong effort to recruit a new director in the last year, even though that effort was ultimately unsuccessful. This effort was yet another manifestation of USC's commitment to the Center. The AC believes that USC's support of the center will continue to be central to the future of SCEC's success and thus we strongly endorse a decision that SCEC remain at USC for SCEC4.

The AC is delighted that Tom Jordan has committed to continue to lead SCEC through the SCEC4 proposal process. However, with Tom Jordan's stated desire to step down from the directorship after the SCEC4 proposal process is complete, the challenges of attracting a new director remain. The AC strongly recommends that a plan be defined as soon as possible for recruiting a new director, keeping in mind that the plan could not be fully executed until after the SCEC4 proposal process is complete. We recommend that the plan be clear cut, with a specific time table. The plan should also include strategies for cultivating a pool of potential candidates such as engaging them in SCEC by inviting potential candidates to serve on the Advisory Council, or by inviting them to attend SCEC meetings and workshops. It will also be important to consider alternate leadership structures for the future as an element of this succession planning. For example, the leadership should consider the possibility that there should be separate directors of special projects that are not funded through the core science budget. This kind of thinking might be important both to the future growth of SCEC and to attracting a new director with management strengths different from the current director.

Visibility and Vital Role of Workshops Within SCEC and Increasing Awareness of Their Outcomes

SCEC is filling a tremendous need for the community by facilitating easy-to-convene topical workshops in a very short time frame—as evidenced by the requests for many more such workshops in the coming year. The Advisory Council noted that while many SCEC members were aware of recent workshops in a related area, in general they were not very aware of the workshop outcomes if they did not personally attend.

Last year the Advisory Council recommended:

1. Continued SCEC-wide promotion of workshop opportunities, this part of the process seems to be working well.
2. Workshop conveners be required to prepare a brief summary for posting on the SCEC website shortly (within 30 days?) after the workshop, with email notification to the SCEC community containing a link to the summary.

We understand from Director Jordan's report that the above recommendations are being implemented, but since they had not yet happened as of the Annual meeting they are repeated here for completeness.

Science Plan Discussions at the Annual Meeting

The AC was very impressed with the format of this year's meeting and noted a significant improvement from the preceding year. Last year AC report noted a wide variability in format and level of interaction in the Focus Groups' science planning sessions. This year's format of a single plenary talk for each session unified the diverse aspects of SCEC and fostered collaboration. AC applauds SCEC planning committee for making this change. They should ensure, however, that in the future there is adequate seating in all the plenary sessions.

Success of plenary sessions was due, in large part, to the outstanding speakers. The presentations were excellent in terms of content, timeliness and accessibility for the entire audience. Despite the disparate backgrounds of AC members, all felt they learned from the presentations. The presentations also laid a solid foundation for the science discussions to follow.

Framing the science plan discussions in terms of a few provocative questions was effective for promoting focused discussion. Audience participation was impressive. Discussion leaders do, however, need to be

vigilant in preventing a few members from dominating discussion and should continue to encourage participation from as many SCEC members as possible.

Evaluating SCEC's Progress Towards Its Goals and Documenting and Disseminating SCEC3 Accomplishments

In the AC deliberations this year, it became apparent to us that in addition to the myriad of SCEC scientific and outreach accomplishments, the center itself has become an extremely successful and effective national model for interdisciplinary collaboration and its system-level scientific approach. We therefore recommend that:

1. SCEC seize the opportunity to document and highlight their role as an extremely effective and vital interdisciplinary science center in a national forum, perhaps in a Perspective piece for Science. Such exposure would be well-timed moving towards SCEC4 proposal submission.

In 2008 the Advisory Council was told that the SCEC Planning Committee would be tracking progress toward the achievement of Center objectives. We have yet to receive the results of this tracking and report on the status of progress on the various goals, we look forward to receiving status synthesis and assume that creating it will be part of the SCEC4 planning process.

Documenting the accomplishments of the earthquake system science done by the SCEC community is challenging—both in determining the appropriate medium for such interdisciplinary work and in capturing the full impact of the contributions. Despite these challenges, the Advisory Council continues to believe that creating an integrated synthesis of contributions by SCEC3 will be a critical part of the Center's legacy, not just within the earth sciences—but in the broader scientific community.

The Advisory Council reiterates our previous recommendations that:

2. SCEC soon to produce an integrated (but not exhaustive) accomplishment synthesis (monograph) that focuses on the progress made towards the 3 or 4 main goals of SCEC3. We believe that the synthesis required to produce such a document will be essential to the SCEC4 planning--- and such a report will be an important supporting document for the SCEC4 proposal.
3. Venues and formats outside of traditional publication medium should be explored-- however, independent and stringent peer review must be assured.
4. A speakers program to broadly disseminate the results of all aspects of SCEC work be established. (We understand that the speaker's program has now been organized, but we decided to again include this recommendation until it is actually implemented).

SCEC4 Planning

SCEC3 will mark 20 years of investment in a focused attack on a complex scientific problem with a unique interdisciplinary, system-level approach. Both the funders and the broader Earth Science community will expect products and deliverables commensurate with such a 20 year investment. SCEC4 presents an exciting opportunity to build upon a number of major scientific products and contributions of SCEC3 as well as the huge outreach and preparedness success of ShakeOut.

There is no question that SCEC has been successful in advancing system science in general and earthquake science, in particular. We think a compelling case for SCEC4 must be based on demonstrating the impact of SCEC's interdisciplinary approach focused on building system-level community community models – a demonstration that these models and new understanding are changing the way both earthquake scientists and earthquake engineers solve problems and approach their research.

It is fair to ask if the SCEC scientific accomplishments have made the impact on both the scientific community and practitioners (engineers, planners, public officials) that a 20 - year investment would warrant. Certainly, as noted previously, for the CEO program the answer is a resounding "yes'. An important aspect of documenting the accomplishments of SCEC3 will be to identify other specific areas in which the broader impact can clearly be demonstrated. If it is determined that the impact has been less than

desired in some areas, are there additional scientific challenges that remain to be met? How will SCEC4 improve upon the translation of that science into practice?

Obviously, SCEC is a big tent and has many diverse aspects. But it is important for documenting the success of SCEC3 and proposal of SCEC4 to avoid the impression of going in too many directions. SCEC should avoid the impression (and reality) of going in too many (e.g., 19) directions. We suggest that a better impact and marketing strategy for SCEC4 would be to organize around 2 to 4 main themes or grand challenges. With regard to overall SCEC4 planning, the AC recommends that:

1. SCEC distill its diverse aspects into a unifying and clearly articulated vision. AC suggests that this can best be done by identifying a few overarching goals and showing how the collaboration of the individual focus groups and disciplinary groups supports these goals.
2. Expanded partnerships may be essential for both increasing SCEC's impact and developing additional funding sources, particularly In the current funding environment. Collaboration or interaction with other agencies could provide additional core support for the proposed SCEC activities or leverage SCEC activities with modest support levels. For example:
    a. NASA Earth Sciences had indicated strong support for research in prediction of natural disasters. Last year's AC report endorsed "a joint SCEC-NASA workshop to explore potential guidelines for engaging space-based earthquake forecasting techniques in CSEP's rigorous and independent testing environment."
    b. Other possible partnerships include FEMA in the area of preparedness and mitigation, NIST or NSF Engineering and PEER in engineering practice, and private sector affiliates for special projects.

Obviously, the planning for SCEC4 should strongly be built on the experience and framework of SCEC3. This framework includes technology transfer across disciplines, consolidation and synthesis of results into accessible databases, encouragement of collaborations with international research groups, and finally a reassessment of staffing needs and tasks – especially in views of the demanding job to manage special projects. With regards to these topics, the AC has several additional recommendations:

3. ***Technology transfer: High performance computing.*** The successful application of high-performance computing to ground motion simulations highlights the unique position of SCEC's scientists in large-scale earthquake simulation and ground motion prediction. As part of SCEC4, we recommend that other SCEC disciplines and focus areas evaluate the potential role of high-performance computing to accelerate their investigations while leveraging the experience and technical framework of the ground motion group.
4. ***Consolidation and Synthesis.*** A key benefit of SCEC that should be trumpeted in the SCEC4 proposal has been the creation of major databases, community models, and community software. Initiatives should be proposed for SCEC4 that will further enhance the value of these important products, and extend the reach of SCEC to a wider audience. This could involve development of user-tools to make databases, software and models more accessible and user-friendly – including to non-SCEC scientists and to engineers. There could also be a link with CEO activities here, in devising new educational activities that utilize SCEC databases.

An important issue in SCEC4 planning will be to elucidate the role for international collaborations, while still maintaining the traditional southern California natural laboratory focus of SCEC that has made it so successful. CSEP in particular is an obvious project in which international collaboration will be important to the success and significance of the project. Defining how this collaboration will be fostered and managed will be a significant challenge in SCEC4.

5. ***International collaborations.*** The CSEP experience highlights the critical role of international collaborations to achieve synergies within the scientific community. SCEC4 could build on this experience and evaluate the feasibility of establishing international collaborations within other SCEC projects or working groups. The identification of suitable international collaborations could be focused on projects which can benefit from relevant datasets, technology and research framework already in place or under development outside the US.

Finally, throughout its history as a center SCDEC has been blessed with a small but extraordinarily effective staff. Looking forward to SCEC4 we recommend:

6. ***Staffing needs.*** While the SCEC program has largely benefited from the success in bringing in special projects, the achievement of a sustainable growth should be high priority. The management of scientific research within large-scale collaborations requires a lot of "behind-the-scene" work and effort by staff members. A careful examination of future staffing needs and resources should be part of SCEC4 planning.

High Risk / High Return Research Opportunities

The AC encourages SCEC to recognize and identify high risk/high return activities in order to continue moving forward and remaining at the forefront of earthquake science. For example, the Keck Foundation provided funding for CSEP precisely because it recognized it as a high risk/high return opportunity. SCEC's access to a large scientific community is a unique asset to support research in potentially controversial topics such as CSEP. The AC encourages SCEC to consider the following recommendations although it recognizes that neither will be easy to implement.

The AC recommends:

1. SCEC should try to identify other research opportunities that would be attractive to organizations focused on funding these high risk research activities. One idea would be to find a mechanism to generate a small pool of "venture" funds dedicated to explore and develop such projects.
2. SCEC needs to establish a process to leverage the results of some high risk projects to create a self-sustaining system or a platform for generating further funding.

Final Comments

It is the current sense of the Advisory Council that the researchers and, particularly, the senior leadership of SCEC are doing an outstanding job. The many individuals now leading committees and focus groups constitute a broadly diverse, extremely able, and committed group, including a number of rising stars. The Advisory Council applauds SCEC's continued role in catalyzing and supporting special projects such as UCERF3, high performance computing, and CSEP. Developing new support for these kinds of activities are essential to growing the community of scientists who are engaged in earthquake science and to leverage the knowledge and understanding developed in SCEC.

The Advisory Council is pleased to continue to provide assistance to SCEC in its efforts to formulate and accomplish the center's major goals. At any time the Council welcomes comments, criticism, and advice from the seismological community, including individuals and groups both inside and outside SCEC membership, on how best to provide that assistance.

Finally, the Advisory Council welcomes new members Jim Goltz of CALEMA and Steve Mahin from PEER. We congratulate and regretfully say goodbye to Kate Miller, new Dean of Geosciences at Texas A&M University. As TAMU is a SCEC -affiliated organization, Kate must cycle off the Advisory Council. She has been a valuable member of AC for a number of years and be will miss her input and perspective. We look forward to working with SCEC leadership assist in SCEC4 planning and to help ensure that the products and progress of the center in the SCEC3 era continue to be commensurate with agency and community investment.

SCEC Communication, Education, and Outreach

Mark Benthien / Robert de Groot
CEO Director for SCEC / CEO Education Programs Manager

Introduction

The SCEC Communication, Education, and Outreach (CEO) program has four long-term goals:

- Coordinate productive interactions among a diverse community of SCEC scientists and with partners in science, engineering, risk management, government, business, and education;
- Increase earthquake knowledge and science literacy at all educational levels, including students and the general public;
- Improve earthquake hazard and risk assessments; and
- Promote earthquake preparedness, mitigation, and planning for response and recovery.

These goals are pursued through activities organized within four CEO focus areas: ***Research Partnerships*** coordinated within the SCEC Seismic Hazard & Risk Analysis focus group; ***Knowledge Transfer*** activities with practicing professionals, government officials, scientists and engineers; ***Public Outreach*** activities and products for the general public, civic and preparedness groups, and the news media; ***Education*** programs and resources for students, educators, and learners of all ages, including the Experiential Learning and Career Advancement office which coordinates undergraduate and graduate internships and support for early career scientists. Many activities span more than one CEO focus area.

Partnerships are key to achieving SCEC's mission, research objectives, and outreach goals. These partners include other science organizations (e.g. IRIS, EarthScope, and UNAVCO), engineering organizations (e.g. PEER and EERI), education organizations (e.g. Los Angeles County Unified School District, California Department of Education, museums, and the National Association of Geoscience Teachers), and public service / risk management organizations (e.g. California Office of Emergency Services, the California Earthquake Authority, FEMA, and the American Red Cross).

Immediately following the 2009 SCEC Annual Meeting, a major review meeting was held of the SCEC CEO program. An extensive evaluation document was prepared in summer 2009 by evaluation consultants, which an external review panel used as the basis of its analysis. The review panel's report was quite thorough and provided several excellent recommendations. Overall, they concluded that "It is the strong consensus of the review committee that the SCEC CEO program has been an overwhelming success both in terms of breadth and impact." The SCEC Advisory Council commented that "the review strongly indicates that SCEC has demonstrated success in meeting the Broader Impacts criterion of NSF reviews, has become a leading force in education and outreach efforts related to earthquake science in Southern California, and has set a standard for others to emulate in all of California or elsewhere." The review was very important to the SCEC4 proposal process and was supported with funding from the NSF.

The following are highlights of SCEC's Public Outreach and Education activities in the last year.

Public Outreach Activities

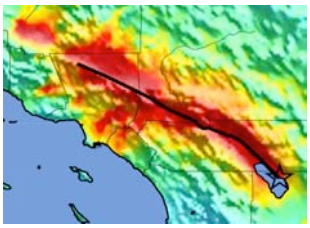

Great (Southern & Statewide) California ShakeOut. A major focus of the CEO program in 2008 and 2009 has been organizing the inaugural ShakeOut drill for Southern California on November 13, 2008, and the first statewide ShakeOut drill planned for October 15, 2009. The purpose of the Shakeout is to motivate all Californians to practice how to protect ourselves during earthquakes ("Drop, Cover, and Hold On"), and to get prepared at work, school, and home.

2009 Great California ShakeOut and Beyond. Immediately following the 2008 ShakeOut (initially conceived as a "once-in-a-lifetime" event), participants began asking for the date of the 2009 ShakeOut. After significant discussion among ECA partners and state agencies, the decision was made to organize an annual, statewide Shakeout drill to occur on the third Thursday of October (October 15 in 2009). This date is ideal for our school partners and follows National Preparedness Month in September, which provides significant exposure prior to the drill.

Expanding statewide has been much more complicated than simply deleting the word "Southern" from all materials and webpages. The 2008 ShakeOut was based on a single earthquake scenario, which does not apply to the entire state. Thus, 11 "ShakeOut Information Areas" were created, based on earthquake hazards, geography, media markets, and other factors, to provide local hazard information for participants throughout California. The redesigned *ShakeOut.org* website contains a description of each area's earthquake hazard and ShakeOut registration statistics down to the county level.

In addition, expanding statewide required considerable partnership development with state agencies and regional alliances. As described below, the Earthquake Country Alliance, which has also expanded statewide, is the primary organization behind the ShakeOut, connecting four regional alliances. The group works together to coordinate messaging and develop resources.

6.9 million people participated in the 2009 ShakeOut. Many of the 2008 participants registered again, along with new participants from all 58 of California's the states 58 counties. 5 million of the participants were staff and students from K-12 schools, but the rest were people and organizations that typically do not have earthquake drills.

Recruitment is well underway for the 2010 ShakeOut, with over 5.1 million participants registered as of August 31. The goal is to exceed at least 8 million.

In 2009 SCEC also created and hosted the website for "New Zealand Great West Coast Shakeout." Over 27 percent of the region's 30,000 residents participated. The British Columbia ShakeOut on January 26, 2011 will be the next non-California drill, along with a local drill in Oregon (Washington may join in 2012 as part of a Cascadia ShakeOut). In April, 2011, the Great Central US ShakeOut will be held as part of the lead up to the New Madrid Bicentennial. And in 2012 Utah and possibly New Zealand (nationwide) will launch ShakeOut drills. ShakeOut has really changed the way people and organizations are approaching the problems of earthquake preparedness.

SCEC is hosting the website for each of these drills, to maintain consistency in the brand and work towards unified earthquake messaging worldwide.

Putting Down Roots in Earthquake Country. In 1995 SCEC, the USGS, and a large group of partners led by Lucy Jones (USGS) developed and distributed 2 million copies of a 32-page color handbook on earthquake science, mitigation and preparedness. Funding was primarily from the National Science Foundation and USGS. The booklet was distributed through libraries, preparedness partners, cities, companies, and directly to individuals through SCEC.

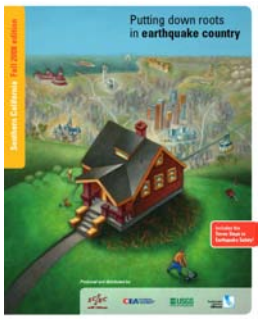

The creation of the Earthquake Country Alliance in 2003 was concurrent with the desire to update *Putting Down Roots* in advance of the 10th anniversary of the Northridge earthquake. The process brought the ECA together to develop consensus messaging and notably introduced the "Seven Steps to Earthquake Safety," which has become a standard approach to organizing earthquake preparedness messaging. Since 2004, the booklet has undergone five additional revisions and printings, the latest of which was finalized in October, 2008, and included the ShakeOut Scenario and an overview of the Uniform California Earthquake Rupture Forecast study led by SCEC. A new version is being worked on currently, to be printed in Fall, 2010, and will include new tsunami science and preparedness content.

Putting Down Roots has been widely distributed through newspaper inserts, museums, schools, at events organized by SCEC and ECA partners, and via an online order form. Over 2.3 million copies have been distributed since 2004, and an additional 1.25 million copies in Spanish have been distributed. Printing and distribution of the booklet was made possible by generous support of the California Earthquake Authority and additional funding from the Federal Emergency Management Agency (FEMA), and the USGS. The handbook is available at *www.earthquakecountry.info/roots* as an online version and downloadable PDF, and printed copies can be ordered for free through an online request form.

Putting Down Roots is the principal SCEC framework for providing earthquake science, mitigation, and preparedness information to the public. The "Roots" framework extends beyond the distribution of a printed brochure and the online version. For example, the Birch Aquarium in San Diego developed an earthquake exhibit that featured a "Seven Steps" display, similar to SCEC's "ShakeZone" exhibit at the Fingerprints Childen's Museum in Hemet, CA. The Emergency Survival Program (managed by LA County) based its 2006 and 2009 campaigns around the "Seven Steps." Many other adaptations of *Roots* and *Seven Steps* content have been developed by ECA and other partners.

The new version of *Putting Down Roots* was designed to allow other regions to adopt and adapt its structure to create additional versions. The first is a Greater San Francisco Bay Area version produced by a partnership led by the USGS with SCEC, local and state emergency managers, the Red Cross and many other organizations. Over 2.3 million copies have been printed, many distributed in newspapers, with funding from the California Earthquake Authority, USGS, FEMA, Red Cross, OES, CGS, and several others). In addition, a new booklet, *Protecting Your Family From Earthquakes–The Seven Steps to Earthquake Safety*, was produced in 2006 as part of the Putting Down Roots series, in two versions - English and Spanish in one booklet, and English, Chinese, Korean, and Vietnamese in another booklet. All Bay Area booklets can also be accessed from *www.earthquakecountry.info/roots*. All printings of the Bay Area version to date have been coordinated through SCEC.

Two other versions were produced over the last year, and can be downloaded from the Roots website:

- The Utah Seismic Safety Commission in 2008 produced the first version of *Putting Down Roots* outside of California, and discussion for a Central United States version has been moving forward (though slowly).
- *Living on Shaky Ground*, an update to the well-known earthquake booklet for California's North Coast, now including the Seven Steps to Earthquake Safety, has been in development for several years and is subtitled "Part of the *Putting Down Roots* in Earthquake Country Series."

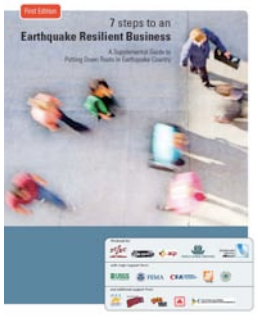

Finally, SCEC and ECA partners have developed a new supplement to Putting Down Roots, titled *The Seven Steps to an Earthquake Resilient Business*, an exciting new 16-page guide for businesses to develop comprehensive earthquake plans, printed in Fall, 2008. This booklet is the first non-regional publication, created as a supplement to all Putting Down Roots or other materials that include the *Seven Steps to Earthquake Safety*. It can be also downloaded and ordered from *www.earthquakecounty.info/roots*.

Earthquake Country Alliance. To coordinate activities for the 10-year anniversary of the Northridge Earthquake in January 2004 (and beyond), SCEC led the development of the "Earthquake Country Alliance" (ECA) beginning in summer 2003. This group was organized to present common messages, to share or promote existing resources, and to develop new activities and products. The ECA includes earthquake scientists and engineers, preparedness experts, response and recovery officials, news media representatives, community leaders, and education specialists. The mission of the ECA is to foster a culture of earthquake and tsunami readiness in California.

In 2006, the ECA launched the Dare to Prepare Campaign, to promote earthquake awareness and preparedness and to mark the 150th anniversary of the January 9, 1857, Ft. Tejon earthquake on the San Andreas Fault. With a strategy of getting southern Californians to "talk about our faults," the campaign acknowledged that "Shift Happens," and if you "Secure Your Space" you can protect yourself, your family, and your property. A new website (*www.daretoprepare.org*) was created, along with public events throughout the region (presentations, preparedness fairs, etc.) and a comprehensive media campaign with television, radio, and print promotion, public service announcements, on-air interviews and much more. A new Spanish-language website, *www.terremotos.org*, was also created and is hosted by SCEC.

The Earthquake Country Alliance is now the primary SCEC mechanism for maintaining partnerships and developing new products and services for the general public. Following the success of developing and implementing the 2008 Great Southern California, the ECA has now been expanded into a statewide organization and currently includes regional stakeholder alliances in southern California, the central coast, Bay Area, and north coast (see map). The statewide ECA, including state agencies, is currently planning the Great California ShakeOut, an annual statewide event in October.

SCEC developed and maintains the ECA website (*www.earthquakecountry.org*), which provides multi-media information about living in earthquake country, answers to frequently asked questions, and descriptions of other resources and services that ECA members provide. The site is set up separately from the main SCEC web pages (though has attribution to SCEC) so that all members of the ECA see the site as their own and are willing to provide content. The site features the online version of *Putting Down Roots* and special information pages that all groups can promote, such as a special page about the "10.5" miniseries and a page about the "Triangle of Life" controversy (see assessments below). The site is being completely redesigned to complement the new design of the *ShakeOut.org* website.

Media Relations. SCEC engages local, regional and national media organizations (print, radio and television) to jointly educate and inform the public about earthquake-related issues. The goal has been to communicate clear, consistent messages to the public–both to educate and inform, and to minimize misunderstandings or the perpetuation of myths. SCEC CEO encourages scientists who are interested in conducting interviews with media reporters and writers to take advantage of short courses designed and taught by public information professionals.

Emergency Survival Program. SCEC serves on the Coordinating Council of the Los Angeles County-led Emergency Survival Program, with emergency managers from all southern California counties, many large cities, the American Red Cross, and Southern California Edison. The primary role of the program is to develop a series of public information materials including monthly Focus Sheets, newsletter articles, and public service announcements related to a yearly theme. In 2006 and 2009 the program focused on earthquakes, with seven of the monthly focus sheets based on the "seven steps to earthquake safety" in *Putting Down Roots in Earthquake Country*. SCEC provided the Spanish version of the seven steps text, and coordinated the translation of the five other monthly focus sheets for 2006.

Use of SCEC Community Modeling Environment (CME) Products. Many SCEC CME products are being used in public presentations, webpages (*scec.org*, *earthquakecountry.info*, etc.), printed publications such as *Putting Down Roots in Earthquake Country* (English and Spanish), our "Earthquake Country – Los Angeles" DVD and in other venues to communicate earthquake hazards and encourage preparedness. These products, including the SCEC TeraShake and ShakeOut simulations, Puente Hills earthquake simulation, and Community Fault Model, have also had extensive media coverage through press briefings, reporters attending the SCEC Annual Meeting, and television documentaries, and have been used frequently as background imagery in many news stories. The visualizations were featured extensively in the National Geographic Channel documentary "Killer Quake," which presented SCEC TeraShake and Puente Hills animations, along with fault movies produced using SCEC's Virtual Display of Objects (SCEC-VDO) software. In June 2009 the Department of Energy honored the most advanced visualization to date of a magnitude 7.8 earthquake on the southern San Andreas Fault as one of this year's best scientific visualizations at the Scientific Discovery through Advanced Computing Conference. The new visualization was created by Amit Chourasia at the San Diego Supercomputer Center in collaboration with SCEC scientists Kim Olsen, Steven Day, Luis Dalguer, Yifeng Cui, Jing Zhu, David Okaya, Phil Maechling and Tom Jordan. The visualizations are featured at *http://www.wired.com/wiredscience/2009/08/visualizations/*.

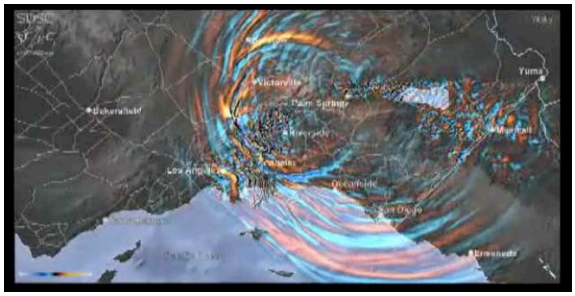

Education Program

SCEC and its expanding network of education partners are committed to fostering increasing earthquake knowledge and science literacy at all grade levels and in a variety of educational environments.

The SCEC Education program uses the research literature (science education, learning psychology, sociology, etc.) and evaluation methodology to:

- Develop new materials and products (e.g. lesson plans, evaluation instruments, websites) where needed.
- Collaborate with partner organizations to enhance existing materials or products to meet the needs for SCEC's Earthquake Program mission.

- Utilize and promote existing materials that coincide with or complement SCEC's earthquake K-12 Education Program mission.
- Provide innovative experiential learning opportunities to undergraduate and graduate students during the summer and year-round.

SCEC Education programs include three internship programs, facilitated activities at museum exhibits, earthquake education workshops, public earthquake talks, and activities at conferences such as the National Science Teachers Association. SCEC Education programs and products are implemented in a variety of educational environments- any place, situation, or context where the transmission of knowledge to learners is taking place.

SCEC Experiential Learning and Career Advancement Programs

Since 1994, SCEC has provided 404 internships to undergraduate and graduate students, with 330 internships since 2002 (charts included here are for 2002-2009 only). SCEC offers two summer internship programs (SCEC/SURE and SCEC/USEIT) and a year-round program for both undergraduate and graduate students (ACCESS). These programs are the principal framework for undergraduate student participation in SCEC, and have common goals of increasing diversity and retention. In addition to their research projects, participants come together several times during their internship for orientations, field trips, and to present posters at the SCEC Annual meeting. Students apply for both programs at *www.scec.org/internships*.

The SCEC Summer Undergraduate Research Experience (SCEC/SURE) has supported **189** students to work one-on-one as student interns with SCEC scientists since 1994 (118 since 2002). SCEC/SURE has supported students working on numerous projects in earthquake science, including the history of earthquakes on faults, risk mitigation, seismic velocity modeling, science education, and earthquake engineering.

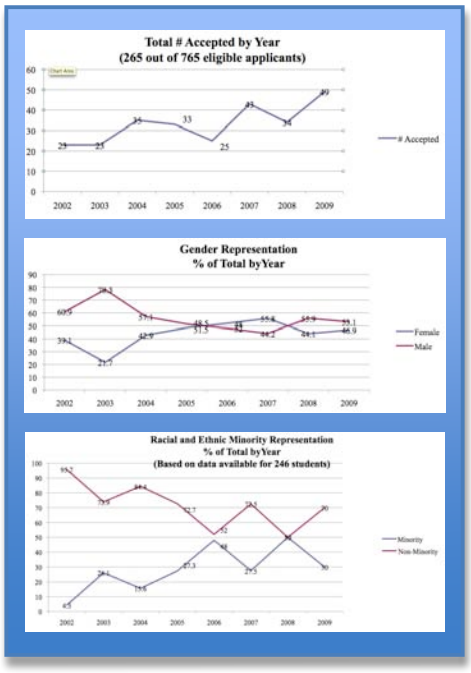

The SCEC *Undergraduate Studies in Earthquake Information Technology* (SCEC/USEIT) program, unites undergraduates from across the country in an NSF REU Site at USC. SCEC/USEIT interns interact in a team-oriented research environment with some of the nation's most distinguished geoscience and computer science researchers. Since 2002, 148 students have participated. Research activities are structured around "Grand Challenges" in earthquake information technology. Each summer the interns build upon the foundation laid by previous intern classes to design and engineer increasingly sophisticated visualization tools.

Our USEIT and CME experience has identified a "weak link" in cyberinfrastructure (CI)-related career pathways: the transition from discipline-oriented undergraduate degree programs to problem-oriented graduate studies in earthquake system science. We address this educational linkage problem through a CI-TEAM implementation project entitled the *Advancement of Cyberinfrastructure Careers through Earthquake System Science* (ACCESS). The objective of the ACCESS project is to provide a diverse group of students with research experiences in earthquake system science that will advance their careers and encourage their creative participation in cyberinfrastructure development. Its overarching goal is to prepare a diverse, CI-savvy workforce for solving the fundamental problems of system science. Undergraduate (ACCESS-U) internships support CI-related research in the SCEC Collaboratory by undergraduate students working toward senior theses or other research enhancements of the bachelor's degree. Graduate (ACCESS-G)

internships support up to one year of CI-related research in the SCEC Collaboratory by graduate students working toward a master's thesis. The SCEC ACCESS program ends in 2010 with 31 internships having been awarded.

Earthquake Exhibits and Museum Partnerships

Recognizing the key role that museums have in engaging communities not often reached by schools, SCEC facilitates a network of museums and other locations interested in providing earthquake education programming. These organizations also serve as a distribution point for SCEC resources such as *Roots*. SCEC has worked with some of these partners for many years, and in summer 2008 they have been organized as Earthquake Education and Public Information Centers (Earthquake EPIcenters). The concept emerged during the planning of the 2008 Great Southern California ShakeOut, and the need to organize museums for the ShakeOut has evolved into a year-round interaction with the ShakeOut being the culminating community event for the year. The ShakeOut has provided a basis for institutions to share resources and expertise

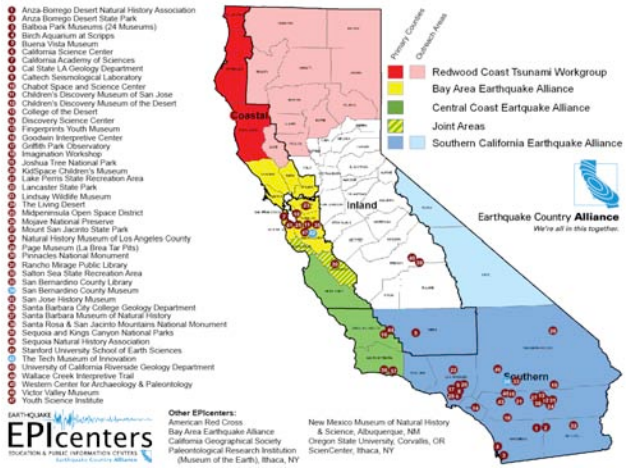

EPIcenters share a commitment to demonstrating and encouraging earthquake preparedness. They help coordinate Earthquake Country Alliance activities in their county or region (including the ShakeOut), lead presentations or organize events in their communities, or in other ways demonstrate leadership in earthquake education and risk reduction. EPIcenters are found in a variety of public meeting places such as museums, science centers, libraries, and universities. Just as the ShakeOut became a statewide effort in 2009 so did the EPIcenter Network. Currently over 50 free-choice learning institutions statewide participate in the ShakeOut and other activities throughout the year. The statewide Network is coordinated by SCEC Education Program Manager Robert de Groot with Kathleen Springer (San Bernardino County Museum) and Candace Brooks (The Tech Museum) coordinating Network activities in Southern and Northern California respectively.

SCEC's first major project in the development of a free choice-learning venue was the *Wallace Creek Interpretive Trail*. In partnership with the Bureau of Land Management (BLM), SCEC designed an interpretive trail along a particularly spectacular and accessible 2 km long stretch of the San Andreas Fault near Wallace Creek. Wallace Creek is located on the Carrizo Plain, a 3-4 hour drive north from Los Angeles. The trail opened in January 2001. The area is replete with the classic landforms produced by strike-slip faults: shutter ridges, sag ponds, simple offset stream channels, mole tracks and scarps. SCEC created the infrastructure and interpretive materials (durable signage, brochure content, and a website at *www.scec.org/wallacecreek* with additional information and directions to the trail). BLM has agreed to maintain the site and print the brochure into the foreseeable future.

The *ShakeZone Earthquake Exhibit* at Fingerprints Youth Museum in Hemet, CA was developed originally in 2001 and was redesigned in 2006. The current version of the exhibit is based on SCEC's *Putting Down Roots in Earthquake Country* handbook. Major partners involved in the exhibit redesign included Scripps Institution of Oceanography and Birch Aquarium at Scripps. With funding from the United Way and other donors ShakeZone will be expanded in 2010 to include a section on Earthquake Engineering.

In 2006 SCEC has embarked on a long-term collaboration with the San Bernardino County Museum (SBCM) in Redlands, California. SCEC participated in the development and

implementation of *Living on the Edge Exhibit*. This exhibit explains and highlights natural hazards in San Bernardino County (e.g. fire, floods, and earthquakes). SCEC provided resources in the development phase of the project and continues to supply the exhibit with copies of *Putting Down Roots in Earthquake Country*.

As a result of the successful collaboration on *Living on the Edge*, SCEC was asked to participate in the development of SBCM's *Hall of Geological Wonders*. To be completed in 2011, the Hall is a major expansion of this important cultural attraction in the Inland Empire. One of the main objectives of the Hall is to teach about the region from a geologic perspective. The museum is devoting a large space to the story of Southern California's landscape, its evolution and dynamic nature. SCEC has played an ongoing advisory role, provided resources for the development of the earthquake sections of the exhibit, and will have an ongoing role in the implementation of educational programming

The most recent debut of a SCEC earthquake display is the *Earthquake Information Center* at California State University, Los Angeles (CSULA). This exhibit, created in partnership with the geology department at CSULA, features two computer screens showing recent worldwide and local earthquakes. Located in the lobby of the Physical Science Building this exhibit also displays the seven steps to earthquake safety and components of a basic earthquake disaster supply kit. Many hundreds of students pass by the exhibit every day on their way to science classes. Development of other EPIcenter exhibits and resource areas are occurring at the Rancho Mirage Public Library, The California Science Center, Los Angeles, and the Natural History Museum of Los Angeles County.

K-12 Education Partnerships and Activities

Partnerships with Science Education Advocacy Groups and Organizations with Similar Missions. SCEC is an active participant in the broader earth science education community including participation in organizations such as the National Association of Geoscience Teachers, the Coalition for Earth System Education, and local and national science educator organizations (e.g. NSTA). Improvement in the teaching and learning about earthquakes hinges on improvement in earth science education in general. Hence, SCEC contributes to the community through participation on outreach committees wherever possible, co-hosting meetings or workshops, and building long-term partnerships. An example of a current project is a partnership with EarthScope to host a San Andreas Fault workshop for park and museum interpreters that was held in Spring 2009. In 2010 SCEC is collaborating with IRIS and EarthScope in developing the content for the San Andreas fault Active Earth Kiosk. The Active Earth Kiosk is an interactive website where visitors learn about earth hazards in a particular region. EarthScope is creating an Active Earth Kiosk for each of the regions covered by its Interpretive Workshops. Also in 2010 Arizona State University, the OpenTopography Facility, and SCEC developed three earth science education products to inform students and other audiences about LiDAR and its application to active tectonics research. First, a 10-minute introductory video titled *LiDAR: Illuminating Earthquakes* was produced and is freely available online. The second product is an update and enhancement of the Wallace Creek Interpretive Trail website. LiDAR topography data products have been added along with the development of a virtual tour of the offset channels at Wallace Creek using the B4 LiDAR data within the Google Earth environment. Finally, the virtual tour to Wallace Creek is designed as a lab activity for introductory undergraduate geology courses to increase understanding of earthquake hazards through exploration of the dramatic offset created by the San Andreas Fault (SAF) at Wallace Creek and Global Positioning System-derived displacements spanning the SAF at Wallace Creek. This activity is currently being tested in courses at Arizona State University. The goal of the assessment is to measure student understanding of plate tectonics and earthquakes after completing the activity. Including high-resolution topography LiDAR data into the earth science education curriculum promotes understanding of plate tectonics, faults, and other topics related to earthquake hazards.

Teacher Workshops. SCEC offers teachers 2-3 professional development workshops each year with one always held at the SCEC Annual Meeting. The workshops provide connections between developers of earthquake education resources and those who use these resources in the classroom. The workshops include content and pedagogical instruction, ties to national and state science education standards, and materials teachers can take back to their classrooms Workshops are offered concurrent with SCEC meetings, at National Science Teachers Association annual meetings, and at the University of Southern California. In 2003 SCEC began a partnership with the Scripps Institution of Oceanography Visualization Center to develop teacher workshops. Facilities at the Visualization Center include a wall-sized curved panorama screen (over 10m wide). The most recent teacher workshop held in partnership with Mt. San Antonio College was held in April 2010 at the GSA Cordilleran Section meeting.

Since 2009, SCEC has been collaborating with the Cal State San Bernardino/EarthScope RET program led by Sally McGill. During the course of the summer 7-10 high school teachers and their students conduct campaign GPS research along the San Andreas and San Jacinto faults. SCEC facilitates the education portion of the project through the implementation of the professional development model called Lesson Study. This allows for interaction with the teachers for an entire year following their research. For the second year all of the members of the RET cohort participate in the SCEC Annual Meeting by doing presentation of their research, participating in meeting activities such as talks and works culminating in presenting their research at one of the evening poster sessions.

Sally Ride Science Festivals. Attended by over 1000 middle school age girls (grades 5–8) at each venue, Sally Ride Science Festivals offer a festive day of activities, lectures, and social activities emphasizing careers in science and engineering. Since 2003, SCEC has presented workshops for adults and students and participated in the Festival's "street fair," a popular venue for hands-on materials and science activities. At the street fair SCEC demonstrates key concepts of earthquake science and provides copies of *Putting Down Roots in Earthquake Country*. The workshops, presented by female members of the SCEC community share the excitement and the many career opportunities in the Earth sciences.

National Science Teachers Association and California Science Teachers Association. Earthquake concepts are found in national and state standards documents. For example, earthquake related content comprises the bulk of the six grade earth science curriculum in California. SCEC participates in national and statewide science educator conferences to promote innovative earthquake education and communicate earthquake science and preparedness to teachers in all states.

Development of Educational Products

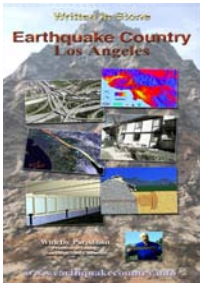

Earthquake Country - Los Angeles Video Kit. The video, produced by Dr. Pat Abbott of SDSU, tells the story of how the mountains and valleys of the Los Angeles area formed, and the important role of earthquakes. The video features aerial photography, stunning computer animations (some produced by SCEC's USEIT interns), and interviews with well-known experts. SCEC developed an educator kit for school and community groups, available online and provided at SCEC's teacher workshops.

Plate Tectonics Kit. This new teaching tool was created to make plate tectonics activities more accessible for science educators and their students. SCEC developed a user-friendly version of the *This Dynamic Earth* map, which is used by many educators in a jigsaw-puzzle activity to learn about plate tectonics, hot spots, and other topics. At SCEC's teacher workshops, educators often suggested that lines showing the location of plate

boundary on the back of the maps would make it easier for them to correctly cut the map, so SCEC designed a new (two-sided) map and developed an educator kit.

Use of SCEC Community Modeling Environment (CME) Products in K-12 Education. SCEC has included CME animations in its teacher education workshops since 2002 with the initial visualization of the Community Fault Model (CFM), and through 2008 with the latest TeraShake and ShakeOut animations. SCEC's "Earthquake Country – Los Angeles" DVD and *Putting Down Roots* handbook are used by teachers throughout Southern California, and both feature CME products. A compilation of CFM visualizations have also distributed on a CD at teacher conferences such as the NSTA annual meeting.

Research Accomplishments

Southern California Earthquake Center

2010 Annual Report

This section summarizes the main research accomplishments and research-related activities during 2008 and the early months of 2009. The research reported here was funded by SCEC with 2008 research funds. While the presentation is organized sequentially by disciplinary committees, focus groups, and special project working groups, it is important to note that most SCEC activities are crosscutting and could be presented under multiple focus groups.

Disciplinary Activities

The following reports summarize recent progress in the three main infrastructural activities and the discipline-oriented research, *Seismology*, *Geodesy*, and *Geology*.

Seismology

Four projects were funded in the Seismology Infrastructure focus group in 2008-09. These were the Southern California Earthquake Data Center, the Borehole Seismometer Network, the Portable Broadband Instrument Center, and a Caltech/UCSD collaboration assembling earthquake catalogs and measuring earthquake properties and structure. In addition, several innovative projects were funded as part of the seismology research effort.

Southern California Earthquake Data Center (SCEDC)

Major 2009 Accomplishments

1. Continued key data-acquisition and archiving functions by maintaining and updating the primary online, near real-time searchable archive of seismological data for southern California. Added 1,229,564 days of continuous data for 387 stations and parametric and waveform data for 16,004 local events and 446 teleseismic earthquakes.
2. The SCEDC purchased 64 2xTB disks to more than double the storage capacity of the waveform archive.
3. In response to user recommendations at the SCEDC town-hall meeting, the SCEDC began continuous archiving of all HN borehole channels as of Oct 1, 2009.
4. The SCEDC continues to make improvements Station Information System (SIS) with the Southern California Seismic Network (SCSN). The SCEDC replaced its single SIS with two Dell Power Edge R610 web servers. The user interface has been improved so that users can store non-response information such as telemetry equipment and layout.
5. The SCEDC hosted a mirror site to the SCEC Earthquake Response Content Management System (ERCMS) for the November 2009 ShakeOut. The SCEDC will continue to host this mirror site for SCEC.
6. The SCEDC has added QuakeML as a catalog search format. Web services for QuakeML format are also now available. Development of these services will serve as a foundation for greater capabilities for users to access data.
7. The SCEDC will continue to serve out fault data to the SCEC WGCEP group. The SCEDC is working with SCEC intern Michael Ihrig to produce a Google Map version of the Clickable Faults Map.

8. SCEDC has released a new version of the STP client that can access both the SCEDC archives in Pasadena, and the NCEDC archives at UC Berkeley, giving SCEC researchers access to continuous waveforms throughout California.

9. As part of a NASA/AIST project in collaboration with JPL and SIO, the SCEDC will receive real time 1 sps streams of GPS displacement solutions from the California Real Time Network (*http://sopac.ucsd.edu/projects/realtime*; Genrich and Bock, 2006, J. Geophys. Res.). These channels will be archived at the SCEDC as miniSEED waveforms, which then can be distributed to the user community via applications such as STP. This will allow seismologists access to real time GPS displacements in the same manner they access traditional seismic data.

10. The SCEDC is now distributing a subset of seismograms (20 km and 40 km spacing) and GPS data computed for the 2008 ShakeOut scenario. The seismic data are velocity waveforms at 40 sps in SAC format. The GPS waveforms are 1 sps displacements in SAC format. Seismic waveforms for GPS station locations are also available.

11. The SCEDC has made an interactive site to view the vertical and horizonal cross sections of the latest tomographic model of Southern California. Users can view vertical cross sections perpendicular to major faults or in north-south, east-west grid. Users can also view horizontal cross sections by different depth intervals as well as play a slideshow of cross sections.

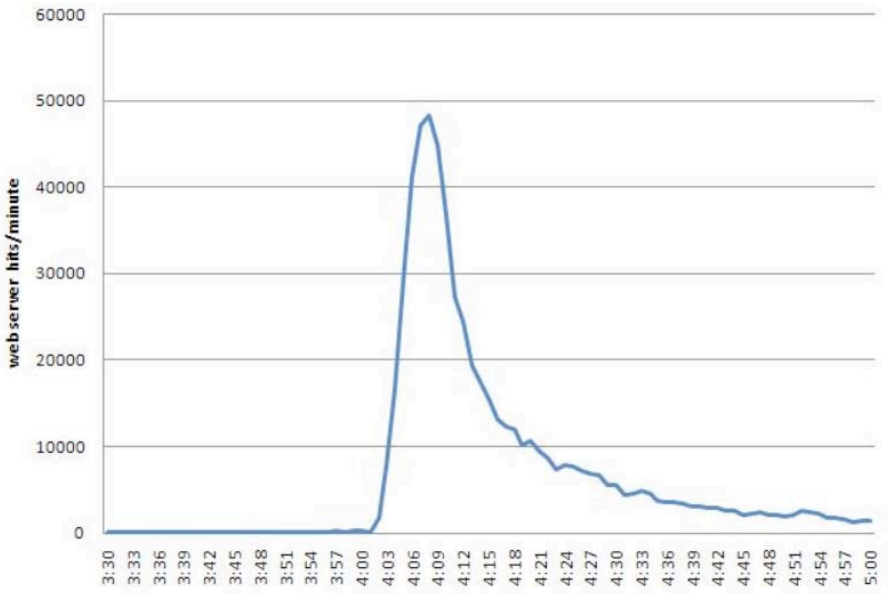

Figure 5. Web hits on SCEDC server showing a large increase in traffic seconds after the M4.4 earthquake in Pico Rivera on March 16, 2010.

The Data Center is a central resource of SCEC and continues to be an integral part of the Center. In 2009, the SCEDC continued to provide online access to a stable and permanent archive of seismic waveforms and earthquake parametric data. The seismological data archive held at the SCEDC has contributed significantly to the publication of many scientific papers pertinent to the region, most of which have SCEC publication numbers. The Caltech/USGS catalog archived by the SCEDC is the most complete archive of seismic data for any region in the United States.

The SCEDC has allowed the data to be distributed to a much broader community of scientists, engineers, technologists, and educators than was previously feasible (Figure 5). The electronic distribution of data allows researchers in the world-wide scientific community to analyze the

seismic data collected and archived in southern California and contribute their results to the SCEC community.

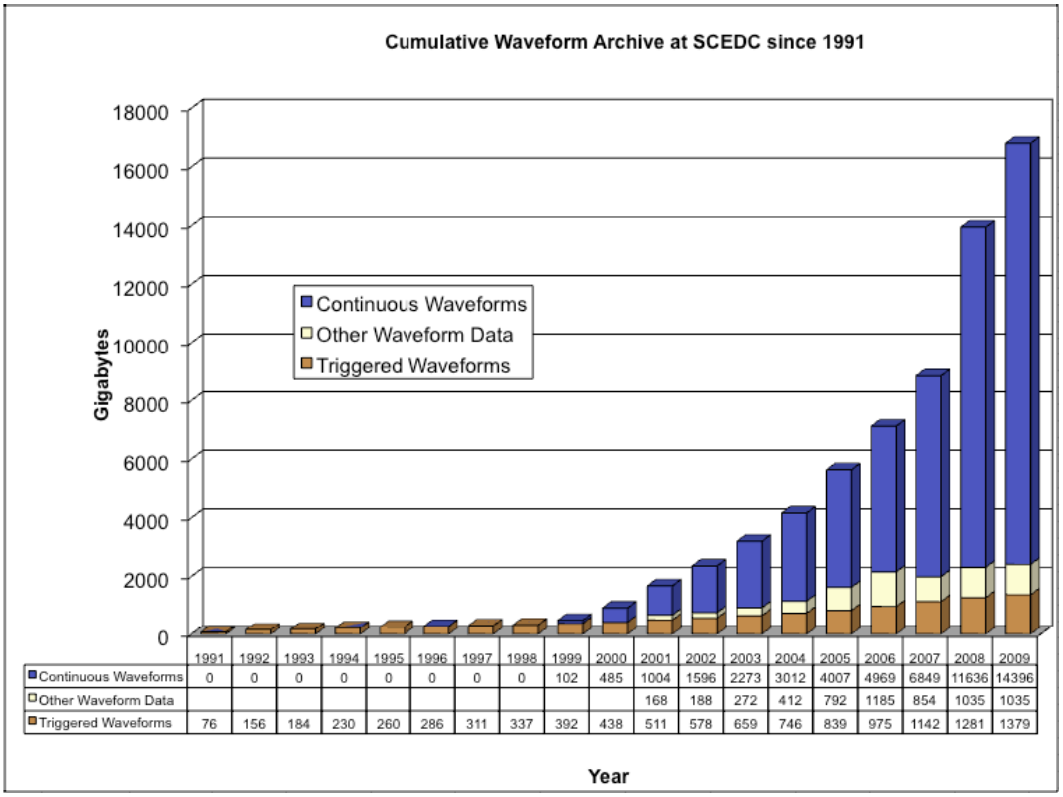

	1991	1992	1993	1994	1995	1996	1997	1998	1999	2000	2001	2002	2003	2004	2005	2006	2007	2008	2009
Continuous Waveforms	0	0	0	0	0	0	0	0	102	485	1004	1596	2273	3012	4007	4969	6849	11636	14396
Other Waveform Data											168	188	272	412	792	1185	854	1035	1035
Triggered Waveforms	76	156	184	230	260	286	311	337	392	438	511	578	659	746	839	975	1142	1281	1379

Figure 6. Cumulative waveform archive at SCEDC since 1991.

The archive at the SCEDC currently has the following holdings:

The Caltech/USGS catalog of over 627,838 earthquakes spanning 1932-present.

- 16.81 terabytes of continuous and triggered waveforms (Figure 6).
- million phase picks.
- 83.4 million triggered waveform segments.
- Nearly 10 years of continuous broadband and high sample short period waveform recording of representing more than 8,745,239 days of continuous waveforms.
- 20.3 million amplitudes available for electronic distribution.
- Triggered data for more than 9,789 significant teleseismic events.

Application of Waveform Cross-Correlation and Other Methods to Refine Southern California Earthquake Data

The ever-expanding waveform archive of over 400,000 local earthquake records provides an invaluable resource for seismology research that has only begun to be exploited; however, efficiently mining these data requires the development of new analysis methods, an effort that goes beyond the limited resources of individual scientists. Through coordinated efforts common tools and data products have been developed that can be used by researchers to accomplish many SCEC goals.

The HASH algorithm (Hardebeck and Shearer, 2002 and 2003) was applied to determine focal mechanisms from the SCSN data set of first motion polarities. Removing azimuth, take-off angle, and distance filters maximized the number of mechanisms. The method developed by Shearer and Hauksson only requires more than 8 first motions for each mechanism and an azimuth gap of less than 180°. This results in 137,000 mechanisms. The algorithm provides the strike, dip, and rake for one of the two planes of each mechanism, as well as error estimates. Error estimates are analyzed to look for obvious trends that would make it possible to determine filtering values to optimize the selection of reliable mechanisms.

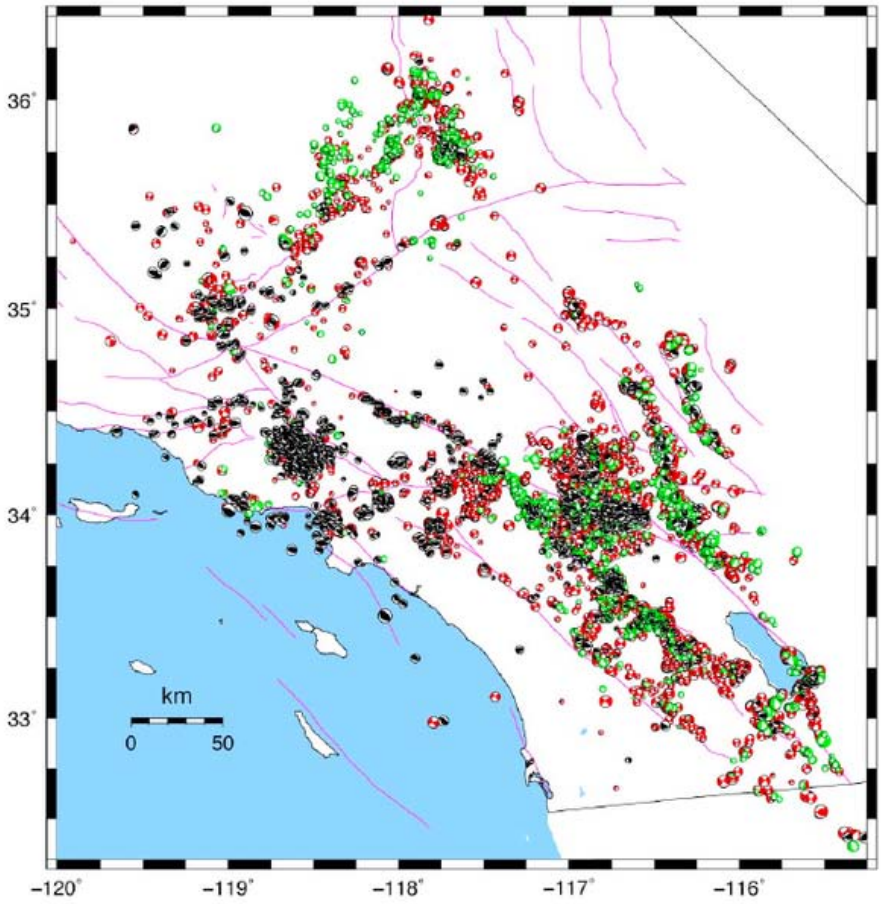

Figure 7. The ~15,000 focal mechanisms (1981 – 2009) (A, B, and C quality) selected using similar criteria as J. Hardebeck used for the previous catalog. First, the strike-slip (red) are plotted. Second, the normal (green), and thrust mechanisms (black) are plotted on top – reducing somewhat the prominence of the strike-slip events.

The average quality of the focal mechanisms and style of faulting has remained similar from 1981 to 2009. The results show that strike-slip faulting mechanisms occur across southern California and are most common along the major late Quaternary faults (Figure 7). Normal faulting mechanisms are dominant along the Salton Trough, and the northern end of the San Jacinto fault, and also occur in the southern Sierra Nevada and Coso regions. Thrust faulting mechanisms occur within the Transverse Ranges, and beneath Banning Pass extending to the west across the Los Angles and Ventura basins.

Overall, Shearer and Hauksson found the plate boundary is characterized by strike-slip faulting with small regions of compression and extension, which results in spatial overlaps of different

types of focal mechanisms. In addition, it was found that normal faulting is more common at depths between 3 and 10 km while thrust faulting is more common 3 to 5 km deeper. The temporal behavior of all the focal mechanism parameters and their errors are very similar from 1981 to 2009. Thus the tectonics of southern California as expressed by ongoing seismicity has remained similar, and the predominant style of faulting changed only during major earthquake sequences.

Analysis of Southern California Seismicity Using Improved Locations and Stress Drops

Using recent dramatic improvements in earthquake locations, focal mechanisms and stress drop estimates, a variety of issues can be addressed, including whether space/time clustering of seismicity obeys ETAS-like triggering relationships, whether precursory seismicity varies as a function of event size, and what are the space-time details of small earthquake stress drops. Preliminary analysis of stress drops reveals no obvious relationship between stress drops and the location of faults and tectonic features. It is not yet understood what may be controlling the large observed variations in stress drop and this will be a focus of future work.

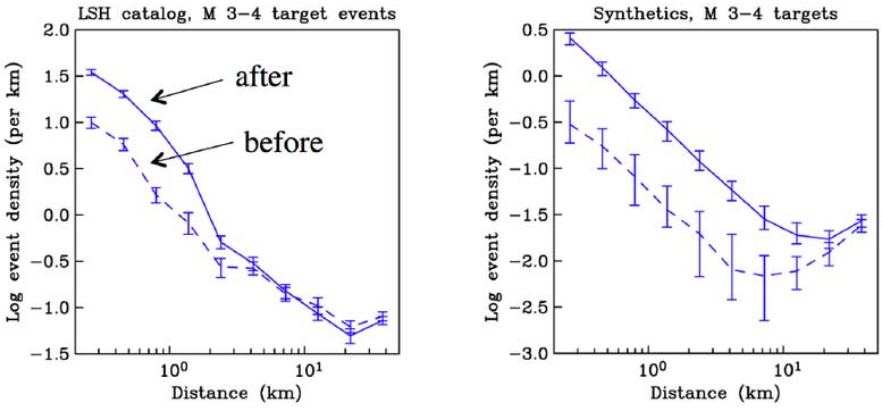

Figure 8. Event density as a function of distance in one-hour windows before and after M 3–4 target earthquakes, comparing the LSH catalog of southern California seismicity (left) with predictions of an ETAS-like triggering model (right). One-standard error bars are computed using a bootstrap resampling method.

Results suggest that there are at least some physical differences in the state existing before larger earthquakes compared to smaller earthquakes. Shearer is building on these results to study the more general problem of determining which features of the space/time clustering observed in seismicity catalogs are well-explained by ETAS-like models and which features more likely reflect underlying physical processes. The results suggest that triggering is only resolvable to distances of about 3 km for M2-4 mainshocks, far less than the distances suggested by Felzer and Brodsky (2006) (Figure 8).

Refining and Synthesis of 3D Crustal Models and Seismicity Catalogs for Southern California

Hauksson et al. analyzed relocated background seismicity (1981-2005), and several geophysical crustal properties to improve our understanding of the brittle part of the crust in southern California, often referred to as the seismogenic zone. Crustal deformation in southern California is dominated by right-lateral shear stress caused by relative motion of the Pacific and North America plates. The major late Quaternary faults are the zones of weakness that accommodate plate boundary deformation. They also control the spatial distribution of seismicity. The dilatational crustal deformation field that causes crustal thinning or thickening is superimposed on the shear deformation but does not seem to have a significant effect on the distribution of earthquakes.

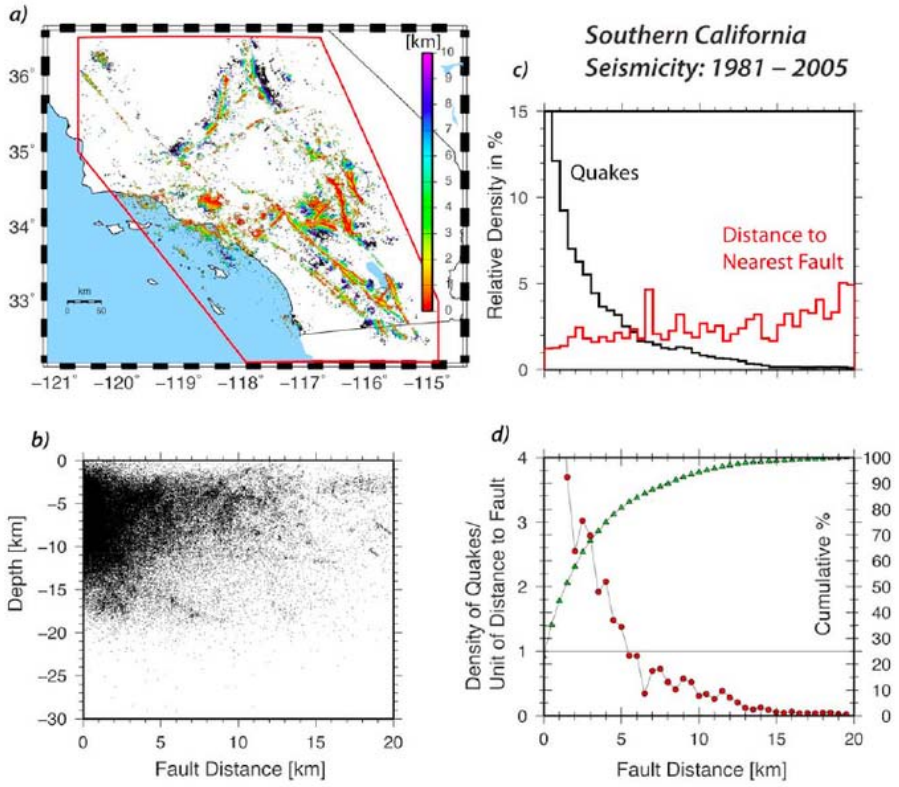

Figure 9. Fault-distance and seismicity. (a) Fault-distances for earthquakes of M≥1.8 are plotted in color. The fault traces are not included. (b) Each hypocenter is plotted at the respective distance from the nearest principal slip-surface of a late Quaternary fault. (c) Relative density of quakes and 'fault-distance' values for each 1 km of distance, and relative density of distances measured from a regular grid across southern California. (d) Normalized density of quakes per 1 km step in fault-distance, and cumulative number of quakes.

Seismicity preferentially occurs near the late Quaternary faults, in crust with average geophysical properties (Figure 9). Density, isostatic gravity, Vp/Vs variations, and volumetric strains affect the locations of seismicity less than proximity of late Quaternary faults. About 90% of the earthquakes occur within the available range of each of the modeled geophysical variables. As an example, the heat flow of 50 to 100 mWm2, isostatic gravity of -50 to 0 mGals and GPS dilatation of -60 to 40 nanostrains/yr. Similarly, they occur at elevations less than 1600 m, depth to Moho, and average crustal Vp/Vs of 1.73 to 1.81. Relatively few earthquakes are present if the crust is too thin or too thick or the elevation is too high. Similarly, if the crust is too thin, the heat flow is very high and the deformation is spread among several faults covering a wider region. If the crust is too dense or there is minimal Quartz content, earthquakes are unlikely. Similarly, if the Vp/Vs, and density are low, and the elevation is high, the crust is too thick to accommodate through going faulting. The dynamic volumetric strains as well as modeling favor earthquakes in extensional regimes, with some earthquakes occurring in compressional regimes provided the strain rate is high enough.

Correlation between seismic clustering properties and regional physical conditions

Enescu et al. (2009) investigate the relations between properties of seismicity patterns in Southern California and the surface heat flow using a relocated earthquake catalog. They first search for earthquake sequences that are well separated in time and space from other seismicity and then determine the Epidemic Type Aftershock Sequence (ETAS) model parameters for the sequences with a sufficient number of events. The productivity parameter α of the ETAS model quantifies the

relative productivity of an earthquake with magnitude M to produce aftershocks. By stacking sequences with relatively small and relatively large α values separately, they observed clear differences between the two groups. Sequences with smaller α have a relatively large number of foreshocks and relatively small number of aftershocks. In contrast, more typical sequences with larger α have relatively few foreshocks and larger number of aftershocks. The stacked pre-mainshock activity for the more typical latter sequences has a clear increase in the day before the occurrence of the main event. The spatial distribution of the α values correlates well with surface heat flow: areas of high heat flow are characterized by relatively small α, indicating that in such regions the swarm-type earthquake activity is more common. Our results are compatible with a damage rheology model that predicts swarm type seismic activity in areas with relatively high heat flow and more typical foreshock-mainshock-aftershock sequences in regions with normal or low surface heat flow. The high variability of α in regions with either high or low heat flow values indicates that at local scales additional factors (e.g., fluid content and rock type) may influence the seismicity generation process.

Zaliapin and Ben-Zion (2010) also examine the relationship between spatial symmetry properties of earthquake patterns along faults in California (CA) and local velocity structure images to test the hypothesis that ruptures on bimaterial faults have statistically preferred propagation directions. The analysis employs seismic catalogs for twenty five fault zones in CA. They distinguish between clustered and homogeneous parts of each catalog using a recently introduced earthquake cluster analysis and calculate an asymmetry index for the clustered portion of each examined catalog. The results indicate strong asymmetric patterns in early-time spatially-close aftershocks along large faults with prominent bi-material interfaces (e.g., sections of the San Andreas fault), with enhanced activity in the directions predicted for the local velocity contrasts, and absence of significant asymmetry along most other faults. Assuming the observed asymmetric properties of seismicity reflect asymmetric properties of earthquake ruptures, the discussed methodology and results can be used to develop refined estimates of seismic shaking hazard associated with individual fault zones.

Quantifying Heterogeneity of Active Fault Zones using Fault Trace and Earthquake Focal Mechanism Data

Wechsler et al. (2010) perform a systematic comparative analysis of geometrical fault zone heterogeneities using derived measures from digitized fault maps that are not very sensitive to mapping resolution. They employ the digital GIS map of California faults (version 2.0) and analyze the surface traces of active strike-slip fault zones with evidence of Quaternary and historic movements. Each fault zone is broken into segments that are defined as a continuous length of fault bounded by changes of angle larger than 1°. Measurements of the orientations and lengths of fault zone segments are used to calculate the mean direction and misalignment of each fault zone from the local plate motion direction, and to define several quantities that represent the fault zone disorder. These include circular standard deviation and circular standard error of segments, orientation of long and short segments with respect to the mean direction, and normal separation distances of fault segments. They also examined the correlations between various calculated parameters of fault zone disorder and the following three potential controlling variables: cumulative slip, slip rate, and fault zone misalignment from the plate motion direction. The analysis indicates that the circular standard deviation and circular standard error of segments decrease overall with increasing cumulative slip and increasing slip rate of the fault zones. In other words, the range or dispersion in the data, which provide measures of the fault zone disorder, vary with cumulative slip and slip rate (or more generally slip rate normalized by healing rate), which is attributable to the fault zone maturity. The fault zone misalignment from plate motion direction does not seem to play a major role in controlling fault trace heterogeneities. The frequency-size statistics of fault segment lengths can be fit well by an exponential function over the entire range of observations.

Bailey et al (2010) present a statistical analysis of focal mechanism orientations for nine California fault zones with the goal of quantifying variations of fault zone heterogeneity at seismogenic

depths. The focal mechanism data are generated from first motion polarities for earthquakes in the time period 1983–2004, magnitude range 0–5, and depth range 0–15 km. Only mechanisms with good quality solutions are used. They define fault zones using 20 km wide rectangles and use summations of normalized potency tensors to describe the distribution of double-couple orientations for each fault zone. Focal mechanism heterogeneity is quantified using two measures computed from the tensors that relate to the scatter in orientations and rotational asymmetry or skewness of the distribution. The relative differences in the focal mechanism heterogeneity characteristics are shown to relate to properties of the fault zone surface traces such that increased scatter correlates with fault trace complexity and rotational asymmetry correlates with the dominant fault trace azimuth. These correlations indicate a link between the long term evolution of a fault zone over many earthquake cycles and its seismic behavior over a 20 year time period. Analysis of the partitioning of San Jacinto fault zone focal mechanisms into different faulting styles further indicates that heterogeneity is dominantly controlled by structural properties of the fault zone, rather than time or magnitude related properties of the seismicity.

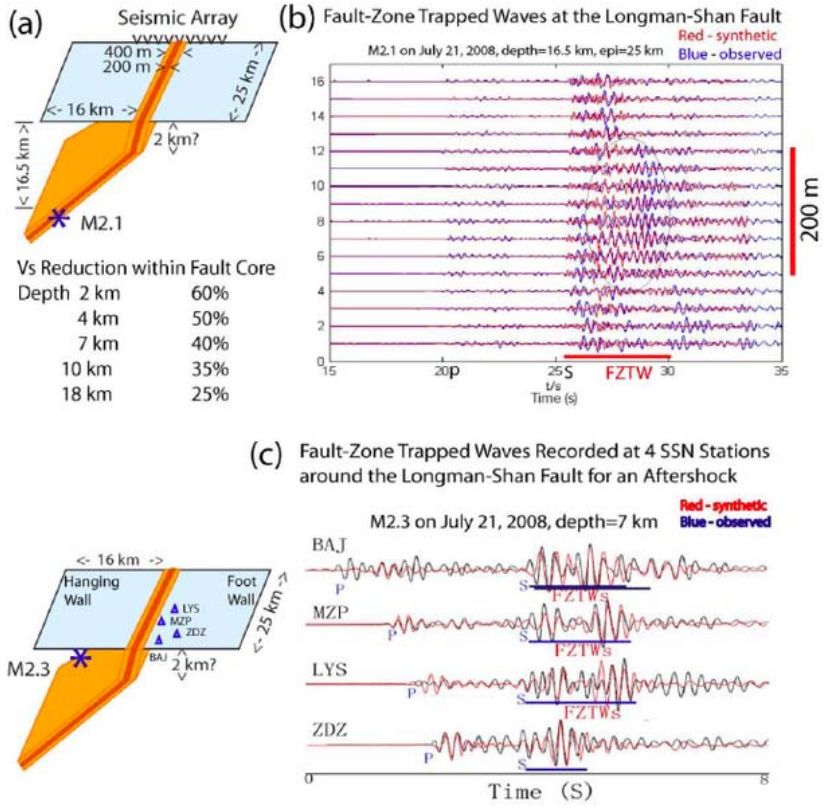

Figure 10. (a) Depth-dependent fault-zone model used to simulate FZTWs recorded at the Longman-Shan fault. The fault dips at 75 degrees above 2 km and then dips at 45 degrees at greater depths. Velocities within the 200-m-wide fault core are reduced by 25-60% from wall-rock velocities, with the maximum reduction at depths above 2 km. The fault core is sandwiched by a 400-m-wide zone with weaker velocity reductions. Q values within the fault zone are 10-60, with the lowest value within the fault core at shallow depth. (b) 3-D finite-difference synthetic seismograms (red lines) and fit to data (blue lines) recorded at the cross-fault dense array for a M2.1 near-fault aftershock occurring at depth of 16.5 km and ~25 km from the array. Seismograms are <3Hz filtered. Prominent fault-zone trapped waves (FZTWs) appear at stations within the fault core. Red bar denotes the time duration of FZTWs.(c) Observed and synthetic seismograms for a M2.3 on-fault aftershock at 7-km depth near the mainshock epicenter show prominent FZTWs with large amplitudes and long wavetrains at stations BAJ, MZP and LYZ located close to the main surface rupture, but short wavetrains after S-arrivals at station ZDZ away from the surface rupture.

A Study of Fault Damage and Healing at the Longmen-Shan Fault That Ruptured in the 2008 M8 Earthquake in China

Li documents the extent of rock damage on the Longmen-Shan fault (LSF) caused by the M8 Wenchuan earthquake and the healing rate after the mainshock by measuring fault-zone trapped waves (FZTWs). They focus on 300 aftershocks recorded at 8 Sichuan Seismological Network stations and a linear seismic array deployed across the LSF after the 2008 Wenchuan earthquake in the source region of the M8 mainshock. They observed prominent fault-zone trapped waves characterized by large amplitudes and long wavetrains after S-waves at station MZP located close to the main rupture along the LSF, but only brief wavetrains at station GHS located on the hanging-wall and away from the LSF for the same events. The wavetrains of FZTWs envelopes increase in duration as traveltimes between station MZP and the aftershocks increase, indicating a low-velocity waveguide that extends at least 25 km along the fault strike and to 10 km depth.

They used a 3D finite difference code to investigate the geometry and material properties along and across strike of the Longmen-Shan fault. Preliminary simulations of FZTWs observed at the southern LSF suggest that the cross section of the fault zone consists of a ~200-m wide fault core sandwiched by the surrounding ~400-m wide damage zone (Figure 10). The damage zone velocities range between 65-75% of wall-rock velocities, while those of the fault core are reduced by 50% compared to intact rock. The width and velocity reduction of the damage zone of the LSF at the shallow depth delineated by the FZTWs are similar to the results from fault zone drilling in the Wenchuan earthquake source region. Preliminary results suggest that seismic velocities within the LSF zone were co-seismically reduced by ~15% or even more due to the rock damage caused by the 2008 M8 mainshock on May 12, 2008. Some healing of the fault zone is observed in the 1.5 years following the mainshock.

Effects of Off-Fault Inelasticity on 3D Dynamic Interaction of En Echelon Strike-Slip Faults

Extensive observational and theoretical studies have focused on the fault zone structure for strike-slip faults. A low-velocity fault zone embedded in the surrounding medium has been identified, which is likely due to repeated damage by historic events on fault. The recent 3D dynamic rupture models incorporating pressure-dependent off-fault yielding have confirmed the 'flower-like' fault zone structure (e.g., Ben-Zion et al., 2003; Rockwell and Ben-Zion, 2007; Cochran et al., 2009) and widespread near-surface inelastic response (e.g., Schaff and Beroza, 2004). The fault zone structure for dipping faults, however, has received much less attention. Very few fault-zone trapped wave studies have been carried out for dipping fault and few theoretical studies have investigated the inelastic off-fault response for dipping faults and explored the distribution of rupture-induced irrecoverable deformation. Here, Ma et al. explore the distribution of inelastic strain induced by rupture propagation on a 30° reverse fault and a 60° normal fault by simulating 2D inelastic dynamic ruptures with a Mohr-Coulomb yield criterion.

Ma (2009) explored the distribution of inelastic strain for reverse and normal faults (Figure 11). For the reverse fault, the hanging wall and footwall is in the compressional and extensional regime of rupture propagation, respectively. The inelastic strain is seen in the footwall only at depth (below approximately 1.2 km depth). In the upper 1.2 km the inelastic zone broadens dramatically in both the hanging wall and footwall due to a smaller confining pressure. This leads to the formation of a highly skewed 'flower-like' structure bounded at the top by the free surface. The inelastic strain is larger and broader in the hanging wall than the footwall even though the hanging wall is in the compressional regime.

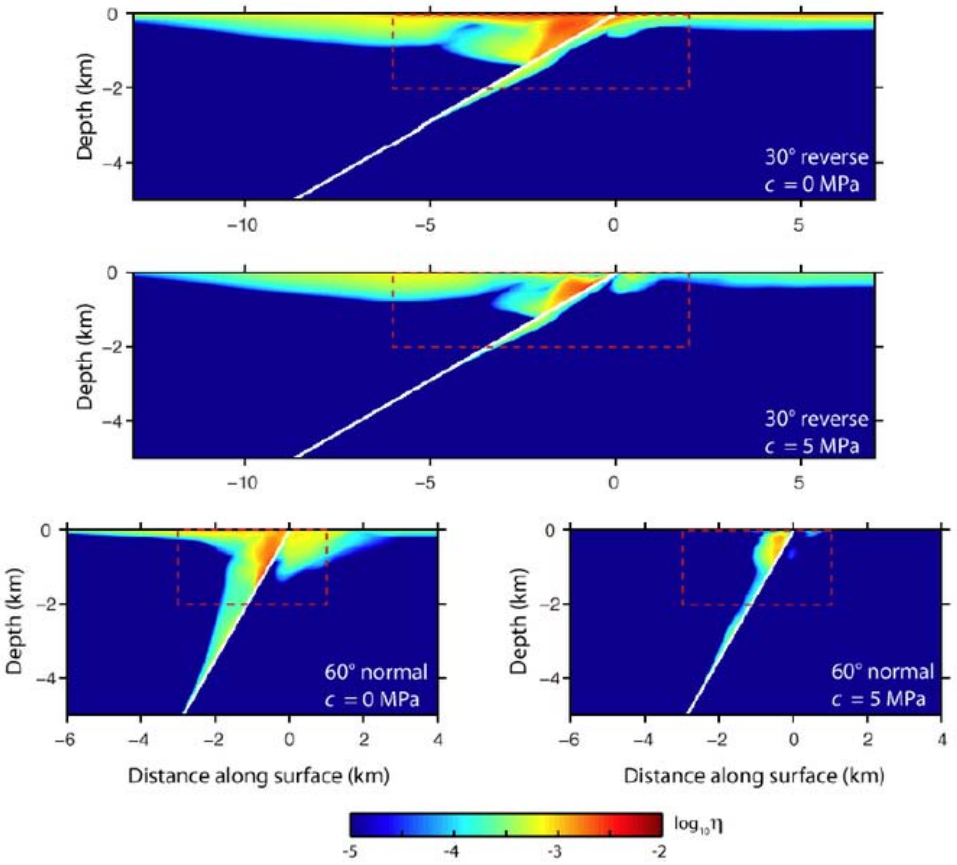

Figure 11. The inelastic strain η is mapped using a logarithmic scale. The inelastic zone widens as it moves up dip, forming a skewed 'flower-like' structure bounded at the top by the free surface. The 'flower-like' structure for the 30° reverse fault is more skewed than the 60° normal fault due to a smaller fault dip. The inelastic zone is larger with higher inelastic strain on the hanging wall than the footwall.

Distribution of Non-Volcanic Tremor Near Anza, California

Cochran and Wang examined surface and borehole seismic data from the region around Anza, California to begin searching for ambient and triggered tremor along the San Jacinto Fault near Anza, California. This region was chosen because there is a dense seismic network and tremor had been previously observed during the passage of the surface waves from the 2002 Denali earthquake. The stations were part of the Anza (AZ) network, the CISN network (CI), and the PBO network (PB). Initial data analysis included orientating the borehole stations and creating an Antelope database of the continuous waveforms.

Data from 2001 to 2008 was examined for tremor triggered by surface waves from teleseismic earthquakes near the Anza gap section of the San Jacinto Fault. Forty-one large earthquakes with magnitudes equal or greater than 7.5 and at a range of back-azimuths were examined. Because of the relatively small amount of data the search was done manually to ensure no episodes of tremor were missed. They found that only the Denali earthquake had triggered tremor (Figure 12), but did find a number of local earthquakes occurred during the passing surface waves of many of the events. Analysis of the fault parallel, fault perpendicular, and vertical teleseismic surface wave amplitudes indicated that Denali earthquake had the highest surface wave amplitude compared to the 40 other events. The period around peak amplitude of Denali surface wave lies within the average of 40 other teleseismic events and is not significantly different.

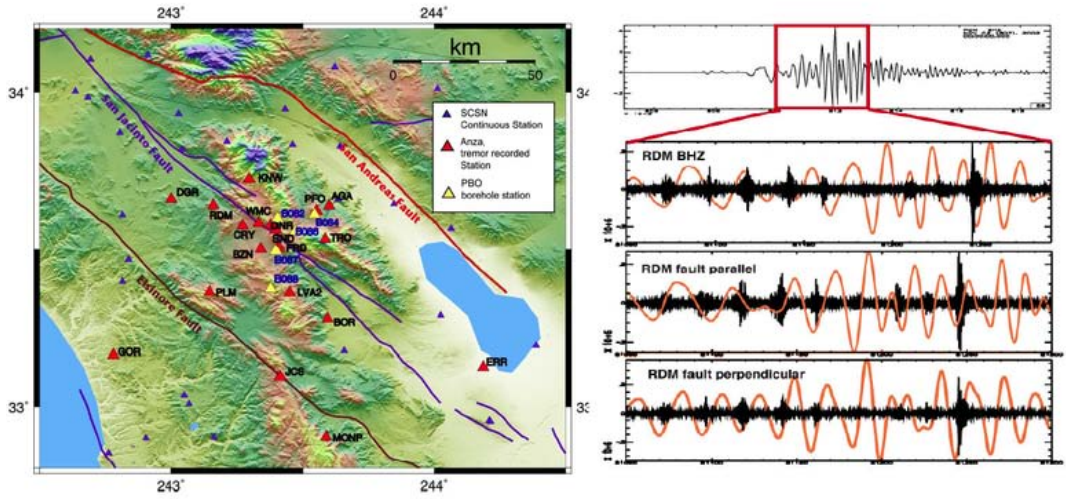

Figure 12. (Left) Map of SCSN and borehole seismic stations (red, blue and yellow triangles, respectively). Selected stations used in constrained tremor detection is shown as red and yellow triangles. (Right)Waveform examples of Denali tremor on station RDM that is triggered by the passing surface waves of the Denali earthquake. The upper panel shows the Denali earthquake recorded on the vertical component of RDM. The region that is expanded in the lower panels is highlighted in red. The lower panels span 250 seconds and show all three components (vertical, fault parallel, and fault perpendicular). The orange curves show the surface waves of the earthquake in nm/sec and the black curves show the data filtered between 2-8 Hz (amplitude is exaggerated by 20,000).

Systematic Analysis of Non-Volcanic Tremor in Southern California

A systematic analysis of non-volcanic tremor in southern California could provide important new information on the fault mechanics on the deep extension of the crustal faults and may shed new light on the predictability of large earthquakes. Zhigang Peng and his colleagues studied 30 large teleseismic events with Mw ≥ 7.5 since 2001, and found that only the 2002 Mw7.8 Denali Fault earthquake triggered tremor in all these regions, including the San Gabriel Mountain (SGM) where neither triggered nor ambient tremor has been observed before. These results suggest a relative lack of widespread triggering in Northern and Southern California (Figure 13), which is in contrast with the finding of multiple events that triggered tremor in Central California, Japan, Cascadia, and Taiwan.

Recently, Aguiar et al. (2009) and Brown et al. (2009b) have detected several cases of triggered tremor by regional and teleseismic events around the SJF and the Calaveras fault based on the waveform matched filter technique (Brown et al., 2008, 2009a). The difference between their results and ours mainly lie in the fact that we are using visual inspection to detect triggered tremor. Hence, we may omit weak triggered tremor signals that are close or below the background noise levels. The tremor observed near the Calaveras fault and SJF appears to be initiated by Love waves, and becomes intensified during the large amplitude Rayleigh waves. The tremor triggered in Simi Valley and SGM only shows weak correlations with the Rayleigh waves. Peng's research group suggests that variability in the background tremor rate or different tremor triggering threshold could be the main cause of the different behaviors.

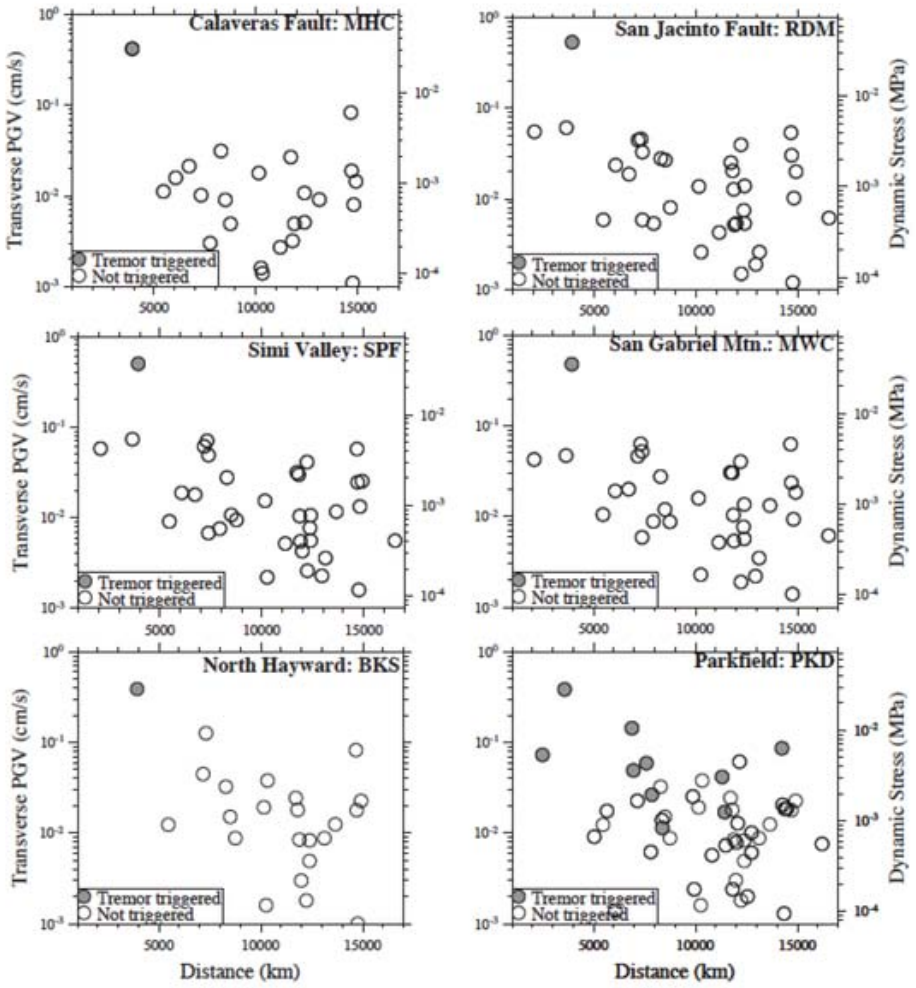

Figure 13. Peak ground velocities (left vertical axis) and related dynamic stresses (right vertical axis) for the transverse components measured at broadband stations in each studied region of California, plotted against the distance from the event to the station specified on plot label. Gray circles are events that caused tremor to be triggered in that area, open circles are events that did not trigger tremor.

Triggering Effect of the 2004 M6 Parkfield Earthquake on Earthquake Cycles of Small Repeating Events

A repeating earthquake sequence (RES) is a group of events that ruptures the same patch of fault repeatedly with nearly identical waveforms, locations, and magnitudes. The recurrence properties of RES are suggestive of a renewal process taking place on the repeatedly rupturing fault patches and thus provide crucial information about the nature of the earthquake cycle and the physics of earthquake rupture. After the 29 September 2004, M 6.0 Parkfield, California earthquake, a large number of postseismic repeats of small earthquakes are observed.

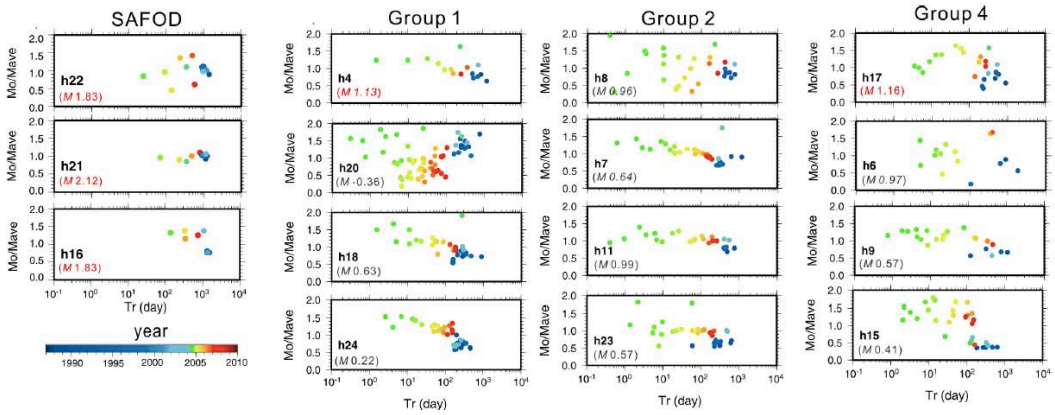

Figure 14. Relative moment as a function of recurrence interval for several groups of repeating earthquake sequences, color coded by the time of repeating events. Blue and green-to-red dots indicate pre- and post- Parkfield events, respectively.

Burgmann et al. analyze a subset of 34 M -0.4 ~ 2.1 repeating earthquake sequences (RES) from 1987-2009 at Parkfield to examine the variation of recurrence properties in space and time. Many of the repeating events strongly accelerated following the Parkfield earthquake with greatly reduced recurrence intervals (Tr) that increase systematically with time following Omori's law (Chen et al., 2010). They find systematic changes in seismic moment (Mo), where many sequences experienced an immediate increase in Mo and subsequent decay as Tr approaches pre-2004 durations (Figure 14). The RES at shallower depth tend to have a larger range in both Tr and Mo, whereas deeper RES shows small variation. These sequences reveal large variation in Tr but small variation in Mo. Earthquake simulations with rate- and state-dependent friction show that slip of velocity weakening asperities surrounded by a velocity strengthening fault is increasingly aseismic as the asperity patch size and loading rate decrease. These models predict that the degree of postseismic variation in Mo and Tr is a function of event size, consistent with the observation of decreasing Mo with increasing Tr for small RES. With a smaller percentage of aseismic slip during rupture, a small asperity appears to grow in Mo under high loading rate, which is contrary to the view that Mo should decrease due to a reduced healing time.

Towards Strong Ground Motion Prediction Using Amplitude Information from the Ambient Seismic Field

Beroza et al. use the ambient seismic field for several aspects of ground motion prediction, including: validation of the ambient-field response against moderate earthquakes, developing a library of Green's functions for improving southern California velocity models, and developing a preliminary attenuation model for the southern California crust. The approach was validated by comparing the amplification effects in sedimentary basins using several well-recorded earthquakes and the ambient seismic field. They use the inter-station complex coherence derived through deconvolution and stacking to extend the analysis that we performed previously for Rayleigh waves on vertical components (Prieto et al., 2009) to all three components, and hence to Love waves. They are currently refining a library of Green's functions to refine crustal wavespeed models in southern California. In addition, they observed some paths with strong sensitivity to sedimentary basins and developed a preliminary laterally varying model of attenuation by quantifying these observations (Figure 15).

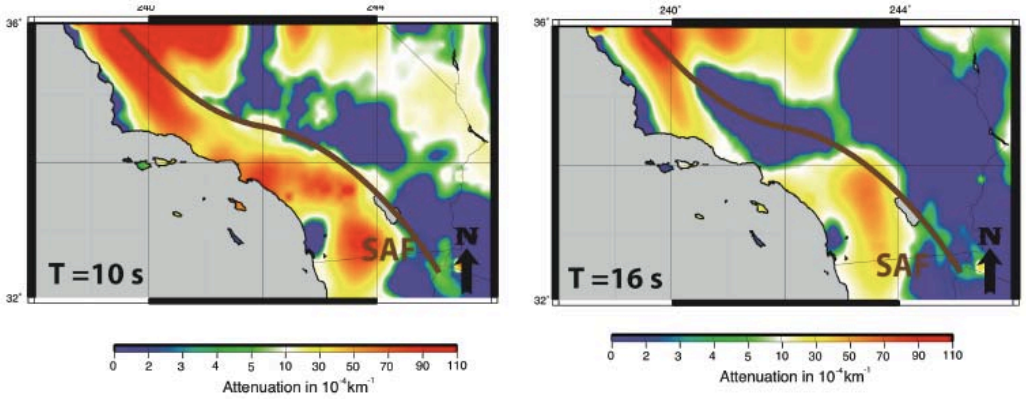

Figure 15. Preliminary maps of attenuation based on analysis of ambient noise vertical component data at periods of T =10 and T=16s.

Using Seismic Noise for the Purpose of Improving Shallow S-Wave Velocity Models

Seismic noise provides important information for shallow S-wave velocity structure. Some parts of noise consist of high-frequency Rayleigh waves (0.1-0.4 Hz) whose properties are sensitive only to shallow depths and thus contamination from deep structure can be avoided without any problems. For the determination of shallow structure, this is an advantage over approaches based on body waves because use of body waves inherently leads to trade-offs between shallow and deep structure.

Tanimoto et al. are combining two analysis methods for seismic noise in order to improve shallow S-wave velocity structure in Southern California: the first is the noise correlation method, which yields Rayleigh-wave phase velocity maps for frequencies 0.1-0.2 Hz. The other is the Z/H method (H/V) for 0.1-0.4 Hz which is particularly useful for constraining even shallower structure. By performing a joint inversion the aim is to obtain an improved, detailed structure for the upper crust (depth 0-10 km). A merit of inverting the two types of data is that depth ranges of sensitivity for phase velocity and ZH ratios complement each other and both are essential to determine S-wave velocity structure in the crust. The S-wave velocity maps at shallow depths show reduced velocities in the Los Angeles Basin and along the Newport-Inglewood fault (Figure 16).

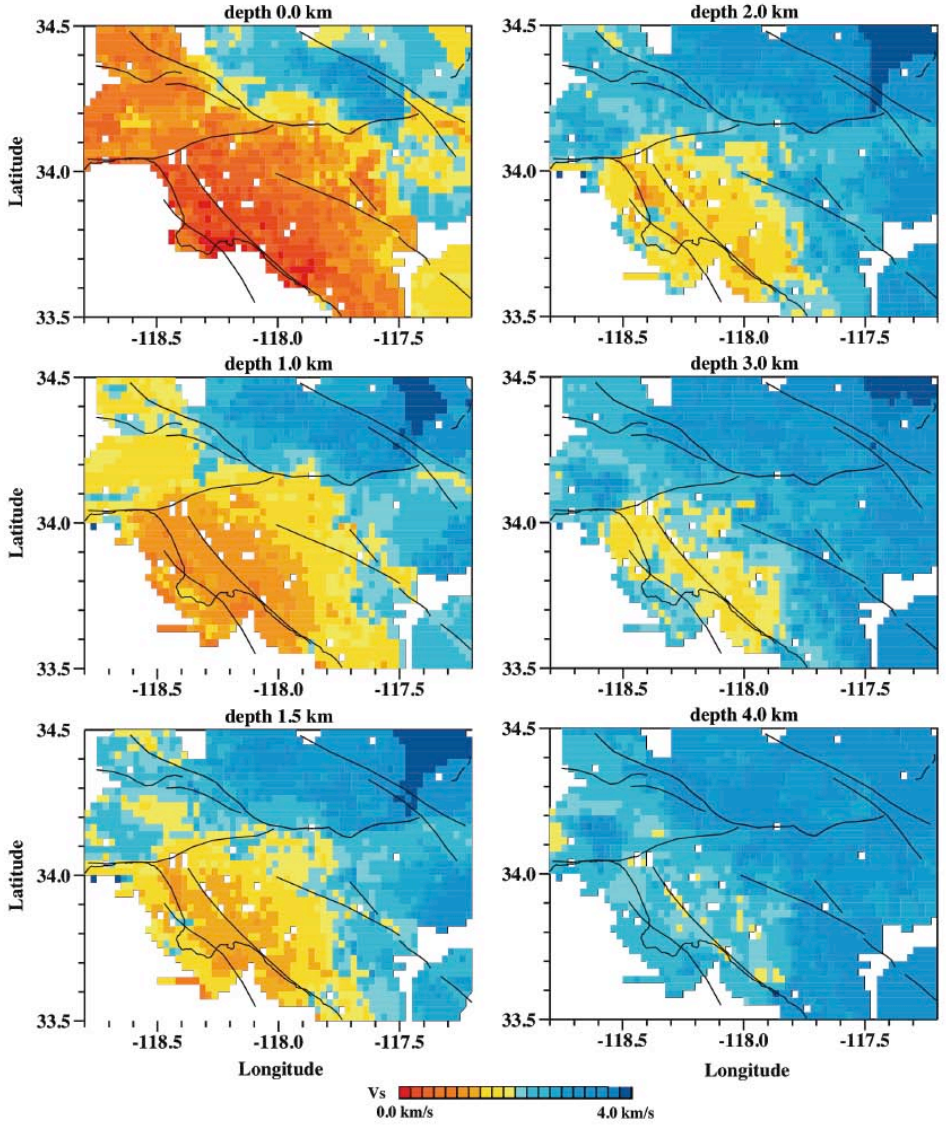

Figure 16. Preliminary results for the seismic noise joint inversion. Slow S-wave velocity in the basin is obvious. In particular, a prominent low-velocity anomaly can be seen along the Newport-Inglewood fault.

What can we learn about the greater Los Angeles Basin from the 2008 July 29 Mw5.4 Chino Hills Earthquake

Lin et al. developed three-dimensional P- and S-wave velocity models for the 2008 Mw5.4 Chino-Hills earthquake region in the greater Los Angeles basin, southern California by using the double-difference tomography algorithm (Zhang and Thurber, 2003). A checkerboard resolution test is used to assess the robustness of the model. They obtain first-arrivals for all local events in the study area from the Southern California Seismic Network (SCSN) and select 2870 events above magnitude 1.0 with more than 8 P and 2 S picks as the master events for the seismic tomographic inversion. In order to improve resolution in the seismically active areas where the differential data provide dense sampling, they also include catalog differential times and assembled P arrival times for 15 active-source data (from the Los Angeles Regional Seismic Experiment (LARSE, Murphy et

al., 1996; Fuis et al., 2001b) in order to constrain absolute event location and shallow crustal structure. They start with a one-dimensional (1D) velocity model derived from the layer-average values of the 3D CVM-H model to solve for new Vp and Vs models.

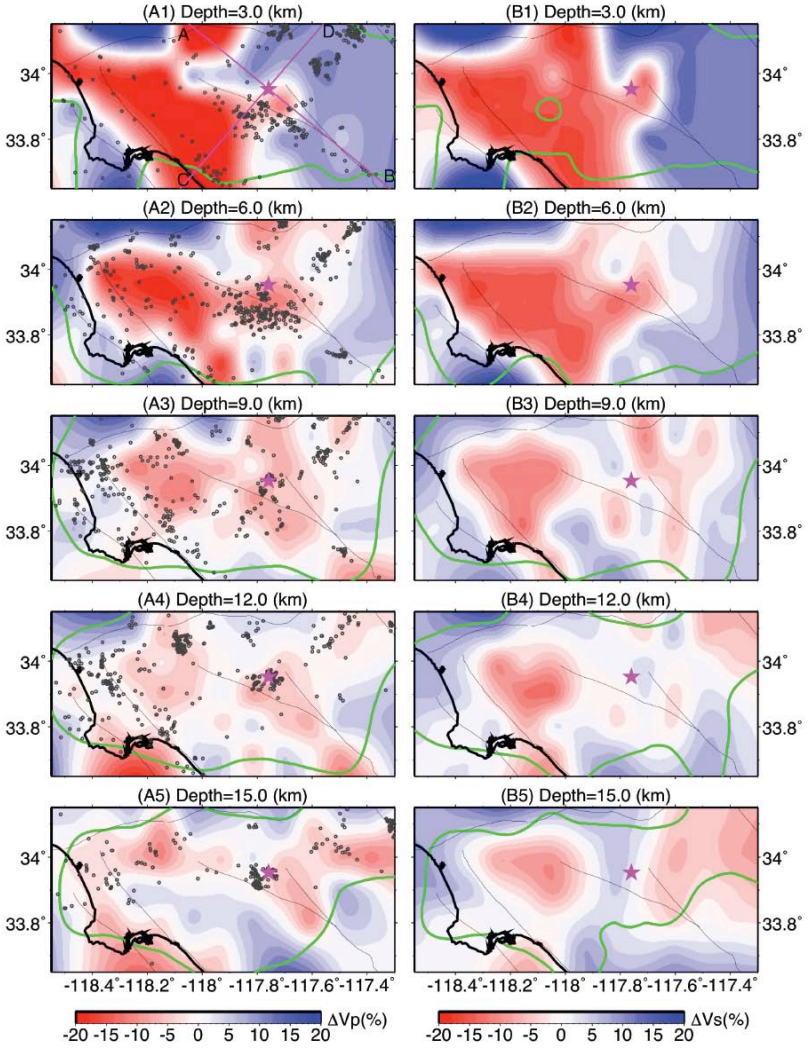

Figure 17. Map views of velocity perturbations relative to layer average at different depth slices. (A1)-(A6): Vp model; (B1)-(B6): Vs model. Black lines denote coastline and surface traces of mapped faults. Black dots represent relocated earthquakes, pink star epicenter of the 2008 Chino earthquake. The green contours enclose the well-resolved area.

The new P and S-wave velocity models, determined from both absolute and differential times, shows strong velocity contrasts around the 2008 Chino Hills mainshock. Figure 17 shows the map view slices of the P-velocity model at different depth slices between 3 and 15 km. The most significant difference between Lin et al.'s model and the CVM-H model is a local velocity contrast around the 2008 mainshock area. The CVM-H model shows a high velocity anomaly starting at 9 km depth from north near the junction between the Hollywood Fault and the Sierra Madre fault zone to the southern section of the Newport-Inglewood Fault. This anomaly cuts the northwest end point of the Whittier Fault, leaving the 2008 earthquake area relatively smooth. Similar high velocity anomalies are also seen in the Lin et al. model, but start at the deeper layer of 12 km,

extending toward the east side and stopping at the location of the 2008 Mw 5.4 Chino Hills mainshock.

References

Aguiar, A. C., J. R. Brown, and G. C. Beroza, Non-volcanic tremor near the Calaveras Fault Triggered by Mw~8 Teleseisms, Eos Trans. AGU, 90(54), Fall Meet. Suppl., Abstract T23E-06, 2009.

Bailey, I. W., Y Ben-Zion, T. W. Becker and M. Holschneider, Quantifying focal mechanism heterogeneity for fault zones in Southern and Central California, Geophys. J. Int., in review, 2010.

Ben-Zion, Y., Z. Peng, D. Okaya, L. Seeber, L. G. Armbruster, N. Ozer, A. J. Michael, S. Baris and M. Aktar, A shallow fault zone structure illuminated by trapped waves in the Karadere-Duzce branch of the North Anatolian fault, western Turkey, Geophys. J. Int., 152, 699–717, doi:10.1046/j.1365-246X.2003.01870.x, 2003.

Brown, J. R., G. C. Beroza, and D. R. Shelly, An autocorrelation method to detect low frequency earthquakes within tremor, Geophys. Res. Lett., 35, L16305, doi:10.1029/2008GL034560, 2008.

Brown, J. R., G. C. Beroza, S. Ide, K. Ohta, D. R. Shelly, S. Y. Schwartz, W. Rabbel, M. Thorwart, and H. Kao, Deep low frequency earthquakes in tremor localize to the plate interface in multiple subduction zones, Geophys. Res. Lett., 36, L19306, doi:10.1029/2009GL040027, 2009a.

Brown, J. R., A. C. Aguiar, and G. C. Beroza, Triggered tremor on the San Jacinto Fault from the 3 August 2009 Mw6.9 Gulf of California earthquake, 2009 SCEC Annual Meeting abstract, 242, 2009b.

Chen, K. H., Bürgmann, R., and Nadeau, R. M., Triggering effect of M 4-5 earthquakes on the earthquake cycle of repeating events at Parkfield, Bull. Seism. Soc. Am., 100, 2, doi:10.1785/0120080369, in proof, 2010.

Cochran, E. S., Y-G Li, P. M. Shearer, S. Barbot, Y. Fialko, and J. E. Vidale, Seismic and Geodetic evidence for extensive, long-lived fault damage zones, Geology, 37, 315-318, doi: 10.1130/G25306A.1, 2009.

Enescu, B., S. Hainzl and Y. Ben-Zion, Correlations of Seismicity Patterns in Southern California with Surface Heat Flow Data, Bull. Seism, Soc. Am., 99, 3114-3123, doi: 10.1785/0120080038, 2009.

Felzer, K.R., and E.E. Brodsky, Decay of aftershock density with distance indicates triggering by dynamic stress, Nature, 441, doi: 10.1038/nature04799, 2006.

Hardebeck, J.L. and P.M. Shearer, A new method for determining first-motion focal mechanisms, Bull. Seismol. Soc. Am, 92, 2264–2276, 2002.

Hardebeck, J.L. and P.M. Shearer, Using S/P amplitude ratios to constrain the focal mechanisms of small earthquakes, Bull. Seismol. Soc. Am., 93, 2434–2444, 2003.

Helmstetter, A., and D. Sornette, Diffusion of epicenters of earthquake aftershocks, Omori's law, and generalized continuous random walk models, Phys. Rev. E., 66, 061104, 2002.

Ma, S., Distinct asymmetry in rupture-induced inelastic strain across dipping faulting: An off-fault yielding model, Geophys. Res. Lett., 36, L20317, doi:10.1029/2009GL040666, 2009.

Ogata, Y., Seismicity analysis through point-process modeling: a review, Pure Appl. Geophys., 155, 471–507, 1999.

Prieto, G. A., J. F. Lawrence, G. C. Beroza, Anelastic Earth Structure from the Coherency of the Ambient Seismic Field, J. Geophys. Res., 114, B07202, doi:10.1029/2008JB006067, 2009a.

Rockwell T. K., Y. Ben-Zion, High localization of primary slip zones in large earthquakes from paleoseismic trenches: Observations and implications for earthquake physics, J. Geophys. Res., 112, B10304, doi:10.1029/2006JB004764, 2007.

Schaff, D. P., G. C. Beroza, Coseismic and postseismic velocity changes measured by repeating earthquakes, J. Geophys. Res., 109, B10302, doi:10.1029/2004JB003011, 2004.

Shearer, P. M., and G. Lin, Evidence for Mogi doughnut behavior in seismicity preceding small earthquakes in southern California, J. Geophys. Res., 114, doi: 10.1029/2009JB005982, 2009.

Wechsler, N., Y. Ben-Zion and S. Christofferson, Evolving Geometrical Heterogeneities of Fault Trace Data, Geophys. J. Int., in review, 2010.

Zaliapin, I. and Y. Ben-Zion, Asymmetric distribution of early aftershocks on large faults in California, Geophys. J. Int., in review, 2010.

Tectonic Geodesy

Transient Detection

The transient detection exercise supported through most of SCEC 3 has the goal of identifying promising algorithms for the detection of temporal fluctuations in the geodetically measured strain field. This effort began with a short workshop in the summer of 2008, and has continued with an exercise involving the analysis of synthetic data by a number of groups pursuing a wide range of detection strategies. A second workshop, where participants presented methodologies and results, was held at the SCEC annual meeting in September, 2009.

Part of the effort involved funding for Duncan Agnew to generate realistic synthetic data sets, a process that has evolved over the course of the three test phases to date, as participants request progressively more sophisticated synthetic data. The most recent iteration of the freely available code for generating this data (FAKENET), includes secular velocities, data gaps, white, flicker and random-walk noise, common-mode seasonal noise dependent on the distance between stations, and tectonic transients that have temporal and spatial variability (i.e., that can propagate along the fault).

All groups detected the transients in Phase I and Phase II group A when the signal was large and had a short timespan relative to the length of the time series. One category of approaches encompasses those involving only characteristics of the signal, such as principle component or multi-trend time series analysis (Ji and Herring, Kreemer and Zaliapin) and the use of wavelets to model spatially or temporally coherent patterns in displacement data (McGuire and Segall, Simons and Zhan). Another category requires some model of the physics driving ground deformation (e.g., Meade, Segall et al.).

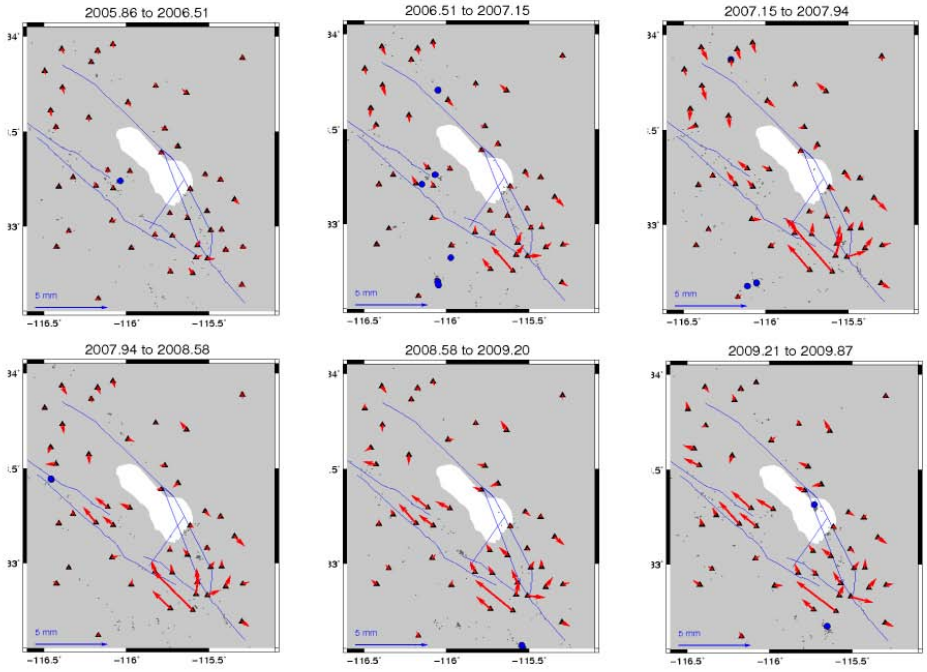

Figure 18. Transient displacement field detected by the Network Strain Filter from 2006-2009 using SCIGN+PBO data.

Advances for this year include McGuire and Segall's application of their Network Strain Filter, which now includes regularization, to real data (Figure 18). They detect several-month-long signals along the Superstition Hills and San Jacinto faults, as well as 1-2 mm offsets associated (but not co-located) with the 2009 Bombay Beach earthquake swarm and the 2008 Cerro Prieto earthquake swarm. In addition to the Network Strain Filter, Segall et al. further developed two other approaches to identify transients. The first detects changes in the time-variable fault slip estimated using a Kalman filtering approach (the Network Inversion Filter). The second uses a Monte Carlo Mixture Kalman Filter (MCMKF) and identifies transients at times when the size of the random walk parameter controlling fault slip exceeds a threshold to a statistically significant degree. Meade developed an alternative to the computationally expensive MCMKF, named the Covariance Candidate Filter, which tracks the statistical behavior of particles rather than having to store the exact behavior of each particle as it runs through the filter. Simons and Zhan extended earlier work to develop an event detector based on detection of transient signals in time series followed by multi-scale wavelet analysis of the transient trends to identify spatially-coherent signals. Herring and Ji continued work on an approach which applies principal component analysis to time series from which trends and seasonal terms have been removed using a first-order Gauss-Markov smoothing algorithm. Kreemer and Zaliapin focused on refinements to their multi-trend analysis detection algorithm.

Other groups have explored facets of the problem of detecting transients with geodetic data without participating in the official exercise. Thurber and colleagues developed a workflow for inverting for slip on faults and identifying whether the error bounds on the signal were larger than the data noise, and applied their approach to data spanning postseismic deformation associated with the 2004 Parkfield earthquake. Lohman worked on developing a synthetic test that would assess whether the addition of InSAR observations from a dense temporal stack of SAR imagery can improve Kalman Filter-based analyses of continuous GPS data.

The next phase of work involves the use of a more realistic synthetic data set and real data provided by Tom Herring. Some effort was put into making it not immediately obvious which of the test datasets used real vs. synthetic data, although it is likely that most of the groups were able to figure out which was which. The results will be unveiled at the SCEC annual meeting in September 2010.

A related effort involved the generation of GPS time series products that merge all of the available data from PBO and SCIGN under a uniform processing scheme. This is of key importance to the ultimate goal of the transient detection exercise, which involves implementing a transient detector on real data.

Acquisition and Interpretation of New Data

Shen et al. completed the compilation of a new velocity field which they have named the Southwest US Crustal Motion Map version 1.0 (SWUS CMM1) (Figure 19). This data product covers an area spanning from 31° to 44°N and 114°-125°W and includes all survey-mode GPS data collected between December 1986 and March 2009. These data were reprocessed and the solutions merged with the SOPAC solutions for continuous GPS sites in this region. Velocities were estimated using a Kalman filter and accounting for the effects of major earthquakes.

Fialko and colleagues expanded the spatial and temporal coverage of their analysis of SAR data for the Coachella Valley-San Bernardino-Mojave segments of the southern San Andreas Fault and Eastern California Shear Zone. By stacking the data to reduce atmospheric noise they have produced line-of-site time series useful for studying secular deformation. Using these data they have estimated the rate and depth-extent of creep on the Superstition Hills Fault and observed a slow slip event that occurred there in 2006.

The Tectonic Geodesy group participated actively in the SCEC response to the El Mayor-Cucapah earthquake of April 4, 2010, helping to coordinated geodetic data collection conducted by several groups. A number of PIs are currently conducting investigations related to this earthquake as noted below.

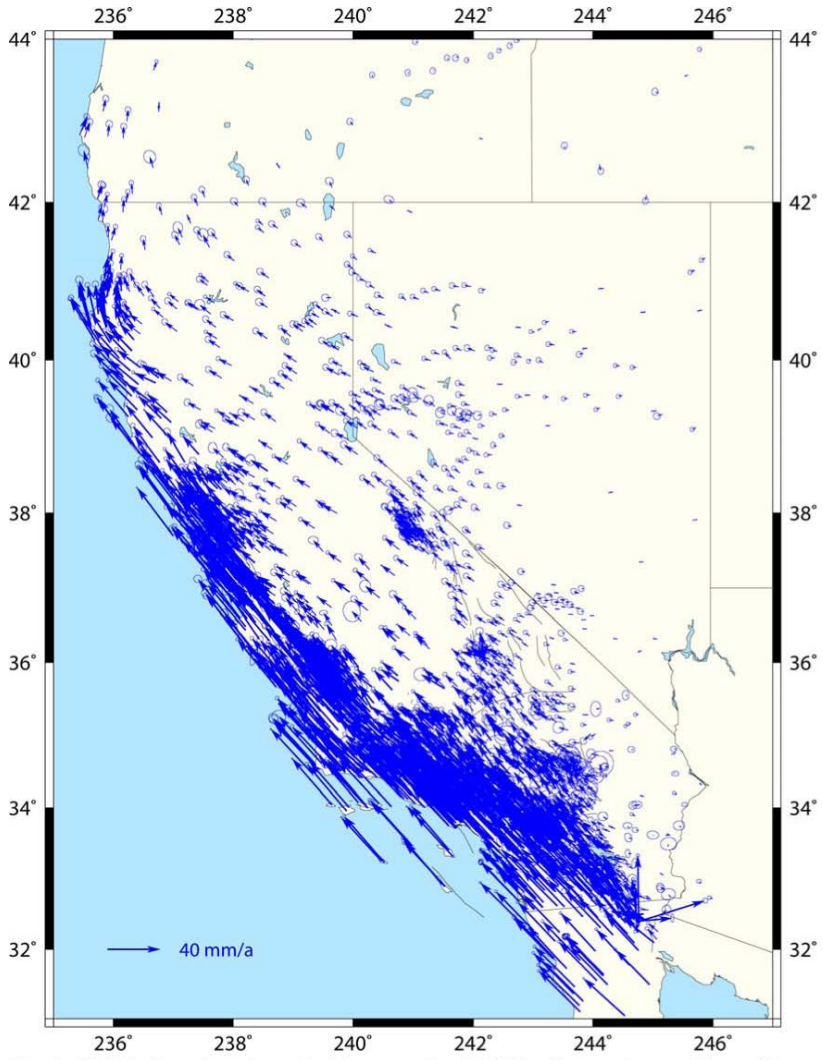

Figure 19. Crustal Motion Map. GPS horizontal station velocities with respect to the SNARF reference frame. Error ellipses represent 95% confidence.

This year, SCEC continued support of the strainmeters at Piñon Flat observatory. 2009 proved to be an interesting year with a long-term fluctuation across the three strainmeters that may be consistent with slip on the San Jacinto fault. The laser and borehole strainmeters also captured offsets (on the BSMs) and dynamic strains from the El Mayor-Cucapah earthquake.

Data from the B4 lidar project received additional attention this year, with Lynch, Hudnut and Bevis combining field projects with use of the lidar data set, and Oskin, Cowgill and Kreylos developing a tool that identifies fault offsets with cross-correlation approaches. They are currently applying their approach to data spanning the El Mayor-Cucapah earthquake in Baja California.

Sandwell and colleagues are continuing their campaign surveys of geodetic benchmarks within the Imperial Valley, exploring both the deformation associated with the 2008 seismic swarm at Obsidian Buttes, and new monuments across the Imperial fault near Mexicali. They also responded to the El Mayor-Cucapah earthquake.

Modeling of Deformation (Crustal and Uppermost Mantle)

SCEC continued support of the summer workshop on numerical modeling of crustal deformation. The workshop includes two days of intensive tutorials on meshing packages and numerical modeling approaches, followed by three days of scientific talks, which help motivate discussions of where the modeling efforts should focus in the future. SCEC also funded several studies that explore what models of ground deformation can tell us about the relative importance of various driving forces, why fault slip rates inferred from geodetic data are often significantly different from geologically-constrained rates, and how geodetic data can be used more fully in hazard assessments such as UCERF3.

Becker and colleagues developed visco-plastic, 3D models for regional deformation modeling that incorporate the effects of gravitational potential energy and buoyancy forces due to density variations, viscous flow in the lower crust and uppermost mantle and edge driving forces. Their work explores whether regions such as the Transverse Ranges would be expected to be under tension or compression in various regimes where they vary the strength of surrounding fault zones and compare buoyancy forces due to crustal and mantle topography with those expected from mantle flow. They find that mantle flow is a secondary effect given the range of parameters examined in their study.

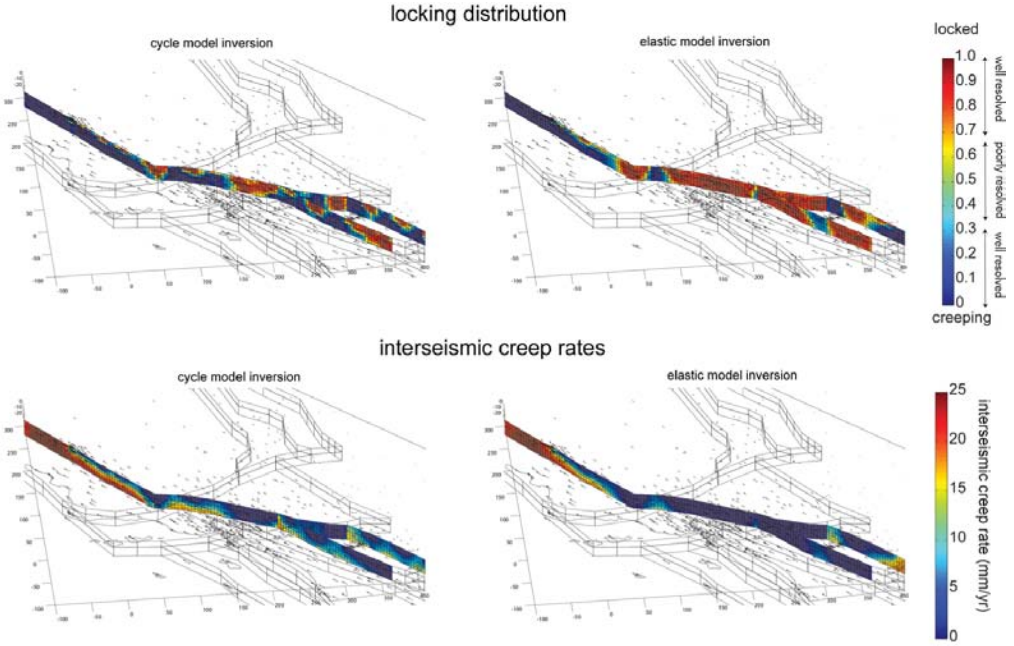

Figure 20. Distribution of locked and creeping patches and interseismic creep rates for viscoelastic cycle model and elastic half space model. Locking/creeping values and interseismic creep rates are the mean values from many thousands of Monte Carlo samples.

Johnson and Chuang explore a similar question and assess the impact of ignoring mantle flow on block models based on geodetic data. Their model with an elastic crust overlying a Maxwell viscoelastic lower crust and mantle does a good job of reproducing fault slip rates that are compatible with geologic estimates. They also find that the elastic-only models typically predict deeper locking depths than their viscoelastic model (Figure 20).

Smith-Konter and colleagues validated their stress accumulation model, both by compiling a more complete archive of slip models, and comparing their fault geometry to other data sets. They are also preparing for efforts to combine GPS and InSAR observations.

Charles Williams applied the Pylith finite element code to a 3000-year history of simulated earthquakes, after improving the computational efficiency of the code to the point where such an exercise became feasible. He has now compared the response of heterogeneous and homogeneous elastic and Maxwell viscoelastic spaces using the SCEC community velocity and fault models when appropriate. They identify regions where the geodetic velocities would differ significantly for ten years or more after an 1857 event, depending on the constitutive properties applied during their modeling.

Steven Ward continued development of methods for including geodetic data in earthquake simulators by developing the software infrastructure for, and conducting a joint inversion of, geodetic and geological data.

Earthquake Geology

The SCEC geology disciplinary group coordinates diverse field-based investigations of the Southern California natural laboratory. The majority of Geology research accomplishments fall under two categories: (1) focused studies of the southern San Andreas and San Jacinto faults in coordination with the SoSAFE (Southern San Andreas Fault Evaluation) special project; and (2) studies of other portions of the southern California fault network aimed at a better understanding fault system behavior. Geology also continues efforts to characterize outstanding seismic hazards to the urban region, and supports field observations related to several focus-group activities (e.g., USR, WGCEP, FARM, GMP, LAD, CDM). Additional goals include longer-term slip rates and deep-time, multi-event paleoseismologic records that have a high impact on seismic hazard assessments. In support to these efforts the Geology group coordinates geochronology infrastructure resources that are shared among various SCEC-sponsored projects.

Southern San Andreas Fault Evaluation (SoSAFE)

The primary goal of the Southern San Andreas Fault Evaluation (SoSAFE) project is to document the timing of large paleoearthquakes and amount of slip released by the southern San Andreas and San Jacinto faults over the past 2000 years. Additional goals include examination of longer-term slip rates and modeling studies that directly impact seismic hazard assessments. SoSAFE is funded by SCEC, leveraging funding from the USGS Multi-hazards Demonstration Project. Research includes earthquake trenching studies, radiocarbon dating supported through the geochronology infrastructure funding, geomorphic studies using lidar and other aerial imagery data in tandem with field measurements, and examination of new methods for analyzing and incorporating neotectonic data. A workshop, led by Kate Scharer and Tom Rockwell, highlighting the 2008-2009 accomplishments was held during the SCEC Annual Meeting in September, 2009 and attracted ~125 attendees. The workshop ended with a discussion aimed at generating new ideas for integrating paleoseismic data along the fault and use of such models in formal earthquake hazard assessments (e.g. UCERF).

SCEC researchers made significant advances at several sites along the northern San Jacinto Fault in 2009 and 2010. Intriguing new results from trenches excavated Nate Onderdonk and Rockwell across an ephemeral sag at Mystic Lake revealed six paleoearthquakes on the Claremont fault since ~300 A.D. Three of these events are of similar age to earthquakes documented at the Hog Lake site, raising the possibility of fault interaction between the Claremont and the Clark fault. At the Quincy site, Sally McGill and Onderdonk excavated an offset paleo-channel that provides a new slip rate of 9.5 to 23 mm/yr; the preferred offset of 17+/-2 mm/yr is consistent with the displacement of five nearby channels. Two additional offset landslides have been mapped and upcoming 10Be dating should provide slip rates for this part of the fault.

Farther south, on the Clark strand of the San Jacinto fault, field and B4 lidar measurements of 55 offset features reveal the slip distribution of past ruptures to the north and south of Anza. These measurements suggest that the Clark fault experiences average displacements of ~3 m, and may have generated the 1918 M6.9 earthquake. A study of longer-term slip rate variability along the Clark fault based on 10Be and U-series dating of offset alluvial fans shows decreasing slip on the Clark fault towards its southern end, and a sum rate of slip on the Clark and Coyote Creek faults of

10 to 14 mm/yr (Blisniuk et al., 2010). Work in progress on the Clark fault suggests that its late Holocene slip rate may be faster than the average Pleistocene rate. Similar temporal variations on the Coyote Creek fault suggest that both faults have experienced a concomitant change in the loading rate at depth.

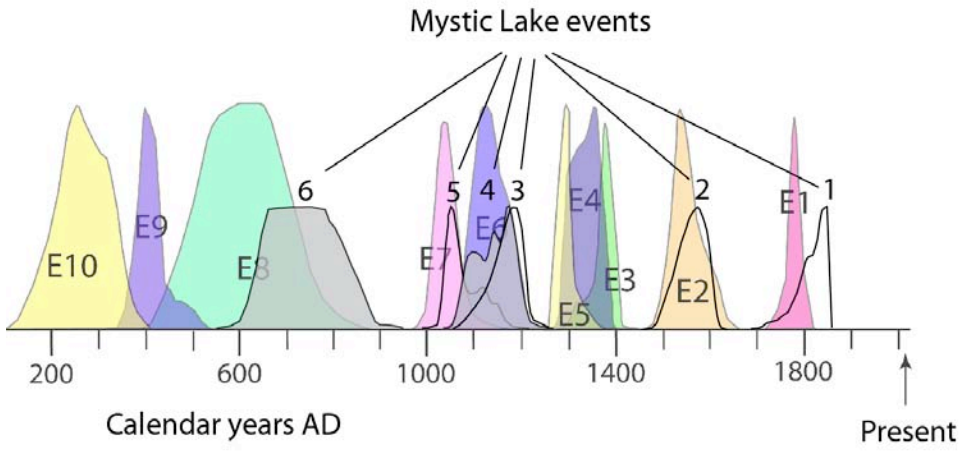

Figure 21. This figure compares the earthquake rupture record from Mystic Lake and Hog Lake along the San Jacinto fault (SJF). The two sites are separated by the Hemet Step-over, a several km-wide releasing step that has been attributed as the segmentation point along the northern SJF, with the Clairemont strand to the NW and the Casa Loma-Clark strand to the SE. In other words, the Hemet Step-over has been interpreted as the likely structural barrier to rupture that segments the central and northern SJF zone. The new Mystic Lake observations suggest that, for the past 1200-1500 years, as many as five earthquakes may have ruptured through the step, whereas at least four did not. These new data suggest that the entire central and northern SJF may rupture together in some events, resulting in a surface rupture of as much as 175 km. Combined with the new B4 LiDAR observations of displacement per event along the Clark fault, which suggest 3-4 m of slip per event, these new data suggest that earthquakes as large as Mw7.5 have occurred along the north-central SJF during the late Holocene.

Several SoSAFE research projects on the San Andreas fault were published this year. For example, a study to examine recurrence patterns showed that the published Wrightwood series is statistically more periodic than would be expected to arise from a random (Poisson) series (Scharer et al., 2010). A new study using AMS-derived radiocarbon dates from the Pallett Creek site showed a similar coefficient of variation (0.68), suggesting that the Mojave section of the fault is weakly time-dependent and not clustered; this paper will be submitted in the fall of 2010. Three important papers on fault offsets and earthquake ages in the Carrizo Plain were published (Akciz et al., 2010; Grant Ludwig et al., 2010, and Zielke et al., 2010) and have generated significant discussion and renewed interest in this section of the fault. Collectively, these results have significantly revised our understanding of the behavior of this key portion of the San Andreas, suggesting that great earthquakes on this part of the fault may be more frequent, and generate less surface slip, than had been thought previously.

Fault System Behavior

The second major emphasis of the Geology group has been to characterize patterns in fault system behavior that could significantly affect earthquake hazards. As a part of this effort, SCEC researchers continue to tease out the record of long-term earthquake clustering in southern California. The eastern California shear zone and the conjugate Garlock fault offer the most compelling examples of clustered earthquake behavior and its potential relationship to anomalously elevated fault loading (Dolan et al., 2007; Oskin et al., 2008; McGill et al., 2009; Ganev

et al., 2010). New work by James Dolan and Eric Kirby on the Panamint Valley fault, a dextral-normal fault that lies just to the north of the Garlock fault, suggests that it has ruptured twice in the last ~1000 years, concurrent with the well-documented cluster of activity on dextral faults in the Mojave Desert (Rockwell et al., 2000). The antepenultimate event occurred 3,300-3,700 years age, during a quiescent period in the Mojave. This event, however, overlaps with the age of the penultimate earthquake on the Owens Valley fault, though the paleoseismologic record on dextral faults north of the Garlock fault is not yet sufficient to address possible clustering isolated to this section of the eastern California shear zone.

As this report is being written, high-resolution seismic reflection data are being acquired by Dolan, John Shaw, and Tom Pratt across the zone of most recent folding above the Ventura Avenue anticline, as well as the blind western strand of the San Cayetano fault. These data will provide targets for borehole and potential trench studies to determine Holocene-Pleistocene slip rates, slip-per-event, and earthquake age data. These observations will be critical for testing the possibility that these large thrust-fault ramps can sometimes connect together to produce great (M~8) earthquakes beneath the central and western Transverse Ranges.

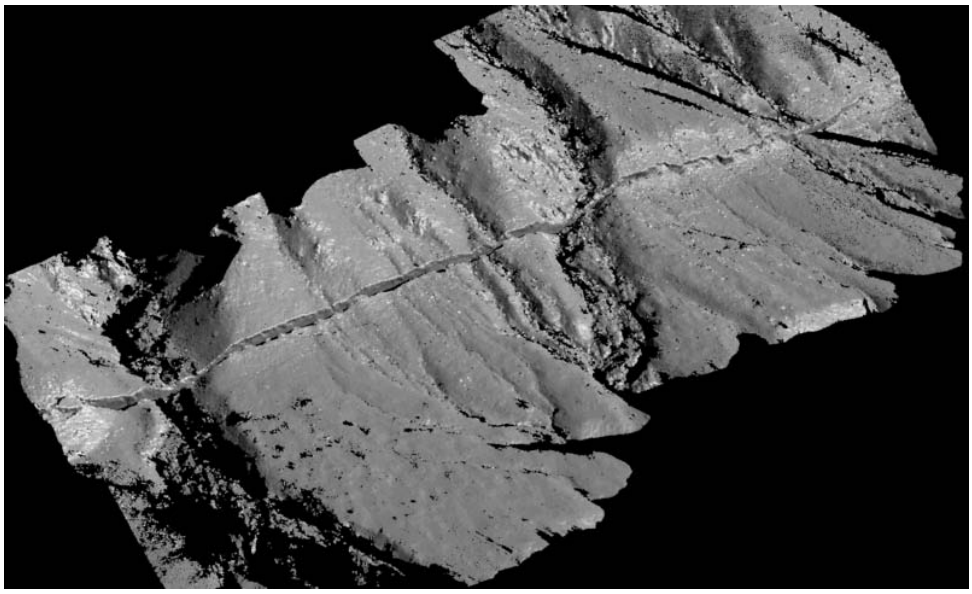

Figure 22. Oblique view of an ultra high-resolution terrestrial lidar scan of a 250 meter-long section of the Borrego fault rupture formed during the 4 April 2010 El Mayor-Cucapah earthquake. A total of 1 km of rupture were scanned immediately after the earthquake, capturing fine, ephemeral details of the rupture including abundant secondary faulting and warping. Data resolution approaches one point per square centimeter on the fault plane, sufficient to resolve striations on its surface.

Earthquake Response

The occurrence of the 4 April 2010 El Mayor-Cucapah earthquake in northernmost Baja California gave SCEC the opportunity to exercise its post-earthquake scientific response plan. A geology field team, led by John Fletcher from CICESE (Ensenada, Baja California) and Tom Rockwell commenced mapping of this complex earthquake rupture within a day of its occurrence. This was yet another unusual magnitude 7+ earthquake. As during the Landers (1992) and Hector Mine (1999) earthquakes, the 2010 event connected smaller fault segments to produce a large, complex rupture. The 2010 rupture was also unusual in that it ruptured a fault immediately adjacent (<1 km distant) to the 1892 Laguna Salada earthquake (Mueller and Rockwell, 1995; Hough and Elliott, 2009). Understanding the relationship between these two closely spaced earthquakes may lead to new understanding of the stress state and post-seismic reloading of faults. This earthquake presents the first opportunity to gather a comprehensive high-resolution topographic image of a

fault rupture. Within two weeks of the earthquake, teams from UC Davis led by Mike Oskin, and from UNAVCO/University of Kansas/UCLA led Mike Taylor, were gathering ultra-high-resolution scans of portions of the surface rupture with ground-based lidar, revealing subtle and highly ephemeral features of the surface rupture in unprecedented detail. An airborne lidar survey of the entire surface rupture and the 1892 scarps will be acquired in mid-August 2010 (the day after this report was submitted). This survey is supported through an NSF RAPID grant to Mike Oskin and Ramon Arrowsmith, and augmented by additional funding from SCEC. Once completed these data will provide a permanent archive of the rupture for future study and comparison to field measurements. Pre-event low-resolution lidar gathered by INEGI (the Mexican cartographic agency) will enable the first-ever fine-scale analysis of distributed vertical motions surrounding the rupture.

Interdisciplinary Focus Areas

Within the new SCEC structure, the focus groups are responsible for coordinating interdisciplinary activities in six major areas of research: *Unified Structural Representation*, *Fault and Rupture Mechanics*, *Crustal Deformation Modeling*, *Lithospheric Architecture and Dynamics*, *Earthquake Forecasting and Predictability*, *Ground Motion Prediction*, *and Seismic Hazard and Risk Analysis*. The following reports summarize the year's activities in each of these areas.

Unified Structural Representation

The Unified Structural Representation (USR) Focus Area develops models of crust and upper mantle structure in southern California for use in a wide range of SCEC science, including strong ground motion prediction, earthquake hazard assessment, and fault systems analysis. These efforts include the development of Community Velocity Models (CVM & CVM-H) and Community Fault Models (CFM & CFM-R), which together comprise a USR. The Focus Area also seeks to evaluate and improve these models through ground motions simulations, 3D waveform tomography, earthquake relocations, and fault systems modeling in partnership with other working groups in SCEC.

This past year's accomplishments include:

1. Development of a new version of the SCEC Community Velocity Model (CVM-H 6.2), which directly incorporates 3D waveform tomographic results (Tape et al., 2009);
2. Development of a SCEC computational platform to evaluate the CVM and CVM-H models by comparisons of the recorded seismograms with synthetics, with demonstration for the 2008 Mw5.4 Chino Hills earthquake (Olsen and Mayhew, 2010);
3. Enhancements to the code that delivers the CVM-H, and optimized, parallel extraction software for CVM4 and CVM-H, in partnership with the SCEC CME group;
4. Development of a statewide Community Fault Model (SCFM); and
5. Improvement of the southern California Community Fault Model (CFM) using precisely relocated seismicity (Hauksson and Shearer, 2005; Shearer et al., 2005; Nicholson et al., 2008).

Community Velocity Models (CVM, CVM-H)

SCEC has developed two crust and upper mantle velocity models (CVM, Magistrale et al., 200; and CVM-H, Suess & Shaw, 2003) for use in strong ground motion simulation and seismic hazard assessment. The community velocity models consist of basin descriptions, including structural representations of basin shapes and sediment velocity parameterizations, embedded in regional tomographic models.

The latest release of the CVM-H (6.2) is an important milestone for SCEC, as it represents the integration of various model components, including fully 3D waveform tomographic results (Plesch et al., 2009). The CVM-H consists of basin structures defined using high-quality industry

seismic reflection profiles and tens of thousands of direct velocity measurements from boreholes (Plesch et al., 2009; Süss and Shaw, 2003). These basin structures were then used to develop travel time tomographic models of the crust (after Hauksson, 2000) extending to a depth of 35 km. This model was then used to perform a series of 3D adjoint tomographic inversions that highlight areas of the model that were responsible for mismatches between observed and synthetic waveforms (Tape et al, 2009). Sixteen tomographic iterations, requiring 6800 wavefield simulations, yielded perturbations to the starting model that have been incorporated in the latest model release (Figure 23). CVM-H 6.2 also incorporates a new Moho surface (Yan and Clayton, 2007) and a series of other upgrades to the basement geotechnical layer and the Vp-density scaling relationship.

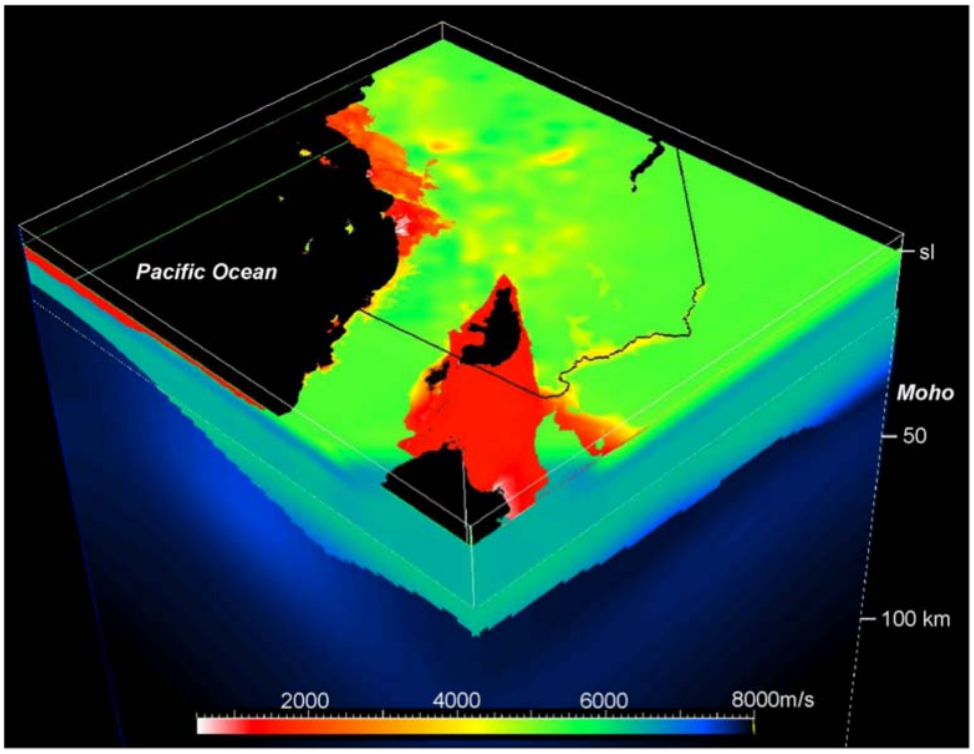

Figure 23. Perspective view of CVM-H 6.2, which includes basin structures embedded in a tomographic model that extends to 35 km depth, which is underlain by a teleseismic surface wave model that extends to a depth of 300km. This latest release of the model includes results from 3D tomographic waveform inversions (Tape et al, 2009). Vs is shown.

Comparisons of observed and synthetic waveforms for earthquakes in southern California demonstrate that the SCEC Community Velocity Models (Magistrale et al., 2000; Süss and Shaw, 2003; Plesch et al., 2009) perform much better than simple 1-D velocity models (Figure 24) (e.g., Komatitsch et al., 2004; Chen et al., 2007; Olsen and Mayhew, 2010). Furthermore, the new 3D waveform tomographic inversion methods offer a comprehensive way to evaluate and iteratively improve velocity models. For example, the adjoint tomographic results included in the CVM-H 6.2 include significant changes (±30%) from the starting models based on travel-time tomographic methods. Such strong perturbations resulted in dramatically improved fits to full-length three component waveforms (Tape et al., 2009, 2010).

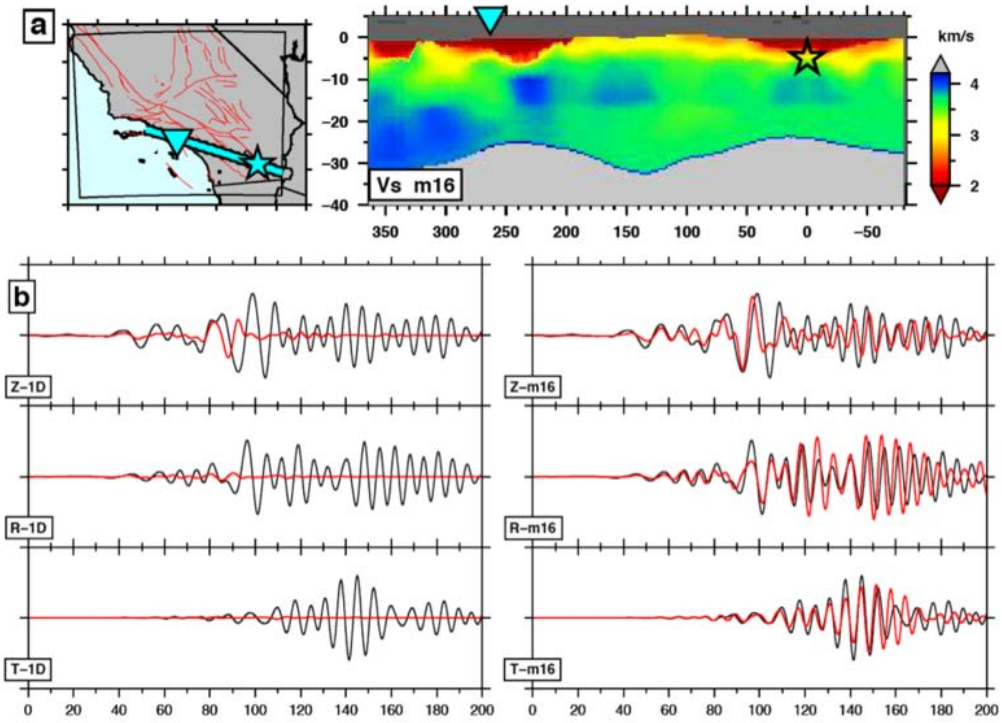

Figure 24. The influence of 3D velocity structure on the seismic wavefield based on the 3D adjoint tomographic analysis of Tape et al. (2009, 2010). (a) Cross section of the final 3D Vs crustal model (m16), containing the path from event 14179736 (I; Mw 5.0, depth 4.9 km), beneath the Salton trough, to station LAF.CI (∇; distance 263.5 km), within the Los Angeles basin. (b, left column) Data (black) and 1D synthetics (red). (b, right column) Data (black) and 3D synthetics for model m16 (red). The seismograms are bandpass filtered over the period range6–30 s. Z, vertical component, R, radial component, T, transverse component.

Coincident with the release of the latest CVM-H model, we also worked in partnership with the SCEC CME group to enhance the code that delivers the model to users. Specifically, we added the capability to extract velocity values below the topographic land surface or relative to a sea level datum. This change helps facilitate the different needs of finite-difference- and finite-element-based wave propagation codes. We also made a number of additional modifications to the code that help facilitate parameterizing grids and meshes, and summarized these enhancements in an updated instruction manual that includes training datasets.

Optimized code for delivering the CVM'S

During the past year, the SCEC CME group (Small, Ely, Maechling) made important progress on speeding up the process of delivering extractions of the CVMs to the ground motion modelers. The developed C/MPI code is called cvm2mesh and is meant for fast mesh generation from either CVM4 or CVM-H. The program operates by partitioning the mesh region into a set of slices along the z-axis as illustrated in Figure 25. Each slice is assigned to an individual core for extraction from the underlying CVM. The partitioning and extraction is an embarassingly parallel operation as the cores do not need to communicate with each other, and they only indirectly interact through the filesystem when the slices are merged into the final mesh file. Each core contributes its slice to the final mesh by computing the offset location of the slice within the greater file, and uses efficient MPI I/O file operations to seek to that location and write the slice data.

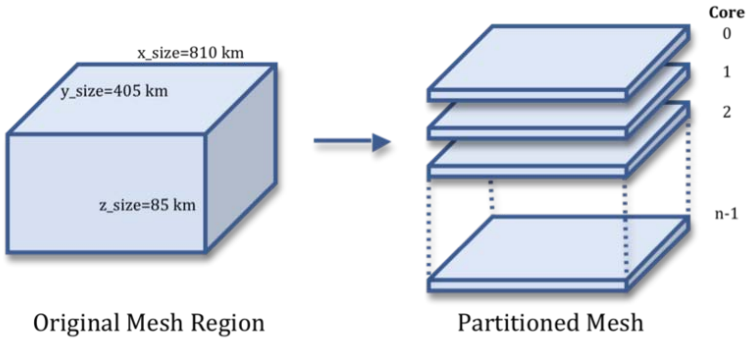

Figure 25. The 3-D mesh region is partitioned into slices along the z-axis. Each slice is assigned to a core in the MPI job, and each core queries the underlying CVM for the points in its slice only.

Using this procedure, cvm2mesh extracted input mesh for the M8 simulation (Cui et al., 2010, finalist for the Gordon Bell Prize 2010) from CVM-4 with ~436 billion points in under five hours while running on 2125 cores. The equally-sized input mesh extracted from CVM-H was generated in under one hour on 425 cores. The cvm2mesh program can scale up to a maximum of n cores, where n is defined by the relationship: n = z_size (m) / spacing (m). Thus, the maximum parallelism that can be achieved for the M8 mesh extractions is 85000 m /40 m = 2125 cores.

The parallel code applied to CVM-H has also been extended to allow for 'topography flattening', used by the ground motion modelers omitting surface topography in their simulations. Querying can be done using either (lat, lon) or UTM coordinates. Finally, the code allows for a user-defined 1-D background model for CVM-H. Derivation of a Vs30-based near-surface velocity model.

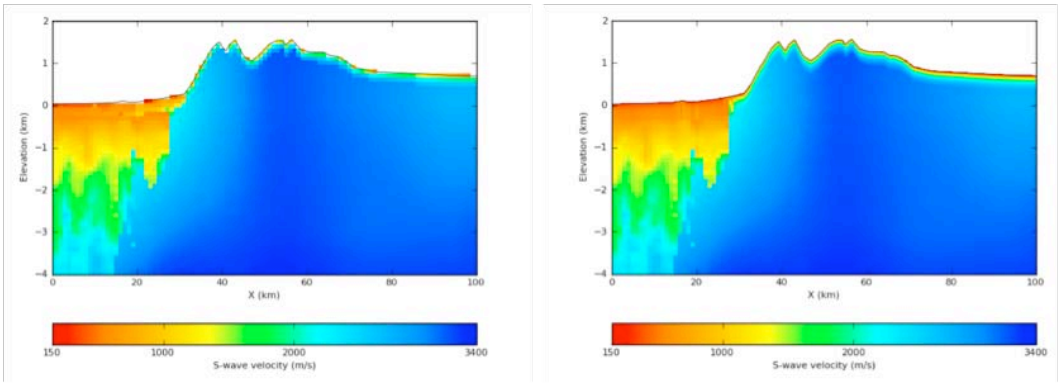

Figure 26. Cross sections from CVM-H (left) without and (right) with the proposed Vs30-based near-surface velocity model.

Additional efforts are ongoing from SCEC CME (Geoff Ely and Phil Maechling) to derive a Vs30-based near-surface velocity model for the CVMs (Ely and Maechling, 2010). The approach generates a supplementary geotechnical layer (GTL) model derived from available maps of VS30 (the average shear-velocity down to 30 meters). The approach also minimizes rasterization artifacts in the near-surface due to sample depth dependence on local topographic elevation (nearly 50 percent of CVM-H does not reach the ground surface at all) (Figure 26).

Evaluating the Community Velocity Models (CVM, CVM-H)

The SCEC CME group initiated development of a platform to examine systematically the goodness-of-fit (GOF) between seismic data and synthetics generated from CVM4 and CVM-H (Small and Maechling, 2010). Current status for the platform includes an estimate of the bias between observed and simulated response spectral accelerations for all included stations, demonstrated for 60+ records of the 2008 Mw 5.4 Chino Hills event. Planned use of the platform includes GOF estimates for future updates of the CVMs, as compared to previous versions. Future efforts will consider adaptation of the GOF method by Olsen and Mayhew (2010), which includes a set of user-weighted metrics such as peak ground motions, response spectrum, the Fourier spectrum, cross correlation, energy release measures, and inelastic elastic displacement ratios.

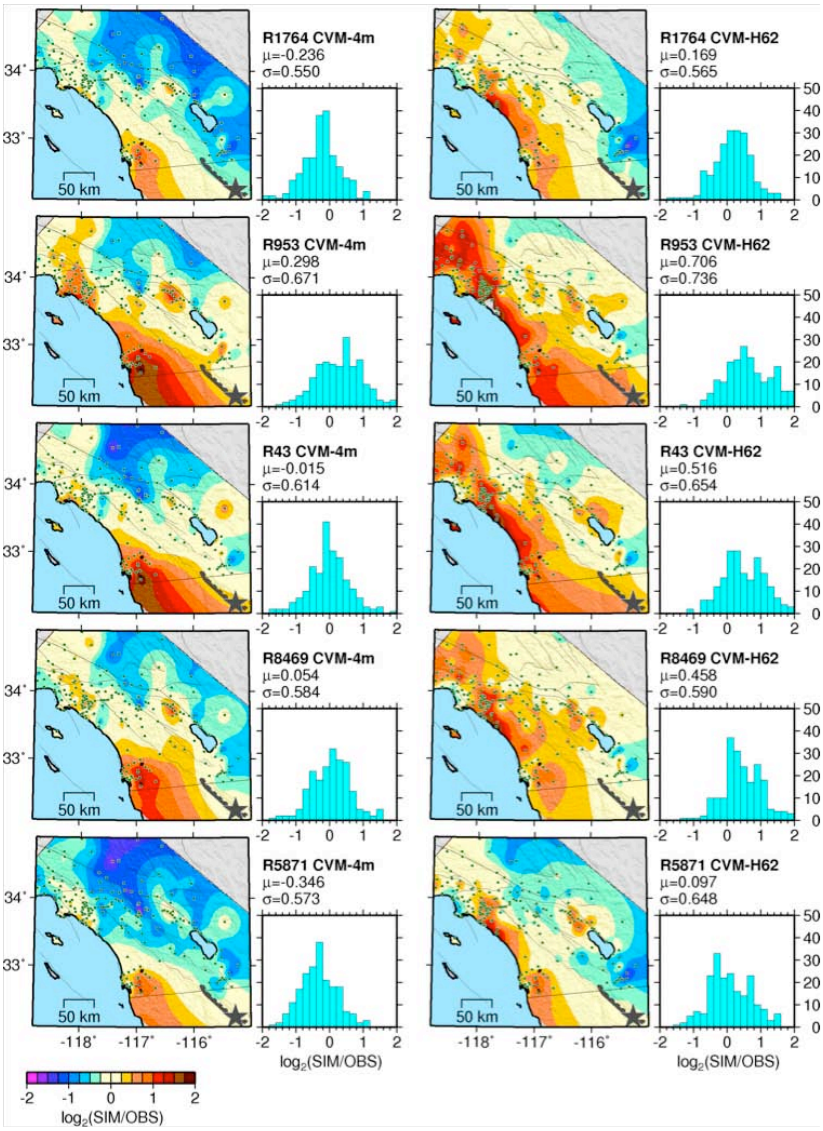

Figure 27. Residuals of simulated and observed PGV for the five rupture scenarios of the Mw 7.2 El Mayor-Cucapah event, using seismic velocity models CVM-4m (left column) and CVM-H62 (right column). For each case, results are displayed as the base 2 logarithm of the ratio of the simulated to observed value computed for each recording site in both map view and histogram, with the mean (m) and standard deviation (s) of the residuals indicated above the histogram. From Graves and Aagaard, 2010).

Additional comparisons of CVM-H and CVM-S were carried out by Robert Graves and Brad Aagaard (2010), using 5 long-period (>2s) kinematic rupture descriptions of the 4 April 2010 M7.2 El Mayor Cucapah earthquake (Figure 27). While the details of the motions vary across the simulations, the median levels match the observed motions reasonably well with the standard deviation of the residuals generally within 50% of the median. Simulations with the CVM-4m model yield somewhat lower variance than those with the CVM-H62 model. Both models tend to over-predict motions in the San Diego region and under-predict motions in the Mojave Desert. Within the greater Los Angeles basin, the CVM-4m model generally matches the level of observed motions whereas the CVM-H62 model tends to over-predict the motions, particularly in the southern portion of the basin. Future work will analyze the causes of these differences, and use the aftershocks of the El mayor-Cucapah event to explore the predictive capability of the two CVMs.

Community Fault Model (CFM)

The SCEC Community Fault Model (CFM) is an object-oriented, 3D representation of more than 140 active faults in Southern California, and includes direct contributions from more than twenty SCEC investigators (Plesch et al., 2007). The model consists of triangulated surface representations (T-surfs) of major faults, which are defined by surface geology, seismicity, well logs, seismic reflection profiles, and geologic cross sections. These 3D fault representations are intended to support SCEC research efforts in fault system modeling and earthquake rupture propagation, as well as to serve as a basis for regional seismic hazards assessment.

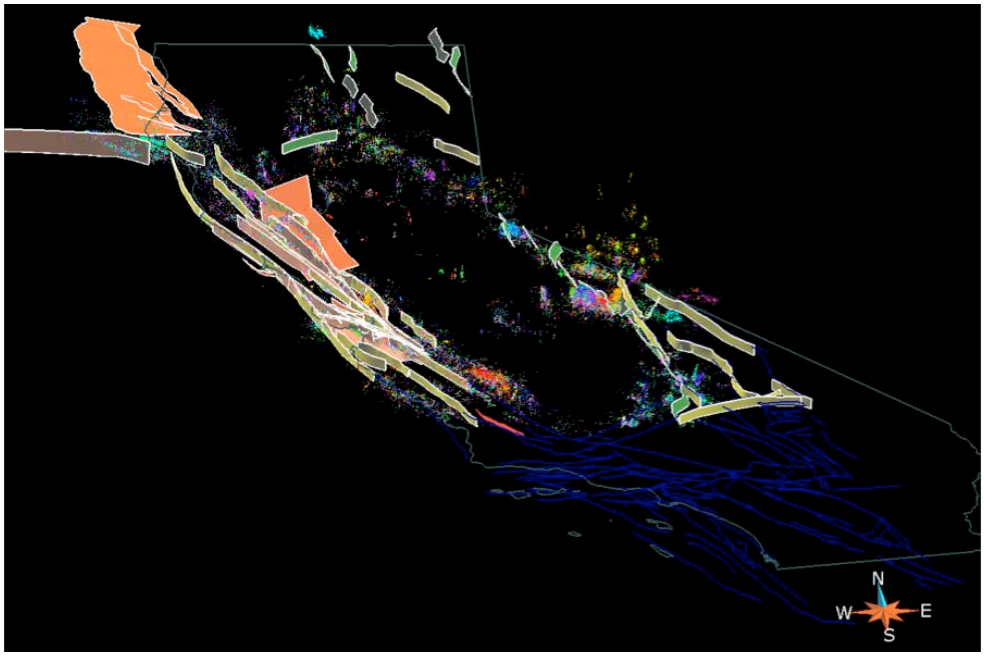

Figure 28. Perspective view of the Statewide CFM (SCFM 1.0), which includes the SCEC CFM 4.0 (Plesch et al., 2007), and the USGS San Francisco bay region fault model (Brocher et al., 2005). New faults added to the model this past year are highlighted in colors.

This past year, we completed a major expansion of the CFM by developing the first generation Statewide Community Fault Model, SCFM 1.0. The statewide model is comprised of the southern California CFM 4.0 and more than 150 additional fault representations for northern California (Figure 28). Geologic models of the greater San Francisco Bay area, developed largely by the U.S.G.S. (Menlo Park), serve as the basis for most representation in that area of northern California (e.g., Brocher et al., 2005). The remainder of the new fault representations was developed by integrating geologic maps and cross sections, seismicity, well and seismic reflection data using the

approach of Plesch et al. (2007). Each of the faults are defined by triangulated surface representations, with separate patches that distinguish between interpolated and extrapolated regions of the fault surfaces. This allows users to clearly distinguish portions of the fault representations that are directly constrained by data from those that are inferred or extended from better known parts of the fault. In addition, the model contains alternative representations of many faults. These cases arise when two or more fault interpretations have been made that involve substantial differences in 3D representation (i.e., in dip direction, fault type), and all of them are seemingly consistent with the available data.

Ultimately, this new model will help improve our assessment of seismic hazards in California, and contribute directly to fault systems modeling activities within SCEC. In the latter part of 2010, we plan to facilitate evaluation of the SCFM 1.0 by the SCEC working group, in order to establish preferred and alternative fault representations, assign quality rankings to faults, and identify areas where further improvements to the model are needed.

In a related effort, the CFM in southern California is being systematically re-evaluated using new re-located earthquake catalogs developed by SCEC (Hauksson and Shearer, 2005; Shearer et al., 2005). These new catalogs provide significantly improved resolution of many faults, and are being used to refine interpolated fault patches for many of the representations in the CFM (Nicholson et al., 2008). These updates, which include critical model components such as the San Andreas fault in San Gorgonio Pass, will be incorporated in a new release of the CFM and SCFM.

Community Velocity Models (CVM, CVM-H)

Brocher, T.M., R.C. Jachens, R. W. Graymer, C. W. Wentworth, B. Aagaard, and R. W. Simpson, 2005, A new community 3D seismic velocity model for the San Francisco bay Area: USGS Bay Area Velocity Model 05.00, SCEC Annual Meeting, Proceedings and Abstracts, Volume XV, p. 110.

Chen, P., L. Zhao, Li, T. H. Jordan, 2007, Full 3D tomography for the crustal structure of the Los Angeles region, Bulletin of the Seismological Society of America, vol.97, no.4, pp.1094-1120.

Cui, Y., K.B. Olsen, T. H. Jordan, K. Lee, J. Zhou, P. Small, D. Roten, G. Ely, D.K. Panda, A. Chourasia, J. Levesque, S. M. Day2, P. Maechling (2010). Scalable earthquake simulation on petascale supercomputers, submitted to Super Computing 2010.

Ely, G., and P. Maechling (2010). A Vs30-derived near-surface velocity model, http://earth.usc.edu/~gely/cvmh/

Graves, R.W., and B. T. Aagaard (2010). Testing Long-Period Ground-Motion Simulations of Scenario Earthquakes using the Mw 7.2 El Mayor-Cucapah Mainshock: Evaluation of Finite-Fault Rupture Characterization and 3D Seismic Velocity Models, to be submitted to BSSA.

Hauksson, E. and P. Shearer, Southern California Hypocenter Relocation with Waveform Cross-Correlation: Part 1: Results Using the Double-Difference Method, Bull. Seismol. Soc. Am., 95, 896-903, 2005.

Hauksson, E., 2000, Crustal structure and seismicity distribution adjacent to the Pacific and North American plate boundary in southern California, JGR, 105, 13,875-13,903.

Komatitsch, D., Q. Liu, J. Tromp, P. Süss, C. Stidham, and J. H. Shaw, (2004), Simulations of strong ground motions in the Los Angeles basin based upon the spectral element method, BSSA, Vol. 94, No. 1, pp. 187–206.

Lin, G., P. M. Shearer, and E. Hauksson, 2007, Applying a 3D velocity model, waveform cross-correlation, and cluster analysis to locate southern California seismicity from 1981 to 2005, (submitted).

Magistrale, H., S. Day, R. W. Clayton, and R. Graves, 2001, The SCEC Southern California Reference Three-Dimensional Seismic Velocity Model Version 2: Bulletin of the Seismological Society of America, v. 90, no. 6B, p. S65-S76.

Nicholson, C., E. Hauksson, A. Plesch, G. Lin, and P. Shearer, 2008, Resolving 3D fault geometry at depth along active strike-slip faults: simple or complex?, 2008 SCEC Annual Meeting, Palm Springs, CA.

Olsen, K.B., and J.E. Mayhew, J.E. (2010). Goodness-of-fit criteria for broadband synthetic seismograms, with application to the 2008 Mw5.4 Chino Hills, CA, earthquake, Seism. Res. Lett , in press.

Plesch, A., John H. Shaw, Christine Benson, William A. Bryant, Sara Carena, Michele Cooke, James Dolan, Gary Fuis, Eldon Gath, Lisa Grant, Egill Hauksson, Thomas Jordan, Marc Kamerling, Mark Legg, Scott Lindvall, Harold Magistrale, Craig Nicholson, Nathan Niemi, Michael Oskin, Sue Perry, George Planansky, Thomas Rockwell, Peter Shearer, Christopher Sorlien, M. Peter Süss, John Suppe, Jerry Treiman, and Robert Yeats, 2007, Community Fault Model (CFM) for Southern California, Bulletin of the Seismological Society of America, v. 97, no. 6.

Plesch, A., C. tape, and J.H. Shaw, 2009, CVM-H 6.0: integration of adjoint-based tomography, the San Joaquin basin and other advances in the SCEC community velocity model, SCEC Annual Meeting, Palm Springs, CA.

Shearer, P., E. Hauksson, and G. Lin, Southern California hypocenter relocation with waveform cross correlation: Part 2. Results using source-specific station terms and cluster analysis, Bull. Seismol. Soc. Am., 95, 904-915, doi: 10.1785/0120040168, 2005.

Small, P. and P. Maechling (2010). SCEC Platform for testing the accuracy of CVMs. http://earth.usc.edu/~patrices/cvmh_sim/work/html/cvmh-sim.html.

Süss, M. P., and J. H. Shaw, 2003, P-wave seismic velocity structure derived from sonic logs and industry reflection data in the Los Angeles basin, California, Journal of Geophysical Research, 108/B3.

Tape, C., Q. Liu, A. Maggi, and J. Tromp, 2010, Seismic tomography of the southern California crust based on spectral-element and adjoint methods, Geophys. J. Int., 180, 433–462.

Tape, C., Q. Liu, A. Maggi, and J. Tromp, 2009, Adjoint tomography of southern California, Science, vol 325, p. 988-992.

Yan, Z., and R. W. Clayton, 2007, Regional mapping of the crustal structure in southern California from receiver functions, J. Geophys. Res., 112, B05311, doi:10.1029/2006JB004622.

Fault Rupture and Mechanics

A large number of projects were funded as part of the Fault and Rupture Mechanics focus group this past year reflecting the continuing need for, and strong community interest in, this area of research. These projects address a broad spectrum of SCEC3 goals that overlap the other SCEC focus and disciplinary group activities. FARM-related research continued to emphasize several critical topics, including understanding the relative importance of different dynamic weakening mechanisms, characterizing the properties of fault cores and damage zones, formulating constitutive laws for use in dynamic rupture models, and comparing the results with both repeatable computer simulations, and laboratory and field observations to assess their impacts on crustal, fault-zone, and earthquake behavior. This section only provides a brief summary of some of the accomplishments and research-related activities reported during 2009 and the early months of 2010. Additional related accomplishments are reviewed in other sections of this report. For a complete review of all FARM-related activities please see the individual PI annual reports posted on the SCEC website.

Frictional Strength of Faults During Earthquake Slip

The concept that most earthquake slip seems to occur in extremely thin zones, suggesting intense thermal effects during rupture, continues to drive laboratory experiments that investigate physical effects at realistic earthquake slip rates. These laboratory studies have revealed a rich array of new physics of dynamic fault zone weakening, including flash heating, thermal pressurization of native fluids or of volatiles liberated by decomposition reactions, possible silica gel lubrication, and as yet poorly understood, nano-particle weakening. A SCEC-led workshop, convened by Dunham and Chester, and with 127 participants, was devoted to reviewing recent experimental results concerning fault friction at coseismic slip rates and associated modeling efforts. Most experiments presented show extreme weakening of friction at speeds exceeding ~0.1 m/s for a wide variety of rock types. Some experiments show friction to be proportional to the inverse of slip velocity, consistent with the theoretical flash heating model, while others show less velocity dependence. Di

Toro presented a compilation of results for a variety of rock types showing how universal dynamic weakening is, even though most of the experiments reviewed were run at either low normal stresses or at slip rates just approaching the coseismic range. Prakash presented data produced at much higher normal stresses and velocities that show extremely low friction coefficients. A topic of discussion is occurrence of oscillations often attributed to machine compliance and Goldsby illustrated how changing machine stiffness influences the amplitude of these oscillations. Reches and Lockner reported results from a new high-speed friction apparatus that show weakening of friction down to ~0.3 at ~0.01 m/s followed by strengthening to ~0.7 at ~0.1 m/s. In addition to fault weakening due to flash heating, distributed high strain-rate plastic flow at asperity contacts (Brown) and the production of nanoscale particles that adhere to the sliding surfaces were offered as alternative mechanisms. Establishing a theoretical understanding of experimental results and identifying distinguishing characteristics of dynamic weakening that can be mapped in the field both remain top research priorities.

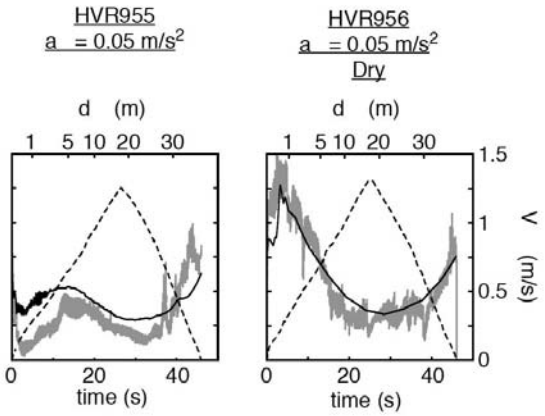

Figure 29. Results of thermal-, mechanical-, and fluid flow-coupled FEM models for constant acceleration experiments on wet gouge, HVR955gb, and on room-dry gouge, HVR956gb. The reduction in strength of the wet gouge relative to the dry gouge, particularly at small displacement, reflects weakening by thermal pressurization. The magnitude of the pore fluid pressurization diminishes with slip because pore fluid escapes (the gouge layer is not sealed) and the rate of temperature increase is reduced. Black and gray solid lines represent the model-calculated torque and the measured torque, respectively, plotted as a function of time. The dashed black lines represent the equivalent velocity.

Although thermal pressurization is becoming more widely used in the modeling community, this mechanism has yet to be documented in laboratory experiments under carefully controlled conditions. Kitajima et al. (in press) links the onset of dynamic weakening to the development of distinct structural units within the sheared layer. The microstructure evolves as slip-rate and temperature increase from distributed shearing flow at low temperatures to fluidized flow associated with the formation of an extremely localized slip zone and dynamic weakening at high temperature. Thermal-, mechanical-, and fluid-flow-coupled FEM models, based on the temperature-dependent friction constitutive relation and that treat thermal pressurization of pore water, successfully reproduce the frictional response in all experiments (Figure 29). Kitajima et al. (2010) hypothesize that thermal pressurization is important at high slip rates and small displacements as temperature rapidly increases. The critical displacement for dynamic weakening is approximately 10 m or less, and can be understood as the displacement required to form a localized slip zone and achieve a steady-state temperature condition. The observed relationship between steady state friction and slip rate is consistent with predictions from micro-mechanical models of flash heating.

At the workshop, constitutive equations discussed describing dynamic weakening ranged from physics-based descriptions of melting and shear of viscous melt layers at asperity contacts

(Rempel) to more empirical formulations capturing a broad set of experimental results (Beeler). Rice presented results of numerical simulations of rupture propagation with flash heating and thermal pressurization using parameters derived directly from laboratory measurements. While computational constraints limit the analysis to very small earthquakes, the resulting stress drop and scaling of slip with propagation distance appear to be consistent with natural events, lending support to the dynamic weakening model of fault mechanics. Lapusta and Noda's work on earthquake cycle simulations with rate-and-state friction and thermal pressurization, showed how dynamic weakening from thermal pressurization can permit ruptures to propagate on rate-strengthening portions of the fault. Using numerical simulations, Joe Andrews suggested that efficient thermal pressurization in the shales at the north end of the Chi-Chi earthquake might explain the low levels of spectral acceleration relative to spectral velocity observed in strong ground motion records.

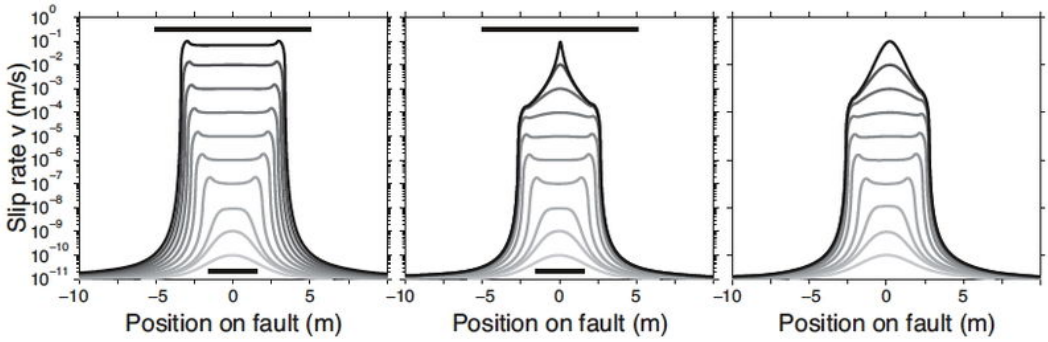

Figure 30. Results from aging law simulations in the isothermal (left) and thermal pressurization (middle and right) cases. In these simulations, a/b = 0.8, dc = 100 μm, and (σ - po) = 140 MPa. Lines are snapshots of slip speed for each tenfold increase in maximum slip speed. (a) Snapshots of slip speed for isothermal, drained, aging-law nucleation. Bottom scale bar shows 2Lmin [Dieterich, 1992]; top scale bar shows 2L∞ [Ampuero & Rubin, 2008]. (b) Snapshots of slip speed with thermal pressurization, with α = 0. Comparing to (a), note that at early times (low slip speeds) the profiles are similar to the isothermal simulation. At about 10-5 m/s, the profiles start to diverge. By about10-4 m/s, the profiles have distinctly different forms. The sharp peak at higher slip speeds indicates how slip is evolving toward a singularity of high slip over a zero-width area. (c) Snapshots of slip speed with thermal pressurization and the Linker & Dieterich [1992] effect with α = μ0 = 0.6. The inclusion of this effect prevents the development of a slip singularity.

Exploring the notion that thermal pressurization also can be significant during slow slip, Segall and others are extending their earlier models of a 2D elastic, diffusive system with a 1D fault to include a finite-width shear zone. To date, using a zero-width shear zone approximation, they have demonstrated that thermal pressurization is significant during the late stages of earthquake nucleation following a period dominated by rate- and state-dependent friction. For an aging friction law they find that thermal pressurization is an important process at slip-speeds of 0.02-2.0 mm/s, and for pulse-like slip it dominates at speeds of 1-100 mm/s (Figure 30).

To understand and characterize the effects of elastic-plastic interaction with pore fluids and determine the pore pressure along the rupture plane, Viesca et al. (2009) and Viesca and Rice (2009, 2010) have extended previous models to include the poro-elastic-plastic response. The interaction between dynamic rupture, inelastic deformation, and changes in the near-fault pore fluid pressure, permeability and storage coefficients predicts a different pore pressure evolution on each side of a planar fault surface, a greater degree of plastic straining behind the rupture front along one side of the slip-weakening zone, and a narrow lobe of plastically active material that extends outward into the surrounding material (Figure 31). With plastic deformation, changes in permeability and compliance modify the magnitude of pore pressure at rupture (Figure 32).

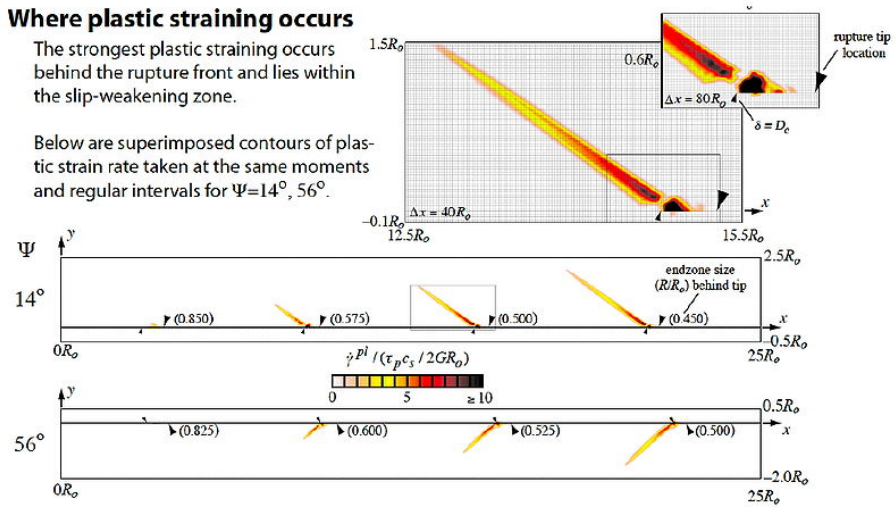

Figure 31. Fine resolution poro-elastic-plastic solution (based on procedures of Viesca et al., [JGR, 2008]) for dynamic shear rupture propagation in a fluid-infiltrated Drucker-Prager material. Note that the most intensive plastic straining occurs along one side of the slip-weakening zone in these examples.

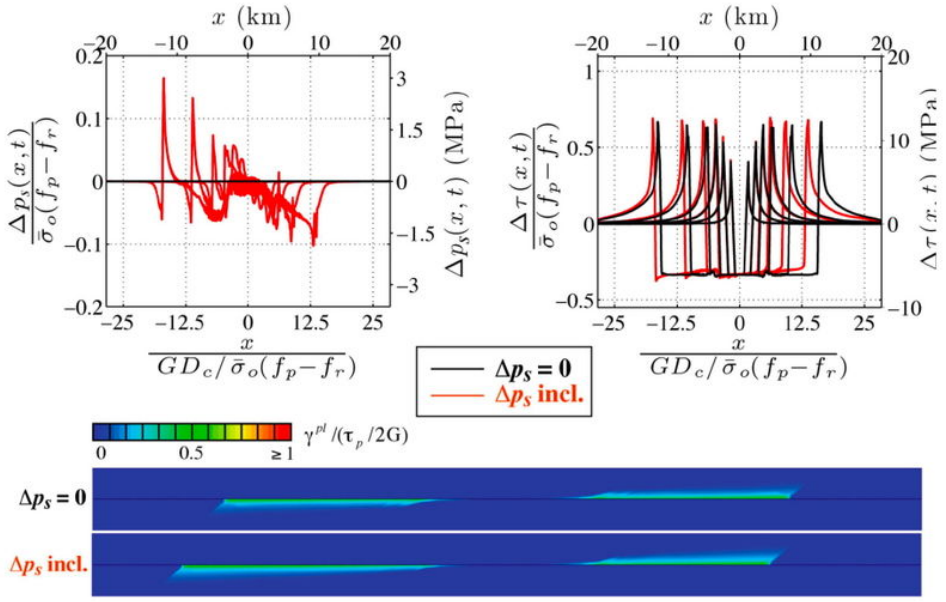

Figure 32. Example of poro-elastic-plastic rupture, with (curves in red) and without (in black) inclusion of procedure for calculation pore pressure changes at the slip surface and including it in the fully coupled dynamic analysis, with undrained conditions assumed everywhere except in the diffusive boundary layer along the slip surface.

Geometric Complexity, Off-fault Damage, and Earthquake Rupture Dynamics

An emerging focus of SCEC in 2009 was directed at understanding the geometric complexity of faults and the implications for earthquake phenomenon. In an attempt to quantify the geometric heterogeneity in California faults over a range of spatial and temporal scales, Wechsler et al (2010) characterized the surface expression of fault displacement accumulated over tens of thousands of

years and found that frequency-size statistics of all fault segment lengths can be fit well by an exponential function. To characterize geometric heterogeneity as a function of seismogenic depth, Bailey et al (2010) used focal mechanism data from 0 to 15 km depth for the period of 1983 to 2004 and illustrated a clear link between the long term evolution of the fault and its seismic behavior over a 20 year interval, and that the partitioning of faulting styles suggests that focal mechanism heterogeneity is primarily controlled by the structural characteristics of the fault.

In the same way that SCEC is pushing the development of advanced experimental techniques to investigate microscale physics and constitutive behaviors, SCEC is making progress testing and advancing computational methods and efficiency for modeling rupture propagation, and incorporating the geometric roughness of faults into modern rupture dynamics simulations to provide insight on high-frequency ground motion and aftershock localization. These community-wide advances have been catalyzed by dedicated workshops and annual meeting topical sessions over the past year.

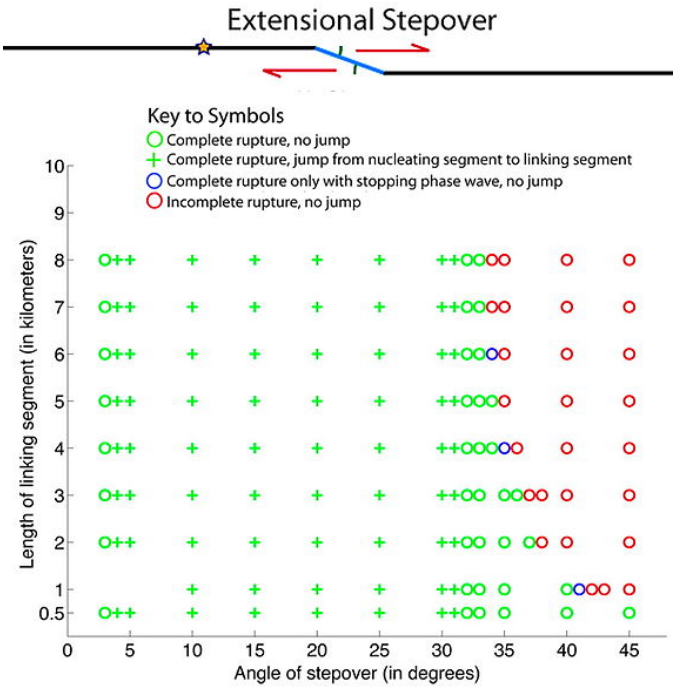

Figure 33. Cartoon of fault geometry and results for an extensional stepover. The blue line represents the linking segment, which is variable in length. The green arcs show the stepover angle, taken relative to the strike of the parallel end segments; this angle also is variable. The red arrows represent the direction of slip. The star marks the nucleation point, 7 km along the nucleating segment of the fault. The lengths of the nucleating and far segments, in black, are constant at 10 km each.

An approach to understand the effects of geometric complexity of fault surfaces, on rupture propagation, is to identify and examine specific classes of geometric features. For example, in 2009, Oglesby and Wesnousky examined double-bends (linked stepovers) in strike-slip faults (Figure 33). They found that for very long linking-faults, the likelihood of a simulated rupture propagating through a stepover is determined by the static favorability of the linking segment (i.e., static stress change due to the main rupture, on the linking segment). They also found that for smaller linking fault lengths, it is possible for simulated ruptures to propagate even though the linking faults might seem to be 'unfavorable'. This study provides insight into the relative contributions of dynamic versus static changes in stress on rupture propagation through geometric complexities.

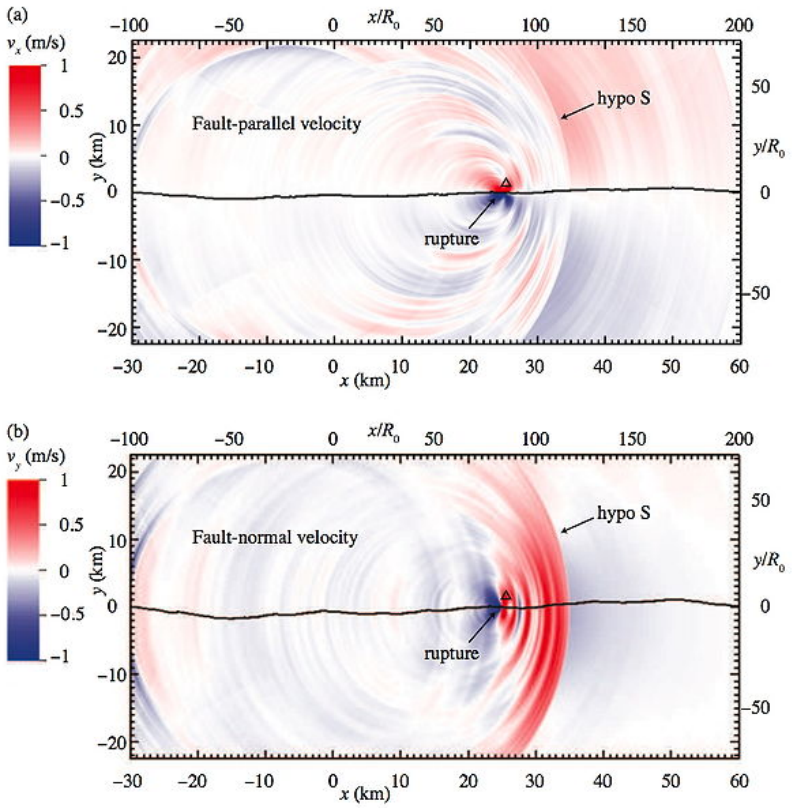

Figure 34. Snapshots of the velocity field radiated by a ruture on a band-limited self-similar fault. a) fault-parallel (vx); (b) fault-normal (vy). The hypocentral shear wave is marked as hypo S.

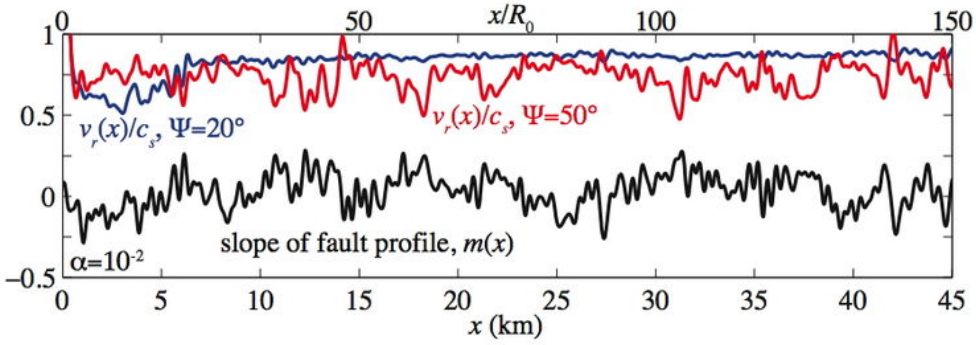

Figure 35. Influence of the orientation of the initial stress field on fluctuations in rupture velocity for self-similar rough faults. Slope of fault profile for amplitude to wavelength ratio of 10^-2 for orientation of the initial stress field at 20 and 50 degrees. The orientation specified by the angle between the maximum compressive stress and the plane defining the average surface of the fault.

While Oglesby and Wesnousky looked at larger scale geometrical features and their effects on the propagation of earthquake rupture, Dunham and Brodsky looked at smaller scale features and their effects on ground motion. Decades ago, U.S. and Japanese researchers hypothesized the effects of small scale fault heterogeneity on high-frequency ground motions, but the computational capabilities to explore this were not yet available, and so most studies assumed flat faults with heterogeneous stresses and slip distributions. Now, with more field-based observations available,

along with impressive computational platforms, these calculations are viable. Dunham and Brodsky did 2D numerical simulations assuming strong rate-weakening friction laws. They showed that the radiated velocity field is affected when assuming rupture on a band-limited self-similar fault, rather than a simple planar fault, and that high-frequency shear waves are emitted every time the simulated rupture accelerates or decelerates (Figure 34 and Figure 35). These studies, which will likely continue in 2010, are an important step towards including not only stress heterogeneity on faults, but also including geometrical complexity.

Significant advances also have been realized in understanding the origin of fault-bordering damage zones, the characterization of their properties by field geologic studies and by seismic analysis of fault-zone trapped waves (including post-rupture time-dependence of their speeds as a window on healing), and understanding how they interact with rupture propagation (e.g., with their inelastic response putting a limit on maximum local slip velocity at the rupture front, compared to modeling which assumes elastic off-fault response). Shallow drilling and coring of the pulverized zone adjacent to the San Andreas Fault at Little Rock is the first attempt to distinguish rock damage caused by near-surface weathering from fracture generated by repeated earthquakes (Weschler et al., 2009). Although addressed theoretically for some time, Biegel et al. (in press) and Bhat et al. (in press) demonstrate in laboratory experiments that the presence of damage adjacent to the rupture surface has a significant effect on dynamic rupture characteristics.

Multi-Investigator Collaborative Projects

A highlight of SCEC is its dedication to multi-investigator collaborative studies (referred to as "Technical Activity Groups" or TAGs in the SCEC4 proposal) that help organize, catalyze, and focus diverse research groups in the earthquake science community. The SCEC workshops are a critical part of this collaborative interaction, and for FARM, the workshop described earlier in this section demonstrates the clear advances in understanding that can be made only in a group event setting. In addition, SCEC hosts large multi-PI science projects. Among these are the computational exercises where a number of researchers agree to tackle a mutually agreed upon science problem to make sure that their science is repeatable. Here we highlight some recent group efforts, as well as the multi-year dynamic rupture code validation computational exercise.

A SCEC collaborative group project that is making much progress is the Transient Detection collaboration (described in detail under the Geodesy section of this report), led by Murray-Moraleda and Lohman. In addition, a new SCEC group in 2009, with goals that will help FARM better understand the physics of coseismic rupture, is the Source Inversion Validation Exercise (SIV), led by Mai, Page, and Schorlemmer. Although tackling the difficult earthquake-source inverse problem that is inherently non-unique, the SIV exercise is showing much promise, and its success would lead to improved views of the earthquake source that are critical to our science overall and especially important for FARM, Ground Motion Prediction, and Seismic Hazard Analysis groups.

Another collaborative exercise in SCEC is the earthquake simulator exercise. Led by Tullis, the simulator group aims to compare computer codes that simulate multiple earthquake cycles on multiple faults, with the dynamic rupture process and dynamic wave propagation simplified to a quasi-static form. In 2009 group progress included meetings to decide on specific benchmarks to run and discussions about appropriate formats for comparison of results. In 2010 the group aims to finalize decisions about implementing a statewide fault geometry, in addition to finalizing decisions about comparison metrics.

In 2009, Harris and co-PI's continued the SCEC dynamic earthquake rupture exercise of computer code validation. The multiple spontaneous-rupture codes used by SCEC PI's and other interested international researchers are tested to determine if the results produced by the different codes are consistent. In particular, the on-fault rupture evolution and simulated ground motion results from the different codes are compared. In 2009, two normal-fault benchmarks designed by Joe Andrews were implemented; both benchmarks were designed to test hypotheses by Andrews et al. (2007) about extreme ground motion near the nation's formerly-proposed nuclear waste repository at Yucca Mountain (see Figure 36for the regional setting and idealized fault geometry). The normal-

Figure 7. Color orthophoto map of the Yucca Mountain area with surface fault traces from figure 2 of Whitney, Taylor, and
shown in the smaller boxed area. Numbers show locations of observed maximum-slip values of 1.3 m on the Solitario Canyon f
the Fatigue Wash fault, and 1.0 m on the Windy Wash fault at the time of the Lathrop Wells eruption. The footprint of the propos
is approximate.

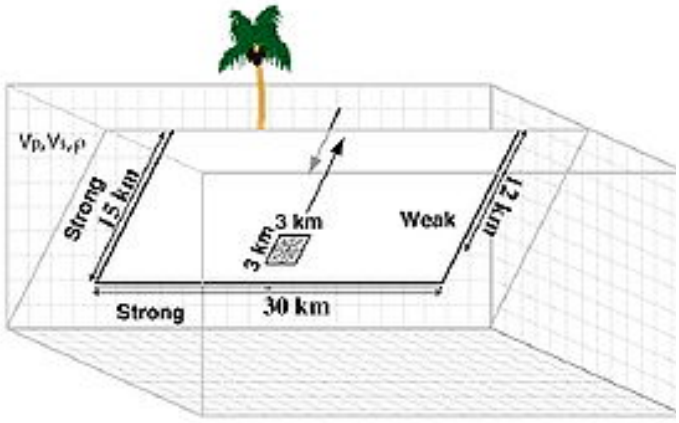

Figure 36. (Top) Geological setting of the Yucca Mountain repository region (figure 7 from Andrews et al., 2007), with the dashed area indicating the repository site. (Bottom) A sketch of the fault model that was used for the Harris et al. 3D TPV12 and TPV13 dynamic rupture code verification benchmarks. The 2D simulations used the centerline of the fault.

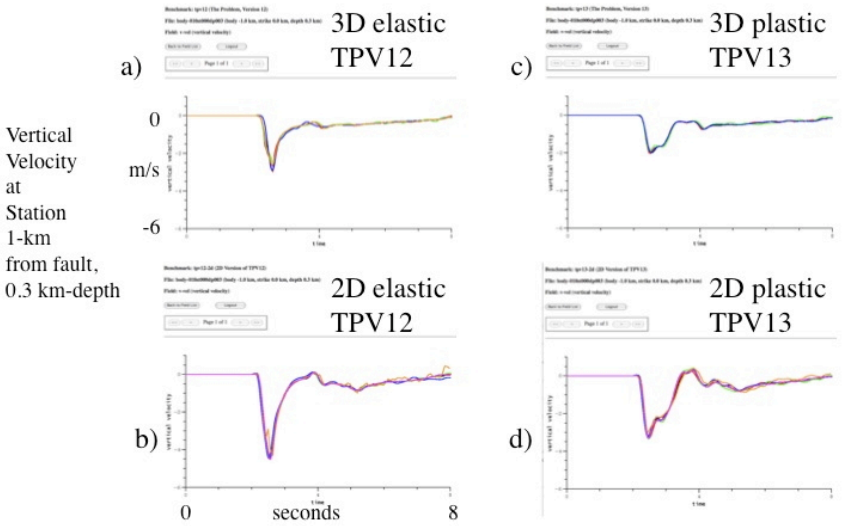

Figure 37. Ground motion simulation results for the Harris et al. TPV12 (elastic) and TPV13 (inelastic) rupture dynamics code verification benchmarks. For each simulation, the filtered vertical velocity results for just one site are presented, with the site located 1-km from the fault, at 0.3km depth. For more results, and a complete benchmark description, please visit the SCEC code verification website. a) TPV12-3D case. b) TPV12-2D case. c) TPV13-3D case. d) TPV13-2D case.

fault benchmarks consisted of 2D and 3D extreme-stress drop, supershear, dynamic-rupture scenarios, that were simplifications of the scenarios presented in 2D in Andrews et al. (2007). For one benchmark (TPV12), the off-fault response was assumed elastic; in the second benchmark (TPV13), the off-fault response was assumed inelastic. Good agreement was found for the simulated ground motions (see Figure 37for some examples) and fault-rupture evolution among most of the participant codes that conducted the benchmarks, and the findings verified the hypothesis of Andrews et al. (2007) that 2D numerical simulations produce higher extreme-ground-motions than 3D calculations. In addition, the elastic simulations generally produced higher ground motion values than those that assumed inelastic off-fault response. In 2010 the code validation group will move into non-planar fault geometry benchmarks, starting with a study of branched strike-slip faults. A spinoff project occurring in 2010, that is based on the results of the 2009 normal-fault benchmarks, is the '100 runs' exercise, with three code-validation participants whose 3D codes agreed well in TPV12 and 13, running cases of heterogeneous initial stresses to generate scenario M6.5 events on a normal fault.

In work related to both the Extreme Ground motion project and FARM, in 2009, dynamic rupture code-validation participants Duan and Day wrapped up a project where they investigated the physical limits to ground motion near Yucca Mountain when off-fault yielding is included for the Solitario Canyon fault. Rather than assuming the simplifications of the TPV12 and TPV13 code verification benchmarks mentioned above, Duan and Day more fully incorporated the Andrews et al. (2007) assumptions, and in addition investigated sophisticated variations on the Andrews et al. (2007) parameters. All of this was done in 2D with the goal of checking the sensitivity of the ground motion results to possible variations in the actual faulting behavior during 'extreme ground motion' events. Duan and Day found that 1) if there is a shallow dip at depth, as earlier studies by Brocher et al. (1998) indicated there might be, and if the cohesion near the Earth's surface is higher than that used by Andrews et al., (2007), then the simulated peak velocities in the ground motion can be larger than those calculated in Andrews et al. (2007), 2) inclusion of a 100-m wide symmetric low-velocity damage zone has little effect on the 'extreme, complete stress drop calculation', and 3) inclusion of time-dependent pore-pressure has little effect on the ground motion calculations (Figure 38 and Figure 39; Duan and Day (2009)).

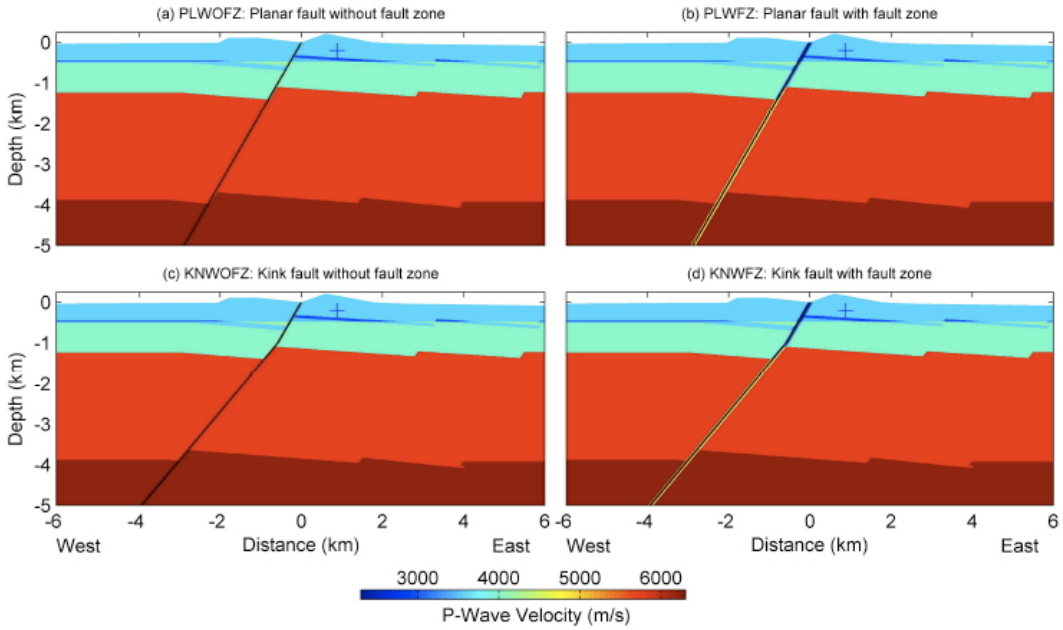

Figure 38. Different fault models to examine effects of fault geometry and fault zone structure of the Solitario Canyon fault (black line) on ground motion at the site (plus sign). A) PLWOFZ and b) PLWFZ are planar fault models, while c) KNWOFZ and d) KNWFZ are kinked fault models with a change in dip from 60 degrees to 50 degrees at a depth of 1 km. The fault zone is absent in a) and c), while a 100-m wide fault zone bisected by the fault is present in b) and d). In the fault zone, seismic wave velocities (both P and S) of the rock are reduced 20 percent relative to those of lateral surrounding wall rock. (From Duan and Day, 2009).

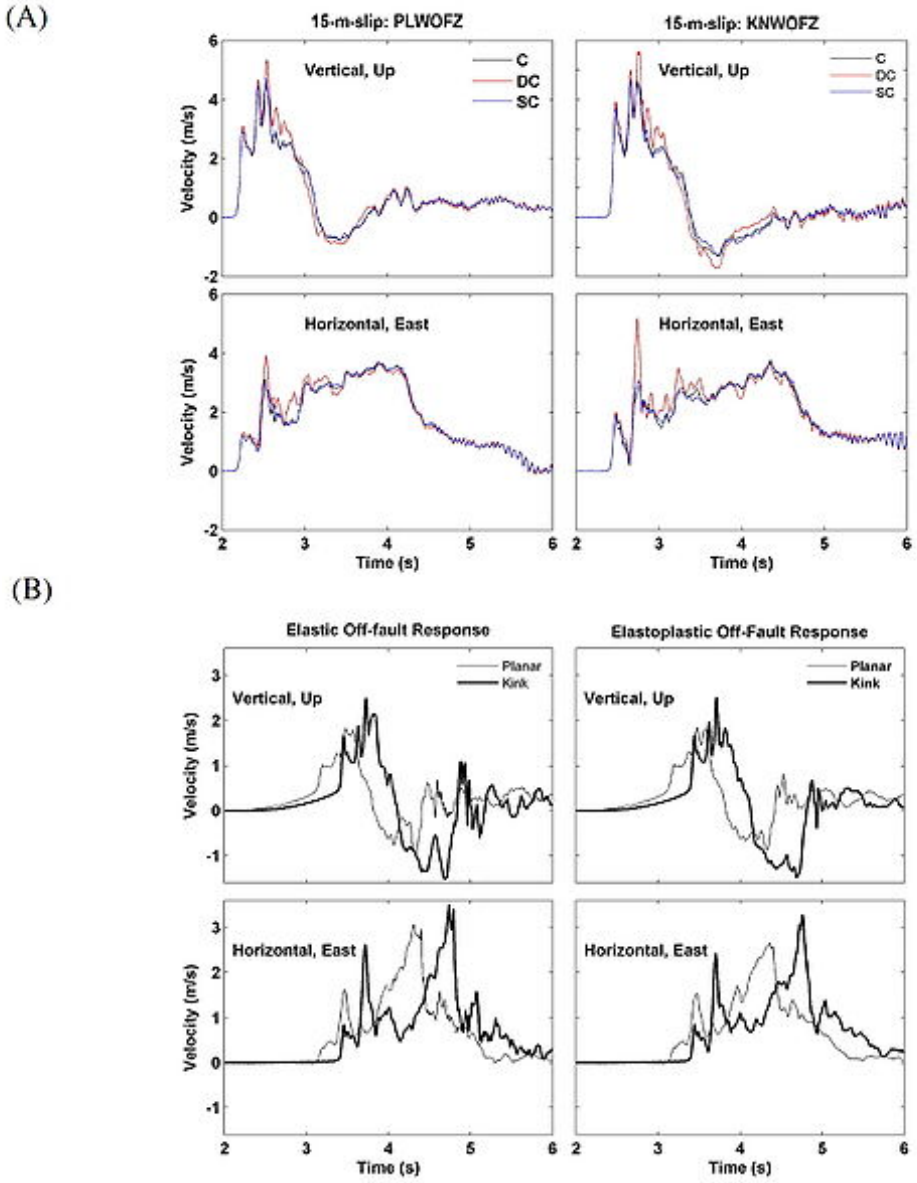

Figure 39. Effects of fault geometry and material strength on ground motion at the site. A) A shallower dip of the Solitario Canyon fault at depth and doubled cohesion values at shallow depth (red on right panel, DC) results in considerably higher peak ground velocities at the site, compared with the reference case (black on left panel, C) in the nearly complete stress drop scenario. B) Effects of a shallower dip (kink) of the Solitario Canyon fault at depth on ground motion with elastic (left panel) or elastoplastic (right panel) off-fault response, compared with the reference fault (planar).

References

Andrews, D.J., T.C. Hanks, and J.W. Whitney (2007), Physical limits on ground motion at Yucca Mountain, Bulletin of the Seismological Society of America; December 2007; v. 97; no. 6; p. 1771-1792; DOI: 10.1785/0120070014.

Bailey, I., T. W. Becker, and Y. Ben-Zion (2009), Patterns of co-seismic strain computed from southern California focal mechanisms, Geophys. J. Int., 177, 1015–1036.

Biegel, R. L., Bhat, H. S., Sammis, C. G., Rosakis, A. J. (in press), The effect of asymmetric damage on dynamic shear rupture propagation I: No mismatch in bulk elasticity, Tectonophysics.

Bhat, H. S., Biegel, R. L., Rosakis, A. J., Samms, C. G. (in press), The effect of asymmetric damage on dynamic shear rupture propagation II: With mismatch in bulk elasticity, Tectonophysics.

Brocher, T. M., W. C. Hunter, and V. E. Langenheim (1998), Implications of seismic reflection and potential field geophysical data on the structural framework of the Yucca Mountain-Crater Flat region, GSA Bulletin, v. 110, no. 8, 947-971.

Duan, B., and S. M. Day, Sensitivity study of physical limits on ground motion at Yucca Mountain, Bull. Seismo. Soc. Am., submitted Dec. 2009.

Dunham, E. M., D. Belanger, L. Cong, and J. E. Kozdon (2010), Earthquake ruptures with strongly rate-weakening friction and off-fault plasticity: 1. Planar faults, Bull. Seism. Soc. Am., submitted.

Dunham, E. M., D. Belanger, L. Cong, and J. E. Kozdon (2010), Earthquake ruptures with strongly rate-weakening friction and off-fault plasticity: 2. Nonplanar faults, Bull. Seism. Soc. Am., submitted.

Harris, R.A., M. Barall, R. Archuleta, E. Dunham, B. Aagaard, J.P. Ampuero, H. Bhat, V. Cruz-Atienza, L. Dalguer, P . Dawson, S. Day, B. Duan, G. Ely, Y. Kaneko, Y. Kase, N. Lapusta, Y. Liu, S. Ma, D. Oglesby, K. Olsen, A. Pitarka, S. Song, E. Templeton (2009), The SCEC/USGS Dynamic Earthquake Rupture Code Verification Exercise, Seism. Res. Lett., vol. 80, No. 1, pages 119-126, doi: 10.1785/gssrl.80.1.119.

Kitajima, H., F. M. Chester, and J. S. Chester, Dynamic weakening of gouge layers by thermal pressurization and temperature-dependent friction in high-speed shear experiments, J. Geophys. Res., submitted, July 2010.

Kitajima, H., J. S. Chester, F. M. Chester, and T. Shimamoto (in press), High-speed friction of disaggregated ultracataclasite in rotary shear: Characterization of frictional heating, mechanical behavior, and microstructure evolution, J. Geophys. Res., doi:10.1029/2009JB007038.

Murray-Moraleda, J.R., and R. Lohman, Workshop Targets Development of Geodetic Transient Detection Methods, EOS, TRANSACTIONS AMERICAN GEOPHYSICAL UNION, VOL. 91, NO. 6, P. 58, 2010, doi:10.1029/2010EO060008.

Viesca, R. C., E. L. Templeton, E. M. Dunham and J. R. Rice (2009), Plasticity in rupture dynamics: what role does pore fluid play?, Computational Infrastructure for Geodynamics Workshop on Numerical Modeling of Crustal Deformation and Earthquake Faulting, Golden, CO, 22-26 June 2009.

Viesca, R. C., and J. R. Rice (2010), Modeling slope instability as shear rupture propagation in a saturated porous medium, in Submarine Mass Movements and Their Consequences (Proc. 4th Int'l. Symp., Austin, Texas, 8-11 November 2009), eds. D. C. Mosher, R.C. Shipp, L. Moscardelli, J. D. Chaytor, C. D. P. Baxter, H. J. Lee, and R. Urgeles, Advances in Natural and Technological Hazards Research, Vol. 28, Springer-Verlag New York, pp. 215-223, 2010.

Viesca-Falguières, R. C., and J. R. Rice (2009), Growing a surface-parallel shear crack by a gradual pore pressure increase: At what point is it unstable?, Eos Trans. AGU, 90(52), Fall Meet. Suppl., Abstract NH41C-1272.

Wechsler, N., Chester, J., Rockwell, T.K., and Ben-Zion, Y. (2009), Particle size distributions, microstructures and chemistry of fault rocks in a shallow borehole adjacent to the San Andreas Fault near Little Rock, CA, Eos Trans. AGU, 90(52), Fall Meet. Suppl., Abstract T54A-01.

Crustal Deformation Modeling

This past year, several Crustal Deformation Modeling Group (CDMG) researchers have used detailed 3D viscoelastic models incorporating the SCEC CFM to address first-order scientific questions. Other CDM researchers have continued to focus their investigations on problems involving earthquake-cycle models with single faults, or postseismic deformation. Below, we showcase some exciting, representative results from various research groups in both categories. This is not meant to be a comprehensive overview of the full range of CDMG research activities, rather it is meant to highlight some of the last year's progress on important issues.

Multiple-fault models

Bridget Smith-Konter (UTEP) and David Sandwell (Scripps) have used semi-analytical models to investigate how differences in earthquake chronologies can affect estimates of stress accumulation, focusing on the Carrizo Plain, Imperial Valley, and Mojave sections of the SAF. This is an important point to address because: (1) revised earthquake chronologies are available for several southern California faults (e.g., Acsiz et al., 2009) and (2) it has been demonstrated that timing of earthquakes, even prior to the ultimate large event, can influence surface velocities predicted with viscoelastic models (Hetland and Hager, 2005). Even though Smith-Konter and Sandwell's models assume a simple viscoelastic structure (50 km thick elastic plate over a uniform viscoelastic halfspace), this is the first investigation of its kind to incorporate multiple faults and competing earthquake chronologies. The models show that large differences in slip history scenarios can result in large uncertainties (1 to 5 MPa) in interseismic stress accumulation estimates (Figure 40). This underlines the need for a comprehensive and conclusive paleoseismic database. Smith-Konter and Sandwell's modeled Coulomb stress accumulation rates range from 0.5-7 MPa/100 years vary as a function of fault locking depth, slip rate, and fault geometry, and are inversely proportional to earthquake recurrence intervals.

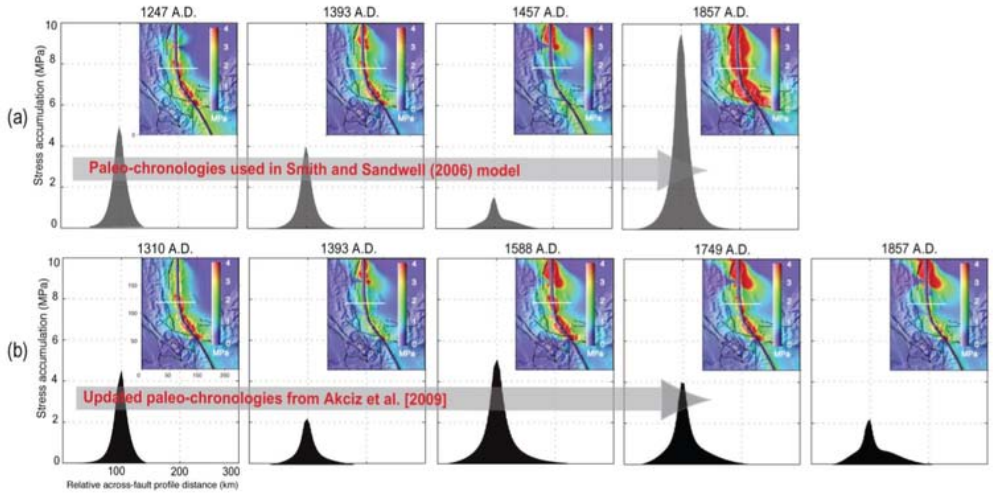

Figure 40. Comparison of hindcast stress accumulation models based on historical and prehistorical earthquake activity of the Carrizo section of the SAFS. Profile locations are represented by the solid white line in each panel. (a) Pre-event stress model results from Smith and Sandwell (2006) based on paleoseismic data (slip events at 1247, 1393, 1457, and 1857 A.D.) available at the time of publication. Each panel represents a snapshot of the accumulated stress field 1 year prior to the estimated slip event. (b) New stress model results calculated from updated data provided by Akciz et al. (2009) (slip events at 1310, 1393, 1588,1749, and 1857 A. D.)

Kaj Johnson (Indiana) and his PhD student Ray Chuang have continued to apply 3D, viscoelastic block models to the interpretation of the southern California GPS velocity field. These models incorporate earthquake chronology information for each fault segment, including repeat time and time since the most recent large earthquake (Figure 41). They have shown that when viscoelastic relaxation is incorporated into these block models, GPS-inferred slip rates on the SAF, ECSZ faults, and the Garlock Fault change dramatically relative to values inferred from elastic block models. In many areas, incorporating viscoelasticity brings the GPS-inferred rates closer to the geological estimates (Figure 42). A grid search suggests that the optimal value of effective viscosity for the lower crust throughout the modeled region is 2x10^20 Pa s, an estimate which is consistent with recent studies (e.g., Bürgmann and Dresen, 2008). Johnson and Chuang also show that inferred locking depths for some faults are lower when viscoelasticity is incorporated in block models (so locking depths inferred from elastic models may be biased upward). Currently, Johnson and

Chuang are addressing whether their findings hold true for a range of admissible lithosphere-asthenosphere viscosity profiles.

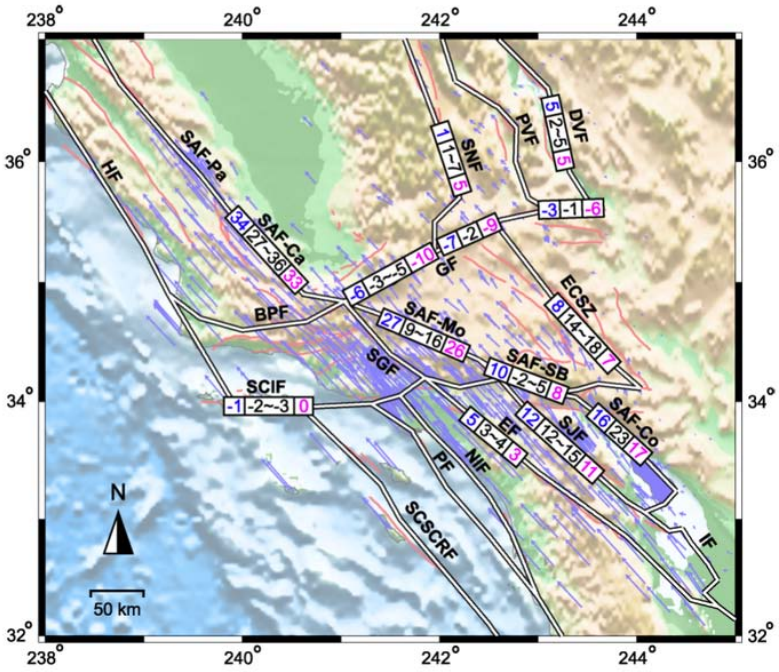

Figure 41. Comparison of geologic fault-slip rates (blue, mm/yr) used in the model, the range of the estimates from elastic block models (black) of Becker et al. (2004) and Meade and Hager (2005), and estimates from our block model (purple) along major faults. Light red lines are surface fault trace, and white thick lines are model blocks. Fault segments and geometry are constructed according to SCEC CFM-R. Blue arrows are crustal deformation velocities from SCEC CMM 3 with respect to the stable North America. BPF: Big Pine fault; DVF: Death Valley fault; ECSZ: eastern California shear zone; EF: Elsinore fault; HF: Hosgri fault; IF: Imperial fault; NIF: Newport – Inglewood fault; PF: Palos Verdes fault; PVF: Panamint Valley fault; SAF: San Andreas fault, Pa: Parkfield segment, Ca: Carrizo segment, Mo: Mojave segment, SB: San Bernardino segment, Co: Coachella segment; SCIF: Santa Cruz Island fault; SCSCRF: Santa Cruz – Santa Catalina Ridge fault; SGF: San Gabriel fault; SJF: San Jacinto fault; SNF: Sierra Nevada fault.

Charles Williams (GNS Science, NZ) has developed a finite-element (FE) model of southern California, incorporating 55 of the SCEC CFM faults. In their models, these faults define the boundaries of 11 blocks. Recurrence interval, time of most recent earthquake, and slip rate for each fault are based on WGCEP values, where available and deformation is modeled over a 3000-year interval (300 years for models incorporating power-law rheologies). Like Johnson and Chuang, Williams shows that viscoelastic relaxation adds a long-wavelength contribution to the surface velocity field, which is absent from the elastic (block-model) results. This effect is particularly apparent after large earthquakes (e.g. the 1857 SAF event). For a similar model incorporating a Burger's rheology with two Maxwell times (one the same as before, and another a factor of ten lower) the long-wavelength deformation component is greater. Together, these results suggest that "ghost transients" associated with viscoelastic relaxation from large earthquakes could pollute the southern California GPS velocity field, and that if two relaxation times are present, Maxwell viscoelastic models incorporating just the slower relaxation time may underestimate the magnitude of viscoelastic contributions to the GPS velocity field. Work on a wider variety of viscosity models is underway, as well as an effort to address whether power-law flow may be adequately mimicked with linear rheologies. The latter project is important because FE models incorporating power-law flow run very slowly, and semi-analytical or block models do not incorporate power-law flow.

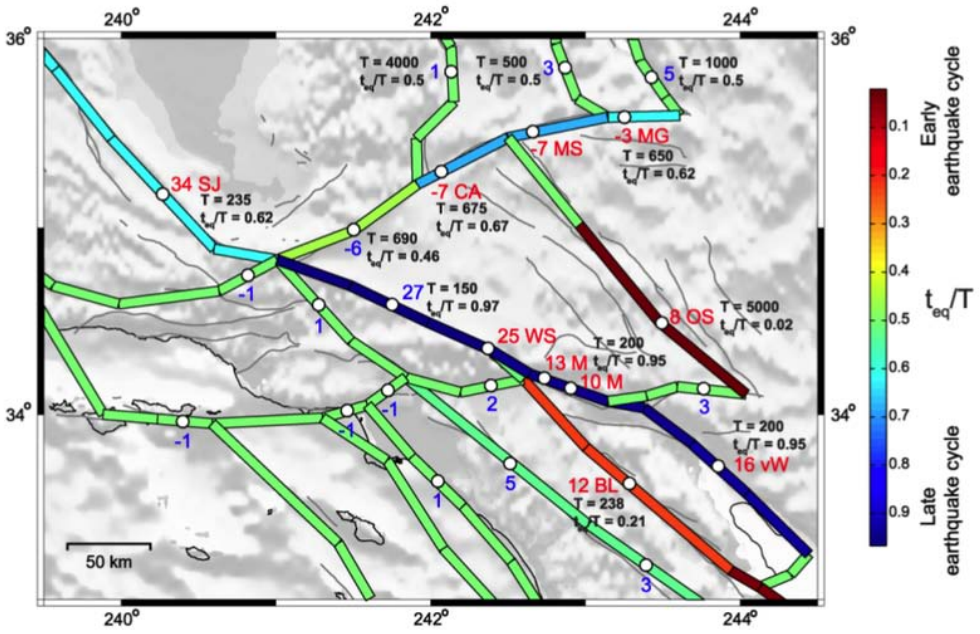

Figure 42. Summary of geologic rates, recurrence interval (T), and time since last earthquake (teq) in southern California used in our models. Blue numbers are geologic rates from WGCEP (2008) and red numbers are rates from other paleoseismology data. The color of each rupture segment represents the ratio of time since last earthquake and recurrence interval. Hot colors show segments are in early earthquake cycle, and cold colors show late earthquake cycle. Light grey lines are surface fault trace.

We also note that our past funding has borne fruit: at the 2010 CFEM workshop in Golden, Colorado, Williams, Brad Aagaard, and their colleagues distributed a version of PyLith that incorporates frictional faults and Drucker-Prager plastic rheology. This allows us to accurately model long sequences of earthquakes (large deformations) in areas with geometrically complex and kinematically imperfect fault systems, and to compute absolute crustal stresses.

Single-fault models

Yuri Fialko (Scripps) and his PhD student Sylvain Barbot improved their semi-analytical deformation code for modeling postseismic deformation, by adding stress-driven afterslip and power-law viscoelastic relaxation. They applied their technique to model coseismic stress-driven afterslip following the 2004 Parkfield earthquake. Their calculations show that the geodetic data are best explained by a rate-strengthening model with frictional parameter $(a - b) = 7 \times 10^{-3}$ and afterslip in areas of low coseismic slip and low seismicity. This is broadly consistent with past findings from Parkfield (Johnson et al., 2006), which were obtained using a different approach.

Elizabeth Hearn (UBC) and PhD student Ali Vaghri modeled the effects of lateral contrasts in viscosity structure on surface deformation around a strike-slip fault. For models with a plate thickness contrast across the fault or a contrast in viscosity below the elastic plate, they found that the sense of asymmetry in surface velocity profiles reverses during the interseismic interval, allowing the integrated interseismic displacement profile to be symmetric about the fault, like the coseismic displacements (Figure 43). For moderate to high substrate viscosity values, which are required for strain to localize around a fault late in its interseismic interval, asymmetry in surface velocities is modest. This suggests that strongly asymmetric surface deformation around major strike-slip faults cannot be explained in terms of viscosity contrasts or plate thickness variations. Models of fault formation and evolution by PhD student Yaron Finzi, which incorporate a brittle

damage rheology, show that asymmetric interseismic surface velocity profiles may result from viscosity contrasts. In these models power-law viscosity is assumed and the creeping fault zone at depth develops at a position which is offset from the material (or plate-thickness) contrast. Damage occurs preferentially in the weak (or thin-plate) side, resulting in asymmetric deformation relative to the fault. The UBC group's findings, and bounds on admissible, large-scale elasticity contrasts in crustal rocks, suggest that asymmetric deformation around strike-slip faults may reflect geometrical effects (e.g., offsets between the surface trace and the creeping fault at depth, perhaps due to deviations from vertical fault orientation) rather than material contrasts.

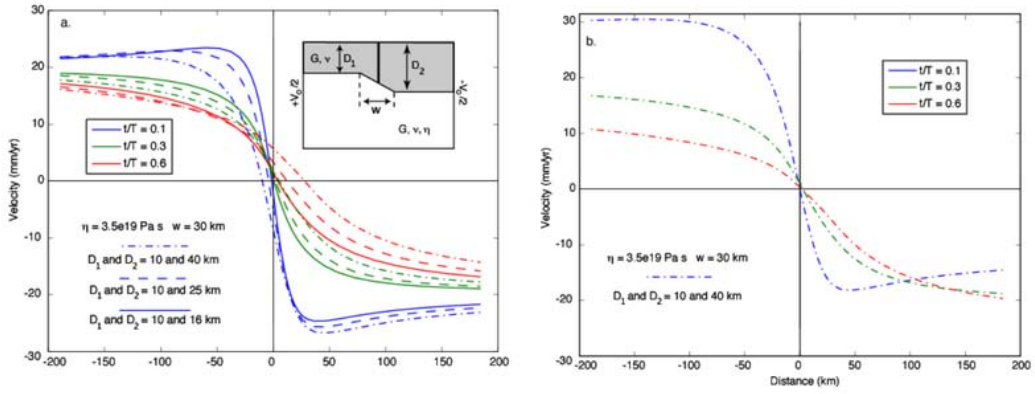

Figure 43. Earthquake-cycle models with a contrast in elastic plate thickness across the fault. (a) Results at three times in the earthquake cycle (t/Tcycle = 0.1, 0.3, and 0.6) for three models. (b) Velocity profiles plotted relative to a point on the fault for the model with the most extreme plate thickness contrast. Note the change in the sense of asymmetry with time. Tcycle = 200 years, TMaxwell = 50 years, G = 40 GPa, and Poisson's ratio = 0.25.

References

Akciz, S. O., L. Grant Ludwig, and J. R. Arrowsmith, J. Geophys. Res., 114, doi:10.1029/2007JB005285, 2009.

Bürgmann, R. and G. Dresen, Ann. Rev. Earth Plan. Sci., 36, 531-567, 2008.

Hetland, E. and B. Hager, J. Geophys. Res., 110, B10401, doi:10.1029/2005JB003689 2005.

Johnson, K., R. Bürgmann, and K. Larson, Bull. Seis. Soc. Am., 96, S321-S338, 2006.

Meade, B.J., and Hager, B.H., 2005, Block models of present crustal motion in southern California constrained by GPS measurements: Journal of Geophysical Research, v. 110, B03403, doi: 10.1029/2004JB003208.

Becker, T.W., Hardebeck, J.L., and Anderson, G., 2004, Constraints on fault slip rates of the southern California plate boundary from GPS velocity and stress inversion: Geophysical Journal International, doi: 10.1111/j.1365-246X.2004.02528.x.

Lithospheric Architecture and Dynamics

Three Dimensional Vp Vs Vp/Vs Structure

Gene Humphreys' group has accomplished a long-standing goal of constructing a tomographic image of southern California upper mantle using modern methods and data, including use of: (1) finite-frequency sensitivity kernels, (2) all available P and S wave data (to hundreds of kilometers from southern California), (3) the SCEC crustal velocity model (crustal velocities and Moho depths), and (4) spatially variable meshing of tomography nodes. The results were published in G-Cubed (Schmandt and Humphreys, 2010). Together, these improvements contribute to a significantly better resolved and accurate upper mantle P-wave model, which in turn provides

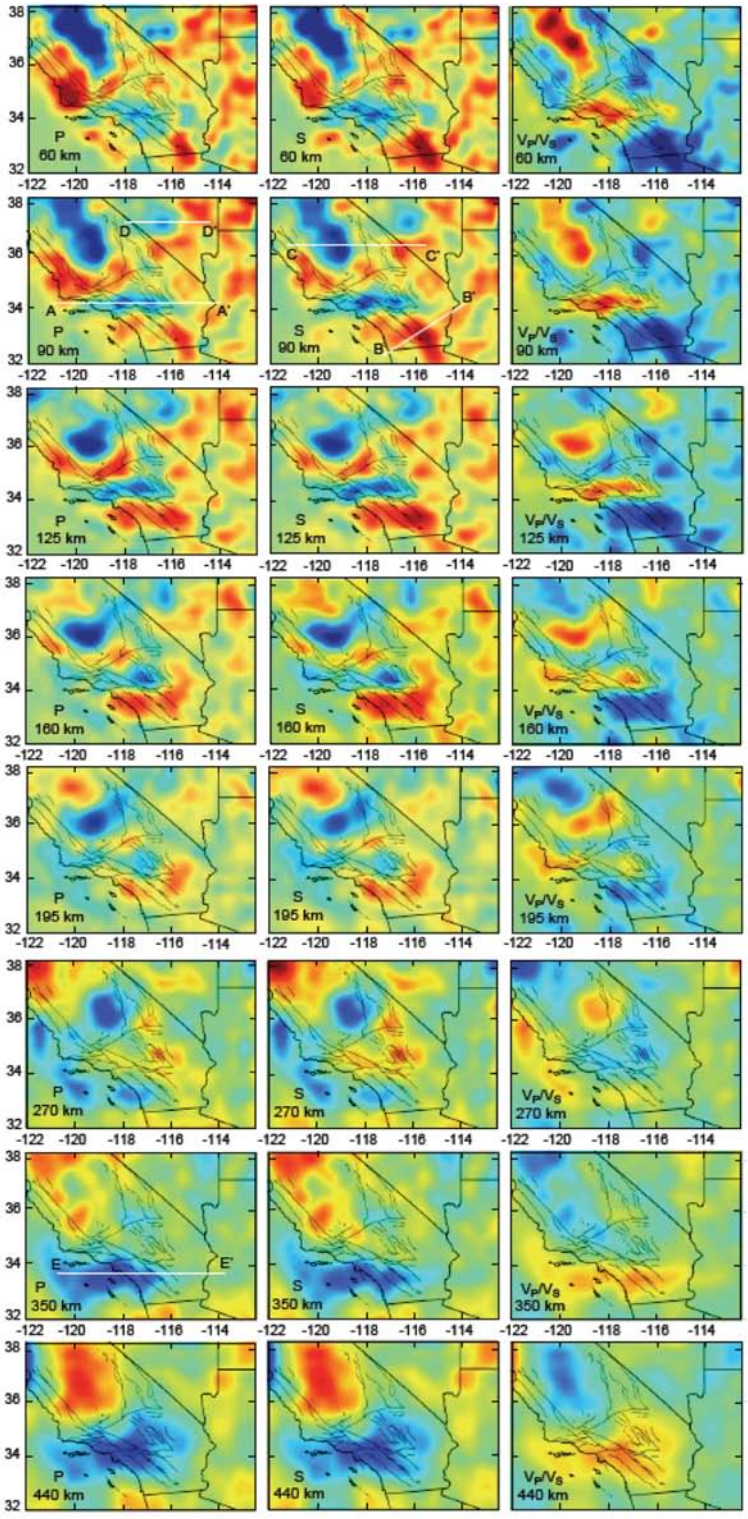

Figure 44. Map-view finite frequency P and S velocity model and Vp/Vs ratios (from Schmandt and Humphreys, 2010).

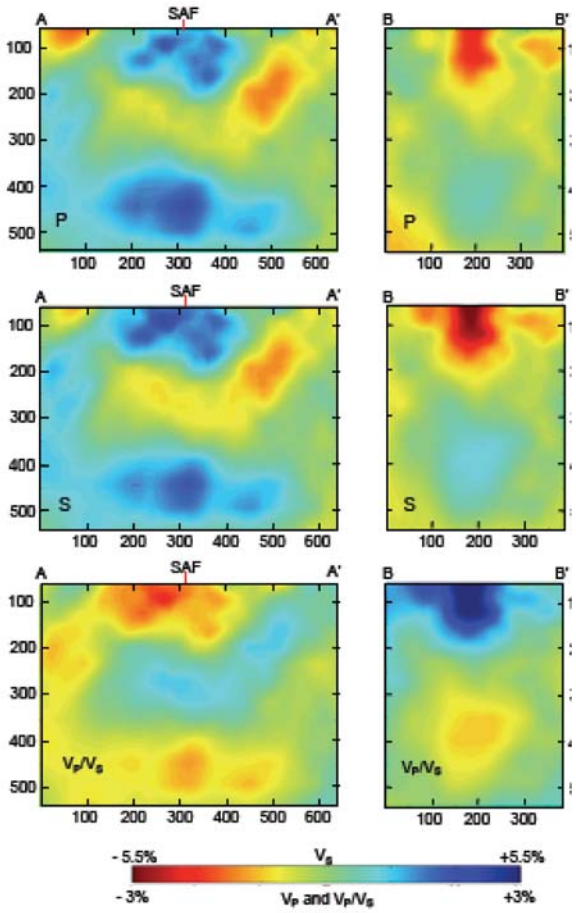

Figure 45. Finite frequency P and S velocity model cross-sections at depth (km) along profiles across the Transverse Ranges (LHS) and Salton Sea (RHS) (from Schmandt and Humphreys, 2010).

better constraints for geodynamic and tectonic models. Beyond improved resolution of the geometry and amplitude of the P-wave structure, other important results include: a companion S-wave tomography model (of resolution better that the previous P-wave model); a well-behaved Vp/Vs model, from which partially molten mantle is inferred beneath the Salton Trough to depths of ~125 km; resolution of high velocity structures within the transition zone that reasonably are fragments of previously subducted ocean lithosphere. Results are shown in map view in (Figure 44) and selected cross-sections beneath the Transverse Ranges and Salton Sea in (Figure 45). The regional tomography shows that the Transverse Ranges high velocity anomaly extends to a depth of 200 km but the southern Sierras anomaly is significantly stronger.

SKS Splitting

A paper on SKS splitting and surface wave comparison is under revision (Kosarian et al., 2010). SKS splitting parameters were calculated for all available data from the California Integrated Seismic Network. In southern California, where the density of stations is greatest, azimuthal anisotropy in the upper 100 km was estimated using surface waves. The inferred splitting from surface waves in the mantle lithosphere is small (on average 0.2 sec) compared with SKS splitting (1.5 sec) and obtains a maximum value (0.4 sec) in the transpressive region of the Big Bend, south of, and aligned with, the San Andreas Fault. In contrast, the SKS splitting is aligned approximately E-W and is relatively uniform spatially on either side of the Big Bend (Figure 46 and Figure 47).

These differences suggest that most of the SKS splitting is generated deeper, perhaps in the asthenosphere. Fast SKS directions align with absolute plate motions (APM) in northern and southeastern California but not in southwestern California. The authors interpret the parallelism with APM as indicating the SKS anisotropy is caused by cumulative drag of the asthenosphere by the over-lying plates. The discrepancy in southwestern California is interpreted as arising from the diffuse boundary there compared to the north, where relative plate motion has been concentrated near the SAF system. In southern California the relative motion originated offshore in the Borderlands and gradually transitioned onshore to the SAF system. This has given rise to smaller displacement across the SAF (160-180 km) compared with central and northern California (400-500 km). Thus, according to this view in southwestern California the inherited anisotropy from prior North American plate motion has not yet been overprinted by Pacific plate motion.

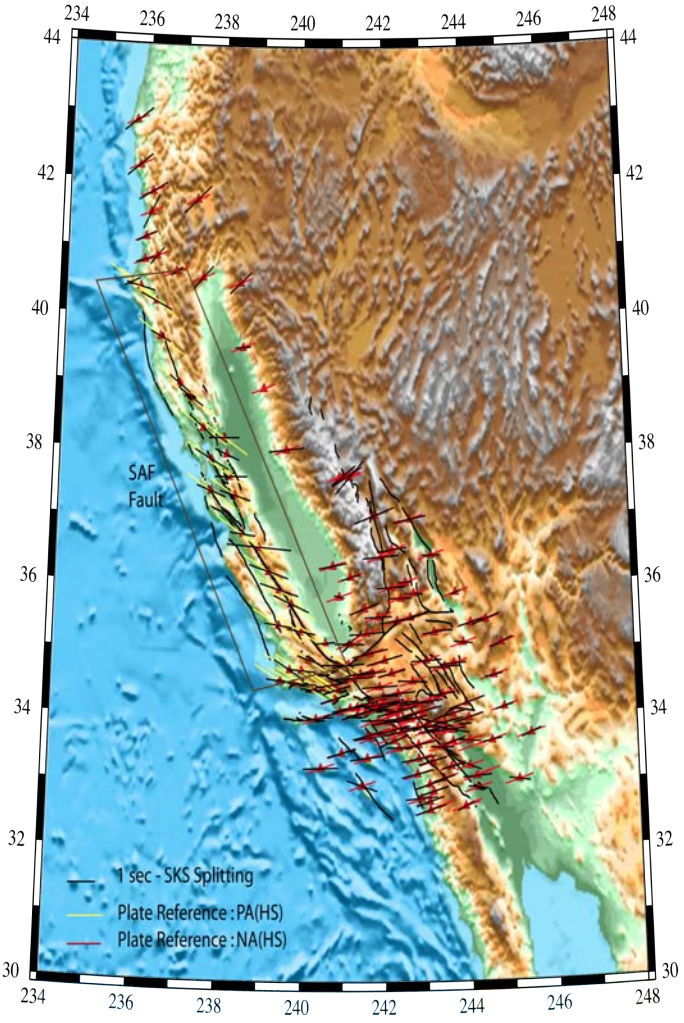

Figure 46. Comparison between APM (absolute plate motion) and splitting variations of the SKS phase for California Stations. Yellow lines give Pacific plate APM from the Nuvel 1A model (Gripp and Gordon, 2002). Red lines denote North American APM and black lines are SKS splitting fast directions. The brown box shows stations that have splitting directions that are rotated towards Pacific plate APM consistent with the 400-500 km of relative motion across the San Andreas Fault system that has occurred after plate capture. In southwestern California the onshore relative motion west of the SAF has been less than half this amount, insufficient to rotate the fast directions.[Kosarian et al., 2010].

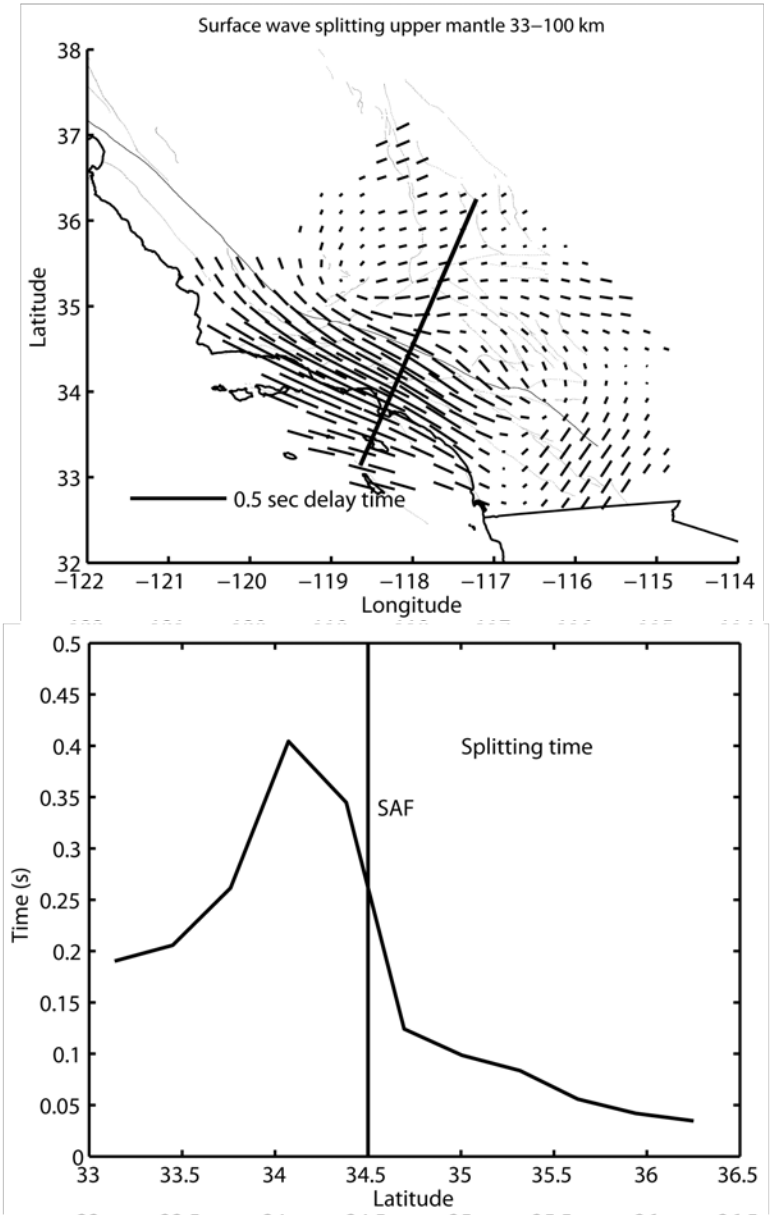

Figure 47. Predicted splitting times from surface wave analyses from mantle lithosphere (33-100 km). The other layers ([0-33, 100-150] km) give negligible effects. The surface waves fast axes are parallel to the San Andreas Fault (curved dark line) and obtain maximum values in the region of high topography associated with the Big Bend south of the fault. A cross-section illustrating this is shown in the lower panel along the line in the upper panel.

Receiver Functions (Lower Crust Anisotropy)

Zandt is examining receiver functions (RFs) in order to obtain seismic properties of the lower crust including anisotropy. He identified a lower crustal anisotropic zone, present in much of southern California (Figure 48). For this work he calculated teleseismic receiver functions for 38 broadband seismic stations in southern California and rotated the anisotropy measurements back to their orientations at 36 Ma. Results reveal a signature of pervasive seismic anisotropy in the lower crust that is consistent with the presence of schists emplaced during Laramide flat-slab subduction.

Anisotropy is identified in receiver functions by the large amplitudes and small move-out of the diagnostic converted phases. Within southern California, the similarity of data patterns on widely separated stations also supports an origin primarily from a basal crustal layer of hexagonal anisotropy with a dipping symmetry axis. Neighborhood algorithm searches (Frederiksen et al., 2003) for depth and thickness of the anisotropic layer and the trend and plunge of the anisotropy symmetry (slow) axis have been completed for the stations. The searches produced a wide range of results, but a dominant SW-NE trend of the anisotropy symmetry axis emerged among the station measurements.

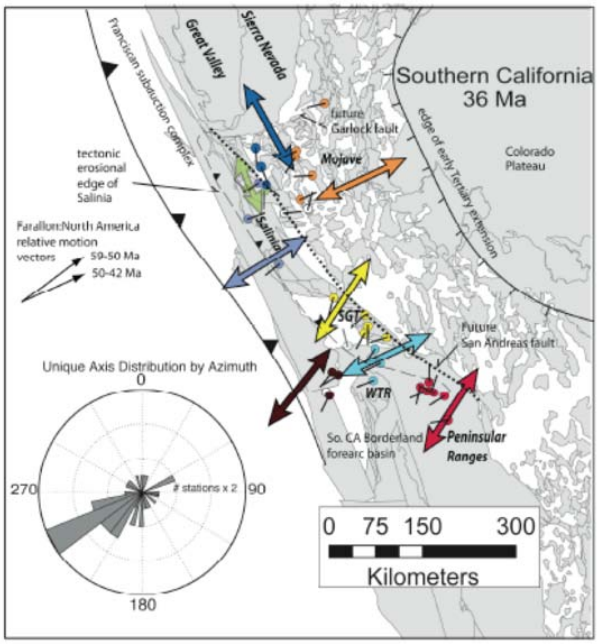

Figure 48. Map of station locations and unique lower crust anisotropy axis orientations at 36 Ma based on the reconstruction of McQuarrie and Wernicke (2005). Station color-coding corresponds to the crustal blocks. The large arrows show the best fitting block trend-lines rotated back to their orientation at 36 Ma. The rose diagram shows the number of stations with anisotropy trends within each 10° bin when rotated back to their 36 Ma orientations. Vectors show Early Tertiary Farallon-North America relative motion vectors from Saleeby (2003). [Zandt 2010].

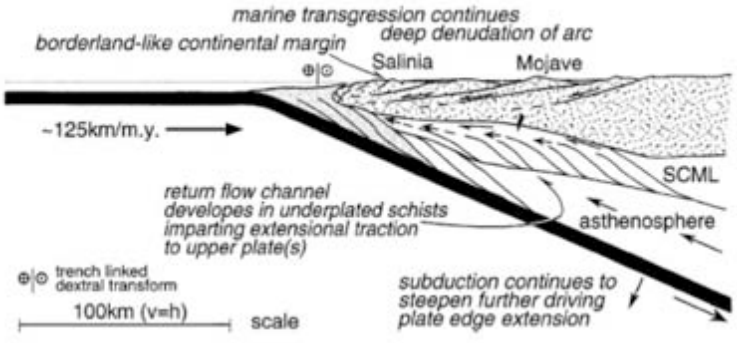

Figure 49. Interpretation of lower crustal anisotropy based on Saleeby model. Under-plated schist associated with relative motion of the Farallon slab and NA plate develops a fabric that can explain tangential energy in receiver functions.

When the results are divided into crustal blocks and restored to their pre-36 Ma locations using the reconstruction of McQuarrie and Wernicke (2005), the regional-scale SW-NE trend becomes even more consistent, though a small subset of the results can be attributed to NW-SE shearing that may be related to San Andreas transform motion. They interpret this dominant trend as a fossilized fabric within schists, created from a top-to-the-southwest sense of shear that existed along the length of coastal California during pre-transform, early Tertiary subduction. The mechanism is described in (Figure 49).

Regional Surface Wave Analysis

The discrepancy between SKS splitting and anisotropy from surface waves in the upper 100 km still remains. The surface wave anisotropy is too small and in the wrong orientation to explain the splitting. Both Tanimoto and Davis groups are examining very long period surface waves to see if the SKS anisotropy could be located deeper; however, achieving the required accuracy to detect anisotropy in (>150s) long period waves is proving difficult. Tanimoto used a beamforming approach in order to completely remove complications and doubts on the surface wave results from complex wave propagation effects. The whole earthquake data sets from 190 events from 1999 to 2008 were reanalyzed by the beamforming method. Figure 50 shows some examples of beamforming for selected earthquakes. In order to determine anisotropy refractions must be taken into account that cause incoming waves to depart from great circle azimuths by as much as thirty degrees. They make phase velocity measurements from the maximum beam locations. In Figure 51, they show the azimuthal variations of Rayleigh wave phase velocities obtained from beams. One hundred ninety events were selected to cover the entire azimuth as uniformly as possible. There are some azimuths for which it is hard to find earthquakes. Two prominent results are (i) 4-theta variations are much smaller than 2-theta variations. This has been assumed since the beginning of this type of study in the mid 1980s but has never been shown directly from data. (ii) The fast axis is in the azimuth of 290-300 degrees, clockwise measured from north. The main results unequivocally show the azimuthal variation of Rayleigh-wave phase velocities. The dominant component is in the 2-theta component, as has always been assumed, but this is perhaps the first result that shows the 4-theta components are small. The fast axis is in the azimuth 290-300 degrees (Figure 52. The fast phase velocity axis for the surface wave analysis is basically in the direction of WNW-ESE. The azimuth is 290-300 degrees. Red lines give regional fast axis for different Rayleigh frequencies. Unlike SKS which has fast directions ~E-W the surface wave fast directions are aligned with the San Andreas Fault (WNW-ESE).). Therefore, previous estimates (Prindle, 2006) for the fast axis is consistent with the current results.

In summary anisotropy in southern California can be separated into at least 4 layers (1) the upper crust with about 0.1 sec splitting with fast axis north-south, possibly associated with cracks and structures related to N_S compressive stresses, (2) lower crust with a similar splitting value oriented NE associated with underplaying of schists such as Catalina etc., at the time of subduction, (3) Mantle lithosphere with variable fast directions, but a coherent pattern in the Big Bend region aligned with structures caused by the transpression and (4) deeper asthenospheric values that amount to 1.5 s splitting and for most of the State are aligned with absolute plate motion, but in southern California is at a large angle to Pacific plate motion, for reasons we do not completely understand. The location of SKS anisotropy has not been found, but appears to be deeper than 150 km. Its parallelism to APM suggest it is upper mantle. The fact that is appears undetectable by surface waves of periods 100 sec and longer begs the question as to whether the strain associated with APM extends to depths of several hundred km.

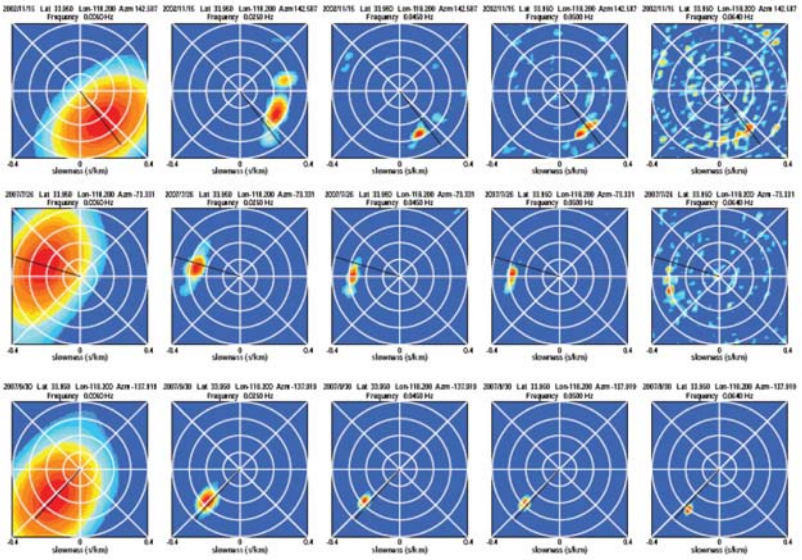

Figure 50. Beamforming analyses for three earthquakes (each row). From left to right, the results at frequencies 0.005 Hz, 0.025 Hz, 0.045 Hz, 0.05 Hz, and 0.064 Hz are shown. Black line from the center shows the (back-) azimuth of source location (along great circle path). At higher frequencies, systematic deviations between the beam locations (orange) and the black lines are obvious. Phase velocity measurements from the beam locations are free from such complications of surface wave refraction.

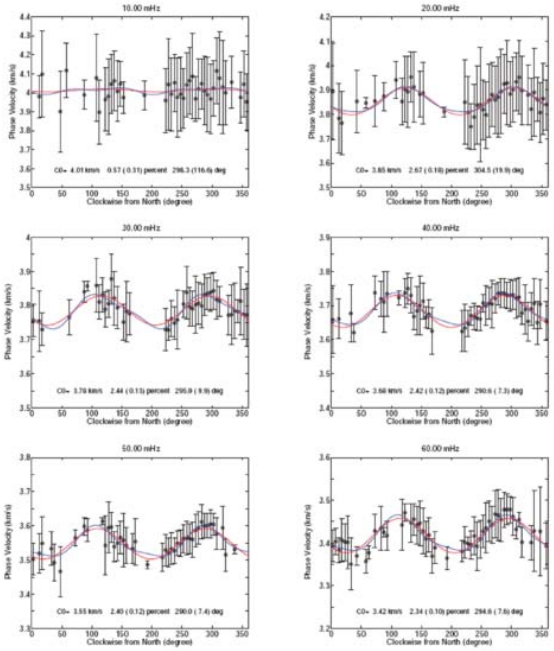

Figure 51. Azimuthal variations of Rayleigh wave phase velocity measurements from beam locations. Note the 100 sec waves indicate very low anisotropy, which is a puzzle when we try to explain SKS splitting.

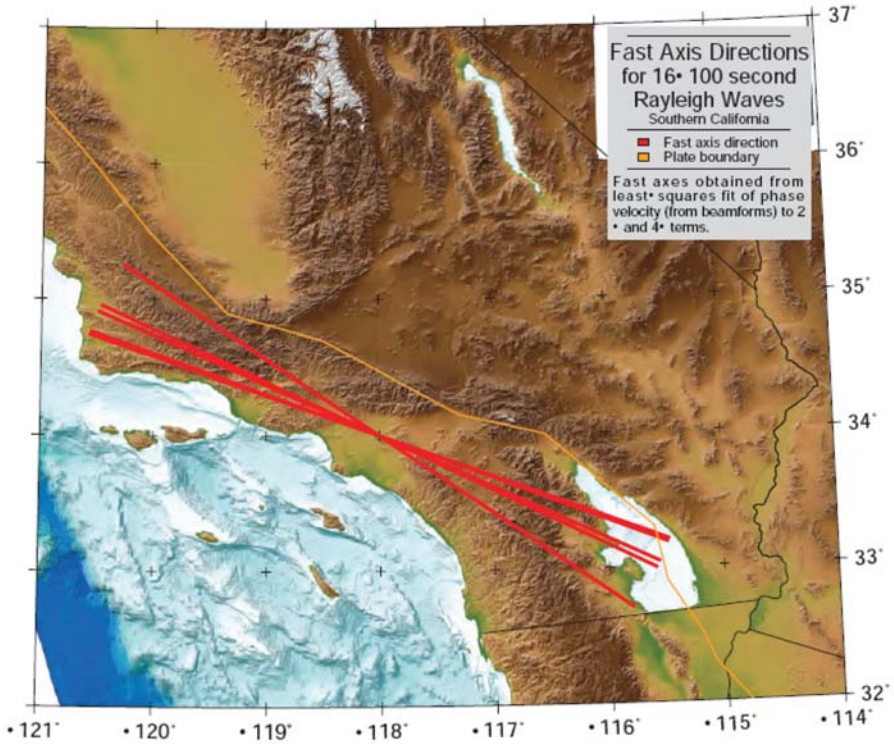

Figure 52. The fast phase velocity axis for the surface wave analysis is basically in the direction of WNW-ESE. The azimuth is 290-300 degrees. Red lines give regional fast axis for different Rayleigh frequencies. Unlike SKS which has fast directions ~E-W the surface wave fast directions are aligned with the San Andreas Fault (WNW-ESE).

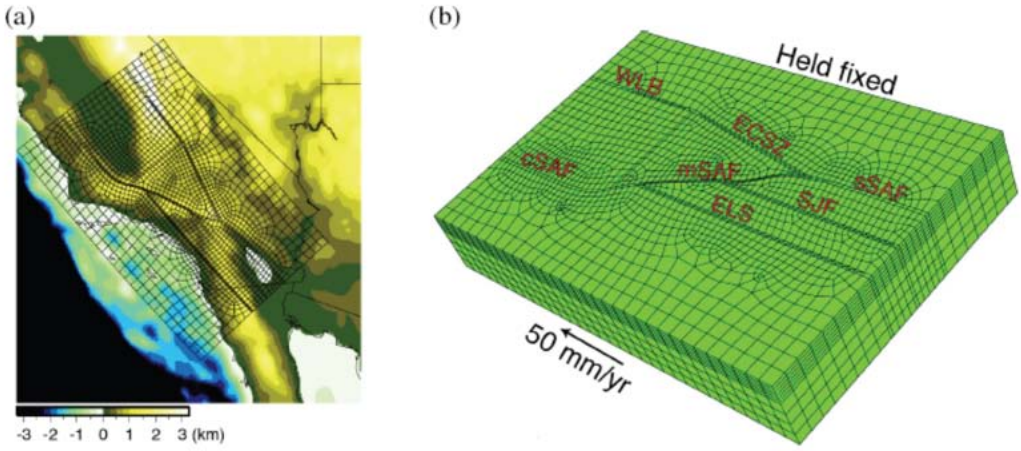

Figure 53. Map of the regional model study area (topography) with finite element domain overlain,focusing on southern California. (b) 3D perspective view of the finite element grid, major fault zones in southern California are marked. WLB: Walker Lane Belt; SAF: San Andreas Fault; cSAF: Central SAF; mSAF: Mojave section of the SAF; sSAF: southern SAF (Carrizo segment); SJF: San Jacinto Fault; ELS:Elsinore fault; Other abbreviations used in text: TR: Transverse Ranges; ECSZ: Eastern California Shear zone.

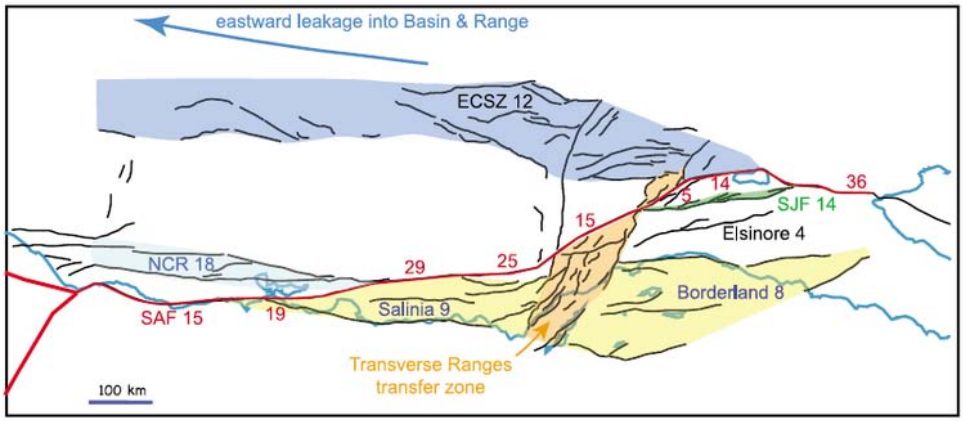

	offshore	SAF	RC/M	Bartlett Sp	NCR total	ECSZ	B&R	TOTAL
Profile 6	3	15	7	11	18	3	10	49
Profile 5	1	19	Hayward 9	Calaveras 6	15	5	9	50
Profile 4	4	29				9	7	49
Profile 3	2	Rinconada 7		SAF 25		12	3	49
Profile 2	3		WTR 12		SAF 15	15	3	48
Profile 1	8		Elsinore 4	SJF 14	SoSAF 14	4	3	48

Figure 54. Slip rate budget for California, showing major faults and bands of grouped faults, with interpreted slip rates. (bottom) The slip rates in tabular form for each profile, including the additional slip rate at the ends of each profile needed to bring the total to the Pacific–North America relative plate velocity. The color bands show schematically how the slip is transferred along strike. (top) Map showing in simplified form how the slip is distributed among the different parts of the system, together with their linkages. [From Platt and Becker, 2010]

Dynamic Models of Lithospheric Deformation

Becker's group is developing finite element models (SMOG3D) to understand driving forces, fault strength and rheology (Figure 53 and Figure 54). They model curved faults with large off-fault strain similar to that observed geodetically and the interaction of the San Andreas, San Jacinto (SJF) and Elsinore (ELS) faults and conclude that if only fault strength is varied to accommodate the geodetically observed distribution of slip-rates, the strength of the ELS must be larger than that of the SJF, which must be larger than that of the SAF Indio by at least a factor of 3 and 2, respectively. The results show that the models can be used to test several suggested forces acting upon southern California faults include in crustal as well as mantle tractions.

Analysis of geodetic velocities

Platt and Becker [2010] substantiate that the zone of highest geodetically defined strain rate in California does not everywhere coincide with the surface trace of the San Andreas Fault (SAF). To determine whether this reflects the pattern of long-term, permanent deformation, they analyzed the velocity field on swaths across the transform, located so as to avoid intersections among the major fault strands. Slip rates and flexural parameters for each fault were determined by finding the best fit to the velocity profile using a simple arctan model, representing the interseismic strain accumulation. Their slip rates compare well with current geologic estimates (Figure 55), which suggests that the present-day velocity field is representative of long-term motions. Platt and Becker find that the transform is a zone of high strain rate up to 80 km wide that is straighter than

the SAF and has an overall trend closer to the relative plate motion vector than the SAF. Most sections of the SAF take up less than half of the total slip rate, and slip is transferred from one part of the system to another in a way that suggests that the SAF should not be considered as a unique locator of the plate boundary. Up to half of the total displacement takes place on faults outside the high strain rate zone, distributed over several hundred kilometers on either side. Platt and Becker's [2010] findings substantiate previous suggestions that the transform has the characteristics of a macroscopic ductile shear zone cutting the continental lithosphere, around which stress and strain rate decrease on a length scale controlled by the length of the transform [e.g. Platt et al., 2008].

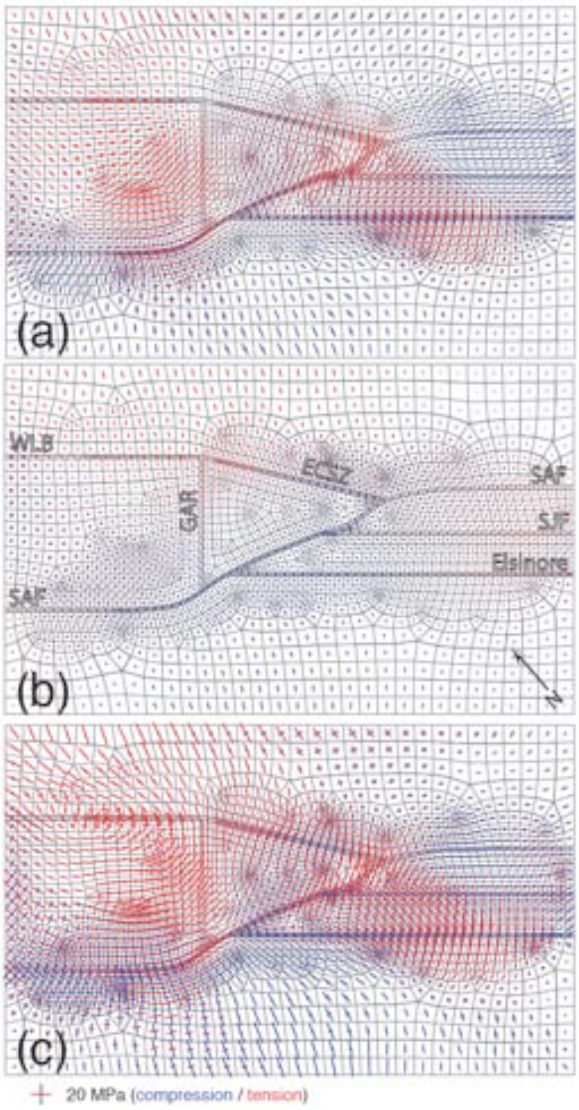

Figure 55. Estimated stress field, from body forces associated with topography, Moho variation and mantle loads inferred from tomography. Horizontal deviatoric principal stress field at 7.5 km depth caused by buoyancy heterogeneity. Blue bars indicate compression, red indicate tension. (a) Stress field caused by lateral variation in crustal thickness. Moho depth taken from receiver function studies [Zhu and Kanamori, 2000; Yan and Clayton, 2007] (b) Stress field caused by anomalous upper mantle density structure and tractions caused by density driven upper mantle flow [Fay et al., 2008]. SAF, San Andreas fault trace. (c) Total stress field (c = a + b) caused by crustal and upper mantle density variations. In the vicinity of the eastern and central Transverse Ranges the stress field is dominantly N-S compression and E-W tension [from Fay et al., 2009].

Tractions from Global Mantle Flow

To place the regional modeling for southern California into a broader context, and to check the consistency of the mantle loading that was explored in the regional finite element models, Becker's group also explores plate-wide models with high enough resolution to incorporate the western US. Earlier studies (Humphreys and Coblentz, 2007) have argued for the importance of shear tractions beneath the continent, but at a reduced amplitude from those predicted by Becker and O'Connell(2001); however, these tractions did not take into account the existence of lateral viscosity variations (LVVs) beneath North America, resulting from strong cratonic root and weak plate margin (cf. Conrad and Lithgow-Bertelloni, 2006; Becker, 2006). They evaluate the tractions and the resulting stresses over North America by incorporating LVVs in a global, high resolution, finite-element convection code, CitcomS (Zhong et al., 2000) (Figure 56). Since one of their goals is to match observables, such as plate motions and geoid, in addition to stresses, they perform a global inversion for both radial and lateral viscosity variations and choose the viscosity structures that yield a good fit simultaneously to both the global geoid and plate motions. They evaluate the tractions and corresponding stress field from those models. Recently they have also incorporated the effects of gravitational potential energy in their convection model by applying the GPE gradients as a stress boundary condition throughout the lithosphere. The GPE induced stresses from the flow model are benchmarked with vertically integrated deviatoric stresses obtained from a thin sheet model (Ghosh et al., 2009). They are in the process of refining the representation of plate boundaries (thinner weak zones), and intend to explore further the role of regional and global tomographic models for mantle tractions.

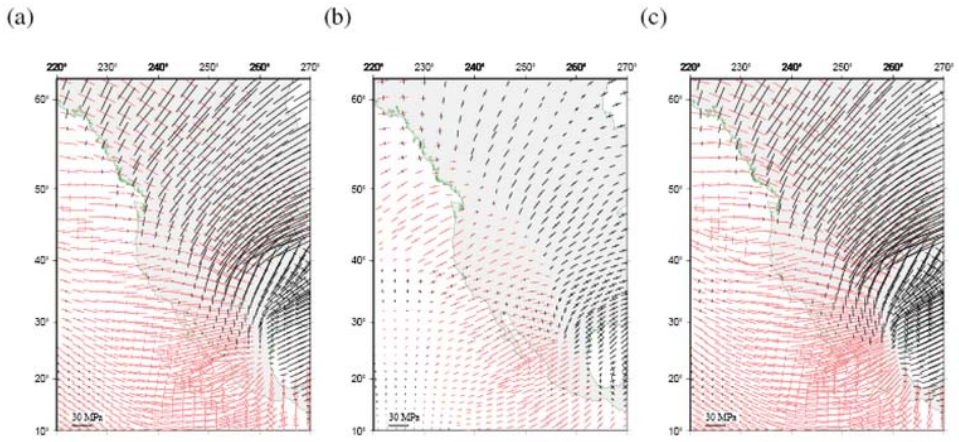

Figure 56. Lithospheric stress fields as predicted from a preliminary global, viscous flow computation (cf.Becker, 2006; Ghosh et al., 2009); red and black sticks indicate the orientation of the tensional and compressional axes, respectively. (Strike-slip style of stresses are correspondingly represented a pair of stresses.) (a)Deviatoric stress prediction from density driven flow model with lateral viscosity variations (LVVs). The tomography model used is the composite SMEAN (Becker and Boschi, 2002). LVV models are based on the best-fitting viscosity structure that matches both global geoid (correlation of 0.82) and plate motions(correlation of 0.85, both up to spherical harmonic degree 20) well (Ghosh et al., 2009). The LVVs are generated by weak plate boundaries (reduced viscosity), strong keels and temperature dependent viscosity.Most of the western US exhibits strike slip style of deformation, but note artifacts from the NW-SE trending weak zone which is at present too wide. (b) Deviatoric stresses from gravitational potential energy (GPE)differences. GPE is calculated based on the CRUST2.0 model of crustal structure, and the gradients of GPE are applied as traction boundary condition throughout the lithosphere. The resultant stress field is due to the instantaneous flow induced by these tractions alone. Tensional stresses mostly occur in the Great Valley and Sierra Nevada region where the GPE is relatively high, mainly due to topography. The stress field is dominated by either pure extension or compression. (c) Deviatoric stresses from GPE differences and density driven flow combined. Strike-slip stresses dominate in most areas except for the westernmost part.

References

Becker, T. W., On the effect of temperature and strain-rate dependent viscosity on global mantle flow, net rotation, and plate-driving forces, Geophys. J. Int., 167, 943–957, 2006.

Becker, T. W., and L. Boschi, A comparison of tomographic and geodynamic mantle models, Geochemistry, Geophysics, Geosystems, 3(1), doi:10.1029/2001GC000168, 2002.

Becker, T. W., Schulte-Pelkum, V., Blackman, D. K., Kellogg, J. B., and O'Connell, R. J.: Mantle flow under the western United States from shear wave splitting, Earth Planet. Sci. Lett., 247, 235-251, 2006.

Conrad, C. P., and C. Lithgow-Bertelloni, Influence of continental roots and asthenosphere on plate-mantle coupling, Geophys. Res. Lett., 33, doi:10.1029/2005GL02562, 2006.

Fay, N. P., R. A. Bennett, J. C. Spinler and E. D. Humphreys, Small-scale Upper Mantle Convection and Crustal Dynamics in Southern California, Geochem. Geophys. Geosyst., 9, Q08006, doi:10.1029/2008GC001988, 2008.

Fay N.P., Becker, T.W., and Humphreys, E. D.: Toward quantifying the state of tectonic stress in the southern California crust. Annual Meeting of the Southern California Earthquake Center Abstract Volume, p. 251, Southern California Earthquake Center, Los Angeles CA, 2009.

Ghosh, A., Becker, T. W., and Zhong, S.: Effects of lateral viscosity variations on the geoid. Geophys. Res. Lett., 37, L01301, doi:10.1029/2009GL040426,2009.

Humphreys, E. D., and D. Coblentz, North American dynamics and western U.S. tectonics, Rev. Geophys., 45(RG3001), doi:10.1029/2005RG000181, 2007.

Kosarian, M., P. M. Davis, T Tanimoto and R. Clayton, The Relationship Between Upper Mantle Anisotropic Structures Beneath California, Transpression and Absolute Plate Motions, Under Revision J. Geophys. Res., 2010.

McQuarrie, N., and B. P. Wernicke, An animated tectonic reconstruction of southwestern North America since 36 Ma Geosphere, 1(3), 147–172. doi: 10.1130/GES00016.1, 2005.

Saleeby, J., Segmentation of the Laramide Slab-evidence from the southern Sierra Nevada region, Geol. Soc. Am. Bull, 115(6), 655-668. doi: 10.1130/0016-7606(2003)115<0655:SOTLSF>2.0.CO;2, 2003.

Platt, J. P. and Becker, T. W.: Where is the real transform boundary in California? Geochem., Geophys., Geosys., 11(Q06013), doi:10.1029/2010GC003060, 2010.

Platt, J. P., Kaus, B. J. P. and Becker, T. W.: The San Andreas Transform system and the tectonics of California: An alternative approach. Earth Planet. Sci. Lett., 274, 380-391, 2008.

Prindle Sheldrake, K., C. Marcinkovich, and T. Tanimoto, Regional Wavefield reconstruction for teleseismic P-waves and Surface waves, Geophys. Res. Lett., 29, 391-394, 2002.

Schmandt, B., and E. Humphreys (2010), Seismic heterogeneity and small-scale convection in the southern California upper mantle, Geochem. Geophys. Geosyst., 11, Q05004, doi:10.1029/2010GC003042.

Silver, P. G., and W. E. Holt, The mantle flow field beneath western North America, Science, 295, 1054-1057, DOI: 10.1126/science.1066878, 2002.

Yan, Z., and R. W. Clayton, Regional mapping of the crustal structure in southern California from receiver functions, J. Geophys. Res., 112, B05311, doi:10.1029/2006JB004622, 2007.

Zandt, G., Lower Crustal Anisotropy in Southern California: Mapping the Distribution of Underplated Schist Progress Report 2009 SCEC Project #09001, 2010.

Zhong, S., M. T. Zuber, L. Moresi, and M. Gurnis, Role of temperature-dependent viscosity and surface plates in spherical shell models of mantle convection, J. Geophys. Res., 105, 11,063–11,082, 2000.

Zhu, L. and H. Kanamori, Moho Depth Variation in Southern California from Teleseismic Receiver Functions, J. Geophys. Res. 105, 2969-2980, 2000.

Earthquake Forecasting and Predictability

The Earthquake Forecasting and Predictability (EFP) focus group coordinates two types of research projects. The first type encourages the development of earthquake forecasting methods to the point that they can be moved to testing within the framework of the Collaboratory for the Study of Earthquake Predictability (CSEP). The other type of research project encouraged by EFP are those that are far from being ready for testing within the CSEP framework, but that aim to obtain fundamental knowledge of earthquake behavior that may be relevant for forecasting earthquakes.

The Search for Earthquake Precursors

There is a long-standing question as to whether the seismicity prior to a large earthquake contains any precursory signals, such as rate changes over the future fault area or more foreshocks than would be expected from a simple earthquake clustering model. Shearer ("Analysis of Southern California Seismicity Using Improved Locations and Stress Drops") addressed these questions by stacking a large database of small earthquake locations. A subtle but significant signal was found, similar to the classic "Mogi doughnut", where more events occur in the day before a larger earthquake, at distances comparable to its source dimension (Figure 57). Comparing the rate of foreshocks to the rate of aftershocks also shows that there are relatively more foreshocks than would be expected from a self-similar process (Figure 58). These signals are too small to be useful precursors for earthquake forecasting, but provide significant insight into pre-earthquake processes, and highlight the limitations of simple self-similar earthquake clustering models.

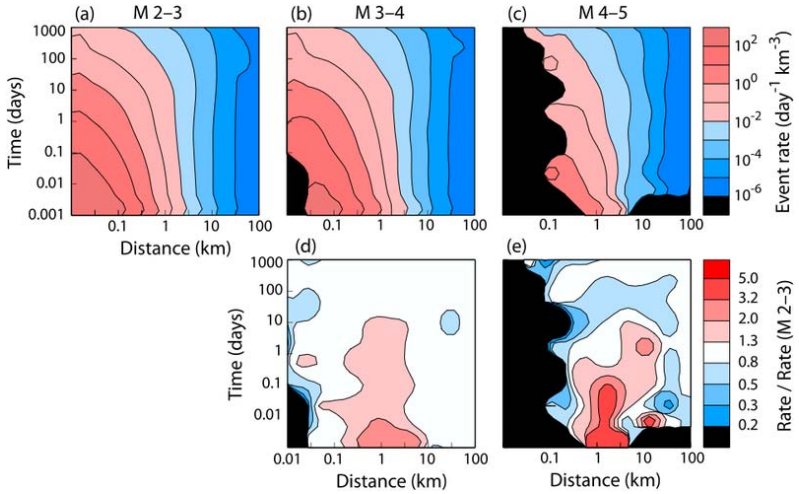

Figure 57. Space/time behavior of precursory seismicity in southern California. (top) The average event rate prior to target earthquakes of (a) M 2–3, (b) M 3–4, and (c) M 4–5, at times from 0.001 day (86 s) to 1000 days prior to the target events at distances from 10 m to 100 km. Contours are uniform in log event density (per day per cubic kilometer). Black shows regions of no data. (bottom) The ratio of precursory seismicity rate for the (d) M 3–4 and (e) M 4–5 target event bins compared to the M 2–3 bin (from: Shearer and Lin, JGR 114, B01318, doi:10.1029/2008JB005982, 2009.)

It has also been proposed that large earthquakes are preceded by a change in the frequency-magnitude distribution, commonly represented by the b-value. Zaliapin ("Investigating temporal changes in the earthquake magnitude distribution") tested for a change in b-value before large earthquakes, as well as changes in the relative number of medium sized earthquakes compared to the number of small earthquake, and changes in the number of earthquakes, fault area, and moment release rate. The ratio of medium sized to small earthquakes appears to increase prior to large earthquakes in California; however, the standard b-value had mixed results, decreasing before large events in northern California while increasing before large events in southern

California. The other statistics were found to have better spatial resolution than temporal predictive power, reflecting spatial variations in earthquake rate. A smoothed seismicity model from this project has been submitted to CSEP testing.

SCEC also supports the operation of the strainmeters at Pinon Flat Observatory (Agnew "Pinon Flat Observatory: Continuous Monitoring of Crustal Deformation"), which are suited to capture precursory slip on the San Jacinto or southernmost San Andreas fault, or at least to constrain the maximum possible precursor if no strain signal is detected.

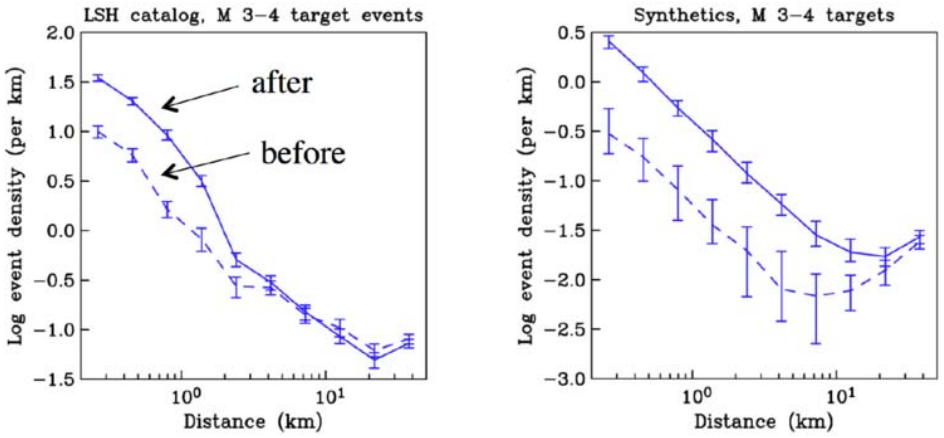

Figure 58. Event density as a function of distance in one-hour windows before and after M 3–4 target earthquakes, comparing the LSH catalog of southern California seismicity (left) with predictions of an ETAS-like triggering model (right). One-standard error bars are computed using a bootstrap resampling method. (From: Shearer, SCEC annual report.)

Testing Earthquake Forecasts

Zechar ("Parkfield microrepeater predictability experiments") attempted forecasts of repeating small earthquakes on the San Andreas Fault near Parkfield, based on the regularity of the events. While retrospective tests indicated that the forecasts based on recurrence times were better than random, the forward tests were unsuccessful. One problem may be the change in rate following the 2004 Parkfield earthquake. Burgmann ("Triggering Effect of the 2004 M6 Parkfield Earthquake on Earthquake Cycles of Small Repeating Events") studied the effect of the Parkfield earthquake on repeating events, and found that after Parkfield, the recurrence intervals decreased dramatically and then started increasing back towards their pre-Parkfield values (Figure 59). Interestingly, the magnitudes also increased for many sequences (Figure 59), a counter-intuitive change that can be explained by post-seismic slip and rate and state friction. For a small velocity-weakening patch embedded in a velocity-strengthening (creeping) fault, at low slip speeds much of the patch slips aseismically, while at higher slip speeds more of the patch participates in stick-slip events. These two studies demonstrate the considerable complexities in the predictability of even the most apparently simple earthquake sources, and the importance of developing a physical basis for the understanding of earthquake behavior.

Several short-term and long-term forecast were submitted to CSEP testing, based on smoothed seismicity and spatial-temporal clustering. These models cover the California-Nevada region and the whole earth (Kagan, "Global and Regional Earthquake Forecasts"; and Jackson, "California Earthquake Forecasts".)

Several proposals supported the CSEP testing centers and implementation of CSEP tests. Gerstenberger's "Developing reference models for earthquake predicitability experiments" addressed the important problem of producing appropriate reference models for testing in CSEP and other testing environments. Gerstenberger's "CSEP Forecast Test Methodology: Development and Participation" supported travel for collaboration and meeting participation for the New

Zealand testing center. Wiemer's "Travel funds for CSEP integration & development" provided similar support for the testing center in Zurich.

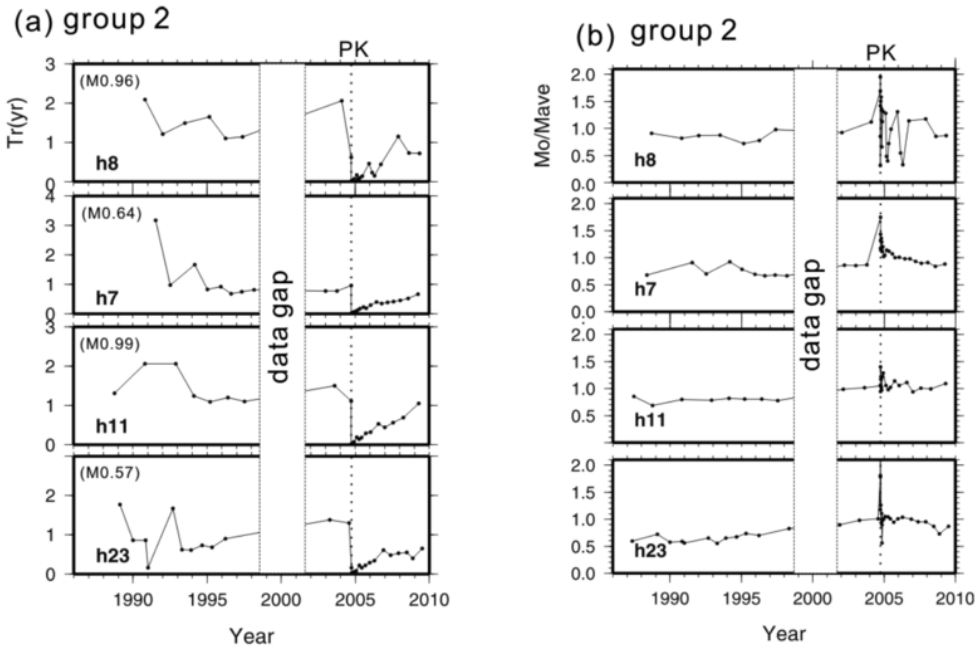

Figure 59. (a) Recurrence interval as a function of time and (b) relative moment variation (ratio of Mo and average Mo of the sequence) as a function of time for repeating sequences on the San Andreas Fault near Parkfield. (From: Burgmann et al., SCEC annual report.)

Observational Constraints

Earthquake forecasts often rely on accurate models of long-term earthquake rates. Zaliapin ("Time-dependent modeling of seismic moment release in San Andreas Fault -- Great Basin System") reconciled apparent differences in moment rate from earthquake catalogs and geodetic information. They demonstrate that moment rate deficits in earthquake catalogs are to be expected due to sampling and clustering affects, and hence can be consistent with geodetic rates. McGill ("Late Quaternary slip rate of the northern San Jacinto fault") studied off-set features along the San Jacinto Fault to better constraint the long-term slip rate. Scharer ("Reducing uncertainties of paleoseismic event dates through critical examination of contributions to the COV") updated the slip history of the San Andreas fault at Pallett Creek using modern dating techniques, and used the revised estimates to better understand the variation of recurrence times.

The multi-disciplinary nature of EFP, and the recognition that certain tests required long-term measurements that may only be accessible through geology, led to support of several other geological studies. Stirling ("Age of precarious landforms near major plate boundary faults in New Zealand: Cross validation of western United States Studies") identified precariously balanced rocks near the Alpine Fault in New Zealand that appear to be old enough to have survived several earthquake cycles, hence potentially placing bounds on the near-field ground motions. Grant-Ludwig ("Constraining the age and renewal rates of precariously balanced rocks (PBRs) in southern California") studied precariously balanced rocks in southern California to constrain better their exhumation history, how this history may affect their apparent age, and how that would feed into their use in testing long-term ground motion predictions.

Earthquake Simulators

Several investigators have conducted research using Earthquake Simulators, including Ward's "ALLCAL -- An Earthquake Simulator for All of California", Tullis's "Quasi-Dynamic Parallel Numerical Modeling of Earthquake Interactions Over a Wide Magnitude Range Using Rate and State Friction and Fast Multipoles", and Dieterich's "Application of a Physics-based Earthquake Simulator to Southern California" and "Stress Heterogeneity and Its Effect on Seismicity". These simulators are numerical models aimed at generating catalogs of simulated earthquakes over a variety of spatial and temporal scales. The aim of these studies is to gain new insight into the behavior of real earthquakes by studying the behavior of simulated earthquakes. For example, one line of inquiry is to see if patterns of simulated seismicity in space and time occur that might also be discovered in real seismicity. If so, forecasting future earthquakes might be done by recognizing ongoing patterns in past and current seismicity. The Earthquake Simulator Comparison Project has recently focused on comparing scaling relationships found from different simulators, including the frequency-magnitude distribution, scaling of the earthquake length with slip and moment, and moment-area relationships (Figure 60).

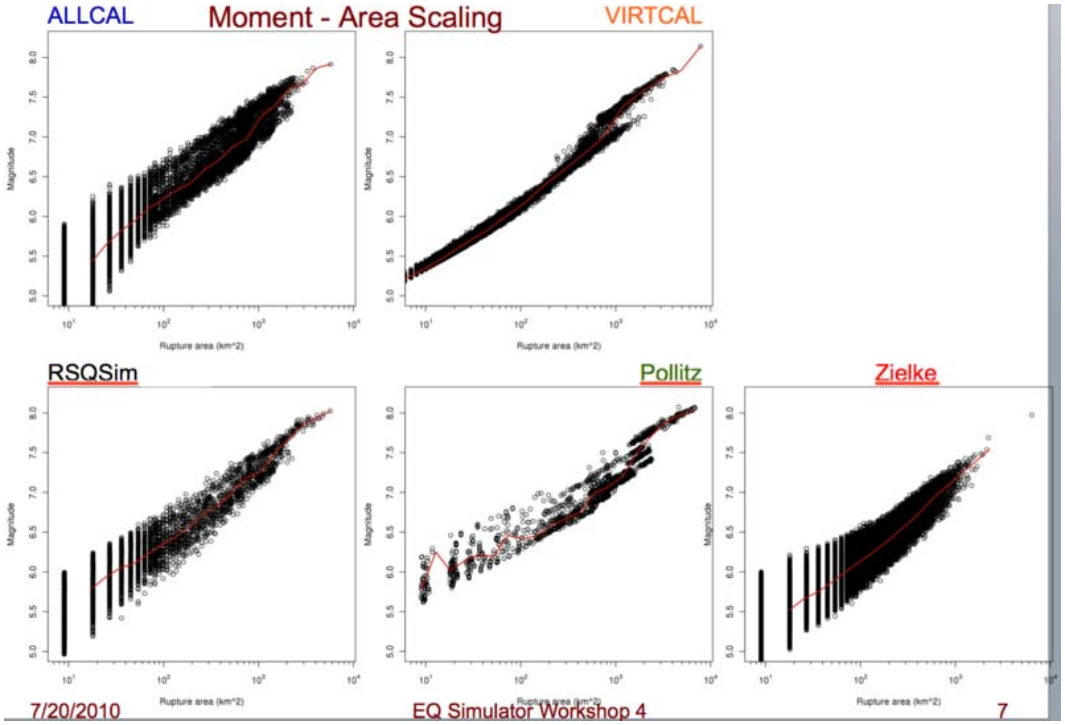

Figure 60. Comparison of moment-area scaling of model earthquakes for Northern California from five different simulators.

There is currently much debate about whether the earthquake frequency-magnitude distribution follows the self-similar Gutenberg-Richter law at large magnitudes, or whether there is a relative surfeit of earthquakes at larger magnitudes. Modeling by Arrowsmith ("The effect of structural complexity and fault roughness on fault segment size and multi-segment rupture probability") demonstrated the effect of fault roughness on the frequency-magnitude distribution. Simulation results show that rough faults produce Gutenberg-Richter distributions, while smooth faults generate characteristic earthquakes, suggesting that both behaviors may be present, and depend on fault maturity (Figure 61).

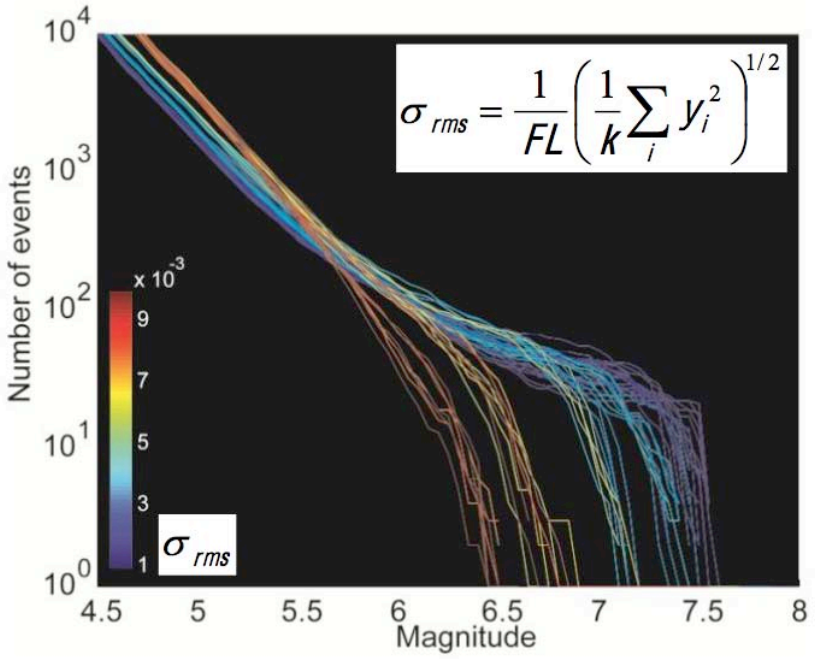

Figure 61. Cumulative magnitude frequency relationship for earthquake simulations along faults with different roughness values. Seismic behavior is becoming increasingly characteristic i.e., bimodal as the fault matures (indicated by decreasing roughness, in cold color.) (From: Arrowsmith and Zielke, SCEC annual report.)

Workshops

The "6th International Workshop on Statistical Seismology" was hosted by SCEC in April of 2009. This 3-day workshop, with approximately 100 participants, included a full day of talks and discussion focused on earthquake forecasting, predictability, and testing, in addition to related topics including earthquake recurrence, earthquake clustering, and earthquake stress interaction.

Ground Motion Prediction

The primary goal of the Ground-Motion Prediction focus group is to develop and implement physics-based simulation methodologies that can predict earthquake strong motion waveforms over the frequency range 0-10 Hz. At frequencies less than 1 Hz, the methodologies should deterministically predict the amplitude, phase and waveform of earthquake ground motions using fully three-dimensional representations of Earth structure, as well as dynamic or dynamically compatible kinematic representations of fault rupture. At higher frequencies (1-10 Hz), the methodologies should predict the main character of the amplitude, phase and waveform of the motions using a combination of deterministic and stochastic representations of fault rupture and wave propagation.

Source characterization plays a vital role in ground-motion prediction and significant progress has been made in the development of more realistic implementations of dynamic and dynamically compatible kinematic representations of fault rupture within ground-motion simulations. Verification (comparison against theoretical predictions) and validation (comparison against observations) of the simulation methodologies continues to be an important component of this focus group with the goal being to develop robust and transparent simulation capabilities that incorporate consistent and accurate representations of the earthquake source and three-dimensional velocity structure. The products of the Ground-Motion Prediction group are designed

to have direct application to seismic hazard analysis, both in terms of characterizing expected ground motion levels in future earthquakes, and in terms of directly interfacing with earthquake engineers in the analysis of built structures. Activities in these areas are highlighted by the projects described below.

Ground-Motion Simulations and Model Validation

Precariously Balanced Rocks. Grant-Ludwig and Rood engaged in collaborative research to develop, refine, and implement the use of precariously balanced rocks (PBRs) for validation of ground-motion studies and seismic hazard analysis. Their work focuses on constraining the age and exhumation or "renewal" rates of PBRs. In previous years they identified PBRs with good potential for cosmogenic nuclide exposure dating at sites that are important for PetaSHA validation and collected >35 samples from rocks at 6 sites. They have analyzed 30 samples for 10Be concentration, obtained preliminary, model-dependent exposure ages of four PBRs near the southern San Andreas fault, and completed a full 3-D model dependent exposure age analysis of a PBR at Grass Valley near the San Andreas and Cleghorn faults as a "proof of concept" (Figure 62).

Figure 62. Sampling profile for Grass Valley Rock GV-2 and the 3D shape model. The 3D modeling effort for GV-2 demonstrates the value of this shape-based method for obtaining exposure ages.

Preliminary results indicate exposure ages correspond with marine isotope stage 2. They hypothesize a causal relationship between climate cycles and PBR formation. The Last Glacial Maximum may have increased soil erosion rates, which rapidly exhumed these PBRs. This hypothesis will be tested when exposure ages are obtained from remaining field sites. If true, regional climatic control on PBR formation would provide high resolution spatial control on unexceeded ground motions since the Last Glacial Maximum. Additionally, the age and location of the Grass Valley PBR is inconsistent with the 2% in 50 year PGA exceedance from the National Seismic Hazard Map. One possibility is that the Cleghorn fault does not have a 3 mm/yr slip rate, as assumed for UCERF-2. Similarly, the slip rate for the Pinto Mountain fault may have been overestimated because PBRs at Yucca Valley and Pioneer Town appear to be inconsistent with the National Seismic Hazard Map. Finally, the Grass Valley rock has experienced shaking from many San Andreas fault ruptures in the last ~18 ka. The enduring stability of this rock indicates persistent low ground motions from San Andreas fault ruptures at this site and suggests a preferred direction, or nucleation region, or upper bound magnitude for past earthquakes.

Ambient Noise Analysis. Beroza, Lawrence, Denolle and Prieto have extended their use of the ambient seismic field for several aspects of ground-motion prediction, including: validation of the ambient-field response against moderate earthquakes, developing a library of Green's functions for improving southern California velocity models, and developing a preliminary attenuation model for the southern California crust. Validation involves using several well-recorded earthquakes that occurred in the vicinity of continuously recording seismic stations to compare amplification effects in sedimentary basins from the ambient field to observed ground motions (Figure 63). Current

work focuses on improving such comparisons by making corrections for earthquake depth and the radiation pattern. Previous analyses were limited to the vertical component (i.e., Rayleigh waves). Utilization of the inter-station complex coherence derived through deconvolution and stacking permits extending the analysis to all three components, and hence to Love waves. This process allows the development of a library of Green's functions that can be applied to refine crustal wavespeed models in southern California. Preliminary results indicate that the horizontal component waveforms appear to have more local noise than the vertical components, which will require an increase in the amount of data being used to construct the ambient-field response to extract the weakly coherent station-to-station signal. Prieto et al. (2009) reported strong differences between paths with strong sensitivity to major sedimentary basins, and paths that have little sensitivity to basins. They have since quantified these observations to develop a laterally varying attenuation model for southern California. Current work focuses on using ambient noise Green's functions in the scattering integral approach for estimating velocity structure.

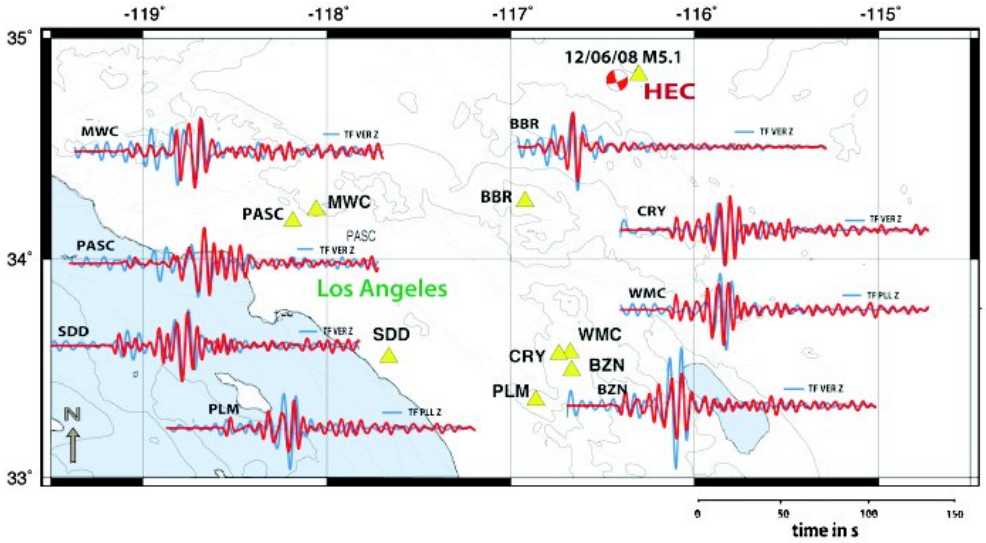

Figure 63. Comparison of vertical component ambient-field ground-motion prediction (blue) with recorded earthquake waveforms (red) for the Mw 5.1 6 December 2008 earthquake. The strong similarity of earthquake and "virtual earthquake" waveforms validates this approach.

Broadband Simulations. Recent work has focused on the development of a Broadband Simulation Platform. This is a collaborative project among Graves and Somerville (URS), Archuleta and Schmedes (UCSB) and Olsen and Mai (SDSU/ETH). Mai and Olsen (2010) developed a method to generate synthetic broadband ground motions by combining low-frequency (f < 1-2 Hz) deterministic simulations and high-frequency (f > 1-2 Hz) point scatterograms based on the theory by Zeng et al. (1991) and Zeng (1993). The two frequency bands are combined at a selected frequency that minimizes the error in both amplitude and phase between the deterministic and stochastic time series (Mai and Beroza, 2003). The scatterograms are generated from values of the elastic scattering coefficient, Kappa, Vs30, and high-frequency attenuation model. Mena et al. (2009) extended this method to distribute the moment of the event to that of a finite-fault and included a dynamically consistent source-time function. Validation has focused on the 1994 Mw 6.7 Northridge earthquake. Using low-pass filtered strong-motion data (to isolate the accuracy of the synthetic high-frequency portion), the method produces a very good fit between observed and synthetic peak ground accelerations, peak ground velocities, and spectral accelerations. Using synthetic low-frequency motions also produces a favorable fit; the broadband synthetics tend to slightly under-predict the strong-motion amplitudes between 2 and 10 Hz, primarily due to lack of complexity in the low-frequency rupture model between 1 and 2 Hz. The response spectra

residuals are significantly smaller as compared to results for the Northridge earthquake using an early approach.

Mayhew and Olsen (2010) have developed a new goodness-of-fit method for the validation of broadband synthetics, consisting of a combination of commonly used metrics such as peak values, Fourier and response spectra, cross correlation, and duration. Additionally, for structural engineering-specific applications, the algorithm includes a comparison of the inelastic/elastic displacement ratios. The method has been applied to broadband synthetics (0-10Hz) generated for the 2008 Mw 5.4 Chino Hills earthquake. The best fits are found for stations SRN and OGC just south of the epicenter, CHF and KIK toward the northwest, and HLL and SMS toward the west. Stations with goodness-of-fit values near or below the proposed acceptable threshold include STS (amplitude and duration under-predicted), and DEC, PDU and RVR (amplitude and duration over-predicted) (Figure 64). Average inelastic/elastic displacement ratios have been computed at short periods (0.2-0.5s), moderate periods (0.75-1.5s) and long periods (2.0-5.0s). At the shorter periods, about 1/3 of the sites (located primarily north of the epicenter, as well as STG, SMS, and WTT) produce inelastic/elastic displacement ratios below the proposed acceptance threshold. On average, the simulated ratios are under-predicting the recorded ratios at the short periods with a large variance. This is in agreement with the findings by Tothong and Cornell (2006) who showed that the inelastic/elastic displacement ratios for oscillators with a short natural period (<0.6s) are highly variable. At moderate periods and long periods, the synthetic ratios tend to have a very good to good fit, suggesting that these ground motions could be used in engineering and hazard analysis applications.

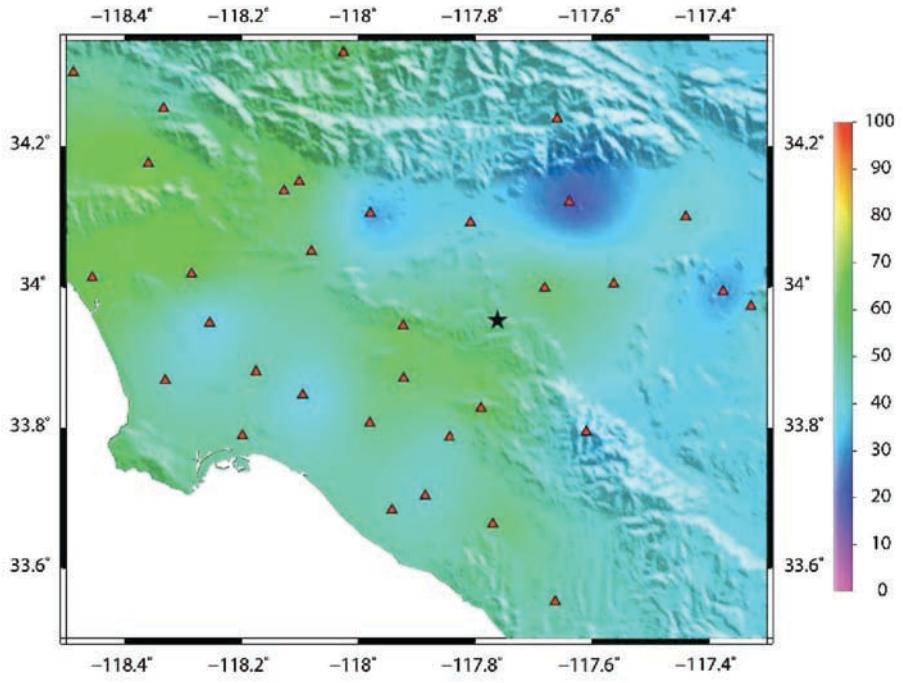

Figure 64. Map of average broadband (0.1-10 Hz) goodness-of-fit for the 2008 Chino Hills earthquake. Triangles depict stations used for comparison, and the star depicts the epicenter.

Seismic Hazard Characterization. As part of the Community Modeling Environment, Graves et al. (2010) are developing the CyberShake Platform, which explicitly incorporates deterministic 3D rupture and wave propagation effects within seismic hazard calculations. The process begins by converting the UCERF-2 rupture definition into multiple rupture realizations with different hypocenters and slip distributions, resulting in about 415,000 scenarios per site. Strain Green

tensors are calculated for the site of interest using the SCEC Community Velocity Model, Version 4 (CVM4), and synthetic waveforms are calculated for each rupture variation using reciprocity. Thus far, ruptures at over 200 sites in the Los Angeles region have been simulated for ground-shaking periods of 2 seconds and longer, providing the basis for the first generation CyberShake hazard maps. These hazard results are much more sensitive to the assumed magnitude-area relations and magnitude uncertainty estimates used in the definition of the ruptures than are the conventional, empirically based ground-motion prediction equation approach. This reinforces the need for continued development of a better understanding of earthquake source characterization and the constitutive relations that govern the earthquake rupture process.

Graves et al. constructed a first generation CyberShake hazard map for the Los Angeles region using the 200+ sites. Figure 65 illustrates the hazard calculated from the CyberShake ground motions with spatial interpolation based on residuals with respect to the Campbell and Bozorgnia (2008) ground-motion prediction equation. The map shows generally elevated hazard for many of the deep basin sites, and a generally reduced hazard level along the San Andreas fault. This highlights the importance of effects such as rupture directivity and basin response on the hazard levels, and demonstrates the potential of using the CyberShake approach for hazard characterization on a regional scale; however, the density of sites (nominally at 10 km spacing) does not provide the resolution needed for detailed interpretation of the results.

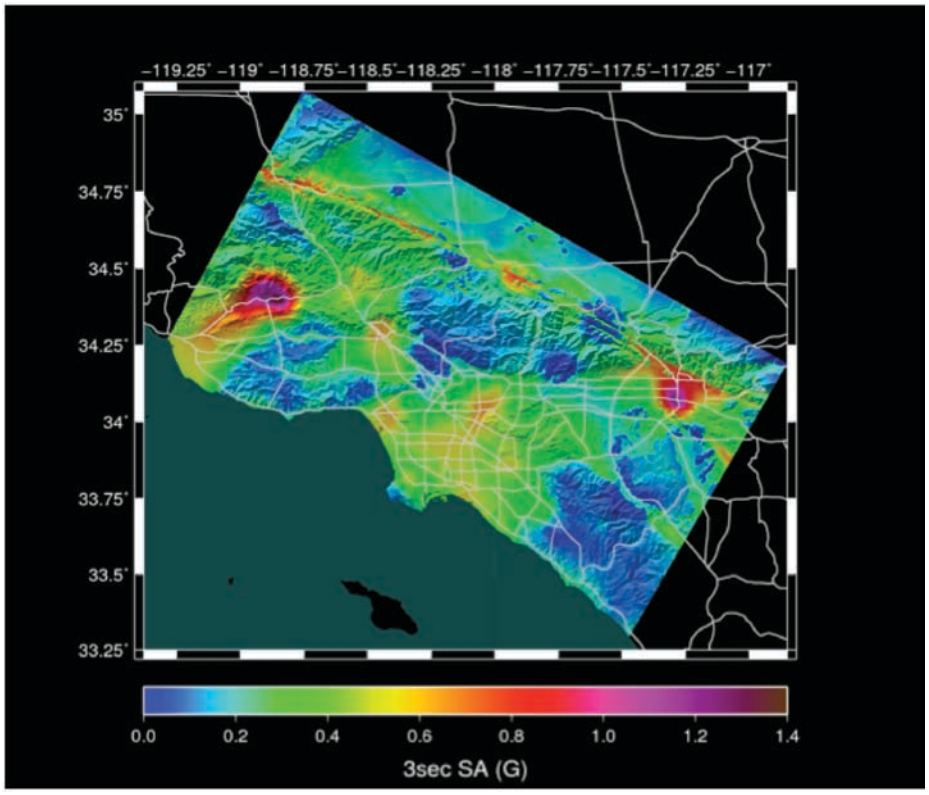

Figure 65. CyberShake hazard map for 3 second SA at 2% probability of exceednace in 50 years derived by interpolating the residual map onto the background map of Campbell and Bozorgnia (2008).

Large-Scale Simulations. Cui et al. (2010) simulated a Mw 8.0 earthquake rupturing the entire southern San Andreas fault (Cholame to Bombay Beach) at frequencies up to 2.0 Hz. The objective was to examine the ground motions over the 800 km by 400 km area, which is home to more than 20 million people and subjected to strong shaking in this scenario. The calculation used a uniform

mesh of 400 billion cubes and ran for 24 hours on 223,074 cores of the NCCS Jaguar to compute waveforms with a duration of up to 360 s. The simulation shows that directivity effects for this scenario may generate similar levels of amplification in the Ventura basin as for southeast-to-northwest ruptures, despite the fact that the wave field enters almost perpendicular to the Ventura basin. Peak motions in the deeper Los Angeles basin are lower and reach about 120 cm/s with 40 cm/s in downtown Los Angeles. San Bernardino appears to be the area with some of the most severe shaking, due to rupture directivity effects coupled with basin amplification (Figure 66).

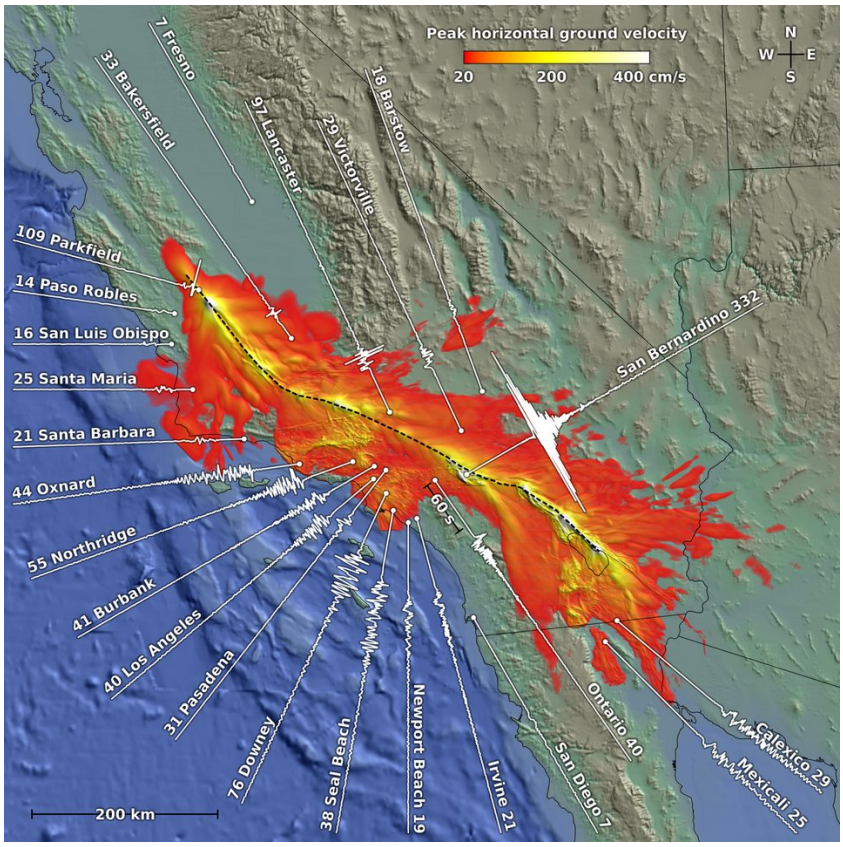

Figure 66. Peak horizontal ground velocity from a simulation for frequencies up to 2.0 Hz for a Mw 8.0 southern San Andreas scenario earthquake. Velocity waveforms (horizontal component in the direction of N46E) are shown at selected locations with their peak velocities (cm/s) listed along the traces.

Earthquake Rupture Characterization

High-Frequency Radiation. Ampuero, Ruiz-Paredes, and Elkoury applied multi-scale signal analysis techniques to identify and quantify signatures of spatial and temporal complexity of rupture propagation in the high-frequency band of strong-motion recordings. The seismic waveform is represented locally as a superposition of a smooth polynomial and a power law singularity using the Wavelet Transform Modulus Maximum (WTMM). This multi-scale technique has been applied in a variety of fields but has not been applied previously to strong-motion data and earthquake rupture processes.

Before applying this technique to strong-motion data, they analyzed 2-D in-plane dynamic rupture simulations using a boundary integral equation method with a slip-weakening friction model. They found that the singularity exponent of the radiated strong phases, measured by the WTMM technique on the seismic potency acceleration, matches the singularity exponent of the initial stress.

This suggests it may be possible to infer the character and spatial distribution of stress singularities from strong-motion data. Applying the technique to strong-motion data sets from the 1999 Mw 7.6 Chi-Chi, 2004 Mw 6.0 Parkfield, and 2008 Mw 5.4 Chino Hills earthquakes suggests the high-frequency wavefield is controlled by a mono-fractal process rather than a multifractal process with smoothing of the wavefield on the scale of the rupture process zone.

Dunham, Kozdon, and Nordstrom have further developed techniques for simulating high-frequency ground motion generated by irregular rupture propagation on nonplanar faults (Figure 67). In their study (Dunham et al., 2010) the faults are modeled as self-similar fractal surfaces with roughness over three orders of magnitude and at scales larger than the maximum slip in a single event. The simulations include off-fault inelastic deformation (via rate-independent plasticity or viscoplasticity) to limit large stress concentrations around bends in the fault surface. Recent work shows that fluctuations in rupture speed and slip associated with the fault roughness excite waves with frequencies up to about 10 Hz. Furthermore, this approach produces synthetic waveforms (Figure 68) qualitatively similar to the Lucerne Valley (LUC) strong-motion record from the 1992 Mw 7.3 Landers earthquake, a typical near-source record from a sub-shear strike-slip rupture. The high-frequency ground motion appears to be most correlated with fluctuations in rupture speed associated with bends in the fault.

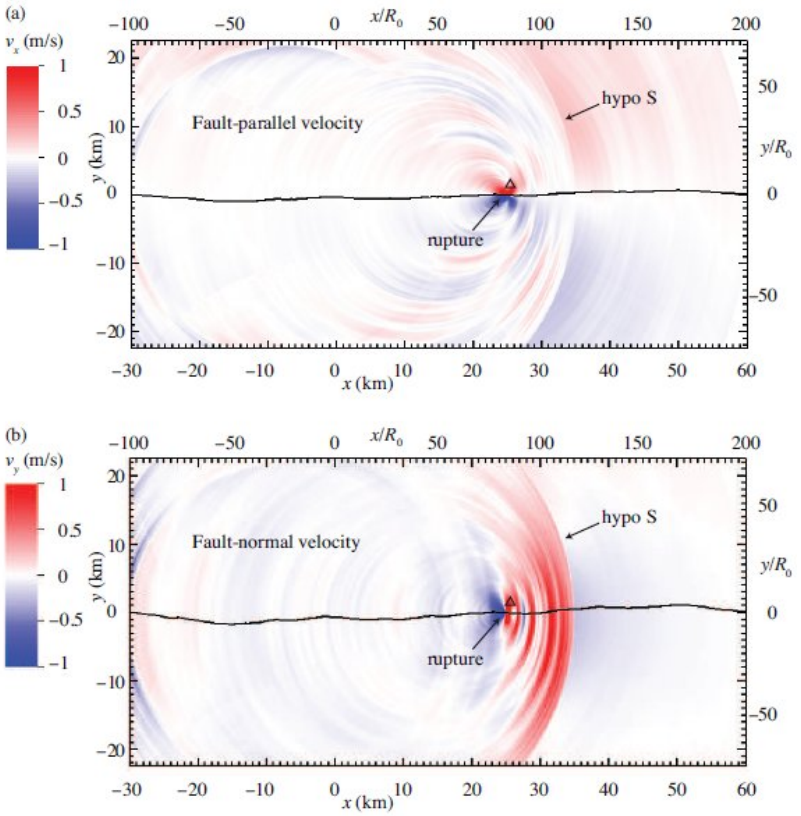

Figure 67. Snapshots of the fault-parallel (top) and fault-normal (bottom) components of the velocity field as the rupture passes the station (triangle) at which waveforms in Figure GMP7 are calculated. The hypocentral shear wave is marked by "hypo S".

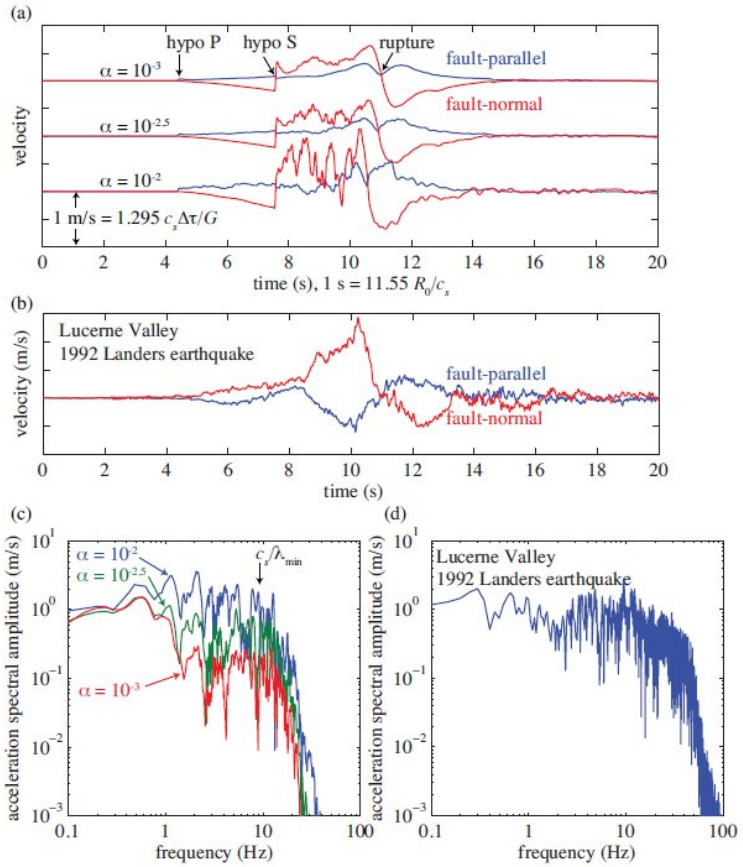

Figure 68. Synthetic velocity waveforms (top) for several values of the amplitude-to-wavelength ratio, alpha. Hypocentral P- and S-wave arrivals are marked. The Lucerne Valley (LUC) record (middle) from the 1993 Mw 7.3 Landers earthquake. Four amplitude spectra of fault-normal acceleration for the synthetic waveforms (bottom left) and the Lucerne recording (bottom right). The minimum wavelength of fault roughness in the model (λ_{min}) prevents excitation of waves at frequencies greater than about $\sim c_s/\lambda_{min}$. A amplitude-to-wavelength ratio of about $10^{-2.5}$ yields waveforms with similar character to the LUC record.

Inelastic Deformation. Two studies have focused on quantifying the effects of off-fault inelastic deformation (plastic yielding) in reducing ground motions with application to dipping faults. Duan and Day (2010) explored the sensitivity of extreme ground-motion estimates at Yucca Mountain to variations in fault geometry, rock strength, fault zone structure, and undrained poroelastic response of the fluid pressure. They found that the peak ground velocity in the limiting cases of nearly complete stress drop on the Solitario Canyon fault is significantly more sensitive to the geometry of the fault at depth and cohesive strength of the rocks at shallow depth than the fault zone structure and pore pressure response. For example, reducing the dip angle of the Solitario Canyon fault at depth while doubling the cohesive strength at shallow depths results in an increase in the vertical PGV values by more than 25% to values over 5 m/s. Figure 69 summarizes the variation in surface slip and peak ground velocity in the study for different cohesion values.

Ma (2009) examined the potential relationship between off-fault inelastic deformation (plastic strain) and the development of a low-velocity zone surrounding the fault for two generic reverse and normal faults. In both cases including the effects of off-fault inelastic deformation reduced the strong asymmetry in peak ground velocity observed for the elastic case while producing asymmetric flower-like plastic strain structures (Figure 70 and Figure 71). These results aid

observational efforts to image shallow low-velocity fault zone structures surrounding dipping faults by providing insight into the physical processes behind the origin of the low-velocity material.

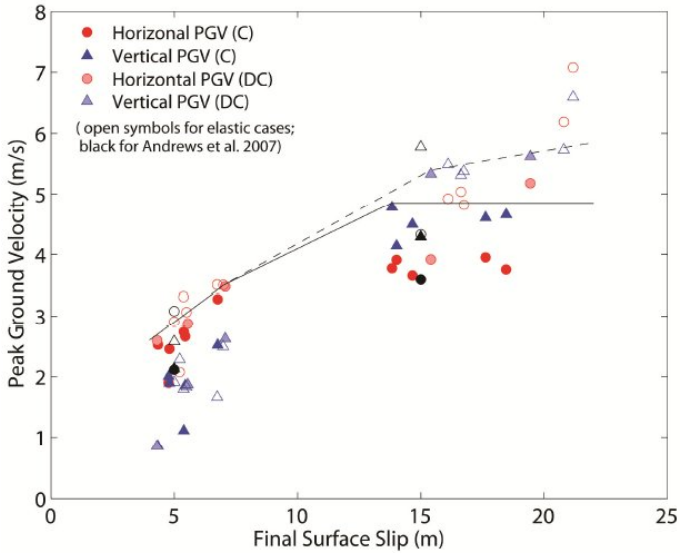

Figure 69. Peak ground velocity (PGV) at the repository site as a function of surface fault slip from 2D dynamic rupture models of scenario earthquakes on the Solitario Canyon fault. Dark shading (C) denotes PGV estimates with Mohr-Coulomb strength parameter values (cohesion and internal friction angle) of Andrews et al. (2007). Light shading (DC) denotes PGV estimates with cohesion values two times larger for the shallow rock units. Open symbols denote PGV estimates with purely elastic response. Including off-fault inelastic deformation reduces the PGV values.

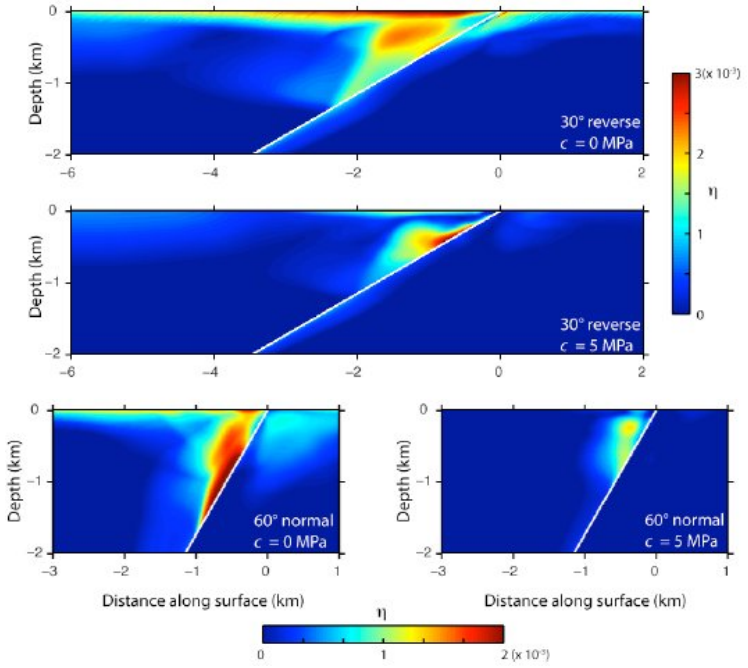

Figure 70. Inelastic strain around the fault tip with strong asymmetric across the fault. As cohesion increases, the inelastic strain near the surface and in the footwall is decreases.

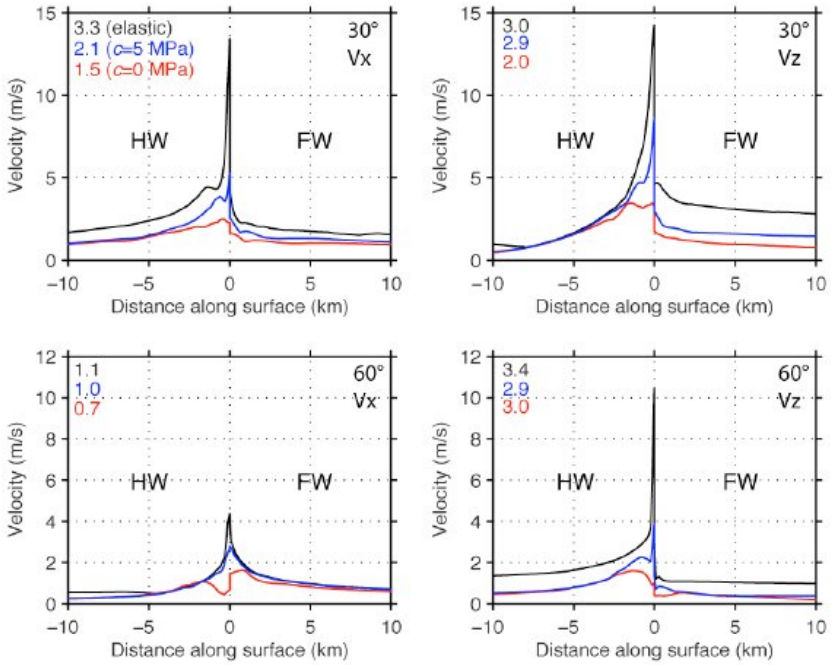

Figure 71. Peak ground velocity (PGV) along the surface for the 30 degree dipping reverse fault (top row) and 60 degree dipping normal fault (bottom row). The ratios of the hanging wall to footwall PGV values are shown in each panel in the upper left corner. The inelastic response reduces the asymmetry and peak motions significantly.

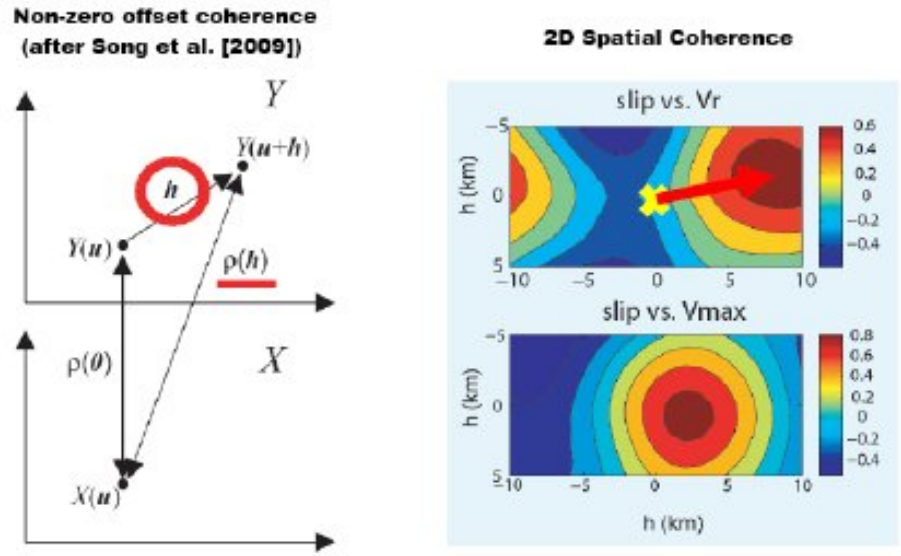

Figure 72. Schematic diagram showing the correlation coefficient as a function of separation vector, h (left) and the 2-D correlograms obtained from a square-shaped asperity rupture model (Song and Somerville, 2010).

Model Parameterization. Efforts to develop methodologies for constructing kinematic rupture models consistent with rupture dynamics continue to advance. Schmedes, Archuleta and Lavallee (Schmedes et al., 2010) analyzed 315 dynamic rupture models to deduce the amplitude distributions and correlations of kinematic rupture parameters. Focusing on subshear rupture they found (1) final slip does not correlate with local rupture speed, (2) final slip correlates with rise time, (3) rupture speed correlates with peak slip rate, (4) rupture speed is controlled by the fracture energy and rate of slip-weakening, and (5) the rupture front becomes more pulse-like away from the hypocenter.

Using a similar approach based on one-point and two-point statistics, Song and Somerville (2010) analyzed kinematic and dynamic rupture models of the 1992 Mw 7.3 Landers earthquake and kinematic rupture models of 1999 Mw 7.6 Izmit earthquake. They demonstrated that the approach quantifies important features of the rupture models. By allowing a spatial offset in the correlation (which was not included in the analysis by Schmedes et al.), they found a correlation between rupture speed and slip; the rupture speed increased after propagation through a region with larger slip (Figure 72). They also found a zero-offset correlation between slip and peak slip rate. Application of this approach to kinematic rupture models highlights the inconsistencies among models for the same event, which are likely due to discretization, regularization, and positivity constraints in the inversion. Song and Somerville are continuing to develop the technique so that it can be used to construct kinematic rupture models consistent with rupture dynamics.

References

Andrews, D. J., T. H. Hanks, and J. W. Whitney (2007), Physical limits on ground motion at Yucca Mountain, Bull. Seis. Soc. Am., 97(6), 1771-1792, doi: 10.1785/0120070014.

Campbell, K. W. and Y. Bozorgnia, (2008), NGA ground motion model for the geometric mean horizontal component of PGA, PGV, PGD, and 5%-damped linear elastic response spectra for periods ranging from 0.01 to 10 s. Earthquake Spectra 24(S1), 139–172.

Cui, Y., K. B. Olsen, T. H. Jordan, K. Lee, J. Zhou, P. Small, D. Roten, G. Ely, D.K. Panda, A. Chourasia, J. Levesque, S. M. Day, P. Maechling (2010), Scalable earthquake simulation on petascale supercomputers, submitted to Super Computing 2010.

Duan, B., and S. M. Day (2010), Sensitivity study of physical limits on ground motion at Yucca Mountain, submitted to Bull. Seis. Soc. Am.

Dunham, E. M., D. Belanger, L. Cong, and J. E. Kozdon (2010), Earthquake ruptures with strongly rate-weakening friction and off-fault plasticity: 2. Nonplanar faults, submitted to Bull. Seis. Soc. Am.

Graves, R., S. Callaghan, E. Deelman, E. Field, T. H. Jordan, G. Juve, C. Kesselman, P. Maechling, G. Mehta, K. Milner, D. Okaya, P. Small, K. Vahi (2010), CyberShake: Full Waveform Physics-Based Seismic Hazard Calculations for Southern California, PAGEOPH, in press.

Ma, S. (2009), Distinct asymmetry in rupture-induced inelastic strain across dipping faulting: An off-fault yielding model, Geophys. Res. Lett., 36, L20317, doi:10.1029/2009GL040666.

Mai, P. M., and G. C. Beroza (2003), A hybrid method for calculating near-source, broad-band seismograms: Application to strong motion prediction, Phys. Earth Planet. Int., 137 (1-4), 183-199.

Mai, M., and K. B. Olsen (2010), Broadband ground motion simulations using finite-difference synthetics with local scattering operators, Bull. Seis. Soc. Am., in revision.

Mayhew, J. E. and K. B. Olsen (2010), Goodness-of-fit criteria for broadband synthetic seismograms, with application to the 2008 Mw5.4 Chino Hills, CA, earthquake, submitted to Seism. Res. Lett.

Mena, B., P. M. Mai, K. B. Olsen, M. D. Purvance, and J. N. Brune (2010), Hybrid broadband ground motion simulation using scattering Green's functions: application to large magnitude events, Bull. Seis. Soc. Am., accepted for publication.

Prieto, G. A., J. F. Lawrence, G. C. Beroza (2009), Anelastic Earth Structure from the Coherency of the Ambient Seismic Field, J. Geophys. Res., 114, B07202, doi:10.1029/2008JB006067.

Schmedes, J., R. J. Archuleta, and D. Lavalle (2010), Correlation of earthquake source parameters inferred from dynamic rupture simulations, J. Geophys. Res., doi: 10.1029/2009JB006689.

Song, S. G. and P. Somerville (2010), Physics-based earthquake source characterization and modeling with geostatistics, Bull. Seis. Soc. Am. 100(2), 482-496, doi: 10.1785/0120090134.

Tothong, P., and C. A. Cornell (2006), An empirical ground-motion attenuation relation for inelastic spectral displacement, Bull. Seis. Soc. Am. 96, 2146-2164.

Zeng, Y. H., F. Su, and K. Aki (1991), Scattering wave energy propagation in a random isotropic scattering medium 1. Theory, J. Geophys. Res. 96 (B1), 607-619.

Zeng, Y. H., K. Aki, and T. L. Teng (1993), Mapping of the high-frequency source radiation for the Loma Prieta earthquake, California, J. Geophys. Res. 98 (B7), 11981-11993.

Seismic Hazard and Risk Analysis

The purpose of the Seismic Hazard and Risk Focus Group is to apply SCEC knowledge to the development of information and techniques for quantifying earthquake hazard and risk. Projects in this focus group can have relationships with most of the other focus groups. The most direct linkages are with the Ground Motion Prediction Focus Group, as well as to SCEC special projects such as the Extreme Ground Motion Project, and to PEER special projects such as the Tall Buildings Initiative. Projects that involve interactions between SCEC scientists and members of the community involved in earthquake engineering research and practice are especially encouraged in SHRA. A very large number and variety of SCEC projects relate in some way to the goals of SHRA. This report briefly reviews a selection of projects that span this wide range of topics.

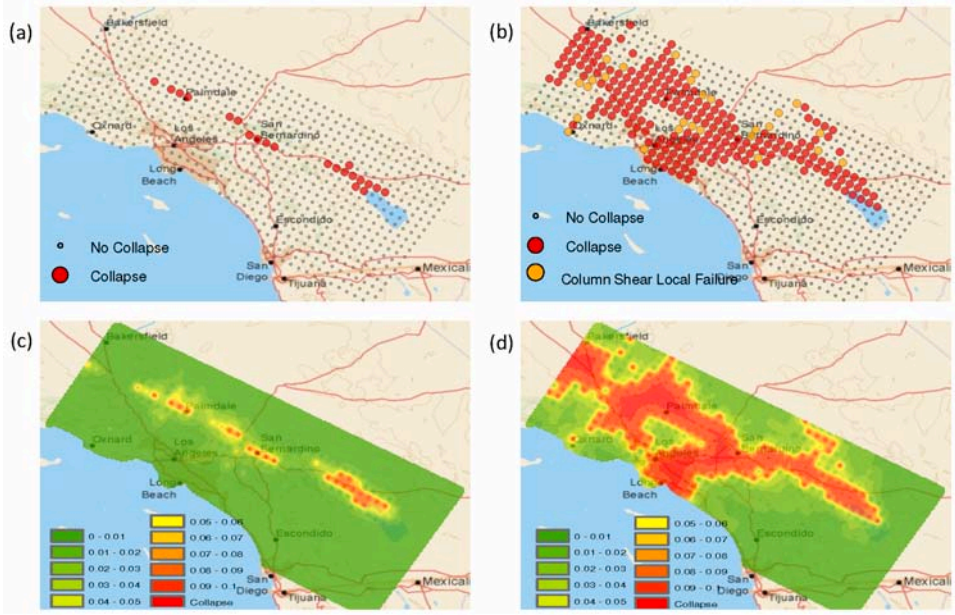

Figure 73. Seismic performance predictions for 4-story modern, (a) and (c), and older, (b) and (d), space frames indicated by collapses and interstory drift ratios.

Seismic Performance of Reinforced Concrete Frame Buildings in Southern California Due to the Magnitude 7.8 Shakeout Scenario Earthquake

(Liel). Because of the prevalence of reinforced concrete frames in Southern California, it is important to understand their response in the event of a large earthquake. This study examines both older, nonductile, RC frames and their modern counterparts to determine the building response due to the ShakeOut scenario earthquake. Results from the seismic analysis indicate that older, nonductile, RC frames are much more susceptible to collapse during large earthquakes than those designed to current code provisions. Although results varied according to height and framing system, on average, the older 6 RC buildings were predicted to collapse at 22% of 735 case

study sites, compared to 4% of sites for the modern RC frame buildings. Predicted areas of significant seismic risk for older nonductile RC frame buildings extend along the entire San Andreas Fault line, including San Bernardino and Palm Springs. Based on this analysis, sites analyzed in downtown Los Angeles and Hollywood, where the largest concentration of nonductile RC buildings exist, are predicted to have a collapse rate of approximately 30-40%. Based on the available inventory data and mapped collapse risk a rough estimate of 50 to 300 collapsed nonductile RC frame buildings could occur during the ShakeOut scenario earthquake. This study is specific to the building type, region and scenario earthquake event, but illustrates a prototype study that can be conducted for different buildings, earthquake scenarios or regions - as a tool for mitigation and emergency response planning to improve the level of seismic readiness in our communities. This type of research is made possible by combining advanced ground motion simulations, such as those that are the focus of SCEC efforts, with robust nonlinear building analysis models, in an effort to better understand how a given earthquake event will affect losses and vulnerability (Figure 73).

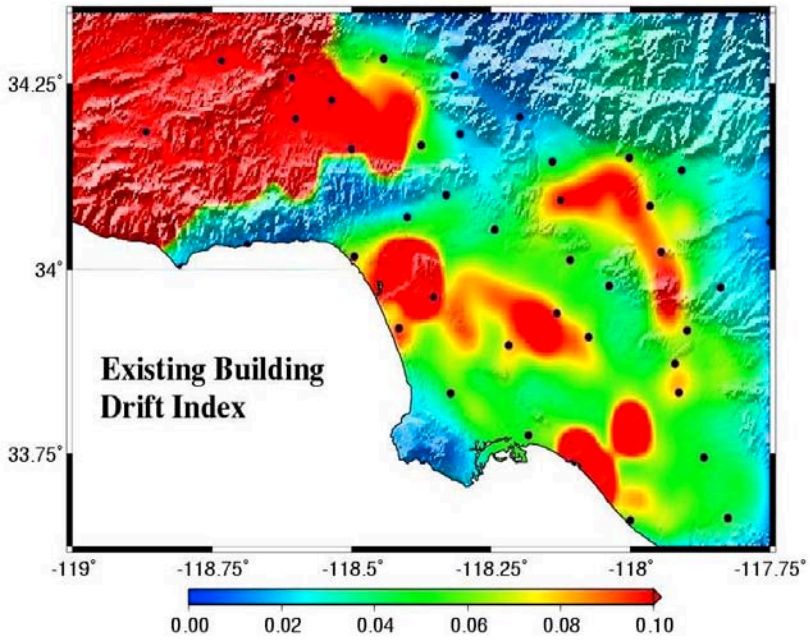

Figure 74. Interstory Drift Ratios (IDR's) in an existing 18-story steel moment frame building subjected to the calculated ground motions from a 1857-like hypothetical magnitude 7.9 earthquake on the San Andreas fault, initiating at Parkfield and rupturing in a southeasterly direction with a peak displacement of 2 m and peak velocity of 2 m.s−1. The color bar refers to the peak IDR at each site.

How Would Tall Steel Moment Frame Buildings Collapse Under Seismic Loading

(Krishnan). This study pursued the question of how tall steel moment frame buildings would collapse under seismic loading. The distribution of moments in a steel moment frame subjected to lateral loads is such that it produces double curvature in all the columns and beams resulting in shear-racking of the frame. Thus, shear deformation and not flexural deformation dominates moment-frame response. Strain doubling occurs due to constructive interference of the reverse phase of the incident wave with the forward phase that is reflected off the free end, similar to the behavior of an ideal beam. Such strain doubling can lead to damage localization, which in turn can result in the formation of a shear-compliant block collapse mechanism, consisting of column yielding at floors corresponding to the top and bottom of the shear-compliant block, with significant yielding of the beams or columns or panel zones at each joint in each of the intermediate floors. For moderate loading (motions that are not strong enough to cause structural collapse), the

Confines of the Most Pronounced Localization of Yielding (CoMPLY) is controlled by the period of the input ground motion relative to the fundamental period of the structure. However, the response to "collapsogenic" input motions shows a "convergence" of the CoMPLY to the same few stories, rendering it invariant with respect to different measures of the ground motion. This implies that there is a characteristic mechanism of collapse for a given building regardless of the frequency-duration characteristics of the incident ground motion (Figure 73). This characteristic collapse mechanism is a function of the structural system alone and can be predicted using its basic properties. The ability to predict these characteristics encourages exploration of possible local retrofitting measures to reduce the collapse potential of these structures. Arnar Bjorn Bjornsson, who is a graduate student at Caltech, has been exploring simple retrofitting measures using steel braces. He has successfully demonstrated the increased collapse resistance of a model of an existing 18-story steel moment frame building using such a retrofit measure (Figure 74).

Trimming the Hazard Logic Tree, Phase 2

(Porter, Scawthorn). This is the second year of an effort to test and depict the sensitivity of societal risk estimates to branches in the UCERF hazard logic tree. The work is not yet complete. In this phase, probabilistic seismic vulnerability functions have been created that relate building repair costs to shaking intensity, by structure type and occupancy classification. Intensity is measured using a vector measure: 5%-damped elastic spectral acceleration response at 0.3-sec and 1.0-sec periods, also conditioned on magnitude, distance, site soil classification, and tectonic regime. Casualty-rate seismic vulnerability functions were previously created for another (USGS) project and both mean and probabilistic seismic vulnerability functions of repair cost were created for SCEC under the SCEC 2008 year. In the current year, a portfolio of assets exposed to seismic risk was also estimated, in work for this 2009 SCEC project and another USGS project. (The USGS work quantified indoor occupants; the SCEC work added square footage and replacement costs, by census tract, occupancy classification, and structure type.) A component of the OpenRisk software, designed for SCEC in previous work and developed in collaboration with USGS programmers, will be used to carry out the loss calculations. The sensitivity analysis, not yet begun, will employ a tornado-diagram-analysis approach developed for decision analysis and applied and extended in the last 10 years by SPA personnel and others for use in earthquake engineering loss estimation. Examples of trends in damage-factor uncertainty versus mean damage factor are shown in (Figure 75).

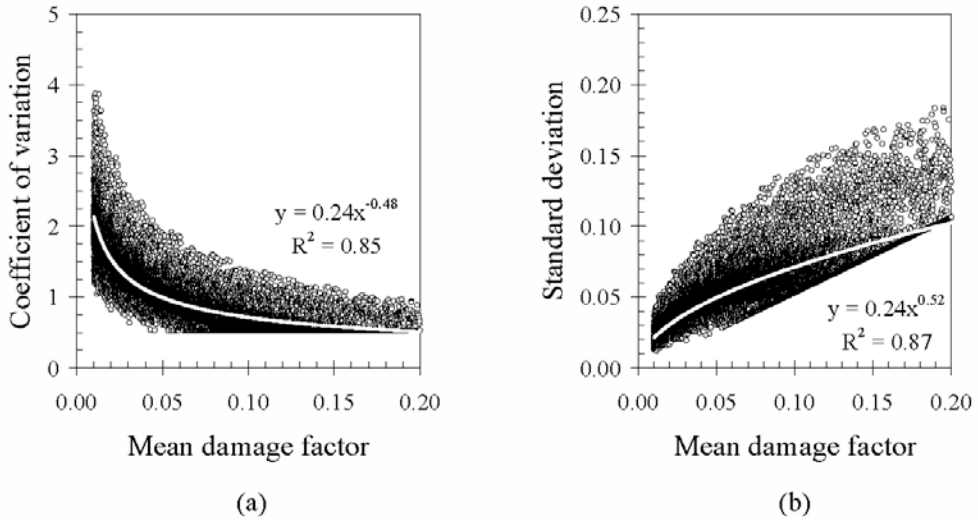

Figure 75. Trends in (a) COV versus MDF and (b) standard deviation versus MDF

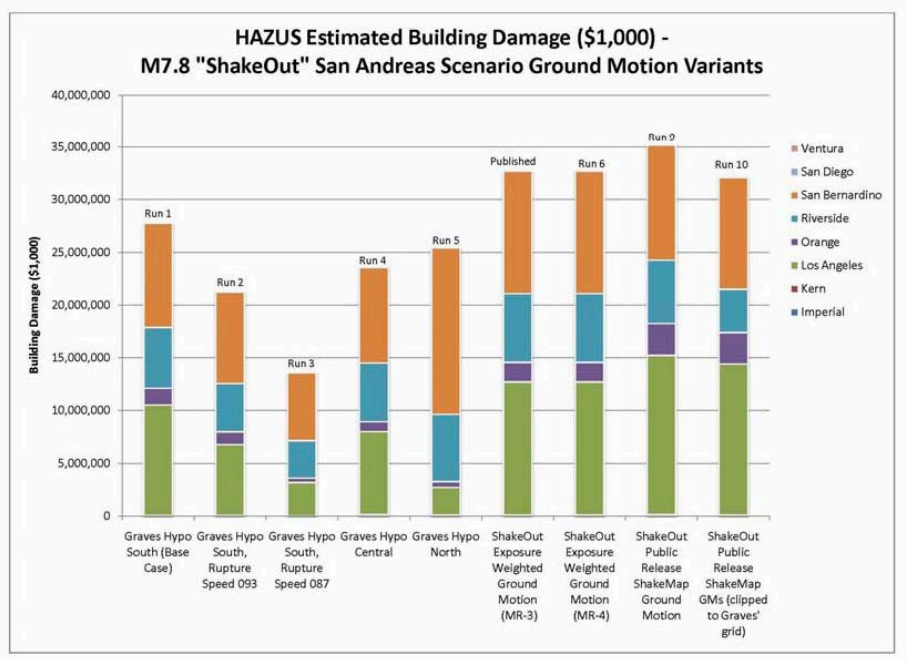

Figure 76. HAZUS® Estimates of Building Damage for the ShakeOut Scenario Ground Motion Variants

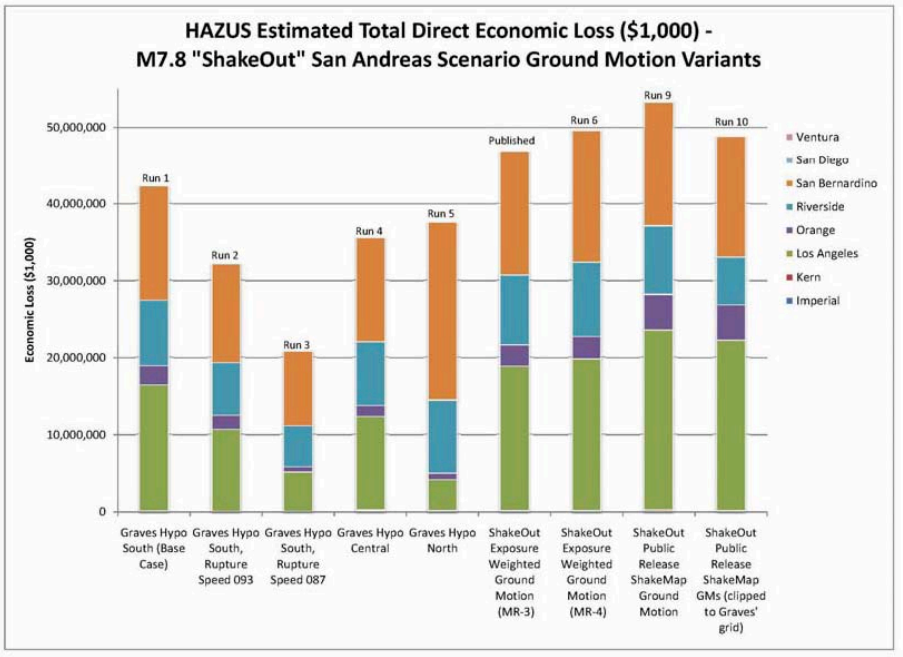

Figure 77. HAZUS® Estimate of Total Direct Economic Loss for the ShakeOut Scenario Ground Motion Variants

Sensitivity Analyses of HAZUS®' Loss Estimates for the ShakeOut Scenario: Assessment of the Impact of Ground Motion Variation on Loss

(Seligson). The "ShakeOut scenario" – a comprehensive impact assessment for a M 7.8 earthquake on the Southern San Andreas Fault – was developed by a regional, multi-disciplinary team of scientists and engineers. The scenario's regional building damage and loss estimates were developed using FEMA's nationally applicable loss estimation software HAZUS®MH (HAZards U.S. Multi-Hazard). The objective of the study was to assess the potential variation in loss resulting from different ground motion representations, including both kinematic simulations (Graves et al., 2008) and dynamic simulations (Olsen et al., 2009). Comparisons of estimated building damage and total direct economic loss using the various ground motion data sets analyzed to date are provided in Figure 76 and Figure 77. Within HAZUS®, total direct economic loss includes building and content losses, as well as inventory loss and income losses (which include relocation costs, proprietor's income losses, wage losses and rental income losses). As shown in Figure 76, there is no discernible difference between the building damage estimated using HAZUS®MH MR-3 ("Published") and MR-4 (Run 6). However, MR-4 included a methodological change in the estimation of relocation loss. The impact of this change is visible in Figure 77 as a 5.8% increase in overall total direct economic loss for the MR-4 run. The reduction in loss associated with limiting the analysis to the area within the Graves analysis grid is small, but not insignificant for the publicly released ShakeMap ground motion data (Run 10 vs. Run 9); an 8.8% reduction for building damage alone, and 8.5% for total direct economic loss overall. For the exposure weighted ground motions, the difference is insignificant; less than 0.1% for both building damage and total direct economic loss (Run 6 vs. Run 7, not shown on charts). As shown in Figure 76 and Figure 77, the baseline kinematic simulation data (Run 1) yields results on the order of 13 – 15% smaller than either the grid-limited exposure weighted ground motions (Run 7, not shown, but approximately equal to Run 6) or the grid-limited publicly-released ground motions (Run 10). Changes in rupture speed can be seen to have a significant impact on losses; a 7% reduction in rupture speed (speed 0.93, Run 2) results in a 24% reduction in both building damage and total direct economic loss, while a 13% reduction in rupture speed (speed 0.87, Run 3) results in a 51% reduction in loss. Changes to the hypocenter location have a smaller impact on loss than rupture speed variation. Relative to the southern base case (Run 1), losses resulting from a scenario with a central hypocenter location (Run 4) are 15% smaller, while losses from a northern hypocenter (Run 5) are 10% smaller than the base case (Figure 76 and Figure 77).

Characterization of Earthquake Slip Distribution of the Central San Jacinto Fault

(Salisbury, Rockwell, Hudnut). The south-central San Jacinto Fault (SJF) from Hemet southeastward to Clark Valley represents the longest and straightest contiguous segment of the SJF zone. It is exceptionally well localized (Rockwell and Ben-Zion, 2007) and is easily identifiable in the geomorphology. The "Anza Seismicity Gap" falls in the middle of this section of the fault with microseismicity to nearly 20 km depth on the edges of the gap. The Hog Lake trench site, located in the Anza Seismic Gap, records the timing of the past 18 surface ruptures in the past 3800 years with an average return period of about 210 years. Work at Hog Lake dates the most recent event (MRE) at ca. 1790, suggesting this was the November 22, 1800 earthquake. In 2006, Middleton evaluated the southern 55 km of the Clark strand of the SJF for offset features using a combination of aerial photography, field techniques, and B4 LiDAR imagery. Displacement estimates show that the MRE produced an average of 2.7 m of dextral slip, with a maximum of 4 m near Anza to less than a meter near the southeast termination of the fault. For this continuation project, the work begun by Middleton was completed by mapping the detailed tectonic geomorphology along the remaining 25 km section of the Clark Fault (NW of the Anza Seismicity Gap to Hemet) using aerial photography, B4 LiDAR data, and field techniques. Together, these data provide a robust assessment of the slip distribution for the entire Clark fault in the last few events. This project involved mapping of small geomorphic offsets for 75 km of the Clark fault from the southern end of Clark Valley (east of Borrego Springs) northwest to the mouth of Blackburn Canyon near Hemet. To the northwest, the flat valley bottom and young aggradation makes additional measurements

with LiDAR impossible. Nevertheless, these data argue that much or all of the Clark fault, and possibly also the Casa Loma fault, tends to fail from end to end in large earthquakes. They also recognize the likely rupture from the 1918 earthquake, which broke a short ~15 km section of the fault in Blackburn Canyon, perhaps due to lower displacement in that area in the ca 1800 event. Figure 78.

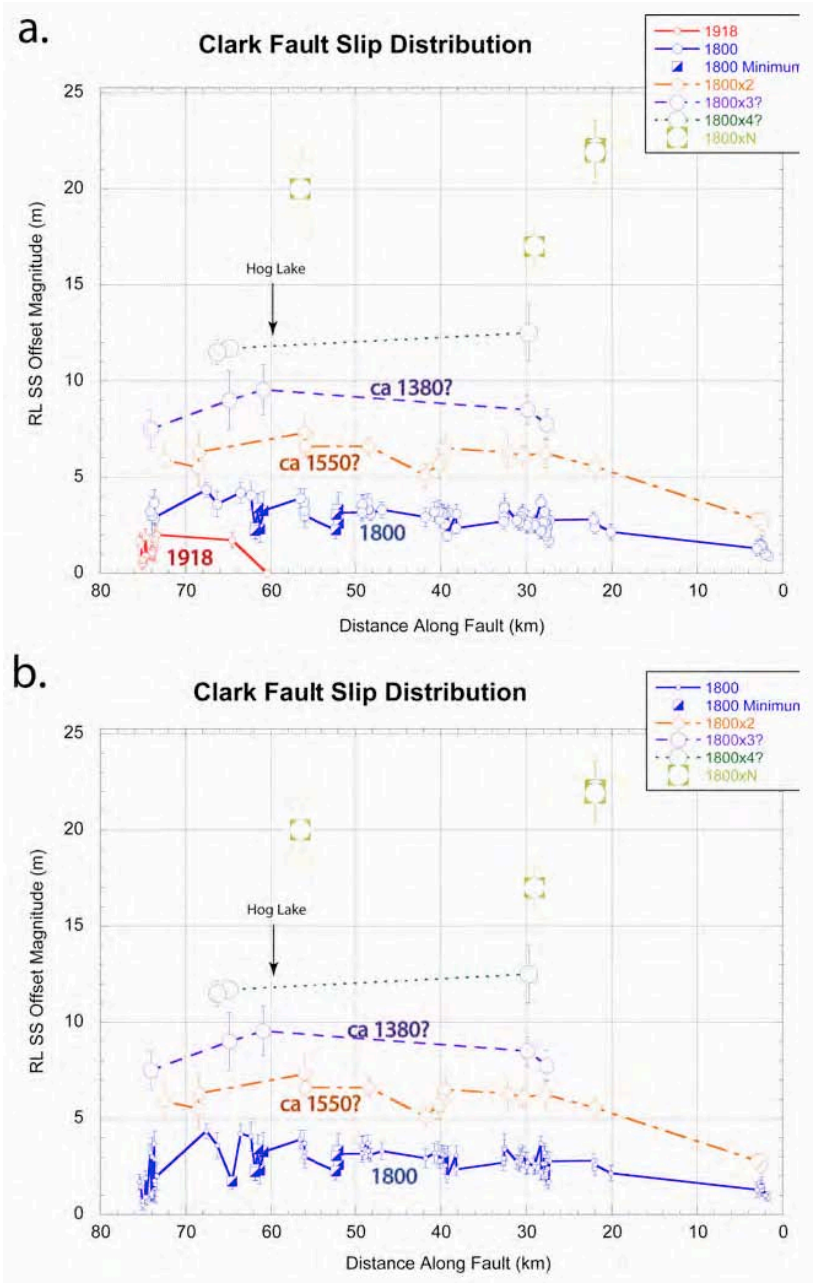

Figure 78. Slip distribution models for geomorphic offsets collected along the Clark strand of the San Jacinto fault from highway S22 northwest to Blackburn Canyon, southeast of Hemet.

Special Projects

In addition to the disciplinary groups, and cross-cutting focus groups, SCEC has undertaken a number of special projects, which are focused on problems with well-defined short-term research objectives, but are nevertheless consistent with SCEC goals. These include the *Southern San Andreas Fault Evaluation* (SoSAFE), the *Collaboratory for the study of Earthquake Predictability* (CSEP), the *Working Group on California Earthquake Probabilities* (WGCEP), the *Extreme Ground Motion Project* (ExGM), and the *Community Modeling Environment* (CME).

Southern San Andreas Fault Evaluation

The primary goal of the Southern San Andreas Fault Evaluation (SoSAFE) project is to document the timing of large paleoearthquakes and amount of slip released by the southern San Andreas and San Jacinto Faults over the past 2000 years. Additional goals include examination of longer-term slip rates and modeling studies which directly impact seismic hazard assessments. SoSAFE is funded through SCEC by the U.S.G.S. Multi-hazards Demonstration Project. Research included earthquake trenching studies, radiocarbon dating supported with Geology infrastructure funding, geomorphic studies using LiDAR and other aerial imagery data in tandem with field measurements, and examination of new methods for analyzing and incorporating neotectonic data. A workshop highlighting the 2008-2009 accomplishments was held during the SCEC Annual Meeting in September, 2009 and attracted ~125 attendees. The workshop ended with a discussion aimed at generating new ideas for integrating paleoseismic data along the fault and use of such models in formal earthquake hazard assessments (e.g. UCERF). Research accomplishments of SoSAFE researchers are addressed in the Section 1.3 under Earthquake Geology.

Working Group on California Earthquake Probabilities

Formulated the "UCERF3 Project Plan", available at *http://www.wgcep.org*.

Collaboratory for the Study of Earthquake Predictability

The CSEP collaboration continues to expand, not only including a wider group of national and international scientists, but also covering more and more topics regarding earthquake predictability and its relation to seismic hazard assessment. The CSEP collaboration is now involved in the research into the physical basis for earthquake predictability, implementation of earthquake prediction algorithms as computer software, and the development of new earthquake prediction evaluation techniques.

The physical infrastructure for SCEC's CSEP activities are housed in the W.M. Keck Testing Center at USC. This facility includes computer resources, data storage devices, custom CSEP software designed to automate the running of earthquake prediction algorithms, and seismological application codes. The CSEP systems are designed to be modular, reliable, and low-cost to acquire and operate. A development system is available to CSEP scientists for the development and testing of forecasting algorithms. Access to the operational system, which runs all model codes and tests, is restricted to ensure the integrity of the evaluation process. A certification system is used to test model codes and testing center codes for proper functionality before deployment to the operational system. The SCEC web server hosts the CSEP web pages for all testing centers.

CSEP Software Development

Many improvements have been made to the CSEP software system since it went into operation in September, 2007. The development has been structured such that the software can be installed in a regional testing center with only minimal changes required to adapt to the specific testing region. To broaden the user base, we have also developed the so-called miniCSEP distribution, which allows researchers to use the CSEP outside of the testing center environment; e.g., as research and teaching tools. The CSEP webpages have been redesigned to include content of all testing centers and to be the portal for a wide variety of CSEP-related information.

The W.M. Keck CSEP Testing Center software has been released under the open-source General Public License and is freely available for use by other research groups. The distribution system has been designed such that the CSEP Testing Center software can be easily updated through periodic releases of the latest version to other testing centers around the world.

New Regions Under Test

The SCEC Testing Center has supported the RELM experiment and placed new classes of time-dependent forecasts for California under test. Because large magnitude events are rare in California, we have been cooperation with foreign research groups to expand the testing program to other regions. Testing centers have been established at GNS Science in Wellington, New Zealand; at the Earthquake Research Institute (ERI) of the University of Tokyo, Japan; and at ETH Zürich in Switzerland. Testing programs are now operational in New Zealand (since January, 2008), Japan (since September, 2008), and Italy (since September, 2009), and plans are underway to begin testing in China's South-North Seismic Belt during the next year, which will be managed by a new testing center at the CEA Institute of Geophysics in Beijing.

In 2008, a testing program was initiated in the western Pacific, and during the past year, this program has been extended to global earthquake forecasting. The global program currently tests forecast models registered on a 1° x 1° grid that target shallow earthquakes of magnitude 5.95 and larger. Efforts are underway to refine global testing using higher-resolution grids and a greater range of focal depths.

New Earthquake Forecasting Models and Testing Procedures

The initial CSEP models, which included 5-year forecasts from the RELM Project, were grid-based models; i.e., they were formulated as expected rates of events on a geographical grid. The original RELM model class has been supplemented by new model classes, including time-dependent forecasts updated on 1-day, 3-month, and 1-year intervals. These models are mostly seismicity-based forecasts, although the RELM set includes models that forecast future seismicity from geodetic and geologic data.

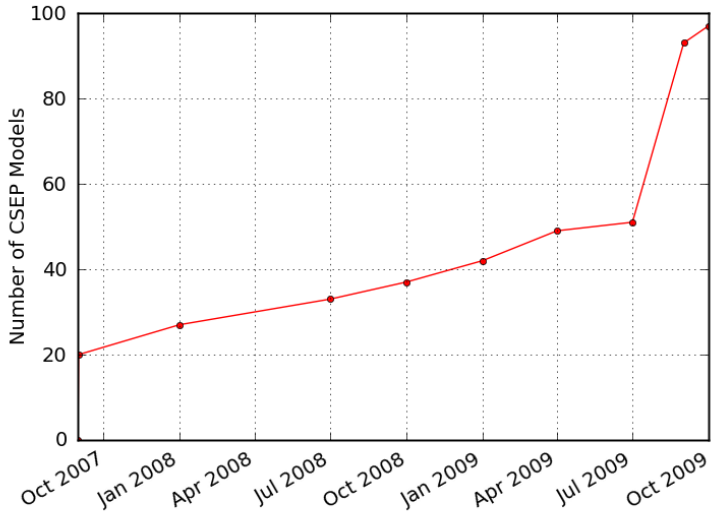

Figure 79. Number of models in all CSEP testing centers over time. The largest additions of models are in October 2007 (RELM models) and September 2009 (5-year models in Italy).

Alarm-based forecasts were introduced as a new class of models during the last year. Alarm-based forecasts do not provide forecast rates per grid cell but monitor input data for particular signals and issue space-time alarms for target events if they detect one or more signals. Several new alarm-based tests (ASS, ROC, Molchan) were developed and implemented to assess this model class. New tests (S- and M-Test) have also been devised for likelihood scoring. These tests allow the likelihood score to be separated into components characterizing earthquake number, spatial distribution, and magnitude distribution. The number of models under CSEP testing worldwide is growing rapidly, as illustrated in Figure 79.

Extreme Ground Motion Project

Extreme ground motions are the very large amplitudes of earthquake ground motion that can arise at very low probabilities of exceedance, as was the case for the Yucca Mountain PSHA when extended out to hazard levels of 10-8/yr. The Extreme Ground Motion project (ExGM) has been a 5-year, $5M research program funded by the Department of Energy to investigate the origin, nature, and physical plausibility of extreme ground motions along three different avenues: physical limits to earthquake ground motion, unexceeded ground motions, and "event frequencies," the frequency of occurrence of very large ground motions or of earthquake source parameters (such as stress drop and faulting displacement) that cause them.

The Cooperative Agreement with DOE ends on September 30, 2010, and ExGM activities in the past year have been concentrated on writing the Final Report, currently in its final stages of preparation. The report's authors are the members of the Extreme Ground Motion Committee [ExGMCom, T.C. Hanks (chair), N.A. Abrahamson, J.W. Baker, D.M. Boore, M. Board, J.N. Brune, and J.W. Whitney] all of whom have participated extensively in SCEC activities over the past five years.

The agreement with DOE called for an independent review by a team of SCEC scientists, composed of G.C. Beroza (chair), S.M. Day, L. Grant-Ludwig, R.B. Smith, and R.J Weldon. ExGMCom hosted a field trip for the SCEC Review Team April 7-10, 2010, so that they could observe in the field some of the more relevant and dramatic geologic and geomorphic observations that are part of the Final Report. These include cliffs of densely welded tuffs shattered by the extreme ground motions of underground nuclear explosions on Pahute Mesa, precarious rocks on the west face of Yucca Mountain, and the evidence for the "million-year-old" landscape on and around Yucca Mountain. See photos below. Upon its completion, the SCEC Review Team will provide a written review of the Final Report

Figure 80. ExGMCom and the SCEC Review Team at the "Grandstand," the viewing area for atmospheric nuclear tests in the 1950s, for the April 2010 field review.

Figure 81. Google Earth image of the crater of the UNE Boxcar (left), the nation's first megaton nuclear device detonated April 26, 1968, and Boxcar Bluff (right), cliffs of densely welded tuffs shattered by Boxcar (**Figure 82**). The crater is about 400 m in diameter.

Figure 82. Looking up at the shattered cliffs of Boxcar Bluffs, scientist for scale at top.

Figure 83. The "clean" west face of Yucca Mountain. The boulders in the foreground have rolled down from the cliffs of Tiva canyon Tuff on the Yucca Mountain crest (skyline). They have surface-exposure ages in excess of 200 ka.

Figure 84. The precarious rock (stack) Tripod, with Jim Brune, Tom Jordan, and Greg Beroza for scale.

The Final Report will recount the major advances in earthquake science driven by ExGm over the past six years, to all of hich SCEC scientists have contributed. They include:

- Delineating the ground motions and faulting displacements that accompany spontaneous, dynamically-propagating, complete stress-drop earthquake models.
- Understanding the causes and effects of non-linear stress-wave propagation in rock and how this leads to physical limits of ground motion.
- Refining the toppling probabilities for and the fragility ages of precariously balanced rocks (PBR), thus allowing better probabilistic portrayals of unexceeded ground motions. These methods are general; the ExGM applications have been to PBRs on the west face of Yucca Mountain.
- Quantifying the spectacular morphological differences of the UNE-shattered cliffs (extreme geomorphology) and the comparatively "clean" west face of Yucca Mountain.
- Determining the surprising antiquity of the Yucca Mountain landscape (the "million-year-old landscape") through many new surface-exposure ages.
- Developing the Points-in-Hazard-Space methodology, allowing a great variety of geologic, geomorphic, and geophysical hazard data and constraints to be placed in a single graphic.
- Developing arms stress drops from the global mb-M database and determining that the distribution of these stress drops for 441 crustal earthquakes is log-normal to more than 2 sigma at its upper end.
- Compiling a global database of the largest surface-faulting displacements for normal-faulting earthquakes, both historic and late-Pleistocene (paleoseismic) events.
- Documenting the magnitude-independence of apparent stresses in the western United States.

Community Modeling Environment

Overview of SCEC Community Modeling Environment (CME) Collaboration

The Southern California Earthquake Center (SCEC) Community Modeling Environment (SCEC/CME) collaboration is an inter-disciplinary research group that includes geoscientists and computer scientists from University of Southern California, San Diego State University, University of Wyoming, Stanford University, San Diego Supercomputer Center (SDSC), the University of California at San Diego, Carnegie Mellon University (CMU), Pittsburgh Supercomputer Center (PSC), and USC Information Sciences Institute (USC/ISI). The CME collaboration develops computational models of earthquake processes and uses high performance computing (HPC) systems to run these predictive numerical models and produce physics-based seismic hazard estimates for California.

Many SCEC research areas require the use of computer modeling and the CME collaboration helps to develop the scientific computing systems SCEC needs. CME researchers are working to improve a broad range of predictive seismic hazard parameters include scenario ground motion maps (used in emergency management exercises), scenario broadband seismograms (used in seismic engineering of tall buildings), and probabilistic seismic hazard curves (used in insurance loss estimations). The CME integrates new SCEC science results into highly-scalable computational models and runs large-scale physics-based seismic hazard calculations using national open-science supercomputer facilities.

SCEC, as a system science organization with broad research goals, has a wide variety of computational science research needs. The CME provides the computer science capabilities for SCEC to conduct one of the largest and most comprehensive seismic hazard computational research activities. SCEC has developed one of the most world's most computationally scalable wave propagation codes (AWP-ODC) and one of the largest and most complex scientific workflow systems (CyberShake1.0) in existence. The CME full 3D Tomography research establishes SCEC as one of the most data intensive computational groups in any NSF research domain. The CME research program has helped to establish a leadership role for SCEC in national scientific computing. CME project members regularly present SCEC research at computer science and HPC conferences such as Supercomputing and TeraGrid. CME research projects typically require both geoscientific and computer science expertise. Each year, the CME works to improve the accuracy, scale, efficiency of our seismic hazard modeling software. Then we apply these new computational capabilities to important SCEC research questions.

Computational tool developments by the CME this year include significant performance improvements in our highest performance earthquake wave propagation codes AWP-ODC and Hercules. The CME has collaborated with the CVM-H development group on the CVM-Toolkit which is a set of software tools for constructing very large meshes using SCEC CVM-H. The CME also performed collaborative development of the second generation SCEC Broadband platform by integrating SCEC scientific codes into a computational system that provides interoperability between codes including rupture generators and non-linear site effect models.

Several seismic hazard research studies were run this year using CME computational capabilities. Three CME modeling groups ran 1Hz+ wave propagation validation simulations of the M5.4 Chino Hills earthquake (Figure 85). SDSU and SDSC ran an ensemble of three magnitude 8.0+ spontaneous rupture simulations with a rupture length exceeding 500km and an ensemble of three San Andreas Wall 2 Wall simulations at 1Hz. Geoff Ely at USC ran an Elsinore Fault rupture and wave propagation simulation which is part of what we call the SCEC Big Ten simulation effort. A collaborative group lead by Y. Cui at SDSC and K. Olsen at SDSU ran the SCEC M8 simulation, a scenario M8 San Andreas event simulation using a dynamic rupture source at frequencies up to 2Hz. The SCEC M8 simulation ran on the largest open-science computer in the world (NCCS Jaguar) and is one of the largest earthquake wave propagation simulations ever performed.

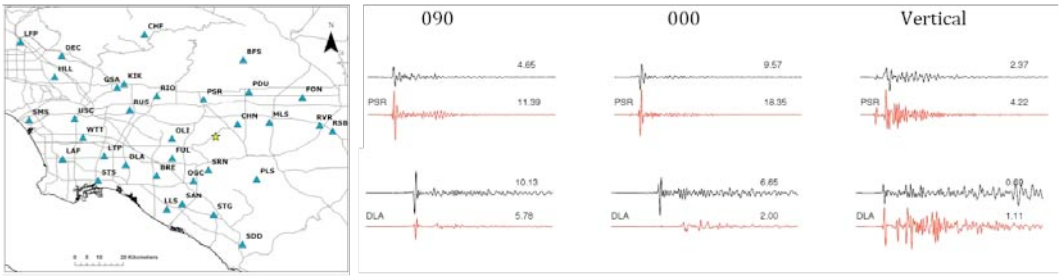

Figure 85. The Chino Hills M5.4 event is used in validation of wave propagation simulations because it just outside the Los Angeles Basin and is well centered within the CISN network. Waveform comparisons using Olsen-AWP (0.1 – 2.0Hz with min Vs = 500m/s - Data black, Simulation red) show good fit for some components at stations to the north of the event, and mismatches between direct S-Waves and observed S arrivals at station DLA as the seismic waves cross the Los Angeles Basin structure. As we push to higher frequencies, we must understand the causes of these mis-matches from source descriptions, velocity models, minimum Vs parameters and local site effects to continue increases in deterministic simulation frequencies.

Development of the CVM-Toolkit (CVM-T)

The CME has worked this year to develop new software tools to help SCEC HPC modeling groups build 3D velocity meshes. The SCEC Community Velocity Model Toolkit (CVM-T) enables earthquake modelers to quickly build, visualize, and validate large-scale meshes using SCEC CVM-H or CVM-4. CVM-T is comprised of three main components: (1) the most current version of the CVM-H community velocity model for Southern California, (2) tools for extracting meshes from this model and visualizing them, and (3) an automated test framework for evaluating new releases of CVM's using SCEC's AWP-ODC forward wave propagation software and one, or more, ground motion goodness of fit (GoF) algorithms.

CVM-T is designed to help SCEC modelers build large-scale velocity meshes by extracting material properties from an extended version of Harvard University's Community Velocity Model (CVM-H). The CVM-T software provides a highly-scalable interface to CVM-H 6.2 (and later) voxets. Along with an improved interface to CVM-H material properties, the CVM-T software adds a geotechnical layer (GTL) to CVM-H 6.2+ based on Ely's Vs30-derived GTL. The initial release of CVM-T also extends the coverage region for CVM-H 6.2 with a Hadley-Kanamori 1D background. Our goodness-of-fit measures include map-based measure which shows variations in matches across a simulation region.

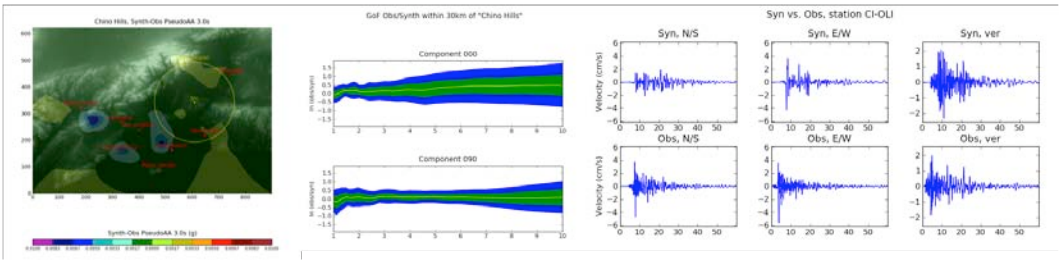

Figure 86. To support modifications and improvements to SCEC Community Velocity Models (CVM's), we have developed an automated CVM evaluation that builds a mesh from the CVM under tests and runs a 1Hz Chino Hills M5.4 event. The automates the running and post processing for this reference event and produces validation information as goodness-of-fit measures. (a) map-based goodness-of-fit, (b) bias comparison for synthetics, and (c) comparison of synthetic and observed seismograms.

The CVM-T system automates the processing needed to configure and run a 1Hz Chino Hills simulation and post-process the results into standard goodness-of-fit reports as shown in Figure 86. The goodness-of-fit algorithms we have developed help identify critical areas in need of improvement in the Community Velocity Model (CVM), and to help SCEC researchers assess the accuracy of different velocity models.

Development of the Second Generation Broadband Platform

The SCEC Broadband platform development involves SCEC researchers, graduate students, and the SCEC/CME software development group. The SCEC Broadband Platform integrates SCEC scientific modeling codes into a system capable of computing broadband seismograms (0-10 Hz) for scenario earthquakes in California. Scientific codes integrated into the SCEC Broadband Platform include pseudo-dynamic rupture generators, low frequency deterministic seismogram synthesis, high frequency stochastic seismogram synthesis, and non-linear site effect modeling codes. The Broadband Platform is designed to be used by both scientific and engineering groups and is designed to be portable and easy-to-use. Users may calculate broadband seismograms for both historical (validation events including Northridge, Loma Prieta, and Landers) earthquakes, as well as user-defined (scenario) earthquake. For each simulation, users may also select among various codebases for rupture generation, 1D low-frequency synthesis, high-frequency synthesis, and incorporation of non-linear site effects, with the option of running a goodness-of-fit comparison against observed or simulated seismograms. The platform produces a variety of ground motion-related data products, including broadband seismograms, rupture visualizations, and goodness-of-fit plots.

Ensemble of Southern San Andreas Wall to Wall Simulations at 1Hz

Large magnitude earthquake (e.g. > M8.0) simulations are computationally demanding because the affected regions are large and the frequencies of interest are high. Much of the seismic hazard in southern California, however, comes from rare, but very large, scenario earthquakes. In a magnitude 8, the San Andreas Fault might rupture for 500km. The area affected by such a wall-to-wall earthquake is large (~800 km by 400 km), and until recent advances in parallel computation, simulations of this scale have been out of reach.

To study these large events, CME researchers have developed the scientific and computational tools needed to simulate a set of Mw 8.0 earthquakes on the southern San Andreas Fault at 1Hz. Based on earlier SCEC research, dynamic rupture-based source descriptions provide source complexity needed for large-scale wave propagation simulations at higher frequencies. CME researchers optimized both the dynamic rupture modeling algorithms and the wave propagation software in our AWP-ODC software. Then, using NICS Kraken, we simulated three Mw8.0 wall-to-wall scenarios in a 32 billion grid point (800 km by 400 km by 100 km with a grid spacing of 100m) subset of the SCEC Community Velocity Model (CVM) V4 with a minimum shear-wave velocity of 500 m/s up to a maximum frequency of 1 Hz. We modeled for 3 wall-to-wall source realizations, namely two uni-lateral (southeast-to-northwest and northwest-to-southeast) ruptures, and a bi-lateral rupture starting in the center of the fault as shown in Figure 87.

The Wall-2-Wall simulations were run using 96,000 processor cores (out of 99,072) on the TeraGrid Kraken Cray XT5 supercomputer. Each run required 2.6 hours wall clock time, obtaining 53 sustained Teraflops. Peak ground motion maps produced by these simulations are shown in Figure 87. All realizations are characterized by strong directivity effects of the rupture, with highly variable pattern of the strong ground motion, and 'sun-bursts' radiating from the fault due to the complexity in the temporal evolution of rupture. All source realizations generated large amplitudes in the Los Angeles and Ventura basins, with the most localized 'pockets' of amplification in Los Angeles for the uni-lateral rupture.

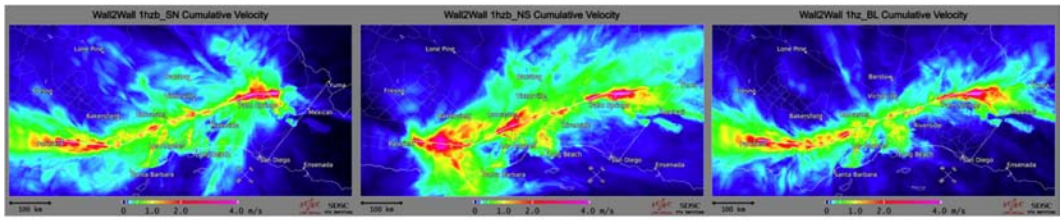

Figure 87. These maps show peak ground velocities for 3 Wall-2-Wall scenario events at 1Hz for M8.0 southern San Andreas ruptures showing the effects of alternative rupture directions. All ruptures are equivalent magnitudes with different rupture directions (left) southeast-northwest; (center) northwest-southeast; and (right) bi-lateral ruptures.

SCEC Big Ten Event Simulations

The SCEC Big Ten project is working to simulate ten of the most probable large (M > 7) ruptures in Southern California, with the objective of understanding how source directivity, rupture complexity, and basin effects affect ground motions. The ruptures and moment-magnitudes are selected from events with relatively high probability rates in the Uniform California Earth¬quake Rupture Forecast, Version 2 (UCERF2) model. The initial Big Ten simulations are being done using a newly developed, second order, mimetic dynamic rupture and wave propagation code. The SORD code supports greater complexity in our fault models but they are less scalable than our finite difference codes at this time and we are working to improve their capabilities. Simulation results from low frequency simulation of M7+ rupture on the Elsinore Fault were performed this year with our recently improved SORD code.

SCEC M8 Simulation

SCEC HPC computational groups at San Diego Supercomputer Center, San Diego State University, Pittsburg Supercomputer Center, and Carnegie Mellon University made outstanding progress this year improving SCEC HPC code performance. The CME research groups have obtained access to large, open-science, computer clusters at TACC, NICS, Argonne, and Oak Ridge. A combination of larger computers and significant software improvements has lead to great improvements in computational capabilities for SCEC wave propagation software, as shown in Figure 88. Wave propagation software performance improvements are critical to SCEC research, because wave propagation codes are used in many of the CME's most common seismic hazard modeling calculations.

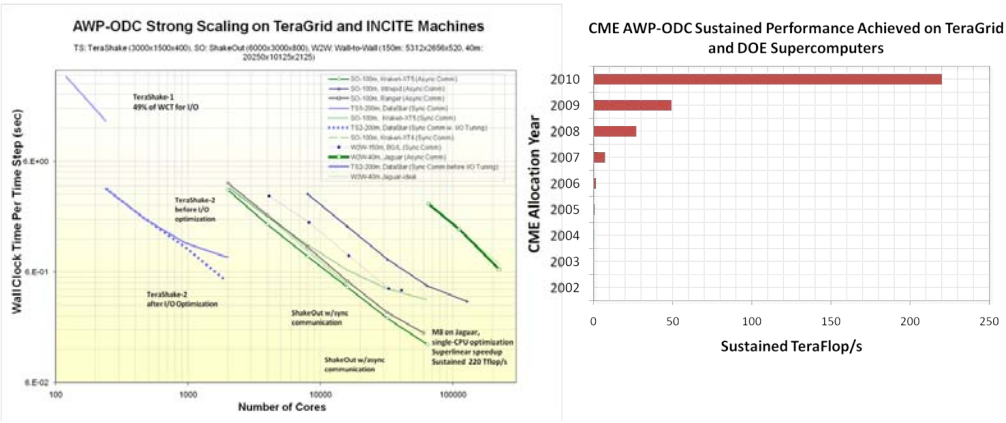

Figure 88. Improvement to SCEC's AWP-ODC software are showing in scaling diagram (a) and sustained performance (b). AWP-ODC, a fourth order, finite difference code, shows excellent scalability on all the largest NSF Track 2 machines, as well as the DOE INCITE computers. On right,

the great performance improvements in AWP-ODC between 2009 and 2010 is a result of communications improvements and access to more cores on Jaguar.

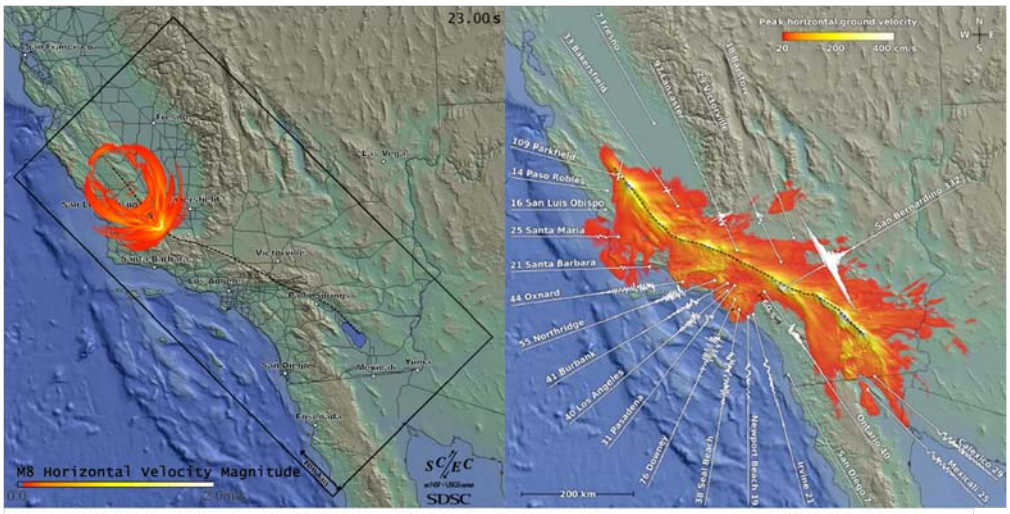

Figure 89. SCEC M8 Simulation Results: (a) View of the M8 simulation showing super-shear rupture with the Mach cone entering the 'Big Bend' section of the San Andreas Fault. Our dynamic rupture-based sources provide evidence of a physical basis for super-shear rupture during large events with slip-weakening friction laws. Further dynamic rupture modeling, investigating alternative friction laws will help identify the causes of super-shear rupture (b) PGVH's derived from M8 superimposed on the regional topography. N46E component seismograms are added at selected locations, with their peak velocities (cm/s) listed along the traces.

CME progress in several areas made it possible for our group to design and run the SCEC M8 simulation, one of the largest wave propagation simulations ever performed. The science and computational performance of the M8 simulation is based on our high frequency validation Chino Hills simulation results, our ensemble Wall-2-Wall San Andreas simulations at 1Hz, our TeraGrid and DOE INCITE allocations of computer time, data storage, and other computer resources, and recent significant performance improvements to our AWP-ODC software.

Our M8 study uses a two-step simulation process in which a dynamic rupture simulation is run to create a physically realistic earthquake slip-time history. This slip-time history is then used as the earthquake source description in the second step, a deterministic earthquake wave propagation simulation. Use of dynamic rupture simulation to generate the M8 source descriptions is one of the reasons that M8 represents a state-of-the-art seismic hazard research simulation. The M8 dynamic rupture simulation models friction on the fault with a slip-weakening law. The output from this dynamic rupture simulation represents an earthquake slip time history dataset which is a required input for the M8 wave propagation simulation. We transferred this dynamic rupture simulation result from NICS Kraken to NCCS Jaguar, and ran the M8 wave propagation simulation on Jaguar. Figure 89 shows (left) an snapshot of the M8 rupture propagating south on the San Andreas Fault, and (right) an M8 peak ground velocity map with seismograms at specific sites overlaid on the map.

The SCEC M8 simulation represents a technological accomplishment that greatly increases the efficiency of SCEC's fundamental seismic hazard calculations. These results will have significant, long-term, impact on SCEC research as we migrate the efficient improvements made to our AWP-ODC code for use in M8 into routine PSHA calculations needed to develop a accurate and precise understanding of seismic hazards.

Upcoming CME Research

The CME helps to implement SCEC's comprehensive, physics-based, system science approach to probabilistic seismic hazard analysis. CME researchers will continue to integrate better physics into seismic hazard calculations by integrating research results from various SCEC research groups together into CME computational tools. Over the next few years, CME researchers will work to improve SCEC ground motion modeling through improved dynamic rupture models, more accurate wave propagation simulations, physics-based probabilistic seismic hazard analysis, and 3D velocity model development. CME researchers expect to contribute to the development by SCEC 4 of time-dependent seismic hazard analysis techniques.

Selected CME-Related Publications

Graves, R. W., B. T. Aagaard, and K. W. Hudnut (2010). The ShakeOut Earthquake source and ground motion simulations, Earthquake Spectra, in press.

Cui, Y., K. B. Olsen, T. H. Jordan, K. Lee, J. Zhou, P. Small, D. Roten, G. Ely, D.K. Panda, A. Chourasia, J. Levesque, S. M. Day, P. Maechling (2010), Scalable Earthquake Simulation on Petascale Supercomputers, Proceedings of the SC10 International Conference for HPC, Networking and Analysis. (Accepted as SC10 Gordon Bell Finalist).

Taborda, R., J. López, H. Karaoglu, J. Urbanic and J. Bielak (2010), Speeding Up Wave Propagation for Large-Scale Earthquake Simulations, Proceedings of the SC10 International Conference for HPC, Networking and Analysis. (Submitted for publication).

Callaghan, Scott, Ewa Deelman, Dan Gunter, Gideon Juve, Philip Maechling, Christopher Brooks, Karan Vahi, Kevin Milner, Robert Graves, Edward Field, David Okaya, Thomas Jordan (2010), Scaling up workflow-based applications, J. Computer System Science, special issue on scientific workflows, in press.

Graves, R., T. Jordan; S. Callaghan; E. Deelman; E. Field; G. Juve; C. Kesselman; P. Maechling; G. Mehta; K. Milner; D. Okaya; P. Small; and K. Vahi (2010). CyberShake: A Physics-Based Seismic Hazard Model for Southern California, Pure Applied Geophys., accepted for publication

Moczo, P., J Kristek, P Franek, E Chalub, PY Bard, S Tsune, F Hollender, T Iwata, A Iwaki, E Priolo, P Klin, S Aoi, C Mariotti, J Bielak, R Taborda, H Karaoglu, V Etienne, J Virieux (2010), Numerical Modeling of Earthquake Ground Motion in the Mygdonian Basin, Greece: Verification of the 3D Numerical Methods, Proc. of the Annual Meeting of the Seis. Soc. of America.

Olsen, K.B., and J.E. Mayhew (2010). Goodness-of-fit Criteria for Broadband Synthetic Seismograms with Application to the 2008 Mw5.4 Chino Hills, CA, Earthquake, Seism. Res. Lett., accepted for publication.

Cruz-Atienza, V.M. and K.B. Olsen (2010). Supershear Mach-Waves Expose the Fault Breakdown Slip, Tectonophysics, in revision for the special volume on 'Supershear Earthquakes'.

Juve, G., Ewa Deelman, Karan Vahi, Gaurang Mehta, Bruce Berriman, Benjamin P. Berman, Phil Maechling (2010), Data Sharing Options for Scientific Workflows on Amazon EC2, 22nd IEEE/ACM Conference on Supercomputing (SC10), New Orleans, Louisiana, November 2010

Juve, G., Ewa Deelman, Karan Vahi, Garuang Mehta, Bruce Berriman, Benjamin P. Berman and Phil Maechling (2009), Scientific Workflow Applications on Amazon EC2, Workshop on Cloud-based Services and Applications in conjunction with 5th IEEE International Conference on e-Science (e-Science 2009), Oxford UK, December 2009.

Lee, K., Cui, Y., Maechling, P., Olsen, K. and Jordan, T., Communication Optimizations of SCEC AWP-Olsen Application for Petascale Computing (accept, Supercomputing 09, Portland, 2009; Lee, K., Cui, Y., Kaiser, T., Maechling, P., Olsen, K. and Jordan, T., IO Optimizations of SCEC AWP-Olsen Application for Petascale Earthquake Computing (both FINALISTS of Best Posters), SC09, Portland, 2009.

Rojas, O., E. Dunham, S.M. Day, L.A. Dalguer, and J.E. Castillo (2009). Finite difference modeling of rupture propagation with strong velocity-weakening friction, Geophys J. Int., in review.

Bielak, J., R.W. Graves, K.B. Olsen, R. Taborda, L. Ramírez-Guzmán, S.M. Day, G.P. Ely, D. Roten, T.H. Jordan, P.J. Maechling, J. Urbanic, Y. Cui, G. Juve, "The ShakeOut earthquake scenario:

Verification of three simulation sets," Geophysical Journal International doi: 10.1111/j.1365-246X.2009.04417x, 2009.

Maechling, P., E. Deelman, Y. Cui (2009), Implementing Software Acceptance Tests as Scientific Workflows, Proceedings of the IEEE International Parallel & Distributed Processing Symposium 2009, Las Vegas Nevada, July, 2009 (published)

Doser, D.I., K.B. Olsen, F.F. Pollitz, R.S. Stein, and S. Toda (2009). The 1911 M~6.6 Calaveras earthquake: Source parameters and the role of static, viscoelastic and dynamic Coulomb stress changes imparted by the 1906 San Francisco earthquake, Bull. Seis. Soc. Am. 99, 1746-1759.

Cui, Y., Chourasia, A., Moore, R., Olsen, K., Maechling, P., Jordan, T., The TeraShake Computational Platform, Advances in Geocomputing, Lecture Notes in Earth Sciences 119, DOI 10.1007/978-3-540-85879-9_7, pp229-278, editor H. Xing, Springer-Verlag Berlin Heidelberg, 2009.

Draft 2011 Science Plan

SCEC Planning Committee

September 2010

I. Introduction

On February 1, 2002, the Southern California Earthquake Center (SCEC) changed from an entity within the NSF/STC program to a freestanding center, funded by NSF/EAR and the U.S. Geological Survey. SCEC2 was funded for a five-year period, February 2002 to January 2007. SCEC was renewed for the period February 2007 through January 2012, referred to now as SCEC3. This document solicits proposals from individuals and groups to participate in the fifth and final year of the SCEC3 research program.

II. Guidelines for Proposal Submission

A. ***Due Date.*** Friday, November 5, 2010, 5:00 pm PST. Late proposals will not be accepted. Note the different deadline for submitting annual progress reports below.

B. ***Delivery Instructions.*** Proposals must be submitted as PDF documents via the SCEC Proposal web site at *http://www.scec.org/proposals*. Submission procedures, including requirements for how to name your PDF files, will be found at this web site.

C. Formatting Instructions.

Cover Page. The cover page should be headed with the words "2011 SCEC Proposal" and include the project title, Principal Investigator(s), institutional affiliation, amount of request, and proposal categories (from types listed in Section IV). List (in order of priority) three science objectives (Section VII) that your proposal addresses, for example A3, A5 and A11. Indicate if the proposal should also be identified with one or more of the SCEC special projects (see Section VIII). Collaborative proposals involving multiple investigators and/or institutions should list all Principal Investigators. Proposals do not need to be formally signed by institutional representatives, and should be for one year, with a start date of February 1, 2011.

Technical Description. Describe in up to five pages (including figures) the technical details of the project and how it relates to the short-term objectives outlined in the SCEC Science Objectives (Section VII). References are not included in the five-page limit.

Budget Page. Budgets and budget explanations should be constructed using NSF categories. Under guidelines of the SCEC Cooperative Agreements and A-21 regulations, secretarial support and office supplies are not allowable as direct expenses.

Current Support: Statements of current support, following NSF guidelines, should be included for each Principal Investigator.

2010 Annual Report: Scientists funded by SCEC in 2010 must submit a report of their progress by 5:00 pm PST February 28, 2011. 2011 proposals approved by the PC will not be funded until all progress reports are submitted. Reports should be up to five pages of text and figures. Reports should include bibliographic references to any SCEC publication during the past year (including papers submitted and in review), including their SCEC contribution number. Publications are assigned numbers when they are submitted to the SCEC publication database at *http://www.scec.org/signin*.

Special Note on Workshop Reports. Reports on results and recommendations of workshops funded by SCEC in 2011 are to be submitted no later than 30 days following the completion of the workshop. The reports will be posted on the SCEC web site as soon as possible after review by the directors.

Labeling the Submitted PDF Proposal. PI's must follow the proposal naming convention. Investigators must label their proposals with their last name followed by 2011, e.g., Beroza2011.pdf. If there is more than one proposal, then the file would be labeled as: Beroza2011_1.pdf (for the 1st proposal) and Beroza2011_2.pdf (for the 2nd proposal).

D. ***Principal Investigator Responsibilities.*** PI's are expected to interact with other SCEC scientists on a regular basis (e.g., by attending workshops and working group meetings), and contribute data, analysis results, and/or models to the appropriate SCEC data center (e.g., Southern California Earthquake Data Center—SCEDC), database, or community model (e.g., Community Velocity Model—CVM). Publications resulting entirely or partially from SCEC funding must include a publication number available at *http://www.scec.org/signin*. By submitting a proposal, investigators are agreeing to these conditions.

E. ***Eligibility.*** Proposals can be submitted by eligible Principal Investigators from:

- U.S. Academic institutions
- U.S. Private corporations
- International Institutions (funding will mainly be for travel)

F. ***Collaboration.*** Collaborative proposals with investigators from the USGS are encouraged. USGS employees should submit their requests for support through USGS channels. Collaborative proposals involving multiple investigators and/or institutions are strongly encouraged; these can be submitted with the same text, but with different institutional budgets if more than one institution is involved.

G. ***Budget Guidance.*** Typical SCEC grants funded under this Science Plan in the past have fallen in the range of $10,000 to $35,000. This is not intended to limit SCEC to a fixed award amount, nor to a specified number of awards, rather it is intended to calibrate expectations for proposals written by first-time SCEC investigators.

Special note 1. The cooperative agreements from the National Science Foundation and the United States Geological Survey that fund the SCEC3 core research program will end on January 31, 2012. No-cost extensions are NOT allowed on cooperative agreements. Therefore any funds awarded under this science plan MUST be expended by January 31, 2012.

Special Note 2. CSEP global travel grants from 2006 to 2010 were funded with a grant from the W. M. Keck Foundation. The Keck grant will end in early 2011 and future funding for CSEP global travel has not yet been obtained at the time of the release of this document.

H. ***Award Procedures.*** All awards will be funded by subcontract from the University of Southern California. The Southern California Earthquake Center is funded by the National Science Foundation and the U.S. Geological Survey.

III. SCEC Organization

A. ***Mission and Science Goal.*** SCEC is an interdisciplinary, regionally focused organization with a mission to:

- Gather data on earthquakes in Southern California and elsewhere

- Integrate information into a comprehensive, physics-based understanding of earthquake phenomena
- Communicate understanding to the world at large as useful knowledge for reducing earthquake risk

SCEC's primary science goal is to develop a comprehensive, physics-based understanding of earthquake phenomena in Southern California through integrative, multidisciplinary studies of plate-boundary tectonics, active fault systems, fault-zone processes, dynamics of fault ruptures, ground motions, and seismic hazard analysis. The long-term science goals are summarized in Appendix A.

B. ***Disciplinary Activities.*** The Center sustains disciplinary science through standing committees in seismology, geodesy, and geology. These committees will be responsible for planning and coordinating disciplinary activities relevant to the SCEC science plan, and they will make recommendations to the SCEC Planning Committee regarding support of disciplinary research and infrastructure. High-priority disciplinary activities are summarized in Section VII.A.

C. ***Interdisciplinary Focus Areas.*** Interdisciplinary research is organized within seven science focus areas: 1) Unified Structural Representation (URS), 2) Fault and Rupture Mechanics (FARM), 3) Crustal Deformation Modeling (CDM), 4) Lithospheric Architecture and Dynamics (LAD), 5) Earthquake Forecasting and Predictability (EFP), 6) Ground Motion Prediction (GMP) and 7) Seismic Hazard and Risk Analysis (SHRA). High-priority activities are listed for each of these interdisciplinary focus areas in Section VII.B.

D. ***Special Projects.*** SCEC supports eight special projects that will advance designated research frontiers. Several of these initiatives encourage further development of an advanced IT infrastructure for system-level earthquake science in Southern California. High-priority initiatives are listed and described in Section VIII.

E. ***Communication, Education, and Outreach.*** SCEC maintains a strong Communication, Education, and Outreach (CEO) program with four principal goals: 1) coordinate productive interactions among SCEC scientists, and with partners in science, engineering, risk management, government, business, and education; 2) increase earthquake knowledge and science literacy at all educational levels; 3) improve earthquake hazard and risk assessments; and 4) promote earthquake preparedness, mitigation, and planning for response and recovery. Opportunities for participating in the CEO program are described in Section IX. Current activities are described online at *http://www.scec.org/ceo*.

IV. Proposal Categories

A. ***Data Gathering and Products.*** SCEC coordinates an interdisciplinary and multi-institutional study of earthquakes in Southern California, which requires data and derived products pertinent to the region. Proposals in this category should address the collection, archiving and distribution of data, including the production of SCEC community models that are on-line, maintained, and documented resources for making data and data products available to the scientific community.

B. ***Integration and Theory.*** SCEC supports and coordinates interpretive and theoretical investigations on earthquake problems related to the Center's mission. Proposals in this category should be for the integration of data or data products from Category A, or for general or theoretical studies. Proposals in Categories A and B should address one or more of the goals in Section VII, and may include a brief description (<200 words) as to how the proposed research and/or its results might be used in a special initiative (see Section VIII) or in an educational or outreach mode (see Section IX).

C. ***Workshops.*** SCEC participants who wish to host a workshop between February 2011 and January 2012 should submit a proposal for the workshop in response to this RFP. This includes workshops that might be organized around the SCEC annual meeting in September. Workshops in the following topics are particularly relevant:

- Organizing collaborative research efforts for the five-year SCEC program (2007-2012). In particular, interactive workshops that engage more than one focus and/or disciplinary group are strongly encouraged.
- Engaging earthquake engineers and other partner and user groups in SCEC-sponsored research.
- Participating in national initiatives such as EarthScope, the Advanced National Seismic System (ANSS), and the George E. Brown, Jr. Network for Earthquake Engineering Simulation (NEES).

D. ***Communication, Education, and Outreach.*** SCEC has developed a long-range CEO plan and opportunities for participation are listed in Section IX. Investigators who are interested in participating in this program should contact Mark Benthien (213-740-0323; *benthien@usc.edu*) before submitting a proposal.

E. ***SCEC/SURE Intern Project.*** If your proposal includes undergraduate funding, please note this on the cover page. Each year SCEC coordinates the SCEC Summer Undergraduate Research Experience (SCEC/SURE) program to support one-on-one student research with a SCEC scientist. See *http://www.scec.org/internships* for more information. SCEC will be recruiting mentors in November, 2010, and will request descriptions of potential projects via email. In December, these descriptions will be published on the SCEC Internship web page to allow applicants to identify their preferred projects.

Mentors will be required to provide at least $2500 of the $5000 intern stipend, and SCEC will pay the balance. Mentor contributions can come from any source, including SCEC-funded research projects. Therefore, interested SCEC scientists are encouraged to include at least $2500 for an undergraduate intern in their 2011 SCEC proposals, and then respond to the recruitment emails.

Questions about the SCEC/SURE Intern Project should be referred to Robert de Groot, *degroot@usc.edu*.

F. ***SCEC Annual Meeting participation.*** Investigators who wish to only request funding to cover travel to the annual meeting can participate in a streamlined review process with an abbreviated proposal. Investigators who are already funded to study projects that would be of interest to the SCEC community, and investigators new to SCEC who would benefit from exposure to the Annual Meeting in order to fine-tune future proposals are encouraged to apply.

V. Evaluation Process and Criteria

A. Proposals should be responsive to the RFP. A primary consideration in evaluating proposals will be how directly the proposal addresses the main objectives of SCEC. Important criteria include (not necessarily in order of priority):

1. Scientific merit of the proposed research
2. Competence and performance of the investigators, especially in regard to past SCEC-sponsored research
3. Priority of the proposed project for short-term SCEC objectives as stated in the RFP

4. Promise of the proposed project for contributing to long-term SCEC goals as reflected in the SCEC science plan (see Appendix).
5. Commitment of the P.I. and institution to the SCEC mission
6. Value of the proposed research relative to its cost
7. Ability to leverage the cost of the proposed research through other funding sources
8. Involvement of students and junior investigators
9. Involvement of women and underrepresented groups
10. Innovative or "risky" ideas that have a reasonable chance of leading to new insights or advances in earthquake physics and/or seismic hazard analysis.

B. Proposals may be strengthened by describing:

1. Collaboration
   - Within a disciplinary or focus group
   - Between disciplinary and/or focus groups
   - In modeling and/or data gathering activities
   - With engineers, government agencies, and others. (See Section IX)
2. Leveraging additional resources
   - From other agencies
   - From your institution
   - By expanding collaborations
3. Development and delivery of products
   - Community research tools, models, and databases
   - Collaborative research reports
   - Papers in research journals
   - End-user tools and products
   - Workshop proceedings and CDs
   - Fact sheets, maps, posters, public awareness brochures, etc.
   - Educational curricula, resources, tools, etc.
4. Educational opportunities
   - Graduate student research assistantships
   - Undergraduate summer and year-round internships (funded by the project)
   - K-12 educator and student activities
     - Presentations to schools near research locations
     - Participation in data collection

C. All research proposals will be evaluated by the appropriate disciplinary committees and focus groups, the Science Planning Committee, and the Center Director. CEO proposals will be evaluated by the CEO Planning Committee and the Center Director.

D. The Science Planning Committee is chaired by the Deputy Director and comprises the chairs of the disciplinary committees, focus groups, and special projects. It is responsible for recommending a balanced science budget to the Center Director.

E. The CEO Planning Committee is chaired by the Associate Director for CEO and comprises experts involved in SCEC and USGS implementation, education, and outreach. It is responsible for recommending a balanced CEO budget to the Center Director.

F. Recommendations of the planning committees will be combined into an annual spending plan and forwarded to the SCEC Board of Directors for approval.

G. Final selection of research projects will be made by the Center Director, in consultation with the Board of Directors.

H. H. The review process should be completed and applicants notified by the end of February, 2011.

VI. Coordination of Research between SCEC and USGS-EHRP

Earthquake research in Southern California is supported both by SCEC and by the USGS Earthquake Hazards Reduction Program (EHRP). EHRP's mission is to provide the scientific information and knowledge necessary to reduce deaths, injuries, and economic losses from earthquakes. Products of this program include timely notifications of earthquake locations, size, and potential damage, regional and national assessments of earthquakes hazards, and increased understanding of the cause of earthquakes and their effects. EHRP funds research via its External Research Program, as well as work by USGS staff in its Pasadena, Menlo Park, and Golden offices. The EHRP also supports SCEC directly with $1.1M per year.

SCEC and EHRP coordinate research activities through formal means, including USGS membership on the SCEC Board of Directors and a Joint Planning Committee, and through a variety of less formal means. Interested researchers are invited to contact Dr. Ken Hudnut, EHRP coordinator for Southern California, or other SCEC and EHRP staff to discuss opportunities for coordinated research.

The USGS EHRP supports a competitive, peer-reviewed, external program of research grants that enlists the talents and expertise of the academic community, State and local governments, and the private sector. The investigations and activities supported through the external program are coordinated with and complement the internal USGS program efforts. This program is divided into six geographical/topical 'regions', including one specifically aimed at Southern California earthquake research and others aimed at earthquake physics and effects and at probabilistic seismic hazard assessment (PSHA). The Program invites proposals that assist in achieving EHRP goals.

The EHRP web page, *http://earthquake.usgs.gov/research/external/*, describes program priorities, projects currently funded, results from past work, and instructions for submitting proposals. The EHRP external funding cycle is several months offset from SCEC's, with the RFP due out in February and proposals due in May. Interested PI's are encouraged to contact the USGS regional or topical coordinators for Southern California, Earthquake Physics and Effects, and/or National (PSHA) research, as listed under the "Contact Us" tab.

USGS internal earthquake research is summarized by topic at *http://earthquake.usgs.gov/research/topics.php*.

VII. SCEC3 Science Priorities

The research objectives outlined below are priorities for SCEC3. They carry the expectation of substantial and measurable success during the coming year. In this context, success includes progress in building or maintaining a sustained effort to reach a long-term goal. How proposed

projects address these priorities will be a major consideration in proposal evaluation, and they will set the programmatic milestones for the Center's internal assessments. In addition to the priorities outlined below, the Center will also entertain innovative and/or "risky" ideas that may lead to new insights or major advancements in earthquake physics and/or seismic hazard analysis.

There are four major research areas with the headings A, B, C and D with subheadings given by numbers. The front page of the proposal should specifically identify subheadings that will be addressed by the proposed research.

A. Develop an extended earthquake rupture forecast to drive physics-based SHA.

A1. Define slip rates and earthquake history of southern San Andreas fault system for the last 2000 years

A2. Investigate implications of geodetic/geologic rate discrepancies

A3. Develop a system-level deformation and stress-evolution model

A4. Statistical analysis and mapping of seismicity and source parameters with an emphasis on their relation to known faults

A5. Develop a geodetic network processing system that will detect anomalous strain transients

A6. Test scientific prediction hypotheses against reference models to understand the physical basis of earthquake predictability

A7. Determine the origin, evolution and implications of on- and off-fault damage

A8. Test hypotheses for dynamic fault weakening

A9. Assess predictability of rupture extent and direction on major faults

A10. Develop statistical descriptions of heterogeneities (e.g., in stress, strain, geometry and material properties), and understand their origin and implications for seismic hazard by observing and modeling single earthquake ruptures and multiple earthquake cycles.

A11. Constrain absolute stress and understand the nature of interaction between the faulted upper crust, the ductile crust and mantle, and how geologic history helps to resolve the current physical properties of the system.

B. Predict broadband ground motions for a comprehensive set of large scenario earthquakes.

B1. Develop kinematic and dynamic rupture representations consistent with seismic, geodetic, and geologic observations.

B2. Investigate bounds on the upper limit of ground motion.

B3. Develop high-frequency simulation methods and investigate the upper frequency limit of deterministic ground-motion predictions.

B4. Validate ground-motion simulations and verify simulation methodologies.

B5. Improve our understanding of site effects and develop methodologies to include these effects in broadband ground-motion simulations.

B6. Collaborate with earthquake engineers

C. Improve and develop community products (data and descriptions) that can be used in system-level models for the forecasting of seismic hazard. Proposals for such activities should show how they would significantly contribute to one or more of the numbered goals in A or B.

D. Prepare post-earthquake response strategies.

Some of the most important earthquake data are gathered during and immediately after a major earthquake. Exposures of fault rupture are erased quickly by human activity, aftershocks decay rapidly within days and weeks, and post-seismic slip decays exponentially. SCEC solicits proposals for a workshop to plan post-earthquake science response. The goals of the workshop would be to: 1) develop a post-earthquake science plan that would be a living document such as a wiki; 2) identify permanent SCEC and other science facilities that are needed to ensure success of the science plan; 3) identify other resources available in the community and innovative ways of using technology for coordination and rapid data processing that will allow for rapid determination of source parameters, maps, and other characteristics of the source and ground motion patterns; 4) develop plans for use of simulations in post-earthquake response for evaluation of short-term earthquake behavior and seismic hazards; and 5) develop mechanisms for regular updates of the SCEC post-earthquake response plan.

VIII. Disciplinary Activities

The Center will sustain disciplinary science through standing committees in seismology, geodesy, and geology. These committees will be responsible for planning and coordinating disciplinary activities relevant to the SCEC science plan, and they will make recommendations to the SCEC Planning Committee regarding the support of disciplinary infrastructure. High-priority disciplinary objectives include the following tasks:

A. Seismology

Objectives. The objectives of the Seismology group are to gather data on the range of seismic phenomena observed in southern California and to integrate these data into physics-based models of fault slip. Of particular interest are proposals that foster innovations in network deployments, data collection, real-time research tools, and data processing. Proposals that provide community products that support one or more of the numbered goals in A, B, C or D or those that include collaboration with network operators in Southern California are especially encouraged. Proposers should consider the SCEC resources available including the Southern California Earthquake Data Center (SCEDC) that provides extensive data on Southern California earthquakes as well as crustal and fault structure, the network of SCEC funded borehole instruments that record high quality reference ground motions, and the pool of portable instruments that is operated in support of targeted deployments or aftershock response.

Research Strategies. Examples of research strategies that support the objectives above include:

- Enhancement and continued operation of the SCEDC and other existing SCEC facilities particularly the near-real-time availability of earthquake data from SCEDC and automated access.
- Real-time processing of network data such as improving the estimation of source parameters in relation to known and unknown faults (A3, A4, A10), especially evaluation of the short term evolution of earthquake sequences and real-time stress perturbations on nearby major fault segments (D).
- Enhance or add new capabilities to existing earthquake early warning (EEW) systems or provide new EEW algorithms. Develop real-time finite source models constrained by incoming seismic and GPS data to estimate evolution of the slip function and potentially damaging ground shaking (D).
- Advance innovative and practical strategies for densification of seismic instrumentation, including borehole instrumentation, in Southern California and develop innovative algorithms to utilize data from these networks. Develop metadata, archival and distribution models for these semi-mobile networks.
- Develop innovative new methods to search for unusual signals using combined seismic, GPS, and borehole strainmeter data (A5, A6); collaborations with EarthScope or other network operators are encouraged.

- Investigate near-fault crustal properties, evaluate fault structural complexity, and develop constraints on crustal structure and state of stress, and (A7, A10, C).
- Collaborations, for instance with the ANSS and NEES projects, that would augment existing and planned network stations with downhole and surface instrumentation to assess site response, nonlinear effects, and the ground coupling of built structures (B4, B6).
- Preliminary design and data collection to seed future passive and active experiments such as dense array measurements of basin structure and large earthquake properties, OBS deployments, and deep basement borehole studies.

Priorities for Seismology in 2011.

1. ***Earthquake early warning research.*** In the next few years, earthquake early warning (EEW) systems will be installed in California. The seismology group seeks proposals that will provide new algorithms, enhance or add new capabilities to existing EEW algorithms. The development of Bayesian probabilities that would take advantage of the extensive knowledge developed by SCEC about fault structures and spatial and temporal seismicity patterns are needed to make EEW algorithms more robust. Similarly, high-sample rate GPS 1 second solutions are being made available real-time for EEW development. Using these new data to develop new EEW algorithms for finite sources is a new area of research for SCEC scientists.
2. ***Community seismic networks.*** Several community seismic networks using low cost sensors are being developed in California. We seek proposals that would address development of seismological algorithms to utilize data from these networks in innovative ways. We also seek proposals that would develop metadata and archiving models for these new semi-mobile networks, as well as archive and serve these data to the SCEC user community.
3. ***The 2010 M7.2 El Mayor-Cucapah Earthquake Sequence.*** The El Mayor sequence ruptured for a distance of more than 120 km, and large data sets were recorded by the SCSN, RESNOM, portable temporary networks, and GPS networks. Proposals that seek to analyze these data and other relevant data sets in the context of SCEC research priorities are welcome.

B. Tectonic Geodesy

Objectives. The broad objective of SCEC's Tectonic Geodesy disciplinary activities is to foster the availability of the variety of geodetic data collected in Southern California and the innovative and integrated use of these observations, in conjunction with other relevant data (e.g., seismic or geologic information), to address the spectrum of deformation processes affecting this region. Topics of interest include, but are not limited to, rapid earthquake response, transient deformation, anthropogenic or nontectonic effects, and the quantification and interpretation of strain accumulation and release, with one goal being the increased use of insights from geodesy in seismic hazard assessment. Proposed work may overlap with one or more focus areas.

Research Strategies. The following are research strategies aimed at meeting the broad objective:

- Develop reliable means for detecting, assessing, and interpreting transient deformation signals and for using this information in monitoring and response activities. (A5).
    - Extend algorithms that have demonstrated their reliability during synthetic tests to real data.
    - Incorporate other data types into monitoring systems in addition to or instead of GPS.
    - Participate in, and generate sets of real or synthetic GPS or other types of data for, the Transient Detection Blind Test Exercise.

  - Investigate processes underlying detected signals and/or their seismic hazard implications.

- Extend methods for estimating crustal motion and refine such estimates for southern California (A1, A2, A3, B1, C, D). In all cases, work should include assessment of the sources of uncertainty in the analysis and results. Proposals for the development of new data products or collection of new data must explicitly motivate the need for such efforts and state how the resulting data or products will be used. Data collected with SCEC funding must be made publicly-available in an online archive within two years of its collection, although PIs may choose to share data on a case-by-case basis earlier than the two-year deadline.
  - Collaborate on the generation and maintenance of an up-to-date consensus velocity field with estimates of uncertainties for southern California.
  - Improve vertical velocity estimates and their uncertainties, for example by refining or extending data processing and analysis strategies or approaches for the combined use of multiple data types.
  - Develop methods for combining data types (e.g., GPS, InSAR, strainmeter, and/or other data) that have differing spatial and temporal apertures, sampling frequencies, and sensitivities, and assess the utility of such combinations for interpreting tectonic or nontectonic signals.
  - Further develop approaches for incorporating geodetic slip and strain rate estimates into the UCERF3 assessment including, but not limited to, the refined assessment of the uncertainties in these quantities due to possible trade-offs among model parameters, postseismic and earthquake cycle perturbations, and choice of data and fault geometry used in modeling. Quantitative comparison among models and development of new models where warranted are also encouraged.
  - Develop tools for using high-rate and real-time GPS positions and demonstrate application of these data to address topics such as rapid earthquake response, postseismic analysis, or the combined use of GPS and seismic data.
- The 2010 M7.2 El Mayor-Cucapah Earthquake Sequence. (B1, C, D) Tectonic Geodesy priorities for response to this event include:
  - Acquisition of data that constrains the coseismic and postseismic deformation field.
  - Integration of geodetic observations with constraints from field geology, seismology, etc, with particular focus on the potential for a large aseismic signal associated with this earthquake.
  - Evaluation of the impact that geodetic observations have on estimates of loading of regional faults by this earthquake.

C. Earthquake Geology

Objectives. The Earthquake Geology group promotes studies of the geologic record of the Southern California natural laboratory that advance SCEC science. Geologic observations can provide important contributions to nearly all SCEC objectives in seismic hazard analysis (A1-A3, A6-A11) and ground motion prediction (B2-B5). Studies are encouraged to test outcomes of earthquake simulations and crustal deformation modeling. Earthquake Geology also fosters data-gathering activities that will contribute demonstrably significant geologic information to (C) community data sets such as the Unified Structural Representation. The primary focus of the Earthquake Geology is on the Late Quaternary record of faulting and ground motion in southern

California, including data gathering in response to major earthquakes. Collaborative proposals that cut across disciplinary boundaries are especially competitive.

Research Strategies. Examples of research strategies that support the objectives above include:

- Paleoseismic documentation of earthquake ages and displacements, including a coordinated effort to develop slip rates and earthquake history of southern San Andreas fault system (A1).
- Documentation and analysis of surface ruptures and distributed deformation resulting from the 4 April 2010 El Mayor-Cucapah earthquake.
- Evaluating the potential for 'wall-to-wall' rupture or a brief cluster of major earthquakes on the San Andreas fault system (A1, A9).
- Investigating the likelihood of multi-segment and multi-fault ruptures on major southern California faults, including possible sources of great earthquakes in off of the San Andreas fault (A1, A9).
- Testing models for geologic signatures of preferred rupture direction (A9).
- Development of slip rate and slip-per-event data sets, taking advantage of newly collected GeoEarthScope LiDAR data, and with a particular emphasis on documenting patterns of seismic strain release in time and space (A1-A3, A5, A6, A9).
- Development of methods to evaluate multi-site paleoseismic data sets and standardize error analysis (A1, A9).
- Characterization of fault-zone geology, material properties, and their relationship to earthquake rupture processes, including studies that relate earthquake clustering to fault loading in the lower crust (A7, A8, A10).
- Quantitative analysis of the role of distributed deformation in accommodating block motions, dissipating elastic strain, and modifying rheology (A2, A3, A7, A10, A11).
- Development of constraints on the magnitude and recurrence of strong ground motions from precarious rocks and slip-per-event data (B2-B5).

Geochronology Infrastructure. The shared geochronology infrastructure supports C-14, optically stimulated luminescence (OSL), and cosmogenic dating for SCEC-sponsored research. The purpose of shared geochronology infrastructure is to allow flexibility in the number and type of dates applied to each SCEC-funded project as investigations proceed. Investigators requesting geochronology support must estimate the number and type of dates needed in their proposal. For C-14 specify if sample preparation will take place at a location other than the designated laboratory. For cosmogenic dating, investigators are required to arrange for sample preparation. These costs must be included in the proposal budget unless preparation has been pre-arranged with one of the laboratories listed. Investigators are strongly encouraged to contact the investigators at the collaborating laboratories prior to proposal submission. Currently, SCEC geochronology has established relationships with the following laboratories:

- C-14: University of California at Irvine (John Southon, *jsouthon@uci.edu*) and Lawrence Livermore National Laboratory (Tom Guilderson, *tguilderson@llnl.gov*).
- OSL: University of Cincinnati (Lewis Owen, *lewis.owen@uc.edu*) and Utah State University (Tammy Rittenour, *tammy.rittenour@usu.edu*)
- Cosmogenic: Lawrence Livermore National Laboratory (Tom Guilderson, *tguilderson@llnl.gov*).

Investigators at collaborating laboratories are requested to submit a proposal that states the cost per sample analysis and estimates of the minimum and maximum numbers of analyses feasible for the upcoming year. These investigators are also strongly encouraged to request for funds to

support travel to the SCEC annual meeting. New proposals from laboratories not listed above will be considered, though preference will be given to strengthening existing collaborations.

Investigators may alternatively request support for geochronology outside of the infrastructure proposal for methods not listed here or if justified on a cost-basis. These outside requests must be included in the individual proposal budget. Please direct questions regarding geochronology infrastructure to the Earthquake Geology group leader, Mike Oskin (*meoskin@ucdavis.edu*).

IX. Interdisciplinary Focus Areas

Interdisciplinary research will be organized into seven science focus areas: 1) Unified Structural Representation (USR), 2) Fault and Rupture Mechanics (FARM), 3) Crustal Deformation Modeling (CDM), 4) Lithospheric Architecture and Dynamics (LAD), 5) Earthquake Forecasting and Predictability (EFP), 6) Ground Motion Prediction (GMP) and 7) Seismic Hazard and Risk Analysis (SHRA). ***High-priority objectives are listed below for each of the seven interdisciplinary focus areas. Collaboration within and across focus areas is strongly encouraged.***

A. Unified Structural Representation (USR)

The Structural Representation group develops unified, three-dimensional representations of active faults and earth structure (velocity, density, etc.) for use in fault-system analysis, ground motion prediction, and hazard assessment. This year's efforts will focus on making improvements to existing community models (CVM-H, CFM) that will facilitate their uses in SCEC science, education, and post-earthquake response planning.

- ***Community Velocity Model (CVM).*** Improve the current SCEC CVM-H model, with emphasis on more accurate representations of Vp, Vs, density structure, and basin shapes, and derive models for attenuation. Generate improved mantle Vp and Vs models, as well as more accurate descriptions of near-surface property structure that can be incorporated into a revised geotechnical layer. Develop (preferably standardized/automated) procedures to evaluate the existing and future iterations of the CVMs with data (e.g., waveforms, gravity) to distinguish alternative representations and quantify model uncertainties; apply these methods for well-recorded small earthquakes in southern California (including aftershocks of the 4 April Mw7.2 El Mayor Cucapah earthquake) to delineate areas where CVM updates are needed. Establish an evaluation procedure and benchmarks for testing how future improvements in the models impact ground motion studies. Special emphasis will be placed on developing and implementing 3D waveform tomographic methods for evaluating and improving the CVM-H.
- ***Community Fault Model (CFM).*** Improve and evaluate the CFM, placing emphasis on defining the geometry of major faults that are incompletely, or inaccurately, represented in the current model. Evaluate the CFM with data (e.g., seismicity, seismic reflection profiles, geodetic displacement fields) to distinguish alternative fault models. Integrate northern and Southern California models into a statewide fault framework, and update the CFM-R (rectilinear fault model) to reflect improvements in the CFM.
- ***Unified Structural Representation (USR).*** Develop better IT mechanisms for delivering the USR, particularly the CVM parameters and information about the model's structural components, to the user community for use in generating and/or parameterizing computational grids and meshes. An example of such IT mechanism is a web-based system that allows plot and download of profiles and cross sections of the CVMs and related data (i.e., Vs30) at desired locations. Another example is a fast and user-friendly method to extract a sub-volume of the CVM and formatting the results for use by the ground-motion modelers. Generate maps of geologic surfaces compatible with the CFM that may serve as strain markers in crustal deformation modeling and/or property boundaries in future iterations of the USR.

B. Fault and Rupture Mechanics (FARM)

The primary mission of the Fault and Rupture Mechanics focus group in SCEC3 is to develop physics-based models of the nucleation, propagation, and arrest of dynamic earthquake rupture. We specifically solicit proposals that address this mission through field, laboratory, and modeling efforts directed at characterizing and understanding the influence of material properties, geometric irregularities, and heterogeneities in stress and strain over multiple length and time scales (A7-A10, B1, B4), and that will contribute to our understanding of earthquakes in the Southern California fault system.

For the final year of the SCEC3 research program we solicit proposals that will finalize ongoing research or make significant progress on the following goals:

- Investigate the relative importance of different dynamic weakening and fault healing mechanisms, and the slip and time scales over which these mechanisms operate (A7-A10).
- Determine the properties of fault cores and damage zones and characterize their variability with depth and along strike to constrain theoretical and laboratory studies, including width and particle composition of actively shearing zones, signatures of temperature variations, extent, origin and significance of on- and off-fault damage, healing, and poromechanical behavior (A7-A11).
- Determine the relative contribution of on- and off-fault damage to the total earthquake energy budget, and the absolute levels of local and average stress (A7-A11).
- Develop realistic descriptions of heterogeneity in fault geometry, properties, stresses, and strains, and tractable ways to incorporate heterogeneity in numerical models of single dynamic rupture events and multiple earthquake cycles (A10-11, B1, B4).
- Understand the significance of fault zone characteristics and processes on fault dynamics and formulate constitutive laws for use in dynamic rupture models (A7-11, B1, B4).
- Assess the predictability of rupture direction and directivity of seismic radiation by collecting and analyzing field and laboratory data, and conducting theoretical investigations to understand implications for strong ground motion (A7-A10, B1).
- Evaluate the relative importance of fault structure, material properties, interseismic healing, and prior seismic and aseismic slip to earthquake dynamics, in particular, to rupture initiation, propagation, and arrest, and the resulting ground motions (A7-A10, B1).
- Characterize earthquake rupture, fault loading, degree of localization, and constitutive behavior at the base of and below the seismogenic zone. Understand implications of slow events and non-volcanic tremors for constitutive properties of faults and overall seismic behavior. Use these data to evaluate seismic moment-rupture area relationships (A3, A11).

C. Crustal Deformation Modeling (CDM)

We seek proposals aimed at resolving the kinematics and dynamics of southern California lithosphere over time scales ranging from hours to thousands of years. Our long-term goal is to contribute to the SCEC objective of developing a physics-based probabilistic seismic hazard analysis for southern California by developing and applying system-wide deformation models of processes at time-scales of the earthquake cycle. Our immediate goals include assessing the level of detail necessary in deformation models to achieve the broader SCEC objectives. Collaborations with geologists and researchers in other SCEC groups are strongly encouraged, as is research that ties in with UCERF3.

System-Wide Deformation Models

- Develop kinematic and mechanical models of interseismic deformation or the earthquake cycle to estimate slip rates on primary southern CA faults, fault geometries at depth, and

spatial distribution slip or moment deficits on faults. Compare with or refine SCEC CFM and assess discrepancies of the kinematic models with geodetic, geologic, and seismic data (A1, A3).

- Develop a system-wide model of southern California faults, incorporating the SCEC CFM, properties derived from the SCEC CVM, and realistic inferred rheologies, to model interseismic deformation, including transfer of stress across the fault system (A3).
- Develop simpler models to compare with the system-wide deformation model above for benchmarking purposes and to assess the degree of detail needed to adequately represent interseismic deformation and stress transfer. Various modeling approaches are requested and might include boundary element methods, 2D simplifications, and analytical or semi-analytical methodology (A10, A3).
- Use system-wide models to estimate southern California fault slip rates, locking depths, and stressing rates for use in UCERF3.
- Address the following problems of interest to WGCEP in development of UCERF3: 1. Quantify the amount of on-fault and off-fault deformation, 2. Constrain slip rates on faults lacking geologic slip rate data, 3. Provide estimates of slip rates on closely spaced faults, 4. Constrain slip rate variations along strike, 5. Constrain distribution of aseismic and seismic slip on faults, and 6. Estimate long-term after-effects of large earthquakes.
- Assess whether stress transfer implicitly assumed in earthquake simulator models is similar to stress transfer estimated from either category of deformation model mentioned above (A11).

More Focused Deformation Models

- Determine the extent to which rheological heterogeneity (including damage) influences deformation and stress transfer at various spatial and temporal scales. What level of detail will be required for the system-wide model (A7, A10, A11, A3)?
- Evaluate spin-up effects for viscoelastic models and methods to accelerate this process. How much does deep viscoelastic relaxation influence interseismic deformation and stress transfer? Can it be neglected or "worked around" in a southern-California-wide stress transfer model (A11, A3)?
- Evaluate whether nonlinear rheologies be represented with heterogeneous distributions of linearly viscoelastic material (A11, A3).
- Investigate causes of discrepancies between geologic and geodetic slip rate estimates (for example, different assumptions about fault geometry, or viscoelastic relaxation) (A2).
- Investigate possible causes and effects of transient slip and earthquake clustering (A1, A11).
- Estimate impact of postseismic deformation from recent large earthquakes on the southern California GPS velocity field and strain rates.

D. Lithospheric Architecture and Dynamics (LAD)

The lithospheric architecture and dynamics group (LAD) seeks proposals that will contribute to our understanding of the structure, geologic provenance and physical state of the major southern California lithospheric units, and how these relate to absolute stress in the crust and the evolution of the lithospheric system (A3, A11).

The principal objective of this group is to understand the physics of the southern California system, the boundary conditions and internal physical properties. Special attention is given to constraining the average absolute stress on southern California faults. Our general approach is to use 3D geodynamic models to relate the various forces loading the lithosphere to observable fields such as geodetic and geologic strain, seismic anisotropy and gravity. Of particular importance are: how

flow in the sub-seismogenic zone and the asthenosphere accommodates plate motion, constraints on density structure and rheology of the southern California lithosphere, and how the system loads faults.

Physics models will be developed that use the paleo-history of the 3D geology to infer how present physical conditions were created, such as depths of Moho, the seismogenic layer, base of the lithosphere, topography and basin depths, rock type, temperature, water content, rheology and how these relate to mantle flow, velocity, anisotropy and density.

The LAD work will interface with the geology group to better understand crustal structure and North America mantle lithosphere. Of particular interest are the distribution of the underplated schist and the fate of Farallon microplate fragments and their relation to inferred mantle drips. We will interact with FARM to obtain constraints on rheology and stress (absolute and dynamic), with the USR and seismology groups on 3D structure, and CDM on current stress and strain rates.

In this context, proposals are sought that contribute to our understanding of geologic inheritance and its relation to the three-dimensional structure and physical properties of the crust and lithosphere. Proposals should indicate how the work relates to stress evolution (A2, A3, A11) as well as the current geological structure (C). A primary goal is to generate systems-level models that describe southern California dynamics against which hypotheses can be tested regarding the earthquake mechanism, fault friction, seismic efficiency, the heat flow paradox and the expected evolution of stress and strain transients (A5).

The LAD group will be involved in the USGS-NSF Margins/Earthscope Salton Trough Seismic Project and will interface to the southern California offshore seismic (OBS) experiment, and will consider proposals that piggyback these experiments and integrate the results into LAD goals.

E. Earthquake Forecasting and Predictability (EFP)

In general we seek proposals that will increase our understanding of how earthquakes might be forecast and whether or not earthquakes are predictable (A6). Proposals of any type that can assist in this goal will be considered. We are especially interested in proposals that will utilize the Collaboratory for the Study of Earthquake Predictability (CSEP). In order to increase the number of earthquakes in the data sets, and so decrease the time required to learn about predictability, proposals are welcome that deal with global data sets and/or include international collaborations.

For research strategies that plan to utilize CSEP, see the description of CSEP under Special Projects to learn of its capabilities. Successful investigators proposing to utilize CSEP would be funded via core SCEC funds to adapt their prediction methodologies to the CSEP framework, to transfer codes to the externally accessible CSEP computers, and to be sure they function there as intended (A6). Subsequently, the codes would be moved to the identical externally inaccessible CSEP computers by CSEP staff who will conduct tests against a variety of data as outlined in the CSEP description. In general, methodologies will be considered successful only if they do better than null hypotheses that include both time-independent and time-dependent probabilities. Proposals aimed toward developing useful measurement/testing methodology that could be incorporated in the CSEP evaluations are welcomed, including those that address how to deal with observational errors in data sets.

Proposals are also welcome that assist in attaining the goals of these two Special Projects: WGCEP (the Working Group on California Earthquake Probabilities) and SoSAFE (the Southern San Andreas Evaluation), especially if the proposals focus on understanding some physical basis for connections between earthquakes. Proposals to utilize and/or evaluate the significance of earthquake simulator results are encouraged. Investigation of what is an appropriate magnitude-area relationship, including the maximum depth of slip during large earthquakes, is encouraged. Studies of how to properly characterize the relationship between earthquake frequency and magnitude for use in testing prediction algorithms are also encouraged.

Proposals that can lead to understanding whether or not there exists a physical basis for earthquake predictability (A6) are welcome, even if they are not aimed toward, or are not ready

for, tests in CSEP, or are not aimed toward assisting WGCEP or SoSAFE. For example, proposals could include ones that connect to objectives A1, A2, A3, A5, A9, A10 and A11, as well as ones focused on understanding patterns of seismicity in time and space, as long as they are aimed toward understanding the physical basis of some aspect of extended earthquake predictability (A6). Development of methods for testing prediction algorithms that are not yet in use by CSEP is encouraged.

Proposals for workshops are welcome. Specific workshops of interest include one on earthquake simulators and one on setting standards that could be used by CSEP for testing and evaluation, data, and products.

F. Ground-Motion Prediction (GMP)

The primary goal of the Ground Motion Prediction focus group is to develop and implement physics-based simulation methodologies that can predict earthquake strong-motion waveforms over the frequency range 0-10 Hz. Source characterization plays a vital role in ground-motion prediction. At frequencies less than 1 Hz, the methodologies should deterministically predict the amplitude, phase and waveform of earthquake ground motions using fully three-dimensional representations of Earth structure, as well as dynamic or dynamically-compatible kinematic representations of fault rupture. At higher frequencies (1-10 Hz), the methodologies should predict the main character of the amplitude, phase and waveform of the motions using a combination of deterministic and stochastic representations of fault rupture and wave propagation.

Research topics within the Ground-Motion Prediction program include:

- Developing and/or refining physics-based simulation methodologies, with particular emphasis on high frequency (1-10 Hz) approaches (B3)
- Incorporation of non-linear models of soil response (B2, B4, B5);
- Development of more realistic implementations of dynamic or kinematic representations of fault rupture. In collaboration with FARM, this research could also include the examination of current source-inversion strategies and development of robust methods that allow imaging of kinematic and/or dynamic rupture parameters reliably and stably, along with a rigorous uncertainty assessment. (B1, B2).
- Verification (comparison against theoretical predictions) and validation (comparison against observations) of the simulation methodologies with the objective of being to develop robust and transparent simulation capabilities that incorporate consistent and accurate representations of the earthquake source and three-dimensional velocity structure (B4, C).

It is expected that the products of the Ground-Motion Prediction group will have direct application to seismic hazard analysis, both in terms of characterizing expected ground-motion levels in future earthquakes, and in terms of directly interfacing with earthquake engineers in the analysis of built structures (B6). Activities within the Ground Motion Prediction group will be closely tied to several special projects, with particular emphasis on addressing ground motion issues related to seismic hazard and risk. These special projects include the Extreme Ground Motion Project and the Tall Buildings Initiative (see SHRA below).

G. Seismic Hazard and Risk Analysis (SHRA)

The purpose of the SHRA Focus Group is to apply SCEC knowledge to the development of information and techniques for quantifying earthquake hazard and risk, and in the process to provide feedback on SCEC research. Projects in this focus group will in some cases be linked to the Ground Motion Prediction Focus Group, to SCEC special projects such as the Extreme Ground Motion Project, and to Pacific Earthquake Engineering Research Center (PEER) special projects such as the Tall Buildings Initiative (TBI) and Reference Buildings and Bridges Project. Projects that involve interactions between SCEC scientists and members of the community involved in

earthquake engineering research and practice are especially encouraged. Examples of work relevant to the SHRA Focus Group follow:

Improved Hazard Representation

- Develop improved hazard models that consider simulation-based earthquake source and wave propagation effects that are not already well-reflected in observed data. These could include improved methods for incorporating rupture directivity effects, basin effects, and site effects in the USGS ground motion maps, for example. The improved models should be incorporated into OpenSHA.
- Use broadband strong motion simulations, possibly in conjunction with recorded ground motions, to develop ground motion prediction models (or attenuation relations). Broadband simulation methods must be verified (by comparison with simple test case results) and validated (against recorded strong ground motions) before use in model development. The verification, validation, and application of simulation methods must be done on the SCEC Broadband Simulation Platform. Such developments will contribute to the future NGA-H Project.
- Develop ground motion parameters (or intensity measures), whether scalars or vectors, that enhance the prediction of structural response and risk.
- Investigate bounds on the variability of ground motions for a given earthquake scenario.

Ground Motion Time History Simulation

- Develop acceptance criteria for simulated ground motion time histories to be used in structural response analyses for building code applications or risk analysis.
- Assess the advantages and disadvantages of using simulated time histories in place of recorded time histories as they relate to the selection, scaling and/or modification of ground motions for building code applications or risk analysis.
- Develop and validate modules for the broadband simulation of ground motion time histories close to large earthquakes, and for earthquakes in the central and eastern United States, for incorporation in the Broadband Platform.

Collaboration in Building Response Analysis

- Tall Buildings. Enhance the reliability of simulations of long period ground motions in the Los Angeles region using refinements in source characterization and seismic velocity models, and evaluate the impacts of these ground motions on tall buildings. Such projects could potentially build on work done in the TBI Project.
- End-to-End Simulation. Interactively identify the sensitivity of building response to ground motion parameters and structural parameters through end-to-end simulation. Buildings of particular interest include non-ductile concrete frame buildings.
- Reference Buildings and Bridges. Participate with PEER investigators in the analysis of reference buildings and bridges using simulated broadband ground motion time histories. The ground motions of large, rare earthquakes, which are poorly represented in the NGA strong motion data base, are of special interest. Coordination with PEER can be done through Yousef Bozorgnia, *yousef@berkeley.edu*.
- Earthquake Scenarios. Perform detailed assessments of the results of scenarios such as the ShakeOut exercise, and the scenarios for which ground motions were generated for the Tall Buildings Initiative (including events on the Puente Hills, Southern San Andreas, Northern San Andreas and Hayward faults) as they relate to the relationship between ground motion characteristics and building response and damage.

Ground Deformation

- Investigate the relationship between input ground motion characteristics and local soil nonlinear response, liquefaction, lateral spreading, local soil failure, and landslides. Investigate hazards due to surface faulting and to surface deformation due to subsurface faulting and folding.

Risk Analysis

- Develop improved site/facility-specific and portfolio/regional risk analysis (or loss estimation) techniques and tools, and incorporate them into the OpenRisk software.
- Use risk analysis software to identify earthquake source and ground motion characteristics that control damage estimates.

Other Topics

- Proposals for other innovative projects that would further implement SCEC information and techniques in seismic hazard and risk analysis, and ultimately loss mitigation, are encouraged.

X. Special Projects and Initiatives

A. Southern San Andreas Fault Evaluation (SoSAFE)

The SCEC Southern San Andreas Fault Evaluation (SoSAFE) Project will continue to increase our knowledge of slip rates, paleo-event chronology, and slip distributions of past earthquakes, for the past two thousand years on the southern San Andreas fault system. From Parkfield to Bombay Beach, and including the San Jacinto fault, the objective is to obtain new data to clarify and refine relative hazard assessments for each potential source of a future 'Big One.' Past SoSAFE workshops have led to a focused research plan that responds to the needs and opportunities identified across existing research projects. We strongly welcome proposals that will help to improve correlation of ruptures over the past 2000 years. This includes short-term (3-5 earthquake) and slip-per-event data from paleoseismic sites, but can include longer-term rates (60,000 years) in some cases. Use of novel methods for estimating slip rates from geodetic data would also potentially be supported within the upcoming year. Lengthening existing paleoearthquake chronologies or starting new sites in key locations along the fault system is encouraged. It is expected that much support will go towards improved dating (e.g., radiocarbon and OSL) of earthquakes within the past 2000 yrs., so that event correlations and coefficient of variation in recurrence intervals may be further refined. We welcome requests for infrastructure resources, for example geochronology support. That is, an investigator may ask for dating support (e.g., to date 12 radiocarbon samples). Requests for dating shall be coordinated with Earthquake Geology and a portion of SoSAFE funds will be contributed towards joint support for dating. However, we also welcome proposals which seek to add other data (such as climate variations) to earthquake chronologies, which may be used to improve age control or site-to-site correlation of events. We also welcome proposals that investigate methodologies for integrating paleoseismic and geologic data into rupture histories. For example, ongoing interaction between SoSAFE and the scenario rupture modeling activities of SCEC continue beyond the ShakeOut, as we continue to develop constraints such as dating or slip data that can be used to eliminate the scenario of a "wall-to-wall" rupture (from Parkfield to Bombay Beach). SoSAFE will also work to constrain scenario models by providing the best possible measurements of actual slip distributions from past earthquakes on these same fault segments as input, thereby enabling a more realistic level of scenario modeling. Research will address significant portions of the fault system, and all investigators will agree to collaboratively review one another's progress. Research by single or multi-investigator teams will be supported to rapidly advance SCEC research towards meeting priority scientific objectives related to the mission of the SoSAFE special project. SoSAFE objectives also foster common longer-term research interests and engage in facilitating future collaborations in the broader context of a decade-long series of interdisciplinary, integrated and complementary studies on the southern San Andreas fault system. The fifth year of SoSAFE may again be funded at $240K by USGS, depending on 1) the report on progress in the first three years, 2) effective leveraging of USGS funds with funds from other

sources, 3) level of available funding from USGS for the year, and 4) competing demands for the USGS Multi-Hazards Demonstration Project funding.

B. Working Group on California Earthquake Probabilities (WGCEP)

Following the 2008 release of the Uniform California Earthquake Rupture Forecast version 2 (UCERF2), the WGCEP is now working on adding some major enhancements, in UCERF3. Our primary goals are to relax segmentation, add multi-fault ruptures, and include spatial-temporal clustering (earthquake triggering). As the latter will require robust interoperability with real-time seismicity information, UCERF3 will bring us into the realm of operational earthquake forecasting. This model is being developed jointly by SCEC, the USGS, and CGS, in close coordination with the USGS National Seismic Hazard Mapping Program. The following are examples of SCEC activities that could make direct contributions to WGCEP goals:

- Reevaluate fault models in terms of the overall inventory, and specify more precisely fault endpoints in relationship to neighboring faults (important for multi-fault rupture possibilities)
- Reevaluate fault slip rates, especially using more sophisticated modeling approaches (e.g., that include GPS data, generate kinematically consistent results, and perhaps provide off-fault deformation rates as well).
- Help determine the average along-strike slip distribution of large earthquakes, especially where multiple faults are involved (e.g., is there reduced slip at fault connections?)
- Help determine the average down-dip slip distribution of large earthquakes (the ultimate source of existing discrepancies in magnitude-area relationships).
- Contribute to the compilation and interpretation of mean recurrence-interval constraints from paleoseismic data.
- Develop earthquake rate models that relax segmentation and include multi-fault ruptures.
- Develop ways to constrain the spatial distribution of maximum magnitude for background seismicity (for earthquakes occurring off of the explicitly modeled faults).
- Answer the question of whether every small volume of space exhibits a Gutenberg Richter distribution of nucleations?
- Develop methods for quantifying elastic-rebound based probabilities in un-segmented fault models.
- Help quantify the amount of slip in the previous event (including variations along strike) on any major faults in California.
- Develop models for fault-to-fault rupture probabilities, especially give uncertainties in fault endpoints.
- Determine the proper explanation for the apparent post-1906 seismicity-rate reduction (which appears to be a statewide phenomenon)?
- Develop applicable methods for adding spatial and temporal clustering to the model.
- Develop easily computable hazard or loss metrics that can be used to evaluate and perhaps trim logic-tree branch weights.
- Develop techniques for down-sampling event sets to enable more efficient hazard and loss calculations.

Further suggestions and details can be found at *http://www.WGCEP.org*, or by speaking with the project leader (Ned Field: *field@usgs.gov*; (626) 644-6435).

C. Next Generation Attenuation Project, Hybrid Phase (NGA-H)

The NGA-H Project is currently on hold, but it is hoped that it will go forward at some point in the future in conjunction with PEER. It will involve the use of broadband strong motion simulation to generate ground motion time histories for use, in conjunction with recorded ground motions, in the development of ground motion attenuation relations for hard rock that are based on improved sampling of magnitude and distance, expecially large magnitudes and close distances, and improved understanding of the relationship between earthquake source and strong ground motion characteristics. Broadband simulation methods are verified (by comparison of simple test case results with other methods) and validated (against recorded strong ground motions) before being used to generate broadband ground motions for use in model development. These simulation activities for verification, validation, and application are done on the SCEC Broadband Simulation Platform. The main SCEC focus groups that are related to this project are Ground Motion Prediction and Seismic Hazard and Risk Analysis.

D. End-to-End Simulation

The purpose of this project is to foster interaction between earthquake scientists and earthquake engineers through the collaborative modeling of the whole process involved in earthquake fault rupture, seismic wave propagation, site response, soil-structure interaction, and building response. Recent sponsors of this project have been NSF (tall buildings) and CEA (woodframe buildings), and new sponsors are being sought. The main SCEC discipline and focus groups working on this project are Geology, especially fault models; Unified Structural Representation; Faulting and the Mechanics of Earthquakes; Ground Motion Prediction; Seismic Hazard and Risk Analysis; and PetaSHA – Terashake and Cybershake.

E. Collaboratory for the Study of Earthquake Predictability (CSEP)

CSEP is developing a virtual, distributed laboratory—a collaboratory—that supports a wide range of scientific prediction experiments in multiple regional or global natural laboratories. This earthquake system science approach seeks to provide answers to the questions: (1) How should scientific prediction experiments be conducted and evaluated? and (2) What is the intrinsic predictability of the earthquake rupture process? Contributions may include:

1. Establishing rigorous procedures in controlled environments (testing centers) for registering prediction procedures, which include the delivery and maintenance of versioned, documented code for making and evaluating predictions including intercomparisons to evaluate prediction skills;
2. Constructing community-endorsed standards for testing and evaluating probability-based and alarm-based predictions;
3. Developing hardware facilities and software support to allow individual researchers and groups to participate in prediction experiments;
4. Providing prediction experiments with access to data sets and monitoring products, authorized by the agencies that produce them, for use in calibrating and testing algorithms;
5. Intensifying the collaboration between the US and Japan through international projects, and initiating joint efforts with China;
6. Developing experiments to test basic physical principles of earthquake generation (e.g., models for estimating the largest possible earthquake on a given fault are important to earthquake scenarios like ShakeOut and to earthquake hazard models. We seek proposals to develop quantitative tests of such models); and

7. Conducting workshops to facilitate international collaboratories.

A major focus of CSEP is to develop international collaborations between the regional testing centers and to accommodate a wide-ranging set of prediction experiments involving geographically distributed fault systems in different tectonic environments.

Special Note. CSEP global travel grants from 2006 to 2010 were funded with a grant from the W. M. Keck Foundation. The Keck grant will end in early 2011 and future funding for CSEP global travel has not yet been obtained at the time of the release of this document.

F. National Partnerships through EarthScope

The NSF Earthscope project provides unique opportunities to learn about the structure and dynamics of North America. SCEC encourages proposals to the NSF Earthscope program that will address the goals of the SCEC Science Plan.

G. Extreme Ground Motion Project (EXGM)

Extreme ground motions are the very large amplitudes of earthquake ground motions that can arise at very low probabilities of exceedance, as was the case for the 1998 PSHA for Yucca Mountain when extended to 10**-8/yr. This project investigates the credibility of such ground motions through studies of physical limits to earthquake ground motions, unexceeded ground motions, and frequency of occurrence of very large ground motions or of earthquake source parameters (such as stress drop and faulting displacement) that cause them. Of particular interest to ExGM (and more generally to ground-motion prediction and SHRA) is why crustal earthquake stress drops are so independent of earthquake size (amidst considerable scatter) and so much less than the frictional strength of rocks at mid-crustal depths.

Since the summer of 2005, the DOE-funded Extreme Ground Motion (ExGM) program has supported research at SCEC, both institutionally and individually. ExGM funding has been dramatically cut in the current year, and prospects for the future are uncertain. Available funds will be directed to ground-motion simulations in accord with the original ExGM prospectus and schedule. While the status of ExGM as a separately funded, Special Project is thus uncertain, the research imperatives of ExGM remain significant to several of the SCEC focus and disciplinary groups, including, Geology – especially fault zone geology; Faulting and Mechanics of Earthquakes, Ground-Motion Prediction, and Seismic Hazard and Risk Analysis. This project is also discussed above within SHRA.

H. Petascale Cyberfacility for Physics-Based Seismic Hazard Analysis (PetaSHA)

SCEC's special project titled "A Petascale Cyberfacility for Physics-based Seismic Hazard Analysis" (PetaSHA) aims to develop and apply physics-based predictive models to improve the practice of seismic hazard analysis. This project will utilize numerical modeling techniques and high performance computing to implement a computation-based approach to SHA. Three scientific initiative areas have been identified for this project to help to guide the scientific research. The PetaSHA initiative areas are: (1) development of techniques to support higher frequencies waveform simulations including deterministic and stochastic approaches; (2) development of dynamic rupture simulations that include additional complexity including nonplanar faults, a variety of friction-based behaviors, and higher inner /outer scale ratios (e.g. (fault plane mesh dimension) / (simulation volume dimension)); and (3) physics-based probabilistic seismic hazard analysis including probabilistic seismic hazard curves using 3D waveform modeling. All of these modeling efforts must be accompanied by verification and validation efforts. Development of new techniques that support the verification and validation of SCEC PetaSHA modeling efforts are encouraged.

The SCEC PetaSHA modeling efforts address several of the SCEC3 objectives. Development of new verification and validation techniques (B4) are common to each of the PetaSHA initiative areas.

Research activities related to the improved understanding and modeling of rupture complexity (A8, B1) support the PetaSHA initiatives. In addition, research into the upper frequency bounds on deterministic ground motion predictions (B2, B3) are SCEC3 science objectives that are important work areas in the PetaSHA Project.

XI. SCEC Communication, Education, and Outreach

SCEC maintains a Communication, Education, and Outreach (CEO) program with four long-term goals:

- Coordinate productive interactions among a diverse community of SCEC scientists and with partners in science, engineering, risk management, government, business, and education.
- Increase earthquake knowledge and science literacy at all educational levels, including students and the general public.
- Improve earthquake hazard and risk assessments
- Promote earthquake preparedness, mitigation, and planning for response and recovery.

Short-term objectives are outlined below. These objectives present opportunities for members of the SCEC community to become involved in CEO activities, which are for the most part coordinated by CEO staff. As project support is very limited, budgets for proposed projects should be on the order of $2,000 to $5,000. Hence proposals that include additional sources of support (cost-sharing, funding from other organizations, etc.) are highly recommended. Smaller activities can be supported directly from the CEO budget and do NOT need a full proposal. Those interested in submitting a CEO proposal should first contact Mark Benthien, associate SCEC director for CEO, at 213-740-0323 or *benthien@usc.edu*. There may be other sources of funding that can be identified together.

CEO Focus Area Objectives

1. ***SCEC Community Development and Resources*** (activities and resources for SCEC scientists and students)

   SC1 Increase diversity of SCEC leadership, scientists, and students

   SC2 Facilitate communication within the SCEC Community

   SC3 Increase utilization of products from individual research projects

2. ***Education*** (programs and resources for students, educators, and learners of all ages)

   E1 Develop innovative earth-science education resources

   E2 Interest, involve and retain students in earthquake science

   E3 Offer effective professional development for K-12 educators

3. ***Public Outreach*** (activities and products for media reporters and writers, civic groups and the general public)

   P1 Provide useful general earthquake information

   P2 Develop information for the Spanish-speaking community

   P3 Facilitate effective media relations

   P4 Promote SCEC activities

4. ***Knowledge transfer*** (activities to engage other scientists and engineers, practicing engineers and geotechnical professionals, risk managers, government officials, utilities, and other users of technical information.

I1 Communicate SCEC results to the broader scientific community

I2 Develop useful products and activities for practicing professionals

I3 Support improved hazard and risk assessment by local government and industry

I4 Promote effective mitigation techniques and seismic policies

APPENDIX: SCEC3 Long-Term Research Goals

This section outlines the SCEC science priorities for the five-year period from February 1, 2007, to January 31, 2012. Additional material on the science and management plans for the Center can be found in the SCEC proposal to the NSF and USGS (*http://www.scec.org/aboutscec/documents/*).

SCEC is, first and foremost, a basic research center. We therefore articulate our work plan in terms of four basic science problems: (1) earthquake source physics, (2) fault system dynamics, (3) earthquake forecasting and predictability, and (4) ground motion prediction. These topics organize the most pressing issues of basic research and, taken together, provide an effective structure for stating the SCEC3 goals and objectives. In each area, we outline the problem, the principle five-year goal, and some specific objectives. We then assess the research activities and the new capabilities needed to attain our objectives.

A. Earthquake Source Physics

Problem Statement. Earthquakes obey the laws of physics, but we don't yet know how. In particular, we understand only poorly the highly nonlinear physics of earthquake nucleation, propagation, and arrest, because we lack knowledge about how energy and matter interact in the extreme conditions of fault failure. A complete description would require the evolution of stress, displacement, and material properties throughout the seismic cycle across all relevant scales, from microns and milliseconds to hundreds of kilometers and many years. A more focused aspect of this problem is the physical basis for connecting the behavior of large ruptures at spatial resolutions of hundreds of meters and fracture energies of megajoules per square meter with laboratory observations of friction at centimeter scales and fracture energies of kilo-joules per square meter. Two further aspects are the problem of stress heterogeneity—the factors that create and maintain it over many earthquake cycles—and the related problem of defining the concept of strength in the context of stress and rheological heterogeneity.

Goal and Objectives. The goal for SCEC3 will be to discover the physics of fault failure and dynamic rupture that will improve predictions of strong ground motions and the understanding of earthquake predictability. This goal is directly aligned with our mission to develop physics-based seismic hazard analysis. Specific objectives include:

1. Conduct laboratory experiments on frictional resistance relevant to high-speed coseismic slip on geometrically complex faults, including the effects of fluids and changes in normal stress, and incorporate the data into theoretical formulations of fault-zone rheology.
2. Develop a full 3D model of fault-zone structure that includes the depth dependence of shear localization and damage zones, hydrologic and poroelastic properties, and the geometric complexities at fault branches, step-overs, and other along-strike and down-dip variations.
3. Combine the laboratory, field-based, and theoretical results into fault constitutive models for the numerical simulation of earthquake rupture, test them against seismological data, and extend the simulation methods to include fault complexities such as bends, step-overs, fault branches, and small-scale roughness.
4. Develop statistical descriptions of stress and strength that account for slip heterogeneity during rupture, and investigate dynamic models that can maintain heterogeneity throughout many earthquake cycles.

B. Fault System Dynamics

Problem Statement. In principle, the Southern California fault system can be modeled as a dynamic system with a state vector S and an evolution law $dS/dt = F(S)$. The state vector represents the stress, displacement, and rheology/property fields of the seismogenic layer as well as its boundary conditions. Its evolution equation describes the forward problem of fault dynamics. Many of the most difficult (and interesting) research issues concern two inference or inverse problems: (1) model building—from our knowledge of fault physics, what are the best representations of S and F?—and (2) data assimilation—how are the parameters of these representations constrained by the data D on the system's present state S0 as well as its history?

The SCEC approach is not to proceed by trying to write down general forms of S and its rate-of-change F. Rather, we use judicious approximations to separate the system evolution into a series of numerical simulations representing the interseismic, preseismic, coseismic, and postseismic behaviors. In particular, the natural time-scale separation between inertial and non-inertial dynamics usually allows us to decouple the long-term evolution of the state vector from its short-term, coseismic behavior. Therefore, in describing many interseismic and postseismic processes, we can treat the fault system quasi-statically, with discontinuous jumps in S at the times of earthquakes. On the other hand, the dynamics of earthquake rupture is clearly important to the basic physics of fault system evolution. In the modeling of stress heterogeneity, for example, the coupling of inertial and non-inertial dynamics must be addressed by integrating across this scale gap.

Goal and Objectives. The principal SCEC3 goal for fault system dynamics is to develop representations of the postseismic and interseismic evolution of stress, strain, and rheology that can predict fault system behaviors within the Southern California Natural Laboratory. The SCEC3 objectives are sixfold:

1. Use the community modeling tools and components developed in SCEC2 to build a 3D dynamic model that is faithful to the existing data on the Southern California fault system, and test the model by collecting new data and by predicting its future behavior.
2. Develop and apply models of coseismic fault slip and seismicity in fault systems to simulate the evolution of stress, deformation, fault slip, and earthquake interactions in Southern California.
3. Gather and synthesize geologic data on the temporal and spatial character and evolution of the Southern California fault system in terms of both seismogenic fault structure and behavior at geologic time scales.
4. Constrain the evolving architecture of the seismogenic zone and its boundary conditions by understanding the architecture and dynamics of the lithosphere involved in the plateboundary deformation.
5. Broaden the understanding of fault systems in general by comparing SCEC results with integrative studies of other fault systems around the world.
6. Apply the fault system models to the problems of earthquake forecasting and predictability.

C. Earthquake Forecasting and Predictability

Problem Statement. The problems considered by SCEC3 in this important area of research will primarily concern the physical basis for earthquake predictability. Forecasting earthquakes in the long term at low probability rates and densities—the most difficult scientific problem in seismic hazard analysis—is closely related to the more controversial problem of high-likelihood predictions on short (hours to weeks) and intermediate (months to years) time scales. Both require a probabilistic characterization in terms of space, time, and magnitude; both depend on the state of

the fault system (conditional on its history) at the time of the forecast/prediction; and, to put them on a proper science footing, both need to be based in earthquake physics.

Goal and Objectives. The SCEC3 goal is to improve earthquake forecasts by understanding the physical basis for earthquake predictability. Specific objectives are to:

1. Conduct paleoseismic research on the southern San Andreas and other major faults with emphasis on reconstructing the slip distributions of prehistoric earthquakes, and explore the implications of these data for behavior of the earthquake cycle and time-dependent earthquake forecasting.
2. Investigate stress-mediated fault interactions and earthquake triggering and incorporate the findings into time-dependent forecasts for Southern California.
3. Establish a controlled environment for the rigorous registration and evaluation of earthquake predictability experiments that includes intercomparisons to evaluate prediction skill.
4. Conduct prediction experiments to gain a physical understanding of earthquake predictability on time scales relevant to seismic hazards.

D. Ground Motion Prediction

Problem Statement. Given the gross parameters of an earthquake source, such as its magnitude, location, mechanism, rupture direction, and finite extent along a fault, we seek to predict the ground motions at all regional sites and for all frequencies of interest. The use of 3D velocity models in low-frequency (< 0.5 Hz) ground motion prediction was pioneered in SCEC1 (§II.A), and this type of simulation, based on direct numerical solution of the wave equation, has been taken to new levels in SCEC2 (§II.B.6). The unsolved basic research problems fall into four classes: (a) the ground motion inverse problem at frequencies up to 1 Hz; (b) the stochastic extension of ground motion simulation to high frequencies (1-10 Hz); (c) simulation of ground motions using realistic sources; and (d) nonlinear wave effects, including nonlinear site response. In addition, there remain scientific and computational challenges in the practical prediction of ground motions near the source and within complex structures such as sedimentary basins, as well as in the characterization of the prediction uncertainties.

Goal and Objectives. The principal SCEC3 goal is to predict the ground motions using realistic earthquake simulations at frequencies up to 10 Hz for all sites in Southern California. The SCEC3 objectives are:

1. Combine high-frequency stochastic methods and low-frequency deterministic methods with realistic rupture models to attain a broadband (0-10 Hz) simulation capability, and verify this capability by testing it against ground motions recorded at a variety of sites for a variety of earthquake types.
2. Use observed ground motions to enhance the Unified Structural Representation (USR) by refining its 3D wavespeed structure and the parameters that account for the attenuation and scattering of broadband seismic energy.
3. Apply the ground-motion simulations to improve SHA attenuation models, to create realistic scenarios for potentially damaging earthquakes in Southern California, and to explain the geologic indicators of maximum shaking intensity and orientation.
4. Investigate the geotechnical aspects of how built structures respond to strong ground motions, including nonlinear coupling effects, and achieve an end-to-end simulation capability for seismic risk analysis.

SCEC Annual Meeting Presentations

Plenary Presentations

SUNDAY, SEPTEMBER 12, 2010 — *Horizon Ballroom I*

17:00 – 18:00 **COMPARISON OF THE 1960 AND 2010 CHILEAN EARTHQUAKES** *H. Kanamori and L. Rivera*

MONDAY, SEPTEMBER 13, 2010 — *Horizon Ballroom*

11:00 – 11:30 **THE JANUARY 12, 2010, MW 7.0 EARTHQUAKE IN HAITI: CONTEXT AND MECHANISM** *E. Calais*

16:00 – 16:30 **PERFORMANCE OF STRUCTURES IN THE 27 FEBRUARY 2010 GREAT MAULE EARTHQUAKE** *J. Restrepo*

TUESDAY, SEPTEMBER 14, 2010 — *Horizon Ballroom*

08:00 – 08:30 **DISTRIBUTION AND KINEMATICS OF SURFACE RUPTURES ASSOCIATED WITH THE EL MAYOR-CUCAPAH EARTHQUAKE SEQUENCE** *J. Fletcher*

10:30 – 11:00 **TRIGGERING BY SEISMIC WAVES AND IMPLICATIONS FOR EARTHQUAKE PREDICTABILITY** *E. Brodsky*

15:30 – 16:00 **BEHAVIOR OF THE DEEP ROOTS OF FAULTS** *G. Hirth*

WEDNESDAY, SEPTEMBER 15, 2010 — *Horizon Ballroom*

08:00 – 08:30 **PETRIFIED EARTHQUAKES: STRUCTURAL PROPERTIES OF DAMAGED ROCKS WITHIN THE SAN ANDREAS FAULT ZONE** *O. Dor*

Poster Presentations

Group 1 Posters

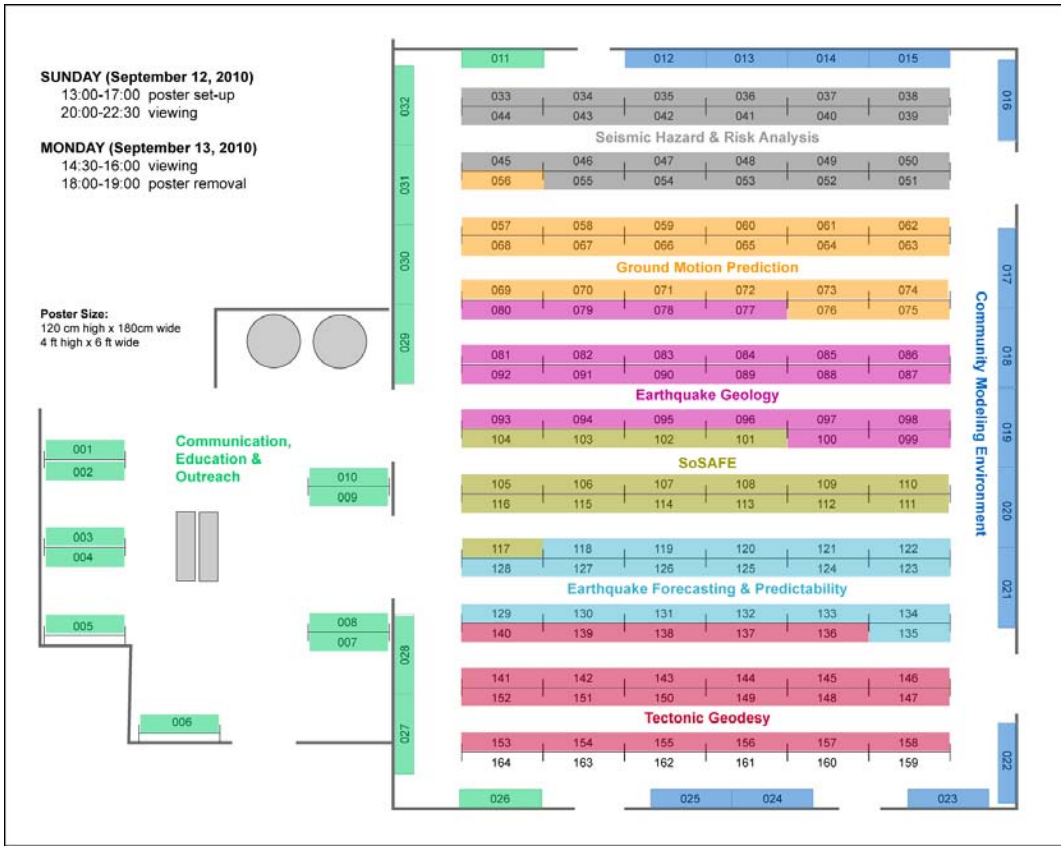

Communication, Education, and Outreach

1-001 **SCEC USEIT MEDIA TEAM** *E. Alaniz, N. Ballew, H. Chen, J. Rodriguez, E. Soto, R. de Groot, T. Jordan, T. Huynh, and M. Ihrig*

1-002 **2010 USEIT DEVELOPMENT TEAM** *B. Siver, C.A. Castro, N. Anderson, and M. Sheehan*

1-003 **2010 VDO-PRODUCTION TEAM** *K. Brunner, L. Gelbach, S. Romero, A. Valencia, B. Walters, T. Jordan, R. de Groot, and M. Ihrig*

1-004 **2010 SCEC USEIT SCIENCE RESEARCH TEAM** *M. Gonzalez, S. Kowalke, S. Lauda, H. Potter, A. Stevens, R. de Groot, T. Jordan, T. Huynh, M. Ihrig, and K. Welch*

1-005 **2010 CMS IMPLEMENTATION** *D. Brown, M. Contreras, A. Deolarte, J. Walker, T. Jordan, R. de Groot, T. Huynh, K. Welch, and M. Ihrig*

1-006 **PRODUCTION OF SOUTHERN CALIFORNIA EARTHQUAKE CENTER VIRTUAL DISPLAY OF OBJECTS (SCEC-VDO) DISPLAYING SEISMIC RISK OF THE ELEVEN SHAKEOUT AREAS WITHIN CALIFORNIA** *S.A. Moreland, M. Benthien, and R. de Groot*

1-007 **FACILITATING INTERACTIVE INFORMATION SHARING: SCEC INTERN EXPERIENCE** *K.B. Welch, T.H. Jordan, T.T. Huynh, R.M. de Groot, and J.S. Montes De Oca*

1-008 **SCEC EDUCATIONAL PRODUCTS AND PROGRAMS** *Y. Robles, R.M. de Groot, B. Dansby, D. Coss y Leon, W. Yamashita, C. Gotuaco, and G. Hwang*

1-009 **EDUCATIONAL PRODUCTS FROM SCEC COMMUNICATION, EDUCATION AND OUTREACH (CEO) PROGRAM: PLATE TECTONICS MAP AND LEARNING KIT** *B.P. Dansby, R.M. de Groot, D. Coss Y Leon, and C.O. Gotuaco*

1-010 **SOUTHERN CALIFORNIA'S NEWEST VENUE FOR TEACHING EARTH SYSTEM SCIENCE: THE SAN BERNARDINO COUNTY MUSEUM'S HALL OF GEOLOGICAL WONDERS** *K. Springer, E. Scott, and J.C. Sagebiel*

1-011 **THE SHAKY TRUTH: DEBUNKING DOUG COPP AND THE TRIANGLE OF LIFE** *A.E. Liang*

1-026 **BUILDING A PHYSICAL "EARTHQUAKE SIMULATOR" TO EXPLORE THE EARTHQUAKE CYCLE IN K12 OUTREACH** *B. Lipovsky, M. Rohrssen, J. Lozos, K. Ryan, C. Neighbors, E. Cochran, C. Meyers, G. Funning, and M. Droser*

1-027 **MAKE YOUR OWN EARTHQUAKE** *S.W.H. Seale, J.H. Steidl, P. Hegarty, and H. Ratzesberger*

1-028 **3DV: INTERACTIVE EARTHQUAKE VIEWER** *E. Boyd, R. Welti, and R. de Groot*

1-029 **DEVELOPMENT OF THE SAN ANDREAS REGION ACTIVE EARTH DISPLAY** *G.P. Hwang, R.M. de Groot, K. Springer, R.J. Lillie, P. McQuillan, E. Scott, and C. Sagebiel*

1-030 **UPDATING AND ENHANCING THE WALLACE CREEK INTERPRETIVE TRAIL (WIT) WEBSITE** *S.E. Robinson, J. Colunga, R. de Groot, and J.R. Arrowsmith*

1-031 **SCEC/SURE: THE IMPACT OF THE EARTHQUAKE COUNTRY ALLIANCE EARTHQUAKE EDUCATION AND PUBLIC INFORMATION CENTERS (ECA EPICENTERS)** *I.N. Gow, R.M. de Groot, K.B. Springer, L. Schuman, J. Sutorus, B. Burrows, and N. Oropez*

1-032 ***GEOCACHE YOUR WAY TO PREPAREDNESS: A SCAVENGER HUNT FOR SAFETY*** *D.N. MacCarthy*

Community Modeling Environment

1-012 **GLYPHSEA: VISUALIZING TIME-DEPENDENT SEISMIC VECTOR FIELDS WITH GLYPHS** *E. McQuinn, A. Chourasia, J-B. Minster, and J.P. Schulze*

1-013 **SCEC/CME SEISMIC HAZARD ANALYSIS COMPUTATIONAL SCIENCE RESEARCH** *T.H. Jordan, G. Beroza, J. Bielak, S. Callaghan, P. Chen, Y. Cui, S. Day, E. Deelman, E. Field, R. Graves, K. Milner, J.B. Minster, K. Olsen, P. Small and the CME Collaboration*

1-014 **SCEC CVM-TOOLKIT (CVM-T) -- HIGH PERFORMANCE MESHING TOOLS FOR SCEC COMMUNITY VELOCITY MODELS** *P. Small, P. Maechling, G. Ely, K. Olsen, K. Withers, R. Graves, T. Jordan, A. Plesch, and J. Shaw*

1-015 **CHALLENGES AND PROSPECTS FOR HIGH PERFORMANCE COMPUTING WITH SORD** *J. Zhou, Y. Cui, K. Lee, G.P. Ely, and P.J. Maechling*

1-016 **RUNNING ON-DEMAND STRONG GROUND MOTION SIMULATIONS WITH THE SECOND-GENERATION BROADBAND PLATFORM** *S. Callaghan, P.J. Maechling, R.W. Graves, P. Somerville, N. Collins, K.B. Olsen, W. Imperatori, M. Jones, R.J. Archuleta, J. Schmedes, and T.H. Jordan*

1-017 **FULL-3D WAVEFORM TOMOGRAPHY FOR SOUTHERN CALIFORNIA** *E. Lee, P. Chen, T.H. Jordan, P.J. Maechling, M. Denolle, and G.C. Beroza*

1-018 **SCEC M8, A REGIONAL SCALE DETERMINISTIC WAVE PROPAGATION SIMULATION USING SCEC AWP-ODC** *Y. Cui, K.B. Olsen, T.H. Jordan, K. Lee, J. Zhou, P. Small, D. Roten, G. Ely, D.K. Panda, A. Chourasia, J. Levesque, S.M. Day, and P. Maechling*

1-019 **MEMORY-EFFICIENT DISPLACEMENT-BASED INTERNAL FRICTION FOR WAVE PROPAGATION SIMULATION** *J. Bielak, H. Karaoglu, and R. Taborda*

1-020 **CUSTOMIZED DYNAMIC RANK ASSIGNMENT FOR IMPROVED EFFICIENCY WITH SEISMIC APPLICATIONS** *K. Lee, Y. Cui, J. Zhou, and P.J. Maechling*

Seismic Hazard and Risk Analysis

1-048 **ANALYSIS OF HIGH-RESOLUTION P-WAVE SEISMIC IMAGING PROFILES ACQUIRED THROUGH RENO, NEVADA FOR EARTHQUAKE HAZARD ASSESSMENT** *R.N. Frary, W.J. Stephenson, J.N. Louie, J.K. Odum, J.Z. Maharrey, M.S. Dhar, R.L. Kent, and C.G. Hoffpauir*

1-049 **RECONNAISSANCE GEOLOGIC CHARACTERIZATION OF THE ONSHORE PALOS VERDES FAULT ZONE, SOUTHERN CALIFORNIA** *P.J. Hogan, S.C. Lindvall, and S.L. Varnell*

1-050 **NON-LINEAR BUILDING RESPONSE SIMULATIONS USING SCEC SIMULATED GROUND MOTIONS** *C.A. Goulet and C.B. Haselton*

1-051 **INFRASONIC OBSERVATIONS OF GROUND SHAKING ALONG THE 2010 MW 7.2 EL MAYOR RUPTURE: A NEW TOOL FOR CREATING GROUND SHAKING INTENSITY MAPS?** *K.T. Walker and C. de Groot-Hedlin*

1-052 **A CYBERSHAKE-BASED SYSTEM FOR OPERATIONAL FORECASTING OF EARTHQUAKE GROUND MOTIONS** *T.H. Jordan, K. Milner, R. Graves, S. Callaghan, P. Maechling, E. Field, P. Small, and the CyberShake Working Group*

1-053 **EVALUATING SEISMIC RISK USING THE FEMA HAZUS-MH MR4 EARTHQUAKE MODEL IN KING COUNTY WASHINGTON** *C.J. Neighbors, G.R. Noriega, Y. Caras, and E.S. Cochran*

1-054 **EARTHQUAKE EARLY WARNING DEMONSTRATION TOOL (EEWDT)** *M. Barba, M. Boese, and E. Hauksson*

1-055 **STYLE OF DEFORMATION AND EARTHQUAKE RISK ASSESSMENT: A COMPARISON BETWEEN CALIFORNIA AND MEDITERRANEAN COUNTRIES** *A. Baltay, M. Nyst, T. Tabucchi, and P. Seneviratna*

Ground Motion Prediction

1-056 **OPENSHA IMPLEMENTATION OF THE GCIM APPROACH FOR GROUND MOTION SELECTION** *B.A. Bradley*

1-057 **BEHAVIOR OF HILL SLOPES DURING STRONG GROUND MOTION AND NONLINEAR ATTENUATION** *N.H. Sleep*

1-058 **APPLICABILITY OF FOREIGN GROUND MOTION PREDICTION EQUATIONS FOR NEW ZEALAND ACTIVE SHALLOW EARTHQUAKES** *B.A. Bradley*

1-059 **STOCHASTIC MODEL FOR EARTHQUAKE GROUND MOTIONS USING WAVELET PACKETS** *Y. Yamamoto and J.W. Baker*

1-060 **LARGE SCALE EARTHQUAKE SIMULATIONS IN THE CENTRAL UNITED STATES** *L. Ramirez-Guzman, O. Boyd, S. Hartzell, and R. Williams*

1-061 **LONG-PERIOD GROUND-MOTION SIMULATIONS OF THE MW 7.2 EL MAYOR-CUCAPAH MAINSHOCK: EVALUATION OF FINITE-FAULT RUPTURE CHARACTERIZATION AND 3D SEISMIC VELOCITY MODELS** *R.W. Graves and B.T. Aagaard*

1-062 **TESTING REGIONAL-SCALE GROUND MOTION ESTIMATES FOR THE CISN SHAKEALERT PROJECT** *P.J. Maechling, M. Liukis, and T.H. Jordan*

1-063 **CONSTRAINING GROUND MOTION IN SEDIMENTARY BASINS USING THE AMBIENT SEISMIC FIELD** *M. Denolle, E. Dunham, J. Lawrence, G. Prieto, and G. Beroza*

1-064 **FREQUENCY DEPENDENCE OF RADIATION PATTERNS AND DIRECTIVITY EFFECTS IN FAR-FIELD GROUND MOTION FROM EARTHQUAKES ON ROUGH FAULTS** *H. Cho and E.M. Dunham*

1-065 **M8** *K.B. Olsen, Y. Cui, T.H. Jordan, K. Lee, J. Zhou, P. Small, D. Roten, G. Ely, D.Kim. Panda, A. Chourasia, J. Levesque, S.M. Day, P. Maechling, and J. Jones*

1-066 **ARRA-FUNDED GEOTECHNICAL CHARACTERIZATION OF SEISMOGRAPHIC STATION SITES** *A. Yong, W. Leith, K. Stokoe, J. Diehl, A. Martin, and S. Jack*

1-067 **CHARACTERISTICS OF LONG-PERIOD (3 TO 10 S) STRONG GROUND MOTIONS OBSERVED IN AND AROUND THE LOS ANGELES BASIN DURING THE MW7.2 EL MAYOR-CUCAPAH EARTHQUAKE OF APRIL 4, 2010** *K. Hatayama and E. Kalkan*

1-068 **NONLINEAR GROUND MOTION AND TEMPORAL CHANGES OF SITE RESPONSE ASSOCIATED WITH MEDIUM-SIZE EARTHQUAKES IN JAPAN AND CALIFORNIA** *C. Wu, Z. Peng, and Y. Ben-Zion*

1-069 **SIMULATION OF GROUND MOTION IN THE IMPERIAL VALLEY AREA DURING THE MW 7.2 EL MAYOR-CUCAPAH EARTHQUAKE** *D. Roten and K.B. Olsen*

1-070 **CHARACTERISTICS OF GROUND MOTION ATTENUATION DURING THE M7.2 EL MAYOR CUCAPA (BAJA) EARTHQUAKE** *E. Kalkan, K. Hatayama, M. Segou, V. Graizer, and V. Sevilgen*

1-071 **STATUS REPORT ON THE PRECARIOUS BALANCED ROCK ARCHIVE** *G.P. Biasi and J.N. Brune*

1-072 **INFERRING SEISMIC HISTORIES FROM THE AGES OF PRECARIOUSLY BALANCED ROCKS** *D.H. Rood, G. Balco, M. Purvance, R. Anooshehpoor, J. Brune, L. Grant Ludwig, T. Hanks, and K. Kendrick*

1-073 **ESTIMATES OF VS100 AT SITES OF PRECARIOUSLY BALANCED ROCKS** *J.N. Louie, J.N. Brune, and S.K. Pullammanappallil*

1-074 **TESTING CONSISTENCY OF PRECARIOUSLY BALANCE ROCKS WITH 2008 PROBABILISTIC SEISMIC HAZARD MAPS AND CYBERSHAKE SA3 VALUES IN SOUTHERN CALIFORNIA** *J.N. Brune, M.D. Purvance, R. Graves, S. Callaghan, E. Deelman, E. Field, T. Jordan, G. Juve, K. Kasselman, P. Maechling, G. Mehta, K. Milner, D. Okaya, P. Small, and K. Vahi*

1-075 **GEOLOGIC AND GEOMORPHIC CHARACTERIZATION OF PRECARIOUSLY BALANCED ROCKS** *D.E. Haddad and J.R. Arrowsmith*

1-076 **PROGRESS IN GAINING AGE CONSTRAINTS FOR PRECARIOUS LANDFORMS IN TEMPERATE ENVIRONMENTS** *M.W. Stirling and D.H. Rood*

Earthquake Geology

1-081 **COMPLEX QUATERNARY DEFORMATION AMONG INTERSECTING SETS OF STRIKE-SLIP FAULTS NEAR TWENTY-NINE PALMS, SOUTHERN CALIFORNIA** *C.M. Menges, J.C. Matti, V.E. Langenheim, S.A. Mahan, and J.W. Hillhouse*

1-082 **TEXTURAL RECORD OF THE SEISMIC CYCLE: STRAIN RATE VARIATION IN AN ANCIENT SUBDUCTION THRUST** *C.D. Rowe, F. Meneghini, and J.C. Moore*

1-083 **MUD VOLCANO RESPONSE TO THE EL MAYOR-CUCAPAH EARTHQUAKE** *M.L. Rudolph and M. Manga*

1-084 **SUBSURFACE EVIDENCE FOR THE PUENTE HILLS AND COMPTON-LOS ALAMITOS FAULTS IN SOUTH-CENTRAL LOS ANGELES** *R.S. Yeats and D.M. Verdugo*

1-085 **COLLISIONAL TECTONICS OF THE SANTA ANA MOUNTAINS AND PUENTE HILLS, ORANGE COUNTY, CALIFORNIA** *E.M. Gath and L. Grant Ludwig*

1-086 **2010 SAN BERNARDINO MOUNTAINS GPS CAMPAIGN** *J.N. Bywater, K.K. Chung, B.J. Anderson, J.C. Duncan, M.R. Swift, S.F. McGill, J.C. Spinler, A.D. Hulett, and R.A. Bennett*

1-087 **HIGH LIFETIME SLIP RATE ACROSS THE SAN JACINTO FAULT ZONE NEAR CLARK LAKE** *S.U. Janecke and D.H. Forand*

1-088 **EVIDENCE FOR VERTICAL PARTITIONING OF STRIKE-SLIP AND COMPRESSIONAL TECTONICS FROM SEISMICITY, FOCAL MECHANISMS, AND STRESS DROPS IN THE EAST LOS ANGELES BASIN AREA, CALIFORNIA** *W. Yang and E. Hauksson*

1-089 **TEMPORAL AND SPATIAL VARIATION IN SLIP ALONG THE SOUTHERN STRAND OF THE KARAKORAM FAULT SYSTEM, LADAKH HIMALAYAS** *W.M. Bohon, J.R. Arrowsmith, and K. Hodges*

1-090 **CHILEAN EARTHQUAKE RECONNAISSANCE: LESSONS LEARNED BY THE JULY 2010 AMERICAN RED CROSS DELEGATION** *D.A. Weiser*

1-091 **THE DEVELOPMENT OF AN INTRODUCTORY VIDEO ON LIGHT DETECTION AND RANGING (LIDAR) AND STUDYING EARTHQUAKE HAZARDS** *S.E. Robinson, A. Whitesides, R. de Groot, J.R. Arrowsmith, and C.J. Crosby*

1-092 **TRIGGERED SURFACE SLIP IN SOUTHERN CALIFORNIA ASSOCIATED WITH THE 2010 SIERRA EL MAYOR-CUCAPAH, BAJA CALIFORNIA, MEXICO, EARTHQUAKE** *M.J. Rymer, J.A. Treiman, K.J. Kendrick, J.J. Lienkaemper, R.J. Weldon, R. Bilham, M. Wei, E.J. Fielding, J. Hernandez, B. Olson, P. Irvine, N. Knepprath, R.R. Sickler, D. Sandwell, X. Tong, and M. Siem*

1-093 **HOLOCENE PALEOSEISMOLOGY OF THE SOUTHERN PANAMINT VALLEY FAULT ZONE: EVALUATING SEISMIC CLUSTERING ALONG THE EASTERN CALIFORNIA SHEAR ZONE NORTH OF THE GARLOCK FAULT** *L.M. McAuliffe, J.F. Dolan, E. Kirby, B. Haravitch, and S. Alm*

1-094 **GROUND PENETRATING RADAR (GPR) SURVEY OF THE SAN ANDREAS FAULT AT THE BIDART FAN AND OTHER POTENTIAL RESEARCH SITES IN THE CARRIZO PLAIN** *S.O. Akciz, L. Grant Ludwig, and R. Kaufmann*

1-095 **USING PHOTOGRAMMETRY TO PRODUCE HIGH-RESOLUTION DEMS OF THE EL MAYOR- CUCAPAH SURFACE RUPTURE** *A.E. Morelan, J.M. Stock, K.W. Hudnut, and S.O. Akciz*

1-096 **AIRBORNE LIDAR SURVEY OF THE 4 APRIL 2010 EL MAYOR-CUCAPAH EARTHQUAKE RUPTURE** *M. Oskin, R. Arrowsmith, A. Hinojosa, J. Gonzalez, A. Gonzalez, M. Sartori, J. Fernandez, Y. Fialko, M. Floyd, J. Galetzka, and D. Sandwell*

1-097 **LATE QUATERNARY SLIP RATE AND EARTHQUAKE CHRONOLOGY OF AN ACTIVE FAULT IN THE KASHMIR BASIN: IMPLICATIONS FOR SEISMIC HAZARDS AND THE EARTHQUAKE CYCLE IN THE NORTHWEST HIMALAYA** *C.L. Madden, D.G. Trench, A.J. Meigs, J.D. Yule, S. Ahmad, and M.I. Bhat*

1-098 **PRELIMINARY RESULTS FROM HOLOCENE SURFACE MAPPING ALONG THE CENTRAL PART OF THE GARLOCK FAULT, SEARLES VALLEY, SOUTHEASTERN CALIFORNIA** *P.N. Ganev, J.F. Dolan, S.F. McGill, and K.L. Frankel*

1-099 **ARE SURFACE DISPLACEMENTS REPRESENTATIVE OF SLIP AT SEISMOGENIC DEPTHS? IMPLICATIONS FOR GEOLOGIC SLIP RATE STUDIES** *B. Haravitch and J. Dolan*

1-100 **OSL AS A DATING TECHNIQUE FOR INVESTIGATING FAULT MOVEMENT** *E. Rhodes*

Southern San Andreas Fault Evaluation

1-101 **AERIAL SURVEYS USING CONSUMER ELECTRONICS: FAST, CHEAP AND BEST OF ALL: USEFUL!** *D.K. Lynch, K.W. Hudnut, and D. Dearborn*

1-102 **NUMERICAL MODELING OF THE SAN ANDREAS FAULT SYSTEM: COMPARISON WITH ANALYTICAL SOLUTIONS AND GEOLOGICAL OBSERVATIONS** *B.P. Hooks and B.R. Smith-Konter*

1-103 **TWO POTENTIAL TRIGGERS FOR LARGE RUPTURES ALONG THE SOUTHERN SAN ANDREAS FAULT: SECONDARY FAULT DISPLACEMENT AND LAKE LOADING** *D. Brothers, D. Kilb, K. Luttrell, N. Driscoll, and G. Kent*

1-104 **AIRBORNE THERMAL INFRARED HYPERSPECTRAL IMAGERY OF SURFACE GEOTHERMAL ACTIVITY IN THE SALTON SEA GEOTHERMAL FIELD AND THE LINK TO SUBSURFACE TECTONISM** *D.M. Tratt, D.K. Lynch, K.N. Buckland, S.J. Young, J.L. Hall, B.P. Kasper, M.L. Polak, J. Qian, P.D. Johnson, and M.G. Martino*

1-105 **PRELIMINARY RESULTS FROM MYSTIC LAKE: A NEW PALEOSEISMIC SITE ALONG THE NORTHERN SAN JACINTO FAULT ZONE.** *N. Onderdonk, S. McGill, G. Marliyani, and T. Rockwell*

1-106 **AN INVESTIGATION OF THE BIRTH AND DEATH OF FAULTS ALONG A RESTRAINING BEND USING CLAYBOX ANALOG MODELS** *J. Moody, M. Cooke, and M. Schottenfield*

1-107 **INTEGRATING NEW SOSAFE PALEO-EVENT CHRONOLOGIES WITH STRESS EVOLUTION MODELS OF THE SAN ANDREAS FAULT SYSTEM OVER THE LAST 2000 YEARS** *T. Solis, G. Thornton, and B. Smith-Konter*

1-108 **SLIP ON FAULTS IN THE IMPERIAL VALLEY TRIGGERED BY THE 4 APRIL 2010 MW 7.2 EL MAJOR EARTHQUAKE** *M. Wei, D. Sandwell, Y. Fialko, and R. Bilham*

1-109 **LIDAR AND FIELD OBSERVATIONS OF EARTHQUAKE SLIP DISTRIBUTION FOR THE CENTRAL SAN JACINTO FAULT** *J.B. Salisbury, T.K. Rockwell, T.J. Middleton, and K.W. Hudnut*

1-110 **ACCELERATED HOLOCENE SLIP ACROSS THE SOUTHERN SAN JACINTO FAULT ZONE INFERRED FROM 10BE AND U-SERIES DATING OF LATE QUATERNARY LANDFORMS** *K. Blisniuk, M.E. Oskin, W. Sharp, K. Fletcher, and T. Rockwell*

1-111 **SUBSURFACE CHARACTERIZATION OF MYSTIC LAKE PALEOSEISMIC SITE ON THE CLAREMONT FAULT USING CPT DATA: EVIDENCE FOR STRAIGHTENING OF THE NORTHERN SAN JACINTO FAULT** *G.I. Marliyani, T.K. Rockwell, N.W. Onderdonk, and S.F. McGill*

1-112 **PALEOSEISMOLOGY AND SLIP RATE OF THE SAN GORGONIO PASS FAULT ZONE: TESTING THE LIKELIHOOD OF THROUGH GOING SAN ANDREAS RUPTURES** *D. Yule, P. McBurnett, and S. Ramzan*

1-113 **10BE DATING OF FLUVIAL TERRACES IN SOUTHERN CALIFORNIA: SUCCESS, FAILURE, AND THE FUTURE…** *R.V. Heermance, K. McGuire, and H. McKay*

1-114 **SEISMOTECTONICS OF THE 2010 EL MAYOR CUCAPAH/INDIVISO EARTHQUAKE** *J. Gonzalez-Garcia and J. Gonzalez-Ortega*

1-115 **SLIP RATE OF THE NORTHERN SAN JACINTO FAULT FROM OFFSET LANDSLIDES IN THE SAN TIMOTEO BADLANDS** *S.F. McGill, L.A. Owen, E.O. Kent, N. Onderdonk, and T.K. Rockwell*

1-116 **PREHISTORIC EARTHQUAKES ALONG THE SAN JACINTO FAULT IN TRENCH 7 AT THE MYSTIC LAKE PALEOSEISMIC SITE** *M.R. Swift, S.F. McGill, N. Onderdonk, T.K. Rockwell, B. Anderson, J. Bywater, K. Chung, J. Duncan, and G.I. Marlyani*

1-117 **CORRELATIONS OF PALEOSEISMIC EVENTS ON THE SOUTHERN SAN ANDREAS FAULT: UPDATE TO WGCEP-2** *G.P. Biasi, K.M. Scharer, and R.J. Weldon*

Earthquake Forecasting and Predictability

1-118 **A FIRST-ORDER TEST TO COMPARE REGIONAL EARTHQUAKE LIKELIHOOD MODELS** *D.A. Rhoades, M.C. Gerstenberger, and A. Christophersen*

1-119 **RANDOM STRESS AND OMORI'S LAW** *Y.Y. Kagan*

1-120 **BUILDING THE COMMUNITY ONLINE RESOURCE FOR STATISTICAL SEISMICITY ANALYSIS (CORSSA)** *A.J. Michael, S. Wiemer, J. Zechar, J. Hardebeck, M. Naylor, J. Zhuang, and S. Steacy*

1-121 **PRELIMINARY RESULTS FOR N CA FROM EARTHQUAKE SIMULATOR COMPARISON PROJECT** *T.E. Tullis, M. Barall, K. Richards-Dinger, S.N. Ward, E. Heien, O. Zielke, F. Pollitz, J. Dieterich, J. Rundle, B. Yikilmaz, D. Turcotte, L. Kellogg, and E.H. Field*

1-122 **CSEP-JAPAN: REPORT ON PROSPECTIVE EVALUATION TEST OF THE 3-MONTH TESTING CLASS** *S. Yokoi, K. Nanjo, H. Tsuruoka, N. Hirata, D. Schorlemmer, and F. Euchner*

Tectonic Geodesy

1-141 **USING GPS TO MEASURE FAULT SLIP-RATES OF THE SAN JACINTO FAULT IN RIVERSIDE COUNTY** *S.L.C. Morton, G.J. Funning, and M. Floyd*

1-142 **BATHYMETRIC SURVEYS OF THE HMS BEAGLE AT SANTA MARIA ISLAND, CHILE, (37°S) AND THE SEISMIC CYCLE** *R.L. Wesson, D. Melnick, M. Cisternas, L. Ely, and M. Moreno*

1-143 **IDENTIFYING GROWTH OF STRUCTURES IN THE ZAGROS FOLD AND THRUST BELT: INITIAL TIME SERIES RESULTS AND EVALUATION OF PRECIPITABLE WATER VAPOR EFFECTS** *W.D. Barnhart and R.B. Lohman*

1-144 **INSAR TIME SERIES IN A FOLD AND THRUST BELT** *A. Huth, R. Lohman, and W. Barnhart*

1-145 **ACCELERATED LOADING OF THE SOUTHERN SAN ANDREAS FAULT DUE TO TRANSIENT DEFORMATION IN THE SALTON TROUGH** *B.W. Crowell, Y. Bock, D.T. Sandwell, and Y. Fialko*

1-146 **UNAVCO RESPONSE TO THE M7.2 EL MAYOR-CUCAPAH EARTHQUAKE** *C. Walls, A. Borsa, S. Lawrence, D. Mann, A. Bassett, M. Jackson, and K. Feaux*

1-147 **LONGBASE STRAINMETER MEASUREMENTS OF DEFORMATIONS AFTER THE CUCUPAH/EL-MAYOR EARTHQUAKE** *F.K. Wyatt and D.C. Agnew*

1-148 **TESTING THE INFERENCE OF CREEP ON RODGERS CREEK FAULT** *L. Jin and G. Funning*

1-149 **SEPARATING SEASONAL, ANTHROPOGENIC, AND TECTONIC DEFORMATION IN THE WESTERN TRANSVERSE RANGES REGION, CA** *S.T. Marshall, S.E. Owen, and G.J. Funning*

1-150 **ATMOSPHERIC ERROR BUDGET IN INSAR DATA AND ITS IMPLICATION TO DESDYNI MISSION FOR CRUSTAL DEFORMATION** *S. Yun, M. Chaubell, E. Fielding, Z. Liu, S. Hensley, F. Webb, and P. Rosen*

1-151 **EXPLORING LITHOSPHERIC DEFORMATION OF WESTERN US WITH GPS TIME SERIES, VELOCITIES, AND STRAIN MAPS.** *S.E. Owen, Y. Bock, F.H. Webb, S. Kedar, D. Dong, P. Jameson, P. Fang, M. Squibb, and B. Crowell*

1-152 **A DENSIFIED GEODETIC VELOCITY SOLUTION FOR THE NORTH SAN FRANCISCO BAY REGION** *M.A. Floyd, G.J. Funning, and B.P. Lipovsky*

1-153 **COSEISMIC DEFORMATION OF THE 2010 SIERRA EL MAYOR EARTHQUAKE FROM ALOS PALSAR IMAGERY** *G.J. Funning*

1-154 **SOUTHERN CALIFORNIA HIGH SCHOOLS CONTRIBUTE TO THE GPS VELOCITY FIELD IN THE INLAND EMPIRE** *S.F. McGill, B. Brownbridge, J. Cooper, A. Foutz, M. Johnson, J.M. Jones, J. Lipow, M. Meijer, T. Ramsey, R. Ruiz, B. Vargas, J. Spinler, and R, Bennett*

1-155 **GPS COSEISMIC AND POSTSEISMIC SURFACE DISPLACEMENTS OF THE EL MAYOR-CUCAPAH EARTHQUAKE** *J. Gonzalez-Ortega, J. Gonzalez-Garcia, D. Sandwell, Y. Fialko, F. Nava, J.M. Fletcher, D. Agnew, and B. Lipovsky*

1-156 **FAULT CREEP OF THE SAN ANDREAS FAULT NEAR THE PAINTED CANYON REVEALED BY GPS SURVEYS** *M. Wei, D. Sandwell, Y. Bock, Y. Fialko, D. Agnew, X. Tong, and B. Crowell*

1-157 **DISTRIBUTED STRAIN AND FAULT SLIP RATES IN SOUTHERN CALIFORNIA INFERRED FROM GPS DATA AND MODELS** *K.M. Johnson and R.Y. Chuang*

1-158 **COMPARISON OF LOCKING DEPTHS ESTIMATED FROM GEODESY AND SEISMOLOGY ALONG THE SAN ANDREAS FAULT SYSTEM** *B.R. Smith-Konter, D.T. Sandwell, and P. Shearer*

Group 2 Posters

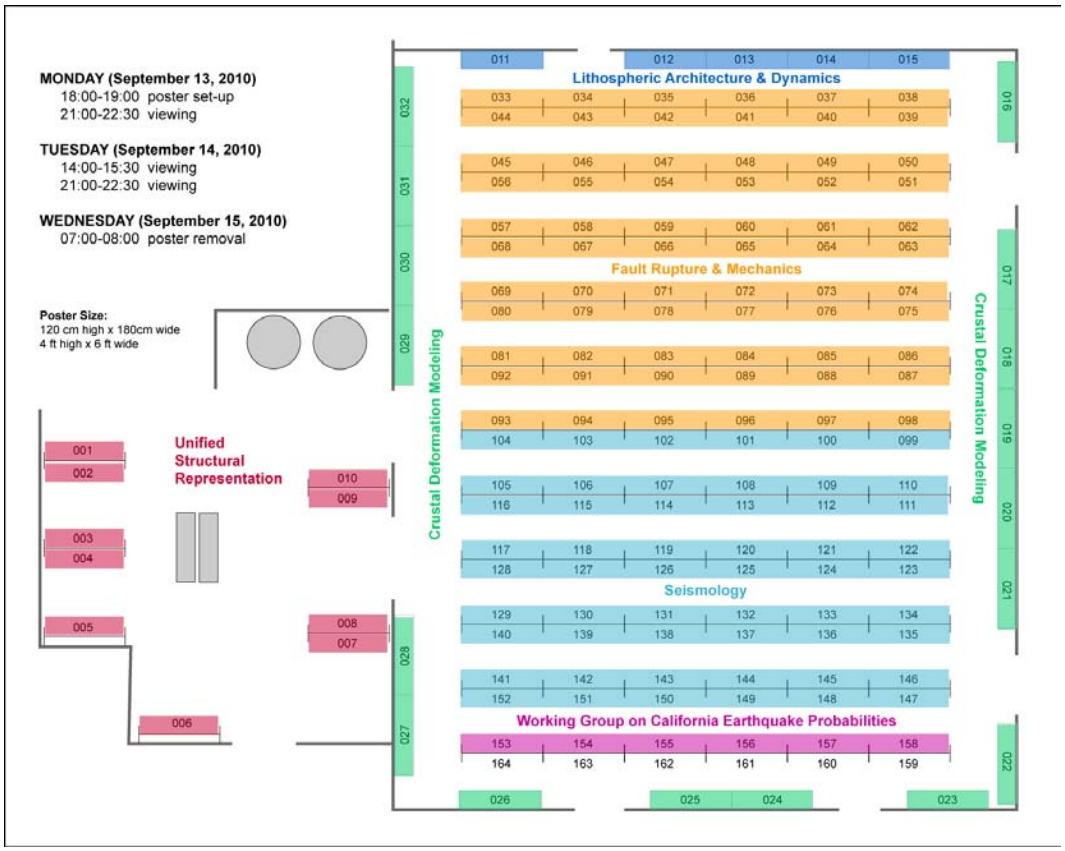

Unified Structural Representation

2-001 **ACTIVE STRIKE-SLIP FAULTING IN THE CALIFORNIA CONTINENTAL BORDERLAND** *M.R. Legg*

2-002 **DEEP STRUCTURE OF LITHOSPHERIC FAULT ZONES** *J.P. Platt and W.M. Behr*

2-003 **NEW DEVELOPMENTS FOR THE SCEC COMMUNITY FAULT MODEL AND ITS ASSOCIATED FAULT DATABASE** *A. Plesch, C. Nicholson, J.H. Shaw, E. Hauksson, and P.M. Shearer*

2-004 **ON THE ACCURACY OF CVM4 AND CVMH-6.2** *K. Withers, K.B. Olsen, P. Small, and P. Maechling*

2-005 **EXPANSION OF CVM-H 6.2 TO OFFSHORE AND CENTRAL CALIFORNIA** *C. Tape, A. Plesch, and J.H. Shaw*

2-008 **TIME REVERSAL SEISMIC IMAGING USING LATERALLY REFLECTED SURFACE WAVES IN SOUTHERN CALIFORNIA** *C. Tape, Q. Liu, J. Tromp, A. Plesch, and J. Shaw*

2-009 **CONSTRAINING SEDIMENTARY BASIN-BASEMENT INTERFACE WITH CONVERTED BODY WAVES** *S. Ni and S. Wei*

2-010 **STATEWIDE COMMUNITY FAULT MODEL (SCFM)** *A. Plesch and J.H. Shaw*

Lithospheric Architecture and Dynamics

2-011 **INVESTIGATING FAULT EVOLUTION AROUND RESTRAINING BENDS WITHIN A CLAYBOX** *M.L. Cooke, M.T. Schottenfeld, and J. Moody*

2-012 **A NATURALLY CONSTRAINED STRESS PROFILE THROUGH THE MIDDLE CRUST IN AN EXTENSIONAL TERRANE** *W.M. Behr and J.P. Platt*

2-013 **THRUST-FOLDING, TILTING AND SUBSIDENCE: CALIFORNIA BORDERLAND AND HAITI** *C. Sorlien, L. Seeber, M-H. Cormier, M. Davis, J. Diebold, N. Dieudonne, S. Gulick, M. Hornbach, C. McHugh, and M. Steckler*

2-014 **P AND S BODY WAVE AND JOINT S BODY WAVE AND RAYLEIGH WAVE TOMOGRAPHY OF THE SOUTHERN CALIFORNIA UPPER MANTLE** *B. Schmandt, E. Humphreys, D. Forsyth, and C. Rau*

2-015 **LITHOSPHERIC DEFORMATION WITHIN SOUTHERN CALIFORNIA: A COMPARISON OF CRUSTAL AND UPPER MANTLE ANISOTROPY MEASUREMENTS** *R. Porter and G. Zandt*

Crustal Deformation Modeling

2-016 **THREE-DIMENSIONAL THERMO-MECHANICAL MODELING OF THE DEATH VALLEY FAULT ZONE** *C. Del Pardo, B.P. Hooks, B.R. Smith-Konter, L.F. Serpa, and T.L. Pavlis*

2-017 **RESOLVING DISCREPANCIES BETWEEN PERMANENT GPS DERIVED AND GEOLOGIC SLIP RATES** *J.W. Herbert and M.L. Cooke*

2-018 **A KINEMATIC FAULT NETWORK MODEL OF CRUSTAL DEFORMATION FOR CALIFORNIA AND ITS APPLICATION TO THE SEISMIC HAZARD ANALYSIS** *Y. Zeng, Z.-Y. Shen, and M. Petersen*

2-019 **SLIP RATES ON MAJOR FAULTS OF THE SOUTHERN SAN ANDREAS FAULT SYSTEM FROM INVERSIONS OF CONTINUOUS GPS DATA** *E. Lindsey and Y. Fialko*

2-020 **QUANTIFYING THERMOELASTIC AND POROELASTIC VARIATIONS FOR SEASONAL CHANGES IN GPS POSITIONS AND SEISMIC WAVE SPEEDS IN SOUTHERN CALIFORNIA** *V.C. Tsai*

2-021 **PYLITH: A FINITE-ELEMENT CODE FOR MODELING QUASI-STATIC AND DYNAMIC CRUSTAL DEFORMATION** *B.T. Aagaard, C.A. Williams, M. Knepley, and S.N. Somala*

2-022 **RECONCILING GEOLOGIC AND GEODETIC FAULT-SLIP-RATE DISCREPANCIES IN SOUTHERN CALIFORNIA: CONSIDERATION OF NON-STEADY MANTLE FLOW AND LOWER CRUSTAL FAULT CREEP** *R.Y. Chuang and K.M. Johnson*

2-023 **STRUCTURAL DEVELOPMENT OF BASINS ASSOCIATED WITH BENDS ON CONTINENTAL TRANSFORMS: THE NORTH ANATOLIAN FAULT IN NW TURKEY AND THE SAN ANDREAS FAULT IN SOUTHERN CALIFORNIA** *H. Kurt, L. Seeber, C.C. Sorlien, M. Steckler, D. Shillington, E. Perincek, D. Timur, and D. Dondurur*

2-024 **HOW MUCH DO LONG-TERM "GHOST TRANSIENTS" FROM PAST EARTHQUAKES CONTRIBUTE TO THE PRESENT-DAY GPS VELOCITY FIELD IN CALIFORNIA?** *F.F. Pollitz, E.H. Hearn, and W.R. Thatcher*

2-025 **BENCHMARKING PYLITH AGAINST ABAQUS FOR PROBLEMS INVOLVING FAULT FRICTION AND INELASTIC DEFORMATION** *C.A. Williams and S.M. Ellis*

2-026 **HORIZONTAL STRAIN RATE ESTIMATION USING DISCRETIZED GEODETIC DATA AND ITS APPLICATION TO SOUTHERN CALIFORNIA** *Z.-K. Shen and Y. Zeng*

2-027 **DEFORMATION ASSOCIATED WITH THE 2010 SIERRA EL MAYOR, BAJA CALIFORNIA EARTHQUAKE FROM CAMPAIGN GPS MEASUREMENTS** *D. Ben-Zion, G.J. Funning, and M.A. Floyd*

2-028 **3D STRESS HETEROGENEITY – POTENTIAL IMPLICATIONS FOR CRUSTAL STRESS PARAMETERS AND STRESS INVERSION RESULTS IN SOUTHERN CALIFORNIA** *D.E. Smith and T.H. Heaton*

2-030 **PROGRESS ON MODELING SURFACE DEFORMATION IN THE NEW MADRID SEISMIC ZONE** *O. Boyd, Y. Zeng, A. Frankel, and L. Ramirez-Guzman*

2-031 **TOMOGRAPHY OF THE MOJAVIAN LITHOSPHERE VISCOSITY FROM SPACE GEODETIC DATA OF THE LANDERS AND HECTOR MINE EARTHQUAKES** *S. Barbot and Y. Fialko*

2-032 **RELATIVE CONTRIBUTION OF STABLE AFTERSLIP AND VISCOELASTIC RELAXATION FOLLOWING THE 2004 PARKFIELD EARTHQUAKE** *S. Barbot, L. Bruhat, and J-P. Avouac*

Fault Rupture and Mechanics

2-033 **HIGH-RESOLUTION IMAGING OF THE SAN ANDREAS FAULT DAMAGE ZONE FROM SAFOD MAIN-HOLE AND SURFACE SEISMIC RECORDS** *Y-G. Li, P.E. Malin, E.S. Cochran, P. Chen, and J.E. Vidale*

2-034 **A DAMAGE MODEL FOR THE ABSENCE OF SIGNIFICANT PRECURSORY SEISMICITY** *Y-T. Lee, D. Turcotte, J. Rundle, and C-C. Chen*

2-035 **SPECIFYING INITIAL STRESS FOR DYNAMIC HETEROGENEOUS EARTHQUAKE SOURCE MODELS** *D.J. Andrews and M. Barall*

2-036 **ANTICIPATED ARREST: INSUFFICIENT CONDITIONS FOR CONTINUED DYNAMIC PROPAGATION OF A SLIP-WEAKENING RUPTURE NUCLEATED BY LOCALIZED INCREASE OF PORE-PRESSURE.** *R.C. Viesca-Falguières and J.R. Rice*

2-037 **SUPERFICIAL SIMPLICITY OF THE 2010 MW 7.2 EL MAYOR-CUCAPAH EARTHQUAKE OF BAJA CALIFORNIA** *S. Wei, E. Fielding, S. Leprince, A. Sladen, J-P. Avouac, D.V. Helmberger, E. Hauksson, R. Chu, M. Simons, K. Hudnut, T. Herring, and R. Briggs*

2-038 **OFF-FAULT YIELDING DURING DYNAMIC RUPTURES: DISTRIBUTION AND ORIENTATIONS** *S. Xu, Y. Ben-Zion, and J.-P. Ampuero*

2-039 **EFFICIENT NUMERICAL MODELING OF SLOW SLIP AND QUASI-DYNAMIC EARTHQUAKE RUPTURES** *A.M. Bradley and P. Segall*

2-040 **FACTORS INFLUENCING STRESS-DROPS OF SMALL EARTHQUAKES IN SOUTHERN CALIFORNIA** *P. Bird and P.M. Shearer*

2-041 **PHASE DIAGRAMS AS METHOD FOR MODEL INTERCOMPARISONS: EARTHQUAKE SIMULATORS PROBLEM 3** *B.E. Shaw, H. Noda, K. Richards-Dinger, S.N. Ward, J.H. Dieterich, N. Lapusta, and T.E. Tullis*

2-042 **MICRO-CRACKS AND VOLUMETRIC STRAIN IN SAPROCK: WORKING TOWARDS AN UNDERSTANDING OF THE EFFECTS OF GROUND SHAKING ON THE DEVELOPMENT OF WEATHERING PROFILES IN SEISMICALLY ACTIVE AREAS** *C.T. Replogle, N.M. Morton, M.T. Buga, B.R. Page, and G.H. Girty*

2-043 **THE EFFECT OF PARTICLE ANGULARITY ON THE TRANSITION TO INERTIAL GRANULAR FLOW** *N.J. van der Elst and E.E. Brodsky*

2-044 **ESTIMATING ABSOLUTE TRACTION FROM SLICKENLINES** *J.D. Kirkpatrick and E.E. Brodsky*

2-045 **RUPTURE DIRECTIVITY OF MICRO-EARTHQUAKES ON THE SAN ANDREAS FAULT FROM SPECTRAL RATIO INVERSION** *E. Wang and A. Rubin*

2-046 **DYNAMIC WEAKENING OF GOUGE LAYERS BY THERMAL PRESSURIZATION AND TEMPERATURE-DEPENDENT FRICTION IN HIGH-SPEED SHEAR EXPERIMENTS** *H. Kitajima, F.M. Chester, and J.S. Chester*

2-047 **INTEGRATING AFTERSHOCK AND SURFACE RUPTURE DATA TO CONSTRAIN 3D STRUCTURE OF THE 1992 LANDERS EARTHQUAKE** *B.H. Madden and D.D. Pollard*

2-048 **DYNAMIC EARTHQUAKE RUPTURE MODELING WITH PYLITH: SCEC BENCHMARKS AND APPLICATION TO TSUNAMIGENIC EARTHQUAKES** *S.N. Somala, B. Aagaard, J-P. Ampuero, and N. Lapusta*

2-049 **PARTICLE SIZE ANALYSIS OF DAMAGE TEXTURES IN FAULT ZONE ROCKS** *N. Wechsler, J.S. Chester, T.K. Rockwell, and Y. Ben-Zion*

2-050 **HOW BARRIERS ENABLE MULTI-FAULT RUPTURE IN A BRANCHED FAULT SYSTEM** *J.M. Tarnowski, D.D. Oglesby, and D. Bowman*

2-051 **FORMATION OF PULSE-LIKE RUPTURES ON VELOCITY-WEAKENING INTERFACES AND ITS RELATION TO STABILITY PROPERTIES OF STEADY-STATE SLIDING** *A.E. Elbanna, N. Lapusta, and T.H. Heaton*

2-052 **A NEW PARADIGM IN MODELING PULSELIKE RUPTURES: THE PULSE ENERGY EQUATION** *A.E. Elbanna and T.H. Heaton*

2-053 **MODELING SHALLOW SLIP DEFICIT IN LARGE STRIKE-SLIP EARTHQUAKES USING SIMULATIONS OF SPONTANEOUS EARTHQUAKE SEQUENCES IN ELASTO-PLASTIC MEDIA** *Y. Kaneko and Y. Fialko*

2-054 **EFFECT OF FAULT SEGMENTATION ON DISPLACEMENT TIME HISTORY** *A.S. Bykovtsev*

2-055 **USING DYNAMIC RUPTURE MODELS WITH OFF-FAULT PLASTIC YIELDING TO INVESTIGATE INELASTIC RESPONSE OF PRE-EXISTING FAULT ZONES TO NEARBY EARTHQUAKES** *B. Duan*

2-056 **DISTRIBUTION OF PLASTIC DEFORMATION DUE TO RUPTURE ON A BIMATERIAL INTERFACE** *N. DeDontney, J.R. Rice, and R. Dmowska*

2-057 **STRAIN LOCALIZATION WITHIN A FLUID-SATURATED FAULT GOUGE LAYER DURING SEISMIC SHEAR** *J.D. Platt, J.R. Rice, and J.W. Rudnicki*

2-058 **PERIODIC, CHAOTIC AND LOCALIZED SLIP PULSE SOLUTIONS WITH DIETERICH-RUINA FRICTION** *B.A. Erickson, D. Lavallee, and B. Birnir*

2-059 **COMPARISON OF PROXIES FOR THE 'VELOCITY STRENGTHENING' ZONE AT SHALLOW DEPTH AND THEIR EFFECT ON RUPTURE DYNAMICS** *Q. Liu, R.J. Archuleta, and R.B. Smith*

2-060 **THE MICROMECHANICS OF FAULT GOUGE AND DYNAMIC EARTHQUAKE TRIGGERING: INVESTIGATION BY DISCRETE ELEMENT METHOD NUMERICAL SIMULATIONS** *M. Griffa, E.G. Daub, R.A. Guyer, P.A. Johnson, C.J. Marone, and J. Carmeliet*

2-061 **A GLOBAL CHARACTERIZATION OF PHYSICAL SEGMENTATION ALONG OCEANIC TRANSFORM FAULTS** *M.L. Wolfson and M.S. Boettcher*

2-062 **ADAPTIVE MESH REFINEMENT FOR DYNAMIC RUPTURE SIMULATIONS** *J.E. Kozdon and E.M. Dunham*

2-063 **FINITE FAULT CO-SEISMIC KINEMATIC AND POST-SEISMIC SLIP DISTRIBUTION MODEL OF THE 2009 MW 6.3 AQUILA EARTHQUAKE FROM JOINT-INVERSION OF STRONG MOTION, GPS, AND INSAR DATA** *T.E. Yano, G. Shao, Q. Liu, C. Ji, and R.J. Archuleta*

2-064 **IDENTIFYING THE UNIQUE GROUND MOTION SIGNATURES OF SUPERSHEAR EARTHQUAKES: THEORY AND EXPERIMENTS** *M. Mello, H.S. Bhat, A.J. Rosakis, and H. Kanamori*

2-065 **STRESS RELAXATION DUE TO SLIP ON GEOMETRICALLY COMPLEX FAULTS: HOW IT AFFECTS FAULT SIMULATORS AND OFF-FAULT MOMENT RELEASE** *D.E. Smith and J.H. Dieterich*

2-066 **SIMULATIONS OF SLOW SLIP EVENTS WITH RSQSIM** *H.V. Colella and J.H. Dieterich*

2-067 **DYNAMICS OF PARALLEL STRIKE-SLIP FAULTS WITH OFF-FAULT PLASTIC YIELDING, FLUID PRESSURE CHANGE AND LOW VELOCITY ZONES** *Z. Liu and B. Duan*

2-068 **OFF-FAULT DAMAGE AND FAULT ZONE COMPLEXITY ASSOCIATED WITH A LOCALIZED BEND IN THE SAN GABRIEL FAULT** *A.W. Becker, F.M. Chester, and J.S. Chester*

2-069 **AN EXPERIMENTAL AND THEORETICAL STUDY OF ASYMMETRIC EARTHQUAKE RUPTURE PROPAGATION CAUSED BY OFF-FAULT FRACTURE DAMAGE** *H.S. Bhat, C.G. Sammis, and A.J. Rosakis*

2-070 **EFFECTS OF HETEROGENEOUS FRICTIONAL PROPERTIES ON DYNAMICS OF GEOMETRICALLY COMPLEX FAULT SYSTEMS: A CASE STUDY OF THE 1999 HECTOR MINE EARTHQUAKE** *J. Kang and B. Duan*

2-071 **THERMAL PRESSURIZATION DURING THE TRANSITION FROM QUASI-STATIC NUCLEATION TO DYNAMIC RUPTURE** *S.V. Schmitt, E.M. Dunham, and P. Segall*

2-072 **ANALYSES OF COSEISMIC SURFACE DEFORMATION USING TERRESTRIAL LIDAR SCANS OF THE 4 APRIL 2010 EL MAYOR-CUCAPAH EARTHQUAKE RUPTURE** *P.O. Gold, A.J. Elliott, M.E. Oskin, M.H. Taylor, A.J. Herrs, A. Hinojosa, O. Kreylos, T.S. Bernardin, and E.S. Cowgill*

2-073 **SUPERSHEAR RUPTURE TRANSITION ON FAULT STEPOVERS USING DIFFERENT FRICTION PARAMETERIZATIONS** *K.J. Ryan and D.D. Oglesby*

2-074 **NUMERICAL MODELS OF THRUST EARTHQUAKES ON HOMALITE FAULTS** *D.D. Oglesby, N. Lapusta, V. Gabuchian, and A.J. Rosakis*

2-075 **EXPERIMENTAL INVESTIGATION OF THRUST FAULTS IN HOMALITE** *V. Gabuchian, A. Rosakis, N. Lapusta, and D. Oglesby*

2-076 **LABORATORY OBSERVATIONS OF THE RESPONSE OF FAULT STRENGTH AS NORMAL STRESS IS CHANGED, AND IMPLICATIONS FOR DYNAMIC RUPTURE** *J.C. Lozos and B. Kilgore*

2-077 **DISCRETE RUPTURE OF ASPERITIES RECORDED ON INSTRUMENTED LABORATORY FAULTS** *G.C. McLaskey and S.D. Glaser*

2-078 **FAULT ROUGHNESS AND BACKGROUND STRESS LEVELS ON MATURE AND IMMATURE FAULTS** *Z. Fang and E.M. Dunham*

2-079 **PROPERTIES OF DYNAMIC SLIP PULSES IN A 2D SLAB** *Y. Huang, J-P. Ampuero, and L.A. Dalguer*

2-080 **DYNAMIC RUPTURE ON FAULTS WITH HETEROGENEOUS STRENGTH DUE TO NON-UNIFORM NORMAL STRESS: THE EFFECT OF STRESS REDISTRIBUTION BY PRIOR EVENTS** *J. Jiang and N. Lapusta*

2-081 **INTERACTION OF SMALL REPEATING EARTHQUAKES IN A RATE AND STATE FAULT MODEL** *T. Chen and N. Lapusta*

2-082 **THE SCEC-USGS DYNAMIC EARTHQUAKE RUPTURE CODE VERIFICATION EXERCISE: REGULAR AND EXTREME GROUND MOTION** *R.A. Harris, M. Barall, R. Archuleta, B. Aagaard, J.-P. Ampuero, D.J. Andrews, V. Cruz-Atienza, L. Dalguer, S. Day, B. Duan, E. Dunham, G. Ely, A. Gabriel, Y. Kaneko, Y. Kase, N. Lapusta, S. Ma, H. Noda, D. Oglesby, K. Olsen, D. Roten, and S. Song*

2-083 **EFFECT OF FAULT ROUGHNESS ON DYNAMIC RUPTURE** *Z. Shi and S. Day*

2-084 **SIMULATIONS OF SLIP HISTORY ON FAULTS WITH HETEROGENEOUS RATE-WEAKENING AND RATE-STRENGTHENING PROPERTIES** *S. Barbot, N. Lapusta, and J.-P. Avouac*

2-085 **SIMULATIONS OF SEISMICITY IN FAULT SYSTEMS – EFFECTS OF INTERACTIONS WITH FAULT CREEP** *K. Richards-Dinger and J. Dieterich*

2-086 **HIGH FREQUENCY VIBRATIONAL WEAKENING OF FAULT ZONES: NEW INSIGHTS FROM HIGH VELOCITY EXPERIMENTS WITH IMPLICATIONS FOR NATURAL EARTHQUAKE FAULT ZONE DYNAMICS** *K.M. Brown and Y. Fialko*

2-087 **ON THE CONTINUITY TO THE NORTHWEST OF THE CERRO PRIETO FAULT** *O. Lazaro-Mancilla, D. Lopez, J.A. Reyes-López, C. Carreón-Diazconti, and J. Ramírez-Hernández*

2-088 **EARTHQUAKE NUCLEATION MECHANISMS AND PERIODIC LOADING: MODELS, EXPERIMENTS, AND OBSERVATIONS** *B. Brinkman, G. Tsekenis, Y. Ben-Zion, J. Uhl, and K. Dahmen*

2-089 **BRITTLE AND DUCTILE FRICTION AND THE PHYSICS OF TECTONIC TREMOR** *E.G. Daub, D.R. Shelly, R.A. Guyer, and P.A. Johnson*

2-090 **CASCADIA TREMOR INSPECTED WITH THE EARTHSCOPE ARRAY OF ARRAYS** *J.E. Vidale*

2-091 **DESIGNER FRICTION LAWS FOR BIMODAL SLOW SLIP PROPAGATION SPEEDS** *A.M. Rubin*

2-092 **DYNAMIC TRIGGERING OF SHALLOW EARTHQUAKES NEAR BEIJING, CHINA** *C. Wu, Z. Peng, W. Wang, and Q. Chen*

2-093 **VARIATIONS IN TREMOR ACTIVITY AND IMPLICATIONS FOR LOWER CUSTAL DEFORMATION ALONG THE CENTRAL SAN ANDREAS FAULT** *D.R. Shelly*

2-094 **EPISODIC TREMOR AND SLIP ON A FRICTIONAL INTERFACE WITH CRITICAL ZERO WEAKENING IN ELASTIC SOLID** *Y. Ben-Zion*

2-095 **THE EFFECT OF WATER ON TRIGGERING OF STICK SLIP BY OSCILLATORY LOADING** *N.M. Bartlow, D.A. Lockner, and N.M. Beeler*

2-096 **INTERMITTENT FAULT SLIP EMBEDDED IN CREEP GENERATES SEISMIC EVENTS: INSIGHT FROM ACOUSTIC AND OPTICAL MONITORING OF CRACK PROPAGATION** *J.E. Elkhoury, O. Lengliné, J.-P. Ampuero, and J. Schmittbuhl*

Seismology

2-099 **DYNAMIC TRIGGERING OF SHALLOW EARTHQUAKES IN THE SALTON SEA REGION OF SOUTHERN CALIFORNIA** *A.K. Doran, Z. Peng, C. Wu, and D. Kilb*

2-100 **NON-VOLCANIC TREMOR CHARACTERISTIC AND LOCATIONS IN ANZA REGION, SOUTHERN CALIFORNIA** *T-H. Wang and E.S. Cochran*

2-101 **HIGH-VP/VS (POISSON RATIO) ZONE ACCOMPANYING SLOW EVENTS AND LOW-VELOCITY LOWER CRUST ALONG ACTIVE FAULTS BENEATH THE SOUTHWESTERN JAPAN** *M. Matsubara and K. Obara*

2-102 **TREMOR EVIDENCE FOR DYNAMICALLY TRIGGERED CREEP EVENTS ON THE DEEP SAN ANDREAS FAULT** *D.R. Shelly, Z. Peng, D.P. Hill, and C. Aiken*

2-103 **A CATALOG OF LOW FREQUENCY EARTHQUAKE ACTIVITY FROM TRIGGERED TREMOR ON THE SAN JACINTO FAULT** *J.R. Brown*

2-104 **ANALYSIS OF TREMOR AND EARTHQUAKE ALONG THE SAN ANDREAS FAULT IN CHOLAME, CA** *C.E. Potier, E.S. Cochran, and R.M. Harrington*

2-105 **SEISMICITY IN COLOMBIA: TOMOGRAPHY, INTERMEDIATE DEPTH EARTHQUAKES, AND QCN** *G.A. Prieto*

2-106 **SEISMIC DOCUMENTATION OF ROCK DAMAGE AND HEAL AT THE LONGMAN-SHAN FAULT RUPTURED IN THE 2008 M8 WENCHUAN EARTHQUAKE FROM FAULT-ZONE TRAPPED WAVES** *Y-G. Li, J.Y. Su, and T.C. Chen*

2-107 **RESULTS FROM QUAKE-CATCHER NETWORK RAPID AFTERSHOCK MOBILIZATION PROGRAM (QCN-RAMP) FOLLOWING THE M8.8 MAULE, CHILE EARTHQUAKE** *A.I. Chung, C. Neighbors, A. Belmonte, M. Miller, A. Sepulveda, C. Christensen, E.S. Cochran, and J.F. Lawrence*

2-127 **AVERAGE STATIC STRESS DROPS FOR HETEROGENEOUS SLIP DISTRIBUTIONS: COMPARISON OF SEVERAL MEASURES AND IMPLICATIONS FOR ENERGY PARTITION IN EARTHQUAKES** *H. Noda, N. Lapusta, and H. Kanamori*

2-128 **SPECTRAL ANALYSIS OF PORE PRESSURE DATA RECORDED FROM THE 2010 SIERRA EL MAYOR (BAJA CALIFORNIA) EARTHQUAKE AT THE NEES@UCSB WILDLIFE FIELD SITE** *D. Lavallee and S.W.H. Seale*

2-129 **THE 2010 OCOTILLO SWARM: PRELIMINARY RESULTS FROM DATA RECORDED AT THE NEES@UCSB WILDLIFE LIQUEFACTION ARRAY** *D.A. Huthsing, S.W.H. Seale, and J.H. Steidl*

2-130 **DOES CASING MATERIAL INFLUENCE DOWNHOLE ACCELEROMETER RECORDINGS? A CONTROLLED STUDY OF EARTQUAKE AND EXPERIMENTAL DATA RECORDED AT THE NEES@UCSB WILDLIFE LIQUEFACTION ARRAY** *D.A. Huthsing, S.W.H. Seale, and J.H. Steidl*

2-131 **SEISMIC REFLECTION STUDY OF THE SALTON SEA** *A.M. Kell-Hills, G. Kent, N. Driscoll, A. Harding, and R. Baskin*

2-132 **UNDERSTANDING PHYSICAL MECHANISMS OF EARTHQUAKE TRIGGERING IN SOUTHERN CALIFORNIA FOLLOWING THE 2010 MW7.2 NORTHERN BAJA CALIFORNIA EARTHQUAKE** *Z. Peng, X. Meng, and A. Doran*

2-133 **BAYESIAN KINEMATIC FINITE FAULT SOURCE MODELS** *S.E. Minson, M. Simons, and J.L. Beck*

2-134 **EXAMINING SEISMICITY IN A COMPLEX FAULT ZONE: THE 2001, 2005, AND 2010 M5+ ANZA EARTHQUAKES AND AFTERSHOCK SEQUENCES** *D.L. Kane, F.L. Vernon, D.L. Kilb, and K.T. Walker*

2-135 **INNOVATIVE REPRESENTATION OF EARTHQUAKE TRIGGERING FROM SONIFICATION/VISUALIZATION OF SEISMIC SIGNALS** *M. Fisher, Z. Peng, D. Simpson, and D. Kilb*

2-136 **TEMPORAL AND SPATIAL ANALYSIS OF ACOUSTIC EMISSION CLUSTERS DURING SLIDING OF ROUGH GRANITE SURFACES** *T.H. Goebel, S. Stanchits, T. Becker, D. Schorlemmer, and G. Dresen*

2-137 **SORD AS A COMPUTATIONAL PLATFORM FOR EARTHQUAKE SIMULATION, SOURCE IMAGING, AND FULL 3D TOMOGRAPHY** *F. Wang, G.P. Ely, and T.H. Jordan*

2-138 **WHAT THE SPICE SOURCE INVERSION VALIDATION BLINDTEST I EXERCISE DID NOT TELL YOU?** *G. Shao and C. Ji*

2-139 **LONG PERIOD (T>1.0-S) SEISMIC RESPONSE OF THE SALT LAKE BASIN FROM EARTHQUAKE SIMULATIONS** *M.P. Moschetti and L. Ramirez-Guzman*

2-140 **ON THE CHARACTERISTICS OF SEISMIC EVENTS WITH MAGNITUDES -5 < M < -1** *K. Plenkers, G. Kwiatek, D. Schorlemmer, M. Nakatani, Y. Yabe, and D. Dresen*

2-141 **SOURCE PROPERTIES OF THE 2010 M7 HAITI EARTHQUAKE ESTIMATED BY BACK PROJECTION OF THE DATA RECORDED BY THE NATIONAL VENEZUELA SEISMIC NETWORK** *L. Meng, J-P. Ampuero, and H. Rendon*

2-142 **RUPTURE PROCESS OF THE 2010 MW 7.3 EL MAYOR-CUCAPAH EARTHQUAKE** *X. Zhao, G. Shao, C. Ji, K.M. Larson, K.W. Hudnut, and T. Herring*

2-143 **FINITE FAULT INVERSION OF MODERATE AND LARGE EARTHQUAKES IN SOUTHERN CALIFORNIA USING NEAR REAL-TIME HIGH RATE GPS AND STRONG MOTION WAVEFORMS** *X. Zhao, G. Shao, X. Li, and C. Ji*

2-144 **GEONET: PLATFORM FOR RAPID DISTRIBUTED GEOPHYSICAL SENSING** *I. Stubailo, M. Lukac, D. McIntire, P. Davis, W. Kaiser, J. Wallace, and D. Estrin*

2-145 **HIGH-FREQUENCY SOURCE PROPERTIES OF THE 2010 M 7.2 SIERRA EL MAYOR EARTHQUAKE FROM LOCAL, REGIONAL, AND TELESEISMIC DATA** *T. Uchide and P.M. Shearer*

Working Group on California Earthquake Probabilities

Abstracts

PYLITH: A FINITE-ELEMENT CODE FOR MODELING QUASI-STATIC AND DYNAMIC CRUSTAL DEFORMATION (2-021)

B.T. Aagaard, C.A. Williams, M. Knepley, and S.N. Somala

We have developed open-source finite-element software for 2-D and 3-D dynamic and quasi-static modeling of crustal deformation. This software, PyLith (current release is 1.5), combines the quasi-static viscoelastic modeling functionality of PyLith 0.8 and its predecessors (LithoMop and Tecton) and the wave propagation modeling functionality of EqSim. The target applications require resolution at spatial scales ranging from tens of meters to hundreds of kilometers and temporal scales for dynamic modeling ranging from milliseconds to minutes or temporal scales for quasi-static modeling ranging from minutes to thousands of years. PyLith development is part of the NSF funded Computational Infrastructure for Geodynamics (CIG) and the software runs on a wide variety of platforms (laptops, workstations, and Beowulf clusters). Binaries (Linux, Darwin, and Windows systems) and source code are available from geodynamics.org. PyLith uses a suite of general, parallel, graph data structures called Sieve for storing and manipulating finite-element meshes. This permits use of a variety of 2-D and 3-D cell types including triangles, quadrilaterals, hexahedra, and tetrahedra.

Current features include prescribed fault ruptures with multiple sequential earthquakes and aseismic creep, spontaneous fault ruptures with a variety of fault constitutive models, time-dependent Dirichlet and Neumann boundary conditions, absorbing boundary conditions, time-dependent point forces, and gravitational body forces. PyLith supports infinitesimal and small strain formulations for linear elastic rheologies, linear and generalized Maxwell viscoelastic rheologies, power-law viscoelastic rheologies, and Drucker-Prager elastoplastic rheologies. Current development focuses on performance improvements and adding additional bulk and fault constitutive models. We also plan to extend PyLith to allow coupling of quasi-static and dynamic simulations to resolve multi-scale deformation across the entire seismic cycle.

GROUND PENETRATING RADAR (GPR) SURVEY OF THE SAN ANDREAS FAULT AT THE BIDART FAN AND OTHER POTENTIAL RESEARCH SITES IN THE CARRIZO PLAIN (1-094)

S.O. Akciz, L. Grant Ludwig, and R. Kaufmann

Excavations of the Bidart Fan reveal evidence of six surface ruptures since ~A.D. 1350 and suggest that the Carrizo section of the San Andreas fault ruptured, on average, every 88 years (45-144 yr for individual intervals) since ~A.D. 1350 (Akciz et al., 2010). Excavations of two deeply incised and offset channels on the Bidart Fan suggest that slip during past earthquakes varied through time, and were not as uniform as previously thought (Grant Ludwig et al., 2010). Higher resolution slip-per-event data is needed to constrain the slip and magnitudes of the last six surface ruptures. Due to logistical restrictions on excavations within the National Monument Land, we are conducting a Ground Penetrating Radar (GPR) survey of the Bidart Fan and other potential research sites to locate subsurface channels and promising stratigraphy for future detailed 3D excavations. GPR uses high frequency electromagnetic waves to acquire subsurface information. Energy is radiated downward into the ground from a transmitter and is reflected back to a receiving antenna. The reflected signals are recorded and produce a continuous cross-sectional "picture" or profile of shallow subsurface conditions. Reflections of the radar wave occur where there is a change in the dielectric constant or electric conductivity between two materials. Changes in conductivity and in dielectric properties are associated with natural hydrogeologic conditions such as bedding, cementation, moisture, clay content, voids, faults, and fractures.

Data will be processed using EKKO VIEW deluxe software (Sensors & Software).Gains and filters will be applied to optimize the reflections in the GPR data. The GPR data will be displayed as cross-sections, with anomalous features such as buried channels and faults annotated on the cross-sections. This abstract is due on the first day of our GPR field work. Results will be presented at the SCEC meeting. If successful, collected subsurface GPR data, combined with our paleoseismic data will provide a unique characterization of the shallow structure of the San Andreas Fault in the Carrizo Plain.

SCEC USEIT MEDIA TEAM (1-001)

E. Alaniz, N. Ballew, H. Chen, J. Rodriguez, E. Soto, R. de Groot, T. Jordan, T. Huynh, and M. Ihrig

The task of the 2010 USEIT Media Team was to capture the experience of the USEIT intern class and demonstrate how students from across the country came together for eight weeks to achieve the Grand Challenge. We collaborated with four other multi-disciplinary teams to accurately portray the roles of each group in achieving the Grand Challenge for this year. The first stage of the movie making process was to create a script. As we revised different editions of the script, we were challenged to effectively describe USEIT and the Grand Challenge. It was important for the Media Team to portray the struggles that the interns faced to show our audience the nature of the USEIT program. Coming from different backgrounds,

the interns learned to collaborate and develop software used by scientists. Footage obtained over the course of the internship was edited and assembled into a final product. In order to accomplish our task, we first learned how to operate the camera and audio equipment as well as how to edit audio and video using a media editing software. To help the interns remember their summer experience, the Media Team facilitated the SCEC Intern T-Shirt design process. We were also responsible for assisting in planning the USEIT poster session at the SCEC Annual Meeting so that the posters and computers were presented in a logical manner.

SEISMIC VELOCITY STRUCTURE OF THE SAN JACINTO FAULT ZONE FROM DOUBLE-DIFFERENCE TOMOGRAPHY AND EXPECTED DISTRIBUTION OF HEAD WAVES (2-150)
A.A. Allam and Y. Ben-Zion

We present initial results of double-difference tomographic images for the velocity structure of the San Jacinto Fault Zone (SJFZ), and related 3D forward calculations of waves in the immediate vicinity of the SJFZ. We begin by discretizing the SJFZ region with a uniform grid spacing of 500 m, extending 140 km by 80 km and down to 25 km depth. We adopt the layered 1D model of Dreger & Helmberger (1993) as a starting model for this region, and invert for 3D distributions of VP and VS with the double-difference tomography of Zhang & Thurber (2003), which makes use of absolute event-station travel times as well as relative travel times for phases from nearby event pairs. Absolute arrival times of over 78,000 P- and S-wave phase picks generated by 1127 earthquakes and recorded at 70 stations near the SJFZ are used. Only data from events with Mw greater than 2.2 are used. Though ray coverage is limited at shallow depths, we obtain relatively high-resolution images from 4 to 13 km which show a clear contrast in velocity across the NW section of the SJFZ. To the SE, in the so-called trifurcation area, the structure is more complicated, though station coverage is poorest in this region. Using the obtained image, the current event locations, and the 3D finite-difference code of Olsen (1994), we estimate the likely distributions of fault zone head waves as a tool for future deployment of instrument. We plan to conduct further studies by including more travel time picks, including those from newly-deployed stations in the SJFZ area, in order to gain a more accurate image of the velocity structure.

OBSERVATIONS OF SURFACE WAVE AZIMUTHAL ANISOTROPY IN SOUTHERN CALIFORNIA (2-152)
C.R. Alvizuri and T. Tanimoto

We use the Southern California Seismic Network as an array and apply a beamforming method to determine the Rayleigh surface wave phase velocities and their arrival directions for 190 teleseismic events. Analysis of the phase velocities reveals the ubiquitous pattern of azimuthal phase velocity variation of Rayleigh waves for an anisotropic medium. Our analysis confirms azimuthal dependence on the 2-theta component. We also confirm the assumption of most studies that the contribution by the 4-theta component is negligible. Though these results are consistent with the theory for weak anisotropic media and results from tomography, we have not seen similar direct measurements reported elsewhere.

We show that anisotropy is present in the period range 15-50 seconds which corresponds approximately to 50-200 km wavelengths, and suggests anisotropy extends to the upper mantle. The array aperture has limited resolution of azimuthal phase velocity variations for periods above 100 seconds. This is evident in the large error bars of measurements in this range. Our analysis shows an prevalent anisotropic fast axis that is oriented along the direction SE-NW (110/290 degrees clockwise from North). This direction is interesting in that it is sub-parallel with the Mohave section of the San Andreas Fault. It is this section of the fault that is misaligned with the general direction of the North America-Pacific Plate boundary. Thus we speculate that the fast axis alignment may be associated with shear and compression of the Transverse Ranges.

GPS MONITORING OF THE SAN BERNARDINO MOUNTAINS AND INLAND EMPIRE FOR SLIP RATE MODELING OF SOUTHERN CALIFORNIA PLATE BOUNDARY FAULTS (1-137)
B.J. Anderson, J.C. Duncan, J.N. Bywater, K.K. Chung, M.R. Swift, S.F. McGill, J.C. Spinler, A.D. Hulett, and R.A. Bennett

Although there has been no major earthquake on the southern San Andreas fault (SAF) in more than two centuries, the surrounding crust still moves. This crustal deformation causes strain accumulation on the SAF as well as the San Jacinto fault (SJF) and many others in the area. To get a better picture of how much strain is currently building on these faults, we used precise Global Positioning System (GPS) surveying to measure site velocities within the San Bernardino Mountains and surrounding areas, and we modeled these data along with site velocities from SCEC's Crustal Motion Model 4 (CMM4) to characterize crustal deformation within a transect across the plate boundary using two-dimensional elastic half-space models in MS Excel. We tested hundreds of thousands of slip rate combinations to find which combinations provide a good fit to the site velocities. From the combinations that produce the best-fitting lines, our results showed that the faults west of the SJF system could have total slip values of 4.5 to 13.5 mm/yr with the individual faults at: San Clemente: 0-1mm/yr, San Diego Trough: 0-1mm/yr, Palos Verdes: 0-5mm/yr, Newport-Inglewood: 0-

3mm/yr, and Elsinore: 0-8mm/yr. The SJF-SAF system could have total slip of 15 to 26 mm/yr with the two faults at: SJF: 2-24mm/yr, SAF: 0-20mm/yr. The Eastern California Shear Zone had totals from 13 to 17 mm/yr with the individual faults at: Helendale: 0mm/yr, Lenwood: 1.5-2mm/yr, Emerson: 6.7-8.7mm/yr, West Calico: 0mm/yr, Pisgah: 2.2-2.9mm/yr, Ludlow: 1.5-2mm/yr, Red Pass Lake: 0.7-1mm/yr, and Baker: 0.4-0.5mm/yr.

DISTRIBUTION OF EARTHQUAKE CLUSTER SIZES IN THE WESTERN UNITED STATES AND IN JAPAN (1-033)
J.G. Anderson and K. Nanjo

Earthquakes occur in clusters, which classically are described as either foreshock-mainshock-aftershock sequences or swarms. A simple algorithm is defined to assign all earthquakes in a seismicity catalog to a cluster, where the minimum cluster size is one earthquake. This was applied to seismicity catalogs for Japan, southern California, and Nevada. Cluster sizes measured by the number of earthquakes in the cluster exhibit an approximately power-law frequency distribution. Cluster durations are bounded by a line asymptotic to K^0.5, where K is the number of earthquakes in the cluster. Normalized to overall seismicity, the frequency of clusters is spatially variable: highest in southern California, intermediate in Nevada, and lowest in Japan.

SPECIFYING INITIAL STRESS FOR DYNAMIC HETEROGENEOUS EARTHQUAKE SOURCE MODELS (2-035)
D.J. Andrews and M. Barall

Dynamic rupture calculations, using heterogeneous stress drop that is random and self-similar, with a power-law spatial spectrum, have great promise of producing realistic ground motion predictions. We present procedures to specify initial stress for random events with a target rupture length and target magnitude. The stress function is modified in the depth dimension to account for the brittle-ductile transition at the base of the seismogenic zone. We have no arbitrary fault barriers; rather, slip stops naturally in regions of shear stress increase. Self-similar fluctuations in stress drop are tied in this work to the long-wavelength stress variation that determines rupture extent. Heterogeneous stress is related to friction levels, in order to relate the model to physical concepts. In a variant of the model, there are high stress asperities with low overall sliding stress. For equal moment and rupture extent, the slip function has higher peaks (a heavier-tailed distribution) in the asperity model.

STYLE OF DEFORMATION AND EARTHQUAKE RISK ASSESSMENT: A COMPARISON BETWEEN CALIFORNIA AND MEDITERRANEAN COUNTRIES (1-055)
A. Baltay, M. Nyst, T. Tabucchi, and P. Seneviratna

Large earthquakes are typically underrepresented in the historical record due to their long return periods. As a result, insurance companies cannot turn to their past loss experiences to understand the financial implications posed by these large earthquakes. Additionally, insurers need to understand the full profile of seismic events that could impact their exposure. For these reasons, insurance companies utilize seismic hazard models to assess risk. In this presentation, metrics employed to quantify risk are used to discuss the impact of various styles of tectonic deformation on earthquake risk assessment. Seismic risk in California is compared to that of Portugal, where risk is determined by long return period, large magnitude events; Italy, where the highest risk is posed by moderate magnitude, relatively frequent events; and Turkey, with an earthquake risk profile similar to that in California. Modern catastrophe models use probabilistic approaches to take into account the full range of event magnitudes, using average annual losses (AAL) and loss-exceedance curves to analyze risk profiles.

AAL is calculated by summing the product of the expected loss level and the annual rate for all possible events affecting the exposure. In many regions, such as Italy, the more frequent moderate magnitude earthquakes will contribute most significantly. Thus, insurers need to quantify the impact of the full range of magnitudes. By annualizing the expected losses due to events of varying severities and recurrence intervals, annual premium rates can be set with longer term risk planning in mind.

The loss-exceedance curve is also derived from the full suite of seismic events that could impact the insured exposure. This curve represents the probability of exceeding a particular loss level in a year, often expressed as return period, the simple inverse of the corresponding probability. Loss-exceedance curves provide insurers with the quantification needed to assess solvency issues and manage their portfolios. Although similar to ground motion hazard curves, a fundamental difference in the loss curve is its link to the spatial distribution of the portfolio. Even in a small region, different exposure concentrations can lead to significantly different risk profiles.

Using these metrics, we compare the risk in three different tectonic regions in the Mediterranean to the risk in California, and highlight the advantages of a probabilistic approach to risk modeling.

EARTHQUAKE EARLY WARNING DEMONSTRATION TOOL (EEWDT) (1-054)
M. Barba, M. Boese, and E. Hauksson

An earthquake early warning (EEW) system may help mitigate the damage expected from a major earthquake. Over the past four years, the California Integrated Seismic Network (CISN) has tested the real-time performance of three algorithms for EEW in California, including the τc-Pd on-site warning algorithm (Kanamori, 2005; Wu et al., 2007; Böse et al., 2009ab).

We have developed the Earthquake Early Warning Demonstration Tool (EEWDT) to assess the potential performance of an EEW system in California based on the τc-Pd algorithm. For a given earthquake scenario, EEWDT displays the real-time P- and S-wave propagation, the stations that have recorded and transferred data (depending on the processing and telemetry delays specified), and the estimated magnitude, epicenter location, and corresponding uncertainties. EEWDT also shows the warning-time available at a given user location, as well as the estimated seismic intensity at this site.

For simulating the performance of the EEW system, we developed error models that were calibrated with real-time and off-line testing observations of the τc-Pd algorithm. The model for magnitude estimation includes both the inter- and intra-event variability of the τc-magnitude relation. We applied the Monte Carlo Method to simulate the potential performance in the EEWDT based on these error models. Statistical error models for other EEW algorithms can be easily incorporated into EEWDT.

EEWDT will aid in optimizing the CISN for EEW and in explaining EEW to potential users.

TOMOGRAPHY OF THE MOJAVIAN LITHOSPHERE VISCOSITY FROM SPACE GEODETIC DATA OF THE LANDERS AND HECTOR MINE EARTHQUAKES (2-031)
S. Barbot and Y. Fialko

We investigate the transient deformation following the 1992 Mw 7.3 Landers and the 1999 Mw 7.1 Hector Mine earthquakes using a combination of GPS and InSAR for an interval spanning 1992 to 2010. We test the possible mechanisms of postseismic relaxation using physically-based time-dependent models of deformation driven by coseismic stress changes. Considered mechanisms include viscoelastic flow, afterslip and poroelastic rebound. We find that both afterslip and viscoelastic relaxation models can explain the horizontal post-Landers GPS data equally well. Afterslip however gives rise to vertical displacements of opposite polarity to the ones measured by GPS. A viscoelastic model marked by a strong (high viscosity) lower crust and weak (low viscosity) upper mantle transitioning at a depth of 40 km gives rise to large wavelength LOS deformation in the near field which is not fully compatible with the InSAR data. Poroelasticity models are consistent with wavelength of InSAR LOS displacements and campaign GPS vertical data, but cannot explain alone the azimuth and amplitude of horizontal displacements. None of these simple models can explain all the available geodetic measurements simultaneously and a more complex explanation is required, involving either multiple mechanisms or more spatial variations in material properties. Assuming that forward models of deformation are separable in space and time we devise a linear inversion to infer the amplitude and location of source mechanisms required by all the geodetic data. For the post-Landers data a model combining viscoelastic relaxation in the lower crust and the upper mantle and poroelastic rebound best reduces the data. Afterslip taking place on the down-dip extension of the rupture may accompany a broader viscoelastic flow but simultaneous inversion of the post-Landers and post-Hector Mine data supports a combination of poroelastic rebound and viscoelastic relaxation in the lower crust and upper mantle as the dominant mechanisms of transient deformation. Resolution of available data is not sufficient to rule out a gentle gradient of viscosity between the lower crust and upper mantle yet the preferred model implies distinct viscous flows in the lower crust and upper mantle (below 50 km) separated by a mantle lid. Lateral variations in viscosity are stronger in the lower crust than in the upper mantle and are marked by a lower-crustal low-viscosity zone in the South West towards the San Bernardino Mountains.

SIMULATIONS OF SLIP HISTORY ON FAULTS WITH HETEROGENEOUS RATE-WEAKENING AND RATE-STRENGTHENING PROPERTIES (2-084)
S. Barbot, N. Lapusta, and J.-P. Avouac

Variations in friction are thought to be an important factor controlling the magnitude and the long-term timing of events in earthquake cycles. Numerous investigators have related spatial variability in interseismic coupling on transform faults and subduction zones to variations in effective friction properties on a fault. Recent findings of the SAFOD experiment on the San Andreas Fault revealed the presence of fault minerals with velocity-strengthening behavior at aseismic slip rates and low static friction coefficients.

Motivated by these observations, we investigate the influence of large variations in frictional properties on the rupture of individual earthquakes and the long-term behavior of faults. To these ends, we consider rate- and state-dependent friction models of earthquake cycles with fully dynamic ruptures. The models include statically weak areas with velocity-strengthening friction neighboring statically strong areas with velocity-

weakening friction. In particular, we concentrate on the transition region from unstable to stable friction assuming a heterogeneous fault with inclusions of stable asperities in the nominal seismogenic zone and inclusion of deeper unstable patches in the creeping domain. We test whether heterogeneous friction properties around the depth of seismic/aseismic transition may explain a wide range of fault slip phenomena from regular earthquakes to slow-slip events. Deeper velocity-weakening patches may also lead to anomalously deep earthquakes or propagation of seismic episodes deeper than the typical depth extension of possible nucleation (and hence microseismicity). Reciprocally, we assess the influence of stable asperities above the bottom of seismicity on the presence of high frequency content of seismograms and hypocenter locations in multiple earthquake cycles. A future goal is to test the hypothesis that the apparent low strength of mature faults is fully or partially due to spatial variations in frictional properties of fault rocks.

RELATIVE CONTRIBUTION OF STABLE AFTERSLIP AND VISCOELASTIC RELAXATION FOLLOWING THE 2004 PARKFIELD EARTHQUAKE (2-032)
S. Barbot, L. Bruhat, and J-P. Avouac

The 2004 Parkfield, CA earthquake was a long-expected event which ruptured the San Andreas fault between the creeping segment, to the North and the locked one to the South. The presence of multiple geodetic and seismic instruments surrounding the epicenter allowed to record in detail many aspects of the rupture and subsequent motion on and surrounding the fault. In particular, many studies have shown the complementary location of coseismic slip and afterslip on the fault plane. The postseismic relaxation following the 2004 event was dominated by afterslip, which cumulated a total equivalent geodetic moment that is comparable to the moment released coseismically. A relatively large postseismic moment is not generally observed at other locations and implies a large area to partake in stable creep. Using all available data, including continuous GPS and synthetic aperture radar interferograms (InSAR), we test whether some of the data may be explained by a viscoelastic relaxation of a weak lower crust or whether the strong inferred postseismic moment is only explained by stable (aseismic) afterslip on the fault plane surrounding the coseismic rupture. We document a strong tradeoff between inferred viscoelastic flow and deep afterslip below the coseismic rupture. Assuming that time series of predicted viscoelastic flow following the 2004 rupture is separable in space and time, we divise a linear inversion scheme that resolves the relative contribution of afterslip and viscoelastic flow as a function of time. We find that models that account for viscoelastic flow may not require slip on a deep extension of the fault plane, as opposed to models that imply afterslip as the only mechanism of postseismic relaxation. Resolution of available data does not allow the discrimination between the so-called ''jelly sandwich'' and ''crême brulée'' models. A viable model, assuming viscoelastic relaxation in the lower crust and upper mantle requires the joint occurrence of some afterslip on the down-dip extension of the fault that ruptured coseismically and viscoelastic flow in the deeper substrate. We therefore conclude that a classic scenario of the earthquake cycle that includes creep on fault roots and stick-slip motion at the surface should be extended to a more general view of the earthquake cycle partitioned into stick-slip motion in the predominantly seismogenic zone, stable creep in a fault root and a transition to broad viscoelastic flow at greater depth.

COSEISMIC OFFSETS ON PBO BOREHOLE STRAINMETERS: REAL, OR SPURIOUS? (1-138)
A.J. Barbour and D.C. Agnew

We have observed coseismic strain offsets during many significant earthquakes, at all locations in the 74-instrument PBO borehole strainmeter (BSM) network. Offsets typically occur during the passage of body waves from local earthquakes, rather than from teleseismic surface waves. The M7.2 El Mayor-Cucapah earthquake of April 4, 2010 induced the largest offsets thus far, on BSMs located within the San Jacinto fault zone - the "Anza cluster". Here we present a preliminary analysis of trends in the observed offsets for these sites, as well as inspection of their inferred borehole lithology. We speculate that these static offsets are controlled more by localized geologic constraints than by triggered fault slip, as has been suggested in previous studies (e.g. Linde and Johnson, 1989).

IDENTIFYING GROWTH OF STRUCTURES IN THE ZAGROS FOLD AND THRUST BELT: INITIAL TIME SERIES RESULTS AND EVALUATION OF PRECIPITABLE WATER VAPOR EFFECTS (1-143)
W.D. Barnhart and R.B. Lohman

The Zagros Fold and Thrust Belt (ZFTB) of western and southwestern Iran accommodates active collision between the Arabian and Eurasian plates. GPS surveys reveal current convergence rates of 25-36 mm/yr, with roughly half of the shortening accommodated in the ZFTB. While rates of seismicity in the ZFTB are high, large (>Mw 7.0), surface rupturing earthquakes are rare, and calculations of seismic moment rates suggest that only 10-30% of the total shortening is accommodated seismically. Thus, a significant amount of strain must be accommodated aseismically, presumably though the growth of the large whale-back anticlines characteristics of the ZFTB. In this work, we present the initial results of an InSAR time series analysis in the Bandar-Abbas region of the southern ZFTB where strain rates calculated from campaign GPS surveys are high relative to regions to the east. We aim to identify interseismic strain accumulation and growth of the folds in order to

better our understanding of the relative roles of seismic and aseismic deformation on the formation of long lived geologic structures. We implement the Small Baseline Subset (SBAS) time series approach to calculate line of sight (LOS) surface velocities from 29 ENVISAT Track 435 acquisitions between May 2003 and May 2010. In addition to a complete time series, we also present pre- and post-seismic time series from the same data set calculated relative to the 25-March 2006 Mw 5.7 Fin earthquake.

A key assumption of SBAS is that correlated atmospheric noise is random in sign in time and should have zero effect on the time series. To investigate if the seasonal distribution of available dates induces a biased atmospheric noise signal that may contribute to our computed LOS velocities, we use MODIS precipitable water vapor data to analyze the potential effects of our data distribution. We create synthetic "interferograms" by differencing MODIS data acquired in the same month as the SAR imagery and compute a time series using the same process as for the ENVISAT data. We begin with an approach in which we use data acquired on the same day as our SAR acquisitions and create the same data pairs that are used in the InSAR time series. We also explore a stochastic approach where we generate many combinations of acquisition dates that are within the same month of the SAR acquisitions.

THE EFFECT OF WATER ON TRIGGERING OF STICK SLIP BY OSCILLATORY LOADING (2-095)
N.M. Bartlow, D.A. Lockner, and N.M. Beeler

Most laboratory stick-slip experiments are conducted with dry samples. However, seismogenic faults likely have hydrostatic or super-hydrostatic fluid pressure. Recent observations that non-volcanic tremor activity can be modulated by earth tides imply that deep fault pore pressure may be near-lithostatic. We are exploring the effect of varying effective stress on stick slip events in simulated faults. Wet cylindrical westerly granite samples containing 30° inclined saw-cuts are deformed in a triaxial apparatus at 50 MPa confining pressure. We impose a constant driving velocity of 0.1 microns/s, superimposed with a sinusoidal driving velocity of varying amplitude and period. This sinusoid is a perturbation to the background stressing rate, such as from the solid earth tides or from a local transient effect. We determine the amplitude that produces stick-slip events that are correlated with the sinusoid at a variety of frequencies. We compare these wet experiments to the previous dry experiments of Lockner and Beeler, JGR, 1999 (further analysis in Beeler and Lockner, JGR, 2003) and find that for 1 atm pore pressure at low frequency, the addition of water does not change the correlation amplitude. At higher frequencies water inhibits correlation and the fault seems immune to the sinusoidal perturbations, even when the amplitude is large enough to induce sizable reversals. This may be an effect of the characteristic diffusion time of the granite causing it to behave as if it is undrained at high frequencies.

Additionally, there are two clear failure modes in both wet and dry experiments; at low frequency we observe threshold failure whereas at high frequency we observe a nucleation-dominated failure mode in which rate-dependent friction becomes important. This is evident in the phase of the oscillatory loading that is correlated with stick-slip. In the threshold failure mode, the stick-slip events are correlated with the peak stressing rate, while in the nucleation-dominated mode they are correlated with the peak stress. We have also found that at all frequencies, the stick-slip events have more consistent amplitudes compared to dry experiments. We hypothesize this is caused by water inhibiting the formation of surface gouge. Finally, we have tested lower effective stress by increasing pore pressure to 20MPa to study the effect of effective stress on triggering. These experiments show smaller stress drops compared to those without imposed pore pressure.

OFF-FAULT DAMAGE AND FAULT ZONE COMPLEXITY ASSOCIATED WITH A LOCALIZED BEND IN THE SAN GABRIEL FAULT (2-068)
A.W. Becker, F.M. Chester, and J.S. Chester

Mechanical models of dynamic fault slip demonstrate the importance of variations in mechanical properties and locally variable stress states in fault-bordering damage zones, and non-planar and discontinuous fault geometries on the propagation and arrest of earthquake ruptures. This study examines the variation in mesoscale damage and structural fabric along a continuous, but non-planar mature fault zone. In particular, we are investigating fault zone structure in the vicinity of a macroscopic-scale bend in the North Branch of the San Gabriel Fault (NBSGF), an extinct branch of the San Andreas Fault located within the San Gabriel Mountains of southern California. The NBSGF is a near-vertical, strike-slip fault with 16 to 22 km of right-lateral displacement that has been exhumed several km and that cuts granodiorite and other rocks of the San Gabriel basement complex. This ongoing field study includes detailed mapping at a scale of 1:10,000 along an 8 km portion of the NBSGF, quantification of the mesoscale fault-density and fault-kinematic data, and collection of oriented hand samples for microstructural analysis. Through mapping we have documented that the NBSGF along the West Fork of the San Gabriel River occurs as two, relatively planar, hard-linked fault segments, each extending 10+ km along strike. The two segments differ in strike by 13˚, from an orientation of 105˚ west of the bend to 092˚ east of the bend. The fault is identified by the local increase in

damage intensity as the fault is approached, and by the juxtaposition of different rock units along the fault surface. The fault surface is defined by an ultracataclasite layer. A series of six exposures of ultracataclasite within a 2 km stretch centered on the bend clearly document the continuity of the fault surface and the change in strike through the bend. Linear fracture density traverses perpendicular and parallel to the fault zone show a general decrease in density with distance from the fault consistent with other studies; however, the fracture density and subsidiary fault kinematics is highly variable on both sides and along strike through the bend of the fault, possibly due to the non-planar fault surface or the variable nature of the host rocks. Current work is focusing on comparing the mesoscale data from different structural domains in the vicinity of the bend, and analyzing the microscale structure of the samples collected from the damage zone of the fault.

A NATURALLY CONSTRAINED STRESS PROFILE THROUGH THE MIDDLE CRUST IN AN EXTENSIONAL TERRANE (2-012)

W.M. Behr and J.P. Platt

We present a method in which paleopiezometry, Ti-in-quartz thermobarometry (TitaniQ), and 2-D thermal modeling can be used to construct naturally constrained stress profiles through the middle crust in areas of exhumed mid-crustal rocks. As an example, we examine the footwall of the Whipple Mountains metamorphic core complex (WMCC). Rocks in the WMCC were initially deformed at ~20 km depth by distributed ductile shear, and were then progressively overprinted by localized ductile shear zones and eventually by discrete brittle fracture as the footwall was cooled and exhumed toward the brittle-ductile transition (BDT). Increasing localization and cooling during exhumation allowed earlier microstructures to be preserved, and rocks in the WMCC therefore represent several 'points' in temperature-stress space (and by inference depth-stress space). We identify enough of these stress-depth points to construct a complete profile of the flow stress through the middle crust to a depth of ~20 km, from which we derive regional estimates of the ambient stresses in the brittle upper crust, the peak strength at the brittle-ductile transition, and the integrated strength of the continental crust in this region during Miocene extension.

Maximum differential stress reached ~130 MPa just below the brittle-ductile transition at a depth of ~9 km; values up to 200 MPa likely reflect transient stresses related to seismic events on the Whipple detachment fault. Stress levels are consistent with Byerlee's law in the upper crust assuming a vertical maximum principal stress and near-hydrostatic pore fluid pressures and suggest a coefficient of friction on the Whipple fault of 0.4. Stress dropped to 15-20 MPa at 18 km depths and 500 C. For strain rates typical of actively deforming regions (10^-12 to 10^-15 /s), our stress profile is bracketed by the Hirth et al. (2001) flow law for wet quartzite, whereas the flow law of Rutter and Brodie (2004) overestimates the strength of this particular region.

DEFORMATION ASSOCIATED WITH THE 2010 SIERRA EL MAYOR, BAJA CALIFORNIA EARTHQUAKE FROM CAMPAIGN GPS MEASUREMENTS (2-027)

D. Ben-Zion, G.J. Funning, and M.A. Floyd

The April 4, 2010 M7.2 Sierra El Mayor, Baja California earthquake occurred close to the mapped Laguna Salada fault system near the international border between the US and Mexico. The objective of this project is to use data gathered south of the border in Baja California to analyze the displacements that occurred during and after the earthquake and hence investigate the properties of the crust near Laguna Salada.We, along with researchers from Scripps Institute of Oceanography and CICESE, surveyed 13 campaign sites in the epicentral region to gather postseismic GPS data several times in the months after the earthquake. The time series that these data will provide will be especially useful for constraining the styles of postseismic deformation in the area. We processed this data using GAMIT/GLOBK software and used GMT plotting utilities to create several time series for post seismic ground motion. We also processed data from these and several other sites in the Southern California region, held in the SCEC archive and elsewhere, to present a map of velocity vectors during the decade of seismic inactivity preceding the earthquake. By combining our processed pre- and post-seismic data, we estimate the displacements due to coseismic fault slip along that region of the Laguna Salada fault. We hope to use the time series derived from the postseismic GPS data to determine the mechanisms of postseismic deformation, and thus the frictional, viscoelastic and/or poroelastic properties of the crust in this area.

EPISODIC TREMOR AND SLIP ON A FRICTIONAL INTERFACE WITH CRITICAL ZERO WEAKENING IN ELASTIC SOLID (2-094)

Y. Ben-Zion

Non Volcanic Tremor (NVT) and related relatively weak and slow slip events, termed jointly Episodic Tremor and Slip (ETS), are observed below the seismogenic sections of numerous subduction zones and major strike-slip faults. These events have several distinguishing characteristics including moment-duration scaling relation with exponent less than 2, intermittency and flickering behavior, relatively small slip, high

susceptibility for triggering, and temporal occurrence with numerous periodicities. Here we show with analytical and numerical results that a frictional fault in elastic solid with a strip below the seismogenic zone having critical zero weakening during slip provides a simple unified explanation for the diverse observed phenomena associated with ETS. The results imply that ETS have little to no predictive power on the occurrence of large events in the overriding seismogenic zone. Additional model predictions that should be tested with future high-resolution observations are fractal slip distributions and failure areas, potency/moment proportional to area and duration proportional to effective source radius (producing together the observed moment-duration scaling), discrete power law frequency-moment statistics with exponent 3/2 and exponential tapering, overall scale-invariant potency/moment time histories, and parabolic (or exponential) source time functions for event sizes measured by duration (or moment).

AN EXPERIMENTAL AND THEORETICAL STUDY OF ASYMMETRIC EARTHQUAKE RUPTURE PROPAGATION CAUSED BY OFF-FAULT FRACTURE DAMAGE (2-069)
H.S. Bhat, C.G. Sammis, and A.J. Rosakis

The interaction between a dynamic mode II fracture on a fault plane and off-fault damage has been studied experimentally using high-speed photography and theoretically using finite element numerical simulations. In the experimental studies, fracture damage was created in photoelastic Homalite plates by thermal shock in liquid nitrogen and rupture velocities were measured by imaging fringes at the tips. Two cases were studied: an interface between damaged and undamaged Homalite plates, and an interface between damaged Homalite and undamaged polycarbonate plates. Propagation on the interface between damaged and undamaged Homalite is asymmetric. A ruptures propagating in the direction for which the compressional lobe of its crack-tip stress field is in the damage (which we term the 'C' direction) is unaffected by the damage. In the opposite 'T' direction, the rupture velocity is significantly slower than the velocity in undamaged plates at the same load. Specifically, transitions to supershear observed using undamaged plates are not observed in the 'T' direction. Propagation on the interface between damaged Homalite and undamaged polycarbonate exhibits the same asymmetry, even though the elastically "favored" '+' direction coincides with the 'T' direction in this case indicating that the effect of damage is stronger than the effect of elastic asymmetry. This asymmetric propagation was also simulated numerically by incorporating the micromechanical damage mechanics formulated by Ashby and Sammis (PAGEOPH, 1990) into the ABAQUS dynamic finite element code. The quasi-static Ashby/Sammis formulation has been improved to include modern concepts of dynamic fracture mechanics, which become important at the high loading rates in the process zone of a propagating rupture.

DO SUPERSHEAR RUPTURES AFFECT AFTERSHOCK STATISTICS? (2-119)
P. Bhattacharya, R. Shcherbakov, K.F. Tiampo, and L. Mansinha

Though supershear ruptures were theoretically predicted more than 30 years ago and first reported about 25 years ago for the 1979 Imperial Valley event, the fact that they are not particularly rare has become clear only recently. Supershear ruptures produce a seismic shock wave, similar to the sonic boom from supersonic airplanes, and possibly increase the destructive potential of the seismic event. It has been recently reported that the aftershocks of all the known supershear earthquakes are distributed preferentially away from the main fault plane due to off fault stress redistributions produced by this supershear boom. The occurrence of supershear ruptures is also generally associated with a region of local high pre-stress and an unusually smooth friction profile over the supershear segment, leading to a conspicuous absence of high frequency ground motions. We have considered the aftershock sequences of five well-known supershear earthquakes from around the world (1979 Imperial Valley, 1992 Landers, 1999 Izmit and Duzce and 2002 Denali earthquakes) to test whether the aftershock statistics around the supershear rupture are different from the statistics in the rest of the region due to the aforementioned stress conditions and redistributions. We have looked at the frequency-magnitude distribution in particular in order to study the variation of the b value for each of the sequences and observe statistically significant variations. In particular, we have determined that the b value is always higher in the supershear segment than in the rest of the aftershock region. The Omori Law, however, does not show such clear trends. This leads us to ask the following question: Does pre-stress on faults control the b-value and/or is it controlled by the post-rupture off-fault stress redistribution? In this light, understanding the details of the supershear process might lead to a greater understanding of the relationship of the b value with seismic rupture.

STATUS REPORT ON THE PRECARIOUS BALANCED ROCK ARCHIVE (1-071)
G.P. Biasi and J.N. Brune

Precariously balanced rocks (PBRs) and geologic features can provide constraints on ground motions when the age and conditions for toppling are known. PBRs provide perhaps the only direct measurements of ground motion covering a sufficient time period to test ground motion predictions of SCEC initiatives such as CyberSHAKE. Preliminary comparisons indicate that PBR fragilities are consistent with mean ground motion predictions, but not with extremes that develop by random sampling of uncertain fault properties.

An archive of PBR images and testing results is being developed at the University of Nevada Reno. About 15,000 digital image files compiled over a period of about 18 years are being organized. The image files include both photos of PBRs, and supporting photos of various types. The digital files also include videos intended for 3-D documentation and photogrammetric analysis. One present thread of archive work includes checking locations of rocks, fixing mis-associations, and linking photos where more than one was taken of a given rock. This effort is completed approximately half of the rocks in the southern California PBR Region.

We have also begun a screening process to get an estimate of how much of the archive might be of value for constraining ground motions. The screening consists of a visual classification of the images into a few basic categories, plus, for photos where the analysis can be conducted, rocking angles (alphas) and static overturning accelerations. We used a 2-D analysis code developed by D. Haddad after modifying it to expedite the analysis and improve record keeping. About 3963 photos have been classified, and 2-D analyses conducted on 1773 of them.

Summarizing the categories for sorted images:

1773 "PBR for 2-D analysis";

943 "Supporting photo or non-fragile direction";

248 "distant view of PBR, stack, or field";

205 "duplicate, alternate view";

157 "fragility not evident in photo";

9 "relevance to archive unclear";

98 "fragile stack";

359 "rocking pts not visible; possible PBR";

149 "slab or leaner; no rocking pts";

22 Other.

Summarizing the static overturning angles for analyzed rocks:

975 have at least one alpha < 20 degrees;

628 with at least one alpha < 15 degrees;

324 with at least one alpha < 10 degrees;

59 with both alphas <15 degrees;

328 have a length scale in them, providing a basis for estimating the frequency of shaking to which the rock would be most susceptible.

CORRELATIONS OF PALEOSEISMIC EVENTS ON THE SOUTHERN SAN ANDREAS FAULT: UPDATE TO WGCEP-2 (1-117)

G.P. Biasi, K.M. Scharer, and R.J. Weldon

Characterization of paleoseismically detected events on the southern San Andreas fault (SSAF) in the Working Group on California Earthquake Probabilities 2 report was based on the pearl-stringing methodology of Biasi and Weldon (2009) and event data published as of 2007. We report on a preliminary update to these results using new event dates from sites in Coachella (Philibosian et al., 2009), Pallett Creek (Scharer et al., in prep), Frazier Park (Scharer, pers. comm.), and Bidart Fan (Aksiz et al., 2010). The WGCEP-2 slip rate and 10% aseismic creep model (m2_1) was assumed. Scenarios were graded based on total rupture displacement compared to expected slip since AD 1200. Rupture displacement is scaled from rupture length using the sinesqrt shape from Biasi and Weldon (2009).

With only 810 years of averaging, the patterns among successful scenarios are somewhat less distinct. Some preliminary conclusions: (1) Wall-to-wall are very difficult to accommodate because of the displacement (slip-rate) constriction through Banning and south San Bernardino. Salt Creek to Frazier ruptures do occur, but in scenarios that over-predict averaged displacement by >3.5 m or more. (2) Good total displacement fits can be achieved with 16-20 events in the post-1200 period. This puts the gross average RI since AD 1200 under 50 years(!). (3) The addition of the Frazier Mountain record increases by 2-3 the number of ruptures needed to fit all reported paleoseismic events. (4) Counting 1857 there tends to be about two mid- to high M7-class events since AD 1200 on the Carrizo to Mojave reach. (5) The southern half of the SSAF seems to be

chaotic, with Thousand and Coachella linking only in 1680 and sometimes around 1500. (6) Few scenarios do a good job of reproducing the slip rate change from Banning Pass to the southernmost SSAF. (7) If all ruptures had a lower profile than in the sinesqrt, fewer, longer ruptures could account for the rupture evidence. This may indicate a lower average stress drop for SSAF earthquakes than is implied in the sinesqrt model.

MEMORY-EFFICIENT DISPLACEMENT-BASED INTERNAL FRICTION FOR WAVE PROPAGATION SIMULATION (1-019)
J. Bielak, H. Karaoglu, and R. Taborda

The incorporation of intrinsic attenuation into time domain simulations of seismic wave fields is a key ingredient for the realistic modeling of transient wave propagation in soil and rock materials. The general subject of intrinsic wave attenuation is vast and has applications in many fields. In recent years, most of the proposed rheological models for anelasticity have been based on first-order mixed velocity-stress formulations of the equations of elastodynamics. While this formulation is extensively used in finite difference and occasionally in finite element approximations, most finite element wave propagation formulations use displacements as the only dependent variables. We present here a new internal friction model with Q as the defining parameter, based on a displacement-only formulation. We describe the model initially for a fiber, and then extend it to three-dimensional elstodynamics. We present the applicability of the proposed anelastic model with two examples which we solved using Hercules—the parallel octree-based finite element simulator developed by the Quake Group at Carnegie Mellon University. Using this model allows us to cover a large frequency range with an almost constant Q value and a maximum error of five percent.

FACTORS INFLUENCING STRESS-DROPS OF SMALL EARTHQUAKES IN SOUTHERN CALIFORNIA (2-040)
P. Bird and P.M. Shearer

Shearer et al. [2006] determined Brune-type stress-drops of 65,564 relocated M ~1.5–3.1 earthquakes in southern California (1989–2001) by using spectral methods with signal/noise quality control, empirical local Green's functions, and source and station corrections. They found that stress-drop appears to increase with depth when it is computed by assuming uniform shear velocity. However, stress-drop is not correlated with magnitude, focal mechanism, or distance from the nearest fault. We begin further analysis by recomputing each stress-drop using the local shear velocity from the Harvard version of the Community Velocity Model. Stress-drop versus burial depth now shows a weak peak at 11 km and another sharp peak (probably an artifact) at 1 km. We use the heat-flow map of Blackwell & Steele [1992] to estimate temperature at each hypocenter, and study the separate effects of temperature (at constant depth) and burial depth (at constant temperature). Median stress drop rises with temperature up to ~250 C, after which it declines. Median stress-drops on the declining branch are positively correlated with burial depth, but those on the rising branch are not. We interpret the rising branch as showing that shallow-crustal stress-drops are proportional to the amount of interseismic fault healing (as in rate-and-state friction theory). This is further supported by a finding that median stress-drops are correlated with tectonic strain-rates from the preferred model of Bird [2009], with exponent of -0.2, when hypocentral temperature is below 200 C. We interpret the depth- and temperature-dependent median stress-drops for temperatures above 300 C to show that these stress-drops are scaled by the preseismic tectonic shear stress around the future hypocenter, which is controlled by temperature and by a gradient of composition (sialic to mafic) with burial depth. Separating stress-drops by tectonic terrane leads to other small differences; in particular, stress-drops are about 75% higher within the Sierra Nevada. Combining all of these predictors, we are still only able to explain ~14% of the variance in log(stress-drop). Post-model residual stress-drop factors have approximately a log-normal distribution with standard deviation of 0.47 decades (if some high-side outliers are discounted). Thus, we have obtained some valuable hints about earthquake physics, but have not achieved a capacity to forecast stress-drops of future earthquakes.

ACCELERATED HOLOCENE SLIP ACROSS THE SOUTHERN SAN JACINTO FAULT ZONE INFERRED FROM 10BE AND U-SERIES DATING OF LATE QUATERNARY LANDFORMS (1-110)
K. Blisniuk, M.E. Oskin, W. Sharp, K. Fletcher, and T. Rockwell

To constrain which mechanisms may govern long-term fluctuations in deformation rate, we combined 10Be surface exposure and U-series dating of faulted landforms to determine geologic slip rates for the Clark and Coyote Creek fault strands of the San Jacinto fault zone. By testing for slip-rate variability on these two parallel strands we may infer whether fault strength or variable loading rate fluctuate over time. Our results from 5 sites - 2 along the Coyote Creek fault, and 3 along the Clark fault - imply that late Quaternary slip rates have varied considerably along strike and in time. Spatial slip rate variability is shown by a pronounced southward decrease of the rate along the Clark fault strand over the past 50-30 kyr, from ~13 mm/yr at Anza to 8.9 ± 2.0 mm/yr at Rockhouse Canyon to 1.5 ± 0.4 mm/yr near the southern Santa Rosa

Mountains, as slip is transferred from the Clark fault strand to the Coyote Creek fault strand and to nearby zones of distributed deformation. Temporal slip rate variability is shown by an apparent increase of slip rates from the ~35-5 ka interval to the ~5-0 ka interval on both these faults. Measurements at Anza, across Rockhouse Canyon and Ash Wash, and the southern Santa Rosa Mountains yield slip rates of 6.2 ± 3.0 mm/yr, 8.7 ± 2.8 mm/yr, and 1.8 ± 0.9 mm/yr, respectively, during the time interval ~35 ka to ~5 ka, and of 16.3 ± 4.7 mm/yr, 12.6 ± 3.8 mm/yr, and 3.1 ± 0.9 mm/yr, respectively, since ~5 ka. Our observed apparent coordinated increase in Holocene slip rate for the Clark and Coyote Creek fault strands may be attributed to cycles of strain hardening and strain weakening of a shared ductile shear zone at the base of the San Jacinto fault zone.

EARTHQUAKE EARLY WARNING IN SOUTHERN CALIFORNIA USING REAL TIME GPS AND ACCELEROMETER DATA: LESSONS FROM THE MW 7.2 2010 EL MAYOR-CUCAPAH EARTHQUAKE (2-122)

Y. Bock, R. Clayton, B. Crowell, S. Kedar, D. Melgar, M. Squibb, F. Webb, and E. Yu

The Mw 7.2 April 4, 2010 El Mayor-Cucapah earthquake demonstrated convincingly the power of dense near-source, high-rate, real-time GPS networks for earthquake early warning and rapid earthquake response. With funding from NASA's Advanced Information System Technologies (AIST) program, a robust set of 1 Hz data was collected from over 100 California Real Time Network (CRTN - http://sopac.ucsd.edu/projects/realtime/) GPS stations in southern California with a latency of about 0.4 seconds. These data were inverted to provide on-the-fly total displacement waveforms, which captured the propagation of the S-wave through the southern California crust at stations up to 450 km from the epicenter. By "total displacement" we mean direct measurement of both static and dynamic displacements, previously relegated separately to geodesy and seismology, respectively. While most broadband seismic stations clipped for this earthquake, including the Pinyon Flat Observatory (PFO) about 180 km from the epicenter (although accelerometers at the same sites did not), the real-time GPS stations did not saturate and continued to provide on-scale data. Compared to the current state of the art in recordings of strong ground motions, total displacement waveforms have the advantages that they are measured directly; their signal-to-noise ratio increases with the intensity of shaking; and they include the static (permanent, coseismic) surface deformation as well as any post-seismic displacements and strain transients whether or not these are accompanied by seismic shaking. The higher frequency range is only limited by the sampling rate of the CGPS instruments, which may be extended by optimal combination with higher-rate accelerometer measurements. We discuss lessons learned from this earthquake and earlier earthquakes, in terms of earthquake early warning, on-the-fly optimal combination of GPS and accelerometer data, and rapid estimation of earthquake magnitude and source parameters. A special portlet has been set up on GPS Explorer (http://geoapp03.ucsd.edu/gridsphere/gridsphere) with information on our response to the El Mayor-Cucapah earthquake. In addition, three component 1 Hz seismograms of CRTN GPS stations for this earthquake are available in SAC format at the Southern California Earthquake Data Center (http://www.data.scec.org/).

TOWARDS CSEP TESTING OF SEISMIC CYCLES AND EARTHQUAKE PREDICTABILITY ON THREE MID-OCEAN RIDGE TRANSFORM FAULTS (1-124)

M.S. Boettcher, J.J. McGuire, and J.L. Hardebeck

By contrast to the repeat times of the largest earthquakes on most faults (50-1000 years), the repeat times of the largest earthquakes on many mid-ocean ridge transform faults (RTFs) are remarkably short. Specifically, the largest earthquakes on a segment of Gofar repeat every ~5.5 years [McGuire, 2008], those on Clipperton repeat every ~20 years, and those on a segment of Blanco repeat every ~13.5 years [Boettcher and McGuire, 2009]. These short recurrence intervals make moderate to fast-slipping (6-14 cm/yr) RTFs ideal for testing the concepts of seismic cycles and the importance of renewal processes, where stress builds up for an extended period of time and then is released suddenly in a large earthquake.

We use the Brownian Passage Time model [e.g. Matthews et al, 2002] together with a scaling relation for repeat time of the largest earthquakes on RTFs [Boettcher and McGuire, 2009], a range of stress drops (1-100 MPa), and coefficients of variation (0-0.5) to construct probability density functions (PDFs) of when the next large earthquakes will occur on segments of Gofar, Clipperton, and Blanco RTFs. Similarly we use a scaling relation for the largest expected earthquake [Boettcher and Jordan, 2004] to construct magnitude PDFs for the next large earthquake on these faults. Finally, we constructed uniform boxes with sizes based on estimates of location error in the Global Centroid Moment Tensor (CMT) catalog, as spatial PDFs. The spatial PDFs are centered on the CMT location of the previous event. Combining these temporal, spatial, and magnitude PDFs, we have developed earthquake predictions for five RTF fault segments. We will be implementing these predictions into the Center for Earthquake Predictability (CSEP) global testing center over the next few months. While these fault segments show quasiperiodic behavior, there is also some natural variability in both the timing and the moment of individual ruptures. This variability presumably results from heterogeneity of material properties along the fault and from time-dependence of both the stressing-rate on

the fault-zone and the fault's strength. Using the CSEP process, we will objectively develop a quantitative understanding of this variability and assess whether a renewal process is active on these RTF segments.

TEMPORAL AND SPATIAL VARIATION IN SLIP ALONG THE SOUTHERN STRAND OF THE KARAKORAM FAULT SYSTEM, LADAKH HIMALAYAS (1-089)
W.M. Bohon, J.R. Arrowsmith, and K. Hodges

The NW-SE striking, dextral Karakoram fault system stretches for more than 1200 km from the Pamirs of Central Asia at least as far SE as the Kailas area of Tibet. Geodetic studies show slip rates between 1-3 mm/yr, studies on offset geomorphic features find slip rates between 4-11 mm/yr while the reconstruction of offset geologic features indicate rates as high as 32 mm/yr. In the Ladakh region of NW India (~ 33°28'N, 78°45'E), the fault system bifurcates into 2 subparallel fault strands bounding the Pangong Range (~110 km along the faults x 10 km wide). Mictrotectonic and thermochronologic studies of ductile deformation fabrics along these strands suggest that slip began in the Miocene, and Brown et al. (2002) documented Quaternary right-lateral slip along the northern strand at ~4 mm/yr on the basis of 2 debris flows offset 1-2 m and 45 m. The lack of documented Quaternary offset along the southern strand has led most researchers to assume that Quaternary slip on the Karakoram fault system in this region was partitioned exclusively to the northern strand.

However, recent field work in the Pangong Range and adjacent Nubra Valley provides the first documentation of significant Quaternary activity along the southern fault strand. Along this strand in the Tangyar Valley surfaces of different ages (dates pending) show varying amounts of displacement. The oldest surface, an incised alluvial fan, has erosional risers offset ~150 m right laterally with east side up (consistent with the sense of motion for the fault system in this region --Searle et al., 1998). On a younger adjacent debris flow-dominated alluvial fan, older debris flows show likely offset and deflection across the fault while younger flows show no disruption. The lack of faulting on the younger surfaces along the southern strand coupled with the evidence of recent faulting along the northern strand may indicate that slip along the southern strand has stopped or significantly decreased and that slip is now partitioned primarily to the northern strand. Unless the slip and displacement from both strands are considered, the overall Quaternary rate of slip and total displacement along this part of the fault system may be underestimated. Determining these slip rates is essential for answering first-order questions about the evolution and behavior of the Karakoram fault system in this region, slip partitioning between subparallel strike-slip faults, and regional seismic hazard potential.

PROGRESS ON MODELING SURFACE DEFORMATION IN THE NEW MADRID SEISMIC ZONE (2-030)
O. Boyd, Y. Zeng, A. Frankel, and L. Ramirez-Guzman

We model the surface deformation and strain rate signal associated with post-earthquake effects and steady-state creep on deeply buried faults beneath the Mississippi embayment and compare these results with geodetic observations. This comparison has yet to be done primarily because of expectations of low signal-to-noise ratio. Improvements in the precision of geodetic monitoring indicate very low rates of surface deformation, which appear to be inconsistent with the return periods of large earthquakes in the New Madrid seismic zone. We build upon previous studies and seek to answer the following questions: How do subsurface faulting and steady-state creep, if present, translate into surface deformation? What are the far- and near-field drivers of stress, and how do they affect surface deformation? The answers to these questions will help us to constrain and address questions significant for earthquake hazard assessments.

We present estimates of constant and time-variable surface deformation. The former results are derived from models in which steady-state creep occurs on lower crustal faults within the New Madrid seismic zone subject to various boundary conditions. The latter, time-variable surface deformation estimates, result from modeling the viscoelastic relaxation in the lower crust/upper mantle after earthquakes on faults within the New Madrid seismic zone. Our best fitting model, 1.5 mm/yr of slip imposed across a discontinuity along the downdip extension of the reverse-slip Reelfoot fault, can explain 43% of the variance in the geodetic observations. In an alternative model, 20% of the variance can be explained by 3.5 mm/yr of slip across the downdip extension of the right-lateral strike-slip Cottonwood Grove fault. If modeled together, 1.5 mm/yr on downdip extensions of both faults best explains the data with 46% variance reduction. For models involving viscoelastic relaxation, our best fitting model has 1 m of slip on both the Reelfoot and Cottonwood Grove faults during the 1811-1812 earthquakes and can explain 18% of the variance in the geodetic observations. We continue this investigation by studying the effect of a finite lower crustal dislocation in the presence of regional and far field drivers rather than imposing slip across the dislocation locally. We also begin to assess the uncertainty in the geodetic observations to better appreciate the amount of signal in the data and whether we can expect to achieve 15 - 45% variance reduction.

3DV: INTERACTIVE EARTHQUAKE VIEWER (1-028)
E. Boyd, R. Welti, and R. de Groot

The 3D Viewer of earthquake data, 3DV, is a collaborative project between the Southern California Earthquake Center (SCEC) and the Incorporated Research Institutions for Seismology (IRIS). The IRIS Interactive Earthquake Browser (IEB) is a two-dimensional Google map that combines the IRIS Data Management Center's extensive database of earthquake epicenters with Google's web interface. As an extension to IEB, 3DV is an interactive web application that displays the same real-time data in a three dimensional environment and is capable of user navigation and rotation.

Because embedded Flash and Java have limited web browser support, a combination of HTML5 and jQuery was the ideal technology for this data visualization tool. HTML5, the new standard for web structuring and design, allows for a rich Internet application. And since jQuery is essentially a JavaScript library, it is a more efficient approach to coding and offers many plug-ins that already handle difficult features.

As a modified and updated version of existing code, 3DV can dynamically load an XML file from IRIS's IEB and display up to a thousand events around the globe. Each event is currently shown as a red sphere and assigned a radius value to reflect its magnitude. The user has the option to rotate the globe around the x, y, and z axes and zoom in and out. In addition, 3DV can present several pre-selected regions of interest and the earthquakes that occur in those regions. With room for expansion, 3DV will eventually incorporate useful features and be used as a learning tool in schools.

EFFICIENT NUMERICAL MODELING OF SLOW SLIP AND QUASI-DYNAMIC EARTHQUAKE RUPTURES (2-039)
A.M. Bradley and P. Segall

We are developing a two-dimensional quasi-dynamic simulation of faulting that includes rate-and-state friction, thermal pressurization, dilatancy (following Segall and Rice [1995]), and flash heating [Rice, 2006]. We hypothesize that at low effective normal stress, dilatancy stabilizes velocity-weakening faults against dynamic slip, while at higher effective stress, thermal pressurization overwhelms dilatancy, which leads to dynamic rupture. We consider half-space models of subduction zones with depth-variable friction (based on lab experiments on gabbro) and low effective stress in the 25-37 km depth range. We find that, generically, a simulated earthquake cycle includes a large dynamic event (DE); a quiescent period; and then, preceding the next DE, a long sequence of slow slip events (SSE) that penetrate updip with time. Predicted behavior bears many similarities to SSE in Cascadia.

Partial differential equations (PDE) in pressure and temperature are solved on profiles normal to the fault. The diffusion equations are discretized in space using finite differences. The mesh is nonuniform with greater density near the fault. The system of equations is a semiexplicit index-1 differential algebraic equation (DAE) in slip, state, fault zone porosity, pressure, and temperature. We integrate state, porosity, and slip explicitly; solve the stress-balance equation on the fault; and integrate pressure and temperature implicitly. For speed, we adaptively switch between this DAE time-integration technique and a pure-ODE approach; the latter is faster but less accurate. We use relative error control to calculate the time step adaptively. The nonlinear equations in pressure, temperature, and slip speed decouple by fault cell and so at each time stage, many relatively small nonlinear equations are solved. The primary work is solving linear systems associated with solving the nonlinear equations. For efficiency, we group fault cells by physical properties, perform only one sparse LU factorization per group, and efficiently update the factorization at each solve, yielding a method that is linear in the number of diffusion profile nodes. We approximate the elasticity matrix relating slip and stress by a hierarchical low-rank representation to speed up matrix-vector products. We parallelize the software to work on a shared-memory system using OpenMP.

OPENSHA IMPLEMENTATION OF THE GCIM APPROACH FOR GROUND MOTION SELECTION (1-056)
B.A. Bradley

Ground motion selection is known to be an important step in seismic hazard and risk assessment. There have been numerous procedures proposed for selecting ground motions ranging from somewhat ad-hoc guidelines specified in seismic design codes to more rigorous approaches which have found favour in the research-community, but are not yet applied routinely in earthquake engineering practice.

The most common method (often specified in seismic design codes) for selecting ground motion records for use in seismic response analysis is based on their 'fit' to a Uniform Hazard Spectrum (UHS). This is despite the fact that many studies have highlighted the differences between the UHS and individual earthquake scenarios, and therefore its inappropriateness for use in ground motion selection.

The reluctance of the earthquake engineering profession to depart from UHS-based selection of ground motions is arguably because of its simplicity to implement relative to methodologies with sounder theoretical

bases. To this end, the aim of the present work was to implement a recently developed Generalised Conditional Intensity Measure (GCIM) approach for ground motion selection (Bradley, 2010) into the open-source seismic hazard analysis software OpenSHA (Field et al. 2003).

APPLICABILITY OF FOREIGN GROUND MOTION PREDICTION EQUATIONS FOR NEW ZEALAND ACTIVE SHALLOW EARTHQUAKES (1-058)

B.A. Bradley

The number of instrumental ground motion records in New Zealand (NZ) has increased significantly in recent years due to an increase in the number and quality of seismometer throughout NZ. Figure 1 provides a comparison between NGA ground motion database and the NZ database developed as part of this study. Despite this increase in instrumental data there is a lack of empirical records from large magnitude events observed at near-source distances. This lack of ground motion records from large magnitude near-source records, which typically dominate seismic hazard analyses, makes it difficult to develop robust ground motion prediction equations used in seismic hazard analysis based on NZ data alone.

In this study an alternative approach to empirical ground motion prediction equation development was taken. Firstly, the applicability of various foreign ground motion prediction equations (derived using plentiful data) to NZ were considered. The consideration was based on both the dependence of the inter- and intra-event residuals as a function of several predictor variables, and also the general predictor variable scaling of the various models. Secondly, the model exhibiting the best applicability to NZ was modified based on theoretical and empirically-driven considerations to better represent the NZ data.

The NZ-specific GMPE developed exhibits large magnitude and near-source scaling based on global ground motions, and small magnitude and large distance scaling constrained by the NZ ground motion database. The developed model is also applicable for 23 vibration periods from 0.01 to 10 seconds making it applicable for emerging displacement-based design procedures.

EARTHQUAKE NUCLEATION MECHANISMS AND PERIODIC LOADING: MODELS, EXPERIMENTS, AND OBSERVATIONS (2-088)

B. Brinkman, G. Tsekenis, Y. Ben-Zion, J. Uhl, and K. Dahmen

The project has two main goals:

(a) Improve the understanding of how earthquakes are nucleated -- with specific focus on seismic response to periodic stresses (such as tidal or seasonal variations)

(b) Use the results of (a) to infer on the possible existence of precursory activity before large earthquakes.

A number of mechanisms have been proposed for the nucleation of earthquakes, including frictional nucleation (Dieterich 1987) and fracture (Lockner 1999, Beeler 2003). We study the relation between the observed rates of triggered seismicity, the period and amplitude of cyclic loadings and whether the observed seismic activity in response to periodic stresses can be used to identify the correct nucleation mechanism (or combination of mechanisms).

A generalized version of the Ben-Zion and Rice model for disordered fault zones and results from related recent studies on dislocation dynamics and magnetization avalanches in slowly magnetized materials are used in the analysis (Ben-Zion et al. 2010; Dahmen et al. 2009). The analysis makes predictions for the statistics of macroscopic failure events of sheared materials in the presence of added cyclic loading, as a function of the period, amplitude, and noise in the system. The employed tools include analytical methods from statistical physics, the theory of phase transitions, and numerical simulations. The results will be compared to laboratory experiments and observations.

TRIGGERING BY SEISMIC WAVES AND IMPLICATIONS FOR EARTHQUAKE PREDICTABILITY (invited talk)

E.E. Brodsky

Triggering by seismic waves has been well-documented since the early 1990's. These situations provide a window into rupture initiation by providing natural experiments during which the triggering stresses in the seismic wave can be measured. We have calibrated a relationship between the seismicity rate change and the amplitude of the perturbing stresses. This relationship provides a measure of the strength distribution on faults and its regional variability. For instance, the degree of triggerability shows that the faults in the Western US as a population are closer to failure than the ones in Japan.

The connection between ground-shaking and seismicity rate change also provides a method of calculating time-dependent earthquake probabilities. Since the ground-shaking increases the probability of an earthquake systematically, using the observed map of shaking can result in a few percent gain in earthquake probability for long-range triggering and much more significant gains in the nearfield. These degrees of

predictability are comparable to the current generation of stochastic (ETAS-like) forecasts and the shaking-based relationship can be shown to be identical in form to the empirical statistical formulations. However, using dynamic triggering relations provides the first forecasting based in part on a physical observable (amplitude of seismic waves).

A final implication of dynamic triggering is that extremely large earthquakes, like the 2004 M9.2 Sumatra event, produce significant enough shaking to trigger earthquakes globally. Since long-range triggering appears to decay following the same, gradual Omori's Law observed for local earthquakes, these farflung sequences can persist and cascade into occasional large events. Using reasonable aftershock productivity and triggering rates, the recent spurt of M8 earthquakes can be explained ass aftershocks of Sumatra.

TWO POTENTIAL TRIGGERS FOR LARGE RUPTURES ALONG THE SOUTHERN SAN ANDREAS FAULT: SECONDARY FAULT DISPLACEMENT AND LAKE LOADING (1-103)
D. Brothers, D. Kilb, K. Luttrell, N. Driscoll, and G. Kent

The southern San Andreas Fault (SSAF) in California has not experienced a large earthquake in approximately 300 years, yet according to paleoseismic studies the average recurrence for the previous five ruptures is about 190 years. As a large SSAF earthquake seems imminent, it is important to understand how crustal stress perturbations can promote or inhibit fault failure(s). This work is aimed at understanding two potential earthquake triggers along a 60 km section of the SSAF that has been periodically submerged during high-stands of the large late-Holocene Lake Cahuilla (LC). A large expanse of LC sediments along with the southern termination of the SSAF are covered by today's Salton Sea. Geophysical surveys and cone penetration tests in the Salton Sea have allowed us to identify LC parasequence sets and correlate onshore and offshore stratigraphy. Detailed analysis of growth faulting provides a robust record of 10-15 paleo-displacement events during the last 14 LC parasequences. Throw-plots show that displacement is discrete and punctuated, and that continuous creep is not a significant contributor to the cumulative throw. Seven events appear coincident across three offshore faults, four of which were potentially synchronous with SSAF ruptures. Observations suggest that each time the Colorado River floods a dry basin (identified by both channelization and coarsening along parasequence boundaries), displacement occurs along each of the three offshore faults. In summary, these records indicate coincident timing between (1) LC flooding and displacement along secondary normal-oblique faults and (2) displacement on secondary faults and paleoearthquakes along the SSAF. To study the potential hazards these phenomena present to the SSAF, we calculate static stress perturbations from LC flooding and rupture of secondary faults beneath the Salton Sea. The geometry of the extensional faults beneath the Salton Sea makes them more sensitive to lake loading effects (increased pore pressure and bending stress). We find that displacement along the offshore faults, whether triggered by lake loading or by tectonic stresses, can increase the coulomb failure stress along the SSAF greater than 0.6 MPa. These results highlight the importance of studying lake level fluctuations and paleoseismic records along secondary faults, as both have the potential to modulate earthquake cycles on major plate boundary faults.

2010 CMS IMPLEMENTATION (1-005)
D. Brown, M. Contreras, A. Deolarte, J. Walker, T. Jordan, R. de Groot, T. Huynh, K. Welch, and M. Ihrig

Undergraduate Studies in Earthquake Information Technology (USEIT) is an undergraduate research internship that is managed by the Southern California Earthquake Center (SCEC) at the University of Southern California. A group of diverse undergraduate students from all over the nation are chosen each year to work as a team to complete a "Grand Challenge." The 2010 Grand Challenge was to develop a Seismic Crisis Visualization System using the Southern California Earthquake Center Virtual Display of Objects (SCEC-VDO) to display information needed for operational earthquake forecasting.

Using an open source content management system called Drupal, the Content Management System (CMS) Implementation Team was able to deliver resources to an array of audiences. As a part of the CMS Implementation Team, our goal was to continue adding content to the already existing USEIT website which can be accessed at http://scec.usc.edu/internships/useit/. One of the features created this year was a progress tracker that informs SCEC's staff and interns on each of the group's progress, goals, tasks, and notes throughout the Grand Challenge. To further our contribution to the Grand Challenge, the CMS Implementation Team was responsible for collaborating with the remaining groups and delivering the content to a broad array of audiences. Collectively gathering SCEC-VDO animations created by the SCEC-VDO Production Team and scientific research information from the Science Research Team gave us the opportunity to create a seismic event page that discusses operational earthquake forecasting and information explaining probabilistic earthquake forecasting. Collaborative efforts with the SCEC-VDO Development Team resulted in developing the ability to live stream the Real-time Earthquake Plug-in. The USEIT intern site is constantly being updated with the ambitions to become a more resourceful site for the general public.

HIGH FREQUENCY VIBRATIONAL WEAKENING OF FAULT ZONES: NEW INSIGHTS FROM HIGH VELOCITY EXPERIMENTS WITH IMPLICATIONS FOR NATURAL EARTHQUAKE FAULT ZONE DYNAMICS (2-086)
K.M. Brown and Y. Fialko

We present evidence that experimental (and natural?) shear zones generate near field high frequency vibrational energy at frequencies of 0.1 to 1 kHz or more. This generates short-lived elevated peak slip and energy dissipation rates on asperity contacts (by potentially >10x above nominal average slip rates) that greatly enhances dynamic fault weakening above that expected for nominal average near seismic slip velocities. Such high frequency vibrational energy should be intrinsic to both experimental and natural systems. The near field frequency distribution is governed by the normal stress, local field wall rock rigidity at the time of slip, nominal average slip velocity, and the velocity weakening process (in addition to fault roughness and other local structural complexes in natural systems). Such high frequency energy (0.1 to > 1kHz) tends to be attenuated rapidly in many sediments or extensive zones of fault damage and we predict essentially comprises a highly significant "hidden weakening term" in the dynamic energy balance of many earthquake faults.

A CATALOG OF LOW FREQUENCY EARTHQUAKE ACTIVITY FROM TRIGGERED TREMOR ON THE SAN JACINTO FAULT (2-103)
J.R. Brown

In this study I catalog swarms of deep low frequency earthquakes within triggered tremor on the San Jacinto fault in southern California. The excitation of tremor waveforms of the following three earthquakes are examined: November 3, 2002 Mw 7.9 Denali, AK; August 3, 2009 Mw 6.9 Gulf of California; and July 7, 2010 Mw 5.4 Collins Valley, CA. Similar to deep tectonic tremor activity in subduction zones (e.g. SW Japan, Cascadia, Costa Rica, Alaska), the triggered tremor in southern California appears to consist of a series of low frequency earthquakes (LFEs). I use a running autocorrelation of 2-hour bandpassed filtered waveforms (1-7 Hz) recorded on the Anza and Plate Boundary Observatory networks starting one hour prior to the origin time of the triggering event. In all three cases there is no evidence of a repeating signal prior to the passing of the surface wave train. After aligning events on their S- and P-wave arrivals I am able to forward calculate a starting position for the candidate events and subsequently update their relative locations using differential times from cross-correlation for high precision relocations using double difference methods. Cross-correlation and relocations of LFEs amongst the three triggering episodes share similar waveform features and a common location pattern between 25 and 31 km depth ~20 km northwest of Borrego Springs, CA on the deep extension of San Jacinto fault zone. The LFE sequences reveal a self-similar location pattern for deep triggering of tremor on the San Jacinto fault. In addition, the deep LFE locations imply the San Jacinto fault is a continuous structure to at least 31 km depth similar to deep tectonic tremor observed elsewhere (e.g. Parkfield, CA). Waveforms from this catalog will be useful for a more comprehensive search of deep, spontaneous occurrences of tremor activity as well.

TESTING CONSISTENCY OF PRECARIOUSLY BALANCE ROCKS WITH 2008 PROBABILISTIC SEISMIC HAZARD MAPS AND CYBERSHAKE SA3 VALUES IN SOUTHERN CALIFORNIA (1-074)
J.N. Brune, M.D. Purvance, R. Graves, S. Callaghan, E. Deelman, E. Field, T. Jordan, G. Juve, K. Kasselman, P. Maechling, G. Mehta, K. Milner, D. Okaya, P. Small, and K. Vahi

In Purvance et al. (2008, Bull. SSA), the overturning fragilities of precariously balanced rocks (PBRs) were parameterized as a function of a vector of the ground motion intensity measures peak ground acceleration (PGA) and response spectra at 1 sec (Sa1). The resulting failure probabilities (OPs) for several of the PBRs were very high, suggesting they were inconsistent with the 2002 USGS ground motions. Here we make an approximate comparison with the 2008 hazard maps by comparing the PGA-Sa1 vector components with the PBR fragility plots. PGA and Sa1 values are taken from the USGS website. A recent draft manuscript by Graves et al. (2010) indicates that the Sa3 values from the 2008 hazard maps and the corresponding Cybershake Sa3 values are about the same for rock sites. For the sake of a rough comparison we assume the same is true for Sa1 values and thus similar conclusions follow whether Sa1 values are estimated from the 2008 maps or extrapolated from Cybershake Sa3 values. PGA values have decreased somewhat between the 2002 and 2008 maps. However, the Sa1 values have decreased significantly, and in some cases this has resulted in a significant decrease in OPs. Approximate changes in OPs for an earthquake with 2% in 50 yr PGA and Sa1 values, from the 2002 to 2008 hazard maps are: Aliso Canyon 2, >>.9 to ~.9; Pacifico 1,~.9 to ~.6; Lovejoy Buttes 12a, >>.9 to ~.9; Lovejoy Buttes s11, >>.9 to ~.9; Black Buttes 1, >>.9 to ~.9; Lake Mirage 1, >.9 to ~ .5; Victorville3, >>.9 >>.9; Victorville 7, >>.9 to~.9; Benton Road, ~.9 to ~.8. Thus, the OPs at many sites remains high, near .9. This suggests that the 2008 2% in 50 yr hazard estimates are still inconsistent with the PBRs. For the 1% maps the discrepancy would obviously be even greater. Since the Cybershake results exclude background seismicity, and assuming the path and site effects are taken care of, we conclude that the earthquake source representation is the primary cause for the remaining discrepancy. We suspect that the reason for this is the large amount of aleatory variation assumed in the UCERF2 source parameterization

(stress drop and magnitude), possibly coupled with assumptions used in generating the CyberShake rupture variations (rupture velocity and rupture direction). This conclusion is also suggested by the great increase in hazard (possibly un-physical) at low probabilities (10-6).

2010 VDO-PRODUCTION TEAM (1-003)
K. Brunner, L. Gelbach, S. Romero, A. Valencia, B. Walters, T. Jordan, R. de Groot, and M. Ihrig

The "Grand Challenge" for the 2010 Undergraduate Studies in Earthquake Information Technology (USEIT) intern class was to develop a Seismic Crisis Visualization System based on Southern California Earthquake Center - Virtual Display of Objects (SCEC-VDO) that can display information needed for operational earthquake forecasting. This includes displaying seismic sequences in real time, kinematic fault rupture models, and probabilities of ruptures on earthquake faults. The Production Team incorporated the above information into animations using SCEC-VDO to be delivered to a wide variety of audiences and organizations. Another responsibility of the Production Team was to work closely with the Development Team to report any bugs with the SCEC-VDO software, test new plug-ins, and identify where existing functionality needed to be improved. The Production Team also collaborated with the Science Research Team to learn about the topics to be displayed in their animations and with the Content Management Team to assemble metadata and publish animations. The Production Team made animations about the 2010 El Mayor-Cucapah earthquake sequence using relocated hypocenter data from Dr. Egill Hauksson at Caltech to depict the northward trend of triggered events. Animations were also created using new plug-ins to demonstrate how CyberShake's theoretical earthquakes would affect the Los Angeles area and to show UCERF participation probabilities on the important faults in Southern California. In addition to those accomplishments, the Production Team also created SCEC-VDO tutorials so that future interns and other users would know how to use the software and the new plug-ins.

DO EARTHQUAKES ON LARGE STRIKE-SLIP FAULTS FOLLOW A GUTENBERG RICHTER DISTRIBUTION? (1-130)
S.A. Bydlon, W.L. Ellsworth, and G.C. Beroza

We address the important question of the magnitude-frequency distribution for large strike-slip faults. Some recent studies have argued in favor of Gutenberg-Richter distribution, while others have argued for statistics that favor large earthquakes of a characteristic size. In an initial examination of this question, we considered the century-long instrumental catalog of earthquakes for two large strike-slip faults that ruptured along most of their length during the 20th century: the Queen Charlotte-Fairweather Fault in western Canada and southeastern Alaska, and the North Anatolian Fault in Turkey. For each of these faults, we analyzed the available earthquake catalogs, took into consideration their detection thresholds, and tested the confidence with which the observed earthquake activity could be considered a realization of a Gutenberg-Richter distribution using the Kolmogorov-Smirnoff test on the cumulative distributions. The relatively inaccurate locations in both areas prevent us from restricting our analysis to earthquakes on the fault itself. Instead, we were forced to consider earthquakes from a band of substantial width (~100 km) astride the fault. We tested over a range of possible b-values to construct a 95% confidence interval bounding an area believed to contain the true b-value if one exists. We found that in both cases the seismicity could be considered a realization of a Gutenberg-Richter distribution. The confidence interval for the Queen Charlotte region spans a b-value range of 0.5-0.63 and for the North Anatolian Fault spans 0.54-0.88. However, the near total lack of moderate earthquakes along the rupture zones of the M 7-8 events suggests that the Gutenberg-Richter distribution may not accurately characterize the size distribution of earthquakes on individual faults.

NONLINEAR VIBRATION AND DYNAMIC STABILITY OF HIGH-RISE SPECIAL STRUCTURE (1-038)
A.S. Bykovtsev, R.A. Abdikarimov, S.P. Bobanazarov, and D.A. Khodzhaev

The new composite materials open amazing opportunity in engineering practice for designing and creation of strong, easy and reliable high-rise special structure. Now the development of effective computing algorithms for solution of nonlinear problems of dynamics of viscoelastic systems with variable rigidity is hot topic. As continuation of previous research (Bykovtsev, Abdikarimov, Hodjaev and Katz 2003) analysis of nonlinear vibrations and dynamic stability of special structure simulated as shells with variable rigidity in geometrically nonlinear statement will be presented. Usually, "special structure'' refers to innovative long-span structural systems, primarily roofs and enclosures to house human activities. More specifically, they include many types of structures, such as: geodesic showground; folded plates; and thin shells. As an example the viscoelastic orthotropic cylindrical shell with radius R, length L and variable thickness h=h(x,y) will be considered in all details. We count, that by the top part of a shell will be operate under wind loads, and the foundation will be operates under seismic load. The weigh of all materials was taken into consideration. For different seismic loads simulation Bykovtsev's Model was used for generating the ground motion (GM) time history. The methodology for synthesizing earthquake GM developed by Bykovtev and based on 2D-analytical solutions by Bykovtsev (1979&1986) and 3D-analytical solutions by Bykovtsev-Kramarovskii (1987&1989) constructed for the single flat fault. This model is based on a kinematics

description of displacement function on the fault and included in consideration of all possible combinations of 3 components of vector displacement (two slip vectors and one tension component). The opportunities to take into consideration both shear and tension vector components of displacement on the fault plane provide more accurate GM evaluations. Radiation patterns and directivity effects were included in the model and more physically realistic results for simulated GM were considered. The equation of movement about a deflection w and displacements u, v was described by system of the nonlinear integro-differential equations in partial derivatives with five various weakly singular kernels of a relaxation. The recurrent formula was received using Bubnov-Galerkin method. The computer codes on algorithmic language Delphi was created and used for research. For real composite materials at wide ranges of change of physical-mechanical and geometrical parameters the behavior of shells were investigated.

EFFECT OF FAULT SEGMENTATION ON DISPLACEMENT TIME HISTORY (2-054)
A.S. Bykovtsev

IS IT APPROPRIATE TO USE SIMPLE BRUNE'S MODEL FOR OBSERVED TIME HISTORY WITH MULTIPLE OSCILLATIONS?

From theoretical point of view the widespread Brune's Model proposed a simple interpretation method for the spectrum of a local small earthquake.

It was OK to characterize the observed spectrum by three parameters:

1. The low-frequency level proportional to the seismic moment.
2. The corner frequency.
3. The power of high-frequency asymptotic decay.

The secondary parameters are usually interpreted by an earthquake source model in which a flat circular rupture plane is formed spreading at a constant speed from the center with a uniform stress drop (Aki 1981).

I see an OUTSTANDING PROBLEM with this approach.

1. The OBSERVED RECORDS in time domain CAN BE QUITE DIFFERENT from those predicted for the FLAT CIRCULAR RUPTURE PLANE MODEL, although the shapes of observed and theoretical amplitude spectra in frequency domain are roughly similar to each other, allowing the source parameter estimation.
2. The simulated time history for displacement of far-field and P and S waves for the flat circular rupture plane is a single spike of a triangle-like shape.
3. However, the OBSERVED TIME HISTORIES are, usually composed of MANY OSCILLATIONS.

Two reasons exist for explanations of these oscillations.

1. Traditional approach: Apparently, the seismic signal arrives along multiple paths due to inhomogeneous structure and spreads over a time length which increases with travel distance. This multipath effect must be modifying the source spectrum in some manner, but the effect has been neglected in the interpretation of the observed spectrum (Aki 1981).
2. New approach based on Bykovtsev's model (Ph.D. Dissertation-1979):

THE OBSERVED TIME HISTORIES OSCILLATIONS REFLECTED MULTIPLE FAULT SEGMENTATIONS!

Effect of fault segmentation on displacement time history of ground motion will be presented for sites located within 6 miles of an active fault. According to AASHTO guide specifications for LRFD seismic bridge design (2009) for sites located within 6 miles of an active fault studies shall be considered to quantify near-fault effects on ground motions to determine if these could significantly influence the bridge response. It will be demonstrated that in near-field (D < 6 miles) ground motion may contain relatively long-duration velocity pulses which can cause severe nonlinear structural response, predictable only through nonlinear time-history analyses.

2010 SAN BERNARDINO MOUNTAINS GPS CAMPAIGN (1-086)
J.N. Bywater, K.K. Chung, B.J. Anderson, J.C. Duncan, M.R. Swift, S.F. McGill, J.C. Spinler, A.D. Hulett, and R.A. Bennett

We conducted a GPS campaign in and around the San Bernardino Mountains, California. Information from these remote sites is filling in a gap where there are little to no recorded velocities. We collected GPS positions from 24 sites over a period of 5 days. Using results from prior years, we calculated velocities for each site, and then used two-dimensional elastic modeling in a spreadsheet to test over a million possible slip rate combinations on 15 faults within a transect that crosses the plate boundary in the vicinity of the San Bernardino Mountains. Using Chi-2 as a criterion, the best-fitting model yielded a slip rate of 5 mm/yr for the San Andreas fault and 16 mm/yr for the San Jacinto fault. However, there is a broad range of San

Andreas and San Jacinto fault slip rates that fit the GPS velocities reasonably well. Among all of the reasonably fitting models, the combined slip rate on the San Andreas and San Jacinto faults is between 15-26 mm/yr. Because these two faults are so geographically close to each other, we found that it is hard to distinguish exactly how much of this strain each fault contributes. We also found that the Eastern California Shear Zone as a whole contributes 13-17 mm/yr of slip, while faults west of the San Jacinto fault contribute 4.5-13.5 mm/yr. Additionally, models using the published geologic slip rates do not fit the GPS velocities at all. This may be because present-day deformation rates, measured by GPS, differ from the long-term averages recorded by geologic offsets.

THE JANUARY 12, 2010, MW 7.0 EARTHQUAKE IN HAITI: CONTEXT AND MECHANISM (invited talk)
E. Calais

[On behalf of colleagues from the Bureau of Mines and Energy and the Universite d'Etat d'Haiti, as well as colleagues and collaborators from several US and French institutions.]

On January 12, 2010, a Mw7.0 earthquake struck the Port-au-Prince region of Haiti, killing more than 200,000 people and causing an estimated $8 billion in damages, ~120% of the country's GDP. Understanding the earthquake and its tectonic context is key to future hazard assessment and robust rebuilding in the region. The earthquake was originally thought to have ruptured the Enriquillo fault of the Southern Peninsula of Haiti, one of two main strike-slip faults accommodating the ~2 cm/yr relative motion between the Caribbean and North American plates.

We will review the tectonic context of the event in the light of a new, comprehensive, GPS velocity field. Together with historical seismicity, GPS-derived fault slip rate estimates confirm that the Southern Peninsula fault zone was -- and remains -- capable of a Mw7.1 or larger event. The data has been integrated in a new seismic hazard map for Haiti which, although still incomplete, provides the first quantitative guidelines for earthquake-safe rebuilding.

The event was followed by a comprehensive data acquisition effort, funded for a large part through NSF's RAPID grant process. We will showcase some of the major science results obtained since the event and discuss their implications for the earthquake source mechanism. Current research shows that the earthquake involved a combination of left-lateral strike-slip and reverse fault slip, consistent with the transpressional nature of regional interseismic strain accumulation. Several models indicate that most of the moment release occurred on an unmapped north-dipping fault, subparallel to -- but different from -- the Enriquillo fault.

RUNNING ON-DEMAND STRONG GROUND MOTION SIMULATIONS WITH THE SECOND-GENERATION BROADBAND PLATFORM (1-016)
S. Callaghan, P.J. Maechling, R.W. Graves, P. Somerville, N. Collins, K.B. Olsen, W. Imperatori, M. Jones, R.J. Archuleta, J. Schmedes, and T.H. Jordan

We have developed the second-generation SCEC Broadband Platform by integrating scientific modeling codes into a system capable of computing broadband seismograms (0-10 Hz) for historical and scenario earthquakes in California. The SCEC Broadband Platform is a collaborative software development project involving SCEC researchers, graduate students, and the SCEC/CME software development group. SCEC scientific groups have contributed modules to the Broadband Platform including rupture generation, low-frequency deterministic seismogram synthesis, high-frequency stochastic seismogram synthesis, and non-linear site effects. These complex scientific codes have been integrated into a system that supports easy on-demand computation of broadband seismograms.

The SCEC Broadband Platform is designed to be used by both scientific and engineering researchers. Users may calculate broadband seismograms for both historical earthquakes (validation events including Northridge, Loma Prieta, and Landers) and user-defined earthquakes. Users may select among various codebases for rupture generation, low-frequency synthesis, high-frequency synthesis, and incorporation of site effects, with the option of running a goodness-of-fit comparison against observed or simulated seismograms. The platform produces a variety of data products, including broadband seismograms, rupture visualizations, and goodness-of-fit plots.

The Broadband Platform was implemented using software development best practices, including version control, user documentation, and acceptance tests, with the aim of ease of use. Users can install the platform on their own machine, verify that it is installed correctly, and run their own simulations on demand without requiring knowledge of any of the code involved. Users may run a validation event, supply their own simple source description, or provide a rupture description in SRF format. Users may specify their own list of stations or use a provided list. Currently the platform supports stations and events in Southern California, the Bay Area, and the Mojave.

In our poster, we will discuss the scientific capabilities of the Broadband Platform. We will describe the software engineering behind the platform development and the rigorous release procedure involved.

Additionally, we will present simulations performed using the platform, including goodness-of-fit results, and discuss potential applications of on-demand broadband seismogram computation.

INTERACTION OF SMALL REPEATING EARTHQUAKES IN A RATE AND STATE FAULT MODEL (2-081)

T. Chen and N. Lapusta

Small repeating earthquake sequences can be located very close, for example, the San Andreas Fault Observatory at Depth (SAFOD) target cluster repeaters "San Francisco" and "Los Angeles" are separated by only about 50 m. These two repeating sequences also show closeness in occurrence time, indicating substantial interaction. Modeling of the interaction of repeating sequences and comparing the modeling results with observations would help us understand the physics of fault slip. Here we conduct numerical simulations of two asperities in a rate and state fault model (Chen and Lapusta, JGR, 2009), with asperities being rate weakening and the rest of the fault being rate-strengthening. One of our goals is to create a model for the observed interaction between "San Francisco" and "Los Angeles" clusters. The study of Chen and Lapusta (JGR, 2009) and Chen et al (submitted to EPSL, 2010) showed that this approach can reproduce behavior of isolated repeating earthquake sequences, in particular, the scaling of their moment versus recurrence time and the response to accelerated postseismic creep. In this work, we investigate the effect of distance between asperities and asperity size on the interaction, in terms of occurrence time, seismic moment and rupture pattern. The fault is governed by the aging version of rate-and-state friction. To account for relatively high stress drops inferred seismically for Parkfield SAFOD target earthquakes (Dreger et al, 2007), we also conduct simulations that include enhanced dynamic weakening during seismic events. As expected based on prior studies (e.g., Kato, JGR, 2004; Kaneko et al., Nature Geoscience, 2010), the two asperities act like one asperity if they are close enough, and they behave like isolated asperities when they are sufficiently separated. Motivated by the SAFOD target repeaters that rupture separately but show evidence of interaction, we concentrate on the intermediate distance between asperities. In that regime, the interaction can be quite complex and varying with time. One of the interesting behaviors is the overlapping rupture areas of events that nucleate on separate asperities. Another interesting behavior is alternating between events that rupture a single asperity and events that rupture both asperities at the same time. These and other features lead to variability of moment and recurrence time for individual repeaters consistent with Parkfield target repeaters.

AN AUTOMATED WAVEFORM WINDOW SELECTION ALGORITHM BASED ON CONTINUOUS WAVELET TRANSFORMS (2-121)

P. Chen and E. Lee

We have developed an algorithm to automatically select waveform windows by using continuous wavelet transform that allows us to analysis waveforms in time-frequency domain. The algorithm is able to select windows from different types of waveforms for full-3D waveform tomography and/or earthquake waveform source inversion. The algorithm has applied on different data types, including earthquake waveforms and ambient noise Green's function waveforms. The process of our algorithm involves four steps: step 1: pre-process waveforms and reject noisy waveforms; step 2: using continuous wavelet transform to convert the input waveforms into time-frequency domain; step 3: applying topological watershed algorithm, a widely used image separation method, on time-frequency spectrum to separate the spectrum into different areas in time-frequency domain; step 4: using inverse continuous wavelet transform to convert the separated areas in time-frequency domain into different windows. For source inversion, we apply the algorithm on data waveforms and select windows of body waves and surface waves to invert optimal source parameters. For waveform tomography, we apply the algorithm both on data waveforms and synthetic waveforms generated from 3-D velocity model and then compare the waveform similarity, phase delay time, amplitude ratio and other properties between data and synthetic windows to select or reject windows.

STUDY OF EARTHQUAKE SOURCE PARAMETERS AND SWARM BEHAVIOR IN SALTON TROUGH (2-110)

X. Chen and P. Shearer

The Salton Trough is located between the southern end of the San Andreas Fault (SAF) and the northern end of the Imperial Fault (IF). The IF to SAF step-over has caused regional subsidence and extension in the southern Salton Sea (Brothers et al., 2009). This region is prone to seismic swarms, some of which are related to aseismic slip (Lohman and McGuire, 2007). In order to constrain the stress state and understand the physical mechanisms of swarms and slow slip events, we analyze the source spectra of earthquakes and study swarm seismicity migration in this region. We obtain Southern California Seismic Network (SCSN) waveforms for earthquakes in the SCEC catalog from 1989 to 2009. We compute displacement spectra, and then isolate source spectra from station terms and path effects using an empirical Green's function (EGF) approach. We obtain stress drops and corner frequencies for 3332 events that have signal-to-noise ratios greater than 3 and are recorded at five or more stations. After applying a spatial-median filter, the spatial

distribution of stress drops is coherent and robust regardless of the EGF used in the calculation. Events in this region generally have stress drops lower than 0.5 MPa. We then search for seismic swarms based on the LSH catalog. We identify 21 seismic clusters, 19 of which are swarms while 2 are mainshock-aftershock sequences. Examination of the temporal-spatial distribution of the events shows that most of the swarms exhibit spatial migration of seismicity. We then develop a robust inversion scheme to solve for the best-fitting 3-D migration vector and velocity. The swarm activities span the Salton Trough region from Bombay Beach to the northern end of the Imperial Fault. The migration vectors have a coherent distribution and their directions are consistent with known plate motions (Brothers et al., 2009). We also study the relationship between swarm properties and stress drop but so far have not found any obvious correlations.

Reference:

Brothers, D. S., N. W. Driscoll, G. M. Kent, A. J. Harding, J. M. Babcock and R. L., Baskin (2009), Tectonic evolution of the Salton Sea Inferred from Seismic Reflection Data, Nature Geoscience, 2(8), 581-584.

Lohman, R. B., and J. J. McGuire (2007), Earthquake Swarms Driven by Aseismic Creep in the Salton Trough, California, J. Geophys. Res., 112, B04405, doi:10.1029/2006JB004596

FREQUENCY DEPENDENCE OF RADIATION PATTERNS AND DIRECTIVITY EFFECTS IN FAR-FIELD GROUND MOTION FROM EARTHQUAKES ON ROUGH FAULTS (1-064)

H. Cho and E.M. Dunham

Primarily unilateral earthquake rupture propagation causes a pronounced directivity effect, where ground motion in the direction of propagation is of larger amplitude than that in the opposite direction. Observations suggest that directivity effects are generally only present at frequencies less than about 1 Hz, and that at higher frequencies, the directivity effect vanishes and the far-field radiation pattern changes from the usual double-couple pattern to an isotropic one. The differences between high and low frequency ground motion have been alternatively explained as either a source effect (with the source losing coherence at short wavelengths) or a path effect (with high frequency waves being preferentially scattered by crustal heterogeneities). In this work we examine whether or not source effects alone can explain the frequency dependence of far-field ground motion. We modeled spontaneously propagating ruptures on rough faults (having self-similar profiles with local slope perturbations of order 10^(-3) to 10^(-2)). The medium was taken to be uniform and isotropic and the simulations were performed in the two-dimensional plane strain geometry. These models produce realistic near-field seismograms with a flat acceleration spectrum at high frequencies. We then constructed an approximate three-dimensional source model by projecting the source onto a high-aspect-ratio fault under the assumption that the rupture process and nonplanar fault topography were everywhere the same across the smaller dimension. We then calculated far-field body wave seismograms and Fourier spectra using the representation theorem. Despite the highly incoherent nature of propagation at short wavelengths (local rupture speeds fluctuate between 0.5 and 1 times the shear-wave speed), the radiation pattern retains the form of a double couple and strong directivity effects are present at all modeled frequencies (up to over 10 Hz). Provided that our representation of the source process and approximations (especially in going from 2D to 3D) have not altered fundamental source properties, then it appears that source effects alone cannot explain frequency-dependent changes in the radiation pattern and directivity effects.

RECONCILING GEOLOGIC AND GEODETIC FAULT-SLIP-RATE DISCREPANCIES IN SOUTHERN CALIFORNIA: CONSIDERATION OF NON-STEADY MANTLE FLOW AND LOWER CRUSTAL FAULT CREEP (2-022)

R.Y. Chuang and K.M. Johnson

In southern California, slip rates derived from geodesy-constrained elastic models are lower than geologic rates along the Mojave and San Bernardino segments of the San Andreas fault and the Garlock fault; in contrast, the summed geodetic rate across the Mojave eastern California shear zone (ECSZ) is significantly higher than the summed geologic rate. We show that geodetic and geologic slip rates in southern California can be reconciled using a viscoelastic earthquake cycle model that explicitly incorporates time-dependent deformation due to non-steady interseismic fault creep in the lower crust and viscous flow in the upper mantle. To reconcile geologic and geodetic rates, our model requires that the southern San Andreas Fault and the Garlock Fault are in the late stages of the earthquake cycle resulting in lower current deformation rates than the cycle-averaged rate. Our model implies that the ECSZ and the San Jacinto faults are in the early stages of the earthquake cycle resulting in high current deformation rates.

RESULTS FROM QUAKE-CATCHER NETWORK RAPID AFTERSHOCK MOBILIZATION PROGRAM (QCN-RAMP) FOLLOWING THE M8.8 MAULE, CHILE EARTHQUAKE (2-107)
A.I. Chung, C. Neighbors, A. Belmonte, M. Miller, A. Sepulveda, C. Christensen, E.S. Cochran, and J.F. Lawrence

Following the 27 February 2010 M8.8 earthquake in Maule, Chile we initiated a QCN Rapid Aftershock Mobilization Program (RAMP). We had an overwhelming number of people eager to participate in the RAMP and rapidly installed 100 USB sensors to record aftershocks. The USB accelerators were deployed in regions directly affected by the mainshock and were densely concentrated in the BioBio region of Chile. Trigger metadata was transferred in real-time and waveform data were recorded continuously at 50 samples per second. Most trigger metadata were received at the QCN server within 7 seconds and waveform data were uploaded in 10 minute-long segments. Using the aftershock trigger data, we refined our triggering and event detection algorithms and tested, retrospectively, whether the network can rapidly and accurately identify the location and magnitude of moderate to large aftershocks (M>4). We are also currently expanding our network in many locations around the world, including Southern California. Because of our low-cost, easy to install sensors, we can quickly deploy a densely distributed network of relatively inexpensive seismic stations throughout a region. Our preliminary results from the data collected from QCN stations around the world suggest that MEMS sensors installed in homes, schools, and offices provide a way to dramatically increase the density of strong motion observations for use in seismic hazard analysis, source rupture imaging, and earthquake early warning.

SIMULATIONS OF SLOW SLIP EVENTS WITH RSQSIM (2-066)
H.V. Colella and J.H. Dieterich

We model slow slip events (SSEs) using the 3D simulation code, RSQSim, which employs rate- and state-dependent constitutive properties to set different modes of fault slip. To develop robust statistical characterizations of slow slip events, we generate long histories consisting of 100,000 events (spanning ~300-500 yrs). For computational efficiency we impose the slip speed for SSEs, otherwise the simulations are fully deterministic in the nucleation, propagation speed, extent of slip, and final distribution of slip. Initial simulations focus on slip along a subduction interface where the mega-thrust is divided into three sections with different sliding characteristics: locked, transition, and continuous creep. The locked zone (<25km depth) corresponds to the section of the mega-thrust that generates great earthquakes, the transition zone (~25-45km depth) corresponds to the section of the mega-thrust that generates SSEs, and the continuous creep zone (>45km depth) corresponds to the section at depth that slides continuously. Based on low stress drops inferred for SSEs, and possible high fluid pressures in this zone, the effective normal stress along the transition zone is assigned a low value of ~3MPa. The simulations generate SSEs with a large range of moments, most of which would be too small to detected geodetically. The largest simulated SSEs are quasi-periodic with equivalent moment magnitudes of M6.5-M7.0. The M>6.5 events are broadly consistent with geodetic and seismic observations for Cascadia SSEs, including total slip, propagation speed, recurrence intervals and scaling of event duration by moment.

INVESTIGATING FAULT EVOLUTION AROUND RESTRAINING BENDS WITHIN A CLAYBOX (2-011)
M.L. Cooke, M.T. Schottenfeld, and J. Moody

We investigate the growth of new faults near a restraining bend within a strike-slip faults system using wet clay analog models. The models simulate conditions similar to that of the southern Big Bend of the San Andreas where new active fault traces have developed within the past 1 My. We explore a range of c restraining bend fault geometries with a servo-controlled claybox. For each experiment, a contraction bend comprised of three kinked segments is cut into the clay. The kink angle and size of the step-over are systematically varied whereas fault dip is vertical in all models. Various basal plate geometries facilitate slip along the kinked fault geometries. During the experiment, the clay is periodically scanned with a 3D laser scanner to document slip, off-fault strain, new fault formation, and uplift. Restraining bends with large kink angle (e.g. 90˚) and large step-over length (e.g. 10 cm) do not exhibit significant strike slip. Instead, new thrust faults develop to form a bivergent pop-up structure that promotes uplift within the contraction bend. Smaller step-over and smaller angle of fault kink promotes strike slip through the restraining bend via the existing fault or the development of new strike-slip faults that splay from the primary fault. The degree of new splay fault development decreases with decreasing step over size and kink angle. The results from this parametric study can be compared to the evolutionary history of the southern Big Bend of the San Andreas to provide insight into the processes controlling abandonment and initiation of active fault strands within this complex system.

ACCELERATED LOADING OF THE SOUTHERN SAN ANDREAS FAULT DUE TO TRANSIENT DEFORMATION IN THE SALTON TROUGH (1-145)
B.W. Crowell, Y. Bock, D.T. Sandwell, and Y. Fialko

The Salton Trough, the transition zone between the spreading center in Baja California and the strike-slip San Andreas fault system, represents one of the most complex zones of active faulting and seismicity in California. It is thought that the southern section of the San Andreas fault may be approaching the end of the interseismic phase of the earthquake cycle, and the Salton Trough may be the nucleation point for the next great earthquake. Throughout 2008 and 2009, we performed 2 rapid static GPS surveys of monuments that stretched from the United States/Mexico border to the northern end of the Salton Sea and had the specific goal of capturing strain transfer through the Brawley Seismic Zone. Here we report on a strain transient centered on the Obsidian Buttes fault just south of the Salton Sea detected from our analysis of a long-history of continuous and campaign GPS measurements. Our best fitting model suggests accelerated slip on the Obsidian Buttes fault between 2001 and 2009, utilizing the Southern California Earthquake Center's Crustal Motion Map 3.0 for temporal comparisons. The associated strain transient has caused an accelerated fault parallel slip rate deficit of 5-7 mm/yr along the southern San Andreas fault near Bombay Beach, corresponding to a Coulomb stress increase since 2001 of ~0.05 MPa/yr centered along the 2009 Bombay Beach seismic swarm. The ongoing strain transient is loading up the transtensional faults in the Salton Sea and the southern San Andreas fault, presumably reducing the time to the expected rupture.

SCEC M8, A REGIONAL SCALE DETERMINISTIC WAVE PROPAGATION SIMULATION USING SCEC AWP-ODC (1-018)
Y. Cui, K.B. Olsen, T.H. Jordan, K. Lee, J. Zhou, P. Small, D. Roten, G. Ely, D.K. Panda, A. Chourasia, J. Levesque, S.M. Day, and P. Maechling

Petascale simulations are needed to understand the rupture and wave dynamics of the largest earthquakes at shaking frequencies required to engineer safe structures (> 1 Hz). Toward this goal, we have developed a highly scalable, parallel application (AWP-ODC) that has achieved "M8": a full dynamical simulation of a magnitude-8 earthquake on the southern San Andreas fault up to 2 Hz. M8 was calculated using a uniform mesh of 436 billion 40-m3 cubes to represent the three-dimensional crustal structure of Southern California, in a 810 km by 405 km area. This production run producing 360 sec of wave propagation sustained 220 Tflop/s for 24 hours on NCCS Jaguar using 223,074 cores. As the largest-ever earthquake simulation, M8 presented tremendous computational and I/O challenges that required collaboration of more than 30 seismologists and computational scientists.

AWP-ODC was composed of pre-processing tools (mesh and dynamic source generator/partitioner), solvers (dynamic fault rupture and wave propagation solvers), and post-processing scripts (validation, derived processing products, data ingestion tool), plus an end-to-end workflow package. AWP-ODC has undergone extensive fine-tuning for M8. On NCCS Jaguar at full system scale, loop-level optimization improved the code performance by 40% (reduced division operations 31%, unrolling 2%, cache blocking 7%), computation/communication overlap by 11%, and reduced algorithm-level communication by 15%. Two other outstanding improvements include the incorporation of an asynchronous communication model (achieved more than ~7x reduction in wall clock time on 223K Jaguar cores) and reduction of I/O time from the original 49% to less than 2% of the wall clock time. Finally, the simultaneous reading of the multi-terabytes mesh/source inputs by thousands of processor cores has reduced initialization time to just a few minutes. The development and improvements to AWP-ODC leading to M8 have created a SCEC community code to perform petascale earthquake simulations.

EDUCATIONAL PRODUCTS FROM SCEC COMMUNICATION, EDUCATION AND OUTREACH (CEO) PROGRAM: PLATE TECTONICS MAP AND LEARNING KIT (1-009)
B.P. Dansby, R.M. de Groot, D. Coss Y Leon, and C.O. Gotuaco

The SCEC CEO program collaborates with educators to develop products for improving the teaching of earthquake science and other standards-based topics. The first phase of this project enhanced the latest version of the USGS "This Dynamic Planet" poster. All of the changes to the map are the direct result of feedback from participants at SCEC-hosted teacher workshops. For example, teachers requested that the details on the front of the map such as the plate velocity vectors be made more visible. Also, conveners of SCEC workshops often heard stories about teachers ruining their maps because the cut lines for the individual plates were hard to discern. This led to the major innovation: plate boundary cut lines on the back of the map. The new back side with boundary lines and pre-labeled plates is easily cut into pieces and the map can be put immediately to use. Additionally, teachers reported losing the smaller plates without having a way to readily replace them, so in many cases, a new map had to be purchased. In response, SCEC developed a downloadable template of "most commonly lost plates" which allows the instructor to easily replace a missing plate such as Juan de Fuca. Phase two of the project is the development of a plate tectonics

learning kit. The kit includes rock samples, videos, and other materials. The goal for both the map and the kit is to implement an effective teaching tool that could be used in a wide variety of learning environments.

BRITTLE AND DUCTILE FRICTION AND THE PHYSICS OF TECTONIC TREMOR (2-089)
E.G. Daub, D.R. Shelly, R.A. Guyer, and P.A. Johnson

Observations of nonvolcanic tremor provide a unique window into the mechanisms of deformation and failure in the lower crust. At increasing depths, rock deformation gradually transitions from brittle, where earthquakes occur, to ductile, with seismic tremor occurring in the transitional region. We show that a physical model that combines both brittle and ductile deformation captures observations of tremor dynamics at Parkfield and provides constraints on the friction and stress in the lower crust. We show that as the strength of the brittle and ductile terms are varied, the model produces various faulting behaviors seen in the earth, including earthquakes, tremor, silent transient slip, and steady creep. Our results show that tremor occurs over a range of brittle and ductile friction values but requires a balance between brittle and ductile processes, which advances our understanding of the basic physics of tremor and earthquakes.

DISTRIBUTION OF PLASTIC DEFORMATION DUE TO RUPTURE ON A BIMATERIAL INTERFACE (2-056)
N. DeDontney, J.R. Rice, and R. Dmowska

Material juxtapositions across faults are a frequent occurrence and previous work has argued that this elastic mismatch results in a rupture that will preferentially propagate in the direction of slip displacement in the more compliant side of the fault. This is due to a reduced clamping stress, but dissimilar poroelastic properties may also contribute to this effect. When off fault damage is considered, there are two ideas about what determines which side of the fault undergoes greater plastic deformation. Studies by Poliakov et al. [JGR 2002] and Templeton and Rice [JGR 2008] on homogeneous materials suggest that the orientation of the pre-stress field is the controlling factor, but Ben-Zion and Shi [EPSL 2005] suggest that for dissimilar materials, damage will predominately occur on the side of the fault with the faster seismic velocity. Their study was done, however, for only a single pre-stress orientation with maximum compression at 45° to the fault (reasonable for the California strike-slip faults studied). Since this result has implications for inferring preferred rupture directions based on observations of damage zone asymmetry [e.g. Dor et al., PAG 2006], we do a complete investigation of the role of the stress state on the distribution of the plastic deformation. We simulate the dynamic rupture propagation using a range of compressive stress orientations and S ratios with a pressure dependent Drucker-Prager elastic-plastic off fault material, implemented with a range of dilatancy angles. We show that there are important factors which change the preferred direction of propagation as well as the side of the fault in which damage predominately accumulates. The orientation of the most compressive stress is the controlling factor in where the plastic deformation occurs, and by changing the orientation, deformation can accumulate in either the more rigid or the more compliant material. For high angles of most compressive stress, the aforementioned Ben-Zion and Shi prediction holds true, but for low angles of most compressive stress, the rupture will preferentially propagate in the direction of slip displacement in the more rigid material. Therefore, we also show that the plastic response may reverse the preferred propagation direction.

THREE-DIMENSIONAL THERMO-MECHANICAL MODELING OF THE DEATH VALLEY FAULT ZONE (2-016)
C. Del Pardo, B.P. Hooks, B.R. Smith-Konter, L.F. Serpa, and T.L. Pavlis

Near surface (~ 10 km), high temperature (~1000°C) intrusions have been suggested to play an important role in the development of surface deformation patterns associated with the Death Valley Fault Zone (DVFZ). This study tests this hypothesis by developing three-dimensional thermo-mechanical numerical models that analyze the strain evolution of the DVFZ driven by thermal perturbations as a result of intrusions. These series of models allow for the study of intrusions' influence on the rheology of the crust and how that affects deformation and strain patterns along the fault system. The DVFZ, located in southeastern California, consists primarily of two dextral strike-slip faults whose motion produced a pull-apart basin that has been extending since its formation approximately 6 Ma. The model consists of a 350 x 500 x 35 km rectangular grid representing the crust within the DVFZ area. A pressure-dependent, non-associative, Mohr-Coulomb plasticity, where post-yield stresses are not maintained, and a temperature-dependent plasticity based upon a power flow law for high-temperature creep are used to define the mechanical behavior of the upper and lower crust, respectively. A basal drag velocity (4.5 mm/yr) is applied in the fault-parallel direction, with a gradient along the same axis, which produces a surface velocity field approximating geodetic velocities spanning the region. Two temperature-variant, intrusive geometries are considered in the model ((1) a pluton denoted by a rectangular shaped box, and (2) a dike represented by a thin square vertical column) and are placed at a depth of 10 km below the area of extension. The driving kinematics, along with the variable temperature thermal sources and mechanical material behavior, are used to analyze the temperature-dependent deformation processes and the extensional structure of the DVFZ.

CONSTRAINING GROUND MOTION IN SEDIMENTARY BASINS USING THE AMBIENT SEISMIC FIELD (1-063)

M. Denolle, E. Dunham, J. Lawrence, G. Prieto, and G. Beroza

In seismic hazard analysis, ground motion is traditionally modeled using parametric scaling relations, commonly known as "attenuation relations." As part of physics-based seismic hazard analysis, SCEC now uses simulations of seismic wave propagation through the geologically complex crust to predict ground motion. Our lack of knowledge of the elastic and anelastic structure of the subsurface limits the accuracy of these simulations and is particularly acute for sedimentary basins, such as in densely populated greater Los Angeles. We show how analysis of the ambient seismic field can improve this situation in several ways.
First, we explore the possibility of using the ambient noise transfer functions (impulse response between two receivers) to model directly ground motion in South California. The recent comparison of first order transfer functions with earthquake records has validated this technique for moderate events in South California. To include the effect of earthquake parameters (depth and radiation pattern), we correct for the source's depth dependence and use the full 3D wavefield to model ground motion. We demonstrate the potential of this method by showing transfer functions from stations temporarily deployed on the San Andreas Fault in Palm Springs area.
Second, we extract the effects of anelastic structure in South California present in our Green's functions. Our method shows little apparent bias due to non-uniform noise excitation and provides new and reliable information on spatially variable attenuation.

UNCERTAINTIES IN CODA MAGNITUDE ESTIMATION FOR SMALL EARTHQUAKES AND DIFFERENCES IN CODA ATTENUATION AT THE SAFOD AND A NEARBY SURFACE STATION (2-148)

L.A. Dominguez-Ramirez and P. Davis

We explored changes in coda attenuation as a function of depth for small earthquakes (Mb<1.0) in the vicinity of the SAFOD station. Initial analysis of the data presented at the SCEC 2009 meeting suggested an unusual population of earthquakes with a characteristic anomalous coda attenuation caused by either intrinsic differences in the nature of the events or path effects. Our method relied on measuring amplitudes of many earthquakes at a given station after normalizing to unit magnitude and comparing them with values expected from geometric spreading and attenuation. Provided the magnitudes are accurate, the method can be used to determine Q as a function of frequency. Last year we found that different populations of earthquakes appeared to have attenuation that differed by an order of magnitude. However, we have subsequently found that the problem was that the reported magnitudes for such small events were in error. We re-estimated the magnitudes based on coda duration which removed the discrepancy. The goal of this study is to test scattering effects as a function of depth in the uppermost section of the crust and to determine the frequency dependence of Q. Our study tests the hypothesis that reverberations due to large impedance contrasts near the Earth's surface may be the main contributor to coda and give rise to frequency-dependent intrinsic and scattering Q. Larger values of attenuation (lower Q) are expected to occur at surface stations compared to borehole stations. Therefore, comparing changes in attenuation from nearby stations both at depth and on surface provides

a method to test models in highly heterogeneous regions. Using the magnitude-corrected data we find, that for both the SAFOD borehole seismometer and the surface station, Q increases with frequency with more attenuation at the surface. For comparison, we also compare results with data from deep borehole and surface stations from the Japanese Hi-Net array.

PETRIFIED EARTHQUAKES: STRUCTURAL AND MECHANICAL PROPERTIES OF DAMAGED ROCKS IN THE SAN ANDREAS FAULT ZONE - AND IN THE LAB (invited talk)

O. Dor

The recognition of pulverized rocks (PR) with minimal fault-parallel shear near the San Andreas Fault (SAF) by Brune in 2001 triggered a series of studies demonstrating the following: PR form due to mechanical breakdown (Wilson et al., 2005; Rockwell et al., 2009) in a ~100 m wide zone parallel to the SAF slip surface (Wilson et al., 2005; Dor et al., 2006) as a systematic damage product during SAF slip events, and are probably the surface expression of a low velocity damage zone (Dor et al., 2006); fracture density decays logarithmically outward from the slip surface (Mitchell et al., 2010); typical particle sizes are in the 10's to 100's of microns range, following a pseudo-power low distribution (Rockwell et al., 2009); PR are asymmetrically distributed with respect to the slip zone, and may be related to the 'bimaterial effect' (Dor et al., 2006; Mitchell et al., 2010); PR form at a shallow depth due to direct compression (Dor et al., 2009) and/or strong tension (Mitchell et al., 2010). The formation of PR may be associated with high strain rates (Reches and Dewers, 2005; Doan and Gary, 2009; Mitchell et al., 2010).

To further investigate the generation mechanism of PR, fracture orientation in quartz grains was analyzed in tens of pulverized granitic samples collected along the SAF. The fractures are fairly steep, showing in most sections two principal orientations: fault-parallel, which is compatible with strong dynamic reduction of normal stress during the passage of earthquake ruptures (Ben-Zion, 2001); and fault-perpendicular, which is compatible with predictions for local maximum compressive stresses due to stress cycling on a rough frictional fault with a high loading angle (Chester and Chester, 2000). The later is supported by Hertzian-type contacts observed in pulverized sandstones near the SAF.

To test whether cyclic fatigue, a possible analogy to stress cycling on a rough fault will result in damage typical for PR, hallow cylindrical samples of Westerly Granite were subjected to cyclic torsional loading in a high pressure rotary double-shear apparatus under displacement servo control, which limited the maximum shear stress. The cyclic loading resulted in strong weakening, which increased as a function of torsional displacement but was insensitive to the loading frequency (ranging 0.001-9.99 Hz). The results support the idea that stress cycling is involved in the damage process of fault zone rocks along the SAF.

DYNAMIC TRIGGERING OF SHALLOW EARTHQUAKES IN THE SALTON SEA REGION OF SOUTHERN CALIFORNIA (2-099)
A.K. Doran, Z. Peng, C. Wu, and D. Kilb

We perform a systematic survey of dynamically triggered earthquakes in the Salton Sea region of southern California using borehole seismic data recordings (2007 to present). We define triggered events as high-frequency seismic energy during large-amplitude seismic waves of distant and regional mainshock events. Our mainshock database includes 10 teleseismic events (epicentral distances > 1000 km; Mw ≥ 7.5), and 26 regional events (epicentral distances 100 - 2000 km; Mw ≥ 5.5). Of these, we find 3 teleseismic and 7 regional events produce triggered seismic activity within our study region. The triggering mainshocks are not limited to specific azimuths. For example, triggering is observed following the 2008 Mw6.0 Nevada earthquake to the north and the 2010 Mw7.2 Northern Baja California earthquake to the south. The peak ground velocities (PGVs) associated with these triggering events are generally larger than 0.03 cm/s, which corresponds to the dynamic stress of ~2 kPa, a value close to the triggering threshold found in the Long Valley Caldera and the Parkfield section of San Andreas Fault. The triggered events occur almost instantaneously with the arrival of large amplitude seismic waves and they appear to be modulated by the passing surface waves, similar to the recent observations of triggered deep "non-volcanic" tremor along major plate boundary faults in California and elsewhere. However, the triggered events found in this study have very short S-P times, suggesting that they likely originated from brittle failure in the shallow crust.

USING DYNAMIC RUPTURE MODELS WITH OFF-FAULT PLASTIC YIELDING TO INVESTIGATE INELASTIC RESPONSE OF PRE-EXISTING FAULT ZONES TO NEARBY EARTHQUAKES (2-055)
B. Duan

The observation of damage to the Johnson Valley fault zone from the nearby Hector Mine earthquake (Vidale and Li, 2003) strongly suggests that response of pre-existing compliant fault zones to nearby ruptures may be well beyond elastic limit. In this study, we use the advanced dynamic source models with off-fault elastoplastic material rheology to investigate conditions under which inelastic strain (i.e., plastic yielding) occurs within compliant fault zones that are about 10 km away from the ruptured fault. We find that response of some portions of the fault zones to the nearby rupture can be inelastic, while the rest of the fault zones deform elastically, when the pre-stress level is close to the strength of fault zone rocks. Decrease in the mean stress in extensional quadrants of the rupture caused by dynamic waves weakens the rock in the fault zones. Under favorable conditions, some portions of the fault zones in these extensional quadrants may yield and inelastic strain accumulates during the dynamic process. While increase in the mean stress in compressional quadrants strengthens the rock, which responds to the nearby rupture elastically. Thus, elastic and inelastic response to nearby ruptures can co-exist along a compliant fault zone. In the static displacement field after the rupture, elastic response results in retrograde motion (i.e., opposite to the long-term slip direction) across the fault zone, while inelastic response gives rise to sympathetic motion (i.e., consistent with the long-term slip direction). Therefore, detection of sympathetic motion of pre-existing fault zones induced by nearby earthquakes from InSAR images may provide us with a means to constrain the pre-stress level in the upper crust, as the strength of fault zone rock can be measured in the laboratory. Dynamic analyses reveal that accumulation of inelastic strain causes dramatic variations in particle velocity across the fault zone, reversing the sense of fault-parallel relative motion from retrograde motion (within elastic limit) to sympathetic motion. These results suggest that re-examination of InSAR observations on the static deformation fields of the 1992 Landers and 1999 Hector Mine earthquakes, using spontaneous rupture models with off-fault elastoplastic response, may provide us with an improved understanding of mechanical response of compliant fault zones to nearby ruptures, relative to the elastic inhomogeneity model proposed by Fialko et al.(2002).

A NEW PARADIGM IN MODELING PULSELIKE RUPTURES: THE PULSE ENERGY EQUATION (2-052)
A.E. Elbanna and T.H. Heaton

Earthquake ruptures are complex processes both spatially and temporally. Seismic source inversions and numerical simulations show that ruptures can occur in one of two primary modes; the slip pulse mode and the expanding crack mode. In order to understand the long time behavior of fault systems sustaining repeated earthquake ruptures we have to run models through hundreds or thousands of events so that the system under consideration evolves into a statistically stable stressed state that is consistent with the assumed friction law. For systems that fail primarily in pulse-like ruptures, the ruptures and the prestress can become very complex at many length scales. With the current computational methods and resources, we are unable to deduce which prestresses are compatible with an assumed friction law.

However, the spatial compactness of slip pulses may provide another alternative approach to simulating many complex events. Here we construct a nonlinear ordinary differential equation that relates the final slip in a pulselike event to the prestress that exists before that event. The differential equation is based on an energy conservation principle for the slip pulse. We illustrate our methodology within the framework of 1D spring block slider system with strong velocity weakening friction. In this system, as the slip pulse propagates, it changes the potential energy of the springs, it loses energy through frictional dissipation, and it possesses a nonzero kinetic energy. The energy conservation dictates that the difference between the change in potential energy and the frictional work dissipated has to be equal to the kinetic energy of the pulse. By expressing the change in the potential energy of the system exactly in terms of slip and prestress, and through approximating the frictional dissipation and pulse kinetic energy as power law functions in the pulse slip (an approximation that is motivated by the approximate self-similarity of the propagating pulse) we arrive at a nonlinear first order differential equation that relates the final slip to the prestress distribution.

Our methodology reduces the complexity of the problem (at least in the framework of the spring block slider model) from solving a number of coupled differential equations equal to the number of blocks to solving a single nonlinear differential equation. This equation predicts the final slip distribution with a considerable saving in the computational time. This direct knowledge of the final slip facilitates modeling repeated ruptures in a much shorter time. We report on our attempts to produce long time statistics from our equation consistent with the long time statistics of the spring block system.

Finally, we think that a similar approach for the more complicated case of ruptures propagating in the continuum may be possible. It is certainly more challenging due to the need of taking into consideration the effect of radiated energy through the transmitted wave field and also the nonlocalization of the potential energy density. However, it may be possible , since similar principles hold in both of the continuum and discrete systems, e.g. energy conservation and spatial localization of slip pulses suggesting that local interaction are of prime importance relative to longer range interaction.

FORMATION OF PULSE-LIKE RUPTURES ON VELOCITY-WEAKENING INTERFACES AND ITS RELATION TO STABILITY PROPERTIES OF STEADY-STATE SLIDING (2-051)
A.E. Elbanna, N. Lapusta, and T.H. Heaton

Prior studies have shown that velocity-weakening interfaces can produce both crack-like ruptures, for higher prestress levels, and pulse-like ruptures, for lower prestress levels and sufficient amounts of weakening. More complex rupture patterns, such as multiple pulses of slip, may result for intermediate levels of prestress. Such multiple pulses occur due to destabilization of steady sliding behind the front of the crack-like rupture that forms after the nucleation stage. The spacing of the multiple pulses can be predicted from linearized stability analysis of the steady sliding; it corresponds to the wavelength of the perturbation with the maximum growth rate. Whether the transition from the crack-like rupture to multiple pulses occurs within the rupture duration depends on the growth rates, which are higher for more pronounced velocity weakening.

Here we explore the possibility that transition from the initial crack-like rupture to a self-healing pulse can also be understood based on such stability analysis. We conduct simulations of dynamic ruptures in a 2D antiplane fault model with rate and state friction that involves enhanced weakening at seismic slip velocities motivated by flash heating. The fault has uniform prestress, except in a small overstressed region with Gaussian prestress distribution used for rupture nucleation. For a range of model parameters that favors slip pulses, we find that the decrease of sliding velocity behind the front of the initial crack causes significant increase in the maximum growth rate of unstable modes and increase in the contrast between their phase velocities. The combined effect of dispersion and mode growth lead to further decrease in the slip rate behind the rupture front. When this slip rate ultimately drops below a certain value, which is dependent on the friction law and the initial pretsress, we observe that several modes grow simultaneously with a growth rate comparable to the mode with maximum growth rate and that many of those modes acquire a zero phase velocity. We hypothesize that this simultaneous growth of the stationary modes leads finally to the local

arrest of rupture and formation of slip pulses. Phase velocities of the growing wavelengths influence the speed of the healing front of the resulting slip pulses and hence influence how the width of the pulse changes with its propagation.

We will report on our current efforts to turn these observations into a predictive theory of rupture mode selection on uniformly pre-stressed velocity-weakening interfaces. The effect of the nucleation procedure, which is clearly present in the formation of self-healing pulses, may be possible to incorporate through the different characteristics of the initial crack-like rupture.

INTERMITTENT FAULT SLIP EMBEDDED IN CREEP GENERATES SEISMIC EVENTS: INSIGHT FROM ACOUSTIC AND OPTICAL MONITORING OF CRACK PROPAGATION (2-096)
J.E. Elkhoury, O. Lengliné, J.-P. Ampuero, and J. Schmittbuhl

Observations of temporal and spatial correlations between slow slip earthquakes and the corresponding tectonic tremor activity suggest a physical relation between these two phenomena. However, detailed descriptions of the mechanisms relating these phenomena are lacking or limited to simply attributing the relation between seismic and aseismic events to fluid mediated processes. Here we present laboratory results of a unique experimental setting aimed at understanding the response to transient loads of a system of small asperities embedded in creep as a model of tectonic tremor activity triggered by slow slip and modulated by tides. Our setup allows for optical and acoustic monitoring of crack propagation at a wide range of rupturing regimes in the absence of fluids. We conducted mode I crack propagation experiments on sandblasted and annealed interfaces of transparent material (Polymethylmethacrylate) where fracture fronts were confined to the weakness plane of the heterogeneous interface. We monitored acoustic emissions (AE) with a linear array of 32 piezo-electric sensors and 10 individual sensors surrounding the crack front. We also optically monitored the rupture front with a fast video camera up to 500 frames per second. Crack front image processing reveals intermittent openings linked to the spatiotemporal clustering of the AE. Using the analogy between mode I and mode III fractures, our results translate into intermittent slow slip on faults linked to clustering of seismic activity produced by the breakage of asperities embedded in the creeping regions with no need of invoking fluid mediated processes. Thus our experiments help reveal the interplay between aseismic and seismic slip on faults.

LIDAR POINT-BASED CROSS-CORRELATION OF OFFSET GEOMORPHIC FEATURES ALONG STRIKE-SLIP FAULTS (1-079)
A.J. Elliott, M.S. Bishop, M.E. Oskin, P.O. Gold, and O. Kreylos

High-resolution topographic data collected by airborne and terrestrial LiDAR scanners resolves subtle geomorphic features that enable precise measurements of fault displacement. To exploit the true resolution of available data, we are developing a tool to perform cross-correlation of laterally offset linear features, such as channels, using raw LiDAR point returns (i.e. the point cloud). This tool is being tested on Earthscope airborne LiDAR of the Lenwood fault in southern California and terrestrial LiDAR of the El-Mayor Cucapah surface rupture of the Borrego fault in northern Mexico. The tool is implemented in the freely distributed 3-D interactive LidarViewer software developed by the UC Davis Keck Center for Active Visualization in the Earth Sciences (KeckCAVES), a collaboration between computer and earth scientists. The tool cross-correlates user-selected swaths of topographic data from one side of a fault to the other and returns an offset distance that corresponds to the most correlative horizontal alignment of the selected topographic swaths. Along the northern half of the Lenwood fault (34.60°N to 34.81°N), where a well expressed fault scarp reflects probable Holocene surface rupture, right-laterally offset features each return a maximum correlation that matches manual LiDAR-based measurements. Calculated offsets range from 2.9 m to 9.2 m, with most under 5 m. The prevalence of <5 m offsets along a 35 km length of fault permits the interpretation of slip from a single event, although additional investigation is required to rule out slip in two events. Cross-correlation of features offset by coseismic displacement along the Borrego fault in northern Mexico complement field measurements at sites where individual piercing lines have been degraded by shaking- or slip-induced collapse. We can cross-correlate the geometry of a deeply incised channel on a coarse alluvial fan that is clearly right-normally offset by the surface rupture. In the field, collapse of the channel walls within 1 m of the scarp precluded precise measurement of lateral offset, but by exploiting the full channel geometry in our point-cloud cross-correlation we may obtain a lateral offset of this substantial feature. Our LiDAR-based correlation tool permits remote measurement of small fault offsets and incorporates the full geometries of displaced features to return a robust estimate of displacement that may not be possible through traditional field survey methods.

A VS30-DERIVED NEAR-SURFACE SEISMIC VELOCITY MODEL (1-021)
G.P. Ely, T.H. Jordan, P. Small, and P.J. Maechling

Shallow material properties, S-wave velocity in particular, strongly influence ground motions, so must be accurately characterized for ground-motion simulations. Available near-surface velocity information exceeds

that which is accommodated by current versions of the SCEC Community Velocity Model (CVM-S4) or the Harvard model (CVM-H6). Additionally, the elevation-referenced CVM-H voxel model introduces rasterization artifacts in the near-surface due to sample depth dependence on local topographic elevation. Nearly 50 percent of CVM-H6 does not reach the ground surface at all. To address these issues, we propose a new algorithm for constructing a near-surface geotechnical layer (GTL) from available maps of Vs30 (the average S-wave velocity down to 30 meters). In our current implementation, the geology-based Vs30 map of Wills and Clahan (2006) is used within California, and is supplemented outside of California with topography-derived Vs30 of Wald, et al. (2007). The new GTL replaces the underlying CVM above a specified transition depth on the order of a few hundred meters. A generic depth dependence is devised for the GTL that is capable of representing a wide range of velocity profile types based on the Vs30 value and a single S-wave velocity value extracted from the underlying CVM at the transition depth. Parameters of the depth dependence are fit to Boore and Joyner's (1997) generic rock profile as well as CVM-4 soil profiles for the NEHRP soil classification types. P-wave velocity and density within the GTL are derived with the help of the scaling laws of Brocher (2005). We present wave propagation simulations for selected events from the SCEC Big Ten scenarios, comparing ground motions modeled with, and without the new GTL implementation.

PERIODIC, CHAOTIC AND LOCALIZED SLIP PULSE SOLUTIONS WITH DIETERICH-RUINA FRICTION (2-058)

B.A. Erickson, D. Lavallee, and B. Birnir

We investigate the emergent dynamics when the nonlinear Dieterich-Ruina rate and state friction law is attached to a Burridge-Knopoff spring-block model. We derive both the discrete and continuous equations governing the system in this framework. The discrete system (ODEs) exhibits both periodic and chaotic motion, where the system's transition to chaos is size-dependent, i.e. how many blocks are considered. From the discrete model we derive the nonlinear elastic wave equation by taking the continuum limit. This results in a nonlinear partial differential equation (PDE) and we find that both temporal and spatial chaos ensues when the same parameter is increased. This critical parameter value needed for the onset of chaos in the continuous model is much smaller than the value needed in the case of a single block and we discuss the implications this has on dynamic modeling with this specific friction law. Most importantly, these results suggest that the friction law is scale-dependent, thus caution should be taken when attaching a friction law derived at laboratory scales to full-scale earthquake rupture models. Furthermore, we find solutions where the initial slip pulse propagates like a traveling wave, or remains localized in space, suggesting the presence of soliton and breather solutions. In the case of a traveling wave we see evidence of a soliton, a wave with permanent form, that is localized in space while it travels at a constant speed through the medium. The breather solution is a time-periodic, exponentially decaying (in space) solution of a nonlinear wave equation. We discuss the significance of these pulse-like solutions and how they can be understood as a proxy for the propagation of the rupture front across the fault surface during an earthquake. We compute analytically the conditions for soliton solutions and by exploring the resulting parameter space, we may determine a range for suitable parameter values to be used in dynamic earthquake modeling.

FAULT ROUGHNESS AND BACKGROUND STRESS LEVELS ON MATURE AND IMMATURE FAULTS (2-078)

Z. Fang and E.M. Dunham

Dynamic weakening mechanisms permit faults to host ruptures at low background stress levels ($\tau^b/(\sigma - p) \sim 0.2 - 0.3$, for shear stress τ^b and effective normal stress $\sigma - p$). Such stresses are inferred to exist around mature faults like the San Andreas. However, the majority of faults operate at higher stress levels ($\tau^b/(\sigma - p) \sim 0.6$). One explanation for this difference is that dynamic weakening mechanisms are active only on mature faults. We offer an alternative explanation, that increased geometric complexity of less mature faults introduces an additional resistance to slip that must be overcome in order for the fault to host ruptures. We idealize faults as self-similar surfaces having slope perturbations α between 10^{-3} (mature faults) and 10^{-2} (immature faults), under the assumption that α decreases as the fault accommodates more slip. Slip on such faults induces stress perturbations that Chester and Chester [2000], assuming ideally elastic response and using a boundary perturbation analysis accurate to $O(\alpha)$, have shown to scale as $\Delta\sigma \sim \alpha G \cdot \Delta u/\lambda_{min}$, where $G \cdot = G/(1 - \nu)$, G is shear modulus, ν is Poisson's ratio, Δu is slip, and λ_{min} is the minimum wavelength of roughness. We extended this analysis to $O(\alpha^2)$ and found that when the first-order stress perturbations are projected onto the nonplanar fault, they generate an additional set of tractions that oppose slip. This additional resistance to slip, which we term "roughness drag," scales as $\tau^{drag} \sim \alpha^2 G \cdot \Delta u/\lambda_{min}$, and exists even if the fault is frictionless. This expression is verified using a spectral collocation method to solve the static problem. We also study dynamic rupture propagation on self-similar faults with strongly rate-weakening fault friction and off-fault plasticity. Dynamic weakening introduces a critical stress level, τ^{pulse}, at which self-sustaining rupture propagation on flat faults is first possible. Roughness increases the critical stress to

roughly $\tau^{pulse} + \tau^{drag}$. For $\alpha \sim 10^{-3}$, $\tau^{drag} \ll \tau^{pulse}$ and faults host ruptures at $\tau^b/(\sigma - p) \sim 0.2 - 0.3$. As α increases to ~ 10^{-2}, $\tau^{drag} \sim \tau^{pulse}$ and larger values of $\tau^b/(\sigma - p)$ are required to propagate ruptures.

SEISMICITY RATES AND MAGNITUDE DISTRIBUTIONS ON THE SOUTHERN SAN ANDREAS FAULT (1-047)
K. Felzer, M. Page, G. Biasi, and R. Weldon

It has been observed that recent seismicity rates on some sections of the Southern San Andreas Fault (SSAF) are low in comparison to estimated geologic slip rates (Allen et al., 1965; Schwartz and Coppersmith, 1984). Two possible explanations are that the fault experiences large swings in seismicity rate as a function of time or that earthquakes smaller than M 7 rarely occur on the SSAF. The latter explanation is commonly referred to as the characteristic earthquake hypothesis (Schwartz and Coppersmith, 1984).

It is well accepted that the Gutenberg-Richter magnitude frequency distribution holds for regions, such as all of southern California. Therefore if there is a lack of small earthquakes on the SSAF in comparison to what the G-R relationship would predict, the rest of Southern California must experience an excess of such events. Alternatively, if off-fault seismicity follows the G-R relationship seismicity on the SSAF must follow the relationship as well; otherwise a G-R relationship for the region as a whole would be mathematically impossible.The Southern California instrumental catalog suggests that off-SSAF seismicity is fit well by a simple G-R relationship, however this catalog contains very few large events. Alternatively, we can use GPS measurements to estimate the rates of M≥4 earthquakes that the G-R and characteristic models would predict. Using the GPS based seismic moment calculations of Ward (1998) , the G-R distribution with b=1, SSAF slip rates from WGCEP 2007, and various assumptions about aseismic deformation, we find that the characteristic model predicts an average of 34.2—39.9 M≥4 earthquakes off of the SSAF/year while the G-R/rate change model predicts 20.2 – 25.9. The observed rate is 23.7 M≥4 off fault earthquakes/year from 1932-2006 (from the WGCEP 2007 catalog), which is within the rate change/G-R model expectations and significantly lower than the rate expected under the characteristic model, even after off-fault rate variability due to aftershock clustering is taken into account ($p<0.02$). This indicates that seismicity rate change with time explains the current low seismicity rate on the SSAF. The idea that SSAF rates change with time agrees with the lack of large earthquakes on the SSAF since 1857 and the suggestion of earthquake clustering in the paleoseismic record.

AZIMUTHALLY ANISOTROPIC PHASE VELOCITY MAPS FOR THE HIGH LAVA PLAINS OF OREGON (2-147)
H. Feng and C. Beghein

This High Lava Plains (HLP), Oregon, is one of the most volcanically active area in the continental United States. It has experienced extensive flood basalt volcanism since the mid-Miocene, and is characterized by a northwest oriented, age-progressive track of silicic volcanism. Unlike the adjacent Yellowstone/Snake River Plains volcanism, the HLP track cannot be explained by regional plate motion. Its origin is still under debate, with hypotheses including a plume related to the presence of the Yellowstone hotspot, slab rollback, back-arc extension, or lithospheric delamination. To shed light on the origin of the HLP volcanism, we measured the dispersion and azimuthal dependence of Rayleigh wave phase velocities using data collected by two dense arrays of seismic stations (HLP and USArray) between periods of 16 and 170s.

At 18 and 20s period, our phase velocity maps do not display significant anisotropy except in the center of the study region, where we find a clear NW trending fast direction for Rayleigh wave phase velocities. Since Rayleigh waves at these periods mostly sample the crust, we suggest that this anisotropy signal is associated with the Brothers fault zone (BFZ), which approximately coincides with the location and direction of fast wave propagation.

Between periods of 25 and 68s, our azimuthally anisotropic phase velocity maps display a clear E-W fast velocity direction in the northern part of the HLP, and phase velocities that are lower than those predicted by our reference model. This is consistent with the presence of a relatively warm uppermost mantle (Warren et al., 2008) and active E-W mantle flow beneath the HLP as concluded from shear-wave splitting analyses (Long et al., 2009). We note, however, that this anisotropy signal appears to be disrupted in the neighborhood of Diamond Crater, which is also associated with localized reduced phase velocities at periods of 102 s and larger. This suggests that the pattern of upper mantle anisotropy in the HLP region is not as simple as previously thought.

STATIC RUPTURE MODEL OF THE 2010 M7.2 EL MAYOR-CUCAPAH EARTHQUAKE FROM ALOS, ENVISAT, SPOT AND GPS DATA (1-139)
Y. Fialko, A. Gonzalez, J. Gonzalez, S. Barbot, S. Leprince, D. Sandwell, and D. Agnew

The April 4, 2010 "Easter Sunday" earthquake on the US-Mexico border was the largest event to strike Southern California in the last 18 years. The earthquake occurred on a northwest trending fault close to, but

not coincident with the identified 1892 Laguna Salada rupture. We investigate coseismic deformation due to the 2010 El Mayor-Cucapah earthquake using Synthetic Aperture Radar (SAR) imagery form ENVISAT and ALOS satellites, optical imagery from SPOT-5 satellite, and continuous and campaign GPS data. The earliest campaign postseismic GPS survey was conducted within days after the earthquake, and provided the near-field cosesmic offsets. Along-track SAR interferograms and amplitude cross-correlation of optical images reveal a relatively simple continuous fault trace with maximum offsets of the order of 3 meters. Also, SAR data indicate that the rupture propagated bi-laterally from the epicenter near the town of Durango both to the North-West into the Cucapah mountains and to the South-East into the Mexically valley. The inferred South-East part of the rupture was subsequently field-checked and associated with several fresh scarps, although overall the earthquake fault does not have a conspicuous surface trace South-East of the hypocenter. It is worth noting that the 2010 earthquake propagated into stress shadows of prior events - the Laguna Salada earthquake that ruptured the North-West part of the fault in 1892, and several M6+ earthquakes that ruptured the South-East part of the fault over the last century. Analysis of the coseismic displacement field at the Earth's surface (in particular, the full 3-component displacement field retrieved from SAR and optical imagery) shows a pronounced asymmetry in horizontal displacements across both nodal planes. The maximum displacements are observed in the North-Eastern and South-Western quadrants. This pattern cannot be explained by oblique slip on a quasi-planar fault. Multi-parametric inversions of the space geodetic data suggest that the El Mayor-Cucapah earthquake occurred on a helix-shaped rupture, with Eastward dip in the Northern section and Westward dip in the Southern section. This interpretation is consistent with field observations of the surface rupture and aftershock data, and provides an explanation for a strong non-double-couple component suggested by the seismic moment tensor solution. The total geodetic moment of our best-fitting model is in a good agreement with the seismic moment.

INNOVATIVE REPRESENTATION OF EARTHQUAKE TRIGGERING FROM SONIFICATION/VISUALIZATION OF SEISMIC SIGNALS (2-135)
M. Fisher, Z. Peng, D. Simpson, and D. Kilb

Sonification of seismic data is an innovative way to represent seismic data in the audible range (Simpson, 2005). Seismic waves with different frequency and temporal characteristics, such as those from teleseismic earthquakes, deep "non-volcanic" tremor and local earthquakes, can be easily discriminated when time-compressed to the audio range. Hence, sonification is particularly useful for presenting complicated seismic signals with multiple sources, such as aftershocks within the coda of large earthquakes, and remote triggering of earthquakes and tremor by large teleseismic earthquakes. Previous studies mostly focused on converting the seismic data into audible files by simple time compression or frequency modulation (Simpson et al., 2009). Here we generate animations of the seismic data together with the sounds. We first read seismic data in the SAC format into Matlab, and generate a sequence of image files and an associated.wav sound file. Next, we use a third party video editor, such as the QuickTime Pro, to combine the image sequences and the sound file into an animation. We have applied this simple procedure to generate animations of remotely triggered earthquakes, and tremor and low-frequency earthquakes in California, and mainshock-aftershock sequences in Japan and California. These animations clearly demonstrate the interactions of earthquake sequences and the richness of the seismic data. The tool developed in this study can be easily adapted for use in other research applications and to create sonification/animation of seismic data for education and outreach (E&O) purpose.

DISTRIBUTION AND KINEMATICS OF SURFACE RUPTURES ASSOCIATED WITH THE EL MAYOR-CUCAPAH EARTHQUAKE SEQUENCE (invited talk)
J.M. Fletcher

Surface rupture associated with the April 4, 2010 El Mayor-Borrego earthquake extends ~100 km from the northern tip of the Gulf of California to the international border and comprises two distinct geomorphologic and structural domains. The southern half of the rupture consists of a zone of distributed fracturing and liquifaction that cuts across the Colorado River delta and its trace is distinct from previously recognized faults like the Cerro Prieto fault and proposed faults that control the eastern margin of Sierra El Mayor. The northern half of the rupture propagated 55 km through an imbricate stack of east-dipping faults in the Sierra Cucapah. In the southern Sierra Cucapah, rupture extends 7 km along the Laguna Salada and is dominated by right lateral displacement (up to 3.3 m), whereas vertical offset is less than 1 m does not show a consistent NE or SW facing direction along strike. From its intersection with the Laguna Salada fault, rupture follows the Pescadores fault to the north for ~13 km, and Right lateral offset (up to 3.7 m) continues to dominate the vertical offset (~1 m), which has a consistent NE-side down sense. This rupture segment terminates in the high elevations of the sierra and steps left through a complex accommodation zone that extends nearly 10 km before rupture consolidates on the structurally lower Borrego fault, which contains the greatest slip magnitudes of 4 m of dextral east down displacement. A low-angle detachment intersects the footwall of the central portion of the Borrego fault at a segment boundary, and rupture bifurcates with a splay that follows the trace of the detachment in a more westerly direction. Over the next 6 km to the north, rupture steps left

across a 2km wide zone before finally consolidating on a fault that we have named the Paso Superior Fault and extends ~10 km to the north. The Paso Superior is well-exposed at Highway 2, where it is clearly a low-angle detachment. Scarps near the fault trace accommodate dip slip and nearly twice as much strike-slip is spread across a 100-150 m wide zone of cracking and secondary faulting to the east. Part of the complexity of the rupture can be attributed to interaction with detachment faults that allow the rupture to expand in the near surface. This rupture illustrates the complexity that can develop when a rupture propagates through a network of high- and-low angle faults that accommodate the three-dimensional strain of transtensional plate margin shearing.

A DENSIFIED GEODETIC VELOCITY SOLUTION FOR THE NORTH SAN FRANCISCO BAY REGION (1-152)

M.A. Floyd, G.J. Funning, and B.P. Lipovsky

A new, densified GPS velocity solution is presented for the area north of San Francisco Bay between the coast and Lake Berryessa, to Healdsburg in the north.

Field work was undertaken by the authors in the summers of 2008, 2009 and 2010, and combined with data from publicly-available sources dating back to 1991.

Our new data support previous models that show the majority of the plate boundary deformation being taken up across the San Andreas Fault. One-dimensional profiles of elastic dislocations indicate that 5-6 mm/yr is taken up across the Rodgers Creek Fault, and is fairly consistent along-strike. The Maacama Fault has little to no significant influence this far south, with at most 3 mm/yr of slip rate deficit.

Further observation work is required and anticipated to allow the bridging of the data gap between the BAVU network to the south and the USGS's Pillsbury network to the north. Furthermore, preliminary data suggest that there is evidence for surface creep on the Rodgers Creek Fault in the vicinity of Santa Rosa though it is, at this time, not resolvable to any significant level.

ANALYSIS OF HIGH-RESOLUTION P-WAVE SEISMIC IMAGING PROFILES ACQUIRED THROUGH RENO, NEVADA FOR EARTHQUAKE HAZARD ASSESSMENT (1-048)

R.N. Frary, W.J. Stephenson, J.N. Louie, J.K. Odum, J.Z. Maharrey, M.S. Dhar, R.L. Kent, and C.G. Hoffpauir

In support of the Western Basin and Range Community Velocity Model and the proposed Reno-Carson City Urban Hazard Maps, the U.S. Geological Survey, University of Nevada, Reno, and nees@UTexas, Austin collaborated on a high-resolution seismic imaging study of the Truckee Meadows basin in Reno and Sparks, Nevada, during June 2009. We acquired two seismic reflection profiles to determine basin structure and fault locations in this area. We used the nees@UTexas minivib I vibrator source with a 12-second linear sweep from 15-120 Hz each, and recorded 2-second records on 144 channels with 5-m geophone intervals. One 6.72-km profile followed the Truckee River through downtown Reno east to Rock Boulevard, and a second 3.84-km profile followed Manzanita Lane, about 4.5 km south of the Truckee River. The second profile crossed several previously-mapped faults, including the Virginia lake fault. The seismic processing was catered to the urban environment and included pre-correlation automatic gain correction and frequency-offset (FX) spatial filtering to mitigate ambient noise. Additionally both post-stack time and pre-stack depth migrations were conducted for comparison. Final depth images of these profiles reveal strong reflections between about 0.2 km and 1.0 km depth. Preliminary interpretation of the Truckee River profile suggests the presence of several possible faults and an eastward-dipping reflection sequence. The Manzanita Lane profile shows reflections across a fault zone with multiple steeply-dipping strands.

COSEISMIC DEFORMATION OF THE 2010 SIERRA EL MAYOR EARTHQUAKE FROM ALOS PALSAR IMAGERY (1-153)

G.J. Funning

The 4 April 2010, M7.2 Sierra El Mayor earthquake ruptured over 50 km of a system of faults located on the western side of the Sierra El Mayor mountains, where they meet the dry lake Laguna Salada. The terrain in the region is mostly poorly vegetated desert, and thus a promising target for InSAR.

Using L-band radar data from the PALSAR instrument on the Japanese ALOS satellite, I processed two coseismic interferograms, from ascending and descending tracks that cover the epicentral region. Coseismic offsets in satellite line-of-sight are in some places greater than 1.5 m, indicating peak right-lateral fault slip of at least double that amount. Azimuth offsets were also calculated at high resolution for the same data, and are used to map the location of the earthquake surface rupture. Preliminary inverse models indicate a oblique-normal mode of slip may provide the best fit to the data, consistent with preliminary focal mechanisms and the local geomorphology; the geodetic moment-magnitude of 7.2 for these models is also in line with those estimated seismically.

EXPERIMENTAL INVESTIGATION OF THRUST FAULTS IN HOMALITE (2-075)
V. Gabuchian, A. Rosakis, N. Lapusta, and D. Oglesby

A sound interplay between experimental observations and numerical simulations can reveal a much greater insight into a scientific problem than either methodology alone, where numerics may direct the next experiment or vise-versa. With this motivation, experiments are designed to study the ground motion of thrust faults near the fault trace and to compare with numerical simulation results. Through the application of an external load with a press to a thin sheet of Homalite, a high-density polymer, and discharging a capacitor across a wire, slip is initiated along a carefully treated interface. Several key parameters such as the angle of the interface and the applied load may be varied to achieve fundamentally different wave phenomenon, namely a super shear or sub-Rayleigh event. Laser vibrometers are used to record the velocity normal to the free surface on the hanging wall and the foot wall. With high-speed cameras, photoelastic fringes are obtained in transmission through the Homalite slab, outputting information about the stress state in the material. Discoveries on the material response to the applied wave field are possible with the information from the photoelastic images in conjunction with the velocity traces, especially in the differences between a super shear and a sub Rayleigh event. Experimental results validate the salient features of the numerical simulations in 2D and even more closely in 3D.

PRELIMINARY RESULTS FROM HOLOCENE SURFACE MAPPING ALONG THE CENTRAL PART OF THE GARLOCK FAULT, SEARLES VALLEY, SOUTHEASTERN CALIFORNIA (1-098)
P.N. Ganev, J.F. Dolan, S.F. McGill, and K.L. Frankel

The tectonic significance of the left-lateral Garlock fault in relationship to the eastern California shear zone (ECSZ) and Pacific-North America plate boundary deformation remains a geologic enigma. Geodetic studies imply that the majority of present-day elastic strain accumulation occurs on strike-slip faults oriented northwest-southeast as part of the ECSZ, almost normal to the orientation of the Garlock fault, while strain accumulation parallel to the Garlock fault is minimal. Yet, a large number of offset alluvial landforms along strike of the fault are suggestive of higher tectonic activity than what geodetic strain accumulation rates imply. In an effort to understand the role of this major fault system in accommodating deformation along the Pacific-North America plate boundary, we are analyzing data from four sites on the central section of the Garlock fault. The sites are located within a 21-km stretch of the fault between Trona Road and Randsburg Wash Road in Searles Valley, California. Three of the sites are offset incised channels, whereas the fourth site is an offset alluvial fan. From west to east, the left-lateral offsets at the sites are 49 +/- 8 m (incised channel), 42 +/- 10 m (incised channel), 58 +/- 8 m (offset alluvial fan), and 13 +/- 2 m (offset incised channel), respectively. Two-meter-deep pits were dug in the offset alluvial deposits and samples were collected for Be-10 depth profile and optically stimulated luminescence dating. Given the range in displacements among the four sites our results will prove helpful in understanding whether strain release has been temporarily and spatially constant, and whether the present-day rate of strain accumulation is similar to the geologically determined strain release rates. Ultimately, these results will provide important information on the interaction between the Garlock fault and other faults in the ECSZ, and the role these structures play in accommodating the Pacific-North America plate boundary deformation.

COLLISIONAL TECTONICS OF THE SANTA ANA MOUNTAINS AND PUENTE HILLS, ORANGE COUNTY, CALIFORNIA (1-085)
E.M. Gath and L. Grant Ludwig

The convergence of the 5-6 mm/yr northwest-vergent Peninsular Ranges (Santa Ana Mountains - SAM) and the ~1 mm/yr south-vergent Transverse Ranges (Puente Hills) lies within the Santa Ana River canyon in the southeastern LA Basin. The collision of these two terranes has had a profound effect on the local geology and geomorphology, and is serving as the driving mechanism for most of the seismic hazard for Orange County. The complexity of this convergence is clearly expressed by E-W trending folds and thrusts on the northern nose of the SAM and the southernmost Puente Hills in the Santa Ana River canyon, and by the dispersed microseismicity within the collisional zone. The model temporally and kinematically explains 1) the right-lateral slip on the Whittier fault as the southern LA Basin escapes westerly, 2) the accelerated uplift and folding within the Eastern Puente and Chino Hills due to the convergence, the oblique, right-lateral, reverse slip on the Chino fault by folding and uplift of the Chino Hills, 3) the uplift and segmentation of Loma Ridge by oblique convergence of the SAM and the southern LA Basin sedimentary fill, 4) the repeated northward offset of Santiago Creek by left-lateral shearing, 5) the uplift of the Coyote Hills by oblique convergence, 6) the folding and uplift of the Anaheim and Peralta Hills by shortening due to compressional over-thrusting, 7) a left-lateral solution for the M5.4 July 29, 2008 Chino Hills earthquake by easterly escape tectonics, and 8) a potential but previously unrecognized left-lateral shear zone along the western side of the Santa Ana Mountains. The concept is essentially an Indian subcontinent indenter model but at a much smaller scale. The significance of this model is that while many of the faults and folds created by the collision are small seismic sources, the concern is that they also pose a myriad of potential surface rupture hazards within this densely urbanized region.

COMPARISON OF CLUSTERING AND EARTHQUAKE RATE VARIATIONS IN SIMULATED AND CALIFORNIA CATALOGS (2-157)
J.J. Gilchrist, J.H. Dieterich, and K.B. Richards-Dinger

We compare the space-time statistics of earthquakes in a simulated catalog with the ANSS California catalog (1911-2010). The simulations employ the 3D boundary element code RSQSim with a version of Steve Ward's All-California fault model to create a synthetic catalog with ~200,000 M≥4 events, spanning ~10,000 years. The catalog includes foreshocks, aftershocks and occasional large event clusters. This clustering is reflected in the inter-event passage time statistics of both catalogs, which have nearly identical distributions with a well-defined power-law decay (slopes of -0.85 to -1.0) at short time intervals and a tail that progressively deviates from an exponential distribution. The power-law and exponential distributions become more distinctly separated with increasing magnitude. In the simulated catalog, deviations of the tail from an exponential distribution arise from changes in event rates through time, which are due to intervals of partial quiescence after large events. Plots of the inter-event distances against inter-event times show two distinct populations. Those populations correspond to the power-law and exponential components of the inter-event passage time distributions. Clustering of large events, such as the Joshua Tree – Landers – Hector Mine sequence, is a characteristic of seismicity that indicates an increased probability of additional large earthquakes, but the California catalog is too short to define clustering statistics. In the 10,000-year span of the RSQSim catalog there were 177 M≥7 events with 23 large event clusters including two 3-event clusters and one 4-event cluster.

SEISMICITY BASED EARTHQUAKE FORECAST REFERENCE MODEL (1-135)
T. Goebel, D. Schorlemmer, M. Gerstenberger, J. Zechar, and T. Becker

Reliable long and intermediate term earthquake forecasts are fundamental in reducing seismic risk, raising public awareness and encouraging the development of emergency responses in case of major earthquakes. Additionally probabilistic earthquake forecasts exhibit the potential of advancing the physical understanding of the faulting process and its possible evolution, if predictions based on differentiable models are made thus allowing for statistical testing against actual observations. Efforts that bridge the gap between physical models and statistically testable predictions are essential to advance this process. We strive to establish basic reference forecasts, which incorporate only physical assumptions of elementary character. Our aim is to provide well documented, easily reproducible models that have been tested extensively hence can serve as possible null hypothesis in proceeding investigations.Starting from a simple uniform rate forecast we advance by introducingand optimizing adjustable parameter stepwise. We develop an uniform averagerate model, weighted activity model and kernel smoothed models with constantand spatially variable bandwidth. We optimize our forecasts retrospectively dividing the available seismic record into a learning, optimization and target period. Model parameter are chosen to maximize the likelihood function of observed and forecast rates assuming a Poissonian distribution. We deploy statistical forecast performance tests as suggested by the Collaboratory Study of Earthquake Predictability (CSEP). Relative and inter-model tests are further extended by introducing flexible learning periods, magnitude specific event forecasts and through evaluating spatial performances in different tectonic regimes of California. Based on the findings of of these tests we create a pseudo prospective forecast for the time period of the Regional Earthquake Likelihood Model (RELM) efforts, enabling a comparison between our and offcially submitted models. Besides the dependence on studios optimization procedures we discover a strong dependence of test results on the input data namely the selected time windows and magnitude range.

TEMPORAL AND SPATIAL ANALYSIS OF ACOUSTIC EMISSION CLUSTERS DURING SLIDING OF ROUGH GRANITE SURFACES (2-136)
T.H. Goebel, S. Stanchits, T. Becker, D. Schorlemmer, and G. Dresen

Number and size of fault plane asperities have a fundamental influence on the frictional properties of faults. We investigate if the roughness of open rock surfaces during laboratory experiments produces specific signals in acoustic emissions and spatial b-value anomalies which then could be used to identify asperities and monitor their temporal evolution.

Our experiments were performed at the German Research Center for Geosciences (GFZ) in Potsdam, utilizing a 4600 kN loading frame that enables hydrostatic and axial loading. We investigate fracture and sliding of fault surfaces under variable confining pressures. We start by creating a fault in an originally intact rock sample without recognizable cracks under low confining pressure (20 MPa). To control the rupture nucleation process, we use an acoustic emission feedback system. After fracturing, the confining pressure is increased to 75 MPa in the attempt to lock the fault, and four characteristic stress drop events are observed during axial loading. We compare temporal occurrences of acoustic emissions with stress level and identify seismic events that are connected to episodes of accelerated stress release. High seismic activity appears to be linked to asperity grinding and sliding which takes place in a steady (approximately continuous sliding) or

accelerated displacement mode. A set of measures including spatial b-value maps, moment release per area, inter event times and distances are introduced to locate regions of increased fault roughness (asperities) which is thought to be the nucleation point for larger slip events. Three of the major stress drop events seem to correspond to the failure of an asperity region which causes slip of the entire fault plane. The temporal evolution of b-values and summed moment release is investigated for events inside the area of large fault roughness. While b -values decrease prior and increase after stress release events, the seismic moment exhibits the opposite trend which indicates that before asperity failures large events are favored while small events are dominant after slip events. AE cluster locations after several mms of displacement have a higher level of localization indicating a tendency of fault plane evolution to a smoother more homogeneous state. The invesigation of AE patterns connected to asperities in laboratory experiments could provide means of broadening the understanding of seismicity in field studies.

ANALYSES OF COSEISMIC SURFACE DEFORMATION USING TERRESTRIAL LIDAR SCANS OF THE 4 APRIL 2010 EL MAYOR-CUCAPAH EARTHQUAKE RUPTURE (2-072)

P.O. Gold, A.J. Elliott, M.E. Oskin, M.H. Taylor, A.J. Herrs, A. Hinojosa, O. Kreylos, T.S. Bernardin, and E.S. Cowgill

High-resolution terrestrial LiDAR (t-LiDAR) datasets collected 12-18 days after the 4 April 2010, Mw7.2 El Mayor-Cucapah earthquake in northern Mexico provide a new opportunity to advance understanding of how earthquakes deform the earth's surface. Three t-LiDAR datasets quantify fresh, meter-scale coseismic surface ruptures and an additional dataset captures the effects of vertical accelerations exceeding gravity along low-slip fractures. We analyze gridded 3 cm-resolution digital elevation models and the full resolution t-LiDAR point clouds using the KeckCAVES immersive 3D virtual reality space and a 3D-enabled desktop computer. Detailed mapping reveals widely variable rupture styles at three locations suggesting that style is dependent on the properties of the material through which a rupture propagates. The surprising extent of centimeter to decimeter scale distributed displacement, observed tens to hundreds of meters from the zone of maximum offset, raises the possibility that displacements measured across older fault scarps may often be underestimated. Lineations on the vertical fault face measured from full resolution t-LiDAR point-cloud data at two sites define two southeast plunging populations with an average difference in rake of ~30°. The shallower set of lineations (~30° rake) closely matches the ~34° rake of the 2010 slip vector we measured from displaced landforms. Thus we conclude that the steeper set of lineations (~55° rake) indicate the slip direction in the penultimate event. We reconstructed the pre-rupture topography and take profiles across a prominent paleo-fault scarp that yield an average vertical offset of ~3.3 m, from which we estimate a right-normal displacement during the penultimate event of ~4 m along a slip vector plunging ~55° SE. Within ~20 cm of low-slip fractures through alluvial fans, populations of pebbles that have been thrown from stable pavement positions reveal evidence of vertical ground accelerations exceeding gravity. Our analysis of one such location, ~100 m from the zone of maximum displacement, suggests that pavement disruption is the result of seismic wave amplification at a free-face and highlights these fractures as potentially more hazardous than previously thought. Rapid post-event acquisition of dense terrestrial LiDAR data has allowed us to capture details of both the most recent and penultimate earthquakes, and serves to digitally preserve sections of the rupture upon which to base future studies.

2010 SCEC USEIT SCIENCE RESEARCH TEAM (1-004)

M. Gonzalez, S. Kowalke, S. Lauda, H. Potter, A. Stevens, R. de Groot, T. Jordan, T. Huynh, M. Ihrig, and K. Welch

The Undergraduate Studies in Earthquake Information Technology (USEIT) program is organized around a scientific "Grand Challenge" proposed by Professor Tom Jordan, director of the Southern California Earthquake Center (SCEC). The interns devoted the majority of the eight-week internship to tackling the challenge. The 2010 Grand Challenge was to develop a Seismic Crisis Visualization System based on SCEC - Virtual Display of Objects (SCEC-VDO) that could display information needed for operational earthquake forecasting, specifically: showing time-dependent earthquake probabilities painted on faults, displaying kinematic fault rupture models, and visualizing earthquakes in real time. The Science Research team's main purpose was providing accurate scientific information for the interns to help them achieve their goals by contacting professionals for first-hand information and by researching scientific articles. For example, the Science Research team compiled information about operational earthquake forecasting to aid the SCEC-VDO Development team and provided literature-based content for the Content Management System Implementation team to add to the USEIT web site. In addition, the Science Research team adjusted data to resolve focal mechanism ambiguity so the information could be included in SCEC-VDO. Another challenge for the team was creating an outline and figures for a multi-author scientific paper about the capabilities of SCEC-VDO, where the team contacted previous interns and asked them to participate in authoring the paper. The Science Research team accomplished their goals by conducting research, initiating the scientific paper, and ensuring the scientific accuracy and validity of all products produced during the Grand Challenge.

SEISMOTECTONICS OF THE 2010 EL MAYOR CUCAPAH/INDIVISO EARTHQUAKE (1-114)
J. Gonzalez-Garcia and J. Gonzalez-Ortega

The so called Eastern Sunday 4th April 2010 Mw 7.2 is the biggest earthquake in ~160 years of earthquake history in the Salton Trough region. It was a benign earthquake because only 2 deaths were related to its occurrence. However, it produced agricultural and ecological prominent changes at the southeastern part of the Mexicali Valley, were a new fault, the Indiviso fault was inferred from InSar teledetection and Land Sat Imagery.

The Earthquake was a complex event and it has at least 3 episodes. It originated as a normal earthquake along the here called El Mayor-Hardy fault with a N-S strike and 18 km length. After 10 seconds, two big burst of energy were dissipated, one to the NW and one to the SE producing the total moment liberation that can be reach Mw 7.25.

The NW surface ruptures reactivated the Pescaderos and Borrego faults with almost no disruption of the Laguna Salada fault. This section had a major right lateral strike slip movement with a NE side down. The SE disruption occurred along the Indiviso fault with a strike slip and SW side down. The epicentral aftershock area, including its main aftershock at the NW is >120 km; the surficial faulting occurs along ~110 km with 4-5 km of ramification to the N-NE in the NW and to the S-SW in the SE.

The surficial rupture resembles a propeller structure activated by the normal earthquake along the N-S El Mayor-Hardy fault that is delineating by frequent M~5-5.5 events.

The El Mayor-Cucapah/Indiviso event complements a Gutemberg-Richter b=1, for 9 earthquakes M>6.5 (SCEC catalog) occurring in a "pure strike slip region" between the head of the Gulf of California and the San Andreas's Big Bend in the last 80 years; this conduct to the possibility of the occurrence of a M~7.5 in this region. The fault zones larger than 200 km with no earthquake rupture in the recent past and with the capabilities of generating an earthquake as big are Elsinore and southern San Andreas.

GPS COSEISMIC AND POSTSEISMIC SURFACE DISPLACEMENTS OF THE EL MAYOR-CUCAPAH EARTHQUAKE (1-155)
J. Gonzalez-Ortega, J. Gonzalez-Garcia, D. Sandwell, Y. Fialko, F. Nava, J.M. Fletcher, D. Agnew, and B. Lipovsky

GPS surveys were performed after the El Mayor Cucapah earthquake Mw 7.2 in northern Baja California by scientists from CICESE, UCSD, and UCR. Six of the sites were occupied for several weeks to capture the postseismic deformation within a day of the earthquake. We calculated the coseismic displacement for 22 sites with previous secular velocity in ITRF2005 reference frame and found 1.160±0.016 m of maximum horizontal displacement near the epicentral area at La Puerta location, and 0.636±0.036 m of vertical offset near Ejido Durango. Most of the GPS sites are located East of the main rupture in Mexicali Valley, 5 are located West at Sierra Juarez and South near San Felipe. We present a velocity field before, along with coseismic displacements and early postseismic features related to the El Mayor-Cucapah earthquake.

ANALYSIS OF SEISMIC ACTIVITY AND POTENTIAL SEISMIC HAZARDS OF THE FONTANA TREND IN SOUTHERN CALIFORNIA (1-034)
M.L. Gooding

Southern California is a seismically active region with a large population. The Study Area is the Fontana Seismic Trend, an area of intense earthquake activity in western San Bernardino County. There has not been much significant work done to quantify the potential seismic hazard posed by it. This presentation will show that there is potential for a moderate seismic event on the Fontana Seismic Trend that will likely cause quite a bit of damage and disrupt lives. The major faults nearby have been studied extensively, but this is not the case for the Fontana Seismic Trend. When plotted on a map, the earthquake epicenters of the Fontana Seismic Trend display a significant linear pattern both two dimensionally and three dimensionally. In this presentation, the location and direction of movement of the underlying fault are identified and configured to fit the earthquake data. Using the plotted fault location, direction of movement and length, the maximum potential event that might occur on this fault was also quantified. HAZUS-MH (a FEMA software extension for ArcGIS) was used to perform a seismic hazard analysis to find out what type of damage and casualties can be expected if a moderate event occurs on this fault. This presentation discusses the methods used to determine the fault parameters and details the results from the seismic hazard analysis.

NON-LINEAR BUILDING RESPONSE SIMULATIONS USING SCEC SIMULATED GROUND MOTIONS (1-050)
C.A. Goulet and C.B. Haselton

Although substantial progress has been made in physics-based ground motion simulations in the recent years, the engineering community is still reluctant to use simulated time series as the basis for structural design. One of the reasons for this is a lack of understanding of how simulated ground motions compare to

recorded ground motions, especially when it comes to their impact on nonlinear structural response. There are on-going efforts to validate and verify simulated ground motions, but these tend to be focused on record properties or on the response of single-degree-of-freedom systems. We are proposing a different approach: we plan to compare the nonlinear structural responses of full multi-story structural models when they are subjected to both recorded and simulated ground motions. For direct comparisons to be possible, we will start with sets of recorded and simulated motions that have similar spectral shapes; this will help us to better understand if there are any differences in the records that affect nonlinear structural response, but that are not expressed in the elastic response spectrum.

The responses of buildings to recorded motions have already been well documented in a project recently completed by the PIs. The recorded set is representative of a magnitude 7.0 earthquake, rupturing an average of 10 km from a site with a Vs30 of 400 m/s (average shear wave velocity of the upper 30 meters of the soil column). Our goal is to select SCEC simulated records (for the same type of event and site conditions) with spectral shapes that are consistent with the recorded sets previously used by the PIs. We will then perform the structural simulations and compare the response predictions from both sets of time series (recorded and simulated). In this poster, we present the approach in more detail and show preliminary record selection results.

SCEC/SURE: THE IMPACT OF THE EARTHQUAKE COUNTRY ALLIANCE EARTHQUAKE EDUCATION AND PUBLIC INFORMATION CENTERS (ECA EPICENTERS) (1-031)
I.N. Gow, R.M. de Groot, K.B. Springer, L. Schuman, J. Sutorus, B. Burrows, and N. Oropez

The Earthquake Education and Public Information Center (EPIcenter) Network shares a commitment to encouraging earthquake preparedness through demonstrated leadership in risk-reduction and earthquake education. The EPIcenter Network, starting as an informal alliance in 2008, is now comprised of over 55 free-choice learning institutions throughout California and elsewhere. Having demonstrated its viability, the Network is building a strategy for sustainability. The purpose of the research is to develop impact measures for the EPIcenter Network through grounded theory. Five Network members were interviewed to further understand their institution's goals and mission. The data were incorporated into 5 logic models, one for each institution. The logic models illustrate how the mission of the EPIcenter Network supports the mission of each institution. The models also show the theoretical outcomes and impact of the Network on each institution and the Network on the communities served by each institution. Although there were differences in inputs and outputs between types of free-choice learning institutions, the theoretical outcomes were similar. The five logic models represent a single focused initiative to measure the impact of the EPIcenter Network. A continued literature review on informal science learning and evaluation methods, increased communication with members of the Network, and increased data collection are needed to continue the impact measurement and development of the EPIcenter Network. A potential product of this research is a rubric that will allow individual institutions and the EPIcenter Network as a whole to measure success and identify areas of improvement.

PRECARIOUSLY BALANCED ROCKS IN THE WESTERN SAN BERNARDINO MOUNTAINS AND THE 1812 EARTHQUAKE ON THE SAN ANDREAS - SAN JACINTO FAULT (1-077)
L. Grant Ludwig and J.N. Brune

The rupture extent of the earliest historic earthquake attributed to the San Andreas fault in AD 1812 is poorly constrained by historic and paleoseismic data. Early earthquake catalogs for southern California attributed it to the Newport-Inglewood fault because it destroyed the Mission at San Juan Capistrano. Since the discovery that trees in Wrightwood, CA were disturbed by the earthquake, it has been assigned to the San Andreas fault, and competing rupture models have been proposed to fit the sparse historic accounts of shaking. Confirmation of the proposed rupture pattern has been elusive because dates of surface ruptures observed in trenches at several locations along the San Andreas fault either cannot be resolved to 1812 within radiocarbon dating uncertainty, or preclude rupture. Here we present data on the distribution of fragile precariously balanced rocks (PBRs) in the western San Bernardino Mountains that are inconsistent with accepted rupture models for the 1812 earthquake. To better fit PBR and paleoseismic data, we present an alternate model of rupture that jumped between the San Andreas and San Jacinto faults in Cajon Pass. This model is consistent with previously enigmatic observations about the stress field in Cajon Pass, activity of the Cleghorn fault, and simulated ground motions of San Andreas fault earthquakes.

LONG-PERIOD GROUND-MOTION SIMULATIONS OF THE MW 7.2 EL MAYOR-CUCAPAH MAINSHOCK: EVALUATION OF FINITE-FAULT RUPTURE CHARACTERIZATION AND 3D SEISMIC VELOCITY MODELS (1-061)
R.W. Graves and B.T. Aagaard

Using a suite of five hypothetical finite-fault rupture models, we test the ability of long-period ($T > 2.0$ s) ground-motion simulations of scenario earthquakes to produce waveforms throughout southern California

consistent with those recorded during the 4 April 2010 Mw 7.2 El Mayor-Cucapah earthquake. The hypothetical ruptures are generated using the methodology proposed by Graves and Pitarka (2010) and require, as inputs, only a general description of the fault location and geometry, event magnitude and hypocenter, as would be done for a scenario event. For each rupture model, two Southern California Earthquake Center (SCEC) 3D community seismic velocity models (CVM-4m and CVM-H62) are used, resulting in a total of 10 ground-motion simulations, which we compare with ground motions recorded at over 200 sites throughout southern California. While the details of the motions vary across the simulations, the median levels match the observed peak ground velocities reasonably well with the standard deviation of the residuals generally within 50% of the median. Considering the entire model region, simulations with the CVM-4m model yield somewhat lower variance than those with the CVM-H62 model. However, for the non-basin regions, simulations with the CVM-H62 model perform significantly better than those of CVM-4m, which we attribute to the inclusion of the Tape et al. (2009) tomographic updates within the background crustal velocity structure of CVM-H62. Both models tend to over-predict motions in the San Diego region and under-predict motions in the Imperial basin and the Mojave desert. Within the greater Los Angeles basin, the CVM-4m model generally matches the level of observed motions whereas the CVM-H62 model over-predicts the motions in the southernmost portion of the basin. Animations of the simulated wave fields demonstrate this over-prediction is created by the sharp impedance contrast along the southern margin of the Los Angeles basin in the CVM-H62 model. For both seismic velocity models, the variance in the peak velocity residuals is lowest for a rupture that has significant shallow slip (less than 5 km depth), whereas the variance in the residuals is greatest for ruptures with large asperities below 10 km depth. Overall, these results are encouraging and provide confidence in the predictive capabilities of the simulation methodology, while also suggesting regions where the seismic velocity models may need improvement.

THE MICROMECHANICS OF FAULT GOUGE AND DYNAMIC EARTHQUAKE TRIGGERING: INVESTIGATION BY DISCRETE ELEMENT METHOD NUMERICAL SIMULATIONS (2-060)

M. Griffa, E.G. Daub, R.A. Guyer, P.A. Johnson, C.J. Marone, and J. Carmeliet

In order to investigate the role of stress waves in the nucleation of earthquakes, shearing experiments on thin granular layers were conducted (Johnson et al, 2008). Sound waves, in the form of both wide-band short and quasi-continuous sources, were applied to the shearing block. Upon application of the sound disturbance, the stick-slip dynamics were disrupted in its regular periodicity and slip events were induced at earlier times than expected when sound was applied.

The experiments provide evidence of dynamic triggering of slip events by stress waves, confirming seismic observations. However, they do not allow access to particle-scale measurements of the granular dynamics during the stick-slip cycle and its perturbation by the stress waves. We expand the insight gained by laboratory experiments by implementing and performing Discrete Element Method numerical simulations of a similar model system.

We present analysis using a mesoscopic metric able to provide information about the development of plastic strain inside the granular layer. We show that externally applied vibration causes localized plastic strain in the granular layer prior to the start of a slip event. This demonstrates that vibration nucleates slip by inducing plastic rearrangements in the gouge, allowing slip to initiate at a reduced shear stress relative to simulations without applied vibration. Our results show that small perturbations applied to granular systems can have a dramatic effect on the macroscopic dynamics of failure and slip, and improve our understanding of the most important physical parameters controlling dynamic earthquake triggering.

GEOLOGIC AND GEOMORPHIC CHARACTERIZATION OF PRECARIOUSLY BALANCED ROCKS (1-075)

D.E. Haddad and J.R. Arrowsmith

Precariously balanced rocks (PBRs) are balanced boulders that serve as in situ negative indicators for earthquake-generated strong ground motions and can physically validate seismic hazard analyses over multiple earthquake cycles. Understanding what controls where PBRs form, when they were formed, and how long they remained balanced is critical to their utility as paleoseismometers. The geologic and geomorphic settings of PBRs are investigated using PBR surveys, slenderness analysis from digital photographs, joint density analysis, and landscape morphometry. An efficient field methodology for documenting PBRs was designed and applied to 261 precarious rocks. An interactive computer program that estimates 2-dimensional (2D) PBR slenderness from digital photographs was developed and tested against 3-dimensional (3D) photogrammetrically generated PBR models. 2D slenderness estimates are accurate compared to their 3D equivalents, attaining <8.8% error in the heights of the estimated PBR centers of mass. The joint density analysis reveals a mean PBR joint density of 0.39 m^-1 with few PBRs formed in joint densities <0.22 m^-1 and >0.55 m^-1. Landscape morphometry shows that PBRs are situated in upper reaches of drainage basins near divides and hillslope crests. Surveyed PBRs are preserved on local hillslope gradients between 10° and 45°, and contributing areas (per unit contour length) between 1 m^2/m and 30

m^2/m. The close comparison between the 2D and 3D PBR stability estimates indicates that our program may be used to efficiently estimate PBR slenderness from digital photographs taken in the field within reasonable accuracy. The joint density results indicate that structural control on the bedrock from which PBRs are produced is critical to their formation and preservation; high joint densities create small boulders that completely decompose prior to exhumation while low joint densities create relatively large boulders that are stable. Morphometry results indicate that the location of a PBR in a landscape controls its formation and preservation potential, and may thus help predict expected locations of PBRs in landscapes. More importantly, they caution that the construction of PBR exhumation rates from surface exposure ages needs to account for their geomorphic location in a drainage basin given that soil production and boulder emergence rates are controlled by the geomorphic state of the landscape.

ARE SURFACE DISPLACEMENTS REPRESENTATIVE OF SLIP AT SEISMOGENIC DEPTHS? IMPLICATIONS FOR GEOLOGIC SLIP RATE STUDIES (1-099)

B. Haravitch and J. Dolan

It has long been observed that surface displacements are in many instances smaller than displacements at depth. This is often interpreted to imply that a significant proportion of the slip at depth is accommodated by distributed deformation near the surface. We hypothesize that the degree to which deformation is localized at the surface is fundamentally controlled by the structure of the near-surface fault zone itself. We study six faults that ruptured in seven large earthquakes (Mw 7.1 – 7.9), ranging from structurally nascent (e.g., the Lavic Lake fault in the 1999 Mw 7.1 Hector Mine earthquake), to structurally immature (e.g., the faults that ruptured in the 1992 Mw 7.3 Landers event), to structurally mature (e.g., the North Anatolian fault in the 1999 Mw 7.5 Izmit and Mw 7.1 Duzce events, the Kunlun fault in the 2001 Mw 7.8 Kokoxili earthquake, and the Denali fault in the 2002 Mw 7.9 Denali earthquake). By comparing surface slip distributions to slip distributions at different depths estimated by inversions of InSAR, GPS, or a combination of these data, we determine areas along the faults where surface slip values are in deficit, surfeit, or agreement with the slip values from depth. We find that the ratio of surface slip to slip at depth varies from less than 10% to over 100%, with average values that correlate in general with relative structural maturity (i.e. cumulative displacement) of each fault. Thus, the average ratio of surface slip to slip at depth is greater for mature faults than for structurally immature faults. This trend is roughly linear across the six faults of variable structural maturity that we examine. Inasmuch as structural maturity is directly related to structural complexity, we interpret these results as indicating that structurally simple parts of faults will exhibit more highly localized deformation at the surface than more structurally complex parts of the faults (e.g. steps, bends, and multiple strands). These observations provide a means of determining the degree to which surface geologic slip rate measurements capture the total slip rate of the fault at depth. Such understanding is critically important for assessing the validity of potential geologic/geodetic rate discrepancies and will provide a set of criteria for determining, in advance, the likelihood that a geologic slip rate study site will allow an accurate measurement of the true fault slip rate.

THE SCEC-USGS DYNAMIC EARTHQUAKE RUPTURE CODE VERIFICATION EXERCISE: REGULAR AND EXTREME GROUND MOTION (2-082)

R.A. Harris, M. Barall, R. Archuleta, B. Aagaard, J.-P. Ampuero, D.J. Andrews, V. Cruz-Atienza, L. Dalguer, S. Day, B. Duan, E. Dunham, G. Ely, A. Gabriel, Y. Kaneko, Y. Kase, N. Lapusta, S. Ma, H. Noda, D. Oglesby, K. Olsen, D. Roten, and S. Song

We summarize recent progress by the SCEC-USGS Dynamic Rupture Code Verification Group. In November 2009 we held our most recent workshop where we examined how SCEC and USGS researchers' spontaneous-rupture computer codes agree (or disagree) when computing benchmark scenarios for dynamic earthquake rupture. Our latest benchmarks are 'regular' dynamic ruptures on a vertical strike-slip fault and on a normal fault, at a range of resolutions, and, 'extreme' dynamic ruptures on a normal fault. The 'extreme' dynamic ruptures were designed as complete stress-drop, supershear ruptures that would be most likely to produce maximum possible ground motions. These simulated ruptures could be thought of as very unlikely, but still possible. Among the 2009 'extreme' dynamic rupture benchmarks were those targeted to test two simplified versions of Joe Andrews' [Andrews et al., BSSA, 2007] numerical simulations for hypothesized maximum-possible ground motion at a site near Yucca Mountain. To test the Andrews et al. methodology, we constructed a benchmark for a planar dipping normal-fault set in a medium where the off-fault response was designated to be elastic (TPV12), and another benchmark where the off-fault response was designated to be plastic (TPV13). Although most of our group's previous benchmarks have concentrated on 3D solutions, both the TPV12 and TPV13 benchmarks were offered with both 2D and 3D options, partly because the Andrews et al. [2007] study was conducted in 2D, and partly because it is important to understand the differences and similarities among 2D and 3D rupture propagation and ground motion predictions. Seven researchers' codes participated in the TPV12 2D benchmark test, seven participated in the TPV12 3D test, six participated in the TPV13 2D benchmark test, and four participated in the TPV13 3D test. Our findings were similar to those hypothesized in the Andrews et al. 2007 publication.

At a proposed site for a nuclear waste repository, that was modeled to be 1-km from the fault, at 300 m depth, our 2D elastic benchmark simulations produced the largest vertical velocity, while our 3D plastic simulations produced the smallest vertical velocity. In the fall of 2010, our group will embark on our next 'regular' benchmark exercises. One new benchmark will involve thermal pressurization on a planar strike-slip fault, and another will involve slip-weakening rupture on branching vertical strike-slip faults.

INSTRUMENTATION AND DATA PROCESSING FOR THE SCEC BOREHOLE INSTRUMENTATION PROGRAM (2-151)
K.J. Harris

We present a testing setup that allows for the rapid and accurate testing of the lightning protection circuits employed by ICS at seismic monitoring stations. These lightning circuits are used to protect sensors (both surface and borehole) and data loggers from the harmful effects of lightning strikes near the monitoring stations. With this new testing apparatus, the response of the circuit to large voltages can be readily observed and compared to the expected response, allowing for easy identification of malfunctioning circuits. The test system consists of a circuit made from off the shelf components and software. The setup also allows the quality of the data signal to be monitored in order to check for undesired activity from the circuits, such as aliasing and digital noise. Further work will continue in ensuring the accuracy of the test results as well as increasing the scope of the test setup to allow for quicker testing through simultaneous testing methods.

We also present the initial stages of a seismic event database web application that provides any interested party with pre-selected data from SCEC borehole monitoring stations in southern California. The chosen waveform data was selected for its error-free qualities and to show cases where the ground deformation as a response to seismic activity was linear as well as non-linear. All the events have been selected and are being complied in an Antelope database. From here the database will be integrated into a website where the general public can download the waveforms.

CHARACTERISTICS OF LONG-PERIOD (3 TO 10 S) STRONG GROUND MOTIONS OBSERVED IN AND AROUND THE LOS ANGELES BASIN DURING THE MW7.2 EL MAYOR-CUCAPAH EARTHQUAKE OF APRIL 4, 2010 (1-067)
K. Hatayama and E. Kalkan

We examined the characteristics of long-period strong ground motions within a period range of 3 to 10 s in and around the Los Angeles (LA) basin during the Mw7.2 El Mayor-Cucapah earthquake. The contour map of the observed peak ground velocity (PGV) values clearly shows that the LA basin significantly amplifies the long-period motions. The largest PGV values observed within the LA basin range from 0.1 to 0.12 m/s, though the basin is around 350 km away from the epicenter. These largest PGV values were recorded at seven stations in the central part of the basin and one station in the western part of the basin. The Fourier acceleration spectra of records from these eight stations are predominant at the periods of 6 to 8 s with the corresponding peak values of 1 to 1.4 m/s. The ratio of Fourier amplitudes with respect to a reference site (STG station of the Southern California Seismic Network, located on hard rock in the southeast edge of the LA basin) show that the spectral amplitudes at these eight stations are 5 to 13 times larger than those at the reference site within a wide period range, 5.5 to 9 s. To understand how the spatial variation of amplification for the long-period motions is related to the basin underground structure, we plotted contours of the amplification factors at 3, 5, 7 and 10 s spectral periods with respect to the reference site (i.e. STG station) onto several different maps, where depths to different S-wave velocities (Vs) are also depicted using the latest SCEC Community Velocity Model (CVM-H 6.2). Comparison of amplification contours with the basin model indicates that for the 10 s spectral period, the largest amplification occurs in the central part of the LA basin where the depth to the Vs of 3.2 km/s reaches to the maximum, 9.5 km. For the 7 s spectral period, the amplification becomes larger in the similar area to the 10 s case and also in the San Gabriel valley where the depth to the Vs of 1.5 km/s reaches to the maximum, 3.7 km. For the 3 and 5 s spectral periods, the spatial depth variation of Vs = 2.5 and 2.8 km/s might correlate with the contour pattern of the spectral amplification, in addition to that of Vs = 3.2 km/s.

THE 2010 MW7.2 EL MAYOR-CUCAPAH EARTHQUAKE SEQUENCE, BAJA CALIFORNIA, MEXICO AND SOUTHERNMOST CALIFORNIA, USA (2-111)
E. Hauksson, J. Stock, K. Hutton, W. Yang, A. Vidal-Villegas, and H. Kanamori

The El Mayor-Cucapah earthquake sequence started with preshocks in March 2010, and a sequence of 15 foreshocks of M>2 (up to M4.4) that occurred during the 24 hours preceding the mainshock. The foreshocks occurred along a north-south trend near the mainshock epicenter. The Mw7.2 mainshock that occurred on the 4th of April exhibited complex faulting, possibly starting with a ~M6 normal faulting event, followed ~15 sec later by the main event, which included simultaneous normal and right-lateral strike-slip faulting. The aftershock zone extends for 120 km from the south end of the Elsinore fault zone at the US-Mexico border almost to the northern tip of the Gulf of California. The waveform-relocated aftershocks form two abutting

clusters, of about equal length of 50 km each, as well as a 10 km north-south aftershock zone just north of the epicenter of the mainshock. The spatial distribution of large aftershocks is asymmetric with five M5+ aftershocks located to the south of the mainshock, and only one M5.7 aftershock but numerous smaller aftershocks to the north. Further, the northwest aftershock cluster exhibits complex faulting on both northwest and northeast planes. The aftershocks also express a complex pattern of stress release along strike. The overall rate of decay of the aftershocks is similar to the rate of decay of a generic California aftershock sequence. The synthesis of the El Mayor-Cucapah sequence reveals transtensional regional tectonics, including the westward growth of the Mexicali Valley as well as how Pacific North America plate motion is transferred from the Gulf of California in the south into the southernmost San Andreas fault system to the north.

APPLICATION OF THE REFRACTION MICROTREMOR METHOD TO MEASUREMENTS OF VS30 ALONG THE SOUTHERN SAN ANDREAS FAULT (1-036)
S.E. Hauksson, M. Thompson, J.N. Louie, S. Pullammanappallil, and A. Pancha

We measured the near surface ground velocity for twenty sites on the Southern San Andreas and Imperial Faults using the Refraction Microtremor (ReMi) method. As has been demonstrated by several pervious studies ReMi arrays provide an inexpensive method for measuring near-surface velocities and are especially effective at estimating the vertically-averaged shear velocity from the surface to 30 meter depth, known as Vs30. Vs30 measurements provide us with important information about the likely intensity of ground shaking due to local site conditions. All sites used a linear array of geophones placed at either 3-meter or 8-meter intervals depending on the local topography. The geophone lines pick up Rayleigh waves generated by background seismic noise. The higher frequency content of the signals was augmented by striking a hammer off one end of the array. These Vs30 measurement sites will provide us with a better map of the ground characteristics and velocities in Southern California, thus giving us better estimates of how the ground will behave and what areas will experience more intense shaking in Southern California.

The data were collected during 2009 from the southern end of the Imperial Valley north to Cajon Pass, with two sites west in the northeast San Gabriel Mountains. The Vs30 values measured at these 20 sites ranged from a low of 200 m/sec to a high of 850 m/sec. The low occurred at a site in the loose sediment in the middle of the Imperial Valley and the high in the hard rock of the mountains east of the Imperial Valley. Other high VS30s were found in the mountains to the west of the Imperial Valley, and in the San Bernardino and San Gabriel mountains. These measurements will now allows us to create a more accurate model of how shaking along the Southern San Andreas will propagate and affect Southern California. However, more measurements are still needed to complete the picture of shallow ground shaking in Southern California.

A METHOD TO DETECT DAMAGE IN STEEL STRUCTURES USING HIGH-FREQUENCY SEISMOGRAMS: A NUMERICAL ANALYSIS (1-046)
V.M. Heckman, M.D. Kohler, and T.H. Heaton

A numerical study is performed to gain insight into applying a novel method to detect high-frequency dynamic failure in buildings. The method makes use of a prerecorded catalog of Green's functions for an instrumented building to detect failure events in the building during a later seismic event by screening continuous data for the presence of waveform similarities to one of the prerecorded events. In the first part of this study, an impulse-like force is applied to a beam-column connection in a linear elastic steel frame. Resulting displacements are recorded at six receiver locations. By using a time-reversed reciprocal method, the recorded displacements are used to determine the absolute time and location of the applied force. In the second part of this study, a steel frame's response to two loading cases, an impulse-like force and an opening crack tensile stress, is computed on a temporal scale of microseconds. Results indicate that the velocity waveform of a tensile crack can be approximated by the velocity waveform of an impulse-like force load applied at the proper location. These results support the idea of using an impulse-like force to approximate a weld fracture damage source to characterize a high-frequency fracture event in the far field. The results pave the way for the use of waveform cross-correlation using a pre-event catalog of Green's functions to determine the location and time of occurrence of a subsequent fracture recorded on a network of vibration sensors.

10BE DATING OF FLUVIAL TERRACES IN SOUTHERN CALIFORNIA: SUCCESS, FAILURE, AND THE FUTURE… (1-113)
R.V. Heermance, K. McGuire, and H. McKay

During the last 15-20 years, cosmogenic 10Be has been widely applied to exposure dating of geomorphic surfaces. Dating of these surfaces, however, has been complicated by a variety of factors including post-depositional inflation and/or deflation of the surface and assumptions regarding the nuclide concentration prior to deposition (ie. inheritance). This abstract reports new data from fluvial terraces within the Ventura Basin, as well as ongoing research of 10Be dating from San Gorgonio Pass. Previous research by Rockwell et

al. (GSAB 1984, v. 95, p. 1466-1474) near the Ventura River suggests ages of 38 ka (Qt6a), 30 ka (Qt5b), 20 ka (Qt5a2), and 15 ka (Qt5a1) for prominent terrace surfaces. 10Be dating of boulders from Qt6a reveals an age of ~34 ka, slightly younger than previous work, although the rounding and weathering of the sandstone boulders suggests that this is a minimum age. Depth profiles from Qt6a and Qt5a1 suggest ~30% younger ages than those determined by other methods, although surface deflation may have compromised these data. Other age discrepancies are apparent between optically stimulated luminescence (OSL) ages of ~25 ka and a 10Be depth profile age of ~75 ka from the same geomorphic surface in Moorpark, CA. In summary, cosmogenic nuclide dating of fluvial terraces in the Ventura Basin is complicated by a variety of factors including rapid erosion of bedrock, surface deflation, and unknown inheritance, such that multiple geochronometers are often inconsistent in their age determination. To better understand these factors, we have initiated a comprehensive 10Be study on the Millard Canyon fan in San Gorgonio Pass. Terrace levels were sampled for both depth profiles and boulder/cobble surface ages. Ages will be combined with a comprehensive study of nuclide inheritance from at least 4 grain sizes within the active channel. Inheritance is hypothesized to vary with grain size due to clast erosion during transport and mixing of proximal hill slope sediments. 10Be terrace ages will be compared with C-14 and soil ages from new fault trenches cut into the terraces. Together, this comprehensive study will allow us to interpret the age of these terrace surfaces within a context of nuclide inheritance and post-depositional erosion.

LIMITATIONS AND TRADEOFFS IN LARGE SCALE EARTHQUAKE SIMULATION (2-153)
E.M. Heien, M.B. Yikilmaz, D.L. Turcotte, J.B. Rundle, and L.H. Kellogg

Earthquake simulation provides a new way of investigating the physics and statistics of earthquake models under different conditions and with different parameters. To properly understand small scale behavior these simulations must use large numbers of elements to represent the faults. As the number of elements grows there are increasing demands placed on computing resources in terms of the processor, memory and in the case of parallel simulations, the network. Here we examine the computational limitations of the Virtual California earthquake simulator for large scale models. We show that memory size and bandwidth is much more of a limiting factor than processor speed or network bandwidth, and investigate the limits on simulation detail in regards to various computing platforms. To overcome these limitations we demonstrate techniques to improve memory usage while studying the tradeoffs in accuracy these entail.

EARTHQUAKE FORECASTS FOR CALIFORNIA BASED ON SMOOTHED SEISMICITY AND RATE-AND-STATE FRICTION (1-126)
A. Helmstetter and M.J. Werner

We present new methods for time-independent and time-dependent earthquake forecasting based on smoothed seismicity. Past earthquakes are smoothed in space and time using adaptive Gaussian kernels. The bandwidths in space and time associated with each event are a decreasing function of the seismicity rate at the time and location of each earthquake, in order to obtain a better resolution in areas of intense seismicity and a smoother density in areas of sparse seismicity. This method can be used for producing time-independent forecast by defining the long-term rate in each cell as the median value of the temporal history of the seismicity rate in this cell. When tested on California seismicity, this model produces slightly better forecasts compared to our previous method based on spatial smoothing of declustered catalogs (Helmstetter et al., 2006, 2007; Werner et al., 2010) and is much simpler (no declustering, less adjustable parameters). Spatio-temporal smoothing of past earthquakes can also be used for time-dependent earthquake forecasting by assuming that the seismicity rate in the future will be constant in time and equal to its present value. When used to produce daily forecast in California, this new method is almost as good as the ETAS model (Helmstetter et al., 2006; Werner et al., 2010). Finally, a more realistic and physical model has been developed based on the rate-and-state model of Dieterich (1994). The rate-and-state model is used to extrapolate the rate beyond its present value (measured by spatio-temporal smoothing of past earthquakes), without the need for any stress calculation. This last model requires only one additional parameter, the nucleation time, which characterizes the time necessary for the seismicity rate to evolve toward its long-term rate.

RESOLVING DISCREPANCIES BETWEEN PERMANENT GPS DERIVED AND GEOLOGIC SLIP RATES (2-017)
J.W. Herbert and M.L. Cooke

The southern Big Bend of the San Andreas fault incorporates numerous non-vertical, non-planar, and intersecting fault surfaces that cannot adequately be represented by rectangular fault segments. Numerical models that neglect the complex geometry of faults in this area are unable to incorporate the spatial variability of fault slip. Additionally, models with simple fault geometry may infer erroneous slip rates if they use only a few GPS data to constrain slip. Differences between such GPS-derived slip rates and longer-term geologic slip rates have been attributed to temporal variations in fault slip rate but instead may owe to inadequate fault complexity within the models and/or lack of GPS constraints near the sites of the geologic slip rates. For example, GPS inversion studies have suggested 12 ± 2 mm/yr of accumulated shear strain

across the northern section the Eastern California Shear Zone in disagreement with geologic slip rates across the central Mojave of ≤6.2± 1.9 mm/yr. Data from new permanent array GPS stations show significantly slower strain rates across the central Mojave in agreement with geologic slip rates. Meanwhile, discrepancies between geologic and GPS-derived slip rates along the San Bernardino strand of the San Andreas fault may owe to over simplified fault configurations. Our 3D models with complex fault configurations show significant spatial variation in both fault slip rates and interseismic velocities along the Earth's surface. We are able to simulate both fault slip rates similar to the geologic rates and horizontal velocities that closely match permanent GPS station velocity data without evoking temporal variations in fault slip rates. We also test the sensitivity of fault slip to the orientation and magnitude of regional tectonic loading.

BEHAVIOR OF THE DEEP ROOTS OF FAULTS (invited talk)
G. Hirth

In this invited talk I will outline several lines of evidence that constrain the rheological behavior of the deep roots of faults, including: (1) microstructural observations of natural faults and shear zones combined with extrapolation of laboratory viscous creep data and (2) extrapolation of laboratory friction data to conditions at the base of the seismogenic zone. I will first show structural data that constrain the creep behavior of gabbroic crustal rocks under both wet and dry conditions. By combining constraints from geothermometry and thermochronology with microstructural data on grain size and crystal orientations, we find excellent agreement between predictions based on extrapolation of laboratory flow laws and geologic observations (Mehl and Hirth, 2008; Homburg, Hirth and Kelemen, 2010). A similar approach provides compelling agreement between natural samples and the extrapolation of quartzite flow laws (e.g., Hirth et al., 2001). These studies provide a benchmark to compare independent constraints on lower crustal flow and strain localization based on geodesy and the spatial/temporal distribution of seismicity. For problems related to extrapolating friction data to natural conditions, I will focus on three issues. First, our analysis of the frictional behavior of olivine aggregates is consistent with independent geophysical observations that indicate that mantle seismicity is limited to temperatures less than ~600oC (Boettcher et al., 2007). At laboratory strain rates, we observe a transition from velocity weakening to velocity strengthening in olivine at a temperature of between 800-1000oC. Analysis of these data supports application of a dislocation-glide asperity creep mechanism (e.g., Rice et al., 2001), which forms the basis for extrapolation to natural conditions based on differences between laboratory and geologic strain rates (rather than differences in displacement rates). Second, I will discuss some implications that arise by invoking a similar constraint for extrapolation of frictional data on crustal lithologies. Third, (time permitting), I will briefly outline some of our recent data on dynamic frictional weakening (Kohli, Goldsby, Hirth and Tullis, 2010) and strain localization (Chernak and Hirth, 2010) of serpentinite to motivate discussion of possible mechanisms for slow slip events at elevated temperatures in the crust and mantle.

RECONNAISSANCE GEOLOGIC CHARACTERIZATION OF THE ONSHORE PALOS VERDES FAULT ZONE, SOUTHERN CALIFORNIA (1-049)
P.J. Hogan, S.C. Lindvall, and S.L. Varnell

The Sanitation Districts of Los Angeles County are evaluating the feasibility of constructing a new tunnel and ocean outfall to serve a large portion of metropolitan Los Angeles. The new tunnel and outfall will extend from Carson to the Continental Shelf south of the Palos Verdes Peninsula or San Pedro. The feasibility/design phases of the project started in 2006 and are planned through 2012, with construction set to begin in 2013.

In late 2009 we performed a geologic reconnaissance to better locate and characterize the Palos Verdes Fault Zone (PVFZ) onshore between the Port of LA and Chandler Quarry. Those segments of the tunnel crossing active splays of the PVFZ may be susceptible to damage resulting from potential future fault rupture displacement.
Fugro obtained a large amount of data in various formats, coordinate systems, and units that were used to refine previous interpretations of the location of and geometry of the PVFZ. These data included historic air photos, gravity, aeromagnetic, Digital Elevation Model (DEM), groundwater information, and seismic reflection datasets. GIS renderings, maps, images, and topographic profiles were used to analyze and present updated information on the PVFZ. A sun-illuminated DEM rendering was created from historical USGS topographic maps, providing a detailed representation of the landscape that predates most modern grading and development.

The most significant results of this study are as follows:

- The geometry, width, amount of offset, and sense of displacement vary along the onshore PVFZ;
- Two primary fault splays of the onshore PVFZ were identified. The two primary fault splays are greater than 6,000 feet apart, and bound the Gaffey Anticline;

- The location of the two primary fault splays is consistent with several previous investigations and published maps;
- The Southern fault Splay is likely active, the zone of deformation may be relatively narrow, and the fault style is right lateral strike slip motion;
- The Northern fault Splay is an active oblique reverse fault. Whilst the primary slip zone is likely narrow, secondary faulting and folding should be expected across a broad zone in the hanging wall to the fault; and
- Minor folding and secondary faulting may occur across the broad Gaffey Anticline in the region between the Southern and Northern fault Splays.

Additional geologic, geophysical and geotechnical studies will be performed prior to final tunnel design to further characterize the activity, sense of slip and potential displacements per event for the Northern and Southern Splays of the PVFZ. In addition, these studies should address the potential for additional secondary, off-fault deformation. Paleoseismic studies should also be considered to better assess the activity and rupture history of the Southern and Northern fault Splays.

NUMERICAL MODELING OF THE SAN ANDREAS FAULT SYSTEM: COMPARISON WITH ANALYTICAL SOLUTIONS AND GEOLOGICAL OBSERVATIONS (1-102)
B.P. Hooks and B.R. Smith-Konter

Long-term (Ma), 3D numerical finite difference modeling of the southern San Andreas Fault System reproduces the deformation patterns observed in geological observations. The models consist of an isotropic geometry encompassing an area from ~N31/W121 to ~N35/W111 (750 km by 750 km in pole of deformation projection) and utilize a pressure-dependent, non-associative plasticity for the upper crust (Mohr-Coulomb constitutive model) and thermally-activated plastic yield lower crust (crystal plastic creep). No initial weaknesses, fault systems, or other heterogeneities are included in the models. All deformation, including the dynamic formation of faults and shear zones, is driven by an estimated mantle kinematic model based on long-wavelength crustal velocities averaged from available GPS datasets (e.g. EarthScope PBO, SCEC CMM). The model results were tested by comparing the model surface velocities with the surface GPS velocity data. The best models result in a pattern of faults similar to the major observed faults within the study area and produce stress and strain rates comparable to analytical models. However, due to the limitations on model grid spacing, smaller scale faults are not produced and those that are have wider zones of strain than observed in either analytical models or geological observations. This strain pattern is a function of the basal driving force and is characteristic of the restraining bend system. The uplift patterns are broadly consistent with the Southern California Geologic Motion Map results. Subsidence is recorded within the Imperial Valley, consistent with observations, and the main area of uplift is spatially consistent with the large scale restraining bend. For the short-term vertical motion record, coastal uplift patterns can be compared with available tidal gauge datasets. Here, the model and geological record closely agree as well. These large-scale, long-term models can be used to estimate total stress and strain accumulation, geologic fault slip and offset, and total deformation (vertical and horizontal) associated with the major fault systems of the San Andreas Fault System.

PROPERTIES OF DYNAMIC SLIP PULSES IN A 2D SLAB (2-079)
Y. Huang, J-P. Ampuero, and L.A. Dalguer

Earthquake ruptures are believed to propagate predominantly as self-healing pulses yet the dynamics of these pulses is not completely understood: what controls their rise time and rupture speed? Large earthquake ruptures (M>7) necessarily behave as pulses due to healing by the waves reflected at the top and bottom of the seismogenic zone. To obtain insight on the dynamics of self-healing pulses on very long faults we studied dynamic ruptures running across the middle longitudinal plane of a 2D elastic slab of finite thickness H. Reflected waves from boundaries are also present in this 2D problem and pulse-like ruptures are naturally produced. We studied this model numerically, applying the spectral element method implemented in the SEM2DPACK code, assuming uniform slip-weakening. We monitored the relation between rupture properties such as final slip, peak slip rate, stress drop, rise time and rupture speed. We found a transition between sustained and dying pulses as a function of slab thickness H, well predicted by a critical ratio of fracture energy to potential energy. The limiting speed of sustained rupture is independent on H and is consistent with analytical results based on a non-classical crack tip equation of motion appropriate for this geometry. In super-shear ruptures rise time approaches the travel time of the reflected phases, but in sub-shear ruptures it decreases continuously to much shorter values due to reflected waves faster than rupture fronts. The rupture arrest transition controlled by H and the supershear transition controlled by background stresses are observed also in 3D ruptures on very long faults (Dalguer et al.). We will also report on pulse properties in an elasto-plastic slab and on non-planar faults.

INSAR TIME SERIES IN A FOLD AND THRUST BELT (1-144)
A. Huth, R. Lohman, and W. Barnhart

The primary objective of this project was to examine the deformation that occurred in the past two decades in the fold and thrust belt between Saudi Arabia and Eurasia, where 2-3 cm per year of convergence is accommodated through folding and faulting. The study focused on analyzing aseismic and coseismic deformation using InSAR data processed with the JPL/Caltech Processing Suite ROI_PAC.

In this project, we:

- Modeled fault geometries and constrained earthquake location
- Constructed InSAR time series aimed at resolving aseismic deformation
- Simulated the impact of atmospheric noise using MODIS data

Conclusions:

- We created a time series with many images, reducing the impact of noise.
- Data for the Fin Earthquake prefers an unrealistically long fault, but we get a reasonable fit when we force a less elongate fault.
- Data in the time series still may be dominated by noise, future data may improve the situation.
- MODIS data appears to be a reasonable way to quantify the impact of atmospheric noise

THE 2010 OCOTILLO SWARM: PRELIMINARY RESULTS FROM DATA RECORDED AT THE NEES@UCSB WILDLIFE LIQUEFACTION ARRAY (2-129)
D.A. Huthsing, S.W.H. Seale, and J.H. Steidl

On 15 June 2010 at 9:26 PM PDT a Mw 5.7 event occurred 7.7 km ESE of Ocotillo, CA. This event is considered to be the largest aftershock to date of the 4 April 2010 M 7.2 Sierra el Mayor earthquake. The Ocotillo event generated its own series of local aftershocks. The NEES@UCSB Wildlife Liquefaction Array (WLA) in the Imperial Basin is located 57 km NE of the Ocotillo event. Since June 15th, hundreds of aftershocks have been recorded at WLA. The events were recorded by three-component strong-motion accelerometers at the surface and in boreholes at various depths. A significant number of these events have magnitude 3.0 and above. As of August 15th, 72 aftershocks greater than M 3.0 were recorded at WLA.

From this unique set of recordings, we have selected 60 events with good signal-to-noise ratio for our study. Of these 60, 25 have M 3.5 and above. Our study examines data recorded by the surface instrument and instruments located in the boreholes. We present a spectral analysis of the main shock compared with the average spectrum of the suite of 60 aftershocks and the average spectrum of the subset of 25 larger aftershocks. We also present spectral ratios of surface to downhole recordings for the main shock and the aftershock data. Consistency of source mechanism is clearly evident in the various spectra plotted for the three components of motion. Our study is ongoing and will incorporate future aftershocks of the Ocotillo event.

DOES CASING MATERIAL INFLUENCE DOWNHOLE ACCELEROMETER RECORDINGS? A CONTROLLED STUDY OF EARTQUAKE AND EXPERIMENTAL DATA RECORDED AT THE NEES@UCSB WILDLIFE LIQUEFACTION ARRAY (2-130)
D.A. Huthsing, S.W.H. Seale, and J.H. Steidl

In 2004, NEES@UCSB outfitted the Wildlife Liquefaction Array (WLA) with new instrumentation and initiated an experiment to test whether casing material influences downhole recordings of strong ground motion. Two 5.5m boreholes were drilled one meter apart. One of the boreholes was cased with traditional rigid PVC and the other with flexible Corex® drain pipe. Three-component strong-motion accelerometers were installed in both boreholes. Recently we have obtained a unique set of data at WLA that has allowed us to conduct a controlled study.

On 15 June 2010, a Mw5.7 event occurred near Ocotillo, CA, 57 km SW of WLA. A set of 60 aftershocks with M>3.0 were recorded at WLA with good signal-to-noise ratios. These data are ideal for our study, as the events are approximately co-located relative to the site and they have similar focal mechanisms.

We computed frequency spectra for the three components of motion for these events and we computed average spectral ratios between the data in the two boreholes. The spectral ratios are not flat (=1): certain frequencies within the range of engineering interest (f <20Hz) recorded in the flexible borehole show amplification and damping relative to the recordings from the rigid borehole. An amplification factor of 1.4 is the maximum in this frequency range.

In May 2010, NEES@UTexas visited WLA with the vibroseis truck T-Rex. We have performed spectral analysis of borehole recordings from 30 T-Rex pulses with frequencies ranging from 3 to 16Hz. We present these spectral ratios for comparison with the ones computed from earthquake data.

DEVELOPMENT OF THE SAN ANDREAS REGION ACTIVE EARTH DISPLAY (1-029)
G.P. Hwang, R.M. de Groot, K. Springer, R.J. Lillie, P. McQuillan, E. Scott, and C. Sagebiel

The Active Earth Display is an interactive, real-time, computer-based display that can be used in free-choice learning institutions such as museums, visitor centers, schools and libraries to present basic earth science information through a computer or stand-alone touch screen kiosk. Since April 2008, EarthScope has been conducting interpretive workshops centered on developing these displays. Each display connects to one of five regions - Cascadia, Basin and Range, San Andreas, Colorado Plateau, or Yellowstone - and explains the general earth science principles underlying that region. The San Andreas region was chosen as a venue for an interpretive workshop because of the plate-tectonic processes that result in earthquakes and the dramatic topography that forms along the actively deforming plate boundary. Building upon the concepts developed from the SCEC/EarthScope Workshop for Interpretive Professionals in the San Andreas Region in April 2009, SCEC is spearheading the development of the Active Earth module for the San Andreas fault. The current display is divided into four categories: the San Andreas Fault, Earthquake Basics, Research Today, and Living in Earthquake Country. Each category is comprised of a set of interactive pages that presents information about topics such as the formation and history of the San Andreas fault, plate tectonics, fault types, recent earthquakes, current research projects, careers in earth science, and earthquake safety and preparedness information through animations, videos, images, and text developed by various institutions.

SOUTHERN CALIFORNIA EARTHQUAKE DATA CENTER CLICKABLE FAULT MAP 2.0 (2-118)
M.J. Ihrig, E. Yu, R. de Groot, and J. Marquis

The clickable fault map, located at www.data.scec.org/faults/faultmap.html, was originally developed in 1997 by John Marquis and was based on the Jennings (1994) fault activity map. At that time, the limited scope of web programming technology necessitated the use of static web pages containing mostly static content. Since then, HTML, CSS, JavaScript, Ajax, PHP and many other web development languages and technologies have both emerged and evolved greatly, precipitating the need for an updated, dynamic version of the clickable fault map.

The revised clickable fault map now incorporates current work from the Working Group on California Earthquake Probabilities (WGCEP) into a fully interactive map utilizing the Google Maps API. A key focus of the project is to provide as much basic fault information as possible within one web interface while seamlessly integrating into the structure and presentational style of the existing web site.

Accompanying the clickable fault map is a control panel. Its features include the ability to add and remove custom placemarks, options to view significant historical seismic events, and to search both the fault and earthquake data alphabetically via associated lists.

Currently, the clickable fault map resides on a development server and is in testing. A second project pertaining to the map will link-in the interactive fault traces to any relevant web pages, both on the data.scec.org web site and externally. Another undertaking is to acquire and incorporate the most current UCERF fault dataset. Other refinements and adjustments in the presentational layer will be made to ready the project for public access.

MONITORING MICROSEISMICITY IN THE NORTHERN DEAD SEA BASIN USING PORTABLE SEISMIC MINI-ARRAYS (2-125)
A. Inbal, A. Ziv, H. Wust-Bloch, and Z. Ben-Avraham

The Dead Sea basin is the largest sedimentary basin along the Dead Sea Transform (DST), an active N-S trending plate boundary between the Arabian plate to the east and the Sinai sub-plate to the west. The current rate of earthquake activity along the DST is by a factor of ten lower than that of the San Andreas transform. Because each unit drop in magnitude yields approximately a tenfold increase in the number of events (Gutenberg and Richter, 1944), one needs to either "wait" ten times longer or, alternatively, look for ways to reduce the magnitude of completeness by one magnitude unit, in order to obtain a seismicity map for our study area that is as detailed as that of California. Currently, the magnitude of completeness of the earthquake catalog issued by the Geophysical Institute of Israel is around 2. In an attempt to locally reduce the magnitude of completeness within the northern Dead Sea basin to about 1, we have deployed three portable seismic mini-arrays within the study area on Nov. 2007. The reduction in the magnitude of completeness is a consequence of both getting closer to the earthquake source, and the use of array analysis approach to locate the earthquake hypocenters.

Owing to the proximity of the mini-arrays, a significant fraction of the detected events have been recorded by more than one array. Hypocentral coordinates of such events were determined in two steps. In the first step, we obtain a crude epicentral location for each event separately. In the second, we use the locations obtained in the previous step as an input for an iterative determination of both the 1-D velocity structure and the hypocentral coordinates (Kissling et al., 1994). Finally, we use this velocity model to locate earthquakes

that were recorded by a single array. We adopt the approach of Ide et al. (2003) for source parameters determination under the assumption of a frequency independent attenuation model, and find that our catalog is complete down to Mw1 at a distance of about 15 kilometers. Most of the located seismicity is confined to depths shallower than 6 kilometers, which may indicate that the locking depth of the mapped faults is abnormally shallow, or that most of the seismicity is due to brittle failure within the uppermost sedimentary cover above a locked seismogenic zone.

CALIFORNIA EARTHQUAKE RUPTURE MODEL SATISFYING ACCEPTED SCALING LAWS (1-129)
D.D. Jackson, Y.Y. Kagan, and Q. Wang

We are constructing an earthquake source model for the UCERF3 project. The basic philosophy is to start with the things we know best: the magnitude distribution for the whole state, Omori's law, total moment rate, distribution of moment rate on major faults, the instrumentally recorded earthquake catalog, long-term strain rate, historic earthquake catalog, and paleo-event catalog, in that order. The model is expressed as earthquake rate per unit area, time, magnitude, and focal mechanism direction, with algorithms to simulate "realized" earthquakes at random. The simulated earthquakes are described as spatially tapered ruptures on hypothetical rectangular fault planes with length, width, depth, strike, dip, and rake specified. Earthquake locations and orientations will approximate those of mapped faults based on empirical studies of actual earthquakes. The simulation scheme will allow temporal and spatial clustering according to the Critical Branching Model of Kagan et al. [2007]

We would identify testable features of the models and devise quantitative prospective and/or retrospective tests as appropriate. We include a rule associating earthquakes with mapped faults based on the proximity of their hypocenters to those faults. In that way we can model fault slip rate and paleoseismic dates and displacements.

Reference: Kagan, Y. Y., D. D. Jackson, and Y. F. Rong [2007]. A testable five-year forecast of moderate and large earthquakes in southern California based on smoothed seismicity, Seism. Res. Lett., 78: 94 - 98..

HIGH LIFETIME SLIP RATE ACROSS THE SAN JACINTO FAULT ZONE NEAR CLARK LAKE (1-087)
S.U. Janecke and D.H. Forand

We determined a right separation across the Santa Rosa segment of the Clark fault based on new mapping of a distinctive marker assemblage of biotite, hornblende-bearing tonalite, marble-bearing metasedimentary rocks, migmatite and mylonite in Coyote Mountain and the southeast Santa Rosa Mountains. We measured the uncertainty of projecting the lithologic contacts across Quaternary cover to the trace of the Clark fault and considered a range of plausible projections that conform with the structural geometry of the adjacent areas. Uncertainties are large (+3.7 km /-6.0 km) with the most likely right slip of 16.8 km. This is > 2.4 km higher than Sharp's (1967) prior estimate which correlated the diffuse western boundary of the Eastern Peninsular mylonite zone. These slip measurements together with Sharp's prior analysis document similar displacements across the Clark or Clark-plus-Coyote-Creek faults from Anza to the Santa Rosa Mountains of 24, 23.2, 21.9, 22.9, 25.6 and 20.3 km. There is no SEward decrease in total slip. The Coyote Creek fault displaces the same distinctive marker assemblage 3.5±1.3 km near Coyote Mountain.

Field and structural analysis show that two important folds within the damage zone of the San Jacinto fault zone predate strike-slip faulting and do not record unaccounted dextral strain. The only likely locus of significant additional right separation is within the Mid Ridge fault zone roughly half way between the Clark and Coyote Creek fault. Its right slip is difficult to constrain but less than 0.5-3 km. Dividing the right separation of the Clark fault near Clark Valley by its age (1.0 to 1.1 Ma; Lutz et al., 2006) yields an average lifetime slip rate of 16.0 +4.5/−6.2 mm/yr. Much lower slip rates since the latest Pleistocene across the central most active strand of the Clark fault zone (8.9 ± 2.0 to 1.5 ± 0.4 mm/yr; Blisniuk et al., 2010) northwest and southeast of Clark Valley, respectively, imply very large temporal changes in slip rate or far more strain in the damage zone of the fault than commonly inferred. Further analysis is needed to identify the cause of this large discrepancy. In contrast, the sum of lifetime slip rates across the two main faults of the San Jacinto fault zone near Coyote Mountain (20.1 +6.4/−7.9 mm/yr) agrees with many GPS and InSAR-based slip estimates.

DYNAMIC RUPTURE ON FAULTS WITH HETEROGENEOUS STRENGTH DUE TO NON-UNIFORM NORMAL STRESS: THE EFFECT OF STRESS REDISTRIBUTION BY PRIOR EVENTS (2-080)
J. Jiang and N. Lapusta

In dynamic rupture simulations, spatial distributions of fault strength and initial shear stress both strongly influence the results but are often assigned independently. However, simulations of multiple earthquake cycles show that the two distributions are related due to prior slip (e.g., Lapusta and Liu, JGR, 2009). Accounting for stress redistribution due to prior slip may be crucial for determining the true effect of fault heterogeneity on rupture propagation and hence on ground motion.

Here we investigate the long-term behavior of faults with heterogeneous fault strength using several scenarios of spatially variable and time-independent effective normal stress, including compact single or multiple stronger patches and sinusoidal variations. In our models, a planar fault segment governed by Dieterich-Ruina rate-and-state friction law undergoes both seismic and aseismic slip under slow tectonic loading. Part of our motivation is to use this model to understand the long-term behavior of slightly non-planar faults that may be well represented by planar faults with variable normal stress. We simulate multiple earthquake cycles while accounting for inertial effects during seismic events using the approach of Lapusta and Liu (2009). Uniform initial conditions, including shear stress, are assigned over most of the fault, as often done in simulations of single dynamic events in the presence of heterogeneity of fault strength.

For each simulation, comparison between the first simulated earthquake and subsequent events shows that shear stress redistribution over time at least partially compensates for the heterogeneity in fault strength, removing or diminishing its effect on seismic events. During the first event, the presence of stronger and weaker fault regions combined with uniform prestress leads to variations in rupture speed, slip rate, and final slip, but such variations diminish or, for cases with mild strength heterogeneity, virtually disappear in subsequent events. Our current work aims to quantify the evolution of mismatch between fault strength and stress and understand the dependence of that evolution on the degree of fault heterogeneity. One of our goals is to provide physical constraints on initial distributions of shear stress consistent with the assumed fault strength for simulations of single dynamic events. Our future work will be simulating more realistic scenarios of fault heterogeneity, and incorporating enhanced dynamic weakening.

TESTING THE INFERENCE OF CREEP ON RODGERS CREEK FAULT (1-148)
L. Jin and G. Funning

The Rodgers Creek fault (RCF), one of the major through-going structures in the northern San Francisco Bay area, links two known active creeping faults – the Hayward fault and the Maacama fault. Historic earthquakes that occurred on the fault prove that this fault is seismically active. However, whether or not it creeps like its neighbors remains a question. A previous study (Funning et al.,2007) identified a right-lateral fault creep at rates up to 6 mm/yr between 1992 and 2001. The estimate remains controversial, however, since the evidence on the ground is limited. Another explanation for the velocity step is a vertical hydrological signal.

Here, we use Permanent Scaterers InSAR data from both ascending and descending viewing geometries to test these two hypotheses. Under the assumption that fault-related deformation acts in the fault-parallel direction, it is possible to separate the deformation measured in the two viewing geometries into its horizontal and vertical components. Therefore, we put our efforts to validate/refute our initial hypothesis of creep on RCF by processing a 38-image ascending track dataset (track 478, frame 765) and a 34-image descending track dataset (track 342, frame 2835) from the ESA Envisat satellite spanning the interval 2003-2010, using the StaMPS/MTI code (Hooper,2008). Assuming there is a creep on RCF, we would expect to see vertical deformations in both datasets but horizontal deformations only in track 342. In order to compare the PS velocities on either side of the fault, we plot cross-fault profiles through both datasets at ~5 km intervals and detrend the profiles by fitting parallel straight lines to windows of datapoints either side of the fault. The gradients of the lines reflect the regional component of deformation, along with any residual error in satellite orbital position, while the separations represent fault offset rates.

Our preliminary results show positive (towards the satellite) velocities in the Cotati Basin and negative (away from the satellite) in the Santa Rosa plain in both datasets. In these areas, we believe, the ground is experiencing vertical deformations due to the subsurface fluid exchanges. Also, the results exhibit velocities change from negative to positive from west to east crossing RCF near the Foutaingrove Lake (FL) and the Annadel State Park (ASP), but in track 342 only. Based on the results, we find that our data are consistent with creep on RCF between FL and ASP from 2003 to 2010.

DISTRIBUTED STRAIN AND FAULT SLIP RATES IN SOUTHERN CALIFORNIA INFERRED FROM GPS DATA AND MODELS (1-157)
K.M. Johnson and R.Y. Chuang

This work addresses the question of how much deformation is localized on major faults in southern California and how much deformation is distribute throughout the crust off of major faults. Our conclusion to date is that the present-day deformation in southern California inferred from geodesy can be reconciled with long-term fault slip rates inferred from geology only if some of the present-day velocity field is accommodated as permanent deformation off of major faults.

Our approach to addressing this problem is to model GPS velocities in southern California using elastic and viscoelastic block models. The model consists of fault-bounded blocks in an elastic crust overlying a Maxwell viscoelastic mantle. It is a kinematic model in which long-term motions of fault-bounded blocks is imposed

as a combination of rigid block motions and distributed deformation parameterized with 3rd order polynomial functions. Interseismic elastic distortion of the crust is introduced through the locking and unlocking of faults throughout the earthquake cycle and associated flow in the mantle. Semi-analytical solutions for dislocations in an elastic plate over a viscoelastic substrate are used for the interseismic deformation calculation.

We first show that the kinematics of an elastic block model that fits the GPS velocity field requires distortion of fault-bounded crustal blocks whether or not the model is consistent with long-term fault slip rates. Our elastic block models require additional off-fault, permanent strain in order to be consistent with both long-term geologic slip rates and the GPS velocity field. Models without the additional off-fault distributed deformation that are consistent with long-term fault slip rates result in large systematic residuals in the regions of the Mojave segment of the San Andreas, the Garlock fault, and the region east of the Eastern California Shear Zone (ECSZ). Earthquake cycle models that account for viscous relaxation following large earthquakes and are consistent with long-term geologic slip rates can account for the observed velocity field in the regions of the Mojave segment of the San Andreas and the Garlock faults without additional off-fault deformation, but result in large systematic misfits east of the ECSZ. Both elastic and viscoelastic cycle models that allow for off-fault deformation can reproduce both long-term geologic slip rates and the present-day GPS velocity field.

SCEC/CME SEISMIC HAZARD ANALYSIS COMPUTATIONAL SCIENCE RESEARCH (1-013)*T.H. Jordan, G. Beroza, J. Bielak, S. Callaghan, P. Chen, Y. Cui, S. Day, E. Deelman, E. Field, R. Graves, K. Milner, J.B. Minster, K. Olsen, P. Small and the CME Collaboration*

The SCEC Community Modeling Environment (SCEC/CME) collaboration performs seismic hazard research using high performance computing. The SCEC/CME seismic hazard research program seeks to develop a predictive understanding of earthquake processes and seismic hazards in California. SCEC/CME research areas including dynamic rupture modeling, wave propagation modeling, probabilistic seismic hazard analysis, and full 3D tomography. SCEC/CME computational capabilities are organized around the development and application of robust, re-usable, well-validated simulation systems we call computational platforms. The CME Collaboration, which is managed as a SCEC Special Project Group, comprises geoscientists from six SCEC institutions and USGS and computer scientists from the San Diego Supercomputer Center, the USC Information Sciences Institute, Colorado School of Mines, and the Carnegie Mellon University.

SCEC/CME research activities this year included the following activities. We extended the OpenSHA software to calculate global seismic hazard curves and to support UCERF3.0 development. Three SCEC/CME modeling groups ran 1Hz+ Chino Hills simulations and validated simulation results by comparing results to observations for this event. We began refinement of the CyberShake 1.0 map by integrating an improved rupture generator into the CyberShake processing system. We have developed the CVM-Toolkit (CVM-T) software to support the use of CVM-H 6.2. A second generation SCEC Broadband Platform, capable of calculating 10Hz broadband seismograms, has been developed. The DynaShake Platform was used to calculate a M8.0+ dynamic rupture-based source description for a San Andreas event with a rupture length exceeding 500km. The SCEC M8 simulation, a regional-scale 2Hz, wave propagation simulation, was run on NCCS Jaguar, to investigate seismic hazards from such an event and to investigate the upper frequency limits of deterministic wave propagation simulations. More information about the SCEC/CME research is available at http://www.scec.org/cme

A CYBERSHAKE-BASED SYSTEM FOR OPERATIONAL FORECASTING OF EARTHQUAKE GROUND MOTIONS (1-052)

T.H. Jordan, K. Milner, R. Graves, S. Callaghan, P. Maechling, E. Field, P. Small, and the CyberShake Working Group

The goal of operational earthquake forecasting (OEF) is to provide authoritative information about the time dependence of seismic hazard to help communities prepare for earthquakes. Statistical and physical models of earthquake interactions have begun to capture many features of natural seismicity, such as aftershock triggering and the clustering of seismic sequences. In some situations, seismicity-based forecasting methods can achieve short-term probability gain factors of 100-1000 relative to long-term forecasts. Unifying long-term and short-term earthquake probability models into a single time-dependent forecast (UCERF3) is the goal of the current Working Group on California Earthquake Probabilities. The UCERF models forecast fault ruptures. However, from an OEF perspective, forecasts are better represented in terms of the strong ground motions that constitute the primary seismic hazard. Moreover, the prospective testing of ground motion forecasts—an essential requirement for OEF—is more straightforward than the testing of rupture forecasts. This approach has been applied in the STEP model, which forecasts exceedance probabilities at the intensity-VI shaking level. A major limitation is that empirical attenuation relations used by STEP do not properly account for the directivity and basin effects for individual fault ruptures.

This limitation can be overcome by the coupling of probabilistic rupture forecasting models with large ensembles of ground motion simulations. In particular, we develop a conceptual framework for OEF based on SCEC's CyberShake simulation platform, which can simulate ground motions in geologically complex environments for rupture ensembles large enough (~106) to sample adequately the statistical variability represented in the UCERF forecasts. We show how local increases in rupture probabilities can be mapped into ground motion probabilities using a CyberShake model for the LA region. Maps of exceedance probabilities for 3-second spectral acceleration at 0.2 g are illustrated for short-term probability variations calculated using Agnew-Jones foreshock statistics. Significant gains in the ground motion probabilities relative to a STEP-type model are obtained, primarily because this calculation accounts for the rupture directivity and basin effects associated with all individual ruptures in the CyberShake model; e.g., the strong directivity-basin coupling previously inferred from the TeraShake and ShakeOut simulations.

RANDOM STRESS AND OMORI'S LAW (1-119)
Y.Y. Kagan

We consider two statistical regularities that were used to explain Omori's law of the aftershock rate decay: Levy and Inverse Gaussian (IGD) distributions. These distributions are thought to describe stress behavior under the influence of various random factors, i.e., post-earthquake stress time history is described by a Brownian motion. Both distributions decay to zero for time intervals close to zero. This feature contradicts the high immediate aftershock level according to Omori's law. We propose that these distributions are influenced by the power-law stress distribution in the neighborhood of the earthquake focal zone and we derive new distributions as a mixture of power-law stress with the exponent psi and Levy as well as IGD distributions. These new distributions describe the resulting inter-earthquake time intervals and they closely resemble Omori's law. The new Levy distribution has a pure power-law form with the exponent -(1+psi/2) and the mixed IGD has two exponents, same as Levy for small time intervals and -(1+psi) for longer times. This power-law behavior should be replaced by even longer time intervals by a uniform seismicity rate corresponding to the long-term tectonic deformation. These background rates are computed based on our former analysis of the earthquake size distribution and its connection to the plate tectonics. We analyze several earthquake catalogs to confirm and illustrate our theoretical results. Finally we discuss how the parameters of random stress dynamics can be determined either through a more detailed statistical analysis of earthquake occurrence or by new laboratory experiments.

CHARACTERISTICS OF GROUND MOTION ATTENUATION DURING THE M7.2 EL MAYOR CUCAPA (BAJA) EARTHQUAKE (1-070)
E. Kalkan, K. Hatayama, M. Segou, V. Graizer, and V. Sevilgen

The magnitude 7.2 El Mayor Cucapa earthquake of April 4, 2010, occurred in northern Baja California, approximately 40 miles south of the US-Mexico border at shallow depth along the plate boundary between the North American and Pacific plates. Ground shaking was recorded by 408 free-field strong motion stations in US territory; these data were processed in order to calculate peak ground acceleration (PGA) and 5 percent damped spectral ordinates at 1, 3, 5, 7 and 10 s. Although ground motion showed faster attenuation from the source, typical for California due to low regional Q-factor, long-period motions were significantly amplified in San Fernando, San Bernardino, Ventura and Los Angeles basins; all of them located more than 300 km away from the source. In this study, five recently developed ground-motion prediction equations (GMPEs) were examined for their relative performance in modeling attenuation of PGA and spectral acceleration at various periods inside and outside of basins. Ground motion prediction equations considered are those of Graizer and Kalkan (2007 and 2009), Abrahamson and Silva (2008), Boore and Atkinson (2008), Campbell and Bozorgnia (2008), and Chiou and Youngs (2008). All these models utilized the NGA database, which includes data from stations in southern California basins. Except for GMPE of Boore and Atkinson, rest of the models accounts for basin amplification. In computing the predictions, Vs30 and basin depth parameters (Z1.0 and Z2.5) specific to each station were considered. We used California site classification map (Kalkan et al. 2010) for Vs30 and the latest SCEC Community Velocity Model (CVM-H 6.2) for deriving the aforementioned basin parameters. Ranking of GMPEs is achieved by using an information-theoretic approach suggested by Scherbaum et al. (2009) and further applied by Delavaud et al. (2009) for the purpose of selecting GMPEs for seismic hazard analysis in California. The resulting data driven rankings show that performance of GMPEs is strongly dependent on both distance and frequency. All five models estimate ground motion in southern California fairly for PGA, 0.3s and 1s for distances up to 350 km from the source. At long periods (5 s and beyond), all models tend to underestimate the significantly amplified ground motions in Los Angeles basins. This underestimation is much less for the GMPE of Abrahamson and Silva.

COMPARISON OF THE 1960 AND 2010 CHILEAN EARTHQUAKES (invited talk)
H. Kanamori and L. Rivera

The 1960 Chilean earthquake (Mw=9.5) is believed to be the largest ever recorded, yet its detailed mechanism is not well understood. Since the 2010 Chilean earthquake (Mw=8.8) occurred just north of the 1960 event

and has been studied in detail with hundreds of seismic stations, comparison of these 2 events can give us an important clue to the mechanism of the 1960 event.

The strainmeter record observed at Isabella (ISA), California, for the 1960 Chilean earthquake (Mw=9.5) is one of the most important historical records in seismology because it provided the first definitive observations of free oscillations of the earth. Because of the orientation of the strain rod with respect to the back azimuth to Chile, the ISA strainmeter is relatively insensitive to Love (G) waves and higher order (order > 5) toroidal modes, yet long-period G waves and toroidal modes were recorded with large amplitude. This observation cannot be explained with the conventional low-angle thrust mechanism typical of great subduction-zone earthquakes, and requires an oblique mechanism with half strike slip and half thrust. We tested the performance of the ISA strainmeter using other events, and found no instrumental problem. Thus, this observation represents the real characteristics of the 1960 Chilean earthquake, rather than an observational artifact. The strain spectrum at Ñaña (NNA), Peru, observed for the 1960 Chilean earthquake supports the oblique mechanism. Combining the results from earlier studies, we suggest that the strike slip deformation may have occurred at depths with a time scale of about 300s or longer. The slip direction of the 2010 Chilean earthquake (Mw=8.8) is rotated by about 10° clockwise from the plate convergence direction suggesting that right-lateral strain comparable to that of an Mw=8.3 earthquake remained unreleased and accumulates near the plate boundary. One possible scenario is that the strike slip strain accumulated over several great earthquakes can lead to the occurrence of an especially large earthquake like the 1960 Chilean earthquake. If this is the case, we cannot always expect a similar behavior for all the great earthquakes occurring in the same subduction zone.

EXAMINING SEISMICITY IN A COMPLEX FAULT ZONE: THE 2001, 2005, AND 2010 M5+ ANZA EARTHQUAKES AND AFTERSHOCK SEQUENCES (2-134)

D.L. Kane, F.L. Vernon, D.L. Kilb, and K.T. Walker

The San Jacinto Fault Zone (SJFZ) features a complex distribution of fault traces and seismic sources. Earthquakes in the SJFZ rarely occur along a linear, well-defined fault trace and instead tend to occupy a volume of the crust. Within the past decade several M4 – M5+ earthquakes have ruptured on or near this fault southeast of the Anza seismicity gap. These events have resulted in several thousand cataloged aftershocks with a diverse distribution of earthquake locations and rupture mechanisms. We analyze the three M > 5 earthquakes occurring in 2001, 2005, and 2010 and assess similarities and differences among these mainshocks and their subsequent aftershock sequences. Our focus is on comparing distributions of event locations, distributions of aftershock focal mechanism heterogeneities, aftershock productivity, mainshock rupture directivity, and mainshock source properties to gain insight into the complex suite of earthquakes occurring in the SJFZ.

MODELING SHALLOW SLIP DEFICIT IN LARGE STRIKE-SLIP EARTHQUAKES USING SIMULATIONS OF SPONTANEOUS EARTHQUAKE SEQUENCES IN ELASTO-PLASTIC MEDIA (2-053)

Y. Kaneko and Y. Fialko

Slip inversions of several large strike-slip earthquakes point to coseismic slip deficit at shallow depths (< 3-5 km), i.e., the amount of coseismic slip sharply decreases towards the Earth surface (e.g., Fialko et al., 2005; Bilham, 2010). Examples include the 1992 M7.3 Landers earthquake, the 1999 M7.1 Hector Mine earthquake, the 2005 M6.5 Bam earthquake, the 2010 M7.0 Haiti earthquake, and the M7.2 Sierra El Mayor (Mexico) earthquake. Determining the origin of shallow slip deficit is important both for understanding physics of earthquakes and for estimating seismic hazard, as suppression of shallow rupture could greatly influence strong ground motion in the vicinity of active faults. Several mechanisms may be invoked to explain the deficit. A widely accepted interpretation is the presence of velocity-strengthening fault friction at shallow depths where the coseismic slip deficit is compensated by afterslip and interseismic creep. However, geodetic observations indicate that the occurrence of interseismic creep and afterslip at shallow depths is rather uncommon, except for certain locations near major creeping segments of mature faults and/or in areas with thick sedimentary covers with overpressurized pore fluids (e.g., Wei et al., 2009). Fialko et al. (2005) proposed that extensive inelastic failure of the shallow crust in the interseismic period or during earthquakes may result in coseismic slip deficit at shallow depths.

In this work, we investigate whether inelastic failure of the shallow crust can lead to shallow coseismic slip deficit using simulations of spontaneous earthquake sequences on vertical planar strike-slip faults. To account for inelastic deformation, we incorporate off-fault plasticity into 2-D models of earthquake sequences on faults governed by laboratory-derived rate and state friction (Kaneko et al., 2010). Our preliminary results suggest that coseismic slip deficit could occur in a wide range of parameters that characterize inelastic material properties. We will report on our current efforts on identifying key parameters of fault friction and bulk rheology that link to the degree of coseismic slip deficit over multiple earthquake cycles.

EFFECTS OF HETEROGENEOUS FRICTIONAL PROPERTIES ON DYNAMICS OF GEOMETRICALLY COMPLEX FAULT SYSTEMS: A CASE STUDY OF THE 1999 HECTOR MINE EARTHQUAKE (2-070)
J. Kang and B. Duan

Spontaneous rupture propagation along geometrically complex faults is an important topic because geometrical complexities may control rupture extent and path. Most of previous dynamic rupture models assume uniform frictional properties along a complex fault system. In this study, we examine how non-uniform frictional properties affect rupture path and extent. In particular, we take the fault geometry of the 1999 Hector Mine earthquake as an example. We investigate what combinations of heterogeneous static and dynamic frictional coefficients allow the rupture to propagate onto the branched and bent fault system as it did in the 1999 event in a 2D plane-strain framework, with an assumption of a uniform regional stress field. We find that smaller dynamic frictional coefficient on the northwest and southeast segments, compared with that on the north segment, can allow rupture to propagate onto most of the fault system (except the north half of the north segment), with a uniform static frictional coefficient on the fault system. We are experimenting other combinations of heterogeneous frictional properties to allow the rupture to propagate onto the entire fault system as it did in the event. In particular, non-uniform static frictional coefficient may be needed along the north segment. We will examine how compliant fault zones surrounding the Calico, Pinto Mountain, Rodman, Landers faults respond to the 1999 Hector Mine rupture using the advanced spontaneous rupture models with off-fault plastic yielding, after we succeed in allowing the rupture to propagate onto the entire fault system in a uniform regional stress field.

SEISMIC REFLECTION STUDY OF THE SALTON SEA (2-131)
A.M. Kell-Hills, G. Kent, N. Driscoll, A. Harding, and R. Baskin

The Salton Trough, in southern California, exhibits two critical structures controlling the tectonic regimes and two styles of deformation including transpression along the southern San Andreas Fault (SAF) giving way to transtension further south. Previous work suggests that this transition occurs at Bombay Beach near the most southern extent of the SAF. Multi-channel seismic (MCS) data collected in May 2010 images an ancestral segment of the SAF off-shore from Bombay Beach allowing an understanding of strain transition from the SAF to the northward propagation of the Imperial Fault (IF). These newly acquired MCS data also expand on previous work by Brothers et al. (2009) in imaging deeper along the divergent wedge in the southern Salton Sea. The right lateral jog of the IF to the south and the SAF engenders transtension and propagation of the depocenter from the Mesquite Basin to the southern Salton Sea. The thickening of the divergent wedge toward the south records the onset of subsidence in the sea and potentially the northward migration of the IF. Based on a Lake Cahuilla sedimentation rates of 1-2 cm/y and a ~100 m thick wedge, the onset of subsidence is estimated to have begun ~10-20 k years ago constraining the timing of northward migration of the IF. Preliminary results suggest that the strain from the SAF was accommodated along the IF and the beginning of northward propagation along the IF began in late Pleistocene to early Holocene.

ESTIMATING ABSOLUTE TRACTION FROM SLICKENLINES (2-044)
J.D. Kirkpatrick and E.E. Brodsky

Slickenlines form during fault slip parallel to the slip direction. We examine slickenlines on an exposed fault surface and relate the slickenline geometry to the tectonic stress resolved on the fault. The fault surface is non-planar, with meso-scale corrugations, or bumps, having aligned long axes that rake approximately 30° down to the northeast. Slickenlines also rake approximately 30°, however, they are deflected around the bumps. This observation suggests that the local traction on the surface is a combination of the resolved tectonic stress and an extra stress due to the topography that causes the slickenline deflection. We use this insight to analyze the shape of slickenlines in combination with the known topography to infer the constraints on the absolute stress. Both the fault surface topography and the shape of slickenlines are measured using ground based light detection and ranging (LiDAR), which allows a large area of fault to be examined.

As expected, the slickenline deflections acquired digitally are connected to the fault topography. However, the correlation with simple parameters like topographic height is not straightforward. Interpretation requires calculating the stress pattern from the topography. As a preliminary analysis, we model the deflecting stresses as due to an elastic compression of the bumps. Using a Hertzian contact solution, we calculate the deflecting stress and show that this derived quantity correlates with the angle of deflection of the slickenlines. Measuring the deflection and calculating the deflecting stress therefore will allow the tectonic stress to be constrained.

DYNAMIC WEAKENING OF GOUGE LAYERS BY THERMAL PRESSURIZATION AND TEMPERATURE-DEPENDENT FRICTION IN HIGH-SPEED SHEAR EXPERIMENTS (2-046)
H. Kitajima, F.M. Chester, and J.S. Chester

Frictional measurements were made on natural fault gouge at seismic slip rates using a high-speed rotary-shear apparatus to study effects of slip velocity, acceleration, displacement, normal stress, and water content. From the experimental results, we derive a two-mechanism, temperature-dependent constitutive relation, in which the coefficient of friction is proportional to 1/T, to describe the frictional behavior at co-seismic slip rates. The constitutive relation describes an increase in friction coefficient with temperature (temperature-strengthening) at low temperature conditions (less than approximately 70 ˚C) and a decrease in friction coefficient with temperature (temperature-weakening) at higher temperature conditions. Thermal-, mechanical-, and fluid-flow-coupled FEM models based on the temperature-dependent friction constitutive relation, and that treat thermal pressurization of pore water, successfully reproduce the frictional response in all shear experiments at different conditions of slip rate, acceleration rate, and water content. Friction coefficient, normal stress, pore pressure, and temperature within the gouge layer vary with position (radius) and time, and largely depend on the frictional heating rate. Thermal pressurization is important at high slip rates and small displacements as temperature rapidly increases. The microstructure of the sheared gouge layers evolves as slip-rate and temperature increases, recording a change in mechanism from distributed shearing flow at low temperature conditions to fluidized flow associated with the formation of an extremely localized slip zone and dynamic weakening at high temperature conditions. The critical displacement for dynamic weakening is approximately 10 m or less, and can be understood as the displacement required to form a localized slip zone and achieve a steady-state temperature condition. The observed relationship between steady state friction and slip rate for the higher temperature regime is consistent with predictions from micromechanical models of flash heating.

ADAPTIVE MESH REFINEMENT FOR DYNAMIC RUPTURE SIMULATIONS (2-062)
J.E. Kozdon and E.M. Dunham

The velocity and stress fields near the leading edge of a propagating rupture front are known to be nearly singular [Freund, 1998]. Within a small process zone around the rupture front, $r < R0$, dynamic friction laws and nonlinear material response prevent a singularity from developing. Laboratory measurements and studies of earthquake nucleation [Rice, 2006; Noda et al., 2009] suggest that $R0 \sim 10$ mm, at least in the early stages of rupture, though this is frequently artificially enhanced by several orders of magnitude, $R0 \sim 100$ m or even larger, for large-scale earthquake modeling. It is possible that this compromise alters the rupture behavior, though this critical issue remains unexplored because the use of laboratory parameters necessitates millimeter-scale grid spacings around the rupture front. With this requirement, it is computationally infeasible to simulate large-scale ruptures with any method based on a uniform mesh.

Problems in which resolution needs are dictated by a small, but dynamically changing, region of the domain are ideally suited for adaptive mesh refinement (AMR) techniques. In this work, we explore the use of the Berger-Oliger AMR framework [Berger and Oliger, 1984; Berger and Colella, 1989] for dynamic rupture simulation. Within this framework, fine scale meshes are added (and removed) dynamically based on the local physics of the problem. Since the meshes are block-structured and overlapping, efficient time integration is possible using local time stepping, that is, each mesh is advanced with a locally optimal time step as opposed to the smallest global time step. Thus the rupture front and sharp wavefronts are resolved using small grid cells and time steps whereas larger grid cells and time steps suffice in areas where the solution is smooth.

Preliminary results suggest that the number of grid cells needed by an AMR method for dynamic rupture modeling is several orders of magnitude lower than for a uniform grid, resulting in massive computational and storage savings that far outweigh the additional overhead associated with the more complicated AMR data structures. These results demonstrate the feasibility of AMR for dynamic rupture simulation and, with the inclusion of more complex physics, should enable the use of more realistic friction parameters in large-scale rupture simulations.

TALL BUILDING EARTHQUAKE RESPONSE: (I) RAPID DAMAGE ESTIMATION AND (II) SENSITIVITY TO GROUND MOTION FEATURES (1-044)
S. Krishnan and M. Muto

An efficient rapid damage estimation procedure has been developed. It involves analyzing structural models under a suite of idealized ground motion waveforms characterized by a period, an amplitude, and a duration represented by the number of cycles. The analyses are performed with excitation applied in either direction and the results are stored in a database. For the estimation of structural response under a measured ground motion record, the idealized waveforms that have the least absolute deviation from the two horizontal components of the record are determined. Structural responses are rapidly estimated by querying the database. A modified approach is necessary to account for special cases involving one big pulse, followed by

several moderate pulses. The response database provides us insights into the sensitivity of ground motion features on the response of tall buildings. Near-source ground motion with pulse-periods longer than 4.5s and PGV greater than 1.625m/s, and 3-cycle motion with cycle-periods longer than 3.25s and PGV greater than 0.75m/s causes collapse in the 18-story steel moment frame buildings considered in this study.

PRECISE RELOCATION OF THE NORTHERN EXTENT OF THE AFTERSHOCK SEQUENCE FOLLOWING THE 4 APRIL 2010 M7.2 EL MAYOR-CUCAPAH EARTHQUAKE (2-114)
K.A. Kroll and E.S. Cochran

Following the 4 April 2010 M7.2 El Mayor-Cucapah earthquake, teams from UC Riverside, UC Santa Barbara, and San Diego State University installed an array of 8 temporary seismometers in the Yuha Desert area north of the Mexican border. This temporary array complemented the existing network stations and continuously recorded data from the aftershock sequence from 6 April through 14 June 2010. SCSN data and the temporary aftershock array will be used to study several aspects of fault structure and behavior, including precise relocation of the aftershock sequence. By relocating aftershocks, we hope to illuminate the network of faults that extend from the Laguna Salada fault in Mexico to its northern extension towards the Elsinore and San Jacinto faults. Right-lateral displacements up to 2 cm were identified on several right- and left-lateral fault segments by the USGS/CGS geologists in the area south of Hwy 98, and into the Pinto Wash (Treiman et. Al. Personal Communication, 2010).

We plan to relocate aftershocks within a 20 km by 14 km region containing 1 network and 5 temporary stations. Within this region over 4,000 aftershocks are in the SCEDC catalog from 6 April to 14 June 2010, during the time the temporary network was installed. The P and S wave arrival times for both the network and temporary stations will be manually picked for each of these events. We will compute the double difference hypocenter locations using the picked phase arrivals in the hypocenter relocation program, hypoDD (Waldhauser & Ellsworth 2000). In the event relocation, we will use the velocity profile for the Imperial Valley from the SCEC Unified Velocity Model (Version 4).

Future work will include detecting and relocating events that are not in the SCEDC catalog using the continuous data from the temporary array. All of the data will then be relocated using waveform cross-correlation in HypoDD to further improve the locations. Since little is known about the fault structure in the Yuha Desert region, we hope that accurate earthquake locations will help illuminate the complex and unmapped fault structure in the area. Additionally, more precise earthquake depths will help determine the extent of the seismogenic zone.

VSHAKER PROJECT: VISUALIZATION OF STEEL BUILDING RESPONSE TO GROUND MOTION TIME HISTORIES (1-023)
S.M. Kumar, P.J. Maechling, S. Krishnan, Y. Cui, K.B. Olsen, A. Chourasia, and G.P. Ely

SCEC researchers perform earthquake wave propagation simulations for both historical and scenario earthquakes that produce ground motion time-histories (seismograms). These synthetic seismograms can be used to model building response to strong ground motions. To support the exchange of ground motion time histories between SCEC ground motion modeling groups and building engineering groups, we have developed new tools for combining simulation-based synthetic seismograms with engineering-based building models.

On our VShaker Project, we have developed an interface between SCEC ground motion seismograms and the scientific gateway, Caltech Virtual Shaker, in order to visualize building response to ground motion time-histories. FRAME3D, the analysis engine for the Virtual Shaker, allows us to perform efficient three-dimensional nonlinear analysis of steel buildings subject to ground acceleration records. VShaker is a set of tools developed at SCEC that (a) provides formatted ground motion time-history input to Frame3D software, and (b) processes and visualizes Frame3D structural analysis output from Virtual Shaker in two steps. The program first combines Frame3D structural model and response data with ground motion synthetics to build three-dimensional geometric representations of the structure at specified time intervals. These geometric representations are output as Wavefront OBJ files - a universal file format supported by major 3D rendering programs. In the next step VShaker combines these snapshots to produce simple animations of structural motion.

We are using our VShaker tools to evaluate the response of two types of steel buildings with fundamental periods of 0.63 and 4.54 seconds subjected to acceleration records from the SCEC M8 Simulation. These buildings are being simulated at eight locations spread out across Southern California. The locations were chosen based on a previous study conducted by Krishnan et al., on the response of tall steel buildings for the magnitude 7.9 1857 southern San Andreas Earthquake.

VShaker has the potential to produce animations of structural motion after a significant earthquake to aid in the identification of damage to structural elements. It can also be used to effectively visualize performance of proposed building models to scenario earthquakes.

STRUCTURAL DEVELOPMENT OF BASINS ASSOCIATED WITH BENDS ON CONTINENTAL TRANSFORMS: THE NORTH ANATOLIAN FAULT IN NW TURKEY AND THE SAN ANDREAS FAULT IN SOUTHERN CALIFORNIA (2-023)

H. Kurt, L. Seeber, C.C. Sorlien, M. Steckler, D. Shillington, E. Perincek, D. Timur, and D. Dondurur

The Quaternary active Tekirdag and Cinarcik basins in Marmara Sea and the Late Miocene Ridge Basin in southern California are representative of basins that developed in the wake of bends along continental transforms, the North Anatolian fault (NAF) and the San Andreas fault (SAF), respectively. These basins are oblique time-transgressive half grabens. They are bordered by the master strand of the transform and display similar asymmetric structure: strata are progressively tilted obliquely toward the bend and toward the border fault, where subsidence is fastest. Yet, nearest the bend is also where the basins are youngest and shallowest. Away from the bend the subsidence rate decreases while basins get deeper and older. This common pattern is accounted for by time-transgressive basin growth. On the transtensive side of the bend, slip on the transform is oblique normal and the hangingwall side subsides forming the basin. Subsidence continues along the fault and the basins get progressively deeper away from the bend. Eventually, the basins reach their maximum depths, but can continue to grow longitudinally along the fault. The asymmetric growth of these basins shows that the bends are fixed to the footwall side of the fault opposite the basins, and that the basins are formed as the hangingwall side of the fault deforms to accommodate the bend.

The Ridge Basin grew 70 km long during 7my in late Miocene on the NE side the San Gabriel segment of the SAF in southern California, downstream of an extensional bend at the NW end of that segment. Progressive tilting was active only in the 15-20 km of the basin closest to the bend. Further from the bend the basin grew only laterally by translation forming the well-known "shingled" sequence. In contrast, the Marmara basins are young and active. They are relatively short, suggesting ≈ 30km of displacement on the NAF since inception.

We use seismic profiles and other data to compare structures in several transform-bend basins along the NAF and the Ridge Basin. Readily observable features are angle of transform bend, dip of basement-sediment unconformity and width of the basin from the hinge to the border fault as a function of distance from bend. Results show that subsidence decreases along the fault away from the bend, even if fault strike is uniform. Basins widen away from the bend thus the hinge that allows the tilting rolls backward away from the fault. Both tilting and rollback contribute to subsidence.

SPECTRAL ANALYSIS OF PORE PRESSURE DATA RECORDED FROM THE 2010 SIERRA EL MAYOR (BAJA CALIFORNIA) EARTHQUAKE AT THE NEES@UCSB WILDLIFE FIELD SITE (2-128)

D. Lavallee and S.W.H. Seale

On 4 April 2010, the M7.2 Sierra el Mayor event occurred in Baja California, Mexico. The NEES@UCSB Wildlife Liquefaction Array (WLA) in the Imperial Basin is located 110 km NNW of the hypocenter. The event was recorded on all channels at WLA: by three-component strong-motion accelerometers at the surface and in boreholes at various depths and by pore pressure transducers located in a saturated, liquefiable layer.

We have computed the spectra of the pore pressure response in the frequency domain for signals recorded at different depths. At each depth, the spectrum is attenuated as a power law with a sharp discontinuity at a frequency close to 1 Hz. We report the value of the exponents that characterize the power-law behavior of these spectra. We also computed cross-spectral analysis of the pore pressure records from different depths. The functional behaviors of the curves of the cross-spectra are similar to that of the original spectra. For comparison, we present the spectrum of each component of the ground motion recorded at a nearby accelerometer.

Partially due to the late arrival of the surface waves, the frequency content of the recorded pore pressure signal is also a function of time. To gain a better understanding of the time-dependence of the frequency content, we performed a spectral analysis of the signal in a moving window. The spectral analysis suggests that, except for high frequencies, the curves exhibit a complex behavior as a function of the window position.

We interpret and discuss the consequences of the estimated spectra and cross-spectra.

ON THE CONTINUITY TO THE NORTHWEST OF THE CERRO PRIETO FAULT (2-087)
O. Lazaro-Mancilla, D. Lopez, J.A. Reyes-López, C. Carreón-Diazconti, and J. Ramírez-Hernández

The need to know the exact location in the field of the Cerro Prieto fault traces has been an important affair due that the topography in this valley is almost flat and fault traces are hidden by plow zone, for this reason, the southern and northern ends of the San Jacinto and Cerro Prieto fault zones, respectively, are not well defined beneath the thick sequence of late Holocene Lake Cahuilla deposits. The purpose of this study was to verify if Cerro Prieto fault is the continuation to the southeast of the San Jacinto Fault proposed by Hogan in 2002 who based his analysis on pre-agriculture geomorphy, relocation and analysis of regional microseismicity, and trench exposures from a paleoseismic site in Laguna Xochimilco, Mexicali. In this study, four radon (222Rn) profiles were carried out in the Mexicali Valley, first, to the SW-NE of Cerro Prieto Volcano, second, to the W-E along the highway Libramiento San Luis Río Colorado-Tecate, third, to the W-E of Laguna Xochimilco and fourth, to the W-E of the Colonia Progreso.

The Radon results allow us to identify in the Cerro Prieto profile three peaks where the values exceed 60 picocuries per liter (pCi/L), these regions can be associated to fault traces, one of them associated to the Cerro Prieto Fault (60 pCi/L) and other related with Michoacán de Ocampo Fault (239 pCi/L). The profile Libramiento San Luis Río Colorado-Tecate, shows four peaks above 200 pCi/L, the highest peak is related to the Michoacán de Ocampo fault. The profile of the Laguna Xochimilco, site used by Hogan et al., (2002), permit us observe three peaks above the 140 pCi/L, we can associate the peak of 184 pCi/L the Michoacán de Ocampo Fault, but none of them to the Cerro Prieto Fault. Finally in spite of the Colonia Progreso is the shortest profile with only five stations, it shows one peak with a value of 270 pCi/L that we can correlate with the Cerro Prieto Fault. The results of this study allow us to think in the possibility that the Michoacán de Ocampo Fault is the Continuation to the South of the San Jacinto Fault, not the Cerro Prieto Fault. We present previous studies that reinforce our conclusions.

RAPID CENTROID MOMENT TENSOR (CMT) INVERSION IN 3D EARTH STRUCTURE MODEL FOR EARTHQUAKES IN SOUTHERN CALIFORNIA (2-120)
E. Lee, P. Chen, T.H. Jordan, and P.J. Maechling

Accurate and rapid CMT inversion is important for seismic hazard analysis. We have developed an algorithm for very rapid CMT inversions in a 3D Earth structure model and applied it on small to medium-sized earthquakes recorded by the Southern California Seismic Network (SCSN). Our CMT inversion algorithm is an integral component of the scattering-integral (SI) method for full-3D waveform tomography (F3DT). In the SI method for F3DT, the sensitivity (Fréchet) kernels are constructed through the temporal convolution between the earthquake wavefield (EWF) from the source and the receiver Green tensor (RGT) from the receiver. In this study, our RGTs were computed in a 3D seismic structure model for Southern California (CVM4SI1) using the finite-difference method, which allows us to account for 3D path effects in our source inversion. By storing the RGTs, synthetic seismograms for any source in our modeling volume could be generated rapidly by applying the reciprocity principle. An automated waveform-picking algorithm based on continuous wavelet transform is applied on observed waveforms to pick P, S and surface waves. A grid-searching algorithm is then applied on the picked waveforms to find an optimal focal mechanism that minimizes the amplitude misfit and maximize the weighted correlation coefficient. The grid-search result is then used as the initial solution in a gradient-based optimization algorithm that minimizes the L2 norm of the generalized seismological data functionals (GSDF), which quantifies waveform differences between observed and synthetic seismograms using frequencies-dependent phase-delay and amplitude anomalies. In general, our CMT solutions agree with solutions inverted using other methods and provide better fit to the observed waveforms.

FULL-3D WAVEFORM TOMOGRAPHY FOR SOUTHERN CALIFORNIA (1-017)
E. Lee, P. Chen, T.H. Jordan, P.J. Maechling, M. Denolle, and G.C. Beroza

We are automating our full-3D waveform tomography (F3DT) based on the scatteringintegral (SI) method and applying the automated algorithm to iteratively improve the 3D SCEC Community Velocity Model Version 4.0 (CVM4) in Southern California. In F3DT, the starting model as well as the derived model perturbation is 3D in space and the sensitivity kernels are calculated using the full physics of 3D wave propagation. The SI implementation of F3DT is based on explicitly constructing and storing the sensitivity (Fréchet) kernels for individual misfit measurements. The sensitivity (Fréchet) kernels are constructed through the temporal convolution between the earthquake wavefield (EWF) from the source and the receiver Green tensor (RGT) from the receiver. Compared with other F3DT implementations, the primary advantages of the SI method are its high computational efficiency and the ease to incorporate 3D Earth structural models into very rapid seismic source parameter inversions. For the first iteration, we used over 3,500 phase-delay measurements from regional small to medium-sized earthquakes to invert for 3D perturbations to the 3D reference model, SCEC CVM4. The updated model, CVM4SI1, reduced the variance of the phase-delay measurements by about 29% and the synthetics generated by the updated model generally provide better fit

to the observed waveforms. In the second iteration, we only used phase-delay measurements made on ambient noise Green's function data and the updated model, CVM4SI2, reduced the variance of phase-delay measurements by about 51%. The synthetic waveforms generated by CVM4SI2 not only improved ambient noise Green's function waveform fittings but also earthquake waveform similarities.

CUSTOMIZED DYNAMIC RANK ASSIGNMENT FOR IMPROVED EFFICIENCY WITH SEISMIC APPLICATIONS (1-020)
K. Lee, Y. Cui, J. Zhou, and P.J. Maechling

In the era of petascale computation, the system efficiency depends on effective concurrency exploitation on given systems. The actual concurrency is significantly impacted by multiple system and application derived characteristics such as skewed communication latencies, large latency variation, and growing system imbalance. As observed in the large-scale M8 earthquake simulation, the system efficiency achieved with 223,074 NCCS Jaguar cores remains around 10% due to more than 30% of communication overhead and severe system imbalance. The AWP-ODC code utilized in M8 simulation incorporates structured mesh and subsequent sub-domains are identically decomposed, constructing highly regular mesh that only requires nearest neighbor communications. However, the default run-time rank assignment for each sub-domain is not always guaranteed to be optimal for overall communication latency among cores. The SMP-style rank assignment option utilized in M8 demonstrated a relatively good behavior comparing to other predefined rank assignment options. However, the absolute communication latency and latency variation still remain high. In this poster, we propose a customized dynamic rank assignment technique to systematically reduce the overall latency, highly dependent on the average number of communication hops, and its associated variation that impose critical system imbalance. Experimental results on NICS Kraken and NCCS Jaguar, both equipped with a high bandwidth 3D torus topology and the SeaStar 2+ router technology, demonstrated a significant amount of reduction in communication latency and associated variation through dynamic rank re-placement, enabling us to improve further seismic simulation efficiency on petascale systems.

A DAMAGE MODEL FOR THE ABSENCE OF SIGNIFICANT PRECURSORY SEISMICITY (2-034)
Y-T. Lee, D. Turcotte, J. Rundle, and C-C. Chen

Acoustic emissions prior to rupture indicate precursory damage. Laboratory studies of frictional sliding on model faults feature accelerating rates of acoustic emissions prior to rupture. Precursory seismic emissions are not generally observed prior to earthquakes. To address the problem of precursory damage we consider failure in a fiber-bundle model. We observe a clearly defined nucleation phase followed by a catastrophic rupture. The fibers are hypothesized to represent asperities on a fault. Two limiting behaviors are equal load sharing (stress from a failed fiber is transferred equally to all surviving fibers) and local load sharing (stress from a failed fiber is transferred to adjacent fibers). We show that precursory damage in the nucleation phase is greatly reduced in the local-load sharing limit. We argue that laboratory experiments on fracture involve near-uniform load sharing whereas actual faults involve local load sharing. When one asperity fails on a fault the force carried by the asperity is transferred to adjacent asperities. We argue that this explains the absence of a well defined nucleation phase prior to an earthquake.

ACTIVE STRIKE-SLIP FAULTING IN THE CALIFORNIA CONTINENTAL BORDERLAND (2-001)
M.R. Legg

The Pacific-North America transform plate boundary is more than 200-km wide in southern California. Major strike-slip faults in the California Continental Borderland have been an active part of the plate boundary since early Miocene time and deformation continues today. As much as 25% of the relative plate motion occurs on faults west of the coastline. Because Borderland basins are depositional environments, the long term deformation is recorded in the basin sediments. Many Miocene transtensional basins have been structurally inverted by subsequent transpression associated with the inland jump of the main transform fault system to the southern San Andreas-Gulf of California fault system. Convergence of Baja California and the Peninsular Ranges batholith with the San Andreas Big Bend and the transrotated Western Transverse Ranges (WTR) has generated a combination of north-directed shortening across the WTR and northeast-directed shortening farther south. Multibeam bathymetry provides high-resolution maps of the seafloor deformation associated with active Borderland strike-slip faults, and multichannel seismic reflection data provide high-resolution images of the subsurface structure and related deformation. The overall pattern of the major offshore San Clemente-San Diego Trough fault system closely resembles that of the San Andreas-San Jacinto fault system onshore. Yet, the offshore system formed more than 10 Million years prior to the southern San Andreas system and remains seismically-active today. Images of the subsurface deformation associated with these major offshore strike-slip fault systems help to better infer the subsurface structure and deformation history of the younger onshore fault systems. For example, the intersection between the San Clemente and Santa Cruz-Catalina Ridge faults is an offshore equivalent to the Cajon Pass region where the San Andreas and San Jacinto faults merge, but apparently do not intersect. Four-dimensional understanding

of these complex fault convergence and divergence zones is necessary to better understand how and why large earthquakes branch and propagate to multiple faults and fault segments. The exploration industry has obtained a few 3D seismic data volumes over coastal fault systems that hold significant hydrocarbon reserves. Ultimately, we hope to obtain high-resolution, multichannel, 3D seismic data volumes over critical active strike-slip fault junctures in the California Continental Borderland

SHEAR WAVE SPLITTING IN THE PARKFIELD PILOT HOLE FROM CROSS-CORRELATION OF SEISMIC NOISE (2-109)
M.A. Lewis and P. Gerstoft

We use cross-correlation of seismic noise recorded at stations in the San Andreas Fault Observatory at Depth (SAFOD) pilot hole to extract P and S waves from a source at depth and measure shear-wave splitting on the horizontal components. The data is recorded at 7 three-component stations at depths from 1857-2097 m in the pilot hole. In late September and early October 2004 drilling noise underneath the stations generates propagating waves in the noise cross-correlations between stations, which are absent in the rest of October. Noise cross-correlations between the deepest station and the other six stations in the pilot hole produce estimates of the P and S wave velocities on the vertical and horizontal components respectively which are consistent with velocity measurements taken directly in the borehole. We observe polarization of the S wave, with a fast polarization direction of 120-130° that is 4% faster than the slow direction. Cross-correlation of seismic noise cannot only accurately determine seismic velocities but also S wave anisotropy.

HIGH-RESOLUTION IMAGING OF THE SAN ANDREAS FAULT DAMAGE ZONE FROM SAFOD MAIN-HOLE AND SURFACE SEISMIC RECORDS (2-033)
Y-G. Li, P.E. Malin, E.S. Cochran, P. Chen, and J.E. Vidale

We use fault-zone trapped waves (FZTWs) generated by earthquakes and explosions and recorded at San Andreas Fault Observatory at Depth (SAFOD) borehole seismographs and along a dense linear surface array across the SAF to document fault zone structure and rock damage at seismogenic depths with high-resolution. The seismograph in the SAFOD main-hole was placed in the fault zone at a depth of ~3 km below ground. The observed FZTWs that feature large amplitudes and long wavetrains at dominant frequencies of 2-10 Hz are modeled here using finite-difference methods. To fit the amplitude, frequency, and travel-time characteristics of the data, the models require a downward tapering 100-200-m-wide low-velocity zone along the SAF at depth, with shear velocities reduced by 25-40% from wall-rock velocities. We observe larger velocity reductions at shallower depths and maximum velocity reductions of up to ~50% in a 30-40-m-wide fault core zone. The results indicate the localization of severe rock damage on the SAF likely reflecting pervasive cracking caused by major earthquakes along the Parkfield segment of the SAF. The width and velocity reduction of the damage zone at 3 km depth, as delineated by fault-zone trapped waves, is verified by the SAFOD drilling and logging studies [Hickman et al., 2007]. These studies show that a ~200 m-wide zone of high porosity material, with multiple slip planes and average velocity reductions of ~30-35% is present at this depth. Further, based on the depths of on-fault earthquakes generating prominent FZTWs, we estimate that the low-velocity waveguide along the fault at SAFOD extends to at least ~7-8 km depth. The damage zone is not symmetric across the main slip plane but extends farther on the southwest side of the main fault trace, implying an evolving damage zone on the SAF that accumulates fracturing and damage during successive earthquakes. We plan to use 3-D wave-equation travel-time tomography and full-waveform tomography for fault-zone velocity structure for additional constraints to improve the understanding of fault-zone processes and remove much of the uncertainty associated with focusing/defocusing and scattering in previous studies using forward modeling of FZTWs.

SEISMIC DOCUMENTATION OF ROCK DAMAGE AND HEAL AT THE LONGMAN-SHAN FAULT RUPTURED IN THE 2008 M8 WENCHUAN EARTHQUAKE FROM FAULT-ZONE TRAPPED WAVES (2-106)
Y-G. Li, J.Y. Su, and T.C. Chen

We examined rock damage and heal on the Longmen-Shan Fault (LSF) that ruptured in the 2008 M8 Wenchuan earthquake using the data recorded at Sichuan Seismic Network and portable stations in the source region where the LSF is characterized by reverse thrusting. The dominating fault-zone trapped waves (FZTWs) have been recognized in seismograms registered at near-rupture seismic stations for on-fault aftershocks. These FZTWs illustrate the coherent interference phenomenon of wave propagation in a highly fractured low-velocity fault zone bounded by high-velocity crustal intact rocks. Preliminary results from observations and 3-D finite-difference simulations of these FZTWs show a distinct low-velocity wave-guide (LVWG) a few hundred-meters wide on the south LSF, in which the maximum velocity reduction is 50% or more at shallow depth. This LVGW likely extends across seismogenic depths at varying dip angles with depth. Because of the sensitivity of trapped wave excitation to the source location from the LVGW, it allows us to depict the main fault slipped in the Wenchuan earthquake at depth inferred by precise locations of after shocks which generated prominent FZTWS. The width, velocity and shape of the LSF at shallow depth

delineated by FZTWS are generally consistent with the results from geological mapping and fault-zone drilling at the southern LSF. We interpreted this LVGW as being a damage zone in dynamic rupture that accumulated damage from historical earthquakes, particularly from the 2008 M8 Wenchuan earthquake. The fault zone co-seismically weakening during the major earthquake and subsequently healing (partially) on the LSF have been studied using similar earthquakes occurring before and after the Wenchuan earthquake. We examined the changes in amplitude and dispersion of FZTWS recorded at the same seismic station for earthquakes at the same places between 2006 and 2009. Results suggest that seismic velocities within the south LSF zone could be co-seismically reduced by ~15-20% due to the rock damage caused by the M8 mainshock on May 12, 2008. The moving-window cross-correlations of waveforms for body waves and FZTWs from repeated aftershocks show that seismic velocities near the LSF increased by 5-6% or even more in the first year after the Wenchuan earthquake, with an approximately logarithmic healing rate with time and the largest healing in the earliest stage, indicating the post-main shock healing with rigidity recovery of fault-zone rocks damaged in the M8 quake. The magnitude of rock damage and heal observed at the Longman-Shan fault is larger than those observed at the San Andreas fault ruptured in the 2004 M6 Parkfield earthquake and also on ruptures of the 1992 M7.4 Landers and 1999 M7.1 Hector Mine earthquakes. This difference is probably related to the different earthquake magnitude, faulting mechanism and stress drop.

THE SHAKY TRUTH: DEBUNKING DOUG COPP AND THE TRIANGLE OF LIFE (1-011)
A.E. Liang

The 'Triangle of Life' theory, advocated by self-proclaimed rescuer Doug Copp, has been in circulation via viral email within the past decade, and it has garnered concerns from many professional disaster organizations about the dangerous recommendations made to the public on the actions to take during an earthquake. This research project was set out to achieve 3 main objectives: to question and refute the validity of Copp's claims and credentials, to correct widespread misinformation regarding Triangle of Life, and to educate the public on the approved "Drop, Cover and Hold On" method of earthquake response through social media outreach. Initial research consisted of cataloguing Doug Copp's claims, which ranged from his featured videos about the Triangle of Life, to his supposed health problems complicated by his rescue effort at the site of 9/11. These claims were categorized and cross-referenced with outside responses from various journalistic resources, news media, and individual testimonies, all to create a comprehensive FileMaker database that can eventually be transformed into an online resource for the public in the long run. The research project also consisted of public outreach and communicating the danger of Triangle of Life to bloggers and other web users who have continued the circulation of Doug Copp's original email. All of these efforts strive for the increase in public knowledge on the Triangle of Life fallacy and the employment of "Drop, Cover and Hold On" as a universal policy for earthquake safety preparedness.

USING LOW-COST MEMS SENSORS TO ESTIMATE SITE RESPONSE IN THE BÍO-BÍO REGION FOLLOWING THE M8.8 MAULE, CHILE EARTHQUAKE (2-116)
E.J. Liao, C.J. Neighbors, A.I. Chung, J.F. Lawrence, and E.S. Cochran

We assess local site response in the Bío-Bío region of Chile using both S-wave and coda-wave methods. Site amplification is the response of seismic waves to local subsurface structure and geologic material, which can result in spatially variable patterns of surface damage following an earthquake. Following the mainshock, it was noted that metropolitan areas suffered a highly variable pattern of structural damage (Geo-Engineering Extreme Events Reconnaissance, 2010). The coastal Bío-Bío region is composed of differing geologic material of variable age including fluvial sediments, sedimentary and metamorphic complexes as well as igneous plutonic suites (Servicio Nacional de Geologia y Mineria, 1982). Site amplification analyses of urban areas that are located on sedimentary basins are important to better understand the spatial variability of amplification to mitigate future seismic hazard.

The February 27, 2010 M8.8 Maule, Chile earthquake was followed by a vigorous aftershock sequence around the mainshock zone. The immediate aftershock sequence was captured by the Quake-Catcher Network (QCN) Micro-electro-mechanical System (MEMS) accelerometers. In the month following the mainshock, over 100 sensors were deployed in central Chile with a high density of stations in the Bío-Bío region. Methods used to determine site amplification effects include analyses of the spectral ratios (amplitude vs. frequency content) of both direct S-waves and coda-waves. The Fourier spectra of the coda waves are calculated using seven 50% overlapping 5 sec windows and a 10 sec time window is used for the S-waves; we only use data with a signal to noise ratio greater than 1.5. Amplification recorded by the QCN stations is compared to published reports of site-specific geologic material and subsurface structure to determine the relative importance of soil type and basin depth. The site response analysis highlights areas of the Bío-Bío region that may be more likely to experience high amplitude ground shaking and that may require better engineering practices to mitigate loss following future large earthquakes.

SLIP RATES ON MAJOR FAULTS OF THE SOUTHERN SAN ANDREAS FAULT SYSTEM FROM INVERSIONS OF CONTINUOUS GPS DATA (2-019)

E. Lindsey and Y. Fialko

We use secular velocities from the continuous GPS data provided by the Plate Boundary Observatory (PBO) and Scripps Orbit Permanent Array Center (SOPAC) to estimate the contemporaneous slip rates and locking depths on the Southern San Andreas fault (SAF), the San Jacinto fault (SJF) and the Elsinore fault. These velocities are systematically lower than the velocities from Crustal Motion Model 3 (CMM3) used in several previous studies. We performed inversions on the data using the Savage dislocation model, and the model parameter space was interrogated using a Gibbs sampler. The employed inversion method naturally approximates the joint probability distribution for the model parameters, allowing for a rigorous evaluation of model uncertainties and trade-offs. Previous geodetic estimates of slip rates in this region based on dislocation models have generally inferred a higher slip velocity on the SAF (21-26 mm/yr), and a lower velocity on the SJF (12-19 mm/yr) (refs. 1-3). These "geodetic" slip rates are generally higher than geologic estimates representing average slip rates on time scales of 10^4-10^6 years. We investigate implications of fault geometry such as a non-vertical SAF (ref. 4) and a "blind" segment of the SJF (ref. 5). Using the fault geometry motivated by these recent studies, we estimate a slip rate of 16(+/-3) mm/yr for the southern SAF, and a combined slip rate of 19(+/-6) mm/yr for the two closely spaced branches of the southern San Jacinto fault (the Coyote Creek fault and the blind southern continuation of the Clark fault). The locking depths are estimated at 10(+/-3) km and 12(+/-7) km for the SAF and SJF, respectively. The data suggest a gradual transfer of slip from the SAF to the SJF system, with the average slip rate on the SAF dropping from 18 to 14 mm/yr and the slip rate on the SJF increasing from 16 to 22 mm/yr, from the San Gorgonio bend in the North toward the Brawley shear zone in the South.

1. Becker, T.W. et. al., Geophys. J. Int. (2005) 160, 634-650.
2. Fay, N.P. and Humphreys, E.D., J. Geophys. Res. (2005) 110, B09401.
3. Meade, B.J. and Hager, B.H., J. Geophys. Res. (2005) 110, B03403.
4. Lin, G. et. al., J. Geophys. Res. (2007) 112, B12309.
5. Fialko, Y., Nature (2006) 441, 968-971.

BUILDING A PHYSICAL "EARTHQUAKE SIMULATOR" TO EXPLORE THE EARTHQUAKE CYCLE IN K12 OUTREACH (1-026)

B. Lipovsky, M. Rohrssen, J. Lozos, K. Ryan, C. Neighbors, E. Cochran, C. Meyers, G. Funning, and M. Droser

We have devised a physical apparatus that simulates the strain accumulation and release cycles of the earthquake cycle. The device uses elastically connected groups of cinder blocks that are pulled across a flat surface in series. Although the load point moves at constant velocity, the frictional contact of the blocks with the ground means that each group of blocks encounter episodes of sliding. Each group of blocks is equipped with a 3D accelerometer of the type used in the Quake Catcher Network (QCN). We use this system as a pedagogical model for the earthquake cycle and present our experiences during a demonstration of its use at a large (~100 student) outreach event.

COMPARISON OF PROXIES FOR THE 'VELOCITY STRENGTHENING' ZONE AT SHALLOW DEPTH AND THEIR EFFECT ON RUPTURE DYNAMICS (2-059)

Q. Liu, R.J. Archuleta, and R.B. Smith

In rupture dynamics as well as rock physics studies, it is believed that the friction on the fault plane is highly velocity dependent while the fault is sliding (e.g. Dieterich,JGR 1979). Based on laboratory experiments, researchers also think that a shallow zone 3-4km thick would act in a velocity strengthening manner. In this zone the friction increases with the slip rate. Thus this zone will inhibit slip (Scholz, Nature 1998)--an observation from many earthquakes such as Loma Prieta, Tottori, Parkfield, L'Aquila. To account for this effect many dynamic rupture studies have introduced techniques that will mimic the 'velocity strengthening' zone and thereby efficiently reduce/eliminate the amount of slip near the free surface. Day and Ely (BSSA 2002) carefully examined this weak zone with numerical simulations. We compare the difference between various numerical implementations (infinite Dc, rate dependent sliding friction coefficient, etc.) for this 'velocity-strengthening' zone. We use a slip-weakening friction law for dynamic simulations of a ~Mw 7 earthquake on a rectangular planar normal fault. We semi-quantitatively investigate how the parameters, such as thickness of the zone and dynamic stress drop level in this layer, influence characteristics of rupture process (e.g., slip rate and total slip) near the free surface. We also look at the near fault ground motion statistics. All the implementations are compared with two commonly used initial stress distributions: uniform distribution and linear depth-dependent distribution.

DYNAMICS OF PARALLEL STRIKE-SLIP FAULTS WITH OFF-FAULT PLASTIC YIELDING, FLUID PRESSURE CHANGE AND LOW VELOCITY ZONES (2-067)

Z. Liu and B. Duan

We use a two-dimensional finite element computer program EQdyna to study the effect of off-fault plastic yielding, time–dependent pore pressure change, and the existence of boarding fault zones on dynamics of two parallel strike-slip faults. Our results generally confirm conclusions in previous studies that a strike-slip earthquake rupture is seldom to jump a step-over wider than 5 km, which is consistent with field observations on moderate to great-sized earthquakes. With relatively weak off-fault yielding, we find the initiation of rupture on the second strike-slip fault across the dilational step-over is slightly delayed, while the influence on the compressional one is minor. We find that the existence of fault zones allows the rupture to jump a wider compression step-over (i.e., from 3 km to 4 km). Time-dependent pore pressure change exerts a more profound influence than the above two factors. In particular, time-dependent pore pressure reduces the maximum width of a dilational step-over (i.e., from 4.5 km to 1.0 km) that can be jumped and increases the time needed for rupture to jump. We also explore schemes that gradually stop a propagating rupture on a planar fault. We find that combination of increase in fault strength (i.e., static friction) and decrease in stress drop (i.e., increase in dynamic friction) appears the best in gradually stopping the rupture along a planar fault with a uniform initial stress field. We will examine effects of gradual arrest of the rupture on dynamics of parallel faults in the following study.

NEW DEVELOPMENTS OF THE COLLABORATORY FOR THE STUDY OF EARTHQUAKE PREDICTABILITY (CSEP) TESTING CENTERS (1-134)

M. Liukis, D. Schorlemmer, J. Yu, P. Maechling, J. Zechar, T.H. Jordan, F. Euchner, and the CSEP Working Group

Southern California Earthquake Center (SCEC) began development of the Collaboratory for the Study of Earthquake Predictability (CSEP) in January of 2006 with funding provided by the W. M. Keck Foundation. Since that time, a large group of scientists and software engineers have translated the scientific and computational concepts of CSEP into several operational testing centers. The initial implementation of the W. M. Keck Foundation Testing Center at SCEC for the California natural laboratory became operational on September 1, 2007 and has since been further improved, optimized, and extended over the past two years. The design and implementation of the SCEC Testing Center have been guided by four design goals that were originally identified as objectives for the Regional Earthquake Likelihood Models (RELM) testing center which are: (1) Controlled Environment, (2) Transparency, (3) Comparability, and (4) Reproducibility. By meeting these goals, the CSEP Testing Center can provide clear descriptions of how all registered earthquake forecasts are produced and how each of the forecasts are evaluated. As of September 2010, there are four testing centers established around the globe. The SCEC Testing Center hosts alarm-based and rate-based forecasts models for California, Western Pacific and global testing regions. The forecasts under evaluation are mostly seismicity-based forecasts models. We describe how the currently operational CSEP Testing Center at SCEC has been constructed to meet the design goals; we also present new capabilities and development of the Testing Center, share our experiences operating the center since its inception and present test results for established experiments within Testing Centers.

INSAR/GPS COMBINATION IN TIME SERIES ANALYSIS (1-136)

R.B. Lohman

We have generated a toy problem that illustrate a particular scenario where the existence of an InSAR time series can inform the analysis of GPS data in the same area. Our synthetic ground deformation included components from a fault-related transient (dip slip on a 60-degree dipping fault, evolving over 8 months) and a spatially variable seasonal vertical deformation field with modulation of the annual amplitude. The sparse acquisitions times of InSAR and data latencies of a month or more preclude the use of InSAR for real-time transient detection at the present time, although proposed SAR sensors on missions such as DESDynI, with possible repeat times of as little as 8 days, may change that status. Even with current data capabilities, InSAR may still be able to improve the process of detecting transients. Typically, GPS time series analyses that incorporate spatial and temporal smoothing, such as the Network Inversion Filter, involve the estimation of a state vector that encompasses both tectonic signals, such as coseismic offsets, station-specific variables, such as random walk characteristics, as well as the contribution of spatially correlated noise that affects sites that are in close proximity to each other.

The discontinuous sampling of GPS means that it is quite possible that a nontectonic signal, such as seasonal drawdown and recharge within an aquifer, may be sampled at less than it's spatial scale, and be aliased or interpreted as if it were a longer-wavelength feature. We explore an extreme example of this, where spatially separated regions of high deformation rates are sampled by GPS, with no stations sampling an intervening region with no deformation, such that the inferred spatial scale of the annual signal would be twice its actual wavelength. A blind application of methods such as the Network Inversion Filter or displacement template approaches might map this (incorrect) spatial correlation length into fault slip if the available fault-based

Green's functions happened to provide a reasonable match. The existence of InSAR imagery-based time series, however, may be able to preclude this mapping due to better spatial sampling of a deformation field, even without the dense temporal sampling of GPS.

ESTIMATES OF VS100 AT SITES OF PRECARIOUSLY BALANCED ROCKS (1-073)
J.N. Louie, J.N. Brune, and S.K. Pullammanappallil

In Purvance et al. (2008, Bull. SSA), the overturning fragilities of precariously balanced rocks (PBRs) were parameterized as a function of a vector of the ground motion intensity measures peak ground acceleration (PGA) and response spectra at 1 sec (Sa1). The resulting failure probabilities (OPs) for several of the PBRs were very high, suggesting they were inconsistent with the 2002 USGS ground motions. Previously, Vs30 values (measured shear velocity averaged to 30 meters depth) at PBR sites were surveyed with refraction microtremor arrays in order to correlate with PGA constraints (Pullammanappallil et al., 2005 SCEC; Purvance et al., 2008 SSA). Vs30 values were near 760 m/s, the value assumed in the "rock" site effects in the latest hazard maps. However Sa1 values may be better correlated with deeper shear wave velocities. Here we examine measurements of Vs100 (average shear velocity to 100 meters depth) at a number of sites on granitic rocks, and compare them with the Vs100 values assumed to apply for the hazard maps, from Boore and Joyner (1997). The results indicate that on average, Vs100 values at granitic outcrop sites typical of PBRs are similar to or higher than assumed in the hazard maps. Five of fifteen sites had Vs100 values lower than the 910 m/s Vs100 of Boore and Joyner's average rock-site model. However, the softest of these granitic rock sites (Anza Hoodoo) showed a Vs100 still at 70% of the Boore and Joyner model's Vs100. Two of the sites have Vs100 measurements exceeding twice the model rock Vs100. Thus, in applying an appropriate correction factor to the OP for a measured site, the third of the sites having lower Vs100 values would be expected to shake at most 20% harder than the model rock site. (The square root of the inverse of 0.70 is 1.20.) Most of the granitic sites would be expected to shake less intensely than the model rock site. The stiffest site of the fifteen measured, Mockingbird Tank, would shake 41% less than the Boore and Joyner (1997) model rock site, all other factors being equal. In sum, deeper shear velocities at PBR sites are not significantly lower than what is predicted by the Boore and Joyner model.

LABORATORY OBSERVATIONS OF THE RESPONSE OF FAULT STRENGTH AS NORMAL STRESS IS CHANGED, AND IMPLICATIONS FOR DYNAMIC RUPTURE (2-076)
J.C. Lozos and B. Kilgore

A pivotal issue for rupture propagation through regions of fault step-over, non-planar fault surfaces, and multi-fault intersections is how fault shear resistance depends on normal stress. Rapid normal-stress changes, which should be common at nonplanar faulting features, could potentially either aid or inhibit rupture propagation. At present we do not know whether shear resistance changes instantaneously with changing normal stress, or whether it is insensitive. Therefore, given a particular natural fault geometry, we cannot assess whether earthquakes can rupture fault segment boundaries or jump from fault to fault.

New laboratory experiments have been performed, using the methods described in Linker and Dieterich, JGR 1992, to examine the effects that static, and transient, changes in normal stress have on fault strength. Improved data recording technology, and new experimental capabilities, permit the careful examination of the response of shear stress, fault closure, and the transmissivity of acoustic signals across the fault, as the magnitude and duration of the changes to the applied normal on the simulated fault are varied. Preliminary results indicate that fault closure and acoustic transmissivity respond nearly instantaneously to any change in normal stress across the fault. However, the shear stress is consistently slow to respond to changes in the applied normal stress. Consistency of these observations with existing the constitutive relations for friction are examined and comparison with previous laboratory data are presented.

AERIAL SURVEYS USING CONSUMER ELECTRONICS: FAST, CHEAP AND BEST OF ALL: USEFUL! (1-101)
D.K. Lynch, K.W. Hudnut, and D. Dearborn

We report results from two low-cost, low-altitude, aerial imaging surveys of the San Andreas Fault (SAF) carried out in late 2009. In total 541 km of the fault was imaged with a ground sample distance (pixel size) of a few cm. The two surveys covered the Carrizo Plain and points north to the Choice Valley on 24 Sep 2009, and the SAF between I-5 (Tejon Pass) and I-15 (Cajon Pass) on 29 Dec 2009. Each area was imaged twice, once on the first pass and a short time later on the return pass. The I-5 to I-15 flight included Lone Pine Canyon east of Wrightwood soon after the Sheep Fire of early Oct 2009. Ground that was normally covered by heavy brush was revealed for the first time in many years.

The data set consists of 5216 ~6Mb jpg photographs (31 Gb total) which were posted on the internet within hours of their acquisition. Shortly thereafter they were placed into PICASA web albums for easy browsing. Total cost for both surveys (excluding camera) was about $5000.

The pictures were taken with a Nikon D90 with an attached GP-1 receiver that wrote the aircraft's position into the EXIF file of each photograph. Organization, manipulation and geolocation of the images were done on a Macintosh laptop.

All photographs are freely available and carry no copyright. They are in the public domain.

SOURCE-SCALING RELATIONSHIP FOR M4.6-8.9 EARTHQUAKES: SPECIFICALLY FOR EARTHQUAKES IN THE COLLISION ZONE OF TAIWAN (2-108)
K-F. Ma and Y.T. Yen

We investigated the source scaling of earthquakes (Mw4.6-8.9) mostly from Taiwan orogenic belt, and made the global compilation of source parameter to discuss the scaling self-similarity. Finite-fault slip models (12 dip-slip and 7 strike-slip) mainly from Taiwan dense strong motion and teleseismic data were utilized. Seven additional earthquakes (M>7) were included for further scaling discussion on large events. Considering the definitive effective length and width for the scaling study, we found M0~L2 and M0~L3 for the events less and larger than the seismic moment of 10**20 Nm, respectively, regardless the fault types, suggesting a non-self similar scaling for small to moderate events and a self-similar scaling for large events. Although the events showed the variation in stress drops, except three events with high stress drops, most of the events had the stress drops of 10-100 bars. The bilinear relation was well explained by the derived magnitude-area equation of Shaw (2009) while we considered only the events with the stress drops of 10-100 bars and the seismogenic thickess of 35km. The bilinear feature of the regressed magnitude-area scaling appears at the ruptured area of about 1000km2, for our seismogenic thickness of 35km. For the events having ruptured area larger than that, the amount of the average slip becomes proportional to the ruptured length. The distinct high stress drops events from blind faults in the western foothill of Taiwan yield local high Peak Ground Acceleration (PGA) as we made the comparison to the Next Generation Attenuation (NGA) model. Regardless the relative small in magnitudes of these events, the high PGA of these events will, give the high regional seismic hazard potential, and, thus, required special attention for seismic hazard mitigation.

GEOCACHE YOUR WAY TO PREPAREDNESS: A SCAVENGER HUNT FOR SAFETY (1-032)
D.N. MacCarthy

Trying to convey preparedness information has always been a challenge, and in today's fast-paced world of constant change and instant data, staying relevant and contemporary is an important part of reaching and informing new, non-traditional audiences. Geocaching is one such method that not only takes natural disaster education into the 21st century, but also makes it accessible and entertaining at the same time.

Geocaching is a high-tech treasure hunting game played throughout the world by adventure seekers equipped with GPS devices. The basic idea is to locate hidden containers, called geocaches, outdoors and then share your experiences online. At present, there are an estimated 4-5 million geocachers worldwide, with over 1 million active caches and more being added every day (geocaching.com).

This project takes the concept of finding hidden items and expands it to include preparedness items and questions about basic earthquake knowledge. The goal for the participants is to collect a set of "cached" items that represent components of earthquake preparedness and safety (flashlights, first-aid equipment, water & food rations, etc.); however, participants must correctly answer one of the earthquake-related questions before learning the location of each cache. As a team-oriented scavenger hunt, it will reach a larger audience and therefore increase overall preparedness education. There will be several prize tiers for those groups who collect the most items in the shortest amount of time, with prizes ranging from emergency supply kits to gift cards.

Many options were considered as to an appropriate scale and location for the activity. In order to ensure a diverse range of ideas, input was solicited from Pasadena City College students, as well as interns at the USGS. Ultimately, Griffith Park was identified as the most suitable locale, particularly due to its established reputation as a popular site for geocaches. Now that initial scoping is complete, we are planning our event in detail and beginning to stage it. The actual hunt will take place during the day, with an awareness and safety celebration to follow in the park.

Input and involvement from the SCEC community is most welcome, as volunteers and sponsors are still needed to help run and provide both physical and monetary support for the event. Interested parties should stop by this poster or contact Dawn MacCarthy, dmaccart@usgs.gov

INTEGRATING AFTERSHOCK AND SURFACE RUPTURE DATA TO CONSTRAIN 3D STRUCTURE OF THE 1992 LANDERS EARTHQUAKE (2-047)
B.H. Madden and D.D. Pollard

The complexity of the surface rupture mapped for the 1992 multi-fault Landers earthquake is great, with strike changing along the extent of the main rupture in addition to extensive secondary faulting.

Segmentation of the surface rupture along the main faults is also visible in large-scale maps. Relocated aftershocks have the potential to reveal if this complexity at the surface is reflected in fault structure at depth. Investigation shows that aftershocks cluster into groups with distinct focal mechanism orientations, providing insight into the spatially varying local stress at depth. Integration of the geological field data and geophysical aftershock data presents new possibility for constraining fault model structure, understanding the level of segmentation that should be incorporated into models built from surface rupture traces, and exploring the nature of complex, multi-fault earthquakes. Three models are compared: 1) a model with faults built from interpretation of mapped surface traces at a scale of 1:100,000, producing continuous faults, 2) a model with faults built from interpretation of mapped surface traces at a scale of 1:50,000, producing segmented faults, and 3) a model with the corresponding faults from the Community Fault Model. This work takes a mechanical perspective on earthquake behavior by utilizing the boundary element program Poly3D to model slip along faults and stress in the surrounding material (Maerten et al 2005). Models are evaluated by their ability to reproduce the compiled right-lateral slip distribution measured at the surface and local stress states at depth, determined by comparison of aftershock orientations and modeled Coulomb failure planes at aftershock locations. In addition to providing new constraint on three-dimensional fault structure, which is critical due to its influence on earthquake rupture (Aochi and Fukuyama 2002, Harris 2004), this approach explores the three-dimensional mechanics of multi-fault ruptures. Such understanding is essential to the incorporation of such events into seismic hazard analyses (Field et al 2009).

LATE QUATERNARY SLIP RATE AND EARTHQUAKE CHRONOLOGY OF AN ACTIVE FAULT IN THE KASHMIR BASIN: IMPLICATIONS FOR SEISMIC HAZARDS AND THE EARTHQUAKE CYCLE IN THE NORTHWEST HIMALAYA (1-097)

C.L. Madden, D.G. Trench, A.J. Meigs, J.D. Yule, S. Ahmad, and M.I. Bhat

In contrast to the central Himalaya, where shortening from the collision of India with Asia is localized at the Himalayan frontal thrust(HFT), distributed deformation characterizes convergence across the northwest Himalaya (NWH). Evidence for distributed deformation in the NWH includes active shortening on a fault system over 40 km northeast of the HFT that includes the Reasi fault zone and the Balakot-Bagh fault, source of the Mw 7.6, 2005 Kashmir earthquake. Active faulting also occurs within the Kashmir Valley (KV), an intermontane basin ~100 km north of the NWH deformation front, as indicated by our new mapping and paleoseismic data. The 45+km-long Balapora fault zone (BFZ) consists of several northeast-dipping, high-angle reverse faults that cut late Quaternary terraces on the southwest side of the KV. An uplifted strath terrace preserved in the hanging wall of a northeast strand of the BFZ, which is exposed in the left bank of the Rambira River (RR), is elevated ~19 m above the bedrock-lined active river channel. Dividing the elevation of the strath surface above active channel by an 82+/-12 ka OSL age for the basal strath deposits yields a 0.2-0.3 mm/yr late Pleistocene incision rate for the RR, a proxy uplift rate for this fault strand. A fault dip of 85 degrees makes the slip rate for this strand nearly identical to the uplift rate. This slip rate is only a minimum because the strath terrace is not exposed across the entire fault zone. Outcrops and paleoseismic trenches demonstrate that fluvial overbank deposits overlying the strath terrace exhibit ~14 m of vertical separation across the entire BFZ. 14C and preliminary OSL ages constrain the age of the base of the overbank deposits to 24-40 ka, yielding an uplift rate of 0.4-0.6 mm/yr over this period. Trench exposures also reveal packages of growth strata ponded against upstream-facing scarps of the BFZ that record a minimum of three surface rupturing events in the last 24-40 ka. Stratigraphic restorations of correlative units across the fault zone show that at least 5.5-8.4 m of vertical separation occurred over one or more events between 1.7 – 15.2 ka. These findings show that the BFZ is a low slip rate fault that produces infrequent large earthquakes, and poses a seismic hazard to the people of the nearby city of Srinagar and the KV. These results along with new GPS results from an ongoing study form the basis for a new model of seismic strain release across the NW Himalaya.

TESTING REGIONAL-SCALE GROUND MOTION ESTIMATES FOR THE CISN SHAKEALERT PROJECT (1-062)

P.J. Maechling, M. Liukis, and T.H. Jordan

Our SCEC research team has developed initial capabilities of the CISN Testing Center (CTC) as a part of the USGS-funded CISN ShakeAlert Project. The CTC is designed to compare regional-scale ground motion estimates, such as peak ground motion estimates, against observed ground motion data, for significant California Earthquakes. The CTC is designed to identify which ShakeAlert ground motion estimation methods produce the best fit to observed ground motions. Scientific goals of the CTC include (a) development of consensus among SCEC researchers on meaningful measures of comparison between ground motion estimates and observations, (b) collection and analysis of ShakeAlert performance information, and (c) integration of standard Probabilistic Seismic Hazard Analysis (PSHA) terms and practices into EEW. The technical goal of the CTC is to develop an automated system that can compare ground motion estimates against ground motion observations. The CTC system used the CSEP testing framework to automate the evaluation of CISN ShakeAlert rapid earthquake parameters including ground motion forecasts for each

event. As part of this year's CTC development, we updated the CSEP Testing Framework to use the USGS ShakeMap RSS Feed as an authorized source of event-based ground motion observations. As ShakeAlert systems produce rapid ground motion estimates for significant California events, the CTC will evaluate those ShakeAlert ground motion estimates against CISN ground motion observations using goodness-of-fit algorithms defined by CISN scientific groups.Our ShakeAlert ground motion forecast testing shares scientific and technical goals with several other SCEC activities including validation of attenuation relationships, synthetic ShakeMaps, velocity model and wave propagation model goodness of fit measures, and short term ground motion forecast testing. The CTC system is designed to support CISN ShakeAlert testing and to also be applicable for evaluation of other ground motion estimation methods.

OSL GEOCHRONOLOGY INVESTIGATIONS BY THE U.S. GEOLOGICAL SURVEY IN SOUTHERN CALIFORNIA: WHAT THE AGES TELL US AND HOW THEY WILL BE USED (1-078)
S.A. Mahan, J. Matti, C.M. Menges, R.E. Powell, and K.J. Kendrick

Over the last several years, the U.S. Geological Survey has investigated the geochronology of surficial deposits associated with the San Andreas Fault Zone (SAF) and the Eastern California Shear Zone (ECSZ) in southern California using optically stimulated luminescence (OSL) dating. These OSL ages elucidate ongoing landscape evolution and active tectonics, especially near intersections between the fault systems, and span multiple physiographic provinces, including the Peninsular Ranges, the Transverse Ranges, the Mojave Desert, and the Salton Trough. More than sixty five OSL ages were generated for this study.

Within the Transverse Ranges, the study areas included the south flank of the Cottonwood Mountains, the Cottonwood Pass in the Cottonwood Springs area and a strand of the Chiriaco Fault where it crosses the north piedmont of the Orocopia Mountains west of Chiriaco Summit. Within the Mojave Desert Province we focused on the Twentynine Palms area, at the intersection between the ECSZ and the Pinto Mountain Fault.

At the boundary between the Transverse Ranges and Peninsular Ranges Provinces, we focused on complexities within the SAF zone associated with San Gorgonio Pass. Sample targets included terraces in the canyons of San Gorgonio River; Little San Gorgonio River; the Banning Bench; the alluviated Beaumont Plain at the west end of the San Gorgonio Pass Fault zone; the intersection of the Yucaipa horst-and-graben complex, and the San Bernardino strand of the SAF (Wilson Creek area); and a nested alluvial-fan complex astride strands of the SAF at the mouth of Mission Creek at the northwestern head of Coachella Valley. Coachella Valley and basins within the sinistral fault complex of the Eastern Transverse Ranges were also dated. Samples were selected to help constrain the age of last movement on the Chiriaco fault, a major sinistral fault zone in the eastern Transverse Ranges province, and to begin to document the ages of major alluvial events in that province.

The OSL age results are variable, but not unexpected. In general, younger earth materials (Holocene and late Pleistocene) yielded OSL ages that are compatible with expectations based on geologic, pedogenic, radiocarbon, and cosmogenic data as well as data obtained within the northern Mojave desert from other USGS studies. However, for some earth materials where other data suggested old ages, we were initially surprised by OSL results that, in comparison, appear to be too young. This suggests either that our pre-existing expectations are wrong, or that the OSL technique yields results that indicate the sediments sampled are complicated and need to be evaluated in context. In addition, we found that for some samples the quartz-grain analysis yielded OSL results that are obviously wrong, whereas feldspar grains yielded more expected and predictable age results. These results suggest that the detrital mineral species analyzed may be more important than first suspected. Our continuing investigations are clarifying some of these scientific questions.

SUBSURFACE CHARACTERIZATION OF MYSTIC LAKE PALEOSEISMIC SITE ON THE CLAREMONT FAULT USING CPT DATA: EVIDENCE FOR STRAIGHTENING OF THE NORTHERN SAN JACINTO FAULT (1-111)
G.I. Marliyani, T.K. Rockwell, N.W. Onderdonk, and S.F. McGill

We collected Cone Penetrometer Test (CPT) data along two transects across a small releasing step over at the Mystic Lake paleoseismic site along the Claremont segment of San Jacinto Fault. The primary reasons for this study are to characterize the Holocene pattern of sedimentation and to locate the most promising areas for additional trenching. At the depth of the trench, CPT data agree well with trench observations to better than 10 cm resolution. The main fault identified in our 2009 trench is clearly the principal dip slip fault at depth, and shows increasing vertical separation with increasing depth. Based on limited shallow age data from the trench, the sedimentation rate varies by a factor of two across the main fault, making this an ideal paleoseismic site. The late Holocene sedimentation rate is 3-4 mm/yr within the small sag depression, with unit 800 present at 4-6 m depth in the sag. As we only trenched to about 2 m depth, the current paleoseismic record of pre-historical events is probably a minimum. The young active fault is about 0.5 km from the basin bounding mapped trace of the Claremont fault, which displays minimal Holocene activity in the 2009 trench.

Along with seismic reflection and seismicity data within the Mystic Lake step over between the Casa Loma and Claremont strands (also referred to as the Hemet step-over), these data suggest that the northern San Jacinto fault is reorganizing and straightening, and will eventually bypass this large releasing step in San Jacinto Valley, thereby lengthening the straight continuous section of San Jacinto Fault. Rupture of the entire Clark-Casa Loma-Claremont fault zone could result in earthquakes as large as Mw 7.6, rivaling the San Andreas fault for hazard to the densely populated Los Angeles and San Bernardino/Riverside areas.

SEPARATING SEASONAL, ANTHROPOGENIC, AND TECTONIC DEFORMATION IN THE WESTERN TRANSVERSE RANGES REGION, CA (1-149)
S.T. Marshall, S.E. Owen, and G.J. Funning

The western Transverse Ranges hosts a network of active oblique reverse faults that produce relatively fast contraction rates across the Ventura basin. In order to better characterize the strain rates, fault slip rates, and seismic hazard of this region, we utilize data from 53 continuous GPS sites in the Plate Boundary Observatory's continuous GPS network. Because GPS sites in southern California record the sum of tectonic, seasonal, and anthropogenic ground motions, we apply several analysis techniques to determine both the tectonic and non-tectonic rates of deformation. We begin with the MEaSUREs combined filtered time series solutions which represent the combination of a GIPSY (JPL) and GAMIT (SOPAC) solution that has had the common mode signal from a large network removed. While the network-wide filtering has already been performed on the MEaSUREs time series, local non-tectonic signals are likely to still be present. Therefore, we perform additional time series analysis on our subset of 53 sites using the software package QOCA (http://gipsy.jpl.nasa.gov/qoca/) in order to remove time series offsets due to coseismic events and equipment changes and annual/semi-annual motions. The resultant velocities are dominantly linear implying constant velocity and successful removal of seasonal deformation. One exception is site CSN1, located near the epicenter of the 1994 Northridge earthquake. This site shows a clearly non-linear time series possibly due to postseismic deformation. To determine which of the remaining non-linear signals are spatially-correlated, we perform Principal Component Analysis on the residual data. We find that only two sites have anomalous motions and so we exclude these sites from our analysis. In the end, we have a regionally filtered data set with dominantly linear time series suggesting that we have successfully removed the non-tectonic signals. The spatial pattern of the resultant velocities clearly shows strain accumulation due to the locked San Andreas fault. Our continuing work will focus on using InSAR imagery to determine if any of the linear motions are anthropogenic in origin. Once we are confident that the resultant velocities represent only tectonic motions, we will remove the strain associated with the San Andreas fault to better understand the strain accumulation due to only the regional faults in the western Transverse ranges.

HIGH-VP/VS (POISSON RATIO) ZONE ACCOMPANYING SLOW EVENTS AND LOW-VELOCITY LOWER CRUST ALONG ACTIVE FAULTS BENEATH THE SOUTHWESTERN JAPAN (2-101)
M. Matsubara and K. Obara

Fine-scale three-dimensional P- and S-wave velocity structures beneath all of the Japanese Islands are revealed using data obtained from the dense high-sensitivity seismograph network (Hi-net) operated by National Research Institute for Earth Science and Disaster Prevention (NIED) (Matsubara et al., 2008). We investigate the relation between the slow events and velocity structure since many slow events are observed beneath southwestern (SW) Japan. Active faults also cover the Japanese Islands. The relation between the active faults and velocity structure is also studied.

Deep low-frequency non-volcanic tremors and short-term slow-slip events (S-SSE) are observed at depths of approximately 30 km along the strike of the Philippine Sea (PHS) plate from the Tokai to western Shikoku regions (Obara, 2002). Some studies revealed that these events are located along a high-Vp/Vs zone by seismic tomography (e.g. Shelly et al., 2006). Long-term slow-slip events (L-SSE) are detected beneath the Tokai region and Bungo channel (e.g. Hirose and Obara, 2005). We refer to all of these three kinds of events as slow events.

Tremors and S-SSEs are located within or at the edge of the high-Vp/Vs zone. This indicates that those events occur where the oceanic crust of the PHS plate has the first contact with the serpentinized wedge mantle of the Eurasian (EUR) plate.

However, the L-SSEs are observed only beneath the Tokai region and Bungo channel where the high-Vp/Vs zone extends seaward at depths of 25-30 km. We consider this high-Vp/Vs zone as the lower crust of the EUR plate with fluid dehydrated from the PHS plate since the velocities are too low to consider this region to be the serpentinized wedge mantle. The existence of a high-Vp/Vs lower crust in the EUR plate may control the occurrence of L-SSEs (Matsubara et al., 2009).

We collect the velocity perturbation at depths of 5, 10, 15, and 20km beneath the active faults. In the SW Japan, the perturbations decrease, in general, with depth for both P- and S-waves. This implies that the

shallow region has a higher velocity and the deeper part has a lower velocity than the surrounding region beneath the fault zone. The high- and low-velocity zones are considered brittle and ductile, respectively. We speculate that the strain produced by the deformation of the ductile lower crust is accumulated at the shallower brittle part of the fault which gradually approaches failure.

HOLOCENE PALEOSEISMOLOGY OF THE SOUTHERN PANAMINT VALLEY FAULT ZONE: EVALUATING SEISMIC CLUSTERING ALONG THE EASTERN CALIFORNIA SHEAR ZONE NORTH OF THE GARLOCK FAULT (1-093)

L.M. McAuliffe, J.F. Dolan, E. Kirby, B. Haravitch, and S. Alm

New paleoseismological data from two trenches excavated across the southern end of the Panamint Valley fault (PVF), the most active of the three major faults in the eastern California shear zone (ECSZ) north of the Garlock fault, reveal the occurrence of at least two, and probably three, surface ruptures during the late Holocene. These trenches were designed to test the hypothesis that the earthquake clusters and intervening seismic lulls observed in the Mojave section of the ECSZ (Rockwell et al. 2000, Ganev et al. 2010) at 8-9.5 ka, 5-6 ka and during the past ~1-1.5 ka, also involved the fault systems of the ECSZ north of the Garlock fault. Well stratified playa sands, silts and clays exposed in the trench allowed precise identification of two event horizons; a likely third event horizon occurred during a period of soil development across the playa. Calibrated radiocarbon dates from 25 charcoal samples constrain the dates of the most recent event (MRE) to ~1450-1500AD and the ante-penultimate event at 3.2-3.6 ka. The penultimate event occurred during a period of soil development spanning ~350-1400AD. The presence of large blocks of soil in what appears to be scarp-derived colluvium in a large fissure opened during this event require that it occurred late during soil development, probably only a few hundred years before the MRE. The timing of the three events indicate that the southern PVF has ruptured at least once, and probably twice during the ongoing seismic cluster in the Mojave region. The PVF earthquakes also are similar in age to the 1872 Owens Valley earthquakes and the geomorphically youthful, but undated MRE in central Death Valley. Although we were unable to excavate deeply enough at this site to expose mid-to lower – Holocene playa strata, the timing of the ante-penultimate earthquake at our site shows that the PVF has ruptured at least once during the well-defined 2-5 ka seismic lull in the Mojave section of the ECSZ. Interestingly the 3.2-3.6 ka age of this event overlaps with the 3.3-3.8 ka age of the penultimate (i.e. pre-1872) rupture on the Owens Valley fault. As yet, there are too few paleo-earthquake data from other faults north of the Garlock fault to test the possibility that the northern part of the ECSZ experienced a system wide cluster of earthquakes at ~3.5 ka. We plan to undertake excavations on other faults in the northern ECSZ to test this idea.

SOUTHERN CALIFORNIA HIGH SCHOOLS CONTRIBUTE TO THE GPS VELOCITY FIELD IN THE INLAND EMPIRE (1-154)

S.F. McGill, B. Brownbridge, J. Cooper, A. Foutz, M. Johnson, J.M. Jones, J. Lipow, M. Meijer, T. Ramsey, R. Ruiz, B. Vargas, J. Spinler, and R, Bennett

A five-day GPS campaign coordinated by California State University, San Bernardino and funded by NSF's EarthScope program, was conducted from July 8-12, 2010. Participants included 5 SCEC interns, 3 other undergraduate students, 10 local high school teachers and 22 high school students. Campaign GPS data were collected from 24 sites in the San Bernardino Mountains, Inland Empire and high desert. These data will be processed by the University of Arizona group using GAMIT/GLOBK. In the meantime, participants analyzed processed data from the 2009 campaign, constructing time-series plots of the north, east, and vertical position and calculating velcoties for each site. Each site was determined to be moving at horizontal rates ranging from 17.0-33.2 mm/year (relative to stable North America) in a horizontal direction ranging from N32.7W to N46.5W. Velocities consistently increased for sites located farther southwest, consistent with elastic strain accumulation between the Pacific and North American plates. Slip rates for the San Andreas and 10 surrounding faults were modeled using a two-dimensional elastic model, with locking depths set to the maximum depth of earthquakes. In one afternoon of ad-hoc testing, the best-fitting curve found by the group had a slip rate of 10 mm/year for the San Andreas fault. However, a wide range of possible slip rates for the San Andreas fault was found that fit the GPS velocities well. More systematic testing of slip rates was conducted by the SCEC interns over the remainder of the summer (see abstracts by Anderson and others and by Bywater and others).

SLIP RATE OF THE NORTHERN SAN JACINTO FAULT FROM OFFSET LANDSLIDES IN THE SAN TIMOTEO BADLANDS (1-115)

S.F. McGill, L.A. Owen, E.O. Kent, N. Onderdonk, and T.K. Rockwell

A small restraining bend in the Claremont fault (northern San Jacinto fault zone) has produced basement uplift in the northern San Timoteo badlands. A number of landslides have occurred from this basement uplift as well as younger, secondary landslides within the older landslide deposits. At least two landslides have been offset a measureable amount across the San Jacinto fault and form the basis for two potential slip rate

measurements. The fault zone is relatively narrow in this vicinity, so a complete estimate of slip since the time of the landslides is possible.

The older of the two offset landslides (here named the Quincy Ridge landslide) is sourced from the basement rock uplift southwest of the San Jacinto fault zone. This slide has not yet been fully mapped. At present, however, its geometry appears rather unusual--a long, thin strip parallel to and offset by the San Jacinto fault. The southeastern edge of this old landslide deposit appears to be offset about 1.0 km across the San Jacinto fault, and the complete offset is probably greater than this because scattered boulders from this landslide deposit are present as float on top of the underlying San Timoteo formation as much as 1.6 km southeast of the southeasternmost outcrops of landslide deposit on the southwestern side of the fault. Samples for Be-10 dating were collected from 6 boulder tops on the least-likely-to-be-disturbed portions of the surface of the slide on the northeast side of the fault, and dates are expected in time for the meeting. This fall, soil pits will be dug and examined near some of these boulders in order to see whether or not the soil has been stripped in these locations, and to collect samples for a Be-10 depth profile.

A younger landslide (the Ebenezer Canyon landslide) is sourced from an older landslide deposit (probably a remnant of the Quincy Ridge landslide) on the southwestern side of the fault. The Ebenezer Canyon landslide deposit crosses the fault and is offset 270 ± 100 meters. Samples for Be-10 dating were collected from 6 boulder tops on the portion of the Ebenezer Canyon slide deposit that is northeast of the fault and that is isolated from any current source of boulders that match the lithologies of the slide deposit. Samples were also collected from 4 boulder tops within the headscarp in an attempt to date the sudden exposure of these boulders during the slump that produced the Ebenezer Canyon slide. Dates are expected in time for the meeting.

DISCRETE RUPTURE OF ASPERITIES RECORDED ON INSTRUMENTED LABORATORY FAULTS (2-077)
G.C. McLaskey and S.D. Glaser

We measure stress waves produced during frictional sliding on cm-scale frictional interfaces using an array of pm-scale sensitivity broadband displacement sensors. Experiments were performed on both basalt and PMMA sliding surfaces. By carefully analyzing the stress waves produced during the initiation of sliding, we are able to separate direct wave phases from reflections and identify discrete events or bursts amid the "noise" produced from gross sliding. The rapid rise time of such bursts enables the spatio-temporal location of these sources to be resolved to ~ 1 mm and ~1 microsecond accuracy. These discrete events are interpreted as the rupture of tiny (~micrometer sized) asperities or junctions which collectively constitute the interface. Using an array of ten sensors, we are able to study the focal mechanism and time history of these ruptures, in order to study the micromechanics of friction. While the rupture of an individual asperity may release less than one percent of the total shear load carried by the interface, if it ruptures rapidly enough, it will produce an identifiable (nano)seismic signature. Thus, the evolution of asperity rupture can be mapped as the interface transitions from "stick" to "slip," offering clues to the dynamics of fault rupture and the production of earthquakes.

GLYPHSEA: VISUALIZING TIME-DEPENDENT SEISMIC VECTOR FIELDS WITH GLYPHS (1-012)
E. McQuinn, A. Chourasia, J-B. Minster, and J.P. Schulze

Simulations of earthquakes produce time-dependent vector fields that contain interesting geophysics. Prior visualization strategies focused on slices and volumetric rendering of scalar fields which reduces the observable phenomena. The results of a ACCESS thesis studies visualization techniques implemented in an interactive glyph visualization application called "GlyphSea" that allows exploration of seismic velocity fields. This work draws from a large body of glyph rendering techniques to focus on time-dependent seismic vector fields. The design decisions are the result of collaboration between domain experts in visualization and seismology.

Through the study of vector visualization, several novel techniques were formed. A novel procedural dipole and cross mark texturing enhancement encodes unambiguous vector orientation on any geometry with volume. A novel lattice method was created to show neighborhood which also enables glyph distinction. Visualization is further enhanced by using screen space ambient occlusion, jitter, halos, and displacement. These techniques are flexibly interchanged with a realtime, fully interactive, cross platform software system that runs on workstations and laptops alike.

IDENTIFYING THE UNIQUE GROUND MOTION SIGNATURES OF SUPERSHEAR EARTHQUAKES: THEORY AND EXPERIMENTS (2-064)
M. Mello, H.S. Bhat, A.J. Rosakis, and H. Kanamori

The near field ground motion signatures associated with sub-Rayleigh and Supershear ruptures are investigated using the Laboratory Earthquake Experiment originally developed by Rosakis and coworkers

(Xia et al., 2004, 2005a, 2005b; Lu et al., 2007; Rosakis et al., 2007). Heterodyne laser interferometers enable continuous, high bandwidth measurements of fault-normal (FN) and fault-parallel (FP) particle velocity "ground motion" records at focused positions on the surface of a Homalite test specimen as a sub-Rayleigh or a supershear rupture sweeps along the frictional fault. Photoelastic interference fringes, acquired using high-speed digital photography, provide a synchronized, spatially resolved, whole field view of the advancing rupture tip and surrounding maximum shear stress field. We have experimentally validated that a rupture traveling at supershear speeds has the following analytically predicted signatures.

1. A dilatational precursor, dominant in the fault parallel component, that arrives in the ground motion records prior to the arrival of the Mach front.
2. Dominance of the fault parallel component over the fault normal component in the supershear speed regime (sqrt(2)Cs < Vr <= Cp).
3. Trailing Rayleigh rupture behind the main rupture tip with a dominant fault normal component. This produces a ground-shaking signature qualitatively similar to a sub-Rayleigh rupture.

We have also conducted experiments to replicate some extent of the 2002 Denali event and have identified two of the three signatures, listed above, both in the experimental and natural earthquake (Pump Station 10) records thus experimentally validating the argument of Dunham and Archuleta (2004) that part of the Denali rupture did indeed travel at supershear speeds. The direct practical consequence of the above observations are that a near field station will first experience the primary Fault Parallel(FP) shaking due to the shock structure and will subsequently feel a primary Fault Normal (FN) shaking of the trailing Rayleigh rupture. The timing between these two occurrences will depend on the location of the near field station relative to the point of sub-Rayleigh to supershear transition. Structures located near a fault hosting such a transition will effectively experience two separate, closely timed and qualitatively different sense of ground shaking.

SOURCE PROPERTIES OF THE 2010 M7 HAITI EARTHQUAKE ESTIMATED BY BACK PROJECTION OF THE DATA RECORDED BY THE NATIONAL VENEZUELA SEISMIC NETWORK (2-141)
L. Meng, J-P. Ampuero, and H. Rendon

Back projection of teleseismic waves based on array processing has become a popular technique for earthquake source inversion. By tracking the moving source of high frequency waves, areas of the rupture front radiating the strongest energies can be imaged. The technique has been previously applied to track the rupture process of the Sumatra earthquake and the supershear rupture of the Kunlun earthquakes. The challenge with the 2010 M7.0 Haiti earthquake is its very compact source region, possibly shorter than 30km. Preliminary results from back projection using US-Array or the European network reveal little detail about the rupture process. In this study, we made an effort towards imaging the Haiti earthquake using multiple seismic array networks, including the USArray and the National Seismic Network of Venezuela run by FUNVISIS. The FUNVISIS network is composed of 22 broad-band stations with an East-West oriented geometry, and is located approximately 10 degrees away from Haiti in the perpendicular direction to the Enriquillo fault strike. This is the first opportunity to exploit the privileged position of the FUNVISIS network to study large earthquake ruptures in the Caribbean. We applied back projection methods based on an novel signal subspace technique, which achieves considerable higher resolution than the classic stacking method. We experimented on various scenarios to quantify the inherent bias of the back projection techniques due to interference of coherent seismic signals. we also incorporated Green's function deconvolution in the array processing. Despite the complicated Pn phases at this distance,we observe an east to west rupture propagation along the fault, consistent with a compact source with two significant asperities. These efforts could lead the FUNVISIS seismic network data to play a prominent role in the timely characterization of the rupture process of large earthquakes in the Caribbean, including the future ruptures along the yet unbroken segments.

COMPLEX QUATERNARY DEFORMATION AMONG INTERSECTING SETS OF STRIKE-SLIP FAULTS NEAR TWENTY-NINE PALMS, SOUTHERN CALIFORNIA (1-081)
C.M. Menges, J.C. Matti, V.E. Langenheim, S.A. Mahan, and J.W. Hillhouse

We present geomorphic, structural, stratigraphic, and geophysical data indicating complex time-variant strain developed in a region of intersecting right- and left-lateral faults in the Eastern California Shear Zone (ECSZ) near Twentynine Palms, CA. Here two NW-trending, right-lateral faults of the ECSZ in the central Mojave Desert, i.e., the Mesquite Lake (MLF) fault on the east and the "airstrip" fault directly to the W, intersect the EW-trending sinistral Pinto Mountain fault (PMF) of the Eastern Transverse Range (ETR) fault domain. Major strain patterns include: (a) mismatches between fault traces and gravity-defined subsurface basins that suggest changes in fault organization and deformational style (from transtension to transpression); (b) transpressive deformation (linear ridges, pop-ups, and tilted or folded sediments) along the eastern PMF and SE part of the MLF; (c) contractional deformation and uplift localized at intersections of the dextral faults with the PMF; (d) significant off-fault deformation (asymmetric uplift and tilting from the

SW to NE block margins, widespread fault-related folding) of the intervening blocks between the dextral faults north of the PMF; and (e) large arch-like regional uplift (>600 m) rising southward from the Mojave lowland across the PMF and the entire northern range front of the ETR. New stratigraphic, structural, geomorphic and geochronologic data suggest that much of this deformation developed after mid-Quaternary time. We propose the following geologic history: (1) deposition of fine-grained muddy and sandy sediment (containing a layer of Bishop Ash (~760 ka age), identified by paleomagnetism and tephrochronology) within a regional depositional system as yet not understood in terms of ECSZ history, but discordant with younger mid-late Quaternary deposits; (2) deposition of gravelly and sandy sediment that spread eastward from the rising San Bernardino Mountains (SBM), probably post 760 ka; (3) disruption of the SBM depositional system by surface deformation and uplift associated with the ECSZ and its intersection with the sinistral faults of the ETR. This latter event clearly is post 760 ka, and probably younger than 300-200 ka. Deformation has spanned late Pleistocene to Holocene time, as indicated by deformed deposits dated using OSL (80 ka to 1 ka).

BUILDING THE COMMUNITY ONLINE RESOURCE FOR STATISTICAL SEISMICITY ANALYSIS (CORSSA) (1-120)
A.J. Michael, S. Wiemer, J. Zechar, J. Hardebeck, M. Naylor, J. Zhuang, and S. Steacy

Statistical seismology is critical to the understanding of seismicity, the testing of proposed earthquake prediction and forecasting methods, and the assessment of seismic hazard. Unfortunately, despite its importance to seismology - especially to those aspects with great impact on public policy - statistical seismology is mostly ignored in the education of seismologists, and there is no central repository for the existing open-source software tools. To remedy these deficiencies, and with the broader goal to enhance the quality of statistical seismology research, we have begun building the Community Online Resource for Statistical Seismicity Analysis (CORSSA). CORSSA is a web-based educational platform that is authoritative, up-to-date, prominent, and user-friendly. We anticipate that the users of CORSSA will range from beginning graduate students to experienced researchers.

More than 20 scientists from around the world met for a week in Zurich in May 2010 to kick-start the creation of CORSSA: the format and initial table of contents were defined; a governing structure was organized; and workshop participants began drafting articles. CORSSA materials are organized with respect to six themes, each containing between four and eight articles. The CORSSA web page, www.corssa.org, officially unveiled on September 6, 2010, debuts with an initial set of approximately 10 to 15 articles available online for viewing and commenting with additional articles to be added over the coming months. Each article will be peer-reviewed and will present a balanced discussion, including illustrative examples and code snippets. Topics in the initial set of articles will include: introductions to both CORSSA and statistical seismology, basic statistical tests and their role in seismology; understanding seismicity catalogs and their problems; basic techniques for modeling seismicity; and methods for testing earthquake predictability hypotheses. A special article will compare and review available statistical seismology software packages.

OPENSHA: OPEN SOURCE SEISMIC HAZARD ANALYSIS (1-037)
K. Milner, P. Powers, and E. Field

OpenSHA is an open-source, Java-based platform for conducting Seismic Hazard Analysis (SHA). As an object-oriented framework, OpenSHA can accommodate arbitrarily complex (e.g., physics based) earthquake rupture forecasts (ERFs), ground-motion models, and engineering-response models, which narrows the gap between cutting-edge geophysics and state-of-the-art hazard and risk evaluations. Over ten years in development, the project has been shaped by numerous scientists, developers, and technical experts in the fields of seismology, computer science, and earthquake engineering. Although primarily focused on California at inception, OpenSHA is now seeing broader, national use via incorporation in the National Sesmic Hazard Mapping (NSHMP) at the USGS, and it is receiving global exposure via the Global Earthquake Model (GEM) project. Recent OpenSHA development has expanded the capabilities of the platform to include: multiple (weighted) intensity measure realtionships (IMRs), the mapping of IMRs to tectonic settings, new global ERFs for use with GEM, and more. Updated applications and documentation are available at http://www.opensha.org.

BAYESIAN KINEMATIC FINITE FAULT SOURCE MODELS (2-133)
S.E. Minson, M. Simons, and J.L. Beck

Finite fault earthquake source models are inherently under-determined: there is no unique solution to the inverse problem of determining the rupture history at depth as a function of time and space when our data are only limited observations at the Earth's surface. Traditional inverse techniques rely on model constraints and regularization to generate one model from the possibly broad space of all possible solutions. However, Bayesian methods allow us to determine the ensemble of all possible source models which satisfy the data and our a priori assumptions about the physics of the earthquake source. Until now, Bayesian techniques

have been of limited utility because they are computationally intractable for problems with as many free parameters as kinematic finite fault models. We have developed a methodology called Cascading Adaptive Tempered Metropolis In Parallel (CATMIP) which allows us to sample very high-dimensional problems in a parallel computing framework. The CATMIP algorithm combines elements of simulated annealing and genetic algorithms with the Metropolis algorithm to dynamically optimize the algorithm's efficiency as it runs. We will present synthetic performance tests of finite fault models made with this methodology as well as a kinematic source model for the 2007 Mw 7.7 Tocopilla, Chile earthquake. This earthquake was well recorded by multiple ascending and descending interferograms and a network of high-rate GPS stations whose records can be used as near-field seismograms.

AN INVESTIGATION OF THE BIRTH AND DEATH OF FAULTS ALONG A RESTRAINING BEND USING CLAYBOX ANALOG MODELS (1-106)
J. Moody, M. Cooke, and M. Schottenfield

Geologic faults within the Earth are not static structures. Some faults cease activity while others initiate and propagate. For example, 500,000 years ago the San Andreas fault, abandoned one kinked fault strand and took up slip along a new, straighter fault strand. The slow evolution of faults in the Earth's crust can be modeled on an observable time-scale using wet clay in a servo-controlled claybox. The length scale of the clay in our claybox is five orders less than the crust so the strength of the clay is five orders smaller than crustal rocks. Basal plates apply strike-slip deformation to the overlying clay. How does changing the rheology of material in the claybox affect the pattern of faults that form within it? In a series of experiments we examine the slip, fault formation, and off-fault deformation that occurs in a claybox with and without a base layer of silicone putty. The putty is expected to produce more slip along secondary faults than clay alone because the putty may distribute the shear applied by the basal plates. We investigate fault evolution using both a complex restraining bend fault geometry that approximates the Mission Creek strand of San Andreas fault, which was active 500,000 years ago, and a simpler restraining bend kink fault geometry. The initial fault geometry was cut into the clay using an electrified probe, and the clay overlies metal plates that are shaped to the initial fault system. In all the experiments (with and without putty), the fault segment within the restraining bend was abandoned and new faults developed to accommodate deformation. We found that the putty produced less overall slip than the experiments without putty, and therefore produced more distributed shear within the clay. We also found that the silicone putty flows in response to the weight of the clay above it, so the putty flows outward away from areas of compression. Consequently, experiments with putty have less uplift than experiments with clay alone.

USING PHOTOGRAMMETRY TO PRODUCE HIGH-RESOLUTION DEMS OF THE EL MAYOR-CUCAPAH SURFACE RUPTURE (1-095)
A.E. Morelan, J.M. Stock, K.W. Hudnut, and S.O. Akciz

We developed a method using high-resolution (and low-elevation) aerial photographs to produce three-dimensional Digital Elevation Models (DEMs) of surface terrain. The area of interest was the rupture zone of the April 4, 2010, El Mayor- Cucapah earthquake (Baja California, Mexico). The protocol developed can rapidly and cost-effectively create DEMs for detailed, remote geologic mapping. This photogrammetric method will be especially important as an alternative to LiDAR (light detection and ranging). LiDAR data are more accurate, but also very expensive and logistically difficult to acquire internationally, whereas aerial images are relatively straightforward to capture. We obtained as high as 0.5m resolution in our DEMs, from aerial photographs taken by both a handheld digital SLR camera (Nikon D5000) and a camera intended for aerial photography (DSS 439). One noteworthy result is that topographic features evident in the resulting DEMs were not always visible in the photographs before they were processed. These DEMs are being integrated with field observations in GIS programs to precisely locate and characterize surface rupture of the El Mayor-Cucapah earthquake. Using the three-dimensional data sets created from aerial photography, we will be able to observe and quantify details including the slip vector (computed from horizontal and vertical displacement values) and the fault scarp's relationship to topography. Ongoing work includes comparison of the photogrammetric point cloud with the recently acquired LiDAR point cloud at specific target sites along the fault. Finally, we still need to assess the elevation accuracy of the photogrammetric method.

PRODUCTION OF SOUTHERN CALIFORNIA EARTHQUAKE CENTER VIRTUAL DISPLAY OF OBJECTS (SCEC-VDO) DISPLAYING SEISMIC RISK OF THE ELEVEN SHAKEOUT AREAS WITHIN CALIFORNIA (1-006)
S.A. Moreland, M. Benthien, and R. de Groot

The Great California ShakeOut began in 2008 as a way to educate the public on earthquake preparedness and emergency management in the event of a large earthquake. In order to implement the drill, California has been divided into eleven regions that have been designated as Shakeout areas. Using the Southern California Earthquake Center Virtual Display of Objects (SCEC-VDO), animations showing the various faults and recorded seismicity have been created for each ShakeOut area. This project developed a suite of 30 second

VDOs that focus on each of the eleven areas. SCEC-VDO is an object-oriented, open source software, that enables interactive 4D display of diverse geo-referenced datasets for analysis, presentation, and publication. Examples of datasets that can be visualized using SCEC-VDO include earthquake events, hypocenters and epicenters, fault systems and fault sections, three-dimensional surface images, tectonic plates and their vectors of motion, as well as political boundaries, cities, and highways. SCEC-VDO visualizations were produced to show past events that occurred in each ShakeOut area, and to educate a variety of audiences on probable threats. A second suite of 30 second VDOs is also created to show an event that occurred in one of the ShakeOut areas, the fault it occurred on, and the aftershocks that followed. These were created in an interactive way that allows them to be linked to other VDOs. Working alongside of ShakeOut projects and The Earthquake Country Alliance, SCEC-VDO visualizations are tools which will be used in teaching and spreading the word on earthquake preparedness.

USING GPS TO MEASURE FAULT SLIP-RATES OF THE SAN JACINTO FAULT IN RIVERSIDE COUNTY (1-141)
S.L.C. Morton, G.J. Funning, and M. Floyd

The San Jacinto Fault, which runs west of the Southern San Andreas Fault and parallel to the Elsinore fault, is considered the most dangerous in Southern California. The fault is not continuous, but comprised of a series of faults that run through San Bernardino, Riverside, San Diego and Imperial Counties. It is also split into three major segments: the Claremont segment, the Clark segment and the Coyote Creek section. After recent earthquakes of magnitudes greater than 6.0, it is important to keep an updated GPS data archive in order to determine how the fault is slipping. This summer, GPS was used throughout Riverside County to measure the precise position of twenty geodetic benchmarks. Each survey was left for data collection for 4-8 hours. The receiver was connected to a GPS antenna, which was mounted on a tripod that overlooked each geodetic benchmark. This data, along with data from the past fifteen years, was processed using the Unix-based program GAMIT. GAMIT used the collected phase data to determine the ground position for each benchmark. These positions from the last fifteen years were compared to give velocities for the ground movement of each station. In order to have optimal results, the data must be reprocessed various times as new coordinates are calculated; these recalculations are still being performed. As of now, the Claremont is believed to have a 16-25mm/year slip rate, the Clark has a 13-18mm/year slip rate and the Coyote Creek has a 3-5mm/year slip rate.

LONG PERIOD (T>1.0-S) SEISMIC RESPONSE OF THE SALT LAKE BASIN FROM EARTHQUAKE SIMULATIONS (2-139)
M.P. Moschetti and L. Ramirez-Guzman

The Wasatch Fault bounds the Salt Lake Basin (SLB), Utah to the east and is capable of producing M7 earthquakes. Because large (M>5) earthquakes in this region occur infrequently, the ground motion estimates required for seismic hazard analyses must be based on empirical results from other regions or from deterministic modeling efforts. Previous and on-going studies (Liu et al., 2010; Roten et al., 2010) examine the earthquake ground motions caused by a simulated M7 event on the Salt Lake Segment of the Wasatch Fault. Although the parameterizations of intrinsic attenuation and seismic wave speed models strongly affect the earthquake ground motions that result from numerical simulations, a comprehensive validation of the WCVM has not yet been performed. We compare the simulated seismic response of the SLB caused by small (3<M<5) earthquakes with recorded seismograms to assess the ability of the Wasatch Community Velocity Model (WCVM) (Magistrale et al., 2006) to reproduce the ground motions observed from these events. Simulations, valid up to 1 Hz frequency, are carried out using the WCVM and the Hercules finite element code (Tu et al., 2006). We model three small earthquakes that occurred outside of the basin and compare the synthetic and observed ground motions. In general, there is a good agreement between the arrival times from the simulated and observed waveforms. However, the peak ground velocities and durations of the synthetic waveforms are generally greater than from the recorded waveforms. These discrepancies suggest that the current velocity and attenuation models do not fully capture seismic parameters required for future hazard analysis. Modifications to the intrinsic attenuation model and to the seismic impedance contrasts that exist at the basement of the basin are likely to result in improved estimates of ground motion. Future work will analyze the effects of these modifications to the model.

USING RUPTURE-TO-RAFTERS SIMULATIONS TO QUANTIFY SEISMIC RISK FROM THE SAN ANDREAS FAULT -- CASE STUDIES OF TALL STEEL BRACED FRAME BUILDINGS. (1-043)
R. Mourhatch and S. Krishnan

The emergence of realistic rupture-to-rafters simulations provides us with a convenient tool for quantifying temporal risk posing existing tall buildings in southern California. We compute probabilistic economic losses given the deterministic structural response under a suite of scenario earthquakes and combine these results with the probabilities of occurrence of each scenario inferred from the Uniform California Earthquake Rupture Forecast (UCERF 3.0) to produce annualized loss regional maps for a given structure over the next

30 years. This end-to-end approach comprises of four major tasks: source model generation, ground motion simulations for aforementioned source models, nonlinear analysis of structures, and probabilistic economic loss analysis. We focus our current study on braced frame buildings in the 20-story class located in southern California and the risk posed by earthquakes on the San Andreas fault, which is capable of generating large magnitude earthquakes (7.5-8.0) with a relatively low recurrence interval of 140 to 200 years (Weldon et al,2005; Sieh 1977,1978). We hypothesize that only earthquakes in the magnitude range of 6--8 occurring on the southern section of the San Andreas fault (Parkfield to Bombay Beach) will cause damage of any significance to structures in southern California.We generate the source models by re-sampling the models from past earthquakes. We are simulating a total of 60 San Andreas scenarios with magnitudes in the 6--8 range, two unilateral rupture directivities, and various hypocenter locations. The probability of occurrence of each scenario over the next 30 years is inferred from UCERF 3.0. The ground motions for each scenario are being generated through SPECFEM3D at 450 stations across Southern California. The simulated ground motions will be used for analyzing nonlinear response of three braced-framed buildings using FRAME3D. Probabilistic economic losses will be determined at each location for each scenario. They will be combined with the 30-year probability of occurrence of each scenario to quantify the risk to these buildings across southern California associated with San Andreas earthquakes over the next 30 years. The study will provide a sound basis for short and long-term risk mitigation strategies.

COLLABORATION AMONG SCIENCE, ENGINEERING, AND SOCIAL SCIENCE: EARTHQUAKE RISK MITIGATION IN THE TOKYO METROPOLITAN AREA (1-039)

K.Z. Nanjo and N. Hirata

Seismic disaster risk mitigation in urban areas constitutes a challenge through collaboration of scientific, engineering, and social-science fields. Examples of collaborative efforts include research on detailed plate structure with identification of all significant faults, developing dense seismic networks; strong ground motion prediction which uses information on near-surface seismic site effects and fault models; earthquake resistant and proof structures; and cross-discipline infrastructure for effective risk mitigation just after catastrophic events. In response to such demands, the special project "Earthquake Disaster Mitigation in Tokyo Metropolitan Area" is under way (2007-2011). Our effort at the Earthquake Research Institute, the University of Tokyo is devoted to conduct scientific research: characterization of the plate structure and source faults in and around the Tokyo Metropolitan area. Assessment in the Kanto of seismic hazards produced by the Philippine Sea Plate (PSP) mega-thrust earthquakes requires identification of all significant faults, possible earthquake scenarios, rupture behavior, regional characterization of the PSP geometry, physical properties of overlying the Honshu arc and local near-surface seismic site effects. To meet the requirement for the scientific research, we are developing a dense network in the urban area with 226 stations. Seismic images with improved spatial resolution beneath the Tokyo Metropolitan Area are obtained to assess source areas of the coming large metropolitan earthquakes. In this presentation, we provide an overview of our scientific results obtained so far and extend our discussion to collaborative research among science, engineering, and social science to mitigate earthquake risks in the Tokyo Metropolitan area.

ANALYSIS OF THE COMPLETENESS MAGNITUDE AND SEISMIC NETWORK COVERAGE OF JAPAN (2-123)

K.Z. Nanjo, T. Ishibe, H. Tsuruoka, D. Schorlemmer, Y. Ishigaki, and N. Hirata

A reliable estimate of completeness magnitude, MC, above which all earthquakes are considered to be detected by a seismic network, is vital for seismicity-related studies. We show a comprehensive analysis of MC in Japan. We use the catalog maintained by the Japan Meteorological Agency (JMA) and also available information on seismic stations that report to JMA. For computing MC, we adopt a commonly-used method based on the Gutenberg-Richter frequency-magnitude law. Presently, MC=1.0 might be typical in the mainland, but to have a complete catalog, one needs to use earthquakes with magnitudes 1.9 or larger. Comparison with the Southern California Seismic Network (SCSN) suggests that the recent event detectability in the mainland generally shows similar completeness levels to that in the authoritative region of SCSN. We argue that the current MC of Japan is due to the success of network modernization over time. Particularly, we show that the spatio-temporal change of MC closely matches the addition of the Hi-net borehole stations to enhancing seismic-station density; it started in October 1997 in southwestern Japan, continuing to northeastern Japan until 2002. As suggested from this matching, we confirm that MC inversely correlates with station density. Further we find that irrespective of the network change after 1997, this correlation is unchanged in time, demonstrating that the influence on MC from factors beyond station density does not vary in time. Contrary to Alaska and California (Wiemer and Wyss, 2000), our results do not attribute such factors simply to anthropogenic noise. Because this is due to the borehole stations that reduce ambient noise, we conclude that in Japan the anthropogenic noise has insignificant effect on MC.

EVALUATING SEISMIC RISK USING THE FEMA HAZUS-MH MR4 EARTHQUAKE MODEL IN KING COUNTY WASHINGTON (1-053)

C.J. Neighbors, G.R. Noriega, Y. Caras, and E.S. Cochran

HAZUS-MH MR4 (HAZards U. S. Multi-Hazard Maintenance Release 4) is a loss-estimation software developed by FEMA to estimate possible losses due to disasters. It is meant to be used by federal, state, regional, and local government for planning related to earthquake risk mitigation, emergency preparedness, response, and recovery (FEMA, 2003). In this study, we look at several parameters used in the HAZUS-MH Earthquake Model to understand how differing user-defined settings affect ground motion analysis, seismic risk assessment and consequently, earthquake loss estimates for the 2001 Mw 6.8 Olympia Earthquake, a subduction zone-related event in the American Pacific Northwest. Inputs include USGS ShakeMaps and a variation of deterministic event scenarios and hazard maps. The earthquake component of HAZUS-MH applies a series of empirical ground motion attenuation relationships developed from source parameters of both regional and global historical earthquakes to estimate strong ground motion. Ground motion and resulting ground failure due to earthquakes are then used to calculate potential earthquake hazard. Finally, direct physical damage is calculated for general building stock, essential facilities, and lifelines, including transportation systems and utility systems. Overall losses are expressed in structural, economic and social losses.

This study is being conducted in collaboration with King County, WA officials to determine the best model inputs necessary to generate robust HAZUS-MH models for the Pacific Northwest. Comparisons between recorded earthquake losses and HAZUS-MH earthquake losses will be used to determine how region coordinators can most effectively utilize their resources for earthquake risk mitigation.

CONSTRAINING SEDIMENTARY BASIN-BASEMENT INTERFACE WITH CONVERTED BODY WAVES (2-009)

S. Ni and S. Wei

Deterministic ground motion simulation in southern California has been quite successful for frequencies below 0.5HZ, and pushing to higher frequency (1Hz or higher) requires better understanding of short scale crust structure. In particular, the velocity structure of sedimentary basins, the velocity contrast across them, and the geometry of the basin-basement interface have a controlling influence on the ground motions. We examined broadband waveforms from aftershocks of the 2008 Chino Hill earthquake, 2009 Inglewood earthquake. Most of the records show clear P and S waves, yet between the P and S arrivals we also observe signals almost as strong as the P waves but weaker than S waves. The horizontal signals appear on both radial and tangential components, suggesting an origin due to non 1D structure. With a dozen events from the 2008 Chino Hills as an "event array", we are able to demonstrate that these signals are converted waves when P and S waves cross the bottom of the Chino basin. The signals on the vertical components are Sp waves (converted to P waves when S crosses the interface), arriving before the S wave, and the signals on the horizontal components are Ps waves, which lag the P wave with almost the same time interval as the interval between Sp and S. The Ps on the tangential component can be explained by a dipping interface. The strong amplitudes of these converted waves indicate a strong velocity contrast across the interface. Finite difference calculations with the SCEC CVM do not adequately match the timing interval between Ps and P (or Sp and S) or the amplitude ratio of Ps/P (or Sp/S). We also attempt to model these converted waves with 3D ray-based synthetic seismograms for a few forward models. For the case of the 2008 Chino Hill earthquake, models of the dipping interface with appropriate velocity contrast will be presented. And for the 2009 Inglewood earthquake, horizontal basin-basement interface can explain converted seismic waves well for stations near the epicenter. Our modeling suggests that deterministic waveform at high frequency (>1HZ) is possible for close-in records where waves are converted only once or twice, when the basin structure is well understood. Conversely, those close-in records are valuable for constraining the geometry of and velocity contrast across basins, thus contributing to more accurate ground motion simulation.

AVERAGE STATIC STRESS DROPS FOR HETEROGENEOUS SLIP DISTRIBUTIONS: COMPARISON OF SEVERAL MEASURES AND IMPLICATIONS FOR ENERGY PARTITION IN EARTHQUAKES (2-127)

H. Noda, N. Lapusta, and H. Kanamori

Static stress drop is often estimated using the seismic moment and rupture area based on a circular crack model; we denote this estimate by DS_M. DS_M is sometimes interpreted as the spatial average of stress change over the ruptured area, denoted here as DS_A, and used accordingly, for example, to constrain the long-term stressing rate [e.g., Shaw et al., this meeting]. DS_M is also used to estimate available energy (defined as the strain energy change computed using the final stress state as the reference one) and radiation efficiency [e.g., Venkataraman and Kanamori, 2004]. In this work, we define a stress drop measure, DS_E, that would enter the exact computation of available energy and radiation efficiency.

The three stress drop measures - DS_M that can be estimated from observations, DS_A, and DS_E - are equal if the stress change is spatially uniform, and that motivates substituting DS_M for the other two quantities in applications. However, finite source inversions suggest that the stress change is heterogeneous in natural earthquakes [e.g., Bouchon, 1997]. Since DS_M is the average of stress change weighted by slip distribution due to a uniform stress drop [Madariaga, 1979], DS_E is the average of stress change weighted by actual slip distribution in the event (this work), and DS_A is the simple spatial average of stress change, the three measures should, in general, be different.

Here, we investigate the effect of heterogeneity aiming to understand how to use the seismological estimates of stress drop appropriately. We create heterogeneous slip distributions for both circular and rectangular planar ruptures using the approach motivated by Liu-Zeng et al. [2005] and Lavalleé et al [2005]. We find that, indeed, the three stress drop measures differ in our scenarios. In particular, heterogeneity increases DS_E and thus the available energy when Mo (and hence DS_M) is preserved. So using DS_M instead of DS_E would underestimate available energy and hence overestimate radiation efficiency. For a range of parameters, DS_E is well-approximated by the seismic estimate DS_M if the latter is computed using a modified (decreased) rupture area that excludes low-slipped regions; a qualitatively similar procedure is already being used in practice [Somerville et al, 1999].

NUMERICAL MODELS OF THRUST EARTHQUAKES ON HOMALITE FAULTS (2-074)
D.D. Oglesby, N. Lapusta, V. Gabuchian, and A.J. Rosakis

It is well known that the rupture, slip, and ground motion patterns of dip-slip faults can be quite different from those of otherwise-equivalent strike-slip faults. The primary reason is the asymmetric geometry where the fault meets the free surface. Numerical models and some observations imply that thrust faults should experience significantly larger motion on the hanging wall than on the footwall, and that this asymmetry is produced by a strong breakout phase from the free surface that propagates back down along the fault and through the surrounding medium. To test these and other predictions, we have performed experimental thrust faulting models using homalite in a laboratory setting (see Gabuchian et al., 2010 [this meeting]). We attempt to fit these experimental models with 2-D and 3-D dynamic finite element models with slip weakening friction. We find that the basic features of the numerical models can be reproduced by 2D models, including the amplitude of slip and slip rate, and the asymmetry between hanging wall and footwall. However, some of the complexity in the laboratory model particle time histories may be explained by 3D effects associated with the homalite sample's finite width, including wave reflections off the edges of the homalite material sample. We will discuss which of the experimental and numerical results are applicable to real earthquakes.

M8 (1-065)
K.B. Olsen, Y. Cui, T.H. Jordan, K. Lee, J. Zhou, P. Small, D. Roten, G. Ely, D.Kim. Panda, A. Chourasia, J. Levesque, S.M. Day, P. Maechling, and J. Jones

In the current Uniform California Earthquake Rupture Forecast, the 30-year probability of a magnitude-8 rupture extending from the Salton Sea to Cholame (the 'wall-to-wall' event) is a modest 3%. Moreover, there is no consensus from paleoseismic studies that the 'wall-to-wall' event has ever happened. However, the paleoseismolgical record is consistent with such an event in the late 1400s, so ground motions from this type of earthquake need to be investigated.

We have simulated 0-2Hz wave propagation for a magnitude-8 earthquake that ruptures the entire southern SAF from Cholame to the Salton Sea—a total fault length of 545 km. This 'wall-to-wall' scenario ('M8'), was computed in a 810 km × 405 km × 85 km volume extracted from the SCEC CVM V.4 with 40-meter resolution, comprising a total of 436 billion cubic elements. M8 used a source generated by dynamic rupture on a planar fault, where the resulting slip time histories were inserted onto a 47-segment vertical approximation of the SAF from the SCEC CFM. The initial shear stress on the fault was derived assuming depth-dependent normal stress and a random stress field with a Von Karman autocorrelation function with lateral and vertical correlation lengths of 50 km and 10 km, respectively. In the top 2 km of the fault, we emulated velocity strengthening by forcing the dynamic friction coefficient to be larger than the static friction coefficient. The simulation of 360 s wave propagation sustained 220 Tflop/s for 24 hours on NCCS Jaguar using 223,074 cores.

The PGVs show patterns in agreement with results from the previous TeraShake and ShakeOut-D simulations, including strong directivity effects and 'sun-bursts' radiating from the fault due to the complexity of the spontaneous rupture propagation. The NW-SE rupture direction for M8 is largely transverse to the waveguides, avoiding the intense focusing effect observed for NW-propagating TeraShake/Shakeout ruptures. Still, extremely large PGVs are obtained near the fault, including basin areas such as San Bernardino and Coachella valley. Some of largest near-fault PGVs occur in connection with patches of super-shear rupture for M8, in particular where the rupture speed increases rapidly from sub-

Rayleigh to super-shear rupture speeds. For most distances from the fault, the M8 and NGA PGVs agree very well, providing independent evidence that the fault area (and therefore the average stress drop) are consistent with a moment magnitude-8 event.

PRELIMINARY RESULTS FROM MYSTIC LAKE: A NEW PALEOSEISMIC SITE ALONG THE NORTHERN SAN JACINTO FAULT ZONE. (1-105)
N. Onderdonk, S. McGill, G. Marliyani, and T. Rockwell

We present preliminary results from a new paleoseismic site along the Claremont strand of the San Jacinto Fault Zone in southern California. The site is located along the northeast edge of the ephemeral Mystic Lake at the north end of the San Jacinto Valley step-over. A small-scale (300 m wide) releasing step-over along the Claremont fault has created a sag depression that can be seen in early aerial photography. An initial locator trench was excavated 400 m across the full width of this sag, exposing multiple faults and a structural depression filled with excellent shallow lake stratigraphy. Three additional trenches were excavated across the main active fault zone that bounds the southwest edge of the sag. This fault is expressed as a zone of progressively folded and displaced strata. Upward terminations, fissures, folding, and growth stratigraphy provide evidence for at least six events in the upper 2 meters of section that was exposed. The stratigraphic relationships suggest a model in which each surface rupture results in subsidence of the sag, followed by clay deposition as the sag is filled in, culminating in a weak surface soil. Radiocarbon dating of 19 samples (out of over 400 that have been collected) was used to develop a preliminary event chronology. The most recent rupture occurred after 1750 AD and the penultimate event occurred between 1502 AD and 1612 AD. There is evidence for a cluster of 3 earthquakes between 1026 AD and 1220 AD, and a sixth event between 620 AD and 864 AD.

The timing of the three events around 800 to 1000 years ago coincides temporally with a cluster of three events that were recorded at the Wrightwood paleoseismic site on the Mojave segment of the San Andreas Fault (SAF). These three events have not been recognized at paleoseismic sites along the San Bernardino segment of the SAF south of the juncture with the San Jacinto Fault, which suggests that some events on the SAF may rupture southward down the San Jacinto Fault (or vice-versa). We also note that the two most recent events at Mystic Lake overlap with the two most recent events at the Hog Lake paleoseismic site, 30 miles to the south along the San Jacinto Fault Zone on the Clark Fault. This observation suggests that either some large San Jacinto events may jump across the San Jacinto Valley releasing step-over that separates the northern and central fault segments, or that stress triggering along one segment causes the other to fail in close succession.

AIRBORNE LIDAR SURVEY OF THE 4 APRIL 2010 EL MAYOR-CUCAPAH EARTHQUAKE RUPTURE (1-096)
M. Oskin, R. Arrowsmith, A. Hinojosa, J. Gonzalez, A. Gonzalez, M. Sartori, J. Fernandez, Y. Fialko, M. Floyd, J. Galetzka, and D. Sandwell

Airborne lidar surveys collected August 16-19, 2010, reveal topographic details of the April 4 El Mayor-Cucapah earthquake rupture zone. 3.8 billion point measurements were obtained with an average density of 11 points per square meter. GPS ground control was provided through a combination of PBO stations north of the international border and occupation of a subset of the post-earthquake campaign sites in the central and southern portions of the rupture zone. Overall, the survey spans 100 km in a NW-SE direction, from just south of the border to the tidal flats of the Colorado River delta at the head of the Gulf of California. The 3 km average width of the survey is designed to capture the complexity of slip transfer between the multiple fault segments that slipped in 2010, as well as the adjacent zone of surface ruptures attributed to the 1892 Laguna Salada earthquake. This data set will provide a new basis for offset measurements to be compared against field data collected immediately following the 2010 earthquake. Additional zones of rupture may be identified in areas of steep relief and distributed deformation between fault segments. The southern half of the lidar survey spans a zone of cryptic dextral deformation, hosted within the thick sedimentary fill, where little surface evidence of tectonic deformation has been recovered to date. Preliminary point-cloud data, processed during the survey with a subset of GPS data, will be available at the SCEC annual meeting. The full 100 gigabyte point cloud will be available online via opentopography.org as soon as processing has been completed.

EXPLORING LITHOSPHERIC DEFORMATION OF WESTERN US WITH GPS TIME SERIES, VELOCITIES, AND STRAIN MAPS. (1-151)
S.E. Owen, Y. Bock, F.H. Webb, S. Kedar, D. Dong, P. Jameson, P. Fang, M. Squibb, and B. Crowell

The advent of large dense GPS networks such as PBO poses a logistical obstacle to scientific studies: how can the scientist best explore the deformation being measured by these networks while not spending all their time analyzing massive quantities of data? In response to this challenge, we have developed an operational system for generating data products useful for the study of lithospheric deformation in the Western U.S. from PBO and other continuous GPS stations in this region. The primary objective of this project, funded

through NASA's Making Earth System data records for Use in Research Environments (MEaSUREs) program, is to generate long-term consistent surface deformation Earth Science Data Records (ESDRs) by infusing science product generation, visualization, and manipulation tools and information technology, prototyped in the past 5 years under a variety of NASA Earth Science programs, into an end-to-end operational Science Data System. The products include geodetic daily position time series, crustal motion velocities, and strain and strain rate maps. By the end of the project these products will provide nearly two decades of consistent and calibrated GPS deformation products. These data products are at the level just below interpretation and will make scientific discoveries from PBO and other networks more accessible to the broad community of geophysics researchers and students by generating high level deformation products from the raw geodetic data and providing the through a science data portal with integrated product exploration and modeling tools.
Data products and web-based modeling tools are made accessible through a portal called GPS Explorer (http://geoapp03.ucsd.edu/gridsphere/gridsphere, see below) that allows scientific users to explore and manipulate these products and data sets in a workbench-like environment. The tools allow users to do custom modeling and filtering of time series from PBO sites and other stations greater western North America region.
We will present examples of GPS results from our project, including results from the recent El Mayor-Cucapah earthquake. We will also have a computer on hand to demonstrate how to use GPS Explorer to access and model the time series, and explore velocities and strain movies.

PRELIMINARY RESULTS ON SEISMICITY AND FAULT ZONE STRUCTURE ALONG THE 1944 RUPTURE OF THE NORTH ANATOLIAN FAULT EAST OF ISMETPASA (2-115)
Y. Ozakin, Y. Ben-Zion, M. Aktar, H. Karabulut, and Z. Peng

The North Anatolian Fault (NAF), a continental plate boundary similar in some respects to the San Andreas Fault (SAF), is of great importance to Turkey in terms of seismic hazard. The geological history, lithology & topography suggest that the NAF is generally a bimaterial interface separating different rock bodies. Theoretical and observational studies suggest that there may be fundamental differences between properties of earthquakes and seismic radiation generated by ruptures along interfaces that separate similar and dissimilar solids (e.g., Weertman 1980; Ben-Zion 2001; Dor et al. 2008; Ampuero & Ben-Zion 2008; Zaliapin & Ben-Zion 2010). High-resolution imaging of the internal fault structure in various locations can be used to test hypotheses associated with bimaterial ruptures, and estimate expected shaking hazard based on the results. It is also important to clarify the geometry and seismic potential of various sections through high-resolution studies of seismicity. To begin such studies, we conducted a pilot seismic experiment east of Ismetpasa on the 1944 rupture of the NAF with a line of 6-11 seismometers that cross the fault. The location was chosen because it is within the area where Dor et al. (2008) found strong asymmetry of rock damage that may reflect repeating ruptures on a bimaterial fault interface. The location also coincides with a section of the NAF that is partially creeping at least at shallow depth. The creep rate decayed from a maximum of 4-5 cm/yr following the 1994 earthquake to a present value of to 0.7 cm/yr (Cakir et al. 2005). The small local network has been operating for ~2.5 yr. Earthquake detection was done by a manual inspection of automatic identification of candidate events. To date we were able to detect only ~235 events in the magnitude range -1 to 2.5 within a radius of 45 km from the center of the network. Using template earthquakes for detecting more events was not successful so far, as the signals produced by the employed events are too similar to the background noise. Only 15-20 events are located within 3 km of the rupture and they all have Ml<1.0. The small number of events is in mark contrast to the numerous microearthquakes along the creeping section of the SAF, suggesting that the NAF east of Ismetpasa does not creep at depth. We are planning to use other potential detection methods to increase the number of events, and to analyze the waveforms for high-resolution local velocity structure.

SOLVING FOR EARTHQUAKE RUPTURE RATES ON A COMPLEX FAULT NETWORK (2-156)
M.T. Page and E.H. Field

We present preliminary results from an inverse method that solves for the long-term rate of all ruptures on the major mapped faults in California. This method is being developed for the 3rd Uniform California Earthquake Rupture Forecast (UCERF3). Building on the work of Andrews and Schwerer (2000), we solve for the rates of ruptures that are consistent with a) slip-rate constraints, b) paleoseismic event rates, and optional constraints such as c) a-priori rupture rate estimates, d) smoothness constraints, and e) constraints on the magnitude distribution. These constraints are linear, and allow us to formulate the system of equations as a matrix equation. Multiple solutions to the inverse problem are then sampled via a simulated annealing algorithm.

Using this inversion methodology, the ruptures themselves (or more specifically, the portions of the faults involved in each rupture) must be specified a priori. This requires generating simple rules to describe which faults or fault segments can rupture together in a single earthquake. We discuss possible criteria and their effect on the size of the solution space and the characteristics of the solution.

UNDERSTANDING PHYSICAL MECHANISMS OF EARTHQUAKE TRIGGERING IN SOUTHERN CALIFORNIA FOLLOWING THE 2010 MW7.2 NORTHERN BAJA CALIFORNIA EARTHQUAKE (2-132)
Z. Peng, X. Meng, and A. Doran

Large shallow earthquakes are typically followed by significant increases of seismic activity around the mainshock rupture region, and sometimes at regional and teleseismic distances. While the change of seismicity rate at large distance is mostly attributed to dynamic triggering, whether earthquakes in the near field are triggered by static, dynamic, or quasi-static stress changes, is still in debate. An improved knowledge of the underlying physical mechanism of earthquake triggering is not only vital for better understanding the fundamental physics of earthquake interaction, but also useful for seismic hazard forecasting and mitigation. The 2010 Mw7.2 Northern Baja California has triggered a widespread change of seismicity pattern in southern California, offering an excellent opportunity to test various models of earthquake triggering. In this study we focus on the San Jacinto Fault (SJF) near Anza and the Salton Sea Geothermal Field in southern California, with high-sensitivity continuous borehole recordings and ample background seismicity. We find an clear increase of seismic activity in both regions immediately following the Baja California mainshock and an Omori-law-type decay afterwards, which is consistent with the facts that both regions are in the rupture propagation direction and have experienced significant dynamic shakings during the mainshock. However, the seismicity rate around Salton Sea drops below the pre-mainshock rate after ~1 month, while the seismicity rate around the SJF remains high, including an Mw5.4 earthquake near the Coyote Creek segment of the SJF on 07/07/2010. The difference could be due to a positive Coulomb stress change near the SJF, and a negative Coulomb stress change (i.e., stress shallow) around the Salton Sea. An alternative explanation is that the SJF experienced larger dynamic stresses than the Salton Sea region. So far the analysis is based on earthquakes listed in the Southern California Seismic Network (SCSN) catalog, which could be incomplete in our study regions due to the enormous aftershock activity near the mainshock rupture zone. Our next step is to apply the recently developed matched filter technique to detect potential missing earthquakes in both study regions and use them to better understand the physics of earthquake triggering in southern California.

DEEP STRUCTURE OF LITHOSPHERIC FAULT ZONES (2-002)
J.P. Platt and W.M. Behr

We offer two fundamentally new concepts that help place constraints on the mechanics and width of plate-boundary shear zones below the brittle-ductile transition. 1. Lithospheric shear zones operate at approximately constant stress at any given depth. This is because shear zones form by microstructural changes that cause weakening and hence strain localization. These changes occur when the ambient stress reaches the yield strength σy of intact rock. As a result, the cumulative width w of shear zones reaches a value such that they can accommodate plate motion at a flow stress equal to σy. 2. The second concept follows from the first. Dislocation creep causes dynamic recrystallization and grainsize reduction. This may result in a switch to one of several types of grainsize-sensitive creep, which is the main cause of weakening and strain localization in shear zones. If shear zones operate at constant stress, the dislocation density in the deforming grains remains the same after the switch. Dynamic recrystallization and grain-boundary migration driven by the dislocation strain energy continue at the same rate as before. This inhibits grain growth driven by surface energy, so that the deformation mechanism switch is permanent.
We calculate shear zone widths at depth in the lithosphere based on these concepts. We use a stress-temperature profile obtained from the Whipple Mountains, California, to constrain the strength of the ductile quartz-rich middle crust, and we estimate stress-T-width profiles through the lower crust and upper mantle using published flow laws. We conclude that the cumulative width of shear zones making up the San Andreas Transform is likely to reach about 6 km in the mid-crust, narrow to a few tens of meters in feldspar-dominated lower crust and olivine-dominated uppermost mantle, and widen to 80 km at 45 km depth. Below about 55 km, we predict that weakening mechanisms do not operate, and hence will not contribute to strain localization.

STRAIN LOCALIZATION WITHIN A FLUID-SATURATED FAULT GOUGE LAYER DURING SEISMIC SHEAR (2-057)
J.D. Platt, J.R. Rice, and J.W. Rudnicki

Observations indicate that seismic shear on a fault is extremely localized, with most strain occurring in a narrow zone less than a few mm wide within a broader ultracataclastic zone (Chester and Chester, Tectonophys.1998; Chester and Goldsby, SCEC 2003; Chester et al., EOS 2003; Heermance et al., BSSA 2003; Wibberley and Shimamoto, JSG 2003; Chester at al., Columbia Un. 2004). Heermance et al. noted that the zone of most intense shear is only 50 to 300 microns wide for the Chelungpu Fault of the 1999 Chi-Chi Taiwan earthquake, as intersected at 350 m depth in a borehole. Also, study (Rice, JGR 2006) of the Chester and Goldsby thin-section micrograph for the surface-exposed Punchbowl fault suggest most shear occurs only over 100 to 300 microns width within a nominal 1 mm wide shear zone.

To investigate factors which might set the scale of this localization process, we model a homogeneous, fluid-saturated gouge layer of width h that is being sheared between two saturated poroelastic half-spaces. If the gouge is non-dilatant and has a friction coefficient which is constant, or rate-weakening, then only two forms of deformation are possible (Rice, 2006): homogeneous shear, or slip on a mathematical plane. By assuming a rate-strengthening friction (appropriate for a fault gouge which has achieved high temperatures by ongoing frictional heating), with logarithmic dependence of friction on strain rate, and otherwise following the thermal pressurization formulation by Lachenbruch (JGR 1980) and Mase and Smith (JGR 1987), we find localization of strain to a finite width band to occur within the gouge layer, provided h is large enough.

We infer the width of this band based on the physical properties of the gouge. For a given shear velocity V accommodated across the gouge layer, the width is shown to be only weakly dependent on h and, within the uncertainty of parameter choices, is predicted to be on the scale of 50 to 100 microns when V = 1 m/s. We also studied the weakening of the gouge layer as a function of time, comparing localized and homogeneous shear, the latter with a constant friction coefficient. We find that the localization process leads to additional weakening of the gouge layer, and examine how this additional weakening is controlled by the properties of the gouge. Future studies of this type should include gouge dilatancy as an additional stabilizing feature which contributes to determining the width of the shear zone.

ON THE CHARACTERISTICS OF SEISMIC EVENTS WITH MAGNITUDES -5 < M < -1 (2-140)
K. Plenkers, G. Kwiatek, D. Schorlemmer, M. Nakatani, Y. Yabe, and D. Dresen

We present the results of in-depth analysis of the characteristics of seismic events recorded with the JAGUARS (Japanese-German Underground Acoustic Emission and Microseismicity Research in South Africa)-network with magnitudes -5 < M < -1. We aim to give new insights into the nucleation and rupture process of seismic events by closing the observational gab between field seismology and laboratory fracture experiments.

The JAGUARS-project measures seismic events with frequencies 0.7 kHz < f < 200 kHz in Mponeng gold mine, Carletonville/Republic of South Africa. The seismic network, combining 1 triaxial accelerometer (sensitivity: 50Hz to 25kHz) and 8 Acoustic Emission (AE)-sensors (sensitivity 1kHz-200kHz), monitors a highly-stressed rock volume of approx. 300 m x 300 m x 300 m at a depth of 3540 m. From June 2007 to June 2008 nearly 500,000 events were successfully recorded including more than 57,000 events with frequency content f > 25 kHz. All seismic events display clear P- and S-wave onsets. An aftershock sequence following a M=1.9 event that occurred 30m from the network was monitored. Approx. 25,000 aftershocks were recorded.

Analysis of the network's detection limits shows that high-frequency waves (f > 25 kHz) are able to travel as far as 100 m. The influence of local geology, engineered structures and exploitation is visible. We present an extended probability-based magnitude of completeness (PMC) method that is able to take into account a complex 3D setting of the monitoring network and analyze the detailed spatial distribution of recording completeness. We find a magnitude of completeness as small as -4.7 in the center of the JAGUARS-network.

We analyze the magnitude-frequency characteristics. We estimate b-values between 1.1 and 1.4. No deviation from the Gutenberg-Richter distribution is visible in the magnitude range studied. Preliminary results of our source parameter study are presented. The source parameter study is so far focused on seismic events with dominant frequencies below 17kHz. We calculate corner frequencies between approx. 1kHz and 10kHz. The stress drop is estimated to about 10MPa.

NEW DEVELOPMENTS FOR THE SCEC COMMUNITY FAULT MODEL AND ITS ASSOCIATED FAULT DATABASE (2-003)
A. Plesch, C. Nicholson, J.H. Shaw, E. Hauksson, and P.M. Shearer

We present a new version of the SCEC Community Fault Model (CFM v.4.0) which incorporates updates on fault representations, a detailed fault surface trace layer, and a new naming and numbering scheme for individual 3D fault models that allows for closer links to the USGS/CGS Quaternary Fault and Fold database (Qfaults) and other SCEC data sets. Available fault representations in CFM are now referenced to the modern WG84 datum, and the new surface layer in CFM allows subsurface 3D fault models to be registered to the more detailed, mapped fault traces from Qfaults and other digital fault map sources. In addition, a new SCEC fault database hierarchical naming and numbering scheme is implemented that provides unique identifiers (number, name, abbreviation) for each level of the fault hierarchy under which a particular fault segment is classified. Levels of fault hierarchy include Fault Area (e.g., Coast Ranges, Mojave, Peninsular Ranges-LA Basin, etc.), Fault Zone or System (e.g., San Jacinto fault zone, Elsinore-Laguna Salada fault zone, San Gorgonio Pass fault system, etc.), Fault Section (e.g., Parkfield, Cholame-Carrizo, Mojave, etc.), Fault Name (Chino, Whittier, Glen Ivy, etc.), Fault Strand or Model, Alternative, and Fault Component (e.g., surface trace, top 100m, extrapolated section, etc.). These additional fault identifiers should allow for more flexible database searches and easier identification of fault components, alternative representations, and possible system-level, regional or tectonic associations of the individual 3D fault elements that comprise

CFM. New 3D fault representations for major active fault zones, including the San Andreas from San Gorgonio Pass to the Salton Sea, the San Jacinto, and Elsinore-Laguna Salada are being added that allow for more non-planar 3D fault geometry, as suggested by the relocated microseismicity. This includes changes in dip and dip direction along strike and with depth. These new revised 3D fault models and interpretations help characterize a more complex pattern of fault interactions at depth between various subsurface fault sets, and may help to explain some of the more enigmatic fault behavior that is otherwise difficult to understand, such as why the 1986 M6 North Palm Springs earthquake failed to trigger a larger, longer rupture of the Southern San Andreas fault.

STATEWIDE COMMUNITY FAULT MODEL (SCFM) (2-010)
A. Plesch and J.H. Shaw

We present our progress toward a comprehensive Statewide Community Fault Model, (SCFM), for California. The statewide model is comprised of the southern California CFM 4.0 and more than 150 additional fault representations for northern California. Geologic models developed largely by the USGS serve as the basis for most fault representations in the greater San Francisco Bay area (e.g., Brocher et al., 2005). Additional new fault representations in northern California were developed by integrating geologic maps and cross sections, seismicity, well and seismic reflection data using the approach of Plesch et al., (2007). Each of the faults are defined by triangulated surface representations, with separate patches that distinguish between interpolated and extrapolated regions of the fault surfaces. This allows users to clearly distinguish portion of the fault representations that are directly constrained by data from those that are inferred or extended from better known parts of the fault. In addition, the model contains alternative representations of many faults. These cases arise when two or more fault interpretations have been made that involve substantial differences in 3D representation (i.e., in dip direction, fault type), and all of them are seemingly consistent with the available data.

The current version of the SCFM (1.5) will be evaluated this Fall through a virtual workshop sponsored by SCEC, in order to establish preferred and alternative fault representations, assign quality rankings to faults, and identify areas where further improvements to the model are needed. This activity will be coordinated with plans by the CGS, USGS, and SCEC to develop the UCERF3 fault model. Ultimately, this new statewide model is intended to help improve our assessment of seismic hazards in California, and contribute directly to fault systems modeling activities within SCEC.

HOW MUCH DO LONG-TERM "GHOST TRANSIENTS" FROM PAST EARTHQUAKES CONTRIBUTE TO THE PRESENT-DAY GPS VELOCITY FIELD IN CALIFORNIA? (2-024)
F.F. Pollitz, E.H. Hearn, and W.R. Thatcher

The steady-state GPS horizontal velocity field provides (1) constraints on the broad-scale seismotectonic framework, (2) estimates of the slip rates on major faults and strain rates elsewhere, and (3) input for probabilistic seismic hazard analysis (PSHA). However, the observed velocity field is contaminated by poorly bounded, long-term, long wavelength viscoelastic transient effects of past earthquakes. Our goal in this study is to carry out simple model calculations that will begin to provide upper limits on the amount the observed field is influenced by these transient effects, with application to UCERF3.
We have run forward models of a single, hypothetical M8 earthquake, and a sequence of such earthquakes, to assess the likely duration and magnitude of postseismic transients. End-member viscoelastic models (Maxwell and Burgers Body) based on recent studies of large earthquakes in California and Turkey are employed.

Average velocity contributions from faults to individual GPS points may be calculated by dividing the site displacement over an interseismic interval by the recurrence interval. We will show that velocity contributions may be much larger than this average early in the interseismic interval, and smaller than this average late in the interseismic interval. Such deviations may affect estimates of slip rate and locking depth based on GPS data (e.g. Johnson et al., 2007), because these estimates are made assuming steady-state slip (using elastic block models or the solution for deformation due to a single, infinite dislocation at depth in an elastic halfspace [Savage and Burford, 1973]).

Results from this exercise and follow-up activities will provide an estimate of the extent to which transient deformation due to viscoelastic relaxation affects the southern California GPS velocity field. We hope that these preliminary results will trigger contributions to this project from SCEC researchers with alternative earthquake-cycle models.
Future steps:

- Test additional, admissible lithosphere models (e.g., models with stratified rheology, power-law flow, and/or afterslip).
- Identify a relationship between (1) earthquake size (2) distance to the rupture and (3) time since the earthquake to determine conditions for which velocity perturbations are negligible.

A GML ENCODING STANDARD FOR INTERCHANGE AND VISUALIZATION OF GEOLOGIC, GEOPHYSICAL AND GEOENVIRONMENTAL DATA (1-022)

D.J. Ponti, L.L. Turner, D.S. Burggraf, and C. Bray

An international standard interchange schema for geologic, geotechnical and geoenvironmental data (called DIGGS - Data Interchange for Geotechnical and Geoenvironmental Specialists; www.diggsml.org) is being developed under the auspices of the U.S. Federal Highways Administration through a collaboration of 11 State Departments of Transportation, several US and UK national agencies, university researchers, and representatives from the geotechnical software industry. The goals of DIGGS are to:

- facilitate exchange of data among different databases within an organization;
- enable oversight and regulatory agencies to receive data from consultants and laboratories in a standardized format;
- facilitate exchange and display of data among practitioners and researchers via the Internet;
- facilitate data QA/QC and help to preserve valuable subsurface data and metadata;
- facilitate exchange of data among commercial software packages; and
- promote the development of data-analysis software products that are more standardized and more compatible.

The exchange standard is an XML-based Geographic Markup Language (GML) application schema and borrows heavily from the Open Geospatial Consortium's (OGC) SensorWeb and Observations and Measurements data models. This approach enables DIGGS encoded data to leverage existing OGC-compliant web services and tools for manipulating and visualizing geospatial information. DIGGS defines surface and subsurface sampling features (boreholes, trench walls, etc.), monitoring installations (eg. wells, inclinometers) and a wide range of associated geoscience observations that are obtained from field observations and in-situ and laboratory tests. Data dictionaries developed by the Association of Geotechnical and Geoenvironmental Specialists in the United Kingdom, COSMOS, and the National Geotechnical Experimentation Sites (NGES) are incorporated into the current version of the DIGGS schema, which itself is easy to extend.

An implementation version of DIGGS is to be released this fall. Along with the release will be a suite of web-based tools for facilitating data translation and display, including a previewer for borehole geologic, geophysical and cone penetrometer graphic logs and a KML translator, to allow 3D data to be viewed in GoogleEarth. In addition, several commercial geoscience software packages, including gINT, EQuIS), and HoleBASE, plan to directly import and export DIGGS-formatted data.

LITHOSPHERIC DEFORMATION WITHIN SOUTHERN CALIFORNIA: A COMPARISON OF CRUSTAL AND UPPER MANTLE ANISOTROPY MEASUREMENTS (2-015)

R. Porter and G. Zandt

The identification and characterization of seismic anisotropy can provide valuable information about deformation within the Earth and help explain how stress is partitioned across major physical boundaries (e.g., the Moho). We examine receiver functions (RFs) for travel time delays and diagnostic converted phases to determine the presence of and characterize anisotropy within the Southern California lithosphere. RFs can be used to determine the depth and thickness of discrete zones of anisotropy, making them an excellent tool for the analysis of anisotropy. Using this technique, we have identified a layer of anisotropic material located at the base of the crust. This material exhibits hexagonal anisotropy with an average unique symmetry axis plunging in the NE-SW direction. Applying the McQuarrie and Wernicke (2005) tectonic reconstruction, we rotated and translated anisotropy measurements back to their pre-36 Ma locations and orientations, which made the NE-SW trend even stronger. We interpret the anisotropy measurements as resulting from a top-to-the-southwest sense of shear that existed along the length of coastal California during pre-transform, early Tertiary subduction. We suggest that the anisotropic layer coincides with a package of schists and related rocks emplaced after the removal of lower crustal rocks during Laramide shallow flat subduction. We are now using RFs to search for zones of seismic anisotropy within the upper mantle, to determine if upper mantle anisotropy exists and if it correlates with crustal anisotropy and shear wave splitting results. A visual analysis of RFs calculated from 41 stations deployed in the region suggests that there may be a layer of anisotropy below some of the stations, at ~40 km to ~80 km depth. We are currently forward modeling upper mantle anisotropy to determine how olivine anisotropy would manifest itself in receiver functions, and if diagnostic phases would be visible above noise. If successful, we will then run a neighborhood algorithm search to further characterize anisotropy and explore the relationship between deformation in the mantle-lithosphere and crust.

ANALYSIS OF TREMOR AND EARTHQUAKE ALONG THE SAN ANDREAS FAULT IN CHOLAME, CA (2-104)

C.E. Potier, E.S. Cochran, and R.M. Harrington

This project investigates tremor on the San Andreas Fault near Cholame, California. Tremor is identified as bursts of 2-8 Hz frequency seismic energy whose envelope is coherent among many stations. It lacks impulsive, body wave arrivals and has a very long duration. Tremor had previously been discovered near

Cholame, California, so a temporary seismic array of thirteen stations was deployed in the area to further investigate the tremor there. We also collected data from stations in the Southern California Seismic Network (SCSN) and the Northern California Earthquake Data Center (NCEDC). In our study we focused on a week of data from 20-28 May, 2010. Visually searching for tremor during that week, an approximately 25 minute segment of time was chosen for further examination. Using a cross-correlation method similar to one used by Brown et al. (2008), the tremor was analyzed and 488 tremor events were detected after the first cross-correlation. In this cross-correlation pass, six second segments of data were cross correlated with the entire 25 minutes of tremor using a half second step. A threshold of 5 times mean average deviation was used to determine possible events. A second cross-correlation was completed on the 488 events, using a four second time window around the highest cross-correlation from the first pass and cross-correlating that with a fifteen second segment around the same high correlation value. The results from the second cross-correlation were grouped into families. Using these families, relative arrival times of the tremor at each station was determined. These relative arrival times will allow us to analyze the tremor for spatial and temporal patterns.

SEISMICITY IN COLOMBIA: TOMOGRAPHY, INTERMEDIATE DEPTH EARTHQUAKES, AND QCN (2-105)
G.A. Prieto

The tectonic setting of Colombia (South America) is complicated. The northern Southamerican plate to the west has the subduction of the Nazca Plate, to the north, the Caribbean plate. A number f conflicting evidence has been proposed to explain the tectonic setting in Colombia. A conspicuous feature of Colombian seismicity is the presence of the Bucaramanga nest (B-nest). The B-nest is a unique concentration of seismic activity with a depth concentration approximately 160 km depth below the Earth's surface. Seismicity there represents about 75% of the Colombian catalog, it is the most active of nests per unit volume and could represent an ideal natural laboratory for studying intermediate-depth earthquakes.

I will present preliminary tomography and earthquake location results using seismic data from the Colombian seismic network. These results suggest a subducting Proto-Caribbean plate, which may be the source of the B-nest activity.

Waveforms belonging to more than 40.000 B-nest earthquakes are being analyzed to better understand intermediate-depth earthquakes. I present examples of earthquake records from the B-nest that show very high waveform similarity. This fact can be used to improve earthquake locations via DD algorithms.

Lastly, using Quake-Catcher Network sensors, we have recorded a recent M5.0 earthquake about 120 km south of the capital. The sensors were located in a 5 story building at the University in Bogotá and important features of the building response can be extracted with these low-cost sensors.

LARGE SCALE EARTHQUAKE SIMULATIONS IN THE CENTRAL UNITED STATES (1-060)
L. Ramirez-Guzman, O. Boyd, S. Hartzell, and R. Williams

The Central United States (CUS) hosts two of the major seismic zones east of the Rockies: the New Madrid and Wabash Valley Seismic Zones. Over the past 4500 years the New Madrid Seismic Zone (NMSZ) has repeatedly produced sequences of large magnitude (M>7) earthquakes. The 1811-1812 NMSZ winter events were the largest intraplate sequence historically recorded in the United States and produced great devastation in the epicentral region, which fortunately at that time was scarcely populated. Even though the seismicity in the 1800's was dominated by the NMSZ activity, magnitude 5 and larger earthquakes in the last 150 years have occurred in the Wabash Valley Seismic Zone (WVSZ) (Bakun and Hopper, 2004). The population density and development of this area has drastically changed from that of the early nineteenth century, and a big earthquake would put at risk the population and infrastructure within the country's heartland. In this study we present two earthquake scenarios that induce large ground motions in populated areas within the Mississippi embayment and other areas within the CUS. The hypothetical scenarios are ruptures taking place in the WVSZ and the southern arm of the NMSZ. Our synthetic ground motions are calculated to a maximum frequency of 1.0 Hz using the Hercules finite element tool-chain (Tu et al., 2006) and a recently developed velocity model of the region (CUSVM1). Our simulations use a minimum shear-wave velocity of 350 m/s and cover a 700 km x 700 km domain which includes Memphis and St. Louis.

MICRO-CRACKS AND VOLUMETRIC STRAIN IN SAPROCK: WORKING TOWARDS AN UNDERSTANDING OF THE EFFECTS OF GROUND SHAKING ON THE DEVELOPMENT OF WEATHERING PROFILES IN SEISMICALLY ACTIVE AREAS (2-042)
C.T. Replogle, N.M. Morton, M.T. Buga, B.R. Page, and G.H. Girty

Saprolitization is generally viewed as an isovolumetric chemical weathering process that preserves the original fabric and texture of the parent rock. However, our recent geochemical and textural studies of saprock-corestone pairs located within ~4 km of the active Elsinore fault reveal an ~13-28% increase in volume as corestone is converted to saprock. The combined effects of fracture development during ground

shaking and chemical weathering were proposed as a plausible explanation for these unusual results. To further test this idea, we selected another site located 18 and 22 km from the Elsinore and San Jacinto faults, respectively, where studies of precariously balanced rocks indicate that seismic accelerations have not exceeded ~0.21-0.34g. Data from this site indicates that the process of saprock development from corestone was accompanied by dilatational volumetric strains of ~17-20%. Chemical weathering of the saprock is evident in thin section where ~22% of initial plagioclase, ~98% of initial biotite, and ~48% of initial amphibole have been weathered to clay minerals. This chemical weathering pattern is accompanied by loss of SiO2, CaO, K2O, Na2O, Co, Sr, and Ba mass, and an increase of average CIA values from ~54.8 in the corestone to ~58.8 in the saprolite. The degree of chemical weathering, however, does not account for the magnitude of measured positive volumetric strain. For example, initial cracking of tonalite bedrock may occur as a result of the oxidation of Fe2+ to Fe3+, which involves a small positive change in volume. However, such a process is commonly associated with isovolumetric weathering and does not yield the high volumetric strains measured in this study. In thin section, volumetric strain in the saprock from this investigation appears to have been accommodated by the production of inter- and intra-granular micro-cracks. These micro-cracks make up on average ~13% of the rock volume. About 66% of these micro-cracks are open and lined with clay, indicating that they were active pathways for fluid migration and clay particle transport. The results of this study indicate that if ground shaking events serve as the mechanism for the opening of fractures in already weathered and weakened saprolite, as is evidenced by the positive volumetric strains measured during this and other studies, then it does so in regions of relatively low seismic hazard, well beyond the principal damage zone of major active strike-slip faults.

PERFORMANCE OF STRUCTURES IN THE 27 FEBRUARY 2010 GREAT MAULE EARTHQUAKE (invited talk)
J. Restrepo

The 27 February 2010 Mw 8.8 Great Maule Earthquake caused strong intensity shaking over a corridor 70 mile wide by 400 mile long in central Chile. This region of the country experienced widespread damage to infrastructure and buildings. About 6 million people live in this area. This area has around 10,000 buildings, with a significant number in the range between 15 and 30 stories high. Many of these buildings have thin reinforced concrete bearing concrete walls. The building code in Chile follows closely ACI 318-05 issued by the American Concrete Institute, with some key changes aimed at constructability. The performance of buildings in this earthquake can be considered quite satisfactory from the engineering standpoint, principally because the demands observed from the recorded motions exceeded those used in design. Nevertheless, in Chile wall crushing, bar buckling and shear failures in walls were common. This prompts the need to review some of the design methodologies for bearing wall buildings that are becoming more attractive in Southern California for the construction of low-cost residential buildings. Damage to nonstructural elements was widespread and caused significant business interruption. It is interesting to note that base-isolated buildings had a outstanding performance overall. This presentation will review the performance of buildings in Chile and will highlight some of the main issues that should receive attention in future design codes in United States.

A FIRST-ORDER TEST TO COMPARE REGIONAL EARTHQUAKE LIKELIHOOD MODELS (1-118)
D.A. Rhoades, M.C. Gerstenberger, and A. Christophersen

The standard statistical test applied by the Collaboratory for the Study of Earthquake Predictability (CSEP) to compare two models is the R-test. The R-test examines the rather complex hypothesis of whether the observed log likelihood-ratio between two models is consistent with each of the models in turn being the correct model. This test can be difficult to interpret when two models mutually reject each other. We propose an alternative test which is more direct and therefore easier to interpret.

The log likelihood-ratio, or, equivalently, the mean information gain per earthquake, can be expressed in the form of a classical paired t-statistic, corrected for the difference in the expected number of target earthquakes under the two models. This statistic is the basis of the proposed "T-test", which answers the simple question: does model A perform significantly better than model B? It sets aside the question of whether either model is completely consistent with the observed earthquakes in the test region, and merely tests whether one model is more informative than the other.

Unlike the R-test, the T-test is not computer-intensive, makes no use of simulated catalogues, and only requires knowledge of the model forecasts for the cells in which the target earthquakes occur and the total expected number of earthquakes of each model. It depends on a normality assumption, but the non-parametric version (Wilcoxon signed-rank test) can be used if this assumption seems to be violated.

Comparisons of T-test and R-test results on retrospective analyses of models submitted to the New Zealand Earthquake Forecast testing center and on the published half-time results of the prospective five year RELM experiment in California, suggest that the T-test rejects models less frequently than the R-test. In particular, it

is less likely to reject one model in favour of another when the difference in their likelihoods is mostly attributable to only one or two of the target earthquakes.

The T-test may be a useful supplement to the battery of tests employed by the CSEP testing centers. Models are bound at some stage to fail other tests (N-test, L-test, R-test) if only because of short-term clustering of earthquakes, the imposed Poissonian assumption, and the limitation that models can only be updated periodically. Therefore a straightforward comparison of two models subjected to the same restrictions, by the T-test, may be easier to interpret than the present CSEP test results.

OSL AS A DATING TECHNIQUE FOR INVESTIGATING FAULT MOVEMENT (1-100)
E. Rhodes

Optically Stimulated Luminescence (OSL) is a dating method applicable to sediments spanning the last 200,000 years or so. Light-sensitive OSL signal components are reset when mineral grains are transported through the environment, and slowly re-grow by interaction with ionising radiation during subsequent burial. This makes the technique ideal for dating sediment deposition in a wide range of geomorphic, environmental and archaeologic contexts. However, approaches to OSL which work well in some environments, for example dating desert sand dunes using quartz, may not work as well in the environments encountered in contexts which relate directly to fault movement such as sag pond deposits, fluvial sediments and small alluvial or colluvial fan deposits. Limitations include incomplete signal zeroing, low signal sensitivity and complex signals with uncertain origins. Experience gained in optimizing OSL dating for archaeology is useful in planning how to get the most from this technique in future paleoseismic applications. Ideas to improve the reliability of OSL applications include:

1) routine in-situ dose rate determination,
2) use of high resolution Ge gamma spectrometry to assess dose rate disequilibrium,
3) higher sampling density to assess reproducibility of results,
4) increased assessment-phase OSL determinations to select optimal approach for each context,
5) use of multiple minerals to overcome mineral-specific limitations,
6) single grain OSL methods to reduce incomplete zeroing problems.

SIMULATIONS OF SEISMICITY IN FAULT SYSTEMS – EFFECTS OF INTERACTIONS WITH FAULT CREEP (2-085)
K. Richards-Dinger and J. Dieterich

The earthquake simulator code RSQSim has been expanded to permit investigation of interactions between earthquake slip and continuous fault creep. Creep in the simulations is represented as steady-state rate strengthening friction as described by the rate- and state-dependent fault constitutive representation of fault friction. The addition of fault creep to the simulations affects fault slip and seismicity in a variety of ways that are not seen in simpler systems. Penetration of slip into the deep creeping sections of seismogenic faults alters moment scaling; and it results in a period of afterslip with accelerated time-dependent stressing following large earthquakes. Simulations of the northern California fault system (with and without deep creep) indicate that rupture penetration into the zone of fault creep has negligible affect on seismic moment of mainshock earthquakes M≤6.5, but increasingly contributes to the seismic moment of larger earthquakes reaching about 20% of total moment for 1906-type M~8 events. However, the moments of immediate aftershocks of large earthquakes often have significantly greater contributions to the total moment from coseismic slip on creeping sections. Both the magnitude-frequency statistics and inter-event waiting time density distributions of the simulated northern California catalog are unaffected by deep fault creep. The simulated catalogs have aftershocks that follow Omori's Law. The decay exponent ($p = -0.8$) is unaffected by addition of deep fault creep, but, overall aftershock productivity and late aftershocks are somewhat greater in the simulations with fault creep. In nature it seems likely that spatial fluctuations of parameters that control the rate-dependence of fault friction (composition, effective normal stresses, temperature variations) can result in intermixing of rate-strengthening (creeping) and rate weakening (seismogenic) areas of faults. Simulations that have progressively increasing percentages of creeping elements (10% to 95%) intermixed with the seismic elements also show systematic variations in the character of the simulated seismicity. In particular, as the area fault creep increases, clustering increases and local swarm-type activity appears. At larger percentages the seismic patches can only weakly interact resulting in the semi-periodic isolated failures that are characteristic of repeating earthquakes.

UPDATING AND ENHANCING THE WALLACE CREEK INTERPRETIVE TRAIL (WIT) WEBSITE (1-030)
S.E. Robinson, J. Colunga, R. de Groot, and J.R. Arrowsmith

The Carrizo Plain in California is world-famous for the dramatic offset features along the San Andreas fault. Sag ponds, linear ridges, beheaded channels, and scarps define the landscape along the fault . One of the most significant features is the offset channel at Wallace Creek. In 1998 SCEC and the Bureau of Land Management developed The Wallace Creek Interpretive Trail (WIT) to highlight and explain the significance

and beauty of this location. In addition to the interpretive trail, an interactive website with online field guides, photos, driving directions to Wallace Creek, educational materials, and scientific papers was launched to promote visits to the trail and allow for deeper virtual investigation of this fascinating region. In 2008 the WIT was incorporated into the Earthquake Education and Public Information Center (EPIcenter) Network thus increasing its visibility as destination for students, educators, enthusiasts, and participants in The Great California ShakeOut. In light of the numerous advances in science and web technology members of the SCEC ACCESS internship program in collaboration with the OpenTopography facility updated and re-imagined the WIT website. The 2010 update includes adding recent scientific papers, new photos and imagery (including B4 LiDAR derived topography), and other updates which improve website navigation and backend design. The updated website will provide visitors with the most recent scientific information about Wallace Creek while making it easy to find current directions and relevant educational materials and imagery. Building on the structure of the 1998 WIT website the updates and enhancements provide a new window into the understanding of earthquake hazards in California. The website is available at www.scec.org/wallacecreek.

THE DEVELOPMENT OF AN INTRODUCTORY VIDEO ON LIGHT DETECTION AND RANGING (LIDAR) AND STUDYING EARTHQUAKE HAZARDS (1-091)
S.E. Robinson, A. Whitesides, R. de Groot, J.R. Arrowsmith, and C.J. Crosby

The use of high resolution topography (meter scale pixels) derived from LiDAR in the study of active tectonics is widespread and it has become an indispensable tool to better understand earthquake hazards. Thus, it is important to inform geology students and the general public of the basic concepts of LiDAR and its uses for studying faults and earthquakes. As part of SCEC's ACCESS internship program and in affiliation with the OpenTopography facility, a 10-minute introductory video on LiDAR and its uses for the study of earthquake hazards was created during the summer of 2010. Illuminating Earthquake Hazards intends to inform students studying earth science and related disciplines and general audiences about LiDAR, how it is collected, and how it is used currently to aid scientists in studying earthquakes. The video is composed of three main chapters: An introduction to the need for up-to-date technology for studying earthquake hazards; an overview of LiDAR data collection, storage, and data products; and the application of LiDAR data to the current study of earthquake hazards. Illuminating Earthquake Hazards includes animations of LiDAR collection, explanations of the uses of LiDAR, and interviews with several leading researchers on LiDAR data collection its use in ongoing earth science research, and its potential to revolutionize earthquake science. Illuminating Earthquake Hazards is available online for free.

SCEC EDUCATIONAL PRODUCTS AND PROGRAMS (1-008)
Y. Robles, R.M. de Groot, B. Dansby, D. Coss y Leon, W. Yamashita, C. Gotuaco, and G. Hwang

To promote improved earthquake awareness and preparedness the SCEC Communication, Education, and Outreach program developed the ShakeOut Curriculum and the Take on the Quake Program. This research project continues the development and refinement of these resources. The ShakeOut Curriculum activities were designed to be used leading up to and after the ShakeOut drill. Significant enhancements to this product included expanding the module from six to ten lessons, the development of a facilitator guide with background information, teaching tips, and suggestions for effective implementation with a variety of learners. Other improvements included aligning the lessons with California Science Content Standards and the National Science Education Standards, making the lessons more inquiry-based, and modifying the overall organization of the curriculum. The Take on the Quake Program is ideal for use in many free-choice learning environments such as museums, scouting, after-school programs, libraries, and in parks. Depending on the time available for instruction the program facilitator may select one of three options: Express (45 minutes), Explore (1 hour, 15 minutes) and Experience (2 hours). Take on the Quake was improved through the development of a facilitator guide and further development of the activities. For both the ShakeOut Curriculum and the Take on the Quake Program special attention was devoted to minimizing the need for consumables allowing for cost-effective implementation while also fostering sustainability. Both products are aligned with Earthquake Country Alliance mission by fostering a culture of earthquake and tsunami readiness in California.

COULOMB STRESS INTERACTIONS BETWEEN SIMULATED M>7 EARTHQUAKES AND MAJOR FAULTS IN SOUTHERN CALIFORNIA (1-127)
J.C. Rollins, G.P. Ely, and T.H. Jordan

We calculate the Coulomb stress changes imparted to major Southern California faults by thirteen simulated worst-case-scenario earthquakes for the region, including the ShakeOut and TeraShake scenarios. The source models for the earthquakes are variable-slip simulations from the SCEC CyberShake project and Ely (2009). We find strong stress interactions between the San Andreas and subparallel right-lateral faults, thrust faults under the Los Angeles basin, and the left-lateral Garlock Fault. M>7 earthquakes rupturing sections of the southern San Andreas generally decrease Coulomb stress on the San Jacinto and Elsinore faults and impart

localized stress increases and decreases to the Garlock, San Cayetano, Puente Hills and Sierra Madre faults. A M=7.55 quake rupturing the San Andreas between Lake Hughes and San Gorgonio Pass increases Coulomb stress on the eastern San Cayetano fault, consistent with Deng and Sykes (1996). M>7 earthquakes rupturing the San Jacinto, Elsinore, Newport-Inglewood and Palos Verdes faults decrease Coulomb stress on parallel right-lateral faults. A M=7.35 quake on the San Cayetano Fault decreases stress on the Garlock and imparts localized stress increases and decreases to the San Andreas. A M=7.15 quake on the Puente Hills Fault increases stress on the San Andreas and San Jacinto faults, decreases stress on the Sierra Madre Fault and imparts localized stress increases and decreases to the Newport-Inglewood and Palos Verdes faults. A M=7.25 shock on the Sierra Madre Fault increases stress on the San Andreas and decreases stress on the Puente Hills Fault. These findings may be useful for hazard assessment, paleoseismology, and comparison with dynamic stress interactions featuring the same set of earthquakes (Ely, in progress).

INFERRING SEISMIC HISTORIES FROM THE AGES OF PRECARIOUSLY BALANCED ROCKS (1-072)
D.H. Rood, G. Balco, M. Purvance, R. Anooshehpoor, J. Brune, L. Grant Ludwig, T. Hanks, and K. Kendrick

Currently, the only tool available to empirically test unexceeded earthquake ground motions over timescales of 10 ky-1 My is the use of fragile geologic features, including precariously balanced rocks (PBRs). The age of PBRs together with their distribution and mechanical stability provide a singularly powerful test to site probabilistic seismic hazard analysis. We develop a robust method to date corestone PBRs in granitic terrains using cosmogenic Be-10 with a numerical model that accounts for nuclide production before, during, and after exhumation of the PBR from the subsurface.

We measured Be-10 concentrations in 30 samples from 8 corestone PBRs that provide constraints on ground motions associated with the San Andreas, San Jacinto, and Elsinore faults in southern California. To constrain the exhumation history of the PBR, we use a forward model and compare our Be-10 data to predicted profiles for a range of surface denudation rates and exposure times. Because the cosmic ray flux is only partly attenuated by the rock, our model includes a shielding correction that accounts for the three-dimensional shape of the PBR. Fitting model to data yields the rate and timing of PBR exhumation and thus the length of time the feature was vulnerable to toppling by earthquake ground motions. We use this method to show that an example PBR near the San Andreas fault in the western San Bernardino mountains (at the Grass Valley site) gives a high-confidence age of 18.1 +/- 2.5 ka (n=4). Another PBR near the San Jacinto fault (at the Beaumont South site) gives an apparent age of 10.5 +/- 1 ka; however, data from this rock (n=3) do not produce a statistically acceptable fit. Our results indicate that a more detailed vertical profile is required to evaluate the effects of unsteady erosion for some PBRs. We are currently refining our dating method, and applying it to numerous PBRs throughout the western US and around the world.

SIMULATION OF GROUND MOTION IN THE IMPERIAL VALLEY AREA DURING THE MW 7.2 EL MAYOR-CUCAPAH EARTHQUAKE (1-069)
D. Roten and K.B. Olsen

The Mw 7.2 El Mayor-Cucapah mainshock of April 4 2010 caused significant shaking in the Imperial Valley and Mexicali area, and was recorded by ~20 strong motion stations located on the Imperial Valley sediments. It provides an excellent opportunity to study wave propagation effects in deep sedimentary basins, to test the accuracy of the basin models, and to test our capabilities to predict strong ground motion from numerical simulations.

We have generated two dynamic rupture models constrained by fault geometry, hypocenter location and reported surface displacement, along a ~105km long stretch of the Borrego and Pescadores faults. Both rupture models feature surface slip of up to 1.5 m NW of the hypocenter, with buried slip under the Colorado River Delta SE of the hypocenter, emulated velocity strengthening in the near-surface, and generally subshear rupture speeds. One rupture model contains very limited slip (< 0.2 m) along the north-central part of the fault system where no surface rupture was observed (model A), while the other (model B) is characterized by a more continuous slip distribution, but less slip toward the SE. We simulate the wave propagation resulting from these two rupture models in the SCEC CVM4 on a 200x175x50 km^3 grid that includes approximations of the Borrego and Pescadores faults, the Imperial Valley and the southern part of the Salton Sea. We use a spatial step of 100 m and a minimum near-surface shear-wave velocity of 819 m/s in the Imperial Valley sediments, which allows us to model frequencies up to 1.5 Hz.

Simulated spectral accelerations (SAs) at periods of 2s, 3s and 5s are generally consistent with the recorded strong motion data, with a slightly better fit for rupture model B than for rupture model A. The simulated SAs at 10s, however, underpredict the observations by up to a factor of 4 for sites located on the deep sediments of the Imperial valley. The velocity waveforms recorded at these sites are characterized by energetic wavetrains with a period of ~8 seconds on the horizontal components which are not reproduced by the simulations. This amplification is likely associated with the deep resonance of the basin, and it implies that the shear-wave velocity of the sedimentary fill might be lower than the values included in the CVM4.

This result is consistent with a lower degree of metamorphosis caused by heat flow in the sedimentary rocks of the Gulf of California rift zone than previously assumed.

TEXTURAL RECORD OF THE SEISMIC CYCLE: STRAIN RATE VARIATION IN AN ANCIENT SUBDUCTION THRUST (1-082)
C.D. Rowe, F. Meneghini, and J.C. Moore

Active faults slip at different rates over the course of the seismic cycle: earthquake slip (~ 1 m/s), interseismic creep (~ 10-100 mm/yr), and intermediate rate transients (e.g. afterslip and slow earthquakes). Studies of exhumed faults are sometimes able to identify seismic slip by the presence of frictional melts, and slow creep by textures diagnostic of rate-limited plastic processes. The Pasagshak Point thrust preserves three distinct fault rock textures, which are mutually crosscutting, and can be correlated to different strain rates. Ultrafine-grained black fault rocks including pseudotachylyte were formed during seismic slip on layers up to 30 cm thick. Well-organized S/C cataclasites 7-31 m thick were formed by slow creep with pressure solution as a dominant, rate-limited mechanism and are interpreted as interseismic creep signatures consistent with plate-rate strain. Disorganized, non-foliated, rounded clast cataclasites were formed at shear rates faster than solution creep and are interpreted as representing shear at intermediate strain rates. These could have formed during afterslip or delocalization of slip associated with an earthquake rupture.

DESIGNER FRICTION LAWS FOR BIMODAL SLOW SLIP PROPAGATION SPEEDS (2-091)
A.M. Rubin

A striking observation from both Cascadia and Japan is that the tremor associated with slow slip often migrates along strike at speeds close to 10 kilometers per day, but up- and down-dip at speeds approaching 100 kilometers per hour. Here I examine how such bimodal propagation speeds might arise in models of rate- and state-dependent friction. The underlying premise is that although the chance of any of the commonly-used friction laws being the "correct" one is close to zero, we can still use observations of slow slip to characterize some attributes of the friction laws that must be operating. A simple relation, relying only on kinematics and elasticity, states that for a moving front the ratio of propagation speed to slip speed approximately equals the ratio of the elastic shear modulus to the peak-to-residual stress drop at the front. Thus larger propagation speeds require a combination of larger slip speeds and smaller peak-to-residual stress drops. Here I design a 2-state-variable friction law, including dilatancy, in which the strength drop associated with the main lateral front is much larger than the strength drop for the secondary fronts developing on the active slip surface. Larger strength drops at the main front might arise, for example, from disruption of minerals precipitated since the last slow slip event.

To keep the simulations tractable I run cycles of slow slip events on a 1-D fault, and extract snapshots to use as initial conditions for simulations on a 2-D fault. The 2-D fault is then subjected to a localized perturbation to simulate a "tremor event". Parameter values are chosen with the help of simple analytical rules-of-thumb to generate slip speeds, propagation speeds, recurrence intervals, stress drops, etc., that mimic observed values. The 2-D fault simulations generate secondary fronts that propagate up- and down-dip more than 2 orders of magnitude faster than, and even at some distance from, the main laterally-propagating front. In this sense they validate the rules-of-thumb used to design the friction law, although by no means the law itself.

EXCEPT IN HIGHLY IDEALIZED CASES, REPEATING EARTHQUAKES AND LABORATORY EARTHQUAKES ARE NEITHER TIME- NOR SLIP-PREDICTABLE (1-123)
J.L. Rubinstein, W.L. Ellsworth, N.M. Beeler, K.H. Chen, D.A. Lockner, and N. Uchida

Statistical testing of the time- and slip-predictable models as applied to repeating earthquakes in California, Taiwan, and Japan demonstrates that neither model offers predictive power. In a highly idealized laboratory system, we find that earthquakes are both time- and slip-predictable, but with the addition of a small amount of the complexity (e.g., an uneven fault surface) the time- and slip-predictable models offer little or no advantage over a much simpler renewal model that has constant slip or constant recurrence intervals. Given that repeating natural and laboratory earthquakes fit the assumptions of time- and slip-predictability better than any other earthquakes and still are not well-explained by them, we can conclude that the time- and slip-predictable models are too idealized to explain the recurrence behavior of natural earthquakes. These models likely fail because their key assumptions (1 -- constant loading rate AND 2 -- constant failure threshold OR constant final stress) are too idealized to apply in a complex, natural system. While the time- and slip-predictable models do not appear to work for natural earthquakes, we do note that moment (slip) scales with recurrence time for repeating earthquakes in Parkfield, CA, but not in other locations. While earthquake size and recurrence time are related in Parkfield, the slip-predictable model still doesn't work because fitting a linear trend to the data predicts a non-zero earthquake size at instantaneous recurrence time. This scaling, its presence in Parkfield, and absence elsewhere is presently unexplained

MUD VOLCANO RESPONSE TO THE EL MAYOR-CUCAPAH EARTHQUAKE (1-083)
M.L. Rudolph and M. Manga

Mud volcanoes sometimes respond to earthquakes, but the mechanisms by which earthquakes trigger changes in ongoing eruptions or initiate new eruptions are not completely understood. We measured gas discharge at a field of mud volcanoes near the Salton Sea, Southern California before and after the April 4, 2010 El Mayor-Cucapah Earthquake and observed an increase in gas flux immediately following the earthquake and a subsequent recovery to pre-earthquake values. This earthquake-eruption pair is of particular interest because the earthquake produced large strains, up to 1.2%, near the mud volcano location, allowing us to test two competing triggering mechanisms: (1) shaking-induced bubble mobilization, and (2) permeability enhancement. We measured the rheology of erupted mud from the mud volcanoes to quantify the importance of mechanism (1) and found that this mechanism is unlikely to be important. We therefore favor the explanation that the increased gas flux was caused by a transient increase in permeability.

SUPERSHEAR RUPTURE TRANSITION ON FAULT STEPOVERS USING DIFFERENT FRICTION PARAMETERIZATIONS (2-073)
K.J. Ryan and D.D. Oglesby

It is well known that fault stepovers can under some circumstances allow through-going rupture, and under other circumstances cause rupture termination (e.g., Harris and Day 1993; Kase and Kuge, 1998; Duan and Oglesby, 2006). However, the effect of the stepover on rupture velocity has not been investigated, and there has also not been an investigation of how different frictional parameterizations affect behavior at the stepover. Toward these goals, we model the dynamics of a 2-D fault stepover system with 2 parallel segments, arranged with either a compressional or dilational stress field. We vary the amount of offset, or stepover width, between the two fault segments from 300 meters to 1500 meters. We examine how the dynamics of the stepover system affect the seismic S-factor (strength excess divided by the stress drop) on the secondary fault segment, which in turn affects rupture velocity on the secondary fault segment. In particular, we analyze S values local to the re-nucleation point on the secondary fault segment, in comparison to the well known threshold values for supershear rupture in 2-D models. We utilize both slip-weakening (e.g., Andrews, 1985) and rate-state friction (Dieterich, 1978, 1979). We find that in both frictional parameterizations of the compressional system, there exists a new mode of supershear rupture transition: rupture can reach supershear speed in the compressional case along the secondary fault segment, even if the stress field on the system prior to rupture is such that a standard Burridge-Andrews supershear transition would be precluded. The supershear transition occurs at the same minimum stepover width for both friction parameterizations, implying that the re-nucleation process on the secondary fault is quite similar between slip-weakening and rate-state friction, at least when the slip-weakening model is tuned to correspond closely to the rate-state model. In these models, rupture is delayed on the secondary fault segment, allowing stress waves from the primary fault segment to alter the stress field of the secondary fault segment, making the secondary fault segment more likely to transition to supershear rupture speed once re-nucleation occurs. This mechanism of superhear transition likely requires a crack-like rupture process.

TRIGGERED SURFACE SLIP IN SOUTHERN CALIFORNIA ASSOCIATED WITH THE 2010 SIERRA EL MAYOR-CUCAPAH, BAJA CALIFORNIA, MEXICO, EARTHQUAKE (1-092)
M.J. Rymer, J.A. Treiman, K.J. Kendrick, J.J. Lienkaemper, R.J. Weldon, R. Bilham, M. Wei, E.J. Fielding, J. Hernandez, B. Olson, P. Irvine, N. Knepprath, R.R. Sickler, D. Sandwell, X. Tong, and M. Siem

Surface fracturing (triggered slip) occurred in the central Salton Trough and to the southwest, in the Yuha Desert area—all in association with the 4 April 2010 (Mw7.2) El Mayor-Cucapah earthquake and its aftershocks. Triggered slip in the central Salton Trough occurred on the 'frequent movers': the southern San Andreas, Coyote Creek, Superstition Hills, and Imperial Faults, all of which have slipped in previous moderate to large, local and regional events in the past five decades. Other faults in the central Salton Trough that hosted slip in 2010 include the Wienert Fault (southeastern section of the Superstition Hills Fault), the Kalin Fault (in the Brawley Seismic Zone), and the Brawley Fault Zone; triggered slip had not been reported on these faults in the past. Slip on faults in the central Salton Trough ranged from 1 to 18 mm, and everywhere was located where previous primary or triggered slips have occurred.

Triggered slip in the Yuha Desert area occurred along at least two dozen faults, only some of which were known before the 4 April 2010 El Mayor-Cucapah earthquake. From east to northwest, slip occurred in six general areas; 1) in the Northern Centinela Fault Zone (newly named), 2) along unnamed faults south of Pinto Wash, 3) along the Yuha Fault (newly named), 4) along both east and west branches of the Laguna Salada Fault, 5) along the Yuha Well Fault Zone (newly revised name), and 6) along the Ocotillo Fault (newly named). Faults that hosted triggered slip in the Yuha Desert area include northwest-trending right-lateral slip faults, northeast-trending left-lateral slip faults, and north-south faults, some of which had dominantly vertical slip. Triggered slip along the Ocotillo Fault occurred in association with the 14 June 2010 (Mw5.7) aftershock, which also triggered slip along other faults near the town of Ocotillo. Triggered slip on faults in

the Yuha Desert area was most commonly less than 20 mm. Two significant exceptions to this statement are slip of about 50–60 mm on the Yuha Fault and of about 80 mm on the Ocotillo Fault. All triggered slips in the Yuha Desert area occurred along pre-existing faults, whether previously recognized or not.

LIDAR AND FIELD OBSERVATIONS OF EARTHQUAKE SLIP DISTRIBUTION FOR THE CENTRAL SAN JACINTO FAULT (1-109)
J.B. Salisbury, T.K. Rockwell, T.J. Middleton, and K.W. Hudnut

We mapped the tectonic geomorphology of 80 km of the Clark strand of the San Jacinto fault to determine slip per event for the past several surface ruptures. From the southeastern end of Clark Valley (east of Borrego Springs) northwest to the mouth of Blackburn Canyon (near Hemet), we identify 203 offset geomorphic features from which we make over 560 measurements on channel margins, channel thalwegs, ridge noses, and bar crests using filtered B4 LiDAR imagery, aerial photography, and field observations. Displacement estimates show that the most recent event (MRE) produced an average of 2.5-2.9 m of right-lateral slip, with maximum slip of 3.5 to 4 m at Anza. Double-event offsets for the same 80 km section average ~5.5 m of right-lateral slip. Maximum values near Anza are estimated to be close to 3 m for the penultimate event, suggesting that the penultimate event was similar in size to the MRE. The third event is also similar in size, with cumulative displacement of 9-10 m through Anza for the past three events. Magnitude estimates for the MRE range from Mw=7.2 to Mw=7.5, depending on how far north the rupture continued. Historically, no earthquakes reported along the Clark fault are large enough to have produced the offset geomorphology we observe. However, recent paleoseismic work at Hog Lake dates the most recent surface rupture event at ca. 1790, potentially placing this event in the historic period. A poorly located, large earthquake occurred on November 22, 1800, and is reported to have caused extensive damage (MMI VII) at the San Diego and San Juan Capistrano missions. We infer slightly lower intensity values for the two missions (MMI VI-VII instead of VII) and relocate this event on the Clark fault based on dating of the MRE at Hog Lake. We also recognize the occurrence of a younger offset along ~15 km of the fault in Blackburn Canyon, apparently due to lower slip in that area in the November 22, 1800 event. With average displacement of ~1.25 m, we attribute these offsets to the M6.9 April 21, 1918 event. We present the estimated sizes of the MRE and PE's as minimums, as degradation of fault scarps and offset features has likely occurred. Nevertheless, these data argue that much or all of the Clark fault, and possibly also the Casa Loma fault fail together in large earthquakes.

COMPARISON OF 16 STRAIN RATE MAPS FOR SOUTHERN CALIFORNIA (1-125)
D. Sandwell, T. Becker, P. Bird, J. Bormann, A. Freed, M. Hackl, B. Meade, W. Holt, B. Hooks, S. Kedar, C. Kreemer, R. McCaffrey, T. Parsons, F. Pollitz, Z-K. Shen, B. Smith-Konter, C. Tape, and Y. Zeng

One of the geodetic parameters to be used in UCERF-3 is crustal strain rate. Crustal strain rate is produced by two related processes. Strain rate along faults, which can have large amplitudes (100 - 3000 nanostrain per year), is concentrated within 10-50 km of the fault trace depending on the locking depth of the fault. The second process that produces strain rate is widespread deformation of the crustal blocks. This strain rate generally has much lower amplitude (10 – 100 nanostrain per year) and can be masked by the larger near-fault component. Both of these components of strain rate may help in forcasting earthquakes. Because of inadequate sampling, published strain rate maps sometimes differ by an order of magnitude. To better understand these differences and to determine "best practices" for strain rate estimation, we developed a Strain Rate Estimation Exercise. Sixteen groups submitted their strain rate maps for comparison and evaluation. The poster will display the 16 maps as well as a covariance analysis of the maps. The compiled data are available at ftp://topex.ucsd.edu/pub/sandwell/strain .

GMTSAR: AN INSAR PROCESSING SYSTEM BASED ON GMT (1-140)
D. Sandwell, R. Mellors, X. Tong, M. Wei, and P. Wessel

GMTSAR is an open source (GNU General Public License) InSAR processing system designed for users familiar with Generic Mapping Tools (GMT). The code is written in C and will compile on any computer where GMT and NETCDF are installed. The system has three main components: 1) a preprocessor for each satellite data type (e.g., ERS, Envisat, and ALOS) to convert the native format and orbital information into a generic format; 2) an InSAR processor to focus and align stacks of images, map topography into phase, and form the complex interferogram; 3) a postprocessor, mostly based on GMT, to filter the interferogram and construct interferometric products of phase, coherence, phase gradient, and line-of-sight displacement in both radar and geographic coordinates. GMT is used to display all the products as postscript files and kml-images for Google Earth. A set of C-shell scripts has been developed for standard 2-pass processing as well as image alignment for stacking and time series. ScanSAR processing is also possible but requires a knowledgeable user. Users are welcome to contribute to this effort. In particular contributions using other scripting languages such as PERL and PYTHON are desired. The software and test data are available at ftp://topex.ucsd.edu/pub/gmtsar. The software can be installed on your UNIX computer during the

meeting. The poster will show a mosaic of interferograms for the El Major-Cucupa, Baja California Earthquake.

P AND S BODY WAVE AND JOINT S BODY WAVE AND RAYLEIGH WAVE TOMOGRAPHY OF THE SOUTHERN CALIFORNIA UPPER MANTLE (2-014)
B. Schmandt, E. Humphreys, D. Forsyth, and C. Rau

We present new 3-D compressional and shear velocity tomography models that focus on upper mantle structure beneath southern California. P and S body wave tomography models are derived from measurements of travel-time residuals recorded by the SCSN and NCSN broadband and short-period arrays, the EarthScope Transportable Array, and other temporary deployments. The body wave travel-time tomography method uses frequency dependent 3-D sensitivity kernels to map residual times, measured in multiple frequencies, into velocity structure and recently advanced crust thickness and velocity models to better isolate the mantle component of residual times. In addition to separate Vp and Vs body wave models, we jointly invert the two datasets for Vp/Vs perturbations by imposing a smoothness constraint on the dlnVs/dlnVp field. The joint inversion helps identify regions where non-thermal effects such as partial melt contribute strongly to the imaged velocity structure. In an effort to further improve resolution of upper mantle heterogeneity we are iteratively inverting S body wave and Rayleigh wave data with 3-D starting models in order to exploit the complementary characteristics of their sensitivity kernels. This preliminary attempt at a joint inversion of regional body wave and surface wave data allows quantitative assessment of how well a single 3-D Vs model can fit multi-frequency S body wave travel-times and Rayleigh wave phase and amplitude measurements. Collectively, the suite of tomography models provides an improved perspective on the magnitude and geometry of seismic heterogeneity in the southern California mantle. We plan to continue testing joint body and surface wave inversion methods and ultimately aim to provide a high-resolution mantle component for future versions of the SCEC Community Velocity Model.

THERMAL PRESSURIZATION DURING THE TRANSITION FROM QUASI-STATIC NUCLEATION TO DYNAMIC RUPTURE (2-071)
S.V. Schmitt, E.M. Dunham, and P. Segall

We have begun to investigate the effect of shear heating-induced thermal pressurization as a fault transitions from quasi-static rate/state nucleation to dynamic rupture. Recent work has suggested that, in some cases, shear heating-induced thermal pressurization may become the dominant fault weakening mechanism during the quasi-static nucleation phase. The relative importance of thermal pressurization is controlled by both the fault zone material's heat and pore fluid transport properties and its frictional properties. Numerical simulations of ``aging law'' rate/state-dependent friction coupled to shear heating and heat/fluid transport with diffusivities inferred from laboratory observations of fault zone materials have shown that thermal pressurization dominates at speeds greater than 0.02 to 2 mm/s [Schmitt & others, JGR, submitted]. Such slip speeds are below those typically associated with dynamic rupture, but we find that in some cases, including elastodynamics may affect nucleation behavior. As in prior studies, we use a quasi-static code to model fault slip from the pre-nucleation (that is, below-steady-state) phase into the early stages of nucleation. For the remainder of nucleation and the following early seismic slip, we switch to a fully dynamic code that includes coupled thermal pressurization [Noda & others, JGR, 2009]. We compare the effect of including elastodynamics to prior results that make use of the quasi-dynamic "radiation damping" approximation. Results of simulations like these may have implications for the detection of precursory slip with near-source strainmeters or seismometers.

MAKE YOUR OWN EARTHQUAKE (1-027)
S.W.H. Seale, J.H. Steidl, P. Hegarty, and H. Ratzesberger

Make Your Own Earthquake (MYOE) is a K-6 outreach activity developed by NEES@UCSB. MYOE is presented at local elementary schools and demonstrated at our facilities.

MYOE consists of a Kinemetrics Episensor accelerometer and Q330 datalogger, a laptop computer, and a laser printer. NEES@UCSB has developed the MYOE software. The accelerometer is placed in the classroom and the laptop is nearby. The computer prompts each student to type his/her name and then counts down until the student is instructed to "Jump!" During 10 seconds of jumping, the record of the vertical channel is displayed on the laptop. This record is printed with the student's name. MYOE is a very popular activity and as many as 400 students participate in one session.

In the next year, we will make MYOE a NEES network-wide activity. Instead of expensive field equipment, MYOE will record with Quake Catcher Network (QCN) accelerometers. This accelerometer is a USB device that costs $49 and plugs into any laptop. NEES@UCSB is developing the software for MYOE using the QCN sensor. We will test the activity and write and film a tutorial that will explain the set up and its use. This software and the tutorial will be available on the NEESHUB website.

WHAT THE SPICE SOURCE INVERSION VALIDATION BLINDTEST I EXERCISE DID NOT TELL YOU? (2-138)
G. Shao and C. Ji

Uncertainties of the finite fault inversions using strong motion data are investigated using the BlindTest I exercise of the SPICE earthquake source inversion validation project, motivated by previous counterintuitive results (Mai et al., 2007). The distributions of slip and the shapes of asymmetric cosine slip rate functions (Ji et al., 2003) are simultaneously inverted by matching 10 or 33 broadband 3-component velocity waveforms within the period from DC to 2 Hz, using the finite fault method that carries waveform inversions in wavelet domain. The effects of subfault size, data noise, and the number of stations have been explored. Our results suggest that: 1) Although there are inevitable discrepancies between the inverted model and the target because of ignoring the spatial slip variations within individual subfaults, with precise velocity structure, precise fault geometry and good station coverage, the fault slip and rise time distribution can be well constrained even the data includes 35% Gaussian noise. 2) Inversions using the variance reduction function of velocity waveforms as the objective function have low sensitivities to the total seismic moment and peak slip. The development of new objective functions, which can honor the frequency dependent seismic radiation energy and noise distributions, is then a crucial task for source studies. 3) Though the relative value of the objective function is used to guide the inversion, the absolute value of the objective function associated with an inverted solution cannot be used to evaluate the quality of this model. 4) As the inversion based on the observations on the surface, the spatiotemporal resolution of the source inversion is affected not only by the data quality but also the earthquake itself. For strike slip faulting on a vertical fault, the along-strike resolution is better than that along the down-dip direction.

PHASE DIAGRAMS AS METHOD FOR MODEL INTERCOMPARISONS: EARTHQUAKE SIMULATORS PROBLEM 3 (2-041)
B.E. Shaw, H. Noda, K. Richards-Dinger, S.N. Ward, J.H. Dieterich, N. Lapusta, and T.E. Tullis

Code comparisons when there is a well defined unique and correct answer which all codes are aiming to reproduce as closely as possible, is a well developed and highly fruitful exercise (e.g. SCEC wave propagation and rupture dynamics code verification exercises). Code comparisons when all of the codes, by necessity to make the classes of problems they wish to study tractable, make drastic and very different physical approximations, pose many more challenges. What constitutes agreement or disagreement between codes? What should we be trying to compare?

Given the different physical approximations, even when the simulators can all nominally solve the same problem, it is unlikely that the effective values and sensitivities to the analogous control parameters will all be the same across models. In light of these complications, we suggest that the appropriate comparison be in the form of a phase diagram showing behaviors as various parameters are varied. This has the virtue of addressing both the effective parameter and parameter sensitivity issues, particularly when done as a function of a couple of parameters. Moreover, phase diagrams are helpful in illuminating the potential for more generic behaviors, particularly around bifurcation points where behaviors can cross over in functionally specific ways.

In this context, our earthquake simulator comparisson group has begun an examination of how behaviors in a relatively simple problem change as control parameters change, and comparing the resulting behavior phase diagrams. Earthquake Simulator Problem 3 generalizes an earlier group problem. The initial simulator group problem considered a planar fault problem with two different frictional properties on two halves, with the question being whether the two halves always broke together or sometimes separately, a problem proposed and studied by the UC Davis group [Yiklimaz, et al, 2009] In Problem 3 we generalize the problem by adding the frictional weakening rate as a control parameter on the horizontal axis (the original group problem considered the infinite limit of this parameter). The problem is then to map out a crossover between throughgoing ruptures and ruptures not all breaking the whole fault.

Four groups using very different codes and physical approximations participated in this initial stage of the exercise. Results of this initial stage are presented in the poster.

AN ALTERNATIVE PATHWAY FOR SEISMIC HAZARD ESTIMATES BASED ON SLIP-LENGTH SCALING (2-155)
B.E. Shaw

Standard approaches to estimating seismic hazard use a series of empirical relations linked together to go from an input of slip rates on a system of faults to outputs of distributions of magnitudes of events on those faults. The current standard pathway linking slip rates to event distributions, given full weight in the latest ucerf analysis, does this through a step linking estimated areas of faults which will slip and estimated magnitudes of events of those areas, then doing moment-balancing to ensure long term slip rates are satisfied. While this is a valid methodology, it introduces a few difficulties which are sources of significant

uncertainty in the final hazard estimates. Prominently, differences in proposed empirical magnitude-area scaling laws imply substantial differences in hazard estimates, mainly due to the fact that the moment sum is dominated by the largest events, and differences in magnitude estimates of the largest events in the different empirical relationships end up affecting rates across the whole spectrum of sizes of events. An additional complication in this pathway is the recently raised question of whether or not a significant fraction of the moment may be coming from deeper slip below the seismogenic layer, thereby complicating ways of moment-balancing to ensure long term slip rates are matched.

Here, we propose an alternative pathway linking the same input of fault geometry and slip rates to the same output of distributions of magnitudes of events, but instead of going through the empirical magnitude-area scaling relation step, an empirical slip-length scaling relation step would be used. Linked to this slip-length scaling law would be the balancing of long terms slip rates directly with slip in large events at the surface. This alternative pathway has a number of advantages. First and foremost, it makes geologically observable data central to the estimate, relegating less certain deeper fault effects to scaling relations which do not feed back directly into rate estimates. %(specifically, magnitude-length and magnitude-area scaling relations, which we will discuss further later). Second, by providing an alternative pathway, it helps increase the span of the space of viable models, which helps improve the hazard estimates. Here we present this new alternative pathway, addressing the new issues which arise.

TREMOR EVIDENCE FOR DYNAMICALLY TRIGGERED CREEP EVENTS ON THE DEEP SAN ANDREAS FAULT (2-102)
D.R. Shelly, Z. Peng, D.P. Hill, and C. Aiken

Deep tectonic tremor has been observed along major subduction zones and the San Andreas fault (SAF) in central and southern California. It appears to reflect deep fault slip, and it is often seen to be triggered by small stresses, including passing seismic waves from large regional and teleseismic earthquakes. Here we examine tremor activity along the Parkfield-Cholame section of the SAF from mid-2001 to early 2010, scrutinizing its relationship with regional and teleseismic earthquakes. Based on similarities in the shape and timing of seismic waveforms, we conclude that triggered and ambient tremor share common sources and a common physical mechanism. Utilizing this similarity in waveforms, we detect tremor triggered by numerous large events, including previously unreported triggering from the recent 2009 Mw7.3 Honduras, 2009 Mw8.1 Samoa, and 2010 Mw8.8 Chile earthquakes at teleseismic distances, and the relatively small 2007 Mw5.4 Alum Rock and 2008 Mw5.4 Chino Hills earthquakes at regional distances. We also find multiple examples of systematic migration in triggered tremor, similar to ambient tremor migration episodes observed at other times. Because these episodes propagate much more slowly than the triggering waves, the migration likely reflects a small, triggered creep event. As with ambient tremor bursts, triggered tremor at times persists for multiple days, probably indicating a somewhat larger creep event. This activity provides a clear example of delayed dynamic triggering, with a mechanism perhaps also relevant for triggering of regular earthquakes.

VARIATIONS IN TREMOR ACTIVITY AND IMPLICATIONS FOR LOWER CUSTAL DEFORMATION ALONG THE CENTRAL SAN ANDREAS FAULT (2-093)
D.R. Shelly

Tremor activity patterns can serve to illuminate spatially variable properties and deformation styles of the deep fault. Toward this goal, we use cross-correlation to separate tremor into more tractable individual events, called low-frequency earthquakes (LFEs). We then divide the LFEs into 88 families (groups of similar events) distributed along 150 km of the central San Andreas Fault, beneath creeping, transitional, and locked sections of the upper crustal fault [Shelly and Hardebeck, 2010].

For maximum accuracy, we locate these tremor families using a 3D velocity model and seismogram stacks of up to 400 events. These stacks reveal clear P and S body waves, even on analog surface stations, which tightly constrain event hypocenters. Depths are mostly between 18 and 28 km, in the lower crust, and below the maximum depth of regular earthquakes. Tremor epicenters are concentrated within 3 km of the surface trace, implying a nearly vertical fault. Combined with observations of tremor migration, this suggests that the San Andreas Fault remains a localized, through-going structure at least to the base of the crust in this area.

Using these 88 event families as waveform templates, we systematically scan 9 years of continuous seismic data. We detect more than 550,000 events (LFEs) since mid-2001; typically multiple bursts per day. We find considerable variation in properties among families, including amplitudes, recurrence intervals, responses to the nearby M 6.0 Parkfield and M 6.5 San Simeon earthquakes, and sensitivity to small stresses imparted by the tides and by waves of regional and teleseismic earthquakes. These properties tend to show systematic variation with location, providing hints of lower-crustal heterogeneity. For example, maximum tremor amplitudes vary along the fault by at least a factor of 7, with by far the strongest sources along a 25 km

section of the fault southeast of Parkfield. In addition, shallower sources (i.e. < 23 km depth) have more concentrated (larger, but less frequent) bursts of activity compared to deeper sources, perhaps signaling changing fault strength with depth.

Reference:

Shelly, D. R. and J. L. Hardebeck (2010), Precise tremor source locations and amplitude variations along the lower-crustal central San Andreas Fault, Geophys. Res. Lett., 37, L14301, doi:10.1029/2010GL043672.

HORIZONTAL STRAIN RATE ESTIMATION USING DISCRETIZED GEODETIC DATA AND ITS APPLICATION TO SOUTHERN CALIFORNIA (2-026)
Z.-K. Shen and Y. Zeng

We present an algorithm to calculate horizontal strain rates through interpolation of a geodetically derived velocity field. To derive a smoothly distributed strain rate field using geodetic observations is an under-determined inverse problem. Therefore a priori information, in the form of weighted smoothing, is required to facilitate the solution. Our method is revised from the previous approaches of Shen et al. (1996, 2007). At a given location, the velocity field in its vicinity is approximated by a linear function of positions and can be represented by two velocities, three strain rate components, and a rotation rate at that point. The velocity data in the neighborhood, after re-weighting, are used to estimate the field parameters through a least-squares procedure. Data weighting is done with following considerations: (a) Data are weighted according to either the Voronoi cell area of each neighboring site, or the station azimuthal span of two adjacent neighboring sites. (b) A distance weighting factor is assigned according to site-to-station distances, in the form of either a Gaussian or quadratic decay function. (c) The distance decay coefficient is determined from setting a minimum total weighting threshold which is defined as the sum of the weighting coefficients for all the data input. We also developed an algorithm to exclude contributions of the non-elastic strain associated with fault creep and applied it to the Central California Creeping segment of the San Andres fault system. We apply this method to derive the strain rate field for southern California using the SCEC CMM4 velocity field.

EFFECT OF FAULT ROUGHNESS ON DYNAMIC RUPTURE (2-083)
Z. Shi and S. Day

Natural faults manifest geometric complexities with a broad range of scales ranging from large features such as extensive bending and segmentation spanning over tens of kilometers conspicuous in the field to small topography variations on fault slip surface in microns revealed in the lab. Previous studies have suggested that the geometrical properties of the fault can have strong influence on the static stress distribution around the fault and the dynamic process of earthquake ruptures. With the goal of providing more insights into this problem, we perform 2D and 3D numerical simulations of dynamic rupture along faults with different roughness distributions. We focus on the evolution of pulse-like and crack-like ruptures on faults with roughness distribution of different characteristics. The roles of off-fault plasticity (Drucker-Prager) are also examined. Calculations are carried out using the Support Operator Rupture Dynamics (SORD) code with augmented implementation of physics. Having a highly scalable parallel implementation with MPI, SORD will also allow us to explore roughness models that cover an extended range of length scales by utilizing large high-performance computing clusters.

USING RUPTURE-TO-RAFTERS SIMULATIONS TO QUANTIFY SEISMIC RISK FROM THE SAN ANDREAS FAULT --CASE STUDIES OF TALL STEEL MOMENT FRAME AND DUAL SYSTEM (1-042)
H. Siriki and S. Krishnan

Blind-thrust faults and well-mapped faults such as San Andreas, form a major risk for earthquakes in Southern California. Studies done by Shaw et al. (1996) show that the blind-thrust faults are capable of producing earthquakes in the magnitude range 6.0-7.0, with a recurrence interval ranging from 200 to over 1300 years. Similar studies done by Weldon et al. (2005) for the well-mapped Southern San Andreas fault, show the possibility of high magnitude earthquakes (Mw 7.0-8.0) with a relatively low recurrence periods of about 200 years. This points to the high hazard associated with the San Andreas fault, especially for tall buildings which are more sensitive to long period motions. Until recently, welded steel moment frame buildings were considered to be the most ductile of structural systems. The 1994 Northridge and the 1995 Kobe earthquakes proved otherwise. Fracture occurred in beam-to-column connections in a significant number of moment frame buildings. Motivated by the large number of existing buildings of this type in the Los Angeles basin and the hazard posed by the San Andreas fault, we are conducting a suite of rupture-to-rafters simulations to quantify the risk to these buildings from San Andreas earthquakes over the next 30 years. The procedure outlined by Krishnan et al. (2006) is being followed. A large number of stochastic source models are being generated for earthquakes in the magnitude range of 6.0 - 8.0. Unilateral rupture propagation with rupture directivity from north-south and south-north are considered. Using the open source seismic wave propagation package SPECFEM3D, synthetic seismograms are generated at various sites

across southern California. FRAME3D models of two steel moment frame buildings in the 20-story class and one steel building in the 40-story class (with the dual lateral force-resisting system of braced frame core with perimeter moment frame) will be analyzed under the synthetic 3-component waveforms. Probabilistic economic losses will be computed at each location under each scenario. Finally, annualized losses will be computed by assigning probabilities of occurrence of each scenario over the next 30 years using the Uniform California Earthquake Rupture Forecast (UCERF 3.0).

2010 USEIT DEVELOPMENT TEAM (1-002)
B. Siver, C.A. Castro, N. Anderson, and M. Sheehan

Since 2002, interns in the Undergraduate Studies in Earthquake Information Technology (USEIT) program at the Southern California Earthquake Center (SCEC) have been developing a robust and fully interactive software suite to be used for exploring seismic data in 3D space. Each year, interns in the USEIT program implement new functionality into the Southern California Earthquake Center's Virtual Display of Objects (SCEC-VDO). The software is used for a variety of purposes including scientific research, rendering animations, and spreading earthquake awareness to the general public.

The 2010 SCEC-VDO development team focused on implementing features under the scope of operational earthquake forecasting. One such feature is the real time earthquake plugin, which is capable of displaying and navigating through the most recent earthquakes in 3D space. Data brought in through the California Institute of Technology's web-service is now displayable in real time through this plugin. Furthermore, end users will be able to view a live screencast of this utility via the SCEC website during seismic crises. Another feature added to SCEC-VDO is the animation of kinematic fault ruptures based on data from the CyberShake project. This plugin shows ground displacement in real time as well as total final ground displacement. The ability to view time-dependent rupture probabilities of various points on a fault was also added to SCEC-VDO. Using data from the UCERF-2 model, users can now view the probability of any particular point on a fault participating in ruptures of various magnitudes.

BEHAVIOR OF HILL SLOPES DURING STRONG GROUND MOTION AND NONLINEAR ATTENUATION (1-057)
N.H. Sleep

The shallow subsurface (upper 10s of meters) of hill slopes should exhibit the nonlinear behavior of during strong ground motions. A simple model predicts excessive longterm down-slope movement and constrains the actual properties of brittle hill-slope regolith. S-waves propagating perpendicular to a shallow ~0.1 slope provide simple dimensional expressions. Elastic strain energy and hence anelastic strain are concentrated near the quarter wavelength depth (from a velocity seismogram) or equivalently the scale depth 1/k, the inverse of the wave number, a few tens of meters. Coulomb stress ratios (dynamic shear stress to lithostatic stress) scale with the dynamic acceleration expressed in g's. 1 g is a canonical value for strong motion. Strong nonlinear attenuation implies anelastic strains and displacements scaling with the dynamic ones. Dynamic stresses cause shear tractions on subhorizontal planes that augment or reduce the static shear tractions from gravity. Over many cycles, the hill-slope material behaves like an object on a vibrating ramp with net down-slope movement. The net flux rate of material across a contour line is proportional to twice the dynamic displacement times the slope times the scale depth 1/k and inversely proportional to the recurrence time of strong shaking. Using values from Parkfield California of 0.2 m, 0.1, 30 m, and 30 years yields 0.020 m2 yr-1. This rate is grossly excessive compared to geologically observed rates of ~0.001 m2 yr-1, much of which occurs in shallow soil (Heimsath et al., 2005). The dimensional approximation involves an implicit unknown multiplicative constant and the assumed parameters are uncertain. An excessive creep rate prediction of a factor of a few or even an order of magnitude might be compatible with the simple model. Still it is productive to discuss heterogeneity of the fracture rock. Rapid seismically driven creep does not occur because the shallow brittle subsurface behaves like a wooden jigsaw puzzle. Strong shaking jostles intact blocks of rock, causing slip on fractures and joints. Islands of intact rock coupled with the deeper subsurface lock, limiting the total rate of down-slope creep. The intact rock is significantly stronger than fractures. Linker and Dieterich (1992) relationship represents this effect. Dynamic creep on fractures cushions the intact rock limiting its failure. Still moderately intact rocks should fail at Coulomb ratios of 1.25-1.5 and hence 1.25-1.5 g.

SCEC CVM-TOOLKIT (CVM-T) -- HIGH PERFORMANCE MESHING TOOLS FOR SCEC COMMUNITY VELOCITY MODELS (1-014)
P. Small, P. Maechling, G. Ely, K. Olsen, K. Withers, R. Graves, T. Jordan, A. Plesch, and J. Shaw

The SCEC Community Velocity Model Toolkit (CVM-T) enables earthquake modelers to quickly build, visualize, and validate large-scale meshes using SCEC CVM-H or CVM-4. CVM-T is comprised of three main components: (1) an updated community velocity model for Southern California, (2) tools for extracting meshes from this model and visualizing them, and (3) an automated test framework for evaluating new

releases of CVMs using SCEC's AWP-ODC forward wave propagation software and one, or more, ground motion goodness of fit (GoF) algorithms.

CVM-T is designed to help SCEC modelers build large-scale velocity meshes by extracting material properties from an extended version of Harvard University's Community Velocity Model (CVM-H). The CVM-T software provides a highly-scalable interface to CVM-H 6.2 (and later) voxets. Along with an improved interface to CVM-H material properties, the CVM-T software adds a geotechnical layer (GTL) to CVM-H 6.2+ based on Ely's Vs30-derived GTL. The initial release of CVM-T also extends the coverage region for CVM-H 6.2 with a Hadley-Kanamori 1D background. Smoothing is performed within the transition boundary between the core model and the 1D background. The user interface now includes a C API that allows applications to query the model either by elevation or depth.

The Extraction and Visualization Tools (EVT) include a parallelized 3D mesh generator which can quickly generate meshes (consisting of Vp, Vs, and density) from either CVM-H or CVM-4 with over 100 billion points. Python plotting scripts can be employed to plot horizontal or profile slices from existing meshes or directly from either CVM.

The Automated Test Framework (ATF) is a system for quantitatively evaluating new versions of CVM-H and ensuring that the model improves against prior versions. The ATF employs the CruiseControl build and test framework to run an AWP-ODC simulation for the 2008 Chino Hills event (Mw = 5.39) and perform a goodness of fit statistics calculation on the generated synthetic and recorded observed seismograms using the GoF algorithm, based on comparison of synthetic peak amplitudes to observed peak amplitudes, used in the SCEC Broadband platform. CVM-T produced plots include comparisons of synthetic and observed seismograms, plots of bias versus period, and spatial plots of the pseudo-AA bias over the entire region.

STRESS RELAXATION DUE TO SLIP ON GEOMETRICALLY COMPLEX FAULTS: HOW IT AFFECTS FAULT SIMULATORS AND OFF-FAULT MOMENT RELEASE (2-065)
D.E. Smith and J.H. Dieterich

A form of off-fault stress relaxation, based on rate-state seismicity equations, was developed to resolve several problems associated with geometrically complex faults in elastic media. Slip on geometrically complex faults in elastic media produces fault interaction stresses that non-physically grow without limit. These stresses in turn suppress fault slip and break down the linear slip vs. length scaling for ruptures. In the Earth, these fault interaction stresses cannot grow without limit, and yielding will occur; therefore, we build upon the suggestion by Dieterich and Smith [2009] that off-fault yielding can relieve these stresses in the form of pervasive secondary faulting in the brittle crust. Starting with the rate-state seismicity equations that statistically describe the nucleation of seismicity in the brittle crust, we derive analytical expressions to represent stress relaxation as a time dependent, bulk yielding process. These expressions 1) stabilize the simulations, 2) restore the linear slip vs. length scaling in ruptures, and 3) enable stress asperities to grow and relax about a long-term average instead of growing without limit. In particular, we demonstrate the robustness of this linear slip vs. length scaling in simple fault simulators with stress relaxation. We also map out the off-fault spatial and temporal evolution of stress relaxation with the associated moment release. For example, for a fractal fault with scaling exponent = 1.0 and moderate roughness of beta = 0.03 (rms amplitude of slope deviations) we estimate that the off-fault moment release, integrated up to one fault length away during the aftershock period, is about 5% of the original on-fault rupture moment. If one includes the stress-relaxation due to co-seismic damage processes and inter-seismic seismicity, the off-fault moment is approximately 12% of the original on-fault moment for beta = 0.03. With a more extreme roughness of beta = 0.10, the off-fault moment release approaches 13% for the aftershocks period and 40% for all relaxation processes.

3D STRESS HETEROGENEITY – POTENTIAL IMPLICATIONS FOR CRUSTAL STRESS PARAMETERS AND STRESS INVERSION RESULTS IN SOUTHERN CALIFORNIA (2-028)
D.E. Smith and T.H. Heaton

A 3D, time-varying model of crustal stress with stochastic spatial variations in the stress tensor components is used to generate synthetic earthquake catalogs. These synthetic catalogs in turn are compared to Southern California data to infer crustal stress statistics and potential stress inversion biasing effects. In the crustal stress model, we assume the following: 1) Temporal variations in stress are spatially smooth and are primarily caused by plate tectonics. 2) Spatial variations in stress are the result of past earthquakes and are independent of time for periods between major earthquakes. 3) Heterogeneous stress can be modeled as a stochastic process that is specified by an autocorrelation function. Synthetic catalogs of earthquake hypocenters and their associated focal mechanisms are produced by identifying the locations and times at which the second deviatoric stress invariant exceeds a specified limit within our 3D crustal stress model. This produces a seismicity catalog that is spatially biased, where the only points in the grid that exceed the failure stress are those where the heterogeneous stress is approximately aligned with the stress rate. We

estimate stochastic stress parameters, which generate distance dependent spatial variations in our synthetic focal mechanisms similar to the variations seen in Southern California focal mechanism data. This comparison of focal mechanism catalogs suggests that stress in the crust is strongly heterogeneous. Using this heterogeneous stress model, we generate synthetic spatial variations in borehole breakout data and compare with borehole breakout data measured in the Cajon Pass. Last, using our synthetic focal mechanism catalogs, our best-fit stochastic parameters, and real focal mechanism data, we estimate a percent bias for stress inversions of focal mechanism data in Southern California. If the stress rate is misaligned with regard to the spatially averaged stress, we try to estimate to what degree will stress inversions represent the stress rate rather than the spatially averaged stress.

COMPARISON OF LOCKING DEPTHS ESTIMATED FROM GEODESY AND SEISMOLOGY ALONG THE SAN ANDREAS FAULT SYSTEM (1-158)
B.R. Smith-Konter, D.T. Sandwell, and P. Shearer

Seismic hazard models of the San Andreas Fault System rely on accurate representations of fault depths to properly estimate the earthquake potential of active faults. Independent observations from both seismology and geodesy can provide insight into the depths of faulting, however these depths do not always agree and thus understanding how these parameters are estimated and applied in models is a very important exercise. Here we compare fault depths of 12 segments of the southern San Andreas Fault System estimated from both seismic and geodetic methods. In particular, we inspect variations in locking depths estimated from over 1000 GPS velocities and seismogenic thicknesses derived from over 66,000 relocated earthquake hypocenters. Geodetically-determined locking depths range from 6–22 km (mean of 14 km), while seismogenic thicknesses are largely limited to depths of 11–20 km (mean of 16 km). There is generally good agreement between seismogenic thickness and geodetic locking depth, with nine out of the twelve fault segments analyzed here agreeing to within 2 km. However, three segments (Imperial, Coyote Creek, and Borrego) have significant discrepancies, with seismic estimates that are well outside the error bounds of the geodetic locking depths. In these cases, the geodetically-inferred locking depths are much shallower than the seismogenic depths. We also examine variations in seismic moment accumulation rate per unit fault length as suggested by seismicity and geodesy and find that both approaches yield high rates (~1.8 x 1013 Nm/yr/km) along the Mojave and Carrizo segments and low rates (~0.2 x 1013 Nm/yr/km) along several San Jacinto segments. The largest variation in seismic moment between models is calculated for the Imperial segment, where the moment rate from seismic depths is a factor of ~2.5 larger than that from geodetic depths. Such variability has important implications for the accuracy to which future major earthquake magnitudes can be estimated.

INTEGRATING NEW SOSAFE PALEO-EVENT CHRONOLOGIES WITH STRESS EVOLUTION MODELS OF THE SAN ANDREAS FAULT SYSTEM OVER THE LAST 2000 YEARS (1-107)
T. Solis, G. Thornton, and B. Smith-Konter

A comprehensive paleo-earthquake database is critical for investigating the relationship between stress evolution and occurrence of major earthquakes in southern California. Recent paleoseismic research supported by the Southern San Andreas Fault Evaluation project (SoSAFE) has improved our understanding of the chronology of paleo-events and slip distributions along the San Andreas Fault System (SAFS) over the past 2000 years. These new data are beginning to clarify the sequence of major ruptures along fault segments of the SAFS, the San Jacinto, and the Elsinore faults. Using these data, we assembled a database of fault slip history for 21 fault segments using 100 historical and prehistorical earthquake events reported in the literature spanning the last 2000 years. We include all of these events in a new stress accumulation evolution model of the SAFS that also includes improved fault geometry (geographic representation and fault locking depth). This model allows us to better understand the exchange of stress between parallel faults in southern California over several earthquake cycles and quantifies stress thresholds for repeating earthquakes. As part of this work we are developing 3-D animated simulations of stress evolution to be used as an educational resource for interactive EarthScope kiosk displays.

DYNAMIC EARTHQUAKE RUPTURE MODELING WITH PYLITH: SCEC BENCHMARKS AND APPLICATION TO TSUNAMIGENIC EARTHQUAKES (2-048)
S.N. Somala, B. Aagaard, J-P. Ampuero, and N. Lapusta

PyLith is an open-source, community finite-element code for quasi-static and dynamic tectonic deformation problems. Dynamic fault interface conditions have been implemented in the latest release of PyLith (version 1.5) to enable modeling of earthquake processes via fault constitutive models, including slow quasi-static and fast dynamic slip; previous versions of PyLith were limited to kinematic ruptures. We have implemented various fault constitutive models in PyLith, including slip-weakening and rate-and-state friction. We tested these new features in 2-D and 3-D simulations using two SCEC benchmarks (Harris et al., 2009) (1) slip-weakening friction for a vertical strike-slip fault and (2) slip-weakening for a dipping fault with dip-slip motion. We report on comparisons of our results for these benchmarks using different triangular, quadrilateral, tethrahedral, and hexahedral cells. We have also simulated dynamic rupture in branched fault

systems of subduction earthquakes that trigger slip on secondary splay faults, a process relevant to tsunami hazard. We compared our results to published finite element simulations in 3D (Wendt et al, 2009), which assume a shallow hypocenter and a splay fault reaching the free surface far from the trench (100 km). We also considered a model geometry more typical of splay faulting in the accretionary wedge of the Nankai trough with a deeper hypocenter, and compared the results to spectral element simulations in 2D. Our eventual goal is to create a methodology, based on PyLith, that would be able to simulate long deformation histories of a fault, including quasi-static and dynamic phases, in realistic bulk rheologies.

THRUST-FOLDING, TILTING AND SUBSIDENCE: CALIFORNIA BORDERLAND AND HAITI (2-013)
C. Sorlien, L. Seeber, M-H. Cormier, M. Davis, J. Diebold, N. Dieudonne, S. Gulick, M. Hornbach, C. McHugh, and M. Steckler

Transpression in California Borderlands and along the Caribbean-North America boundary in Haiti is partitioned among strike slip and thrust faults. Anticlines are growing above blind thrust faults along the southern California margin. Oblique thrust slip generally reactivates Miocene extensional faults. Anticline limbs commonly exhibit progressive tilting. In Haiti, 5 mm/yr of contraction is part of the left-lateral plate boundary (Calais, 2010). Offshore seismic reflection profiles and onshore geology document a SSW-verging fold and thrust complex. An anticline forms the WNW-ESE St. Marc Peninsula north of Port-au-Prince. Another 40 km by 150 km-long anticline that includes Gonave Island is between the northern and southern peninsulas of Haiti. Marine terraces are uplifted on both anticlines. The ~120,000 year terrace (Mann et al., 1995) is folded at the St. Marc Peninsula and older terraces above it are progressively tilted. Strata offshore, including the youngest, show progressive tilting on both fore and back limbs. Both anticlines also exhibit evidence of subsidence of their offshore plunge and of their limbs, including unconformities and other planar surfaces now in deep water, and mounds that might be subsided bioherms. If the thrust footwall and basins therein are subsiding, then structural relief growth during thrust-folding is much greater than is uplift of anticline crests with respect to sea level. Offshore seismic profiles image highly extended rocks beneath an unconformity. These profiles also image blind N-dipping faults beneath both anticlines, with evidence for reactivation of normal faults. The unconformity separating the extension and contraction may correlate to an onshore unconformity between Eocene and Miocene rocks. The SSW-verging thrust system intersects a NNE-verging active (oblique?) thrust system and an active left-lateral fault offshore north of the January 2010 earthquake rupture. Thrust aftershocks of the 2010 earthquake occurred on the NNE-verging faults, demonstrating active slip partitioning. Intersections of the folds and thrusts with the left-lateral Enriquillo-Plantain Garden transform fault likely result in growth of bends in the transform, with enhanced transtension or transpression. Thrust-folds in both Haiti and southern California share current oblique convergence with strike-slip faults and re-activate pre-existing extensional faults.

SOUTHERN CALIFORNIA'S NEWEST VENUE FOR TEACHING EARTH SYSTEM SCIENCE: THE SAN BERNARDINO COUNTY MUSEUM'S HALL OF GEOLOGICAL WONDERS (1-010)
K. Springer, E. Scott, and J.C. Sagebiel

The San Bernardino County Museum (SBCM) in Redlands, California is completing exhibits in a new 12,000-square-foot, three-story expansion: the Hall of Geological Wonders. Exhibitions exploring the American southwest from a geologic perspective are united by a consistent emphasis on geologic processes. The richness of our natural resources prescribes regional distribution of floras, faunas, and human populations; our exhibits showcase how geology is ultimately responsible for the distribution of these resources.

Partnering with SCEC's Communication, Education and Outreach Program, and under the Earthquake Country Alliance umbrella, the SBCM and its new Hall of Geological Wonders are the southern California nexus of the EPIcenter (Earthquake Education and Public Information Centers) network. This statewide collaboration of free-choice learning venues such as museums, parks, and libraries is dedicated to the dissemination of earthquake awareness and preparedness information, educating the public on topics related to earthquake science and the Great California ShakeOut. The SBCM is committed to providing visitors with current research answering questions about the titanic geologic forces at work beneath their feet - forces that explain the shape of the Earth, its landforms, and its sometimes-violent nature. Visitors will recognize the significance of these forces in shaping their own region and what it means in their lives.

Our exhibits explain the origin of southern California's striking topography, via the emergence of plate tectonics theory placed in the context of scientific discovery, ultimately revealing our most notorious geologic feature, the San Andreas fault system, as the culprit. Visitors will observe the San Andreas fault zone from our "Earth's Cylinder" – below ground in a re-created paleoseismic trench across the fault, and above ground from a viewing tower. Visitors will also experience a simulated earthquake in our immersive "ShakeOut Cabin". In this manner, the San Andreas fault is interpreted in a way no other museum ever has attempted, while also encouraging earthquake awareness and preparedness in a static museum venue. These exhibits explore the importance of science in everyday life, emphasizing science as a process and encouraging visitors

to become a part of this process through interactives such as "Did You Feel It?" and the Quake Catcher Network, thereby duplicating a real-time earthquake experience in a museum exhibit setting.

PROGRESS IN GAINING AGE CONSTRAINTS FOR PRECARIOUS LANDFORMS IN TEMPERATE ENVIRONMENTS (1-076)
M.W. Stirling and D.H. Rood

Over the last 5 years, studies of precariously balanced rocks (PBRs) in New Zealand have been focused on age determinations of the rocks at near-fault sites. To date, efforts to interpret Be-10 exposure age data on PBRs in central Otago, an area with an equivalent climate to coastal central-to-northern California, have been unable to resolve whether the rocks are of the order 103-104 or 104-105 years of age. Resolution of these differences is critical to determining the utility of PBRs in New Zealand and equivalent temperate environments for constraining seismic hazard models at long return periods.

Present efforts are now focussed on reinterpreting the cosmogenic Be-10 data for "Clyde 6", a PBR that has had eight Be-10 analyses undertaken in recent years (and three additional analyses on nearby outcrops). Samples collected from a vertical profile will be used to interpret the rate of exhumation and thus an age for the PBR. Our dating method combines measured Be-10 concentrations with a numerical model that accounts for nuclide production before, during, and after exhumation of the PBR from the subsurface (see Rood et al. abstract, this meeting). Furthermore, a three-dimensional model constructed from photogrammetry will be used to correct for the shielding of cosmic rays due to the shape of the rock.

AZIMUTHAL ANISOTROPY IN MEXICO OBTAINED FROM RAYLEIGH WAVE PHASE VELOCITY MAPS (2-149)
I. Stubailo, C. Beghein, and P. Davis

We present azimuthally anisotropic fundamental mode Rayleigh wave phase velocity maps for the Mexico area. Body wave tomography in this region reveals the presence of a flat slab under the western part of the MASE seismic array (which ran from Acapulco to Tampico), starting at about 30-50 km depth, and of a steeply dipping slab beneath the center of the array. In addition, preliminary shear-wave splitting (SKS) results in the region did not show any significant difference between measurements made above the slab and away from it. While these SKS splitting observations need to be further refined with stacking, our anisotropic phase velocity maps will help put them in context and constrain the depth of origin of the anisotropy.

We analyzed data recorded at 165 temporary and permanent broadband stations installed in Mexico and Southern USA over a period of 1.5 for 119 teleseismic events of magnitude 6.0 and above. We employed a two station method to measure phase velocity dispersion curves between periods of 16 to 170s, using events located within 3 degrees of the great circle path between the two stations. We then inverted the measurements to obtain azimuthally anisotropic phase velocity maps.

Our results reveal lateral variations in phase velocities consistent with the presence of a slab and in agreement with previous studies. We find velocities larger than average in the south western part of the region, and lower than average north of the MASE seismic line. The lower phase velocities are observed at all periods and coincide with the location of the TransMexican Volcanic Belt, as well as a region of high attenuation.

Our anisotropy maps demonstrate that very little azimuthal anisotropy is present in the forearc between periods of 18 and 54s, which approximately sample the top 80 km. However, at periods of 68s and higher, the forearc is characterized by about 3% anisotropy with a fast direction of propagation roughly perpendicular to the trench, which could indicate active mantle deformation beneath the slab. In the backarc, we find that azimuthal anisotropy is present at all periods up to 85s, with a fast direction of propagation at an angle with the trench. The pattern of anisotropy in that part of the subduction zone is more complicated and difficult to interpret in terms of deformation as the presence of water or partial melt can strongly affect the relation between LPO deformation and seismic wave fast direction.

GEONET: PLATFORM FOR RAPID DISTRIBUTED GEOPHYSICAL SENSING (2-144)
I. Stubailo, M. Lukac, D. McIntire, P. Davis, W. Kaiser, J. Wallace, and D. Estrin

In the GeoNet experiment, the science objective is to use a rapidly installable wirelessly linked seismic network to make near-real time unaliased observations in aftershock or volcanic zones. To accomplish this, we collaborate with Reftek to construct a new generation digital acquisition system (DAS) based on the UCLA-developed LEAP (low-power energy aware processing) system and a newly developed low-power A/D converter from Texas Instruments.

The instrument will have two parts: DAS and a seismic sensor. The DAS would have a solar panel attached on top, battery inside (with external power plug), internal GPS antenna (with a possibility of attaching an external one), external N-type connector for an antenna. Field installation would involve attaching the box to

a post and bury the seismometer. It would then become a node in a wireless network of neighbors, e.g. along a dirt road that could bring event data out in real time, or, in the low power mode, on a duty cycle, e.g., 5 min every hour. The radios would also deliver network time, a backup to GPS.

In a building, the instrument would not need the solar panels, although after an earthquake power may be unavailable. An instrument plus Episensor (or other) would be installed on various floors. Radio connectivity through the floors would be used to provide network time and transport event data. Where available (e.g., near windows) GPS time would calibrate the network time. With no solar energy available, the battery with an active sensor would last 4 days. Longer deployments would require a larger external battery.

At the moment, we have two prototypes that have been tested in short-time field deployments in Palmdale and near the Salton Sea.

PREHISTORIC EARTHQUAKES ALONG THE SAN JACINTO FAULT IN TRENCH 7 AT THE MYSTIC LAKE PALEOSEISMIC SITE (1-116)
M.R. Swift, S.F. McGill, N. Onderdonk, T.K. Rockwell, B. Anderson, J. Bywater, K. Chung, J. Duncan, and G.I. Marlyani

Mystic Lake occupies a closed depression in the San Jacinto Valley within a releasing step-over between the Casa Loma and Claremont faults in the San Jacinto fault zone. In July 2010 we excavated three new trenches (T5, T6 and T7) across the Claremont fault within the deposits of Mystic Lake near the northwestern end of this step-over. This poster presents results from Trench 7, located 5-10 meters northwest of the original trench (T1), which was excavated in October 2009. Six prehistoric faulting events were identified in Trench 1 over the past 1600 years.

In Trench 7 we were able to confirm Event 2 at the same stratigraphic level as in Trench 1, based on a pronounced angular unconformity and a buried graben. Trench 7 also contained evidence (a package of beds thinning against an inferred fold scarp) consistent with an earthquake at the level of Event 3 in Trench 1. Numerous cracks also extended above the Event 2 horizon to the base of a historically deposited layer that contained a tin can (in Trench 1). Stratigraphy was poor in this part of the section, but two white silt layers within 10 cm below the lowest historic deposit were disrupted within the fault zone. This disruption appears to be at a higher stratigraphic level than Event 1 in Trench 1, but additional work will be necessary to test whether this really represents an additional earthquake that was not recognized in Trench 1.

As in Trench 1, there are also a few faults that extend to the ground surface, vertically displacing the historical layers by a cm or two. The lack of historical earthquakes along this portion of the fault, however, suggests that these small offsets are probably due to groundwater withdrawal or creep rather than being related to earthquakes.

Approximately fifty charcoal samples were taken from Trench 7, including samples from most exposed units. In particular, samples from units 390 and 400 in Trench 7 will allow us to bracket the age of event 3, which was not directly datable in Trench 1.

SITE-CITY EFFECTS IN LARGE-SCALE 3D EARTHQUAKE SIMULATIONS (1-024)
R. Taborda and J. Bielak

Using Hercules---the octree-based finite-element earthquake simulator developed by the Quake group at Carnegie Mellon University---we have implemented new computational modules that allow us to incorporate large inventories of idealized buildings in earthquake simulations at scale, using parallel supercomputers. The buildings and their foundation systems are modeled as rectangular prismatic blocks filled with homogeneous material whose properties are set so that the fundamental dynamic properties of the real structures are matched on average. These models consist of the same solid finite-elements as those used for the crust and basin structure of the simulation domain and they are in full contact with the soil. We test our implementation with an inventory of 74 buildings placed near the edge of a realistic basin. Results indicate that the presence of the built environment greatly affects the area up to a perimeter of about 300 to 500 meters around the 'city' boundaries. Within the city, the ground motion exhibits significant changes in the spatial variability of peak response and reductions in the excitations at the base of the buildings. Synthetics exhibit shifts in both the time and the frequency domains. The structural response, in general, is reduced due to soil-structure interaction effects. This study suggests that larger inventories of buildings may have the potential of drastically changing the local and regional ground response and confirms results obtained in previous similar 2D studies.

FULL 3D NONLINEAR SOIL EFFECTS IN LARGE-SCALE GROUND MOTION SIMULATIONS (1-025)
R. Taborda and J. Bielak

We have implemented a rate-dependent plasticity approach to model the plastic behavior of soils in large-scale earthquake simulations using Hercules, the octree-based finite-element earthquake simulator

developed by the Quake Group at Carnegie Mellon University. In this first study we have modeled the soil using the von Mises and Drucker-Prager constitutive equations. We test this new implementation in a realistic basin filled with three layers of soft-soil deposits with shear wave velocities 200, 350, 650 m/s resting on a bedrock of Vs = 2600 m/s. The material within the basin is allowed to deform plastically while the bedrock substrata remains elastic throughout the simulation. Results indicate that there exist 3D effects that cannot be modeled using approximate 2D or 1D approaches. Typical observations from past earthquakes such as permanent deformations, change in the distribution of energy in the frequency domain (reductions in low frequencies and increase of high frequencies), deamplification factors of velocity and accelerations, are all present. In addition, we observe 3D basin, edge, and directivity effects that do not necessarily follow the same patters of linear anelastic simulations. We believe that including the nonlinearity effects of soils in large earthquake ground motion simulations is a key ingredient toward the advancement of computational seismology as a tool for improving seismic hazard analysis of earthquake-prone regions. The present implementation and results are a step forward in that direction.

TIME REVERSAL SEISMIC IMAGING USING LATERALLY REFLECTED SURFACE WAVES IN SOUTHERN CALIFORNIA (2-008)

C. Tape, Q. Liu, J. Tromp, A. Plesch, and J. Shaw

We use observed post-surface-wave seismic waveforms to image shallow (upper 10 km) lateral reflectors in southern California. Our imaging technique employs the 3D crustal model m16 of Tape et al. (2009), which is accurate for most local earthquakes over the period range 2-30 s. Model m16 captures the resonance of the major sedimentary basins in southern California, as well as some lateral surface wave reflections associated with these basins. We apply a 3D Gaussian smoothing function (12 km horizontal, 2 km vertical) to model m16. This smoothing has the effect of suppressing synthetic waveforms within the period range of interest (3-10 s) that are associated with reflections (single and multiple) from these basins. The smoothed 3D model serves as the background model within which we propagate an ``adjoint wavefield'' comprised of time-reversed windows of post-surface-wave coda waveforms that are initiated at the respective station locations. This adjoint wavefield constructively interferes with the regular wavefield in the locations of potential reflectors. The potential reflectors are revealed in an ``event kernel,'' which is the time-integrated volumetric field for each earthquake. By summing (or ``stacking'') the event kernels from 28 well-recorded earthquakes, we identify several reflectors using this imaging procedure. The most prominent lateral reflectors occur in proximity to: the southernmost San Joaquin basin, the Los Angeles basin, the San Pedro basin, the Ventura basin, the Manix basin, the San Clemente-Santa Cruz-Santa Barbara ridge, and isolated segments of the San Jacinto and San Andreas faults. The correspondence between observed coherent coda waveforms and the imaged reflectors provides a solid basis for interpreting the kernel features as material contrasts. The 3D spatial extent and amplitude of the kernel features provide constraints on the geometry and material contrast of the imaged reflectors.

EXPANSION OF CVM-H 6.2 TO OFFSHORE AND CENTRAL CALIFORNIA (2-005)

C. Tape, A. Plesch, and J.H. Shaw

We present four topological surfaces that provide a framework for expanding SCEC CVM-H 6.2 to offshore and central California. The surfaces are constructed from an extensive compilation of previously published data sets and cross sections, as well as seismic reflection profiles and well data within the sedimentary basins. The first surface represents the Moho, which ranges in elevation from -40 km to -8 km (median -26 km) and is constructed from receiver function results and reflection and refraction profiles, including several from offshore California. The second surface represents the top of relict oceanic crust, which ranges from -26 km to -5 km (median -14 km) and is interpreted to underlie the Coast Ranges and offshore California, including the Continental Borderlands. The top of oceanic crust is locally a strong seismic reflector, indicating an impedance contrast from a less dense and seismically slower overburden. The bottom of the relict oceanic crust is interpreted as the Moho surface. The third surface represents the crystalline basement beneath (and east of) the Great Valley. It ranges from -16 km to 1 km (median 6 km) and represents an important velocity interface between sedimentary and crystalline rocks. This surface is largely based on Wentworth et al. (1995), updated to include the 9-km deep Maricopa sub-basin of the southernmost San Joaquin Valley. The second and third surfaces are merged at approximately the San Andreas fault at an elevation of approximately -15 km. The fourth surface represents the base of the Tertiary sedimentary units within the Great Valley. North of the Bakersfield Arch this surface ranges from -7.5 to 0.2 km (median -1.0 km); south of the Bakersfield Arch it ranges from -9 km to 1 km (median -4 km) and is coincident with the crystalline basement defining the Maricopa sub-basin. The vertical separation between the third and fourth surfaces denotes the pre-Tertiary sedimentary rocks. All surfaces are smoothly estimated from the compiled data using spherical wavelets basis functions. Above the fourth surface are the unconsolidated sediments and sedimentary rocks of the San Joaquin basin. We are currently constructing a seismic velocity model for the basin by using sonic logs from approximately 250 wells and stacking velocities along 1200 km of seismic

reflection data. The detailed model of the San Joaquin basin will provide a critical update for the CVM-H model for seismic wavefield simulations in California.

HOW BARRIERS ENABLE MULTI-FAULT RUPTURE IN A BRANCHED FAULT SYSTEM (2-050)
J.M. Tarnowski, D.D. Oglesby, and D. Bowman

We use the finite element method and slip-weakening friction to investigate dynamic rupture propagation on a branched fault system. The system consists of an oblique-normal fault at depth connected to vertical and dipping fault segments near the surface, which accommodate predominately strike-slip and dip-slip motion, respectively. When rupture is nucleated on the basal fault, dynamic unclamping favors rupture propagation to the vertical fault, with no rupture on the dipping fault. However, when a barrier is placed on the vertical fault, the consequent delay of rupture on the vertical fault causes shear stress to increase and normal stress to decrease on the part of the dipping fault overlapping the barrier, facilitating slip on both segments.There is a correlation between barrier area and the ease with which an earthquake at depth propagates to both faults in the branched system, suggesting a critical patch size for nucleation on the dipping fault. The relationship, however, is somewhat complex: barrier width appears to be more important than barrier height in determining whether both segments slip. Keeping all other variables constant while increasing the slip-weakening distance by a factor of √2 produces models that also exhibit this relationship, except with the critical barrier area increased by roughly a factor of 2. This factor is consistent with the relationship between slip-weakening distance and critical nucleation patch size (Day, 1982). Further numerical experiments show that the basic behavior above is relatively general, and does not require finely-tuned stress and frictional parameters.

MODELING EVENTS IN THE LOWER IMPERIAL VALLEY BASIN (2-146)
X. Tian, S. Wei, Z. Zhan, E. Fielding, and D.V. Helmberger

Earthquake records from the Southern Imperial Valley display a great deal of complexity, ie., strong Rayleigh wave multipathing and extended codas. Many of these events such as the recent El Mayor-Cucapah event, also, have complex mechanisms involving a mixture of strike-slip and normal slip patterns. It is difficult to separate these two features because of the lack of stations. However, some of these events have InSar data which can help set their locations and mechanisms. We will present modeling results combining regional and teleseismic data using the CAP codes and finite-fault inversions. We are finding record segments involving Pnl (including depth phases) and some Love waves that appear well behaved, ie., can be approximated by synthetics from 1D local models. Simple events can then be identified along with path calibration. Modeling the more complicated paths can be started with known mechanisms.

DISTRIBUTION OF SEISMIC HAZARD, REGULATION, AND VULNERABILITY IN GREATER LOS ANGELES (1-045)
N.A. Toke, C.G. Boone, and J.R. Arrowsmith

Probabilistic seismic hazard modeling is a powerful tool for understanding the probability, spatial distribution, and magnitude of extreme ground motions due to large earthquakes in a region and over a given time period. Generally, extreme ground motions are likely to be felt close to seismic sources (rupturing faults) and in regions situated on basins filled with unconsolidated sediment, which have the potential to amplify ground shaking.

Ground rupture, associated with the surface trace of a fault, is less widespread than seismic shaking. However, surface ruptures offset structures crossing the fault and therefore also lead to economic and human casualty. California is one of the few places to regulate zoning based upon earthquake hazards. The most mature regulation is the Alquist-Priolo (AP) Earthquake Fault Zones Act. This Act stipulates that construction built for human occupancy cannot occur within an Earthquake Fault Zone. These Fault Zones are defined by geologic mapping of faults and include a setback buffer of at least 50 feet.

The other major factor responsible for determining the outcome of an earthquake, as with all natural disasters, is the social vulnerability of those exposed to the hazard. Here we present geographic information systems (GIS) analyses comparing census block group indicators of vulnerability (e.g., poverty, wealth, ethnicity, age of housing stock) to both probabilistic seismic hazard maps and areas designated as AP Earthquake Fault Zones. Basic statistical comparisons between social vulnerability metrics and areas with a 2% chance of experiencing peak ground accelerations exceeding gravity in the next 50 years show little difference to the social vulnerability of the entire metropolitan area. However, statistical analyses of census block groups within AP fault zones indicate that the regions closest to active faults are occupied disproportionately by the economically privileged. One reason for this result is that slip along faults creates spectacular mountainside landscapes which are sites of desirable real estate. This study confirms that the AP Act has not stigmatized real estate values near faults. Instead it appears that setback requirements are associated with natural and constructed parks that may result in locally-higher prices.

AIRBORNE THERMAL INFRARED HYPERSPECTRAL IMAGERY OF SURFACE GEOTHERMAL ACTIVITY IN THE SALTON SEA GEOTHERMAL FIELD AND THE LINK TO SUBSURFACE TECTONISM (1-104)

D.M. Tratt, D.K. Lynch, K.N. Buckland, S.J. Young, J.L. Hall, B.P. Kasper, M.L. Polak, J. Qian, P.D. Johnson, and M.G. Martino

Two airborne remote thermometric surveys conducted approximately one year apart over the putative surface trace of the Calipatria Fault in the Salton Sea Geothermal Field are described, the latter occurring in the immediate wake of the 4 April 2010 M7.2 El Mayor-Cucapah earthquake. The imagery was acquired using a 7.6-13.5 micron thermal-infrared hyperspectral imager with meter-scale ground sample distance and reveals numerous prominent thermal sources associated with an active fumarole group that has been exposed in recent years by the declining water level of the Salton Sea. Concurrent visible imagery depicts a prolific assemblage of geothermal features in various phases of activity, with the most vigorous erupting plumes of vapor. The fumarole field is roughly coincident with the similarly oriented axis of the Salton Buttes and perpendicular to the Calipatria Fault. The main axis of the hydrothermal vent field strikes approximately N45E, further adding to evidence that volcanic/fumarolic activity is part of a NE-trending spreading center complex that spans the stepover region between the San Andreas and Imperial faults. This spreading center is presumed to be responsible for the Salton Buttes and the localized hydrothermal activity reported here.

FAULT RUPTURE IN THE YUHA DESERT, CALIFORNIA, FROM THE EL MAYOR-CUCAPAH EARTHQUAKE, AND THE CONTRIBUTION OF INSAR IMAGERY TO ITS DOCUMENTATION (1-080)

J.A. Treiman, K.J. Kendrick, M.J. Rymer, and E.J. Fielding

The April 4, 2010 El Mayor-Cucapah earthquake and its aftershocks caused primary and secondary rupture on a broad array of more than two dozen faults in the Yuha Desert, just north of the United States-Mexico border. Field mapping documented maximum displacements of 4-6 cm on branches of the northwest-trending Laguna Salada Fault and on the newly identified and named, northeast-trending Yuha Fault. Lesser displacements, including left-lateral, right-lateral and/or extensional components were mapped on at least twenty other faults, a majority of which are newly identified. Although the principal faults were readily identified and mapped in the field, many of the faults with lower coseismic displacement might not have been mapped had we not had interferometric synthetic aperture radar (InSAR) imagery to alert us to their presence. InSAR images were from data derived from the high resolution NASA/JPL UAVSAR instrument. Fault displacements were discernable from both the primary rupture and the aftershock sequence. Faults with surface displacements as small as a couple of millimeters or less were located and mapped. Several InSAR lineaments are interpreted as faults which had more distributed displacement that was not expressed as brittle surface rupture. InSAR imagery spanning the appropriate time intervals proved invaluable to obtaining a more complete picture of faulting in the Yuha Desert.

QUANTIFYING THERMOELASTIC AND POROELASTIC VARIATIONS FOR SEASONAL CHANGES IN GPS POSITIONS AND SEISMIC WAVE SPEEDS IN SOUTHERN CALIFORNIA (2-020)

V.C. Tsai

It is known that GPS time series contain a seasonal variation that is not due to tectonic motions, and it has recently been shown that crustal seismic velocities may also vary seasonally. In order to explain these changes, a number of hypotheses have been given, among which thermoelastic and poroelastic stresses and strains are leading candidates. In order to test the validity of these two hypotheses, we quantify the displacements and wave speed changes expected from thermoelastic and poroelastic stresses. For these calculations, we rely on well-known expressions for thermoelastic strains given a periodic surface temperature variation. We find that thermoelastic effects can explain a significant fraction (but likely not all) of both the observed annual variation in GPS displacements and the observed annual variations in seismic wave speeds. We find that poroelastic effects may explain the remaining observed variations. However, a number of important thermoelastic and poroelastic parameters must be better determined before definitive conclusions can be made.

PRELIMINARY RESULTS FOR N CA FROM EARTHQUAKE SIMULATOR COMPARISON PROJECT (1-121)

T.E. Tullis, M. Barall, K. Richards-Dinger, S.N. Ward, E. Heien, O. Zielke, F. Pollitz, J. Dieterich, J. Rundle, B. Yikilmaz, D. Turcotte, L. Kellogg, and E.H. Field

It is important to discover how realistic are the long earthquake histories generated from earthquake simulators. One way to do this is to compare their behavior with the limited knowledge we have from the instrumental, historic, and paleoseismic records of past earthquakes. Another, but slow process for large events, is to use them to make predictions about future earthquake occurrence and to evaluate how well the predictions match what occurs. A final approach is to compare the results of many varied earthquake

simulators to determine the extent to which the results depend on the details of the approaches and assumptions made by each simulator.

Five independently developed simulators, capable of running simulations on complicated geometries containing multiple faults, are in use by some of the authors of this abstract. Although similar in their overall purpose and design, these simulators differ from one another widely in their details in many important ways. They require as input for each fault element a value for the average slip rate as well as a value for friction parameters or stress reduction due to slip. They share the use of the boundary element method to compute stress transfer between elements. None use dynamic stress transfer by seismic waves. A notable difference is the assumption different simulators make about the constitutive properties of the faults.

Our project is designed to allow comparisons among the simulators and between the simulators and past earthquake history. The project uses realistic fault geometies and slip rates taken from California. In order to make as close comparisons between the simulators as possible we have developed shared data formats for both input and output and a growing set of tools that can be used to make statistical comparisons between the simulator outputs. To date all five simulators have run a Northern California fault model and are in various stages of working on an All California fault model. The plan in the near future is to run them on the UCERF2 fault model. Initial comparisons show significant differences among the simulators and some differences from observed earthquake statistics. However, it is too early in the process to infer too much from these results. For example, the differences in how each simulator treats fault friction means that they may each need to use values for the assumed stress drops that are better tuned to their approach than are the common values used in the first comparison.

HIGH-FREQUENCY SOURCE PROPERTIES OF THE 2010 M 7.2 SIERRA EL MAYOR EARTHQUAKE FROM LOCAL, REGIONAL, AND TELESEISMIC DATA (2-145)
T. Uchide and P.M. Shearer

The 2010 M 7.2 Sierra El Mayor earthquake was recorded by a wealth of seismic instrumentation at a variety of distances from the event, providing an opportunity to test new analysis methods and to reconcile different constraints on earthquake rupture properties. Here we focus on high-frequency radiation from the event by examining U.S. and Mexican strong motion records, USArray records at regional distances, and teleseismic records from the Global Seismic Network (GSN) and the Japanese Hi-Net array.

Comparisons of Hi-Net and GSN records of the mainshock P wave to M 5–5.7 calibration events in the same region show that the earthquake lasted at least 40 s and that its strongest energy was radiated about 25 s to 35 s after the mainshock origin time. We perform deconvolution experiments using the smaller event records to estimate the high-frequency source-time function of the mainshock. Preliminary results obtained by cross-correlation analysis of the Hi-Net P waves suggest that the large burst of energy at about 30 s was generated near a point about 25 km northwest of the hypocenter. Analysis of the USArray dataset is complicated by the rapidly changing nature of regional phase arrivals, but preliminary analysis of Pn arrivals indicates a large secondary source of energy about 25 s after the first arrivals.

Polarization analysis applied to the initial P-wave in regional strong motion and broadband data can be used to determine approximate origin points for the mainshock source energy. The horizontal components are often slightly rotated, therefore they can be calibrated by the polarization analysis using regional and teleseismic data. So far attempts to resolve rupture directivity using polarization analysis have proven inconclusive.

FLOOR ACCELERATIONS IN HIGH-RISE BUILDINGS UNDER GROUND MOTIONS FROM MODERATE EARTHQUAKES (1-041)
S.R. Uma

Large earthquakes cause damage to buildings and to non-structural components within the buildings, with a larger proportion of loss from the latter. However, under small to moderate earthquakes, buildings that are expected to sustain only minimal structural damage could potentially become unsuitable for occupancy due to extensive damage to non-structural components including building services. Since the majority of non-structural components and contents are sensitive to acceleration (for example, suspended ceilings, electrical and mechanical services mounted on floors or ceilings), a great deal of attention has been given to estimating floor acceleration demands of buildings. Recent studies by Uma et al (as published in NZSEE Bulletin 2010), investigated the response of low and high-rise buildings under moderate earthquakes, and showed that the floor acceleration demands can be markedly high during elastic or near inelastic response of the building, impairing the functionality of non-structural components.

The objective of the work is to investigate floor acceleration demands in tall (10 to 30 storeys) buildings under synthetic ground motions. Building models of 12 and 20 storeys developed by Haselton et al., as a part

of PEER study in 2007, are used for this purpose. In this study, two scenario events are considered to generate synthetic ground motions: (i) Wellington fault event with Mw 7.2; and (ii) Northridge event with Mw 6.7. The broadband synthetics for the scenarios are generated by combining the low-frequency (LF, <~1Hz) finite-difference synthetics with high-frequency (HF, >~1Hz) scattering operators using the hybrid method as reported by Mai and Olsen in BSSA (2009). Floor responses from the above two scenarios are compared.

The work is ongoing. First, low frequency synthetic records from Wellington Fault event (Mw:7.2) are used to generate building responses. Results on structural responses including the distribution of inter-storey drift ratio, residual displacements and spatial distribution of floor acceleration demands due to near fault ground motions with forward directivity and fling effects on high-rise buildings will be presented. Later, effect of broadband synthetic ground motions on building responses will be studied.

THE EFFECT OF PARTICLE ANGULARITY ON THE TRANSITION TO INERTIAL GRANULAR FLOW (2-043)
N.J. van der Elst and E.E. Brodsky

Natural fault zones are filled with granular gouge and are surrounded by granulated damage zones. These granular structures control the strength of the fault and add a degree of complexity to earthquake behavior that may not be captured by planar frictional models. In particular, granular phenomena may explain the susceptibility of faults to triggering by seismic waves, which is not predicted by bare rock frictional experiments. Understanding the implications of granular rheology for the earthquake nucleation process requires a constitutive law for granular flow in the transition from quasi-static to inertial flow regimes, but this transition remains poorly understood. This difficulty arises in part because stresses in granular media are supported by highly heterogeneous networks of grains rather than by simple inter-granular friction. This results in wide variation in rheology for different packing densities, shear rates, and particle characteristics. Most existing theoretical and experimental work on this subject has been focused on the behavior of idealized spherical particles, however, given the complexity of grain interactions, these studies may not be entirely relevant for natural gouges. Here we explore the effect of particle angularity on the transition from quasi-static to intertial flow, using a torsional rheometer at low confining pressures (< 100kPa). We find a shear-rate dependent compaction in the transitional regime that is not observed for smooth or spherical particles, and interpret this behavior in terms of vibration-induced particle reorientation within force chains.

CASCADIA TREMOR INSPECTED WITH THE EARTHSCOPE ARRAY OF ARRAYS (2-090)
J.E. Vidale

Seeking the most intimate details of tremor activity in Cascadia, we installed eight small-aperture seismic arrays in northern Washington in summer 2009. The AoA surrounds a particularly tremor-active region of the Cascadia megathrust, including the area that we previously imaged with a single array in 2008 [Ghosh et al., GRL, 2009, 2010]. Each array consists of 10-20 three-component sensors recording continuously for the year. During the Episodic Tremor and Slip event in August 2010, each array has been augmented by 10 additional single-channel, vertical-component sensors. So far, we have cursorily examined tremor episodes in July 2009 and March 2010, tried to optimize and debug Matlab code, and bought many large hard drives.

We beamform to examine amplitude, slowness and back-azimuth of incident seismic waves from 2 to 15 Hz at each array. During tremor episodes, enough of the arrays show stable slowness, and azimuth over the tremor frequency band. Vertical components show P waves coherently up to 10 Hz and higher, and horizontal components show S waves up to 6 Hz or so, each with their appropriate slowness. Compared to a conventional envelope cross-correlation (ECC) method, our array analysis reveals significantly longer duration of tremor activity, including entire days that remain undetected by ECC. Exploratory perusal of array stacks indicates a complex pattern of tremor activity. Oftentimes, multiple lively tremor sources appear to be active simultaneously. The array of arrays will provide a high-resolution image of tremor source during both ETS, and inter-ETS time period.

We hope to have some preliminary results of the most recent major ETS in Cascadia (August 2010), which is currently ongoing at the time of writing this abstract. Ken Creager is PI, Heidi Houston and I are co-PIs. Steve Malone, Abhi Ghosh and Justin Sweet and several others are actually doing the work.

ANTICIPATED ARREST: INSUFFICIENT CONDITIONS FOR CONTINUED DYNAMIC PROPAGATION OF A SLIP-WEAKENING RUPTURE NUCLEATED BY LOCALIZED INCREASE OF PORE-PRESSURE. (2-036)
R.C. Viesca-Falguières and J.R. Rice

The early earthquake source is a debated issue, particularly whether larger earthquakes originate from larger asperities or whether earthquakes start similarly and their ultimate size is determined by the favorable or unfavorable conditions of heterogeneous stress, pore pressures, and frictional properties. The former is

supported by the reported scaling of the dominant period in an early window of seismic data with final magnitude (e.g., Allen and Kanamori, Science 2003). However, recent studies of the cumulative moment release for earthquakes over several moment magnitudes indicate that growth may be similar (Uchide and Ide, in press JGR 2010). Such behavior is also suggested by the similar early moment rates of the dynamic rupture of big and small events in rate and state friction earthquake cycle models (e.g., Lapusta and Rice, JGR 2003).

Here we consider locally peaked pore pressure distributions and, for simplicity, a slip-weakening fault. We study the quasistatic enlargement of rupture under gradually increasing pore pressures. We show (1) that the pore pressure increase may reach a limit at which the quasistatically calculated crack growth rates become unbounded, corresponding to initiation of dynamic rupture, and (2) that the quasistatic solution at this limit may be nonunique, so that another equilibrium crack length and slip distribution exists which will generally be stable, and the actual dynamic rupture may arrest in that configuration (or one close to it, given frictional inhibition against back-slip), as also shown by Garagash and Germanovich, (2010, priv. comm.). The conditions for (2) are characterized in terms of the background shear stress relative to peak and residual strengths. That is, rupture arrest may occur if the residual friction is too high or if the background stress is too low. We show that the quasi-static predictions are generally comparable to results of elastodynamic initial-value problems, although the results need not agree when the other equilibrium crack length and slip distribution is also near to a configuration at which stability is lost.

Essentially, these results illustrate that two ruptures which have similar nucleation can have very different subsequent extents of propagation, depending on the distribution of pre-stress at positions lying outside the nucleation zone.

INFRASONIC OBSERVATIONS OF GROUND SHAKING ALONG THE 2010 MW 7.2 EL MAYOR RUPTURE: A NEW TOOL FOR CREATING GROUND SHAKING INTENSITY MAPS? (1-051)
K.T. Walker and C. de Groot-Hedlin

The Mw 7.2 El Mayor earthquake in northeast Baja California generated seismic waves that were felt for up to 90 seconds throughout southern California and northern Baja. The locations of the epicenter, aftershocks, and surface rupture suggest that the rupture was not focused at one specific location, but initiated near El Mayor, Mexico and extended northwest for roughly 75 km through the U.S. border. We analyze infrasound and seismic data recorded by three arrays and show that the surface shaking in the vicinity of the rupture also generated infrasound that was detected at least 200 km away to the north and west of the epicentral region, despite winds from the west that only favor eastward propagation. Frequency domain beamforming of infrasound array signals recorded by an array near San Diego (MRIAR) shows a time progression of signal back azimuth that spans the entire rupture length. Ray trace modeling using 4-D atmospheric velocity models suggests that the observed infrasound signals refracted in the thermosphere. The signals have frequencies from 1 to 12 Hz, which is rather high given the level of thermospheric attenuation predicted by traditional models. A secondary infrasound signal that arrived before the epicentral infrasound at MRIAR appears to have originated from an infrasonic radiator, located relatively close to the array, that was excited by the passing seismic disturbance.

Local strong-motion seismometer networks are perhaps the best technology to use for measuring surface shaking intensity. However, budgetary constraints can limit sensor availability and subsequent coverage needed to help with hazard response in many densely populated areas of the world. Regional broadband seismometer networks characterize what occurs inside the solid Earth extremely well. However, even when clipping is not an issue, their value in constraining the intensity of surface shaking that has occurred during a catastrophic earthquake is more limited. From the point of view of infrasound, the Earth's surface is simply a speaker. The fact that epicentral infrasound that radiated from the El Mayor rupture was well recorded and characterized by a regional infrasound array (1) near a noisy city, (2) during the daytime winds, and (3) upwind of the epicentral region suggests that regional infrasound array networks, when used with 4-D atmospheric velocity models, may be useful tools and augment existing technologies in the rapid construction of ground shaking intensity maps.

UNAVCO RESPONSE TO THE M7.2 EL MAYOR-CUCAPAH EARTHQUAKE (1-146)
C. Walls, A. Borsa, S. Lawrence, D. Mann, A. Bassett, M. Jackson, and K. Feaux

UNAVCO, a university consortium and NSF/NASA-funded geodesy facility, supports the research community in the study of significant geophysical events such as the recent M7.2 El Mayor-Cucapah earthquake. Resources include field engineering support; permanent, real-time/high rate, and campaign GPS deployment; data communications and power systems; borehole tiltmeter, strainmeter, and seismometer deployments; ground-based LiDAR measurements and airborne LiDAR project management; InSAR data acquisition; assistance with education and outreach activities; and data processing services.

The El Mayor – Cucapah earthquake occurred close to the Mexico – U.S. border, at the edge of the EarthScope – Plate Boundary Observatory (PBO's) footprint. UNAVCO was one of several community organizations to support event response, providing co-seismic observations from PBO's CGPS stations, borehole strainmeters and seismometers, the shipment of a Terrestrial LiDAR Scanner, and the acquisition of InSAR data through the UNAVCO-hosted WiNSAR consortium. PBO standard 15 second GPS data spanning the event for sites throughout southern California were recorded at 100% data completeness and were used to establish co-seismic displacement hours to days following the earthquake. High-rate (1-5 Hz) GPS downloads were completed with a 97% data return and used by community members to plot co-seismic displacement waveforms. In the months following the event 1Hz GPS data has been collected a disseminated for multiple airborne lidar and photography missions.

CGPS station P796, a deep-drilled braced monument, was constructed in San Luis, AZ along the border within 5 weeks of the event. In addition, UNAVCO participated in a successful University of Arizona-led proposal for the deployment of six continuous GPS stations for post-seismic observations. These stations will be installed, maintained and data analyzed by UNAVCO/PBO in coordination with CICESE, an Associate Member institution in Mexico. At present station reconnaissance is completed with 2 permits accepted and 4 remaining permits in process. Construction of 2 stations is pending at the time of this abstract submission. Details of UNAVCO's earthquake response will be presented.

NON-VOLCANIC TREMOR CHARACTERISTIC AND LOCATIONS IN ANZA REGION, SOUTHERN CALIFORNIA (2-100)

T-H. Wang and E.S. Cochran

Non-volcanic tremor (NVT) is a seismic signal that differs from general earthquakes because of its dominant shear wave energy and low frequency content. Recent observations also suggest NVT is widely triggered by passing teleseismic surfaces waves along several faults across California [e.g. Gomberg et al.,2008; Peng et al., 2008]. The Anza section of the San Jacinto Fault (SJF) is an ideal region for more detailed observation of tremor since there is a densely-spaced seismic network, including borehole stations. We use continuous waveform data, collected by 16 broadband stations of Southern California Seismic Network (SCSN) along with borehole stations from Plate Boundary Observatory (PBO) to search for NVT triggered by teleseismic surface waves. Preliminary observations from 2001 to 2003 of 41 large earthquakes (Mw >=7.5; distance >= 2000 km) suggest that only the Mw 7.8, 2002 Denali earthquake triggered detectable NVT.

More precise arrival-time measurements of each tremor burst are needed to locate the NVTs observed near Anza, California. We identified template NVT within the Denali-triggered NVT episode, using the cross-correlation method developed by Brown et al. [2008]. Recent studies suggest that NVT series consist of swarms of low frequency earthquakes (LFEs). The method by Brown et al. used moving windows to cross-correlate tremor waveforms recorded at different stations, in order to identify identical LFEs within the tremor series. The well-correlated pairs of waveform windows are cross-correlated twice to confirm the arrival times of template LFE. Our first cross-correlation resulted in 259 pairs with correlation coefficient with a correlation threshold over 4 times the mean absolute deviation (MAD). We ran a second cross-correlation and grouped similar correlation pairs into template families of NVTs. These templates help us better define the arrival times of tremor bursts within the triggered NVT episode. We will further locate the triggered NVT hypocenters using the earthquake location package, (GENLOC), provided by the commercial software, Antelope. These template families can then be used to explore the spatial and temporal pattern of triggered non-volcanic tremor near the Anza segment of the San Jacinto fault.

SORD AS A COMPUTATIONAL PLATFORM FOR EARTHQUAKE SIMULATION, SOURCE IMAGING, AND FULL 3D TOMOGRAPHY (2-137)

F. Wang, G.P. Ely, and T.H. Jordan

Earthquake simulations in 3D structures are currently being used for forward prediction of ground motions, imaging of sources, and structure refinement (full-3D tomography). The computational platform for such simulations requires the accurate location of sources and receivers within the computational grid; the flexibility to represent geological complexities, such as topography, non-planar faults, and other distorted surfaces; and the facility to calculate 3D Fréchet kernels for source and structural perturbations. We are adapting the Support Operator Rupture Dynamics (SORD) code for these purposes. SORD is an efficient numerical code developed by Ely, Day, and Minster (2008), which employs a structured but distortable mesh that can handle non-planar surfaces, such as topography. We represent point sources of arbitrary location as mesh-distributed sources of finite duration that match the travel-time and amplitude centroids of radiated waves; similarly, we represent receivers as centroid-preserving summations on a distributed mesh. We compute synthetic seismograms for a 3D reference model of Southern California that includes topography and spherical geometry of the Earth and compare the travel-times and amplitudes with those computed for 3D Cartesian-mesh models, such as the "squashed topography" approximation in common use, and we show the differences can be significant in tomographic inversions. We use SORD and scattering-integral

method (Chen et. al. 2007) to calculate 3D structural (Fréchet) kernels, and illustrate their use in obtaining a physical understanding of seismic wave interference, excitation, and amplification in sedimentary basins, such as Los Angeles basin.

STANDARD ERRORS OF PARAMETER ESTIMATES AND MISSING LINKS IN EARTHQUAKE CLUSTERING MODELS (1-128)
Q. Wang, D. Jackson, F.P. Schoenberg, and J. Zhuang

Point process models like the Epidemic-type Aftershock Sequence (ETAS) model have been widely used to analyze and describe seismic catalogs and to perform short-term forecasting. We use simulations to explore the accuracy of conventional standard error estimates based on the Hessian matrix of the log-likelihood function of the ETAS model. We show that such error estimates from the Hessian matrix are not accurate. Many clustering models imply two kinds of earthquakes: spontaneous ones and those triggered by previous earthquakes. The pair-wise links from earlier to later earthquakes control the estimates of the clustering parameters. However, earthquake catalogs are limited in time, space, and magnitude, so that triggers of some cataloged earthquakes may be unknown. Thus some links are unrecognized and some triggered events appear spontaneous. Here we present a method for identifying such earthquakes and reducing the bias from missing links. We treat earthquakes probably affected by missing links as potential triggers, but we exclude them in evaluating modeled effects. We use an Epidemic-type Aftershock Sequence (ETAS) model to examine specifics. The most affected parameter is the proportion of spontaneous earthquakes. The most important missing links apparently follow earthquakes below the magnitude threshold, before the start, and outside the spatial boundaries of the catalog, in that order.

RUPTURE DIRECTIVITY OF MICRO-EARTHQUAKES ON THE SAN ANDREAS FAULT FROM SPECTRAL RATIO INVERSION (2-045)
E. Wang and A. Rubin

Earthquakes often occur on faults separating materials with different elastic properties (e.g. plate boundaries). On theoretical grounds, it is expected that earthquakes on such bimaterial interfaces might have a preferential rupture propagation direction, that being the direction of motion of the more compliant material. The goal of this study is to determine whether a large sample of natural earthquakes on a bimaterial interface exhibits this tendency. Since the creeping section of San Andreas fault has a large across-fault velocity contrast and has produced thousands of micro-earthquakes over the last few decades, the rupture directions of ~3000 magnitude 0.8~3.0 earthquakes were studied using spectral ratio analysis. The spectral ratios of all earthquake pairs in spatially defined clusters were fitted with synthetic spectral ratios at qualified stations. The synthetics were computed from a simple moving point source model in which each modeled earthquake has four parameters: two rupture lengths (one to the SE and one to the NW) and their propagation velocities. The resolution of rupture directivity increases with event size, such that most of the 1105 events larger than ~70 m appear to be reasonably well resolved. The inversion results suggest that a large proportion of the well-resolved events are roughly bilateral, although more than 75% of the 200 strongly unilateral events (those where the long rupture length is more than twice the shorter) rupture to the SE, consistent with the theoretical prediction. For those rupture halves that were large enough for the propagation speed to be somewhat resolved, that speed was greater by perhaps 10% for those halves propagating to the SE, which is also consistent with numerical simulations. We also found that events with nearby foreshocks within several hours tend to rupture away from those foreshocks, whether to the NW or to the SE, indicating that rupture directivity is influenced by more than just the material contrast.

PARTICLE SIZE ANALYSIS OF DAMAGE TEXTURES IN FAULT ZONE ROCKS (2-049)
N. Wechsler, J.S. Chester, T.K. Rockwell, and Y. Ben-Zion

To determine the character and origin of pulverized granitic rocks outcropping along the southern San Andreas Fault (SAF), we collected a 42 meter-deep core adjacent to the main strand of the fault near Little Rock, CA. Extensive outcrops of granitic rock displaying varying degrees of damage up to a few hundreds of meters from the fault's primary active strand are exposed at the Little Rock site. The cored section is composed of pulverized granites and granodiorites, and is cut by numerous mesoscopic secondary shears. We have characterized the composition, mesoscale and microscale structure, and particle size distribution (PSD) of the cored section using scanning electron microscopy and elemental mapping. Two distinct fault rock types are present: pulverized rocks characterized by extensive, opening-mode microscale fractures, and cataclasites. The pulverized regions are composed of large host-rock crystals that are fractured to produce angular particles ranging from 10-100 microns in diameter. The fractured particles display optical continuity and a high density of fluid inclusion trails suggesting multiple episodes of fracture and healing. The cataclastic regions display smaller (0.5-10 microns) and more rounded grains, greater clay content, and sometimes more than one stage of cementation and shear. The magnitude of shear deformation is heterogeneous. Both damage textures have a PSD that approximates a power-law with exponent-values similar to those of fault rocks produced in experiments and others found in nature. A break in slope is

observed around 2-5 microns in the cataclastic regions only, possibly due to a difference in particle break-up processes at the smallest scale, which we attribute to chemical alteration in these zones. In the pulverized regions, a change in exponent is observed in the coarse fraction, and particle shape analysis shows that the coarse fraction PSD is affected by mineralogy, where breaking along cleavage planes produces more equant particles. The PSDs documented here are mostly consistent with the model of a two-stage fragmentation process in which initial rupturing produces the pulverized textures, and further particle comminution occurs by slip, attrition, shearing or grinding, producing cataclastic textures. Non-self-similar processes can affect the PSD and the particle shape, such as fracture along cleavage and alteration to clay minerals.

SUPERFICIAL SIMPLICITY OF THE 2010 MW 7.2 EL MAYOR-CUCAPAH EARTHQUAKE OF BAJA CALIFORNIA (2-037)
S. Wei, E. Fielding, S. Leprince, A. Sladen, J-P. Avouac, D.V. Helmberger, E. Hauksson, R. Chu, M. Simons, K. Hudnut, T. Herring, and R. Briggs

Major earthquakes can have moment tensors that differ significantly from predictions based on a single planar elastic shear-dislocation. A recent example is the 2010 El Mayor-Cucapah earthquake which ruptured a 120 km straight fault trace, extending the Elsinore-Laguna Salada fault system to the Gulf of California. The sequence was initiated about 15 s prior to the main fault rupture by a moderate normal event along a pull-apart-basin. Although the surface trace is nearly linear, the event involved fault segments with >5 km jogs at depth where the rupture found its way through a complex set of preexisting normal and strike-slip fault segments including undiscovered faults beneath the Colorado River Delta. The inferred complexity of the subsurface fault geometry and the distribution of slip orientation accounts for the large non-double-couple component of the moment tensor.

SLIP ON FAULTS IN THE IMPERIAL VALLEY TRIGGERED BY THE 4 APRIL 2010 MW 7.2 EL MAJOR EARTHQUAKE (1-108)
M. Wei, D. Sandwell, Y. Fialko, and R. Bilham

Radar interferometry (InSAR) and field measurements reveal surface slip on multiple faults in the Imperial Valley triggered by the 2010 Baja M7.2 earthquake. Co-seismic offsets occurred on the San Andreas, Superstition Hills, Imperial, Elmore Ranch, Wienert, Coyote Creek, Elsinore, Yuha Wells, and several minor faults near the town of Ocotillo at the northern end of the mainshock rupture. We documented right-lateral slip (< 40 mm) on northwest trending faults and left-lateral slip (< 40 mm) on southwest trending faults. Slip occurred on 15-km- and 20-km-long segments of the San Andreas Fault in the Mecca Hills (≤ 50 mm) and Durmid Hill (≤ 10 mm) respectively, and 25 km of the Superstition Hills Fault (≤ 37 mm). Field measurements of slip on the Superstition Hills Fault agree with InSAR and creepmeter measurements to within a few millimeters. Dislocation models of the InSAR data on the Superstition Hills Fault confirm that creep in this sequence, as in previous slip events, is confined to shallow depths (< 3 km).

FAULT CREEP OF THE SAN ANDREAS FAULT NEAR THE PAINTED CANYON REVEALED BY GPS SURVEYS (1-156)
M. Wei, D. Sandwell, Y. Bock, Y. Fialko, D. Agnew, X. Tong, and B. Crowell

It is important to establish the style of deformation along the San Andreas Fault since vertical slip could be related to ground water extraction [Fialko, 2006] whereas horizontal deformation is more likely related to shallow strike-slip fault motion [Lyons and Sandwell, 2003]. Previous InSAR data were acquired primarily from descending orbits, so it was not possible to distinguish between vertical and horizontal motion. In 19 Feb 2007 and 19 Feb 2010, we surveyed ~50 GPS benchmarks across the San Andreas Fault at the Painted Canyon, Salton Trough. Most benchmarks are 30 meters apart. GPS data show about 1 cm shallow creep near the location and is consistent with previous estimation of shallow creep rate of 3 mm/yr [Louie et al., 1985; Lyons and Sandwell, 2003]. Our result supports that creep on the Southern San Andreas Fault is mainly horizontal between 2007 and 2010. The slip direction on the SAF over a longer time interval that includes multiple creep events as well as secular creep can be resolved from the analysis of all the ENVISAT data collected in this area over the last 7 years.

CHILEAN EARTHQUAKE RECONNAISSANCE: LESSONS LEARNED BY THE JULY 2010 AMERICAN RED CROSS DELEGATION (1-090)
D.A. Weiser

In July 2010, the American Red Cross (ARC) sent a delegation of 20 experts in disaster response to learn lessons from the Chilean preparation, response, and recovery from the February 27, 2010 M8.8 earthquake and resulting tsunami. We met with key players and affected citizens in the cities of Santiago, Talca, Constitución, Cauquenes, Concepción, Talachauano, and Tumbés. Each of these areas was affected by the earthquake and tsunami; the amount of damage, however, differed greatly. The earthquake rupture plane was offshore and did not extend onshore. Only one town, Constitución, experienced MMI IX shaking. The second largest of city in Chile, Concepción, experienced MMI VIII shaking, while the capital, Santiago,

experienced MMI VI shaking. Thus, three quarters of the country's population was exposed to at least MMI VI shaking, leading to substantial economic losses (30 billion USD) totaling 17% of Chile's GDP.

Our delegation's findings are consistent with the lessons learned from many other major disasters, including challenges from extensive communications failures, inadequate plans, inadequate pre-disaster coordination and slow or poor initial leadership by government officials. Chile performed well with respect to engineered buildings and lifeline systems. Few lifeline systems needed major structural repairs; communications and power supply were back online in some places within a few hours. Many of the communication lines within and between organizations were severed. This hampered recovery efforts and proved to be one of the biggest challenges for emergency responders. Surprisingly few fires were reported, given the size of the earthquake. A significant factor may have been the shutdown of the national electric grid during the early part of the earthquake shaking.

FACILITATING INTERACTIVE INFORMATION SHARING: SCEC INTERN EXPERIENCE (1-007)
K.B. Welch, T.H. Jordan, T.T. Huynh, R.M. de Groot, and J.S. Montes De Oca

SCEC Internships are constantly evolving with the creation of new products and advancements in research. These new deliverables require creditability and support as well as a place to be showcased. With the high turnover of information it is easy to lose information through time and distance. Thus, a framework is needed to capture information and products so that they can be shared with a distributive community.

A content management system is perfect for our use because it allows for a large number of people to contribute and share information. Users can quickly and easily access products and information and can contribute an assortment of content in an organized manner.

A framework was set up in 2009 for the Undergraduate Studies in Earthquake Information Technology (USEIT) internship. It continues to be developed and improved upon today for the Summer Undergraduate Research Experience (SURE) and Advancement of Cyberinfrastructure Careers through Earthquake System Science (ACCESS) internships. These websites allow for the coordination of productive interactions between interns, mentors and the entire SCEC Community.

EXAMINATION ON THE VARIATION OF THE RUPTURE VELOCITIES OF THE 2008 MW=7.9 WENCHUAN, CHINA, EARTHQUAKE (2-124)
Y-Y. Wen and K-F. Ma

The 12 May, 2008 Wenchuan earthquake (Mw=7.9) struck the eastern margin of the Tibetan Plateau in the vicinity of the Sichuan Basin. This great event caused a surface rupture extended laterally about 300 km and was followed by many moderate-size aftershocks in the following days. Because of the complex geological surroundings, the Longmen Shan region is composed of not only the typical thrust faults but also active dextral-slip structures. To retrieve the rupture characters of the 2008 Wenchuan earthquake, we used the empirical Green's function (EGF) deconvolution analysis of teleseismic waveforms to avoid the effect from complicated 3D velocity structure. As the EGF should be near the mainshock and has similar focal mechanism and propagation path, we used three aftershocks for teleseismic P-wave and Rayleigh waves deconvolution analysis. The deconvolved source characters (relative source time function, RSTF) suggested that the dominant rupture characters of thrust slip were in the first 35 sec, then, became strike-slip to the rest of fault rupture, which were consistent with the field investigation. For further understanding on the rupture processes, we then divided the fault into three segments according to the distinct pulses of the average source time function and field observation to obtain a slip model with various rupture velocities. Our inversion result showed that the initial rupture was almost purely thrust motion with a slow rupture velocity of about 1.7 km/s and speed up to 3.2 km/s on the second segment where two parallel faults ruptured simultaneously with largest slip observed in one of the fault, and then slow down to 2.4 km/s on the final strike-slip segment. Overall, the fault extended 305 km with an average rupture speed of 2.6 km/s. The variation in rupture velocity may imply variation in dynamic effects (such as fracture energy) along the fault.

RETROSPECTIVE EVALUATION OF THE FIVE-YEAR AND TEN-YEAR CSEP-ITALY EARTHQUAKE FORECASTS (1-133)
M.J. Werner, J.D. Zechar, W. Marzocchi, and S. Wiemer

On 1 August 2009, the global Collaboratory for the Study of Earthquake Predictability (CSEP) launched a prospective and comparative earthquake predictability experiment in Italy. The goal of the CSEP-Italy experiment is to test earthquake occurrence hypotheses that have been formalized as probabilistic earthquake forecasts over temporal scales that range from days to years. In the first round of forecast submissions, members of the CSEP-Italy Working Group presented eighteen five-year and ten-year earthquake forecasts to the European CSEP Testing Center at ETH Zurich. We considered the twelve time-independent earthquake forecasts among this set and evaluated them with respect to past seismicity data from two Italian earthquake catalogs. We present the results of tests that measure the consistency of the

forecasts with the past observations. Besides being an evaluation of the submitted time-independent forecasts, this exercise provided insight into a number of important issues in predictability experiments with regard to the specification of the forecasts, the performance of the tests, and the trade-off between the robustness of results and experiment duration.

BATHYMETRIC SURVEYS OF THE HMS BEAGLE AT SANTA MARIA ISLAND, CHILE, (37°S) AND THE SEISMIC CYCLE (1-142)
R.L. Wesson, D. Melnick, M. Cisternas, L. Ely, and M. Moreno

We report repeated bathymetric surveys before and after the February 27, 2010 Chilean megathrust earthquake at Santa María Island off the coast of south-central Chile. The island is located approximately 75 km landward of the Chile trench and about 12 km above the megathrust fault. The island was uplifted on February 20, 1835 by the Concepcion earthquake (~M 8.5) and again on February 27, 2010 Maule earthquake (M 8.8). Captain Robert FitzRoy and the HMS Beagle visited Santa María Island in late March-early April, 1835, less than six weeks after the 1835 earthquake and reported 2.4-3 m of uplift on the island, based primarily on his observations of elevated, newly dead, intratidal and subtidal shellfish attached to rocks. The 2010 earthquake produced similar effects. Rada Santa Maria, a bay off the southeastern coast of Santa Maria Island, was surveyed by the Beagle in 1835, soon after the coseismic uplift, using a lead line and pole. On January 13 and 15, 2010, we carried out a simple echo-sounder survey in the same bay. The bay has a smooth and very gently dipping bottom, an average depth of about 8 m, and dimensions of about 3 x 5 km. Comparison of our measured depths with those sounded in 1835, suggests subsidence of 1-2 m. After the February 27 earthquake, on March 23, we resurveyed the same region of the bay and found evidence of about 1.3 m of uplift, which is in good agreement with 1.4 m of coseismic uplift measured at a nearby survey GPS site. We present a sensitivity analysis of our bathymetric survey results to possible sources of error. A detailed 1804-vintage Spanish chart suggests that the elevation of the island at that time was very similar to its state in January 2010. Thus we have information that suggests a probable subsided island in 1804, coseismic uplift in 1835, progressive subsidence between 1835 and 2010, coseismic uplift again in 2010, and now the beginning of intraseismic subsidence from GPS data. This pattern of behavior is consistent with the model of locking the plate interface, the accumulation of inter-seismic strain, and coseismic release, in accord with current ideas about the seismic cycle.

BENCHMARKING PYLITH AGAINST ABAQUS FOR PROBLEMS INVOLVING FAULT FRICTION AND INELASTIC DEFORMATION (2-025)
C.A. Williams and S.M. Ellis

PyLith is a finite element code designed specifically for problems involving crustal deformation, and many of the existing code features have evolved in response to the priorities of the SCEC modeling community. Some of these features have been tested using problems for which there exist either analytical or semi-analytical solutions. Examples include the deformation induced by a fault in an elastic half-space, and the surface deformation resulting from repeated earthquakes on a strike-slip fault in an elastic layer overlying a linear viscoelastic half-space. Such tests are useful; however, as more complex features have been added to PyLith, there are few (if any) analytical solutions against which to compare the finite element solutions. These features generally involve nonlinear behavior, such as power-law and elastoplastic bulk rheologies, as well as fault friction and finite strain. These features are very important in realistic simulations of fault-related deformation in southern California, and it is critical that the implementation and accuracy of these features are verified.

As a first step in testing these new code features, we are developing a set of benchmark tests and comparing the results of PyLith against those of Abaqus, a commercial finite element code. The purpose of these initial benchmarks is to verify that the code features are properly implemented and that the results are accurate. We therefore focus on fairly simple problems, such as the formation of shear bands in a Drucker-Prager elastoplastic material and fault slip on a frictional fault within a viscoelastic medium. We also restrict our attention to quasi-static problems, as the dynamic aspects of PyLith are being tested separately against SCEC dynamic rupture benchmarks. As all aspects of PyLith are extensively tested and verified, the code should become even more useful for problems involving complex fault behavior and rheologies.

ON THE ACCURACY OF CVM4 AND CVMH-6.2 (2-004)
K. Withers, K.B. Olsen, P. Small, and P. Maechling

Small et al. (this volume) presented a new SCEC Community Velocity Toolkit (CVM-T) developed by the SCEC CME collaboration. An important part of CVM-T is the Automated Test Framework (ATF) with the purpose to, in a consistent and semi-automated fashion, estimate the accuracy of the SCEC CVMs in predicting ground motions. Such estimate is warranted in particular when updates to the CVMs are made, to test whether the updated velocity models produce an improved fit between synthetics and data. Here, we use a multi-metric goodness-of-fit measure (GOF, Olsen and Mayhew, SRL, 2010) to estimate the accuracy of

the SCEC CVM V.4 and CVM-H V6.2, by matching recorded data and synthetics produced by CVM-T for the 2008 Mw5.4 Chino Hills earthquake. Metrics used in the GOF estimates include PGA, PGV, PGD, response spectra, energy duration, cumulative energy, and Fourier spectra. We present GIS maps of the GOF estimates using various metrics for CVM-4 and CVM-H V6.2, as well as the difference in GOF for the two CVMs.

A GLOBAL CHARACTERIZATION OF PHYSICAL SEGMENTATION ALONG OCEANIC TRANSFORM FAULTS (2-061)
M.L. Wolfson and M.S. Boettcher

Wesnousky (2006) found that physical fault offsets of 3 - 4 km act as barriers to rupture propagation on continental strike-slip faults. Along oceanic transform faults (OTFs), step-overs, intra-transform spreading centers, and pull-apart basins can divide the fault system into a series of parallel or sub-parallel fault segments. We have characterized the segmentation of OTFs on a global scale and are investigating the effects of this segmentation on seismic behavior. The 1-arcmin Smith and Sandwell global seafloor topography dataset (v. 12.1), comprised of satellite altimetry data blended with depth estimates from ship-borne sonar, was used to measure physical parameters of 200 OTFs. For each OTF, fault length and distance from each endpoint to the nearest ridge discontinuity were measured. The 200 individual fault segments were classified into 101 single-segment faults and 34 multi-segment fault systems, each comprised of between 2 - 7 segments with offsets ≤ 50 km.

Utilizing only ridge-transform-ridge segments, we constructed scaling relations for seismic parameters. To ensure a uniform minimum resolution for our global dataset, where some regions are constrained only by satellite altimetry data, any two adjacent fault segments with an offset ≤ 20 km, were combined into a single segment. The resulting dataset included 155 fault segments. An earthquake catalog was then generated from the global Centroid Moment Tensor database for each individual fault segment. A half-space cooling model was used to calculate the thermal area of contact above the 600-degree isotherm using slip rates acquired from the GSRM plate velocity model. Following the analysis of Boettcher and Jordan (2004), maximum-likelihood estimation was used to determine the largest expected earthquake for fault segments grouped by thermal area. Scaling relations between thermal area and the largest expected earthquake, as well as the seismic coupling coefficient, were calculated. Initial results show no significant differences in the scaling relations derived for the more segmented dataset. Future analyses utilizing OTF structure delineated from higher resolution sonar data will provide additional insight into the underlying mechanics of fault slip on OTFs.

DYNAMIC TRIGGERING OF SHALLOW EARTHQUAKES NEAR BEIJING, CHINA (2-092)
C. Wu, Z. Peng, W. Wang, and Q. Chen

We perform a comprehensive analysis of dynamic triggering around the Babaoshan and Huangzhuang-Gaoliying faults near Beijing, China. The triggered earthquakes are identified as impulsive seismic arrivals with clear P- and S-waves in 5 Hz high-pass-filtered three-component velocity seismograms during the passage of large amplitude body and surface waves of large teleseismic events. We find that this region was repeatedly triggered by 4 earthquakes in East Asia, including the 2001 Mw7.8 Kunlun; 2003 Mw8.3 Tokachi-oki; 2004 Mw9.2 Sumatra; and 2008 Mw7.9 Wenchuan earthquakes. In most instances, the microearthquakes coincide with the first few cycles of the Love waves, and more are triggered during the large-amplitude Rayleigh waves. Such an instantaneous triggering by both the Love and Rayleigh waves is similar to recent observations of remotely triggered 'non-volcanic' tremor along major strike-slip faults and subduction zones, and can be explained by a simple Coulomb failure criterion. We are able to locate 5 of the earthquakes triggered by the Kunlun and Tokachi-oki earthquakes. These events occurred close to the Babaoshan and Huangzhuang-Gaoliying faults at shallow depth (< 5 km). We suggest that these events occur near the transition between the velocity strengthening and weakening zones in the top few kms of the crust, and are likely driven by relatively large dynamic stresses of few tens of KPa.

NONLINEAR GROUND MOTION AND TEMPORAL CHANGES OF SITE RESPONSE ASSOCIATED WITH MEDIUM-SIZE EARTHQUAKES IN JAPAN AND CALIFORNIA (1-068)
C. Wu, Z. Peng, and Y. Ben-Zion

We systematically analyze nonlinear effects and temporal changes of site response associated with medium-size earthquakes in Japan and California, using seismic data recorded by the Japanese Strong Motion Network KIK-Net, and the Southern California Earthquake Center (SCEC) Strong Motion Borehole Sites. We first apply a sliding-window spectral ratio technique to surface and borehole strong motion records at 6 sites in Japan, and stack results associated with different earthquakes that produce similar peak ground acceleration (PGA). In some cases we observe a weak coseismic drop in the peak frequency when the PGA is as small as ~20-30 gal, and near instantaneous recovery after the passage of the direct S waves. The percentage of drop in the peak frequency starts to increase with increasing PGA values. We also observe a coseismic drop in the peak spectral ratio for 2 sites. When the PGA is larger than ~60 gal to more than 100

gal, we observe considerably stronger drops of the peak frequencies followed by logarithmic recovery with time. The observed weak reductions of peak frequencies with near instantaneous recovery likely reflect nonlinear response with essentially fixed level of damage, while the larger drops followed by logarithmic recovery reflect the generation (and then recovery) of additional rock damage. The results indicate clearly that nonlinear site response may occur during medium-size earthquakes, and that the PGA threshold for in situ nonlinear behavior is lower than the previously thought value of ~100-200 gal.

The 2010/04/04 Mw7.2 El Mayor-Cucapah Earthquake in northern Baja California has triggered a widespread increase of moderate-size earthquakes in southern California that are well recorded by many SCEC borehole instruments. We are currently applying the sliding window spectral ratio technique to these newly available data. Our goal is to separate nonlinear site response that is associated with and without material damage and identify the onset of nonlinearity in southern California.

LONGBASE STRAINMETER MEASUREMENTS OF DEFORMATIONS AFTER THE CUCUPAH/EL-MAYOR EARTHQUAKE (1-147)
F.K. Wyatt and D.C. Agnew

The Cucupah/El-Mayor earthquake on 2010:094 (April 4, 2010) produced a rich dataset of continuous strain data from the longbase strainmeters around the Salton Trough. All the strainmeters recorded without interruption, but for these instruments the dynamic strains were so large that the the full coseismic offset cannot be determined, and there is 5 to 10 minute interval during which we do not have a reliable measure of strain. After this, the strainmeters give a continuous record of even small deformations: in all cases there are immediate strain changes at high rates. For the strains at Salton City, closest to the earthquake, the ratio of NS to EW strain is consistent with afterslip on the part of the earthquake rupture with the largest coseismic slip. At Durmid Hill, not much farther away but close to the San Andreas, the data suggest a combination of postseimic slip on the earthquake rupture surface and triggered slip on the San Andreas, the latter appearing both as a gradual change and as rapid steps similar to those observed on these strainmeters between 1997 and 2008. At Pinon Flat (PFO), all longbase instruments (three strainmeters and a tiltmeter) initially show postseismic strains that are roughly consistent, in size and shape, with their source being afterslip from the earthquake rupture. However the later strains do not fit this pattern; instead, the NS and EW show trends of about the same size but opposite sign, while the NW-SE recordings shows less change; we also observe a significant change in trend on the long fluid tiltmeter. These trends largely end by 2010:150. Slip on the San Jacinto fault would produce such strains; the PFO data suggest possible triggered deep slip on this fault.

OFF-FAULT YIELDING DURING DYNAMIC RUPTURES: DISTRIBUTION AND ORIENTATIONS (2-038)
S. Xu, Y. Ben-Zion, and J.-P. Ampuero

We use 2D spectral element code to simulate dynamic ruptures on a fault governed by slip- and velocity-weakening friction with off-fault yielding and possible elastic contrast across the fault. The off-fault yielding is implemented with Mohr-Coulomb plasticity, and a continuum brittle damage that accounts for dynamic changes of elastic properties in the yielding zones (Lyakhovsky et al., 1997). The studies attempt to clarify properties of dynamic ruptures and generated yielding zones for different off-fault rheologies, frictional laws, orientations of the maximum regional compressive stress relative to fault \Psi, values of the seismic S ratio and conditions representing different depth sections. In the current simulations, the damage rheology is used with parameters that prevent off-fault instabilities, leading to results that are generally similar to those obtained with plasticity. The location and extent of the yielding zone are found to depend on \Psi, seismic S ratio and the crack vs. pulse mode of rupture, in agreement with previous theoretical and numerical studies. The off-fault yielding zone is wide for conditions representing shallow depth and becomes progressively localized for conditions representing deeper sections. The intensity of plasticity/damage for both rupture modes is enhanced for larger regional stress, but the width can be suppressed due to higher confining pressure and larger rock cohesion. The angle \Phi representing expected microcrack orientations is generally shallow (<45 degrees) on the compressional side and steep (>45 degrees) on the extensional side. The \Phi values depend also on the S ratio, conditions representing different depth sections, rupture speed, and existence of velocity contrast across the fault. The latter produces steeper angles of \Phi on the compliant side compared to the stiffer side for situations representing the same type (extension or compression) of quadrant.

STOCHASTIC MODEL FOR EARTHQUAKE GROUND MOTIONS USING WAVELET PACKETS (1-059)
Y. Yamamoto and J.W. Baker

For performance-based design, non-linear dynamic structural analysis for various types of input ground motions is required.

Since the number of ground motion recordings is limited for such analysis, synthetic ground motions could be used as additional inputs. Here a stochastic ground motion model with time-frequency nonstationarity is

developed using wavelet packets. Our model is a statistics-based model for modeling ground motion recordings instead of modeling fault rupture and wave propagation in physics-based model. In our model, the wavelet packet transform is employed for analyzing and generating nonstationary time-series data because it can decompose the time-series data into the wavelet packets with constant resolutions in the time and frequency axis, and it can also reconstruct the time-series data from the wavelet packets. The time-frequency characteristics therefore can be modeled intuitively in the time-frequency domain using the wavelet packets. 12 parameters are sufficient to completely describe the time-frequency characteristics of a ground motion in our model, and are thus employed in order to determine the wavelet packets. These parameters can be computed from a specific target ground motion recording or regression analysis based on a large database of recordings.

The simulated ground motions reasonably match the target ground motion recordings in several respects including the elastic and inelastic spectral acceleration, duration, bandwidth, cumulative energy, and time-frequency nonstationarity. In addition, the median and log standard deviation of the spectral acceleration of the simulated ground motions (generated from the parameters from the regression analysis) match those of the published empirical ground motion prediction. These results suggest that the synthetic ground motions generated by our model can be used for the non-linear dynamic structural analysis as the input ground motions.

FAULTING STYLES OF EARTHQUAKE CLUSTERS IN SOUTHERN CALIFORNIA: IMPROVING THE HASH FOCAL MECHANISM METHOD (2-126)
W. Yang and E. Hauksson

We study the faulting styles of earthquake clusters that occurred in the Southern California region between 2000 and 2005. We use clusters identified in the LSH v1.12 relocated catalog and phase picks provided by the SCSN network. We filter the vertical component waveforms in the frequency band of [1 - 10] Hz for the station that recorded the maximum number of waveforms from events in each cluster. To reach a high level of accuracy, we use earthquake clusters satisfying waveforms cross-correlation coefficient values above 0.9 and require a minimum number of three events for each cluster. For each cluster, we apply the HASH method to calculate three sets of focal mechanisms using P-wave polarities, S/P amplitude ratios and both P-wave polarities and S/P amplitude ratios respectively. To calculate the S/P amplitude ratios, we use the waveform peak-to-peak amplitudes in [-0.5 - 1.5] second time windows related to the P and S arrivals after vector summation over three components. We compare the focal mechanism difference in each cluster for the three different approaches, and proposed an improved approach that could minimize the focal mechanism difference. Using the improved HASH method, we calculate faulting styles of earthquake clusters located in areas with different geophysical properties in southern California.

EVIDENCE FOR VERTICAL PARTITIONING OF STRIKE-SLIP AND COMPRESSIONAL TECTONICS FROM SEISMICITY, FOCAL MECHANISMS, AND STRESS DROPS IN THE EAST LOS ANGELES BASIN AREA, CALIFORNIA (1-088)
W. Yang and E. Hauksson

We analyzed earthquake data recorded over the past thirty years (1981 to 2010) in the east Los Angeles basin to determine the characteristics of the seismogenic zone. The seismicity is distributed along the Whittier fault, with the majority of earthquakes located adjacent to the south side, in the depth range from 0 to 9 km, with b-value of 1.1 ± 0.05 and mostly normal and strike-slip faulting. At depths from 9 to 12 km, the seismicity is scattered uniformly across the region, and the b-value is 1.0 ± 0.05 and all three faulting styles present. From 12 to 18 km depth, the seismicity is characterized by a few clusters striking north, with several moderate-sized mainshocks. Also in this depth range, the b-value is 0.78 ± 0.04 and the dominant faulting style is reverse. Inversion for the orientation of the regional stress field showed that the direction of maximum compressional stress rotates from N20°W at shallow depth to due north at the bottom of the seismogenic zone. The results of the P- wave source spectra inversion identified a similar pattern with stress drop generally increasing with depth from around 7 MPa at shallow depth (3 km) to around 53 MPa at the base of the seismogenic zone (17 km). These results that are consistent with existing geological models provide new evidence for the vertical partitioning of styles of deformation and state of stress.

STRESS-INDUCED UPPER CRUSTAL ANISOTROPY IN SOUTHERN CALIFORNIA (2-112)
Z. Yang, A. Sheehan, and P. Shearer

We use an automated method to analyze shear-wave splitting from local earthquakes recorded by the Southern California Seismic Network (SCSN) between 2000 and 2005. The observed fast directions of upper-crustal anisotropy are mostly consistent with the direction of maximum horizontal compression σHmax, suggesting that anisotropy in the top 20 km of crust under southern California is stress-induced anisotropy. At some stations, fast directions are aligned with the trends of regional faulting and local alignment of anisotropic bedrock. Delay times range widely from 0.02 s to 0.15 s. These upper-crustal anisotropy

observations, together with previous studies of SKS shear-wave splitting and receiver functions, show different mechanisms of anisotropy at different depths under southern California. Anisotropy in the upper crust and upper mantle appears to be in response to the current horizontal maximum compression σHmax, whereas lower crustal anisotropy may be caused by the anisotropic schist accreted during the subduction of Farallon plate, which is frozen in the lower crust. We also explore possible temporal variations in upper-crustal anisotropy associated with pre-earthquake stress changes or stress changes excited by surface waves of great earthquakes. However, we do not observe any clear temporal variations in fast directions or time delays.

FINITE FAULT CO-SEISMIC KINEMATIC AND POST-SEISMIC SLIP DISTRIBUTION MODEL OF THE 2009 MW 6.3 AQUILA EARTHQUAKE FROM JOINT-INVERSION OF STRONG MOTION, GPS, AND INSAR DATA (2-063)

T.E. Yano, G. Shao, Q. Liu, C. Ji, and R.J. Archuleta

April 6, 2009 Mw6.3 L'Aquila earthquake occurred in the central Apennines near the medieval town, L'Aquila. The L'Aquila area has been known as one of high seismic risk locations. Historical earthquakes affecting L'Aquila occurred in 1461, 1762, 1916, and 1958 (Rossi et al., 2005).

For near-source strong motion observations of normal faulting the 2009 has the best data set. Seventeen strong motion accelerographs are within 50km of the surface projection of the fault plane. Of these 10 are within 20 km, and five are above the fault plane. The highest accelerations occur for these five stations on the hanging wall with peak horizontal accelerations in the range of 347- 662 cm/s2 and peak velocities in the range of 32-42 cm/s. To understand the earthquake process, we have used the nonlinear inversion method of Ji et al. (2002) to jointly invert the strong motion data and static field measurements, such as GPS and InSAR, for two models: a co-seismic kinematic model and a post-seismic slip distribution. Based on several different inversions we settled on a fault with a dip of 50 degrees to the southwest. We use a strike of 140 degrees which is consistent with the InSAR and with the limited lineament of surface breakage. In our co-seismic model, the rupture initiates at a depth of 9.1 km and then primarily propagates updip and to southeast for more than 20 km with an average velocity of 2.0 km/s along strike and updip. The maximum slip, about 70 cm, occurs in two locations: one near the hypocenter and the other about 6 km southeast of hypocenter. The co-seismic moment is 2.9 x 10**18 Nm. In our post-seismic model, 40 cm slip appears updip from the hypocenter. The seismic moment of the post-seismic model is 1.2 x 10**18 Nm, about 40 % of the co-seismic moment.

SUBSURFACE EVIDENCE FOR THE PUENTE HILLS AND COMPTON-LOS ALAMITOS FAULTS IN SOUTH-CENTRAL LOS ANGELES (1-084)

R.S. Yeats and D.M. Verdugo

We analyzed well data in the vicinity of a deep exploration campaign in 1973-1975 by American Petrofina Exploration Co. to a maximum depth of 6,477 m (American Petrofina Core Hole 1), twice the depth of data from multichannel seismic profiles used in previous studies. The deeper control of the Compton-Los Alamitos (CLA) and Puente Hills reverse faults based on these wells provides evidence of reverse faulting based on repetition of strata on electric logs, abrupt changes of dipmeter-based attitudes, and offset of events on seismic profiles following Avalon Boulevard and Vermont Avenue. Structure contours on the Puente Hills fault are straightforward, whereas contours on the CLA fault are more complex. The presence of faulting at depth leads to the conclusion that the CLA and Puente Hills reverse faults change upward into fault-propagation folds rather than fault-bend folds. The CLA fault marks the northeastern boundary of a broad anticline, called here the Central Uplift anticline, cut along its crest by the right-lateral strike-slip Potrero fault in the vicinity of our study. Structure contours at depth confirm the observations of others that the CLA fault swings westward and steepens in dip toward the NIFZ south of Inglewood oil field. The presence of reverse-fault-plane solutions along the northern NIFZ and evidence for uplift along the CLA fault east of Long Beach and Seal Beach oil fields during the 1933 Long Beach earthquake support an interpretation of faulting along the Newport-Inglewood trend related to strain partitioning, indicating that the NIFZ might generate a Coalinga-type reverse fault as well as a strike-slip event similar to the 1933 earthquake.

A COMPOSITE SIMULATION OF SEISMICITY IN NORTHERN CALIFORNIA (2-154)

M.B. Yikilmaz, E.M. Heien, D.L. Turcotte, J.B. Rundle, and L.H. Kellogg

We generate synthetic catalogs of seismicity in northern California using a composite simulation. The basis of the simulation is the fault based "Virtual California" earthquake simulator. Back-slip velocities and mean recurrence intervals are specified on model strike-slip faults. A catalog of characteristic earthquakes is generated for a period of 100,000 years. These earthquakes are then used to drive the BASS (Branching Aftershock Sequence) model of aftershock occurrence. The BASS model is the self-similar limit of the ETAS (Epidemic Type Aftershock Sequence) model. Families of aftershocks are generated following each Virtual

California (VC) main shock. It is also necessary to generate background seismicity that is random time but spatially associated with the VC model faults. A visual simulation illustrates the resulting seismicity. We generate frequency-magnitude and recurrence interval statistics both regionally and fault specific. We compare our modeled rates of seismicity with observations.

STATISTICS OF A CHARACTERISTIC EARTHQUAKE CYCLE: PARKFIELD 1971 TO 2009 (2-113)
M.R. Yoder, D.L. Turcotte, and J.B. Rundle

The sequence of m≈6 earthquakes that have occurred on the Parkfield segment of the San Andreas fault are often considered the best example of "characteristic earthquakes." The last two of these earthquakes occurred on 28 June 1966 and 28 September 2004. To use the best quality seismic data, we will consider the period 28 June 1971 to 28 September 2009. We study seismicity in the region of aftershocks of the 2004 earthquake. The focus of our studies will be the validity of the Gutenberg-Richter (GR) hypothesis for earthquakes in this region for the period given above. Fitting the GR relation to all earthquakes during the period gives a=5.5 with b=1.0. Full GR scaling would require a=5.97 with b=1.0. Thus, only 34% of the earthquakes required for full GR scaling actually occurred.

CSEP-JAPAN: REPORT ON PROSPECTIVE EVALUATION TEST OF THE 3-MONTH TESTING CLASS (1-122)
S. Yokoi, K. Nanjo, H. Tsuruoka, N. Hirata, D. Schorlemmer, and F. Euchner

The Collaboratory for the Study of Earthquake Predictability (CSEP) is promoting earthquake predictability research by rigorous testing on earthquake forecast hypotheses. The CSEP developed standardized procedures for registering earthquake forecast models, conducting tests, and disseminating results. The underlying testing center software system was deployed in several institutions to host CSEP testing centers. Besides California, testing centers were installed in New Zealand and Europe to host prediction experiments for these regions. The Earthquake Research Institute, the University of Tokyo joined the CSEP and started the Japanese testing center called as CSEP-Japan. This testing center constitutes an open access to researchers contributing earthquake forecast models for applied to Japan. A total of 91 earthquake forecast models were submitted on the prospective experiment starting from 1 November 2009. The models are separated into 4 testing classes (1 day, 3 months, 1 year and 3 years) and 3 testing regions covering Japan, Japan mainland and Kanto. We evaluate the performance of the models in the official suite of tests defined by the CSEP. Here, we provide an overview of the CSEP-Japan and show the evaluation results of the 3-month models for prospectively forecasting earthquakes (4.0<=M<=9.0) that occurred in the mainland during the period from 1 November 2009 to 31 January 2010.

ARRA-FUNDED GEOTECHNICAL CHARACTERIZATION OF SEISMOGRAPHIC STATION SITES (1-066)
A. Yong, W. Leith, K. Stokoe, J. Diehl, A. Martin, and S. Jack

As part of the 2009 American Recovery and Reinvestment Act (ARRA), the USGS received funding to help support research capabilities, as well as improve and upgrade facilities in the bureau. Through this effort, the USGS contracted a consortium consisting of principals from academia and commerce to perform geotechnical site characterization at 189 seismographic station sites—185 in California and four in the central U.S. In this pilot project of the Advanced National Seismic System (ANSS), site characterizations will be conducted at: 130 Southern California Seismographic Network (SCSN), 25 California Geological Survey (CGS), 30 Northern California Seismographic Network (NCSN), and four Central U.S. (CEUS) sites. Each site investigation, involving passive and active surface-wave techniques, includes one or more of established approaches such as the horizontal-to-vertical spectral ratio, 2-D array microtremor, 1-D refraction microtremor (ReMi), spectral analysis of surface wave (SASW), and multi-channel analysis of surface wave (MASW) methods. From this multi-method approach, we determine Vs (shear-wave velocity) profiles and the calculated Vs30 (the average shear-wave velocity in the upper 30 meters depth) for each site. In general, preliminary results based on field reports indicate observed records match expected values for surficial geologic conditions. Unexpected results are typically attributable to inaccurate or coarse map information and alternative explanations are verified through interpretations of local geologic structure observed during field investigations. For example, we find map-based geology to be consistent with observed records at SCSN station CI.PLS, but not the case for CI.CWC, where inaccurate map information are at odds with our recorded velocities. At CI.TIN (near edge of basalt outcrop) and NCSN station NC.MMLB (on rhyolite outcrop), the records observed in the shallow surface do not match expected rock values. Our pilot project ends September, 2011 and an USGS Open File Report describing geology, Vs profile and the calculated Vs30 for each site is expected to follow shortly after.

PRODUCTS AND SERVICES AVAILABLE FROM THE SOUTHERN CALIFORNIA EARTHQUAKE DATA CENTER (SCEDC) AND THE SOUTHERN CALIFORNIA SEISMIC NETWORK (SCSN) (2-117)
E. Yu, S.L. Chen, F. Chowdhury, A. Bhaskaran, S. Meisenhelter, K. Hutton, D. Given, E. Hauksson, and R. Clayton

Currently the SCEDC archives continuous and triggered data from nearly 5000 data channels from 425 SCSN recorded stations, processing and archiving an average of 12,000 earthquakes each year. The SCEDC provides public access to these earthquake parametric and waveform data through its website www.data.scec.org and through client applications such as STP and DHI. This poster will describe the most significant developments at the SCEDC in the past year.

Updated hardware:

- The SCEDC has more than doubled its waveform file storage capacity by migrating to 2 TB disks.

New data holdings:

- Waveform data: Beginning Jan 1, 2010 the SCEDC began continuously archiving all high-sample-rate strong-motion channels. All seismic channels recorded by SCSN are now continuously archived and available at SCEDC.
- Portable data from El Mayor Cucapah 7.2 sequence: Seismic waveforms from portable stations installed by SCEC researchers (contributed by Elizabeth Cochran, Jamie Steidl, and Octavio Lazaro-Mancilla) have been added to the archive and are accessible through STP either as continuous data or associated with events in the SCEDC earthquake catalog. This additional data will help SCSN analysts and SCEC researchers improve event locations from the sequence.
- Real time GPS solutions from El Mayor Cucapah 7.2 event: Three component 1Hz seismograms of California Real-Time Network (CRTN) GPS stations, from the El Mayor-Cucapah earthquake are available in SAC format at the SCEDC. These time series were created by Brendan Crowell, Yehuda Bock, the project PI, and Mindy Squibb at SOPAC using data from the CRTN. The El Mayor-Cucapah earthquake demonstrated definitively the power of real-time high-rate GPS data: they measure dynamic displacements directly, they do not clip and they are also able to detect the permanent (coseismic) surface deformation.

- Triggered data from the Quake Catcher Network (QCN) and Community Seismic Network (CSN): The SCEDC in cooperation with QCN and CSN is exploring ways to archive and distribute data from high density low cost networks. As a starting point the SCEDC will store a dataset from QCN and CSN and distribute it through a separate STP client

New archival methods:

- The SCEDC is exploring the feasibility of archiving and distributing waveform data using cloud computing such as Google Apps. A month of continuous data from the SCEDC archive will be stored in Google Apps and a client developed to access it in a manner similar to STP.

PALEOSEISMOLOGY AND SLIP RATE OF THE SAN GORGONIO PASS FAULT ZONE: TESTING THE LIKELIHOOD OF THROUGH GOING SAN ANDREAS RUPTURES (1-112)
D. Yule, P. McBurnett, and S. Ramzan

Models for the maximum earthquake on the southernmost San Andreas fault hinge upon interpreting the structural complexity and diffuse seismicity of the San Gorgonio Pass (SGP) region. Here strike-slip segments to the north and south intersect with a thrust-dominated fault system, the SGP fault zone. Competing hypotheses assert that the thrust system either prevents or allows a through going San Andreas rupture in the Pass. The 'barrier' model forecasts < M 7.5 earthquakes on either side of the Pass whereas the 'enabler' model envisions a fault system that can generate an ~ M 7.8 rupture that reaches from the Salton Sea to the Mojave Desert. Understanding the behavior of the SGP fault zone can therefore test the likelihood of a San Andreas event that ruptures through SGP. Conflicting data exist from the SGP fault zone and include evidence for two ruptures in the last 700 yrs and a slip rate of 5-7 mm/yr near Cabezon, and evidence for one rupture in the last 3000 yrs and a slip rate of ~1 mm/yr at Millard Canyon. It is difficult to reconcile these different interpretations just 2 km apart from one another. The single detrital radiocarbon age date from the southern splay at Millard Canyon may be reworked from much older terrace deposits nearby. Alternatively the southern splay may be a minor player with most of the slip carried by the northern fault splay at Millard Canyon. We received SCEC funding in 2010 to study the SGP fault zone in Millard Canyon. We recently excavated 60 m-long trenches across a 2.5 m-high scarp of the northern splay. One trench shows a 0.5 - 1 m thick A soil horizon above folded cobble and boulder gravels. A second trench exposes a soil developed atop interstratified sands and fine gravels; these units contain abundant detrital charcoal fragments and show folding and faulting that reflect the surface deformation. Though we have yet to complete detailed trench

logs, the deformed units appear to show growth strata relations that may indicate a multiple event record at the site. Our work plan later this fall includes the cleaning of a natural exposure across the southern scarp at Millard Canyon, pending final approval from landowners, where we hope to log the exposure and recollect charcoal from strata that produced the ~3000 yr age from a study conducted 25 yrs ago. Once completed, our trench logs and charcoal samples should provide new insights on how the SGP fault zone behaves.

ATMOSPHERIC ERROR BUDGET IN INSAR DATA AND ITS IMPLICATION TO DESDYNI MISSION FOR CRUSTAL DEFORMATION (1-150)
S. Yun, M. Chaubell, E. Fielding, Z. Liu, S. Hensley, F. Webb, and P. Rosen

Spatial variation of differential tropospheric delay in interferograms has been known to limit the accuracy of InSAR data for deformation study. The turbulence mixing of the radar signal delay, mainly affected by water vapor content variation, has most energy in long wavelength component. Since the ground deformation often shows strong signal in large scale as well, it is difficult to distinguish the deformation signal from the atmospheric noise. Thus the quantitative analysis on the atmospheric error budget should be implemented at a wide range of distance scale. The derived covariance function and structure function are useful for geophysical modeling and DESDynI (NASA's future L-band InSAR mission) requirements design, respectively. In this study, we characterize the tropospheric delay variation observed in InSAR data in Los Angeles basin area. We used 139 interferometric phase difference maps to estimate the power spectral density functions, covariance functions, and structure functions of the zenith wet delay from the selected area for the time period from 2002/10/28 to 2010/02/27. Then we compare them with a simulated interferometric phase difference map from a magnitude 5.4 from a strike slip fault buried at a depth of 1 km. In this case, we observe that 71 % of data values can be attributed to earthquake deformation with 95 % confidence level. We are testing the usefulness of MODIS (Moderate Resolution Imaging Spectroradiometer) data, which has almost daily global coverage with 2330 km swath, for globally characterizing the atmospheric error budget, working with JPL's OSCAR (Online Services for Correcting Atmosphere in Radar) team.

SEISMIC CLUSTERING AND REGIONAL PHYSICAL PROPERTIES: A STATISTICAL ANALYSIS (1-040)
I. Zaliapin and Y. Ben-Zion

Discovering genuine spatio-temporal seismicity patterns that characterize local regions beyond the classical large-scale average patterns remains an extremely challenging problem. Of particular importance are patterns that can be related to key physical processes associated with specific properties of faults and the lithosphere. This study addresses two related topics: (i) Non-parametric identification of statistically significant seismic clusters, and (ii) Establishing correlations between seismic cluster patterns and regional physical properties. The first issue is solved using a cluster detection technique of Zaliapin et al. (2008), based on bimodality of the 2-D joint distribution of normalized space and time distances between earthquakes. In the second topic we study two types of patterns. First, we examine the relations between symmetry properties of spatial earthquake patterns along various faults in CA and corresponding local velocity structure images. This is done to test the hypothesis that ruptures on bimaterial faults have statistically preferred propagation directions (e.g., Ben-Zion, 2001). The results indicate strong asymmetric patterns in early-time spatially-close aftershocks along large faults with prominent bimaterial interfaces (e.g., sections of the San Andreas fault), with enhanced activity in the directions predicted for the local velocity contrasts; and absence of significant asymmetry along most other faults. Second, we compare seismic productivity within statistically significant clusters in CA with heat flow and general rock type (crystalline vs. deep sedimentary basins), which serve as proxies for the effective viscosity of the crust (Ben-Zion and Lyakhovsky, 2006). We find that (i) relatively cold regions with crystalline rock in the seismogenic zone have high aftershock productivity and low foreshock productivity, and vice versa (ii) regions with high heat flow and deep sedimentary basins have increased foreshock activity and reduced aftershock productivity. The results demonstrate that seismicity patterns do not follow universal power law statistics in all space time domains. Assuming the observed asymmetric properties of seismicity reflect asymmetric properties of earthquake ruptures, and earthquake productivity reflects the local seismic potential of the crust, the discussed methodology and results can be used to develop refined estimates of seismic shaking hazard associated with individual fault zones and regions.

LIKELIHOOD-BASED TESTS FOR EVALUATING SPACE-RATE-MAGNITUDE EARTHQUAKE FORECASTS (1-131)
J.D. Zechar, M.C. Gerstenberger, and D.A. Rhoades

The five-year experiment of the Regional Earthquake Likelihood Models (RELM) working group was designed to compare several prospective forecasts of earthquake rates in latitude–longitude–magnitude bins in and around California. This forecast format is being used as a blueprint for many other earthquake predictability experiments around the world, and therefore it is important to consider how to evaluate the performance of such forecasts. Two tests that are currently used are based on the likelihood of the observed

distribution of earthquakes given a forecast; one test compares the binned space–rate–magnitude observation and forecast, and the other compares only the predicted and observed number of earthquakes. We propose two new tests that isolate the spatial and magnitude component, respectively, of a space–rate–magnitude forecast. For illustration, we consider the RELM forecasts and the distribution of earthquakes observed during the first half of the nearly complete RELM experiment. We show that a space–rate–magnitude forecast may appear to be consistent with the distribution of observed earthquakes despite the spatial forecast being inconsistent with the spatial distribution of observed earthquakes, and we suggest that these new tests should be used to provide increased detail in earthquake forecast evaluation. We also discuss the statistical power of each of the likelihood-based tests and mention the stability (with respect to earthquake catalog uncertainties) of results from the likelihood-based tests.

PRELIMINARY RESULTS FROM THE FIRST 4.5 YEARS OF THE REGIONAL EARTHQUAKE LIKELIHOOD MODELS EXPERIMENT (1-132)
J.D. Zechar, D. Schorlemmer, and M.J. Werner

One of the primary objectives of the Regional Earthquake Likelihood Models (RELM) working group was to formalize earthquake occurrence hypotheses in the form of prospective earthquake rate forecasts in California. RELM scientists developed more than a dozen five-year forecasts; they also outlined a performance evaluation method and provided a conceptual description of a Testing Center in which to perform predictability experiments. Subsequently, researchers working within the Collaboratory for the Study of Earthquake Predictability (CSEP) have begun implementing Testing Centers in different locations worldwide, and the RELM predictability experiment—a truly prospective earthquake prediction effort—is underway within the U.S. branch of CSEP. The experiment, designed to compare time-invariant five-year earthquake rate forecasts, is now approximately ninety percent complete (4.5 out of 5 years). Here, we present the forecasts under evaluation and the preliminary results of this unique experiment. We also discuss the sample of observed target earthquakes in the context of historical seismicity within the testing region.

A KINEMATIC FAULT NETWORK MODEL OF CRUSTAL DEFORMATION FOR CALIFORNIA AND ITS APPLICATION TO THE SEISMIC HAZARD ANALYSIS (2-018)
Y. Zeng, Z.-Y. Shen, and M. Petersen

We invert GPS observations to determine the slip rates on major faults in California based on a kinematic fault model of crustal deformation with geological slip rate constraints. Assuming an elastic half-space, we interpret secular surface deformation using a kinematic fault network model with each fault segment slipping beneath a locking depth. This model simulates both block-like deformation and elastic strain accumulation within each bounding block. Each fault segment is linked to its adjacent elements with slip continuity imposed at fault nodes or intersections. The GPS observations across California and its neighbors are obtained from the SCEC WGCEP project of California Crustal Motion Map version 1.0 and SCEC Crustal Motion Map 4.0. Our fault models are based on the SCEC UCERF 2.0 fault database, a previous southern California block model by Shen and Jackson, and the San Francisco Bay area block model by d'Alessio et al. Our inversion shows a slip rate ranging from 20 to 26 mm/yr for the northern San Andreas from the Santa Cruz Mountain to the Peninsula segment. Slip rates vary from 8 to 14 mm/yr along the Hayward to the Maacama segment, and from 17 to 6 mm/yr along the central Calaveras to West Napa. For the central California creeping section, we find a depth dependent slip rate with an average slip rate of 23 mm/yr across the upper 5 km and 30 mm/yr underneath. Slip rates range from 30 mm/yr along the Parkfield and central California creeping section of the San Andres to an average of 6 mm/yr on the San Bernardino Mountain segment. On the southern San Andreas, slip rates vary from 21 to 30 mm/yr from the Cochella Valley to the Imperial Valley, and from 7 to 16 mm/yr along the San Jacinto segments. The shortening rate across the greater Los Angeles region is consistent with the regional tectonics and crustal thickening in the area. We are now in the process of applying the result to seismic hazard evaluation. Overall the geodetic and geological derived hazard models are consistent with the current USGS hazard model for California.

SEISMIC HAZARD MAPS BASED ON MODELED SLIP RATE DATA AND GPS STRAIN RATE OBSERVATIONS (1-035)
Y. Zeng, Z.-K. Shen, and M. Petersen

In this study, we calculate the seismic hazard map for California and its neighbor states using fault sources with slip rates derived from GPS observations and areal gridded seismic shear sources based on a smoothed residual GPS strain rate map for the region. The GPS observations are from the SCEC WGCEP project of California Crustal Motion Map version 1.0 and the fault model is based on the SCEC UCERF 2.0 fault database. We interpret secular surface deformation using a kinematic fault network model with each fault segment slipping beneath a locking depth. This model simulates both block-like deformation and elastic strain accumulation within each bounding block. We then compute the strain rate for California and its neighbors analytically using Okada (1992) for this fault model. We also compute residual strain rates for all the GPS stations around California based on the difference between the observed GPS velocities and the fault

model predictions. We interpolate those residual strain rates to a uniform grid using a modified approach of Shen et al (1996). This approach introduces an azimuthal weighting scheme based on the area of the Voronoi cells determined for those GPS stations in addition to the Gaussian distance decay function and the GPS velocity error weighting. We then calculate the final residual strain rate map. The predicted strain rate map and the interpolated residual strain rate map were combined to form our final estimate of strain rate for the region. We then developed a preliminary seismic shear source map based on the smoothed residual GPS strain rate map using the Kostrov (1974) formulation to convert strain rate to earthquake recurrence rate. The final seismic hazard maps using the slip rate data obtained from inversion of the GPS data and the seismic shear sources based on the residual strain rate map are compared with the 2008 USGS national seismic hazard estimations.

RUPTURE PROCESS OF THE 2010 MW 7.3 EL MAYOR-CUCAPAH EARTHQUAKE (2-142)
X. Zhao, G. Shao, C. Ji, K.M. Larson, K.W. Hudnut, and T. Herring

We investigate the slip history of the 2010 Mw 7.3 El Mayor-Cucapah earthquake by jointly inverting near-field strong motion records and teleseismic broadband waves, together with GPS static observations and high rate GPS waveforms. We use a local velocity model, averaged from Hauksson's 3D Sothern California model, to approximate the earth structure at the source region and calibrated the arrival times of teleseismic body and surface waves by using the nearby 2009 M5.8 foreshock. Our result reveals a complex rupture process of the 2010 event. It initiated at a depth of 7.3 km on a fault striking 11o with significant normal motion. It first propagated upward along the fault and triggered the other two high-angle faults, striking northwest and southeast, in the beginning 12 s with negligible moment release. It then propagated on those three faults simultaneously and released most (~ 90%) of the seismic moment between 12 s and 40 s. It yielded a total seismic moment of 1.31×1020 N.m with a rupture duration of 60 s and an average rupture velocity of only 1.2 km/s. This earthquake is dominated by the strike-slip motion but with a significant normal motion component below the hypocenter region, resulting a large (31%) CLVD. The slip distribution in the northwest fault segment is well constrained by the GPS statics and waveforms in Southern California. The heterogeneous rupture in the northwest segment, changing from oblique motion to pure strike-slip and to oblique motion from the epicenter to the northwest, is consistent with surface observations.

FINITE FAULT INVERSION OF MODERATE AND LARGE EARTHQUAKES IN SOUTHERN CALIFORNIA USING NEAR REAL-TIME HIGH RATE GPS AND STRONG MOTION WAVEFORMS (2-143)
X. Zhao, G. Shao, X. Li, and C. Ji

We develop the quick finite fault inversion algorithm by incorporating the near real-time high rate GPS waveforms with the CISN strong motion data to routinely study the rupture process of moderate and large earthquakes in Southern California, which can involve more reliable low-frequency signals into the inversion and can better constrain the total seismic moment than the inversion solely based on the strong motion data. We also optimize the inversion algorithm and accelerate the calculation speed by adopting the Open Multi-Processing (OpenMP) technique to take advantage of multi-core CPU. The preliminary test shows that the speed of our finite fault inversion could be easily improved by a factor of two in a Quad-core system. Moreover, an Open Finite Fault Inversion Platform (OFFIP) for wide scientists is under construction by optimizing the web-based IO module and the weight strategy for combining high rate GPS and strong motion waveforms together is explored as well. Finally, we test this new algorithm by using the recent Mw 5.4 Collins Valley earthquake and the Mw 7.2 El Mayor-Cucapah earthquake.

CHALLENGES AND PROSPECTS FOR HIGH PERFORMANCE COMPUTING WITH SORD (1-015)
J. Zhou, Y. Cui, K. Lee, G.P. Ely, and P.J. Maechling

The SORD (Support Operator Rupture Dynamics) code is a generalized finite difference code (Ely, 2008, 2009) used for a growing number of applications within the SCEC community, such as dynamic rupture simulation, wave propagation and ground motion simulation, and full-waveform tomography. As higher resolution and larger size simulation with this code is demanded, system efficiency may deteriorate due to the complex computer architecture (hierarchical cache architecture), limited middle-ware supports (MPI, OpenMP and etc) or even the algorithm design approach (vectorization for big loop). In order to deliver highly optimal code, it is critical to comprehensively examine the data issues in SORD such as the I/O, computation and communication patterns.

To address these challenges, we are redesigning I/O in SORD employing the high performance contiguous I/O and data redistribution scheme, in order to enhance I/O performance, scalability and reliability. After the implementation of the new parallel output scheme, we observe excellent scalability of the code performance with I/O up to 16K cores on NICS Cray XT5 Kraken system. Further improvements are on the way to provide scalable initialization by processing highly contiguous big chunk data instead of multiple fragments and minimizing communication distance to reduce the communication overhead. To improve the

computation efficiency, we propose a hybrid mechanism, incorporating CUDA and asynchronous MPI implementation to speedup the critical computational loop. While CUDA is used for pure computational acceleration, non-blocking MPI message passing is designed to hide the latency by overlapping the times spent during data transfer between CPU and GPU and for MPI communication. The hybrid CPU/GPU programming will significantly improve parallelism and throughput simultaneously in the coming architectures with GPU chips integrated or cohabitated.

Meeting Participants

AAGAARD Brad, *USGS*
AGNEW Duncan, *UCSD*
AGUIAR Ana, *Stanford*
AKCIZ Sinan, *UC Irvine*
ALANIZ Emigdio, *ELAC*
ALLAM Amir, *USC*
ALPERT Lisa, *USC*
ALVAREZ Melva, *PCC*
ALVIZURI Celso, *UCSB*
AMPUERO Jean Paul, *Caltech*
ANDERSON Robert, *CEA*
ANDERSON Greg, *NSF*
ANDERSON Brian, *PCC*
ANDERSON John, *UNR*
ANDREWS Dudley , *USGS*
APPLEGATE David, *USGS*
ARCHULETA Ralph, *UCSB*
ARROWSMITH Ramon, *ASU*
ASPIOTES Aris, *USGS*
ASSIMAKI Dominic, *Georgia Tech*
BAKER Jack, *Stanford*
BALLEW Natalie, *USC*
BALTAY Annemarie, *Stanford*
BARBA Magali, *UC Berkeley*
BARBOT Sylvain, *Caltech*
BARBOUR Andrew, *UCSD*
BARNHART William, *Cornell*
BARRETT Sarah, *Stanford*
BARTLOW Noel, *Stanford*
BEAUDOIN Bruce, *IRIS PASSCAL*
BECKER Andrew, *Texas A&M*
BEELER Nick, *USGS*
BEGHEIN Caroline, *UCLA*
BEHR Whitney, *USC*
BEN-ZION Daniel, *USC*
BEN-ZION Yehuda, *USC*
BENDER Carrie, *CSUN*
BENSON Rick, *IRIS DMC*
BENTHIEN Mark, *SCEC / USC*
BEROZA Gregory, *Stanford*
BHAT Harsha, *USC/Caltech*
BHATTACHARYA Pathikrit, *Western Ontario*
BIASI Glenn, *UNR*
BILHAM Roger, *Colorado*
BIRD Peter, *UCLA*
BISHOP Scott, *UC Davis*
BLANPIED Michael, *USGS*
BLISNIUK Kimberly, *UC Davis*
BOCK Yehuda, *UCSD*
BOETTCHER Margaret, *USGS*
BOHON Wendy, *ASU*
BOORE David, *USGS*
BORSA Adrian, *UNAVCO*
BOUTWELL Christiann, *USC*
BOWMAN David, *CSU Fullerton*
BOYD Oliver, *USGS*
BOYD Elena, *UT Austin*
BRADLEY Andrew, *Stanford*
BRADLEY Brendon, *Canterbury*
BROCHER Thomas, *USGS*
BRODSKY Emily, *UCSC*
BROTHERS Daniel, *USGS*
BROWN Justin, *Stanford*
BROWN Kevin M., *UCSD*
BROWNBRIDGE Brian, *Milor High School*
BRUNE James, *UNRSL*
BUGA Michael, *SDSU*
BÜRGMANN Roland, *Berkeley*
BURTON Jodie,
BWARIE John, *USGS*
BYDLON Samuel, *Penn State*
BYKOVTSEV Alexander, *Construction Testing & Engr*
BYWATER Jamie, *Sonoma State*
CADENA Ana, *CWU*
CALAIS Eric, *Purdue Unviersity*
CALLAGHAN Scott, *SCEC*
CAMPBELL Kenneth, *EQECAT*
CARPENTER Ivy, *UCLA*
CASTIGLIONE Thomas, *J. W. North High School*
CASTRO Saul, *PCC*
CATCHINGS Rufus, *USGS*
CELEBI Mehmet, *USGS*
CHEN Ting, *Caltech*
CHEN Zizhong, *Colorado School of Mines*
CHEN Jiangzhi, *Oregon*
CHEN Xiaowei, *UCSD*
CHEN Hanlong, *USC*
CHEN Po, *Wyoming*
CHESTER Judith, *Texas A&M*
CHIOU Ray, *NAVFAC Command*
CHO Hyunghoon, *Stanford*
CHOI Dong Ju, *SDSC*
CHOURASIA Amit, *SDSC*
CHUANG Yun-Ruei, *Indiana*
CHUNG Angela, *Stanford University*
CHUNG Karina, *Wellesley College*
CIVILINI Francesco, *UCSB*
CLAYTON Robert, *Caltech*
COCHRAN Elizabeth, *UCR*
COLELLA Harmony, *UCR*
COLUNGA Javier, *ASU*
COMBOUL Maud, *USC*
COOKE Michele, *UMass*
COOPER Jacqueline, *PUHSD*
CREMPIEN Jorge, *UCSB*
CROWELL Brendan, *UCSD*
CUI Yifeng, *UCSD*
CURREN Robert, *Kansas State*
DAHMEN Karin, *Illinois*
DANSBY Benjamin, *USC*
DAUB Eric, *Los Alamos National Laboratory*
DAVIS Paul, *UCLA*
DAWSON Timothy, *CGS*
DAY Steve, *SDSU*
DE GROOT Robert, *SCEC*
DEDONTNEY Nora, *Harvard*
DEELMAN Ewa, *ISI*
DEL PARDO Cecilia, *UTEP*
DENOLLE Marine, *Stanford*
DEOLARTE Arnol, *ELAC*
DETERMAN Daniel, *USGS*
DETRICK Robert, *NSF*
DIEHL John, *GEOVision*
DIETERICH James, *UCR*
DILLON Jessica-Ann, *CSUN*
DMOWSKA Renata, *Harvard*
DOLAN James, *USC*
DOMINGUEZ RAMIREZ Luis, *UCLA*
DONOVAN Jessica, *USC*
DOR Ory, *Ecolog Engineering*
DORAN Adrian, *Dartmouth*
DUAN Benchun, *Texas A&M*
DUNCAN John, *Baylor*
DUNHAM Eric, *Stanford*
EISSES Amy, *UNR*
ELBANNA Ahmed, *Caltech*
ELKHOURY Jean, *Caltech*
ELLIOTT Austin, *UC Davis*
ELLSWORTH William, *USGS*
ELY Geoffrey, *USC*
ERICKSON Brittany, *Stanford*
FANG Zijun, *Stanford*
FEAUX Karl, *UNAVCO*
FELZER Karen, *USGS*
FIALKO Yuri, *UCSD*
FIELD Edward, *USGS*
FILSON John, *USGS*
FISHER Meghan, *Bryn Mawr*
FLETCHER John, *CICESE*
FLOYD Michael, *UCR*
FOUTZ Anna, *John W. North HS*
FRARY Roxanna, *UNR*
FREEMAN Stephen, *GeoPentech*
FREYMULLER Jeffrey, *Alaska*
FUIS Gary, *USGS*
FUKUDA Junichi, *Indiana*
FUMAL Thomas, *USGS*
FUNNING Gareth, *UCR*

GABUCHIAN Vahe, *Caltech*
GALETZKA John, *Caltech*
GANEV Plamen, *USC*
GATH Eldon, *ECI*
GEE Robin, *UCSB*
GELBACH Lauren, *USC*
GILCHRIST Jacquelyn, *UCSC*
GOEBEL Thomas, *USC*
GOLD Peter, *UC Davis*
GOLDSBY David, *Brown*
GONZALEZ Marisol, *Chico State*
GONZALEZ-FERNANDEZ Antonio, *CICESE*
GONZÀLEZ-GARCÌA Jose Javier, *CICESE*
GONZALEZ-ORTEGA Alejandro, *CICESE*
GOODING Margaret, *LSA Associates, Inc.*
GORMLEY Deborah, *SCEC*
GOULET Christine, *URS*
GOW Irene, *USC*
GRANT LUDWIG Lisa, *UCI*
GRAVES Robert, *USGS*
HADDAD David, *ASU*
HAGOS Lijam, *CGS/SMIP*
HALLER Kathleen, *USGS*
HANKS Tom, *USGS*
HARAVITCH Ben, *USC*
HARDEBECK Jeanne, *USGS*
HARRIS Karl, *USC*
HARRIS Ruth, *USGS*
HATAYAMA Ken, *USGS*
HAUKSSON Egill, *Caltech*
HAUKSSON Sven, *UNR*
HEARN Elizabeth, *UBC*
HEATON Thomas, *Caltech*
HECKMAN Vanessa, *Caltech*
HEERMANCE Richard, *CSUN*
HEIEN Eric, *UC Davis*
HENRY Pamela, *Fault Line, LLC*
HERBERT Justin, *UMass*
HERRING Thomas, *MIT*
HICKS Andrew, *UNR*
HINOJOSA CORONA Alejandro, *CICESE*
HIRTH Greg, *Brown*
HOGAN Phillip, *Fugro West*
HOIRUP Don, *CA Dept. of Water Resources*
HOLLAND Austin, *Oklahoma*
HOLT William, *SUNY-Stony Brook*
HOOKS Benjamin, *UTEP*
HUANG Yihe, *Caltech*
HUDNUT Kenneth, *USGS*
HUTH Alexander, *Cornell*
HUTHSING Daniel, *UCSB*
HUYNH Tran, *SCEC*
HWANG Grace, *USC*
INBAL Asaf, *Caltech*
JACKSON David, *UCLA*
JANECKE Susanne, *Utah State*
JAYARAM Nirmal, *RMS.*
JI Kang Hyeun, *MIT*
JI Chen, *UCSB*
JIANG Junle, *Caltech*
JIN Lizhen, *UCR*
JOHNSON McKinley, *CSUSB*
JOHNSON Kaj, *Indiana*
JOHNSON Leonard, *NSF*
JOHNSON Marilyn, *PCC*
JONES Megan, *SDSU*
JONES Pierson, *UCI*
JONES Lucile, *USGS*
JORDAN Thomas, *USC*
JORDAN, JR. Frank, *John R. Byerly*
KAGAN Yan, *UCLA*
KALKAN Erol, *USGS*
KANAMORI Hiroo, *Caltech*
KANE Deborah, *UCSD*
KANEKO Yoshihiro, *IGPP / SIO*
KANG Jingqian, *Texas A&M*
KARAOGLU Haydar, *CMU*
KEDAR Sharon, *JPL*
KELL-HILLS Annie, *UNR*
KENDRICK Katherine, *USGS*
KENT Graham, *UNR/NSL*
KILB Debi, *UCSD*
KING Nancy, *USGS*
KIRKPATRICK James, *UCSC*
KITAJIMA Hiroko, *Texas A&M*
KOWALKE Sara, *SDSU*
KOZDON Jeremy, *Stanford*
KREEMER Corné, *UNR*
KRISHNAN Swaminathan, *Caltech*
KROLL Kayla, *UCR*
KUMAR Sandarsh, *USC*
KURT Hulya, *Istanbul Technical*
LAJOIE Lia, *UCSC*
LANGENHEIM Victoria, *USGS*
LAPUSTA Nadia, *Caltech*
LAUDA Samuel, *PCC*
LAVALLEE Daniel, *UCSB*
LAWRENCE Jesse, *Stanford*
LÁZARO-MANCILLA Octavio, *UABC*
LEE Ya Ting, *NCU Taiwan*
LEE Kwangyoon, *SDSC*
LEE En-Jui, *Wyoming*
LEEPER Robert, *USGS*
LEGG Mark, *Legg Geophysical*
LEMERSAL Elizabeth, *USGS*
LEMME Nathan, *NAVFAC ESC/US Navy*
LEWIS Michael, *UCSD*
LI Xiangyu, *UCSB*
LI Yong-Gang, *USC*
LIANG Andy, *USC*
LIAO Eric, *UCR*
LIEL Abbie, *Colorado*
LINDSEY Eric, *UCSD*
LIPOVSKY Brad, *UCR*
LIPOW James, *Valley View High*
LIU Zhen, *JPL*
LIU Zaifeng, *Texas A&M*
LIU Qiming, *UCSB*
LIU Pengcheng, *US Bureau of Reclamation*
LIUKIS Maria, *SCEC*
LOHMAN Rowena, *Cornell*
LOUIE John, *UNR*
LOZOS Julian, *UCR*
LUCO Nicolas, *USGS*
LUNDGREN Paul, *JPL*
LYNCH David, *USGS*
MA Kuo-Fong, *National Central University, Taiwan*
MACCARTHY Dawn, *USGS*
MADDEN Christopher, *Oregon State*
MADDEN Elizabeth, *Stanford*
MAECHLING Philip, *SCEC*
MAHAN Shannon, *USGS*
MAI Paul, *KAUST*
MARLIYANI Gayatri, *SDSU*
MARQUIS John, *SCEC*
MARSHALL Scott, *Appalachian State*
MATSUBARA Makoto, *NIED, Japan*
MAZZONI Silvia, *Degenkolb Engineers*
MCAULIFFE Lee, *USC*
MCBURNETT Paul, *CSUN*
MCCARTHY Jill, *USGS*
MCGILL Sally, *CSUSB*
MCGUIRE Kathleen, *CSUN*
MCGUIRE Jeff, *WHOI*
MCKAY Hannah, *CSUN*
MCLASKEY Gregory, *Berkeley*
MCQUINN Emmett, *UCSD*
MCRANEY John, *SCEC / USC*
MEIJER Michelle, *Eleanor Roosevelt High School*
MELLO Michael, *Caltech*
MELTZER Anne, *Lehigh*
MELTZNER Aron, *Caltech / Earth Observatory of Singapore*
MENG Lingsen, *Caltech*
MENGES Christopher, *USGS*
MERRIAM Martha, *Caltrans*
MICHAEL Andrew, *USGS*
MILETI Dennis, *Colorado*
MILNER Kevin, *SCEC*
MINSON Sarah, *Caltech*
MINSTER Jean, *UCSD*
MONTES DE OCA John, *USC*
MOODY Jessica, *Umass*
MOONEY Walter, *USGS*

MORELAN Alex, *UC Davis*
MORELAND Sarah, *CSU Monterey Bay*
MORTON Nissa, *SDSU*
MORTON Sarah, *UCR*
MOSCHETTI Morgan, *USGS*
MOURHATCH Ramses, *Caltech*
MUELLER Karl, *Colorado*
MURPHY Janice, *USGS*
MURRAY-MORALEDA Jessica, *USGS*
NANJO Kazuyoshi, *Tokyo*
NEE Philip, *UCR / Cornell*
NEIGHBORS Corrie, *UCR*
NI Sidao, *U. Science & Tech, China*
NICHOLSON Craig, *UCSB*
NIGBOR Robert, *UCLA*
NODA Hiroyuki, *Caltech*
NORIEGA Gabriela, *UCI*
NYST Marleen, *RMS, Inc.*
OGLESBY David, *UCR*
OKAYA David, *USC*
OLSEN Anna, *Colorado*
OLSEN Kim, *SDSU*
ONDERDONK Nate, *CSULB*
ORTEGA Gustavo, *Caltrans*
OSKIN Michael, *UC Davis*
OWEN Susan, *JPL*
OZAKIN Yaman, *USC*
PACE Alan, *Petra Geotechnical*
PAGE Morgan, *USGS*
PANDEY Anand, *SDSU*
PANDEY Prabha, *SDSU*
PATINO Alec, *USC*
PAULSON Elizabeth, *USC*
PENG Zhigang, *Georgia Tech*
PEREZ Christy, *Chaffey High*
PLATT John, *Harvard*
PLATT John, *USC*
PLENKERS Katrin, *Karlsruhe Institute of Technology*
POLET Jascha, *Cal Poly Pomona*
POLLARD David, *Stanford*
PONTI Daniel, *USGS*
PORTER Ryan, *Arizona*
PORTER Keith, *Colorado*
POTIER Chelsea, *St. Norbert*
POTTER Hannah, *Cal Poly Pomona*
POUNDERS Erik, *USGS*
POWERS Peter, *USGS*
PRIETO German, *Universidad de los Andes*
PURASINGHE Rupa, *CSULA*
RAMIREZ-GUZMAN Leonardo, *USGS*
RAMSEY Tina, *Montclair High*
RAMZAN Shahid, *CSUN*
REMPEL Alan, *Oregon*
REPLOGLE Crystal, *SDSU*
RESTREPO José, *UCSD*
RHOADES David, *GNS Science*
RHODES Edward, *UCLA*
RICE James, *Harvard*
ROBINSON Sarah, *ASU*
ROBLES Yessenia, *CSULB*
ROCKWELL Thomas, *SDSU*
RODGERS Arthur, *LLNL*
RODRIGUEZ Juan, *ELAC*
ROLLINS John, *USC*
ROMERO Salvador, *PCC*
ROOD Dylan, *LLNL*
ROSE Elizabeth, *USGS*
ROSS Tyler, *US Navy*
ROSS Stephanie, *USGS*
ROTEN Daniel, *SDSU*
ROUSSEAU Nick, *USGS*
ROWE Christie, *UCSC*
ROWSHANDEL Badie, *CGS*
RUBIN Allan, *Princeton*
RUBINSTEIN Justin, *USGS*
RUDOLPH Maxwell, *Berkeley*
RUIZ Ricardo, *Chaffey High*
RUNDLE John, *UC Davis*
RUNNERSTROM Miryha,
RYAN Kenny, *UCR*
RYMER Michael, *USGS*
RYU Hyeuk, *Colorado*
SALISBURY James, *SDSU*
SAMMIS Charles, *USC*
SANDWELL David, *UCSD*
SCHARER Katherine, *Appalachian State*
SCHMANDT Brandon, *Oregon*
SCHMITT Stuart, *Stanford*
SCHORLEMMER Danijel, *USC*
SEALE Sandra, *UCSB*
SEGALL Paul, *Stanford*
SEITZ Gordon, *CGS*
SELIGSON Hope, *MMI Engr*
SEVILGEN Volkan, *USGS*
SHAO Guangfu, *UCSB*
SHARP Warren, *Berkeley Geochronology*
SHAW Bruce, *Columbia*
SHAW John, *Harvard*
SHEARER Peter, *UCSD*
SHEEHAN Michael, *USC*
SHELLY David, *USGS*
SHEN Zheng-Kang, *UCLA*
SHI Zheqiang, *SDSU*
SHIFFERMILLER Barbara, *Chaffey High*
SHOME Nilesh, *RMS*
SICKLER Robert, *USGS*
SIMILA Gerry, *CSUN*
SIMONS Mark, *Caltech*
SIRIKI Hemanth, *Caltech*
SLADEN Anthony, *Caltech*
SLEEP Norman, *Stanford*
SMALL Patrick, *SCEC*
SMITH Deborah, *UCR*
SMITH-KONTER Bridget, *UTEP*
SOLIS Teira, *UTEP*
SOMALA Surendra Nadh, *Caltech*
SOMERVILLE Paul, *URS*
SONG Seok Goo, *URS*
SORLIEN Christopher, *UCSB*
SOTO Elena, *Loyola Marymount*
SPRINGER Kathleen, *SBCM*
SPUDICH Paul, *USGS*
STAR Lisa, *UCLA*
STARK Keith, *SCIGN*
STEIDL Jamison, *UCSB*
STEIN Ross, *USGS*
STEVENS Adam, *PCC*
STIRLING Mark, *GNS Science*
STOCK Joann, *Caltech*
STRADER Anne, *UCLA*
STREIG Ashley, *Oregon*
STUBAILO Igor, *UCLA*
SU Feng, *US Bureau of Reclamation*
SWIFT Mark, *CSUSB*
TABORDA Ricardo, *CMU*
TAKEDATSU Rumi, *SDSU*
TANIMOTO Toshiro, *UCSB*
TAPE Carl, *Harvard*
TARNOWSKI Jennifer, *CSU Fullerton*
THATCHER Wayne, *USGS*
THIO Hong Kie, *URS*
THORNTON Garrett, *UTEP*
THURBER Clifford, *Wisconsin*
TIAN Xiangyan, *Caltech*
TIBULEAC Ileana, *UNR*
TINSLEY John, *USGS*
TODA Shinji, *Kyoto University*
TOKE Nathan, *ASU*
TRATT David, *The Aerospace Corporation*
TREIMAN Jerome, *CGS*
TRENCH David, *Oregon State*
TSAI Victor, *USGS*
TSANG Rebecca, *SDSU*
TULLIS Terry, *Brown*
TURCOTTE Donald, *UC Davis*
UCHIDE Takahiko, *UCSD*
UMA S., *GNS Science*
VALENCIA Aurelio, *ELAC*
VAN DER ELST Nicholas, *UCSC*
VARGAS Bernadette, *Etiwanda High School*
VERDUGO Danielle, *Earth Consultants International*
VIDALE John, *Washington*
VIESCA-FALGUIÈRES Robert, *Harvard*
WALKER Jakayla, *Albany State*

WALKER Brendon, *SDSU*
WALKER Kristoffer, *UCSD*
WALLS Christian, *UNAVCO*
WALTERS Randi, *Stanford*
WALTERS Bryce, *USC*
WANG Enning, *Princeton*
WANG Tien-Huei, *UCR*
WANG Qi, *UCLA*
WANG Feng, *USC*
WANG Wei, *USC*
WARD Steven, *UCSC*
WEAVER Stephanie, *Oregon*
WECHSLER Neta, *SDSU*
WEI Shengji, *Caltech*
WEI Meng, *UCSD*
WEISER Deborah, *USGS/UCLA*
WELCH Kaitlin, *Cincinnati*
WELDON Ray, *Oregon*
WELLER Matthew, *UNR*
WEN Yi-Ying, *UCR*
WERNER Maximilian, *ETHZ*
WESNOUSKY Steven, *UNR*
WESSON Rob, *USGS*
WHITESIDES Andrew, *USC*
WHITNEY John, *USGS*
WILLIAMS Charles, *GNS Science*
WILLIAMS Patrick, *P. Williams Assoc.*
WILLIAMS Chesley, *RMS*
WILLS Chris, *CGS*
WITHERS Kyle, *SDSU*
WOLFSON Monica, *UNH*
WU Chunquan, *Georgia Tech*
WYATT Frank, *UCSD*
XU Shiqing, *USC*
YAMAMOTO Yoshifumi, *Stanford*
YANG Wenzheng, *Caltech*
YANG Zhaohui, *Colorado*
YANO Tomoko, *UCSB*
YEATS Robert, *Oregon State*
YIKILMAZ Mehmet, *UC Davis*
YOKOI Sayoko, *ERI Tokyo*
YONG Alan, *USGS*
YOUNG Karen, *USC*
YU Ellen, *Caltech*
YU John, *USC*
YULE Doug, *CSUN*
YUN Sang-Ho,
ZALIAPIN Ilya, *UNR*
ZANZERKIA Eva, *NSF*
ZAREIAN Farzin, *UCI*
ZECHAR Jeremy, *ETHZ*
ZENG Yuehua, *USGS*
ZHAN Zhongwen, *Caltech*
ZHANG Panxu, *USC*
ZHAO Xu, *UCSB*
ZHONG Jinquan, *SDSU*
ZHOU Jun, *SDSC*
ZIELKE Olaf, *ASU*
ZOBACK Mary Lou, *RMS*